Tropical Cardiovascular Pathology

Autopsy-Based Clinicopathological Cases

Pradeep Vaideeswar
Editor

Springer

Tropical Cardiovascular Pathology

Pradeep Vaideeswar
Editor

Tropical Cardiovascular Pathology

Autopsy-Based Clinicopathological Cases

Springer

Editor
Pradeep Vaideeswar
Department of Pathology (Cardiovascular & Thoracic Division)
Seth Gordhandas Sunderdas Medical College & King Edward Memorial Hospital
Mumbai, India

ISBN 978-981-19-3719-4 ISBN 978-981-19-3720-0 (eBook)
https://doi.org/10.1007/978-981-19-3720-0

This Springer imprint is published by the registered company Springer Nature Singapore Pte Ltd. The registered company address is: 152 Beach Road, #21-01/04 Gateway East, Singapore 189721, Singapore

Preface

With an exponential rise in recent times, cardiovascular disorders have gained notorious recognition as the top killer disease in the Indian subcontinent. Moreover, coronary heart disease affects Indians 5 or 6 years earlier than their western counterparts. Rheumatic heart disease has scourged this part of the world since eternity and continues to be the commonest cardiovascular disease in the young. With a rapidly rising population and a large number of young individuals, congenital heart disease also seems to be more prevalent. In short, the cardiovascular disease burden on the Indian subcontinent is more threatening than ever before. Every effort is being made at every possible level to change this scenario. Though universal health insurance is lacking, various health insurance schemes have been introduced. Skilled manpower and cutting-edge technology are being made available with every passing day. Free or low-cost health camps are being held at grassroots level to address the problem in rural areas. Efforts are being made to catch the disease early to maximize results. Active involvement by a cardiovascular pathologist not only saves the day by examining specimens but also establishes useful feedback mechanisms, which are extremely essential for perpetual quality control. This is particularly true of endomyocardial biopsy that is performed for various myocardial diseases. With the establishment of centers primarily aimed for cardiac care and changing criteria for treatment of various disorders, a surgical pathologist may encounter tissues other than valves, atherectomies or biopsies. Besides, cardiac transplantation has now become fairly well entrenched as a procedure in many institutes.

Apart from the knowledge gained through assessment of surgically excised specimens, examination of the cardiovascular system at autopsy has played a very important role in the understanding of several cardiovascular disorders. Though the rate of clinical autopsy has declined the world over, it nevertheless serves as an important tool of quality assurance in clinical medicine and therefore continues to be relevant in this high technology era. Founded in 1926, the twin institutes of Seth Gordhandas Sunderdas Medical College and the King Edward Memorial Hospital are one of the most important tertiary care and teaching hospitals in Mumbai and have autopsy facility for clinical as well as medico-legal cases. A unique feature is that some of them are performed by experts from Pathology and Forensic Medicine departments, the so-called combined autopsies; effectively around 800 autopsies are performed by the pathology staff. The 2200 bedded hospital has 55 wards and 15 intensive care units for different medical and surgical specialties, treating

about 1.8 million outpatients and 85,000 inpatients annually from across the state and country. It provides low-cost basic care and advanced treatment facilities in all fields of medicine and surgery, and majority of the patients are from low socio-economic strata. Besides illiteracy, a high population density, lack of awareness, inadequate health care system, alcohol and tobacco addiction, the tendency to tolerate symptoms for a long time before seeking medical attention and reliance on traditional medicine add to the problem. Hence, the average clinician across all specialties in India faces a disease process, which is more complex, long-standing and neglected, and hence the natural history of varied cardiovascular diseases along with common and uncommon complications is often encountered at autopsy. This case-based book deals with our experience of cardiovascular diseases at autopsies.

Mumbai, India — Pradeep Vaideeswar
Ahmednagar, India — Sagar Kulat
New Delhi, India — Shashank Tyagi

Contents

Part I Introduction

1 Basic Cardiac Anatomy and Cardiac Dissection 3
Shashank Tyagi and Pradeep Vaideeswar

Part II Pericardial Diseases

2 Tuberculous Pericarditis. 11
Gayathri Amonkar and Pradeep Vaideeswar

3 Pericardial Hemangiomatosis with Cardiac Tamponade 17
Pradeep Vaideeswar, Milind Tullu, and Priyash Tambi

Part III Valvular Heart Disease: Rheumatic

4 Acute Rheumatic Fever: A Fulminant Form 25
Ashutosh Goyal, Pradeep Vaideeswar, Saranya Singaravel, and Girish Sabnis

5 Silent Rheumatic Mitral Stenosis 31
Pawan Daga, Rushabh Shah, and Pradeep Vaideeswar

6 Rheumatic Mitral Stenosis and Anticoagulant Toxicity 39
Amey Rojekar and Pradeep Vaideeswar

7 Rheumatic Mitral Stenosis with Sickling Crisis. 45
Tejaswini Waghmare and Pradeep Vaideeswar

8 Rheumatic Heart Disease and Prosthetic Valvular Thrombosis 49
Supreet P. Marathe and Pradeep Vaideeswar

9 Dominant Rheumatic Aortic Stenosis 53
Pawan Daga and Pradeep Vaideeswar

Part IV Valvular Heart Disease: Non-Rheumatic

10 Mitral Valvular Prolapse and Sudden Cardiac Death. 61
Shashank Tyagi, Manoj Parchake, and Pradeep Vaideeswar

11 Congenital Valvular Mitral Stenosis 65
Pradeep Vaideeswar and Girish Sabnis

12 Senile Calcific Aortic Stenosis 69
Pradeep Vaideeswar and Sagar Kulat

13 Bicuspid Aortic Stenosis 75
Pradeep Vaideeswar

14 Unicommissural Unicuspid Aortic Stenosis with Idiopathic Aortitis 81
Pradeep Vaideeswar

15 Mitral and Aortic Valvular Regurgitation Due To Rheumatoid Arthritis 85
Pradeep Vaideeswar

Part V Valvular Heart Disease: Verrucous Endocarditis

16 Infective Endocarditis Following Balloon Valvotomy for Rheumatic Mitral Stenosis 93
Pradeep Vaideeswar and Girish Sabnis

17 Infective Endocarditis of Normal Native Mitral Valve 99
Heena Desai and Pradeep Vaideeswar

18 Primary Botryomycotic Left-Sided Infective Endocarditis 103
Pradeep Vaideeswar and Sakshi Jain

19 Fungal Endocarditis of Normal Native Mitral Valve in a Renal Transplant Recipient 107
Gwendolyn Fernandes and Pradeep Vaideeswar

20 Right-Sided Infective Endocarditis in a Child 115
Pragati Sathe and Pradeep Vaideeswar

21 Isolated Pulmonary Valvular Infective Endocarditis in a Univentricular Heart 121
Heena Desai and Pradeep Vaideeswar

22 Nonbacterial Thrombotic Endocarditis and Occult Lung Adenocarcinoma 125
Pradeep Vaideeswar

23 Libman-Sacks Endocarditis 133
Smita Divate and Pradeep Vaideeswar

Part VI Ischemic Myocardial Disorders

24 Acute Myocardial Infarction in the Young 141
Shashank Tyagi, Pradeep Vaideeswar, and Girish Tasgaonkar

25 Acute Mitral Regurgitation in Acute Myocardial Infarction . . . 147
Pradeep Vaideeswar

26 Acute Myocardial Infarction with Left Ventricular Free Wall Rupture 151
Ayushi Gupta, Girish Tasgaonkar, and Pradeep Vaideeswar

27 Acute Hemorrhagic Myocardial Infarction 155
Swati Kolhe, Pranita Zare, and Pradeep Vaideeswar

28 Healed Myocardial Infarction with Left Ventricular Mural Thrombus 159
Pradeep Vaideeswar

29 Coronary Stent Infection 165
Saranya Singaravel and Pradeep Vaideeswar

30 Intramural Coronary Arterial Thrombosis and Myocardial Ischemia 171
Pradeep Vaideeswar, Jayashri Chaudhari, and Smita Divate

31 Anomalous Coronary Artery Origin and Sudden Cardiac Death 177
Swati Kolhe, Pranita Zare, and Pradeep Vaideeswar

32 Extensive Myocardial Scarring in a Neonate 181
Pragati Sathe and Pradeep Vaideeswar

Part VII Non-Ischemic Myocardial Disorders

33 Acute Lymphocytic Myocarditis and Sudden Cardiac Death . . 187
Ketan Ingle, Girish Tasgaonkar, and Pradeep Vaideeswar

34 Acute Leptospiral Myocarditis 193
Rachana Binayke, Heena Desai, Pradeep Vaideeswar, and Smita Divate

35 Cardiac Toxoplasmosis 199
Heena Desai and Pradeep Vaideeswar

36 Aspergillous Myocardial Absceses 203
Pradeep Vaideeswar

37 Dual Mycosis of the Heart 207
Jayashri Chaudhari, Pradeep Vaideeswar, Shruti Mondkar, and Milind Tullu

38 Tuberculous Myocarditis 215
Gayathri Amonkar and Pradeep Vaideeswar

39 Isolated Cardiac Sarcoidosis 221
Manoj Parchake, Shashank Tyagi, and Pradeep Vaideeswar

40 Giant Cell Myocarditis 225
Pradeep Vaideeswar and Ketan Ingle

41 Dilated Cardiomyopathy 229
Pradeep Vaideeswar

42 Pheochromocytoma-Induced Cardiomyopathy 233
Pradeep Vaideeswar, Mrinal Sarwate, and Smita Divate

43 Hypertrophic Cardiomyopathy 239
Pradeep Vaideeswar and Shashank Tyagi

44 Arrhythmogenic Cardiomyopathy 243
Pradeep Vaideeswar

45 Restrictive Cardiomyopathy: Loeffler's Endo-Myocarditis 247
Pradeep Vaideeswar and Tejaswini Waghmare

46 Endomyocardial Fibrosis as an Incidental Autopsy Finding . . . 257
Pradeep Vaideeswar and Pranita Zare

47 Cardiac Amyloidosis in an Octagenarian 263
Pradeep Vaideeswar, Girish Sabnis, and Dhiraj Kumar

48 Isolated Fabry Cardiomyopathy 269
Pradeep Vaideeswar and Shobhana P. Pandit

49 Acute Myocardial Calcification: Sepsis-Related? 273
Pradeep Vaideeswar

50 Cardiac Involvement in Primary Hyper-Oxaluria 277
Pradeep Vaideeswar and Gwendolyn Fernandes

51 Endocardial Fibroelastosis 281
Pragati Sathe and Pradeep Vaideeswar

Part VIII Cardiac Tumors

52 Neonatal Multifocal Rhabdomyomas 287
Tejaswini Waghmare and Pradeep Vaideeswar

53 Undifferentiated Pleomorphic Sarcoma Mimicking Left Atrial Myxoma 291
Pradeep Vaideeswar and Amey Rojekar

54 Intracardiac Metastases of Squamous Cell Carcinoma 297
Pradeep Vaideeswar, Anuja Kekatpure, Subhash Yadav, and Neha Lanke

55 Cardiac Posttransplant Lymphoproliferative Disorder 301
Pradeep Vaideeswar, Gwendolyn Fernandes, and Pritam Khairkar

56 Leiomyosarcoma of the Inferior Vena Cava 309
Pradeep Vaideeswar

Part IX Systemic Vascular Diseases

57 Supra-Cardiac Aortic Atherosclerosis 315
Swati Kolhe and Pradeep Vaideeswar

58 Shaggy Aortic Syndrome, Penetrating Atherosclerotic Ulcer, and Rupture 319
Pradeep Vaideeswar and Pranita Zare

59 Atherosclerosis and Neutrophils 323
Pradeep Vaideeswar

60 Acute Aortic Dissection 327
Pradeep Vaideeswar, Girish Sabnis, Charan Lanjewar, and Sarit Kundu

61 Ascending Aortic Aneurysm 333
Pradeep Vaideeswar

62 Long-Segment Aortic Thrombosis with Myoglobinuria and Acute Renal Failure 337
Pradeep Vaideeswar and Balaji Baste

63 Childhood Takayasu's Arteritis 343
Pradeep Vaideeswar

64 Takayasu's Arteritis Manifesting as Intestinal Gangrene 349
Pradeep Vaideeswar

65 Takayasu's Arteritis Complicated by Chronic Aortic Dissection, False Channel Aneurysm, and Aorto-Esophageal Fistula 355
Pradeep Vaideeswar and Subhash Yadav

66 Tuberculous Aortitis with Ruptured Pseudoaneurysm 361
Pradeep Vaideeswar and Gayathri Amonkar

67 Tuberculous Coronary Arteritis and Sudden Cardiac Death . . . 367
Pradeep Vaideeswar and Gayathri Amonkar

Part X Pulmonary Vascular Disorders

68 Chronic Pulmonary Thromboembolism with Membranous Nephropathy 373
Pradeep Vaideeswar and Lovelesh Nigam

69 Pulmonary Tumor Embolism in a Case of Hepatocellular Carcinoma 379
Pradeep Vaideeswar

70 Uterine Choriocarcinoma with Pulmonary Tumor Thrombotic Microangiopathy 383
Pradeep Vaideeswar and Mona Agnihotri

71 Pulmonary Arterial Hypertension in an Infant 389
Pradeep Vaideeswar

72 Porto-Pulmonary Hypertension in Extrahepatic Portal Vein Obstruction 393
Pradeep Vaideeswar, Swati Kolhe, and Manjusha Karegar

73 Takayasu's Disease with Predominant Pulmonary Arterial Involvement 397
Pradeep Vaideeswar

74 Necrotizing Pulmonary Arteritis with Rheumatic Mitral Stenosis. 401
Smita Divate and Pradeep Vaideeswar

75 Pulmonary Arterial Hypertension and Connective Tissue Disorders 407
Pradeep Vaideeswar and Smita Divate

Contributors

Mona Agnihotri Department of Pathology, Seth Gordhandas Sunderdas Medical College and King Edward Memorial Hospital, Mumbai, India

Gayathri Amonkar Department of Pathology, Topiwala National Medical College and BYL Nair Charitable Hospital, Mumbai, India

Balaji Baste Department of Pathology, Seth Gordhandas Sunderdas Medical College and King Edward Memorial Hospital, Mumbai, India

Rachana Binayke Department of Pathology, Grant Government Medical College and JJ Group of Hospitals, Mumbai, India

Jayashri Chaudhari Department of Pathology, Hindu Hriday Samrat Balasaheb Thackeray Medical College, Mumbai, India

Pawan Daga Seth Gordhandas Sunderdas Medical College and King Edward Memorial Hospital, Mumbai, India

Heena Desai Department of Pathology, Topiwala National Medical College and BYL Nair Charitable Hospital, Mumbai, India

Smita Divate Department of Pathology, Seth Gordhandas Sunderdas Medical College and King Edward Memorial Hospital, Mumbai, India

Gwendolyn Fernandes Department of Pathology, Seth Gordhandas Sunderdas Medical College and King Edward Memorial Hospital, Mumbai, India

Ashutosh Goyal Seth Gordhandas Sunderdas Medical College and King Edward Memorial Hospital, Mumbai, India

Ayushi Gupta Seth Gordhandas Sunderdas Medical College and King Edward Memorial Hospital, Mumbai, India

Ketan Ingle Department of Pathology, Seth Gordhandas Sunderdas Medical College and King Edward Memorial Hospital, Mumbai, India

Sakshi Jain Seth Gordhandas Sunderdas Medical College and King Edward Memorial Hospital, Mumbai, India

Manjusha Karegar Department of Pathology, Seth Gordhandas Sunderdas Medical College and King Edward Memorial Hospital, Mumbai, India

Anuja Kekatpure AKMC Pathology Laboratory and Nurture Diagnostics, Nagpur, India

Pritam Khairkar Department of Pathology, Chhindwara Institute of Medical Sciences, Chhindwara, India

Swati Kolhe Department of Pathology, Seth Gordhandas Sunderdas Medical College and King Edward Memorial Hospital, Mumbai, India

Sagar Kulat Director, Rudhira Diagnostics, Ahmednagar, India

Dhiraj Kumar Dr KK Datey Department of Cardiology, Seth Gordhandas Sunderdas Medical College and King Edward Memorial Hospital, Mumbai, India

Sarit Kundu Seth Gordhandas Sunderdas Medical College and King Edward Memorial Hospital, Mumbai, India

Charan Lanjewar Dr KK Datey Department of Cardiology, Seth Gordhandas Sunderdas Medical College and King Edward Memorial Hospital, Mumbai, India

Neha Lanke Department of Pathology, MGM Medical College, Aurangabad, India

Supreet P. Marathe Faculty of Medicine, Queensland Children's Hospital, University of Queensland, Brisbane, Australia

Shruti Mondkar Department of Pediatrics, Seth Gordhandas Sunderdas Medical College and King Edward Memorial Hospital, Mumbai, India

Lovelesh Nigam Department of Pathology, Institute of Kidney disease and Research Center, HL Trivedi Institute of Transplantation Sciences, Gujarat University, Ahmedabad, India

Shobhana P. Pandit Department of Pathology (Cardiovascular and Thoracic Division), Seth Gordhandas Sunderdas Medical College and King Edward Memorial Hospital, Mumbai, India

Manoj Parchake Department of Forensic Medicine and Toxicology, Seth Gordhandas Sunderdas Medical College and King Edward Memorial Hospital, Mumbai, India

Amey Rojekar Department of Pathology, Seth Gordhandas Sunderdas Medical College and King Edward Memorial Hospital, Mumbai, India

Girish Sabnis Dr KK Datey Department of Cardiology, Seth Gordhandas Sunderdas Medical College and King Edward Memorial Hospital, Mumbai, India

Mrinal Sarwate PGY 3, Cleveland Clinic Foundation, Cleveland, OH, USA

Pragati Sathe Department of Pathology, Seth Gordhandas Sunderdas Medical College and King Edward Memorial Hospital, Mumbai, India

Rushabh Shah SRL Dr Avinash Phadke Labs, Mumbai, India

Saranya Singaravel Soleil Diagnostics, Mumbai, India

Priyash Tambi Department of Pediatrics, Seth Gordhandas Sunderdas Medical College and King Edward Memorial Hospital, Mumbai, India

Girish Tasgaonkar Department of Forensic Medicine and Toxicology, Seth Gordhandas Sunderdas Medical College and King Edward Memorial Hospital, Mumbai, India

Milind Tullu Department of Pediatrics, Seth Gordhandas Sunderdas Medical College and King Edward Memorial Hospital, Mumbai, India

Shashank Tyagi Department of Forensic Medicine and Toxicology, Lady Hardinge Medical College and Associated SSK and KSC Hospitals Connaught Place, New Delhi, India

Pradeep Vaideeswar Department of Pathology (Cardiovascular and Thoracic Division), Seth Gordhandas Sunderdas Medical College and King Edward Memorial Hospital, Mumbai, India

Tejaswini Waghmare Department of Pathology, Seth Gordhandas Sunderdas Medical College and King Edward Memorial Hospital, Mumbai, India

Subhash Yadav Department of Pathology, Tata Memorial Hospital, Mumbai, India

Pranita Zare Department of Pathology (Cardiovascular and Thoracic Division), Seth Gordhandas Sunderdas Medical College and King Edward Memorial Hospital, Mumbai, India

About the Editor

Pradeep Vaideeswar completed his postgraduation in the subject of pathology in 1990 from Bombay University, India. After his appointment as Assistant Professor (5 years), Associate Professor (13 years), and Additional Professor (14 years), he currently holds the position of Professor since 2022 in the Department of Pathology, Seth GS Medical College, Mumbai, India. He completed a specialization in cardiovascular and pulmonary/thoracic pathology with a fellowship in cardiovascular pathology at Toronto General Hospital (Toronto, Ontario, Canada) and held a post of visiting clinician in pulmonary pathology at the Mayo Clinic (Scottsdale, Arizona, USA). Dr. Vaideeswar has authored/coauthored more than 100 papers for platform presentations/posters and has 226 international/national publications to his credit. He participated in around 219 presentations as a faculty member in conferences, workshops, CMEs, and slide seminars. He is a life member of the Indian Association of Pathologists and Microbiologists (IAPM), Pediatric Cardiology Society, Society for Human and Animal Mycologists, Indian Society of Hematology and Transfusion Medicine and served the IAPM as its President (2019), Vice-President (2018), Secretary (2014–2016), and Joint Secretary (2011–2013). He is a current councilor of the Asia-Australasia Pulmonary Pathology Society. Dr. Vaideeswar is an Associate Editor of the *Indian Journal of Pathology and Microbiology* and Member of the Editorial Board of *Cardiovascular Pathology* and *Postgraduate Journal of Medicine*, and a reviewer for several national and international journals in pathology, pulmonary medicine, cardiology, and cardiac surgery.

Part I

Introduction

Basic Cardiac Anatomy and Cardiac Dissection

1

Shashank Tyagi and Pradeep Vaideeswar

1.1 Introduction

Diseases of the brain and heart account for the majority of deaths in developed countries. Yet the heart and brain remain very emotive organs for the public and underlie the reluctance of relatives to agree to their retention at autopsy. When conducting an autopsy, particularly in someone who died unexpectedly without a prior illness (most often related to cardiovascular disease, CVD), one must be prepared to look more carefully at the heart. In an approach to autopsy in a deceased with CVD, retention and evaluation of the heart on the part of the prosector is crucial. For a pathological (clinical or academic) autopsy, consent from a relative is required, while in a medicolegal autopsy, consent from relatives is not needed. In a setting of sudden cardiac death, a combined autopsy is recommended where experts from forensic medicine and pathology would work as a team.

1.2 Gross Examination of the Heart

The prosector must examine the heart in such a manner that it exhibits the best alterations of the cardiovascular system caused by the disease. Many dissection methods are available and the prosector must select the right approach for a specific heart disease. Comprehension of the clinical picture is requisite for the preparation of the dissection and assessment method. A systematic approach to the analysis of cardiac specimens is important, regardless of the method selected. Even if there is no evidence of suspected heart disease, prior planning by the expert and team can encourage adequate tissue sampling that could be used for future diagnostic or research purposes such as ultrastructural, immunohistochemical, molecular, and/or genetic analyses. The gross examination of the heart begins with in situ inspection of the heart. After removal of the sternum, it is highly essential to examine the intact pericardium for tamponade evaluation. If tamponade is present, the pericardium will be distended and filled with blood (especially in cases of sudden death) or serofibrinous/serosanguineous fluid. The longitudinal incision is made over the anterior aspect of the pericardial sac and the volume of blood or fluid is collected in a container and measured. Clots, if present, should be weighed. Additionally, the pulmonary trunk and its

S. Tyagi
Department of Forensic Medicine and Toxicology, Lady Hardinge Medical College and Associated SSK and KSC Hospitals, New Delhi, India

P. Vaideeswar (✉)
Department of Pathology (Cardiovascular and Thoracic Division), Seth Gordhandas Sunderdas Medical College and King Edward Memorial Hospital, Mumbai, India

P. Vaideeswar (ed.), *Tropical Cardiovascular Pathology*,
https://doi.org/10.1007/978-981-19-3720-0_1

branches should be palpated and then incised to look for the presence of fatal thromboemboli. At this time too, blood samples can be collected through aseptic techniques for biochemical, serological, or microbiological investigations.

After *en masse* evisceration (a routinely followed procedure), the heart and lung block is separated from the abdominal viscera, which entails cutting the inferior vena cava just above the diaphragm. The heart and the great arteries with their branches are then separated from the lungs by cutting the pulmonary veins and arteries as close to lung hila as possible with separation from the trachea-bronchial tree. The superior vena cava and the left and right brachiocephalic veins are also likewise dissected. If the great arteries are devoid of significant disease, the aorta and the pulmonary trunk are cut transversely about 3 cm above the semilunar valves by putting the index and middle fingers into the transverse sinus of the pericardial cavity. After separation, the heart should be thoroughly washed and the anterior and posterior surfaces (Fig. 1.1) should be carefully inspected for any alterations from normal, which would give clues and guidance for further dissection.

In order to achieve the best examination of the coronary arteries for their abnormalities, it is advisable to perfuse the coronary arteries (and the heart) with buffered formalin through a cannula in the aorta through a motorized pump, under the pressure of 100 mmHg. The coronary arteries would retain their near normal caliber to aid proper assessment of the pathological features, especially for morphometry. In routine autopsies, the prosector will simply cut across the epicardial arteries along their courses at 0.5 cm intervals in the fresh state, with a sharp scalpel blade with a subtle sawing motion to validate any narrowing location and to examine the pathology explicitly. The arteries commonly examined in all hearts include the four major epicardial coronary arteries (Fig. 1.2)—right, left main, left anterior descending, and left circumflex arteries. It is widely accepted that longitudinal cutting of vessels can disrupt thrombi/emboli and make an assessment of stenosis impossible. A four-point system is applied by 25% increments of narrow-

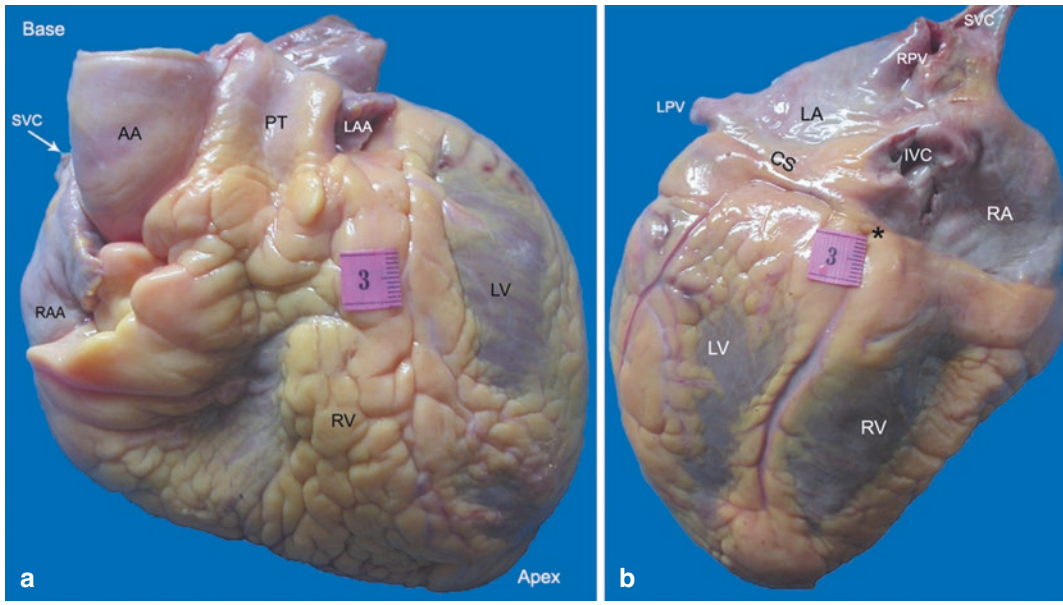

Fig. 1.1 Structures seen on the (**a**) Anterior and (**b**) Posterior surfaces of the heart. Note that the apex is pointing to the left and formed by left ventricle LV. * represents the crux of the heart, a point of convergence of all four chambers (*AA* ascending aorta, *CS* coronary sinus, *IVC* inferior vena cava, *LA* left atrium, *LAA* left atrial appendage, *LPV* left pulmonary vein, *PT* pulmonary trunk, *RA* right atrium, *RAA* right atrial appendage, *RPV* right pulmonary vein, *RV* right ventricle, *SVC* vena cava)

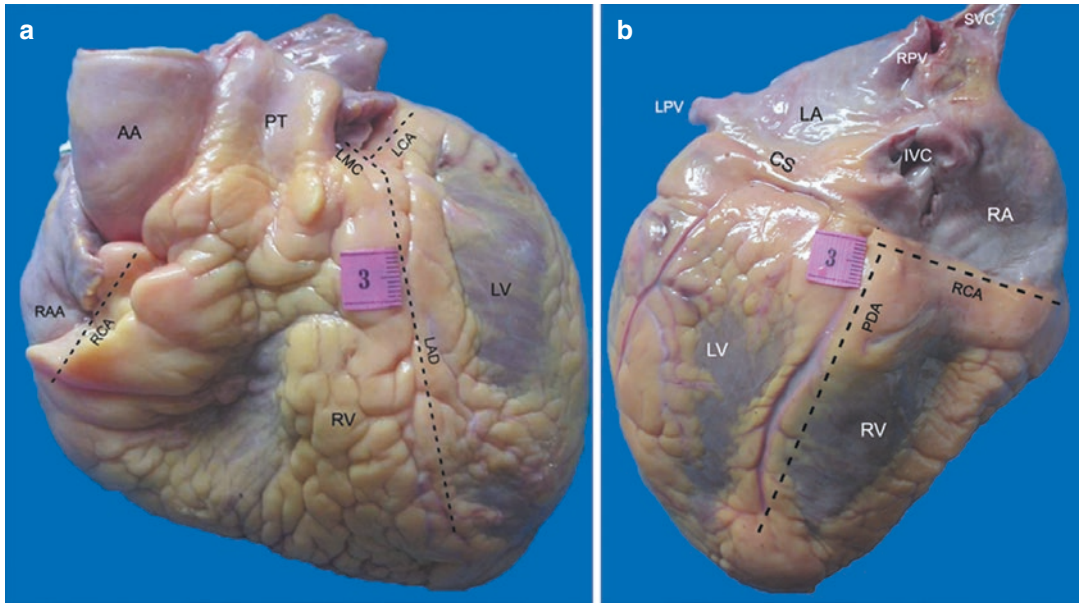

Fig. 1.2 (**a**) The right coronary artery RCA after its origin traverses the right anterior atrio-ventricular groove. The left main coronary artery LMC is a short vessel that divides into left anterior descending artery that courses over the anterior inter-ventricular groove and the left circumflex artery, which enters the left anterior atrio-ventricular groove; (**b**) The RCA continues into the right posterior atrio-ventricular groove and in right dominant circulation terminates as posterior descending artery (PDA)

ing in cross-sectional area. Stenosis of at least 75% is considered severe enough to produce mortality.

1.3 Dissection of the Heart

Dissection techniques are acquired from personal experience and depend not only on the individual autopsy surgeon, but also on the type of CVD. Many older methods are impractical for routine diagnostic pathology. Only the inflow-outflow and short axis (bread slice) techniques have withstood the test of time. For the inflow-outflow method of Virchow, three cuts are applied on either side of the heart (Fig. 1.3a–c). The scissors is used to cut the atria, their appendages, arteries, and veins, while the ventricles are sliced with a scalpel blade or knife. If there is an associated mitral valvular pathology, then a mitral valve-sparing incision (Fig. 1.3d) is taken parallel to the anterior interventricular groove and approximately 1 cm away from it. This curved cut is best achieved with a scalpel; caution should be taken not to cut into either the mitral leaflet or the interventricular septum. Scissors can be used to extend the cut across the aortic valve and ascending aorta.

Once the heart has been cut, the heart should be thoroughly washed and 'persistent' postmortem blood clots should be removed manually. The heart is then weighed (0.25% of the body weight). The chambers and the valves have to be identified through their specific morphology (Figs. 1.4 and 1.5). The atria and the ventricles are described with reference to their cavity size, appearance of endocardium, and thickness of myocardium, particularly for the ventricles (right ventricle ≤0.5 cm and left ventricle ≤1.0–1.5 cm). The atrioventricular valves have to be assessed on the basis of the size of annulus, commissures, leaflets, and the subvalvular apparatus (chordae tendineae and papillary muscles) and the arterial valves are described with respect to their annular size, commissures, cusps, and their number. Always confirm the origin of the right and left coronary arteries from their respective sinuses-of-Valsalva.

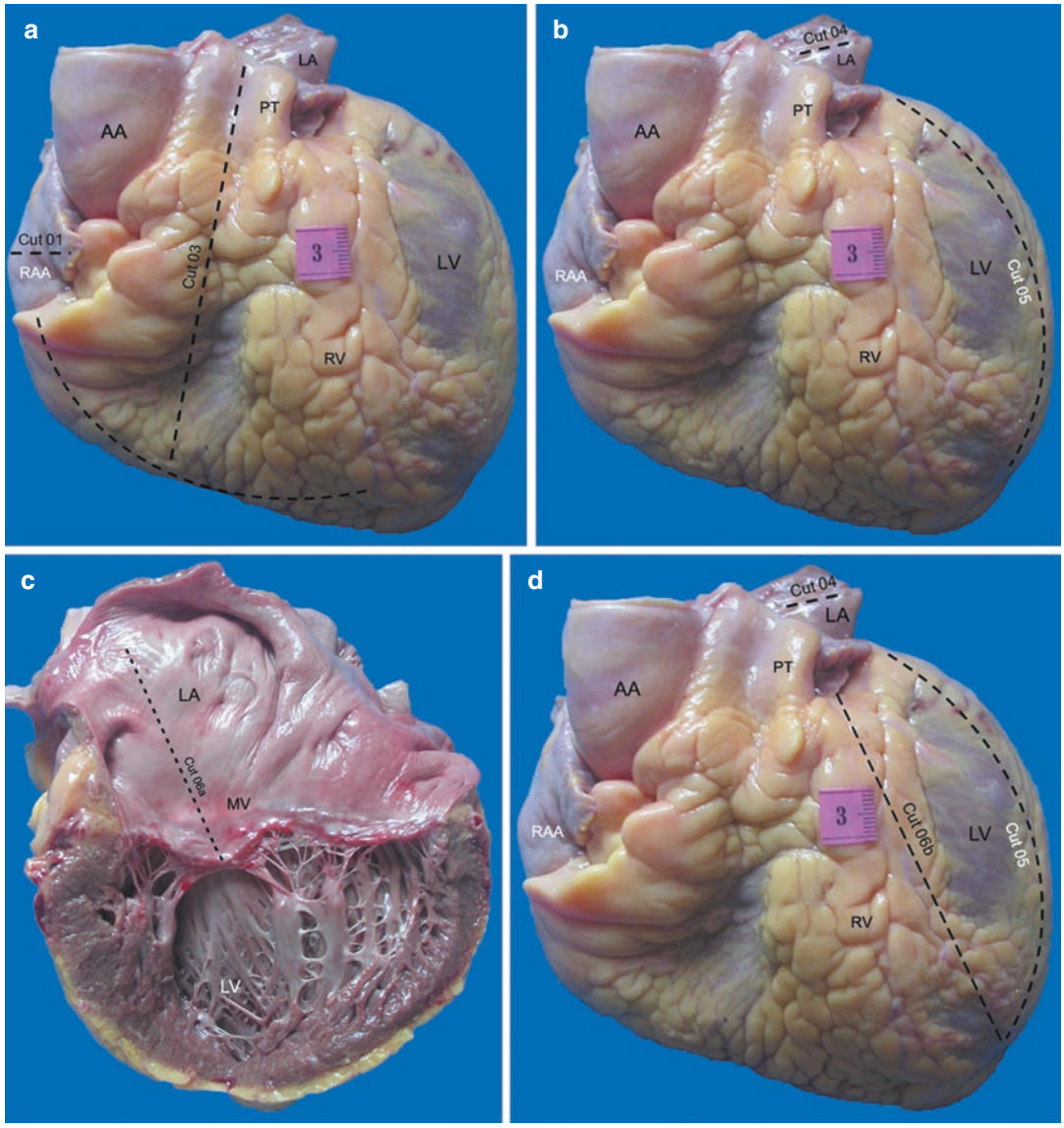

Fig. 1.3 (**a**) The first cut on the right side is made from the inferior vena cava to the right atrial appendage RAA, preserving the superior vena cava with the sinus node region. The right ventricular inflow tract is opened from the right atrium along the right border of the heart through the posterior tricuspid leaflet. The third cut is through the mid-portion of the outflow tract; (**b**) The left atrium LA is opened with scissors between the right and left upper pulmonary veins, while the second cut is through the left border, which goes through the posterior mitral leaflet; (**c**) The third cut is through the anterior leaflet AML of mitral valve and the left atrial LA wall and thence into the ascending aorta AA; (**d**) The mitral valve-sparing incision (*LV* left ventricle, *PT* pulmonary trunk, *RV* right ventricle)

The short axis method (bread loafing) is the method of choice not only for the evaluation of ischemic heart disease as well as for certain non-ischemic myocardial disorders. This is best accomplished using a long, sharp knife on the intact specimen. With the anterior aspect of the heart placed against the cutting board, the cuts are made parallel to the posterior atrioventricular (AV) groove at 1 cm intervals from the apex of the heart to a point approximately 2 cm distal to

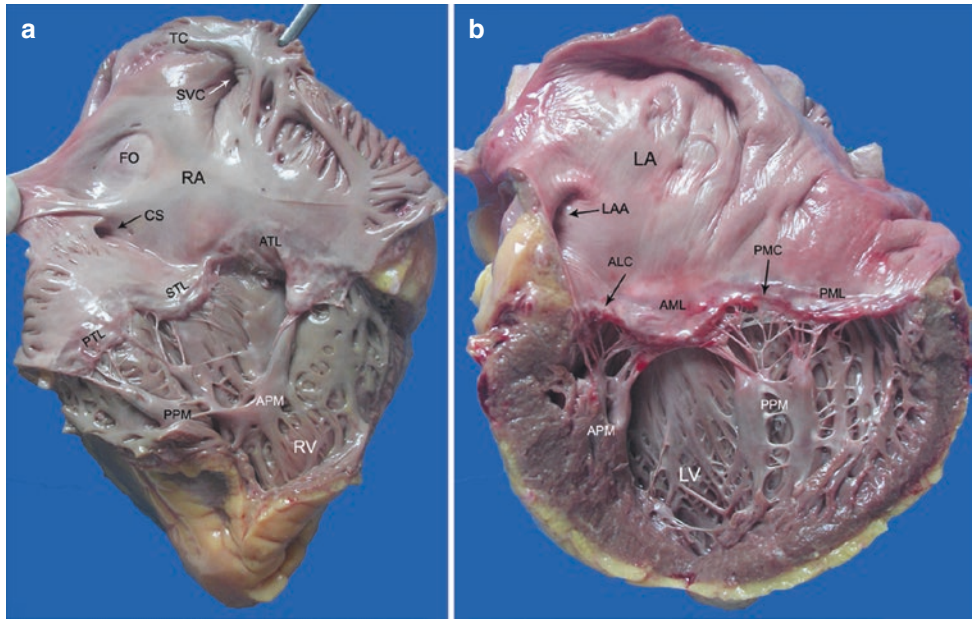

Fig. 1.4 (**a**) The right-sided inflow tract. The right atrium RA has two important landmarks, the fossa ovalis FO and the crista terminalis or terminal crest TC. The tricuspid valve has three leaflets, anterior ATL, posterior PTL, and septal STL leaflets, with three commissures. The anterior APM and posterior PPM muscles are well seen. The right ventricle RV is heavily trabeculated with a thin wall; (**b**) The left-sided inflow tract. The left atrium LA is practically featureless with a thick white endocardial surface. The mitral valve has two leaflets (anterior AML and posterior PML), two commissures (antero-lateral ALC and postero-medial PML), and two beefy papillary muscles (anterior APM and posterior PPM). The left ventricle LV is finely trabeculated with a thick compact myocardium

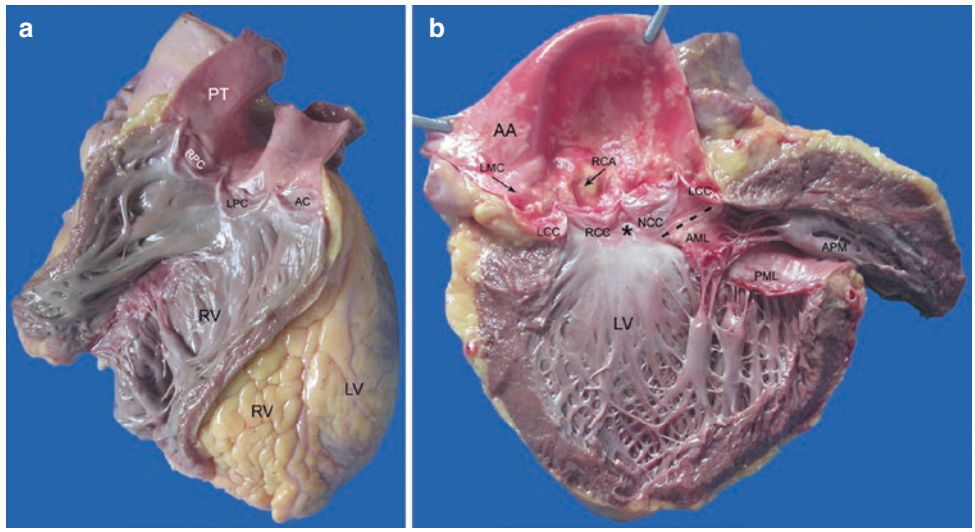

Fig. 1.5 (**a**) The right-sided outflow tract. The right ventricular RV in the outflow tract is also trabeculated. The RV leads to the pulmonary trunk PT via the pulmonary valve. It has three cusps, one anterior APC and two posterior RPC and LPC. (**b**) The left-sided outflow tract. The left ventricular LV outflow is smooth. The cusps of the aortic valve are designated as right coronary RCC, left coronary LCC, and non-coronary NCC cusps. The right and left coronary arterial ostia arise within the sinuses of Valsalva and below a discontinuous ridge transverse ridge, the sino-tubular junction. * is the position of the membranous septum. Dotted line represents the aorto-mitral fibrous continuity

the AV groove. The outcome is a sequential of cross-sections (short axis) across the ventricles, including papillary muscles, leaving the AV valve apparatus intact in the remainder of the specimen. The four-chamber method is advocated in certain types of cardiomyopathies.

The excised heart, which is meticulously grossed, carefully measured and histologically examined with photographic documentation, continues to remain the gold standard. In sudden cardiac death, organ retention and referral should also be considered as the 'gold standard'.

Further Reading

Abdul-Aziz AA, Desikan P, Prabhakaran D, Schroeder LF. Tackling the burden of cardiovascular diseases in India. Circ Cardiovasc Qual Outcomes. 2019;12:e005195.

Buja LM, Barth RF, Krueger GR, Brodsky SV, Hunter RL. The importance of the autopsy in medicine: perspectives of pathology colleagues. Acad Pathol. 2019;6:1–9.

Hull MJ, Nazarian RM, Wheeler AE, Black-Schaffer WS, Mark EJ. Resident physician opinions on autopsy importance and procurement. Hum Pathol. 2007;38:342–50.

Thiene G, Saffitz JE. Autopsy as a source of discovery in cardiovascular medicine. Circulation. 2018;137:2683–5.

Vaideeswar P. Systemic examination–cardiovascular system. In: Lanjewar D, Vaideeswar P, editors. Autopsy practices. 2nd ed. New Delhi: Jaypee Brothers Medical; 2021. p. 38–54.

Vaideeswar P, Tyagi S, Singaravel S, Marathe SP. Sudden cardiac deaths: role of nonischemic myocardial disorders—part 1. Indian J Pathol Microbiol. 2021;64:14–21.

Part II

Pericardial Diseases

Tuberculous Pericarditis

2

Gayathri Amonkar and Pradeep Vaideeswar

2.1 Clinical History

An adolescent female was admitted with chief complaints of progressive shortness of breath for the past 2 months. It was initially grade 2 and progressed to grade 4 with development of paroxysmal nocturnal dyspnea, chest pain, palpitation, and pedal edema. There had been associated mild intermittent fever with chills, dry cough, episodic dull abdominal pain, and loss of weight/appetite. On examination, the general condition was poor with pulse rate of 80 per minute, blood pressure of 90/70 mmHg, and respiratory rate of 34 per minute. She was conscious and well-oriented. Systemic examination revealed audible heart sounds, absent breath sounds in the right lower zone, and tenderness in the right hypochondrium. The clinical diagnosis was possibly viral myocarditis with congestive cardiac failure and superadded bronchopneumonia. The investigations have been tabulated (Table 2.1). She was given antibiotics, inotropes, diuretics, and was mechanically ventilated. She succumbed within 2 days.

Table 2.1 Investigations

Hematological	Hemoglobin 9.1 g/dL Total leukocyte count 10,100/cmm Differential count—Neutrophil predominant (67%) Platelet count 2.5 lakhs/cmm
Biochemical—routine	Blood glucose 91 mg/dL Serum creatinine 1.3 mg/dL Blood urea nitrogen 28 mg/dL Total protein 6.7 g/dL Albumin 2.7 g/dL [a]SGOT 30 U/L [a]SGPT 7.0 U/L [a]Sodium 135 mEq/L [a]Potassium 3.9 mEq/L [a]Chloride 104 mEq/L
Radiological	*ECG*: Low-voltage complexes *X-ray*: Right pleural effusion *USG*: Right pleural effusion, mild pericardial effusion, mild ascites
Others	*Urine*: Normal *Pleural fluid*: Exudate (5.15 g/dL, predominant lymphocytes)

[a]Mean values

2.2 Autopsy Findings

The appearance of the eviscerated viscera is depicted in Fig. 2.1. On gross examination, there was extreme adherence of both the layers of the

G. Amonkar
Department of Pathology, Topiwala National Medical College and BYL Nair Charitable Hospital, Mumbai, India

P. Vaideeswar (✉)
Department of Pathology (Cardiovascular and Thoracic Division), Seth Gordhandas Sunderdas Medical College and King Edward Memorial Hospital, Mumbai, India

P. Vaideeswar (ed.), *Tropical Cardiovascular Pathology*,
https://doi.org/10.1007/978-981-19-3720-0_2

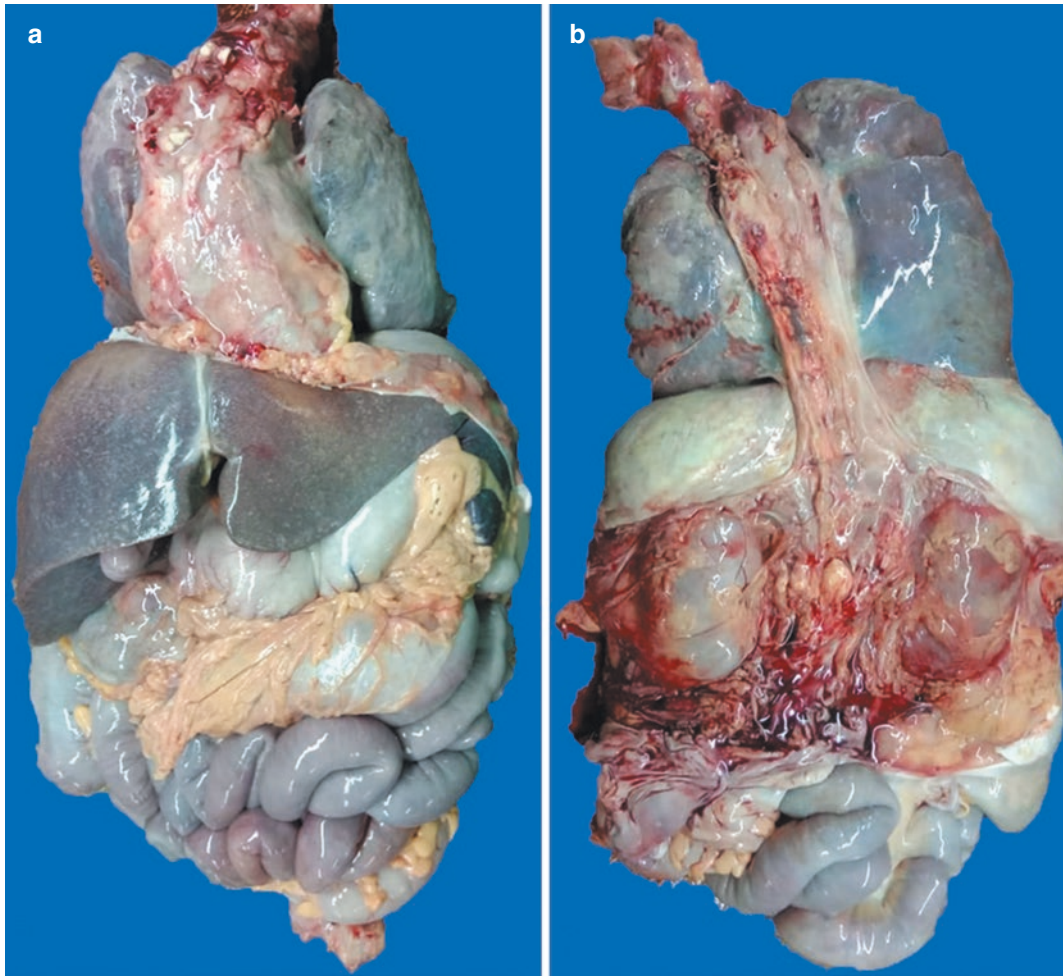

Fig. 2.1 Eviscerated organs as seen from the (**a**) anterior and (**b**) posterior aspects. Note opacification of the parietal pericardium and visceral pleurae with miliary mottling seen in the liver anteriorly and right lung posteriorly

pericardium, along with adherence to the diaphragm. Besides, the grey-white opacification and thickening (Fig. 2.2a), the parietal layer showed the presence of yellowish-white granularity. In this case, the heart could not be opened through the inflow-outflow method and had to be bisected (Fig. 2.2b). There was widening and obliteration of the pericardial cavity (Fig. 2.2b) due to alternate areas of congested granulation tissue, grey-white glistening fibrosis, and soft creamy pale yellow to grey-white caseation necrosis (Fig. 2.3). The thickness of the caseation was maximal over the right side of the heart (1.8 cm, Fig. 2.3a), particularly around the right atrium and both the appendages. The vessels at the base of the heart were also surrounded by similar material till the pericardial attachments. There was hardly any visible adipose tissue. This pathology had produced moderate cardiomegaly (340 g), but the heart itself was normal in size with normal chambers and valves. The histology (Figs. 2.4 and 2.5) revealed several layers of caseation necroses, fibrin deposition, granulomatous reaction, granulation tissue, and hyalinized fibrosis. The stain for acid-fast bacilli (AFB) was negative. The lymph nodes over the arch and in the para-aortic regions were enlarged and frankly caseous; scrape cytology revealed many AFBs. Associated findings were miliary pulmonary tuberculosis, bronchopneu-

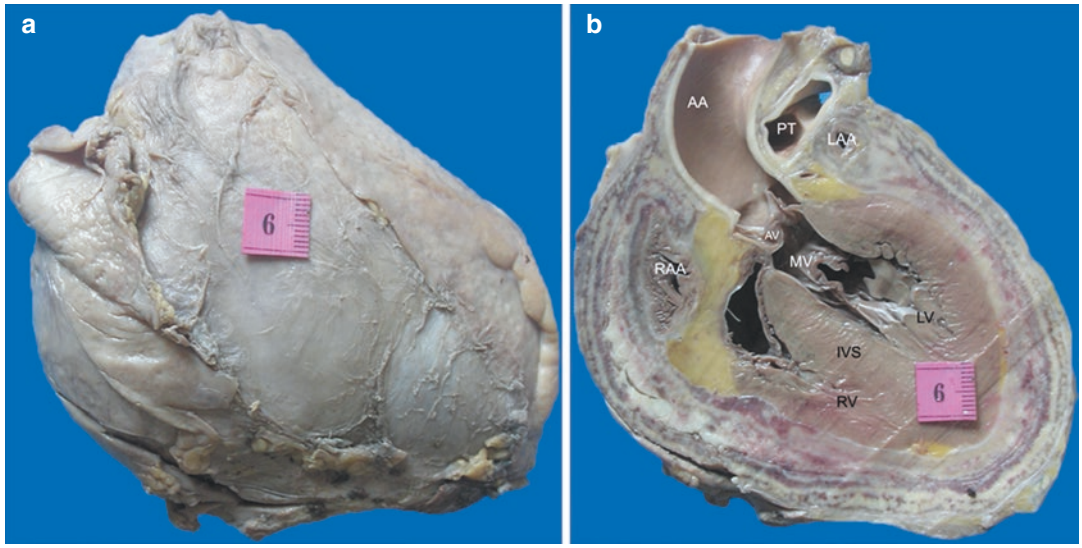

Fig. 2.2 (**a**) The thickened parietal layer of the pericardium could not be separated from the visceral layer; (**b**) Bisected heart showing obliteration of the pericardial cavity by extensive exudative reaction (*AA* ascending aorta, *AV* aortic valve, *IVS* interventricular septum, *LV* left ventricle, *LAA* left atrial appendage, *MV* mitral valve, *PT* pulmonary trunk, *RAA* right atrial appendage, *RV* right ventricle)

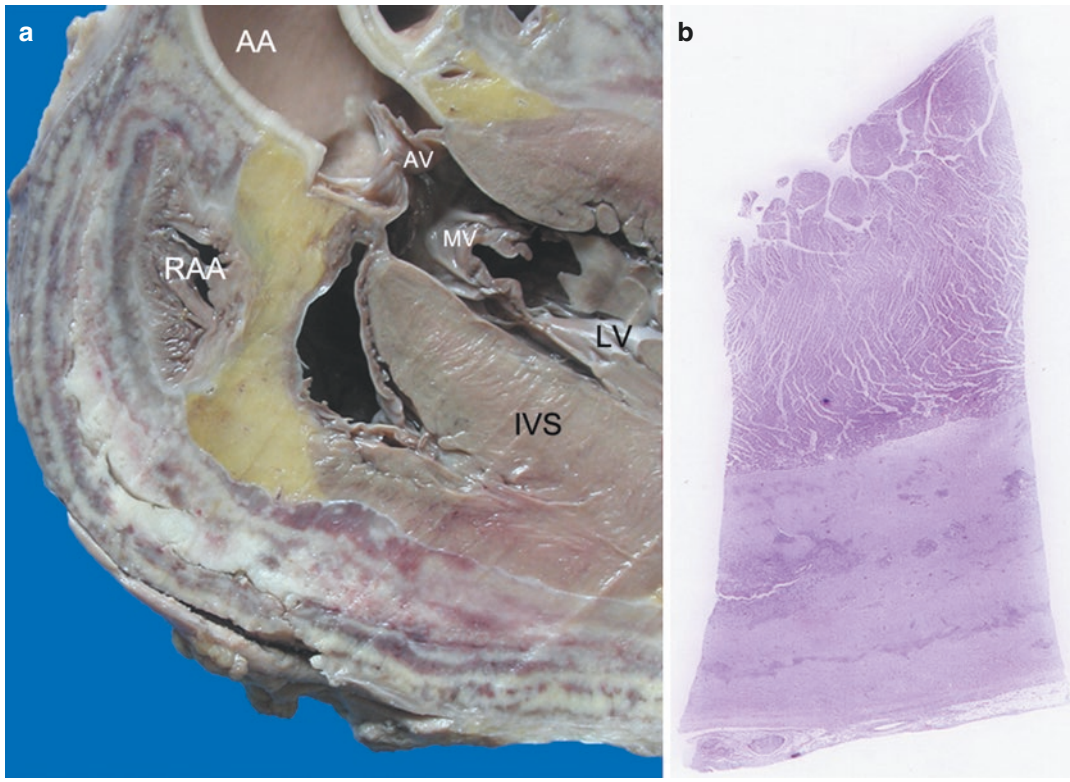

Fig. 2.3 (**a**) Close-up of the right side shows alternate layers of creamy exudates and congested to grey-white tissue (*AA* ascending aorta, *AV* aortic valve, *IVS* interventricular septum, *LV* left ventricle, *RAA* right atrial appendage), which is well brought out in the (**b**) scanner view of the right ventricular section

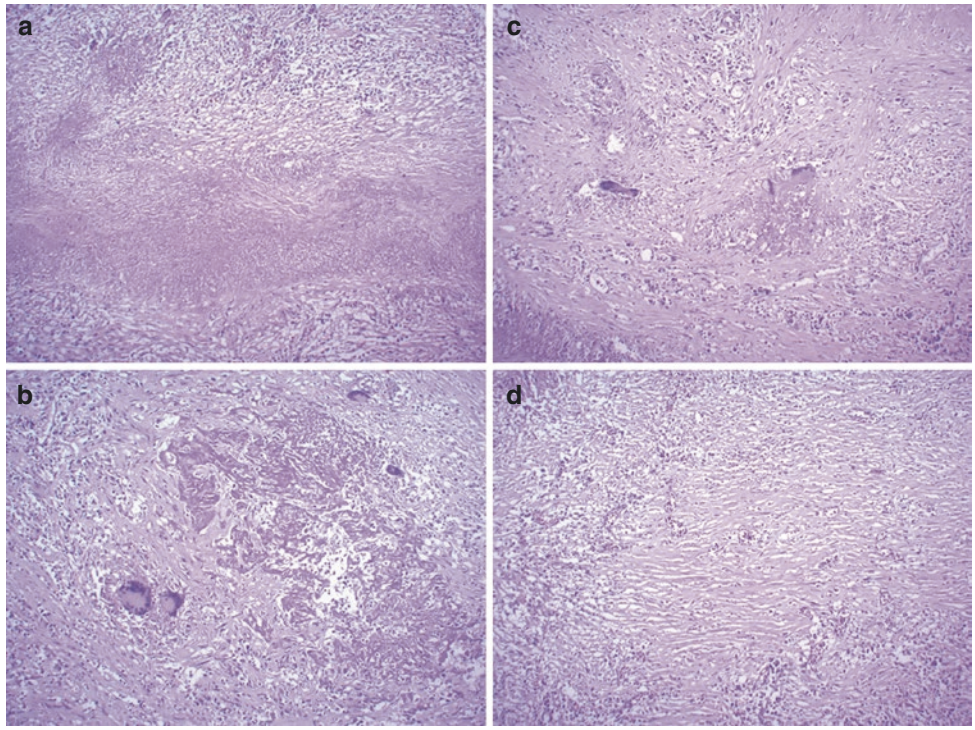

Fig. 2.4 (**a**) Central zone of granular pinkish caseation necrosis flanked by inflammation and fibrotic reaction; (**b**) Granulomatous reaction surrounding darker pink glassy appearing fibrin; (**c**) Caseating granuloma surrounded by areas of granulation tissue; (**d**) Hyalinized collagen infiltrated by mononuclear inflammatory cells (H&E × 250)

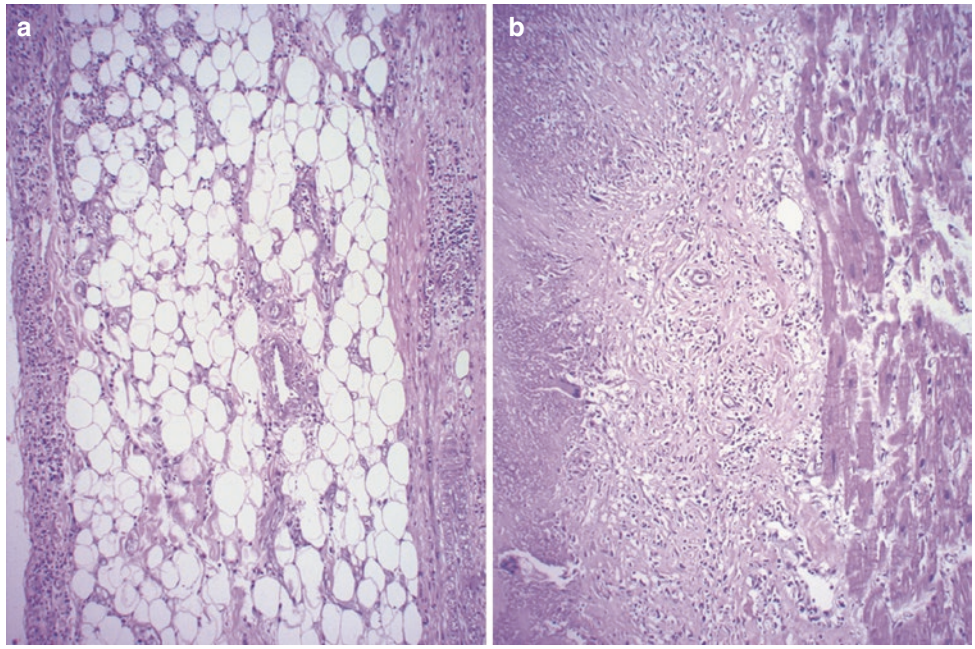

Fig. 2.5 (**a**) The epicardial adipose tissue is enclosed on either side by fibrosis with chronic inflammatory cell infiltrate; (**b**) The zone of caseation necrosis is separated from the myocardium by a layer of granulation tissue (H&E × 250)

monia, centri-zonal hemorrhagic necroses of the liver, splenic miliary lesions, and peripancreatic tuberculous lymphadenitis. The brain was normal; there was no evidence of tuberculous meningitis.

Cause of Death: Tuberculous Pericarditis with Miliary Tuberculosis.

2.3 Discussion

Pericarditis is the most common manifestation of pericardial disease, characterized by inflammation of the pericardial layers and the accumulation of various types and amounts of exudates. It often affects the young population, who present as acute pericarditis, effusion, tamponade, and/or constriction, depending on the etiology. The causes may be infective or noninfective; some of them can cause concomitant involvement of the underlying myocardium (myopericarditis).

In developing countries, where tuberculosis remains a major health concern, tuberculous involvement accounts for more than half of the cases of pericarditis among infectious causes. The pericardium is a critical extrapulmonary site for tuberculosis, and after central nervous system disease, tuberculous pericarditis is responsible for significant morbidity and mortality in the early stage of disease, ranging from 17 to 25% in human immunodeficiency virus (HIV) negative and 34–40% in HIV-positive patients. It has been reported in 1% of all autopsied cases of tuberculosis and 1–2% cases of pulmonary tuberculosis. The tubercle bacilli gain access into the pericardium mainly by retrograde lymphatic spread or direct extension from tuberculous mediastinal, hilar or para-aortic lymphadenitis. Hematogenous dissemination or continuous extension from pleural, pulmonary, or even vertebral lesions is among the other mechanisms. Any one of these mechanisms would have operated in the case described, where there was miliary dissemination.

Four phases of tuberculous pericarditis have been described. It is important to note that these phases can progress at nonuniform pace with skipping of some stages, and the patients too can present at different stages. An initial 'dry' stage is characterized by acute fibrinous pericarditis with a neutrophilic inflammatory response and loose clusters of lymphocytes and macrophages; there would a fair number of mycobacteria. This is followed by the effusive phase in which there is varying accumulation of serosanguineous fluid with dominant lymphocytes and focal granulomatous reaction. The effusion is succeeded by 'absorptive' phase, where there is thickening of the pericardium and obliteration of the cavity by layers of fibrin, caseation necrosis, granulomatous inflammation, granulation tissue, and fibrosis, as seen in the index case. This paves the way for the phase of constrictive pericarditis with fibro-hyalinization and eventual calcification; the heart is then finally encased in a fibro-calcific shell. The transition from effusion to constriction is explained based on delayed hypersensitivity reaction invoked by the subsets of T-lymphocytes. This is associated with the production of increasing concentrations of pro-inflammatory/pro-fibrotic mediators and low levels of anti-fibrotic factors.

The patients with tuberculous pericarditis usually present with pericardial effusion. Constitutional symptoms, features related to the pericardial involvement, and effects of synchronous tamponade and constriction (effusive-constrictive pericarditis) may be seen. Many of these features were present in our patient, but they were mistaken for those associated with viral myocarditis. However, even with the availability of well-established and novel diagnostic modalities, tuberculous pericarditis remains one of the most difficult and challenging aspects and about 20% of the cases are not diagnosed, particularly in resource limited settings. The definitive diagnosis rests on the demonstration of *Mycobacterium tuberculosis* in the pericardial fluid or tissue by either direct examination or culture, but there is now an increasing reliance on Xpert MTB/RIF coupled with biochemical estimations of adenosine deaminase or γ-interferon for early diagnosis.

Further Reading

Chang SA. Tuberculous and infectious pericarditis. Cardiol Clin. 2017;35:615–22.

Howlett P, Du Bruyn E, Morrison H, Godsent IC, Wilkinson KA, Ntsekhe M, Wilkinson RJ. The immunopathogenesis of tuberculous pericarditis. Microbes Infect. 2020;22:172–81.

Imazio M, Gaita F, LeeWinter M. Evaluation and treatment of pericarditis: a systematic review. JAMA. 2015;314:1498–506.

Mutyaba AK, Ntsekhe M. Tuberculosis and the heart. Cardiol Clin. 2017;35:135–44.

Restrepo CS, Gonzalez TV, Brar R, Ocazionez D, Velasco ML, Reyna Lopez RA, Arias L, Baxi AJ, Carrillo J. Thoracic cardiovascular complications of tuberculosis. J Comput Assist Tomogr. 2021;45:157–65.

3 Pericardial Hemangiomatosis with Cardiac Tamponade

Pradeep Vaideeswar, Milind Tullu, and Priyash Tambi

3.1 Clinical History

A 5-month-old male had 3 admissions for recurrent, massive, rapidly filling hemorrhagic pericardial effusion and associated thrombocytopenia. In the first admission (ward stay of 41 days), he had presented with mild intermittent fever, cough, cold, and increased respiratory activity. He was noted to have massive pericardial effusion and thrombocytopenia (mean of 59,000/cmm). The effusion was tapped 6 times and was hemorrhagic; no malignant cells or significant number of inflammatory cells were identified. The child was given fresh frozen plasma, empirical antituberculous therapy, and intravenous immunoglobulin. There was a partial response with hemodynamic stability and he was discharged. However, he was readmitted after 8 days for respiratory distress. During the second admission (ward stay of 21 days), pericardial window with drain and biopsy was performed. However, the histopathology revealed fibro-fatty tissue and skeletal muscle fibers; pericardial tissue was not identified. The etiological workup was negative for infections and hematological, endocrinal, or rheumatological abnormalities. The pericardial drain was removed after a period of 5 days and patient was discharged. After 6 days, he was admitted for the third time with 1 day history of increased respiratory activity. On examination, he had tachypnea, tachycardia, basal crepitations, and tender hepatomegaly. Investigations revealed anemia (mean Hb 9.3 g/dL), neutrophilia (mean total leukocyte count of 23,000/cmm), thrombocytopenia (mean platelet count of 24,000/cmm), hyperbilirubinemia (3.17 mg/dL), and mild elevation of transaminases (plasma aspartate aminotransferase 234 U/L and plasma alanine aminotransferase 245 U/L). There was derangement of the coagulation profile (elevated prothrombin time, activated partial thromboplastin time and thrombin time, reduced fibrinogen, and strongly positive D-dimer). The chest radiograph revealed globular cardiomegaly and the computed tomographic scan showed consolidation of right lung with moderate pericardial effusion (Fig. 3.1a). Pericardial tapping was done thrice in the current admission. He was treated with antibiotics and steroids; antituberculous therapy was continued. However, there was no improvement and child succumbed after 12 days of admission.

P. Vaideeswar (✉)
Department of Pathology (Cardiovascular and Thoracic Division), Seth Gordhandas Sunderdas Medical College and King Edward Memorial Hospital, Mumbai, India

M. Tullu · P. Tambi
Department of Pediatrics, Seth Gordhandas Sunderdas Medical College and King Edward Memorial Hospital, Mumbai, India

P. Vaideeswar (ed.), *Tropical Cardiovascular Pathology*,
https://doi.org/10.1007/978-981-19-3720-0_3

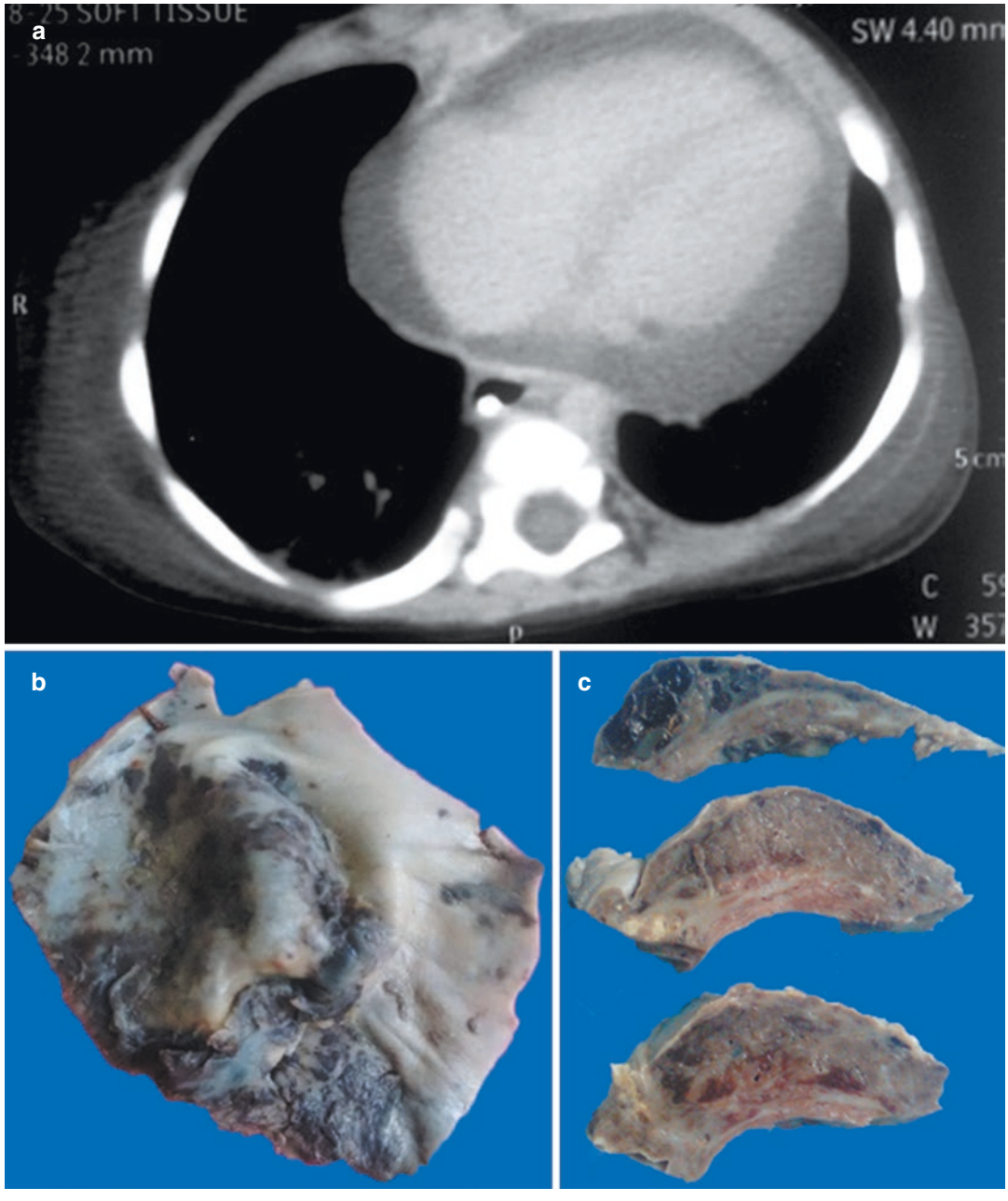

Fig. 3.1 (**a**) Moderate pericardial effusion on the CT scan; (**b**) Focal hemorrhagic appearance of inner aspect of parietal pericardium; (**c**) Pericardial thickening due to spongy hemorrhagic to pale red tissues

3.2 Autopsy Findings

Remarkable findings were present in the mediastinum. The heart appeared enlarged due to hemorrhagic pericardial effusion; 80 mL of fluid was aspirated at autopsy. The inner aspect of the parietal pericardium showed multifocal soft, velvety reddish tissue (Fig. 3.1b). The pericardium in these areas was thickened due to a spongy, hemorrhagic to pale red tissue (Fig. 3.1c). The adventitial aspects of the intrapericardial vascular channels, the tributaries of the superior caval vein, the arch and arch arteries, proximal 4.3 cm of the descending thoracic aorta, the trachea, the main bronchi, and esophagus were covered by a layer soft congested tissue (Fig. 3.2a, b) Similar tissue surrounded the lung hilar structures and had infiltrated the thymus, which was shrunken and densely adherent to the parietal pericardium. On histology, the red brown areas were composed of large and small bundles of proliferating capillaries (Fig. 3.3a). They were lined by plump endothelial cells, devoid of pleomorphism (Fig. 3.3b, c). The trachea revealed extensive squamous metaplasia. The capillary tufts were seen to insinuate between the cartilaginous plates. Apart from the thymus (Fig. 3.4a–d) and trachea, the proliferations were restricted to the surfaces of all the mediastinal structures. The epicardium was covered with fibrinous exudates; the heart was normal. Hemangiomatous foci were not seen in the lungs; bronchopneumonia was present. Other organs, including the liver, were normal.

Cause of Death: Mediastinal and pericardial hemangiomatosis with recurrent, massive pericardial effusion, and cardiac tamponade.

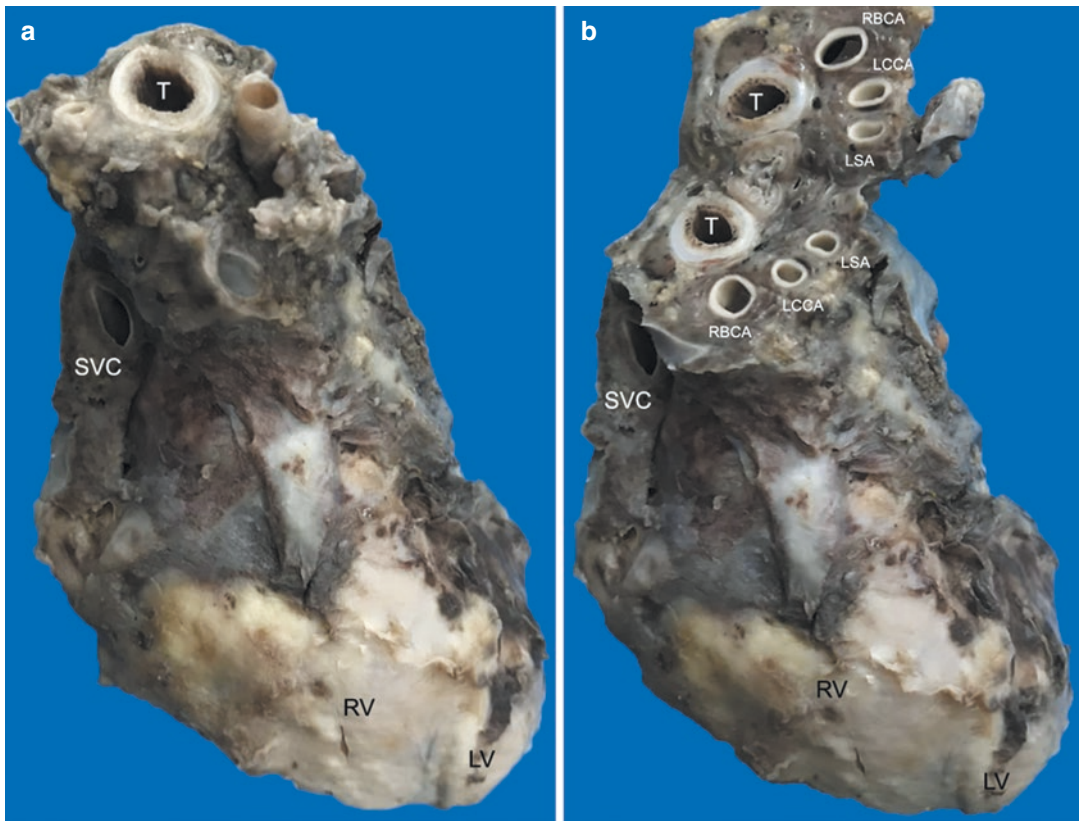

Fig. 3.2 (**a**) and (**b**) Structures in the anterosuperior mediastinum and basal aspect of the heart covered by congested tissue. There is sparing of the apical portion of the heart (*LCCA* left common carotid artery, *LSA* left subclavian artery, *LV* left ventricle, *RBCA* right brachiocephalic artery, *RV* right ventricle, *SVC* superior vena cava, *T* trachea)

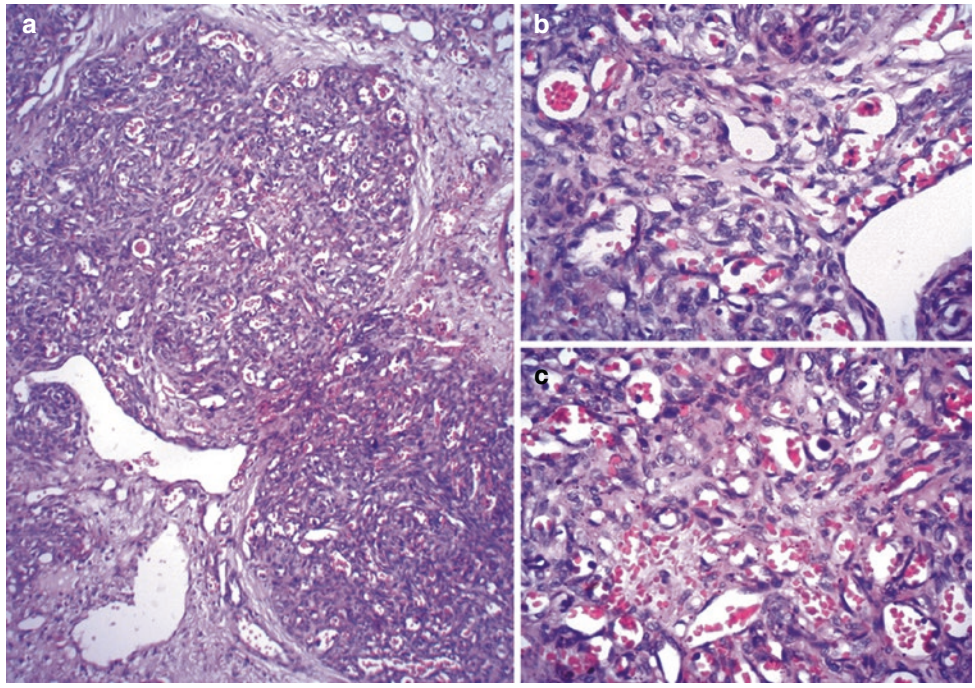

Fig. 3.3 (**a**) The mediastinal connective tissue infiltrated by bundles of capillary channels (H&E × 200); (**b**) and (**c**) Capillary channels lined by plump endothelial cells (H&E × 400)

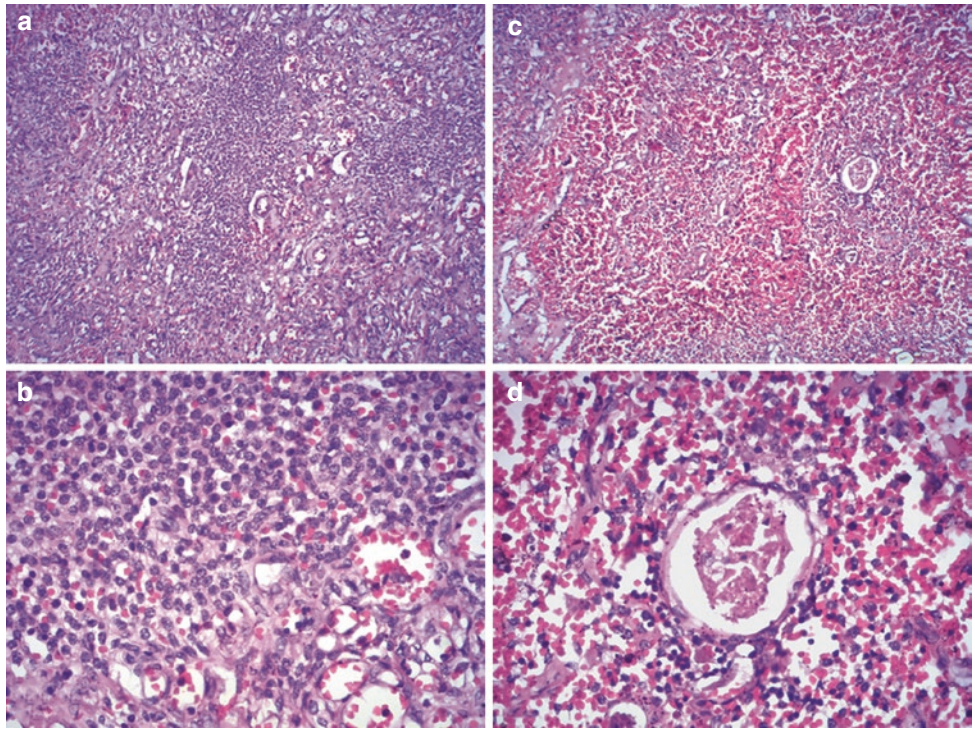

Fig. 3.4 The thymic architecture is replaced by proliferating capillaries with small clusters of lymphocytes (**a**) H&E × 200, (**b**) H&E × 400 and ill-formed Hasall's corpuscles (**c**) H&E × 200, (**d**) H&E × 400

3.3 Discussion

An infant in this illustrated case presented with repeated episodes of hemorrhagic pericardial effusion and unfortunately succumbed due to development of cardiac tamponade. Pericardial effusion, defined by an increase in the physiological amount of fluid within the pericardial cavity, is a rare disease in the pediatric age group. It has varied etiologies, which can primarily be a pericardial disorder or part of a systemic illness. Most often, they are related to infection or appear as a post-cardiac surgery complication; other causes include connective tissue diseases, metabolic disorders, and malignancies. Tuberculosis and bacterial infections are responsible for effusions in the developing countries, while viral infections and post-viral states are the main causes in the high-income countries. In some cases, the reason for the effusion remains unclear, i.e., idiopathic effusions. In such cases, the etiology is frequently presumed to be viral or immune-mediated, but evidence for same is usually not found (because of the expense involved, the inaccessibility of pericardial tissue/fluid, and the time delay or at times the inaccuracy of viral titers). It is even more infrequent to have recurrent, rapidly filling, hemorrhagic pericardial effusions, which are caused by tuberculosis or malignant pericardial infiltration. Furthermore, a progression to cardiac tamponade with ensuing disturbance in the normal hemodynamics is also uncommon. Though our patient was treated with antibiotics, antituberculous drugs, and repeated tapping, the therapy failed to stem the effusion. The biopsy performed was also not representative. It appeared antemortem that the effusion was idiopathic in this case, but the autopsy revealed multifocal capillary proliferations—hemangiomatosis in the mediastinal soft tissue, including the layers of the pericardium.

In general, hemangiomas are the most common vascular tumors that occur in the pediatric population with a prevalence of 4.5% and an incidence ranging from 5 to 10%. In the current backdrop, they are classified into congenital and infantile hemangiomas on the basis of their clinicopathological features, natural history, and their immunohistochemical positivity for glucose transporter 1 protein (GLUT-1). Congenital hemangiomas are GLUT-1 negative and are well-developed in the neonatal period, while infantile hemangiomas are GLUT-1 positive and are well-established in infancy. We considered our case as an infantile hemangiomatous process due to the rapid proliferation and hence an early clinical presentation at the age of 5 months; however, GLUT-1 immunohistochemistry could not be performed.

The natural history of these hemangiomas in infancy usually follows 3 stages—proliferative phase (8–12 months), involuting or stationary phase (1–5 years), and involuted phase (6–12 years). The proliferation occurs due to various vasogenic peptides. Most of the lesions are cutaneous and often multiple (30–50% of the infants). Since they undergo involution, no specific therapy is advocated. If there are more than 5 cutaneous hemangiomas (high-risk tumors), it may represent benign hemangiomatosis, but there is a likelihood of extra-cutaneous or visceral involvement, i.e., diffuse or multifocal infantile hemangiomatosis; such manifestations portend ominous clinical course. Liver is the most common organ to be affected followed by the brain, intestines, and lungs. Apart from hepatic dysfunction and hemorrhage in the affected organs, the shunting leads to high-output cardiac failure and the flow through the tortuous channels causes coagulopathy related to consumption of the coagulation factors and thrombocytopenia. The infant in this case did not have vascular lesions over the skin, but had a dominant involvement of the mediastinum; other organs, particularly the liver and brain, were not affected. The morbidity and mortality were produced by recurrent and massive pericardial effusion. Had the child survived, he may have also developed immunological abnormalities due to thymic affection. Such life-threatening conditions should be recognized early with prompt treatment with beta-blockers like propranolol and steroids, which inhibit proliferation and accelerate the regression of the hemangiomatous process. Surgical excision is performed wherever necessary.

Further Reading

Abdel-Haq N, Moussa Z, Farhat MH, Chandrasekar L, Asmar BI. Infectious and noninfectious acute pericarditis in children: an 11-year experience. Int J Pediatr. 2018;2018:5450697.

Agarwal S, Sharma A, Maria A. Diffuse neonatal hemangiomatosis presenting as congestive heart failure. Dermatol Pract Concept. 2017;7:15.

Bagri NK, Yadav DK, Agarwal S, Aier T, Gupta V. Pericardial effusion in children: experience from tertiary care center in northern India. Indian Pediatr. 2014;51:211–3.

Dotan M, Lorber A. Congestive heart failure with diffuse neonatal hemangiomatosis—case report and literature review. Acta Paediatr. 2013;102:e232–4.

Mayer JLR, Intzes S, Oza VS, Blei F. How we approach hemangiomas in infants. Pediatr Blood Cancer. 2021;e29077.

Nip SYA, Hon KL, Leung WKA, Leung AKC, Choi PCL. Neonatal abdominal hemangiomatosis: propranolol beyond infantile hemangioma. Case Rep Pediatr. 2016;2016:9803975.

Pérez-Casares A, Cesar S, Brunet-Garcia L, Sanchez-de TJ. Echocardiographic evaluation of pericardial effusion and cardiac tamponade. Front Pediatr. 2017;5:79.

Shakti D, Hehn R, Gauvreau K, Sundel RP, Newburger JW. Idiopathic pericarditis and pericardial effusion in children: contemporary epidemiology and management. J Am Heart Assoc. 2014;3(6):e001483.

Part III

Valvular Heart Disease: Rheumatic

4 Acute Rheumatic Fever: A Fulminant Form

Ashutosh Goyal, Pradeep Vaideeswar, Saranya Singaravel, and Girish Sabnis

4.1 Clinical History

A 16-year-old adolescent was referred for mild fever on and off associated with severe pain and swelling of various large joints (knee, elbow, ankle, and wrist in that sequence) over the past 2 months. The fever, joint pain, and swelling had partially responded to nonsteroidal anti-inflammatory drugs. She also complained of effort intolerance and dyspnea on exertion Class II for a month, followed by paroxysmal nocturnal dyspnea for 4 days before admission.

On examination, the pulse rate was 132 per minute and blood pressure 96/60 mmHg. There were distended neck veins with a pulsatile jugular venous pressure of 12 cm and pedal edema; there was no joint swelling but arthralgia was present. Auscultation revealed an audible S_3 gallop with Grade IV/VI pansystolic murmur. Significant laboratory findings were an elevated erythrocyte sedimentation rate (ESR 95 mm after 1 h), raised C-reactive protein (CRP, 42 mg/dL), and a high ASLO titer (1:200). Other hematological and biochemical investigations were normal. Two-dimensional transthoracic echocardiography showed moderate mitral regurgitation with an ejection fraction of 60%. The clinical diagnosis was acute rheumatic fever (ARF) and the patient was administered diuretics and aspirin. There was some gradual improvement with reduced joint swelling and pain, pulse rate to 98 per minute, ESR to 54 mm at the end of 1 h, and CRP to 35 mg/dL. However, she developed sudden severe abdominal pain on the sixth day of admission and sustained a fatal cardiac arrest.

A. Goyal
Seth Gordhandas Sunderdas Medical College and King Edward Memorial Hospital, Mumbai, India

P. Vaideeswar (✉)
Department of Pathology (Cardiovascular and Thoracic Division), Seth Gordhandas Sunderdas Medical College and King Edward Memorial Hospital, Mumbai, India

S. Singaravel
Soleil Diagnostics, Mumbai, India

G. Sabnis
Dr KK Datey Department of Cardiology, Seth Gordhandas Sunderdas Medical College and King Edward Memorial Hospital, Mumbai, India

P. Vaideeswar (ed.), *Tropical Cardiovascular Pathology*,
https://doi.org/10.1007/978-981-19-3720-0_4

4.2 Autopsy Findings

The heart was moderately enlarged in size and weighed 330 g. There was a marked thickening of both layers of the pericardium, between which was present a very thick layer of flaky grayish-white fibrinous exudate. The exudate effectively obscured the normal landmarks of the heart as seen on the external aspect (Fig. 4.1). There was a moderate enlargement of all 4 chambers with patchy endocardial thickening and granularity, and myocardial thinning. Annuli of all valves were dilated. Anteroseptal and postero-septal commissures of the tricuspid valve were fused with mild thickening of the leaflets (Fig. 4.2a). The pulmonary valve appeared normal on gross examination. Both leaflets of the mitral valve were thickened with a row of fine light brown granular vegetations at the lines of closure (Fig. 4.2b). The commissures were mildly fused and chordae only mildly thickened. Endocardial granularity and rugosity—MacCallum's patch was present over the posterior wall of the left atrium. The aortic valve also showed mild commissural fusion and rounding up of free margins of the cusps (Fig. 4.2c). To our complete surprise, we observed the presence of fulminant rheumatic pancarditis on histopathology (Fig. 4.2c) with the presence of numerous Aschoff bodies in the visceral pericardium (Fig. 4.3a–c); in some of the epicardial coronary arterial radicles (Fig. 4.3d, e), all four valves (Figs. 4.4, 4.5 and 4.6), chambers (Fig. 4.7a–d), and papillary muscles. The endocardial granularity noted in the left ventricle was due to protruding Aschoff bodies (Fig. 4.7e). There was no rheumatic pneumonitis; pulmonary edema was present. Other organs were normal.

Cause of Death: Acute rheumatic pancarditis.

Fig. 4.1 Moderately enlarged heart is covered by a very thick flaky grey-white fibrinous exudate. The structures normally seen on the anterior surface are obscured

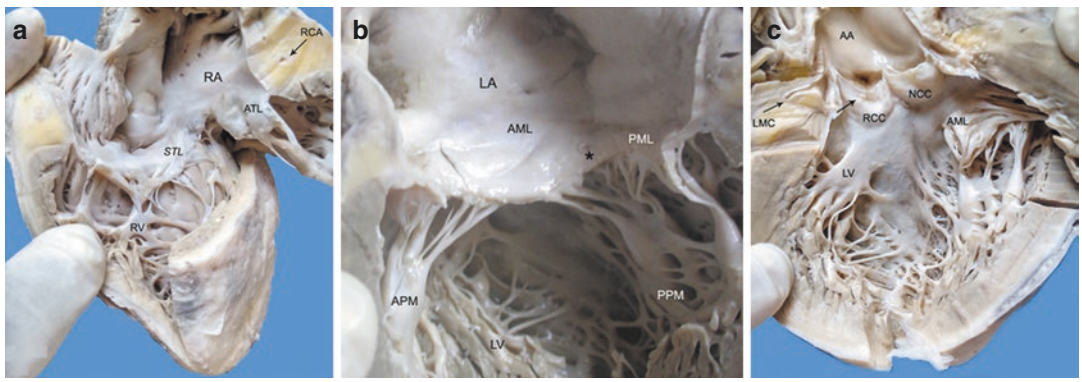

Fig. 4.2 (**a**) Right-sided inflow tract showing mild leaflet and chordal thickening of the tricuspid valve. There is diffuse endocardial thickening of right ventricular RV endocardium; (**b**) There is mild involvement of all the components of the mitral valve. Fine grey-white granularity is present at the lines of closure of the leaflets. * indicates fused posteromedial commissure; (**c**) The aortic valve looks almost normal except for few pin-head sized vegetations close to the nodulus of Arantii of the right coronary cusp RCC (*AA* ascending aorta, *AML* anterior mitral leaflet, *ATL* anterior tricuspid leaflet, *LA* left atrium, *LMC*, left main coronary artery, *LV* left ventricle, *NCC* noncoronary cusp, *PML* posterior mitral leaflet, *RA* right atrium, *STL* septal tricuspid leaflet)

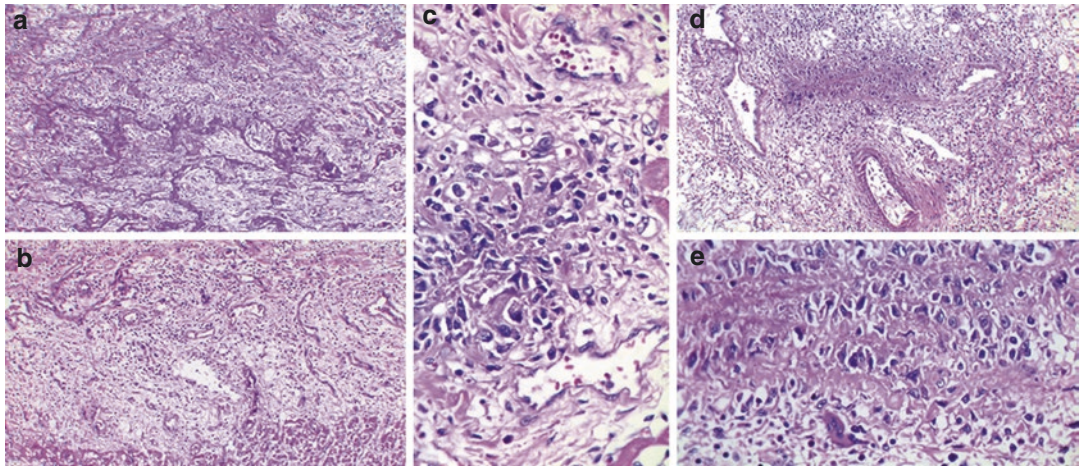

Fig. 4.3 (**a**) Fresh and (**b**) Organizing fibrinous pericarditis (H&E × 250); (**c**) Presence of classic Aschoff body, mainly composed of the uninucleate Anitschkow's cells with intermingled fibrinoid necrosis and other mononuclear inflammatory cells (H&E × 400); Destruction of the epicardial coronary arterial radical by Aschoff body (**d**) (H&E × 250); (**e**) (H&E × 400)

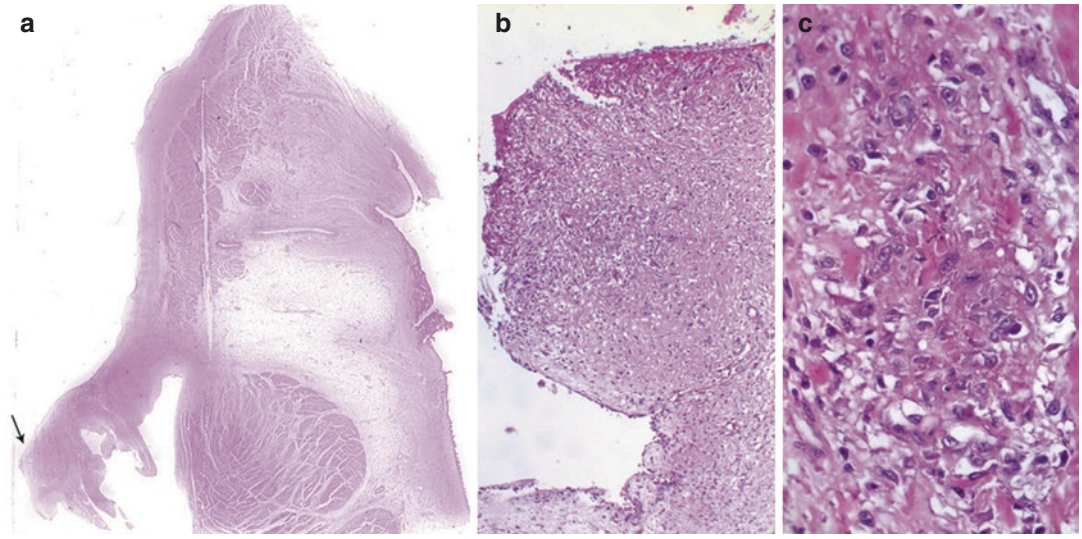

Fig. 4.4 (**a**) Scan of the section showing the left atrium, mitral valve, and left ventricle. Small vegetation (arrow) is seen at the line of closure; (**b**) Vegetation with organization and surface fibrin is accompanied by acute valvulitis (H&E × 250); (**c**) Aschoff body within the valve substance (H&E × 400)

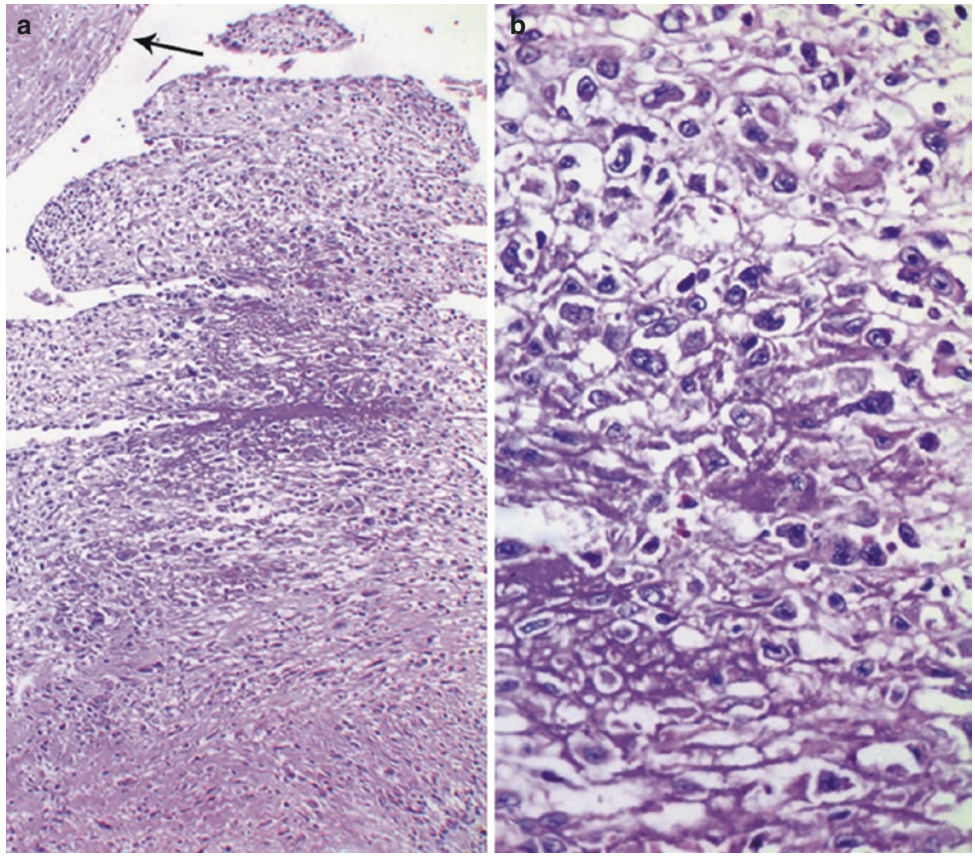

Fig. 4.5 (**a**) Stack of Aschoff's bodies within the sinus-of-Valsalva of the aortic valve. Arrow points to the inflamed non-flow surface of the cusp (H&E × 250); (**b**) Aschoff body (H&E × 400)

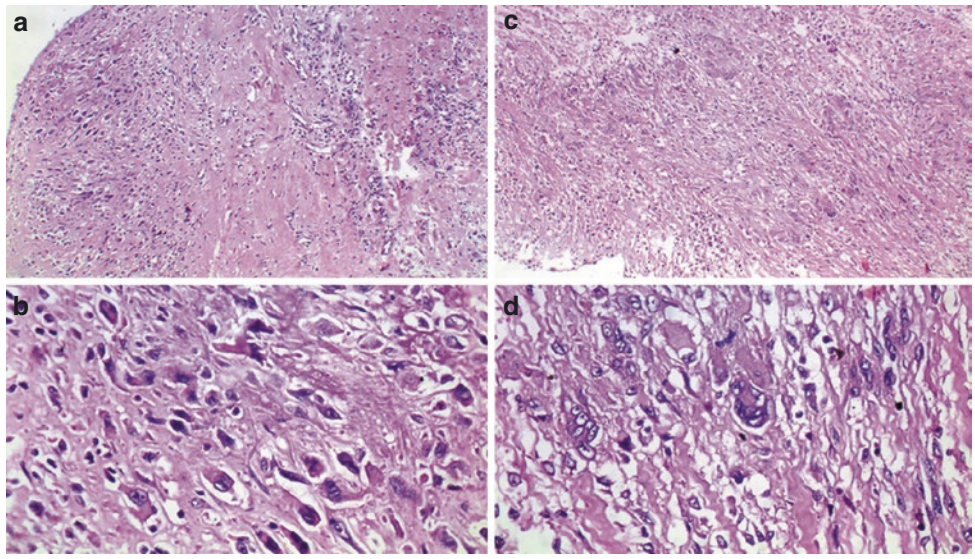

Fig. 4.6 Tricuspid valve showing (**a**) Acute valvulitis (H&E × 250) with many (**b**) Aschoff bodies (H&E × 400); Pulmonary valve showing (**c**) Acute valvulitis, despite normal gross appearance (H&E × 250) with many (**d**) Aschoff bodies with plentiful of Aschoff's giant cells (H&E × 400)

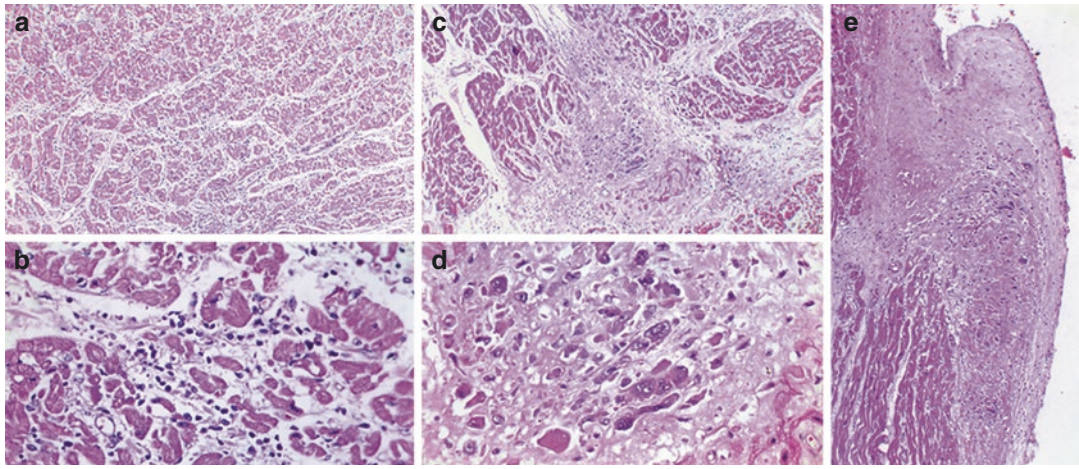

Fig. 4.7 Nonspecific lymphocytic myocarditis (**a**) (H&E × 250), (**b**) (H&E × 400); Granulomatous myocarditis with Aschoff bodies in the interstitium (**c**) (H&E × 250), (**d**) (H&E × 400); (**e**) Aschoff body protruding through endocardium (H&E × 400)

4.3 Discussion

Mortality in the presented case was due to ARF, which is a systemic, nonsuppurative complication of group A beta-hemolytic streptococcal (GAS) infection most frequently in the throat and in some cases possibly the skin. A precursor to the more debilitating valvular deformities, it usually affects children and young adults with an equal gender distribution; however, recurrences can be seen in adults below the age of 35–40 years. The main predisposing factors are linked to poor socioeconomic and environmental conditions. It is not surprising that the disease remains common in low—and middle-income countries and also among the less privileged population in the developed countries. Polymorphisms in the genes that regulate the adaptive immune response have also been shown to play an important role, which explains the occurrence of ARF in around 6% of patients with GAS infections.

In susceptible individuals, ARF develops approximately 2–5 weeks after a pharyngeal (or cutaneous) infection. An immune response that results in the production of antibodies and activation of T-cells against streptococcal antigens such as the M-protein and N-acetyl β D-glucosamine also targets heart proteins (cardiac myosin, valvular endothelium, laminin, and vimentin), brain proteins (lysoganglioside, tubulin, and dopamine receptors) and skin proteins (keratin) due to structural similarity (cross-reactivity or 'molecular mimicry') with consequent autoimmune damage to the host tissue. Such a response is also initiated when streptococcal antigens bind with the host proteins to create 'neo-antigens'. The ensuing tissue damage results in 'fibrinoid necrosis' surrounded by characteristic inflammatory reaction termed as Aschoff bodies or nodules. These nodules develop in 3 distinct phases—the initial (exudative), intermediate (proliferative or granulomatous), and late (healing). All layers of the heart in this case showed Aschoff bodies in the proliferative phase, which are said to occur from the 4th to 13th week of acute illness.

The autoimmune reaction causes systemic effects in the form of migratory arthritis (≥ 75%), clinical carditis (50–65%), chorea (15–20%), erythema marginatum, and subcutaneous nodules (3–10%)—the major Jones criteria, along with constitutional symptoms and alterations in the investigational parameters—the minor criteria, all of which are incorporated in the revised Jones' criteria. The index case, which fulfilled 2 major criteria, was clinically diagnosed as ARF and treated as per protocol. The sine-qua-non for the diagnosis of carditis is valvulitis, which in this case was only represented antemortem as MR;

however, autopsy demonstrated extensive involvement of the other 3 valves as well. Despite florid rheumatic granulomatous myocarditis (another autopsy surprise) that manifested as a fatal ventricular arrhythmia, the left ventricular ejection fraction at the time of diagnosis was surprisingly normal. Though the inflammation was mostly seen in the interstitial connective tissue, the large numbers of granulomas had caused damage to the adjacent cardiomyocytes. It may be speculated that the addition of corticosteroids at presentation as against only salicylates administered in the index case might have ameliorated myocardial inflammation.

Abdominal pain in rheumatic fever (included in the 1944 criteria) is considered a nonspecific symptom and has been attributed to acute localized peritonitis (often mimicking acute appendicitis) or rectus myositis. It is also noteworthy that the pericardial coronary arterial radicles had revealed rheumatic granulomatous vasculitis. In this case, we wonder if it was an example of referred pain of acute myocarditis or myocardial ischemia. This case is remarkable as it so vividly demonstrates the phenomenon of pancarditis with florid myocarditis, in contrast to the recent trends of describing rheumatic carditis solely as a valvular affection.

Further Reading

Cunningham MW. Molecular mimicry, autoimmunity and infection: the cross-reactive antigens of group a streptococci and their sequelae. Microbiol Spectr. 2019;7(4). https://doi.org/10.1128/microbiolspec.GPP3-0045-2018.

Dooley LM, Ahmad TB, Pandey M, Good MF, Kotiw M. Rheumatic heart disease: a review of the current status of global research activity. Autoimmun Rev. 2021;20:102740.

Gewitz MH, Baltimore RS, Tani LY, Sable CA, Shulman ST, Carapetis J, et al. American Heart Association Committee on rheumatic fever, endocarditis and Kawasaki disease of the council on cardiovascular disease in the young. Revision of the Jones criteria for the diagnosis of the rheumatic fever in the era of Doppler echocardiography: a scientific statement of the American Heart Association. Circulation. 2015;131:1806–18.

Liu M, Lu L, Sun R, Zheng Y, Zhang P. Rheumatic heart disease: causes, symptoms, and treatments. Cell Biochem Biophys. 2015;72:861–3.

Peters F, Karthikeyan G, Abrams J, Muhwava L, Zühlke L. Rheumatic heart disease: current status of diagnosis and therapy. Cardiovasc Diagn Ther. 2020;10:305–15.

Watkins DA, Beaton AZ, Carapetis JR, Karthikeyan G, Mayosi BM, Wyber R, et al. Rheumatic heart disease worldwide. JACC scientific expert panel. J Am Coll Cardiol. 2018;72:1397–416.

Silent Rheumatic Mitral Stenosis

5

Pawan Daga, Rushabh Shah,
and Pradeep Vaideeswar

5.1 Clinical History

A 35 years old female, G_4 P_3 L_3 A_1, presented to our hospital on third November in an unconscious state, not responding to deep stimuli and with muffled heart sounds. Her hemoglobin was 9.9 g/dL, total WBC count 26,200/cmm, platelet count was less than 20,000/cmm, blood urea nitrogen 28.1 mg/dL, and serum creatinine 2.5 mg/dL. She succumbed within 3 h despite continuous inotropic support.

She had presented to three different hospitals in the previous 12 days. She initially went to a peripheral hospital on 22nd October with bleeding per vaginum and passage of clots for 4 days associated with abdominal pain, vomiting, and giddiness. Her last menstrual period was in the first week of October. On examination she was afebrile with a feeble pulse of 60 per minute, blood pressure of 90/60 mmHg, and had mild pallor. Systemic examinations were normal. Per vaginal examination had revealed a bulky, 6 weeks size uterus without cervical motion tenderness or forniceal fullness. Her hemoglobin was 11.3 g/dL and β-human chorionic gonadotropin (β-HCG) 4810 mIU/mL. The pelvic ultrasonography was suggestive of products of conception. She was administered intravenous Pause 1 g and was discharged on tablets Methargan, Pause, and Doximate. A β-HCG advised to be repeated after 2 days was 1405 mIU/mL. As the bleeding continued, she was admitted to another nursing home on 31st October. Her hemoglobin was 10.2 g/dL, total WBC count 13,900/cmm, erythrocyte sedimentation rate 62 mm at 1 h, plasma aspartate aminotransferase 55.7 U/L (normal 5–40 U/L), and plasma alanine aminotransferase 72.4 U/L (normal 7–56 U/L)]. Abdominal and pelvic ultrasonography had revealed hepatomegaly, increased cortical reflectivity of both kidneys, and possibly an endometrial polyp or retained products of conception. A

P. Daga
Seth Gordhandas Sunderdas Medical College and King Edward Memorial Hospital, Mumbai, India

R. Shah
SRL Dr Avinash Phadke Labs, Mumbai, India

P. Vaideeswar (✉)
Department of Pathology (Cardiovascular and Thoracic Division), Seth Gordhandas Sunderdas Medical College and King Edward Memorial Hospital, Mumbai, India

P. Vaideeswar (ed.), *Tropical Cardiovascular Pathology*,
https://doi.org/10.1007/978-981-19-3720-0_5

dilatation and curettage was performed under general anesthesia. Postprocedure, she developed an irregularly irregular pulse, hypotension, and bilateral crepitations. She was shifted to the intensive care unit and given injection Amiodarone. However, she took discharge against medical advice. She was admitted to a third nursing home on third November for progressive shortness of breath. At this juncture, her pulse could not be felt and the blood pressure was unrecordable. The heart rate was 186 per minute and the central venous pressure 24–25 cm of water. Inotropic support started, but she developed anuria and was then transferred to our center.

5.2 Autopsy Findings

The heart weighed 290 g and showed moderate cardiomegaly with moderate enlargement of the right-sided chambers (Fig. 5.1a) and marked

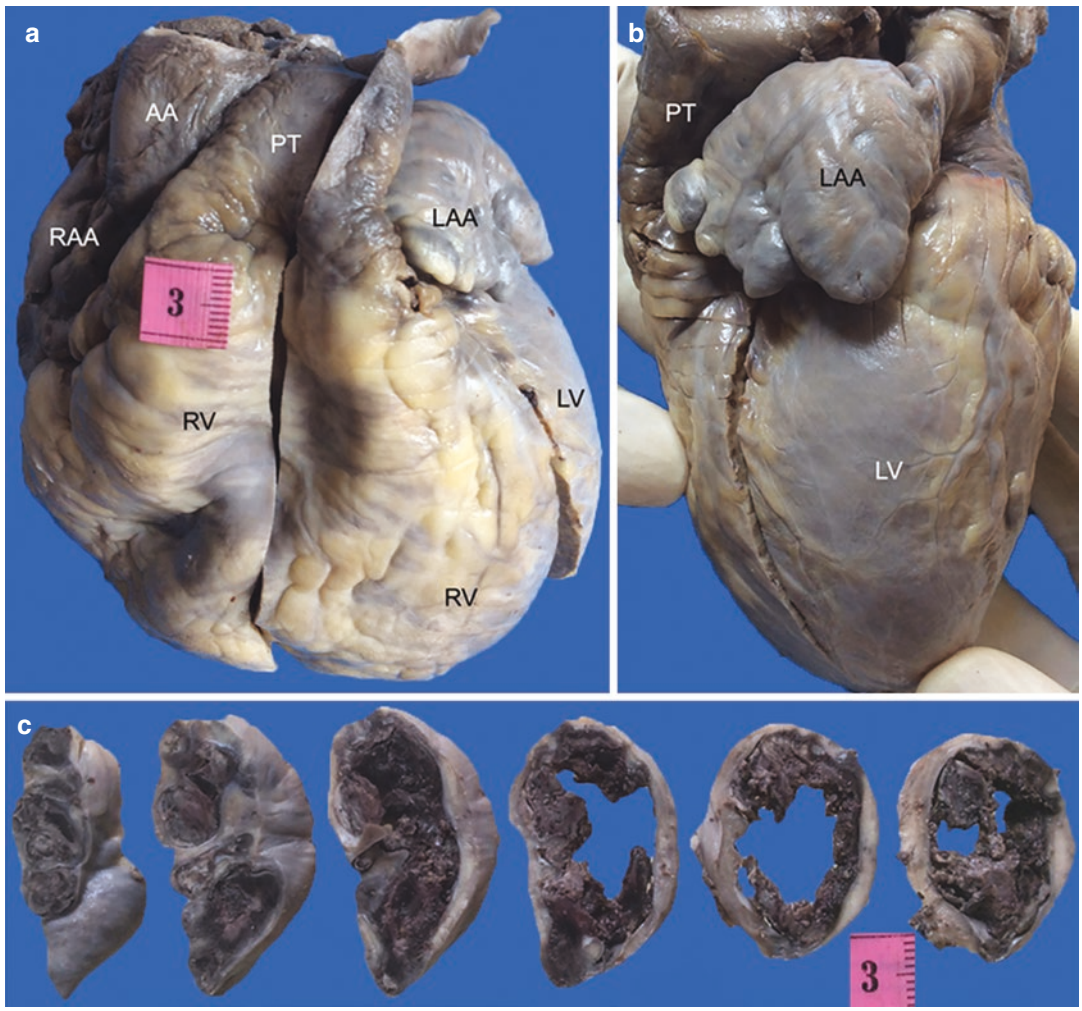

Fig. 5.1 (**a**) Moderate cardiomegaly is produced by enlargement of the right atrium RA and ventricle RV. Note that the apex is formed by the RV and the pulmonary trunk PT is as large as the ascending aorta AA. (**b**) Left lateral view of the heart to show a large and prominent left atrial appendage LAA; (**c**) Serial cross-sections to show fresh occlusive thrombi. Due to friability, the thrombus has dropped off in some of the slices. (*RAA* right atrial appendage)

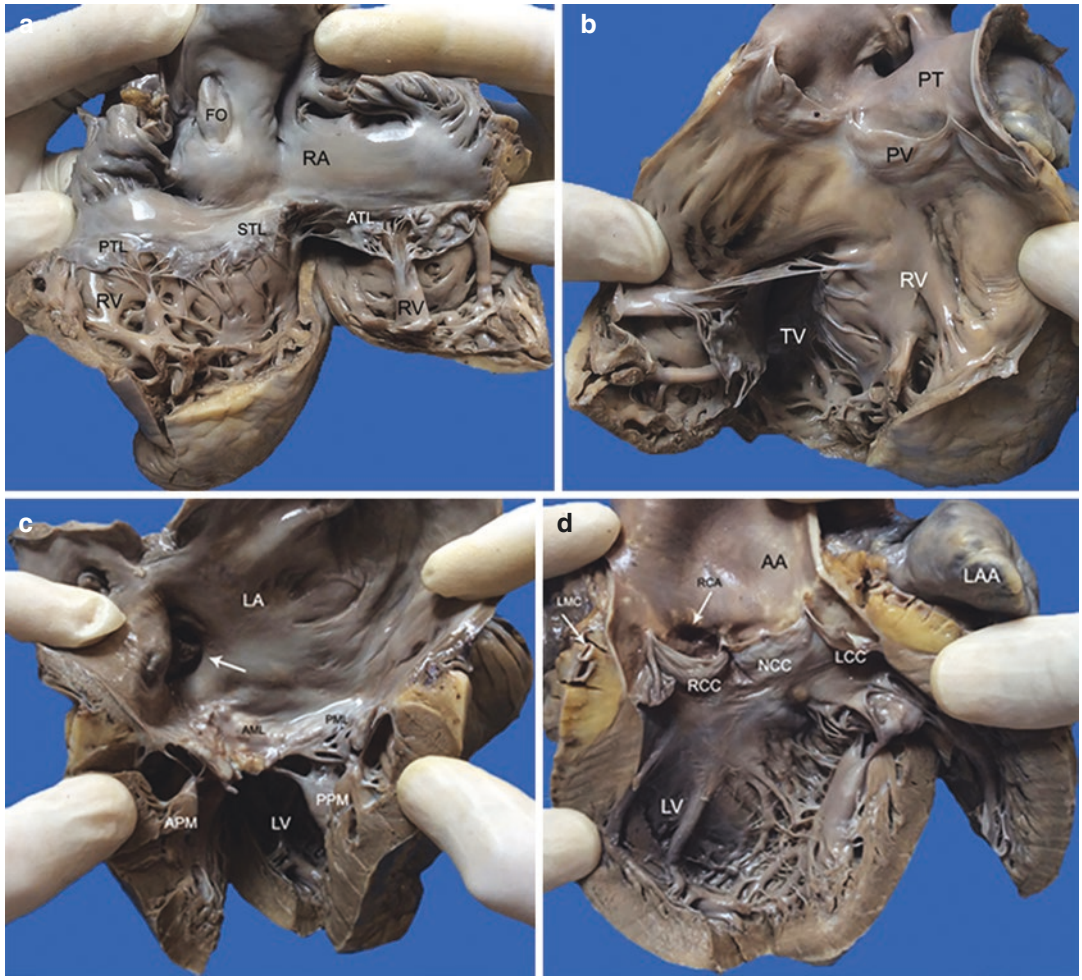

Fig. 5.2 Opened out right ventricular (**a**) Inflow and (**b**) Outflow tracts. The valves do not show any alterations. (**c**) Opened out left ventricular inflow tract. The left atrium LA is dilated. A thrombus protrudes from the appendageal opening (arrow). There is severe mitral stenosis with calcification and severe subvalvular disease. (**d**) Outflow tracts. (*AA* ascending aorta, *AML* anterior mitral leaflet, *ATL* anterior tricuspid leaflet, *FO* fossa ovalis, *LAA* left atrial appendage, *LCC* left coronary cusp, *LMC* left main coronary artery, *LV* left ventricle, *NCC* non-coronary cusp, *PML* posterior mitral leaflet, *PT* pulmonary trunk, *PTL* posterior tricuspid leaflet, *PV* pulmonary valve, *RA* right atrium, *RCA* right coronary artery, *RCC* right coronary cusp, *RV* right ventricle, *TV* tricuspid valve, *STL* septal tricuspid leaflet)

enlargement of the left atrium and its appendage (Fig. 5.1b). The appendage was firm in consistency and the lumen in its entirety was obliterated by a fresh red-brown thrombus (Fig. 5.1c). The tricuspid and pulmonary valvular annuli were dilated with mild right ventricular hypertrophy; however leaflets and cusps were normal (Fig. 5.2a, b). There was marked mitral stenosis (MS, orifice 1.0 cm across) with marked commissural fusion, calcification of the anterolateral commissure, and marked leaflet thickening. The chordae tendineae were thickened, shortened, and almost completely fused with the leaflets. This marked MS had resulted

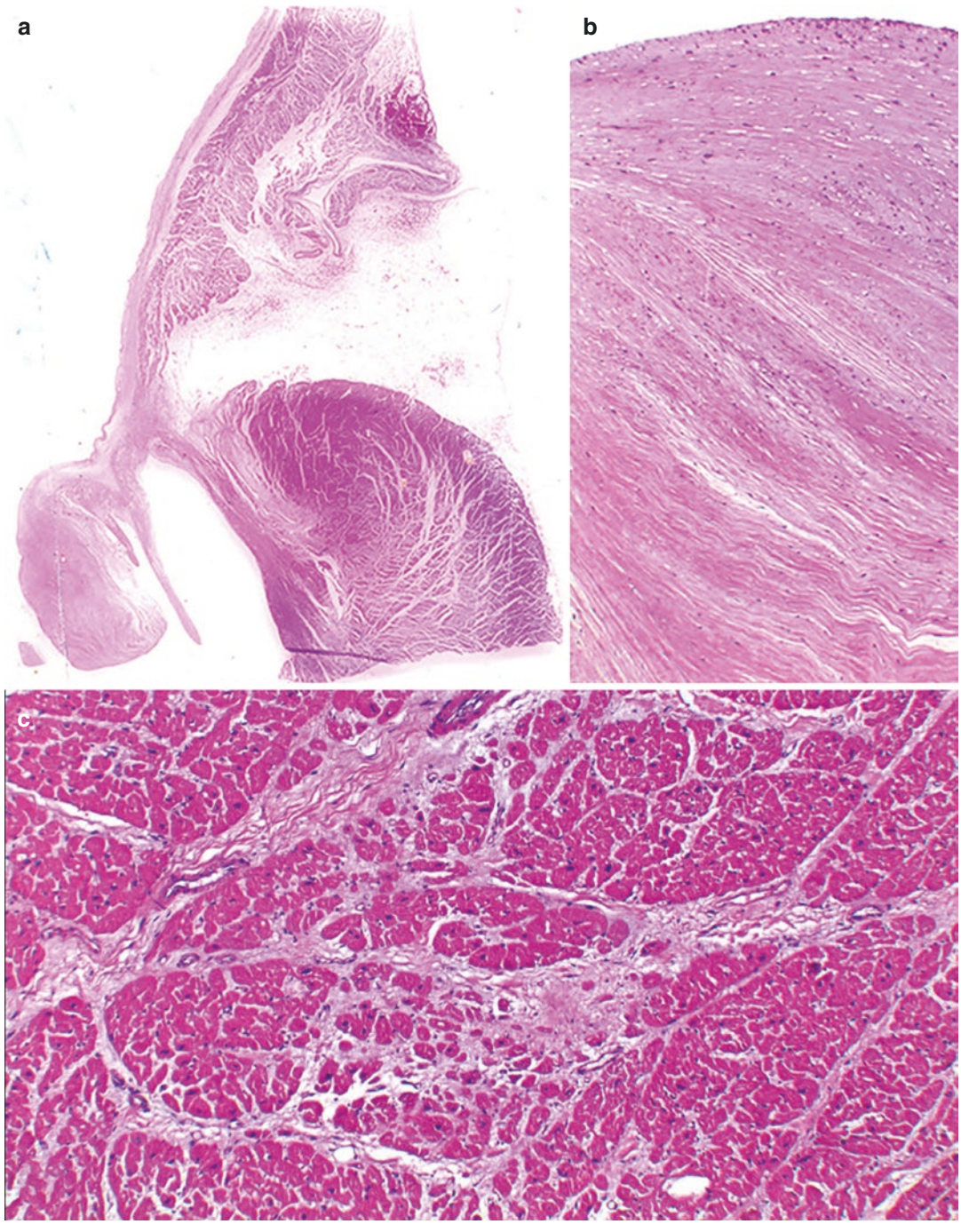

Fig. 5.3 (**a**) Scanned slide of the posterior mitral leaflet; (**b**) Extensive fibrosis of the leaflet (H&E × 250); (**c**) Interstitial and perivascular scars (H&E × 250)

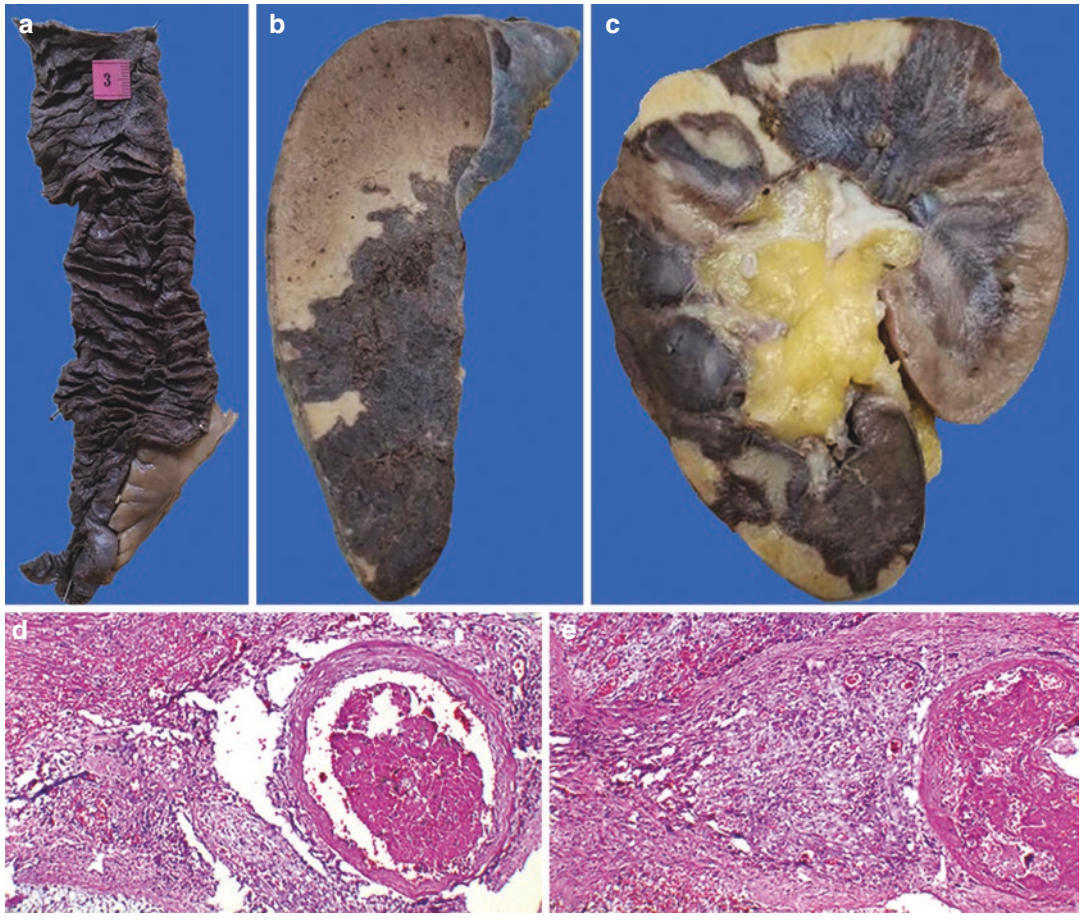

Fig. 5.4 (**a**) Small intestinal gangrene; (**b**) Splenic and (**c**) Renal, infarctions; (**d**) Fresh and (**e**) Fresh and organizing thrombi in the kidney (H&E × 250)

in moderate dilatation of the left atrium (Fig. 5.3c). The left ventricle was of normal size; there was no gross involvement of the aortic valve (Fig. 5.3d). On histopathological examination, the thickened mitral leaflets showed marked fibrosis, and small perivascular and interstitial ischemic scars were seen in the left ventricle. The thromboemboli from the thrombus in the left atrial appendage had resulted in intestinal gangrene, splenic, and bilateral renal infarctions (Fig. 5.4). The lungs showed brown induration, while the liver revealed features of chronic passive venous congestion with focal centrilobular hemorrhagic necroses (Fig. 5.5).

Cause of Death: Multiorgan infarction in a case of rheumatic mitral stenosis with left atrial appendageal thrombus.

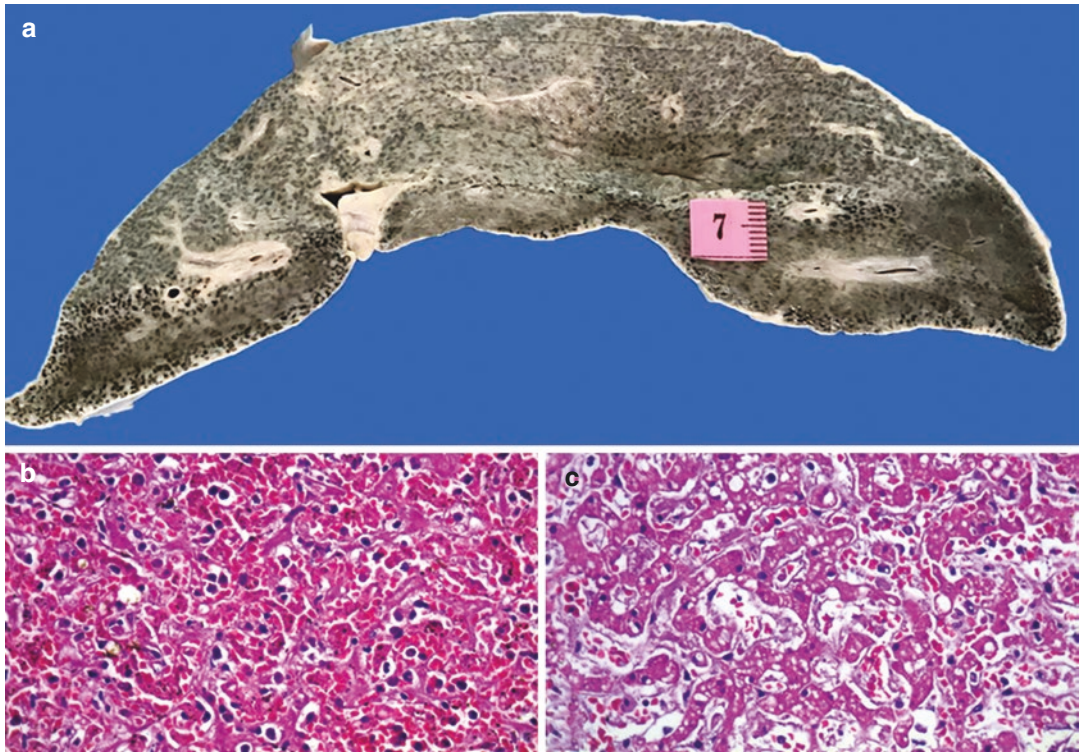

Fig. 5.5 (**a**) Hepatomegaly with an exaggerated nutmeg appearance on the cut surface; (**b**) Centrivenular hemorrhagic necrosis (H&E × 400); (**c**) Fatty change in the midzonal hepatocytes (H&E × 400)

5.3 Discussion

In this young patient, significant narrowing of the mitral valvular orifice MS was observed, which is an example of valvular heart disease (VHD). It results from structural changes or purely functional abnormalities of the atrioventricular and arterial valves; the left-sided valves, i.e., the mitral and aortic valves are chiefly affected. For optimal valvular function, there has to be perfect synchrony of not only the valvular components, but also of the adjacent structures. Disruption of one or more of these components results in stenosis and/or regurgitation of varying proportions. In general, VHD is caused mainly by post-inflammatory or inflammatory (infective or noninfective) conditions affecting the valves or their adjacent structures, degenerative changes, and congenital or heritable conditions.

MS, as seen in this case, is the most common manifestation of chronic rheumatic heart disease (RHD), a major sequel of healing of carditis caused by acute rheumatic fever (ARF, See Chap. 3). However, a history of ARF can be elicited in only half of the cases with chronic RHD. The next common valve affected in RHD is the aortic valve, followed by the tricuspid and rarely the pulmonary. Such preferential involvement of the valves is related to the hemodynamic stress attributable to transvalvular pressure gradients and its effect on transforming growth factor β1. Isolated mitral valvular affliction, as present in this case, occurs in about 70% of cases, while both left-sided valves are affected in about 25% of patients. Rheumatic MS with or without other valvular involvement can follow a single episode of severe carditis, but most often results from recurrent attacks of ARF, leading to cumulative damage and consequent thickening and scarring. The histology is not spectacular and mainly shows fibrosis, neovascularization, and variable degree of chronic inflammation.

The stenotic mitral valve leads to stasis of blood and elevated pressure in the left atrium with subsequent development of chronic passive pulmonary congestion ('brown induration'), pulmonary hypertension, and eventually right heart failure. Most patients present at ages 20–50 years, though some individuals in the Afro-Asian countries develop juvenile MS. However, the clinical scenario depends on the degree of stenosis. Patients with mild to moderate valvular stenosis can go unnoticed clinically, with echocardiography being the only way to identify them (subclinical RHD). Patients having moderate to severe stenosis are usually symptomatic and are readily recognizable on clinical examination. However, in some cases, the auscultatory findings are not easily detectable since severe calcification leads to dampening of the opening snap, and an enlarged right side of the heart leads to displacement of the valve and its associated murmur towards the posterior axillary line, along with shifting of the aorta towards the left sternal border. These are examples of clinically silent RHD and such patients can even remain asymptomatic. Clinically silent cases are detected as a surprise finding at autopsy, as in the case presented.

Women of childbearing age have the highest prevalence of RHD in endemic areas and it is not surprising that rheumatic MS is often the commonest lesion seen during pregnancy. The various pregnancy-related adaptive changes in the maternal cardiovascular system (See Chap. 42) may result in emergence of symptoms of MS for the first time during pregnancy. Furthermore, the risk of cardiac decompensation increases with each subsequent pregnancy as a result of advancement of age and reduction of the cardiac load-bearing capacity. However, early symptoms and signs may be attributed to normal manifestations of pregnancy, resulting in delayed diagnosis that increases the chances of maternal, fetal, and neonatal morbidity and mortality. The presence of other overwhelming diseases too can mask features of RHD. Our case had a silent MS that had gone unnoticed during the previous three pregnancies resulting in first trimester death in the fourth pregnancy. In the natural course of the disease, MS results in severe cardiac failure and can present as postpartum collapse. An important complication in the form of thromboembolism can occur. Stasis of blood in the left atrium and its appendage coupled with atrial fibrillation and pregnancy-associated hypercoagulability predisposes to thrombosis. In the case presented, there was left atrial appendageal thrombosis with embolism and multiorgan infarction that proved fatal.

Further Reading

Bitan A, Mazor-Dray E, Weinstein JM, Carmel S, Ilia R. Rheumatic mitral stenosis: long-term follow-up of adult patients with nonsevere initial disease. Cardiology. 2020;145:155–60.

Bortnick AE, Levine LD. Valvular heart disease in pregnancy. Clin Obstet Gynecol. 2020;63:910–22.

Fessehaye A, Tafere YT, Abate DD. Postpartum maternal collapse—a first-time presentation of severe mitral stenosis: a case report. J Med Case Rep. 2021;15:225.

Karthikeyan G, Fung E, Foo RSY. Alternative hypothesis to explain disease progression in rheumatic heart disease. Circulation. 2020;142:2091–4.

Lewey J, Andrade L, Levine LD. Valvular heart disease in pregnancy. Cardiol Clin. 2021;39:151–61.

Mayosi BM. The challenge of silent rheumatic heart disease. Lancet Glob Health. 2014;2:e677–8.

Peters F, Karthikeyan G, Abrams J, Muhwava L, Zühlke L. Rheumatic heart disease: current status of diagnosis and therapy. Cardiovasc Diagn Ther. 2020;10:305–15.

Wunderlich NC, Dalvi B, Ho SY, Küx H, Siegel RJ. Rheumatic mitral valve stenosis: diagnosis and treatment options. Curr Cardiol Rep. 2019;21:14.

6 Rheumatic Mitral Stenosis and Anticoagulant Toxicity

Amey Rojekar and Pradeep Vaideeswar

6.1 Clinical History

A 21-year-old female had been diagnosed with chronic rheumatic heart disease 15 years ago. She had severe rheumatic mitral stenosis (MS) with atrial fibrillation and had undergone a balloon mitral valvotomy (BMV) 7 years ago. She had developed right-sided hemiparesis 4 months back, when a computed tomographic (CT) scan of the brain had revealed a small acute infarct in the left middle cerebral artery territory. Atrial fibrillation (AF) was also detected and anticoagulant (warfarin) therapy was started. She now presented to our hospital in a poor general condition with barely felt peripheral pulses and recordable blood pressure, following acute severe pain in the abdomen and vomiting. CT of the abdomen performed in the previous evening in a private health-care facility was suggestive of hemoperitoneum due to ruptured left ovarian cyst. The hemoglobin was 4.1 g/dL and prothrombin time was more than 100 s (international normalized ratio >10); other routine investigations had been normal. She expired within an hour of admission.

6.2 Autopsy Findings

A partial chest and abdomen autopsy was performed. The heart weighed 230 g. On external examination, the heart was mildly enlarged (Fig. 6.1a) with moderate enlargement of the right ventricle and left atrium. The right-sided inflow tract (Fig. 6.1b) showed complete obliteration of the septostomy opening (performed for the BMV) in the fossa ovalis region of the interatrial septum, moderate fusion of the anteroseptal commissure of the tricuspid valve, and moderate right ventricular hypertrophy. There was marked mitral stenosis (1 × 0.7 cm, Fig. 6.2a) and the orifice allowed the passage of only the index finger. However, the posteromedial commissure was well split right into the apices of the posterior group of papillary muscles; the anterolateral commissure continued to be markedly fused (Fig. 6.2a). The leaflets were markedly thickened with minimal focal calcification. There was severe subvalvular pathology with hardly any interchordal spaces; the papillary muscles

A. Rojekar
Department of Pathology, Seth Gordhandas Sunderdas Medical College and King Edward Memorial Hospital, Mumbai, India

P. Vaideeswar (✉)
Department of Pathology (Cardiovascular and Thoracic Division), Seth Gordhandas Sunderdas Medical College and King Edward Memorial Hospital, Mumbai, India

P. Vaideeswar (ed.), *Tropical Cardiovascular Pathology*,
https://doi.org/10.1007/978-981-19-3720-0_6

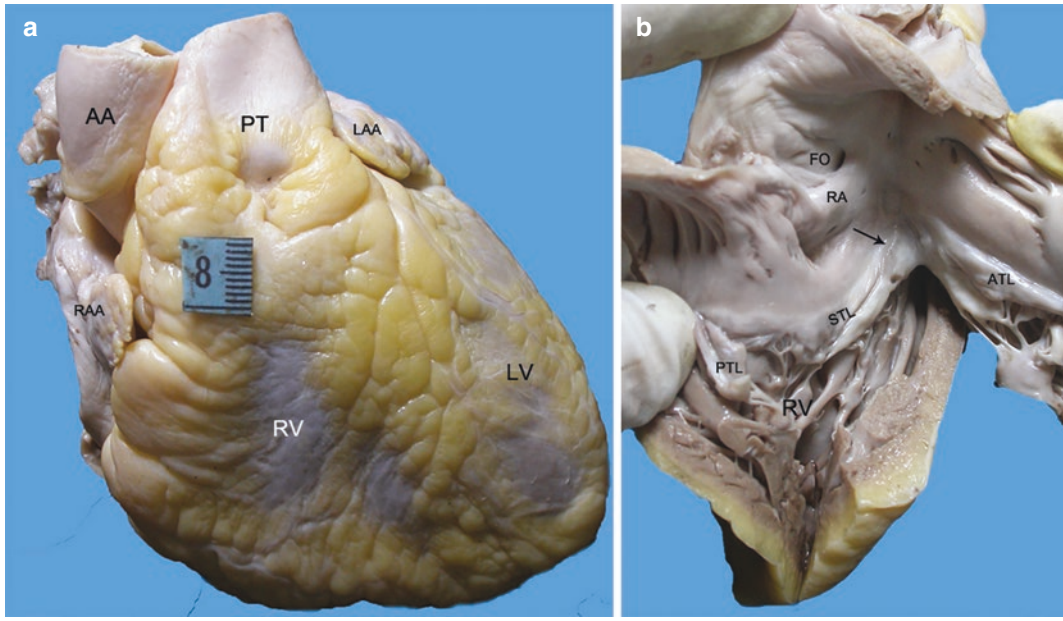

Fig. 6.1 (**a**) Anterior surface of the heart showing moderate enlargement of the right ventricle RV and dilated pulmonary trunk PT, which is larger than the ascending aorta AA; (**b**) Opened out right-sided inflow tract. Note intact fossa ovalis, fused anteroseptal commissure, and RV hypertrophy (*ATL* anterior tricuspid leaflet, *LAA* left atrial appendage, *LV* left ventricle, *PTL* posterior tricuspid leaflet, *RA* right atrium, *RAA* right atrial appendage, *STL* septal tricuspid leaflet)

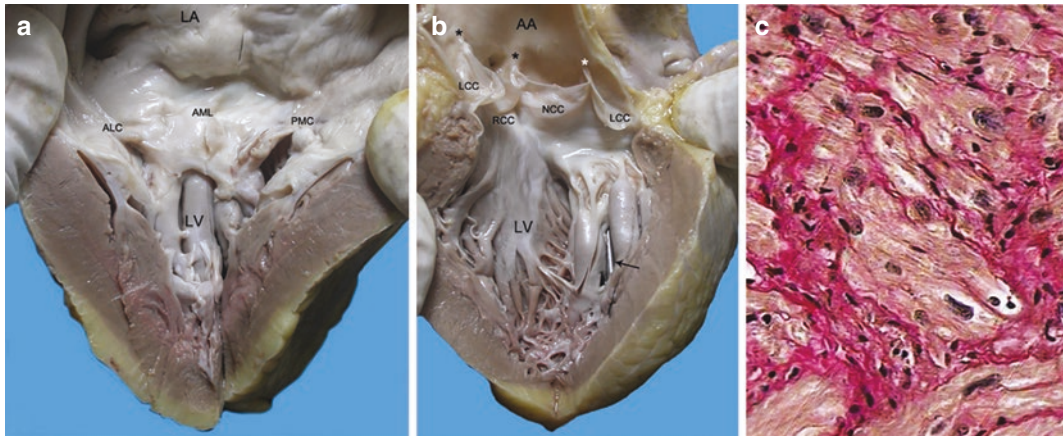

Fig. 6.2 (**a**) There is severe mitral stenosis with involvement of all the components. The anterolateral commissure ALC is well split; (**b**) The papillary muscles appear directly fused with the leaflets. A probe (arrow) has been passed through the stenotic orifice. Commissures * of the aortic valve appear fused. (*AA* ascending aorta, *AML* anterior mitral leaflet, *LA* left atrium, *LCC* left coronary cusp, *LV* left ventricle, *PMC* posteromedial commissure, *NCC* noncoronary cusp, *RCC* right coronary cusp); (**c**) Hypertrophy of the cardiomyocytes with interstitial fibrosis. The collagen is stained bright red (Picro-sirius × 400)

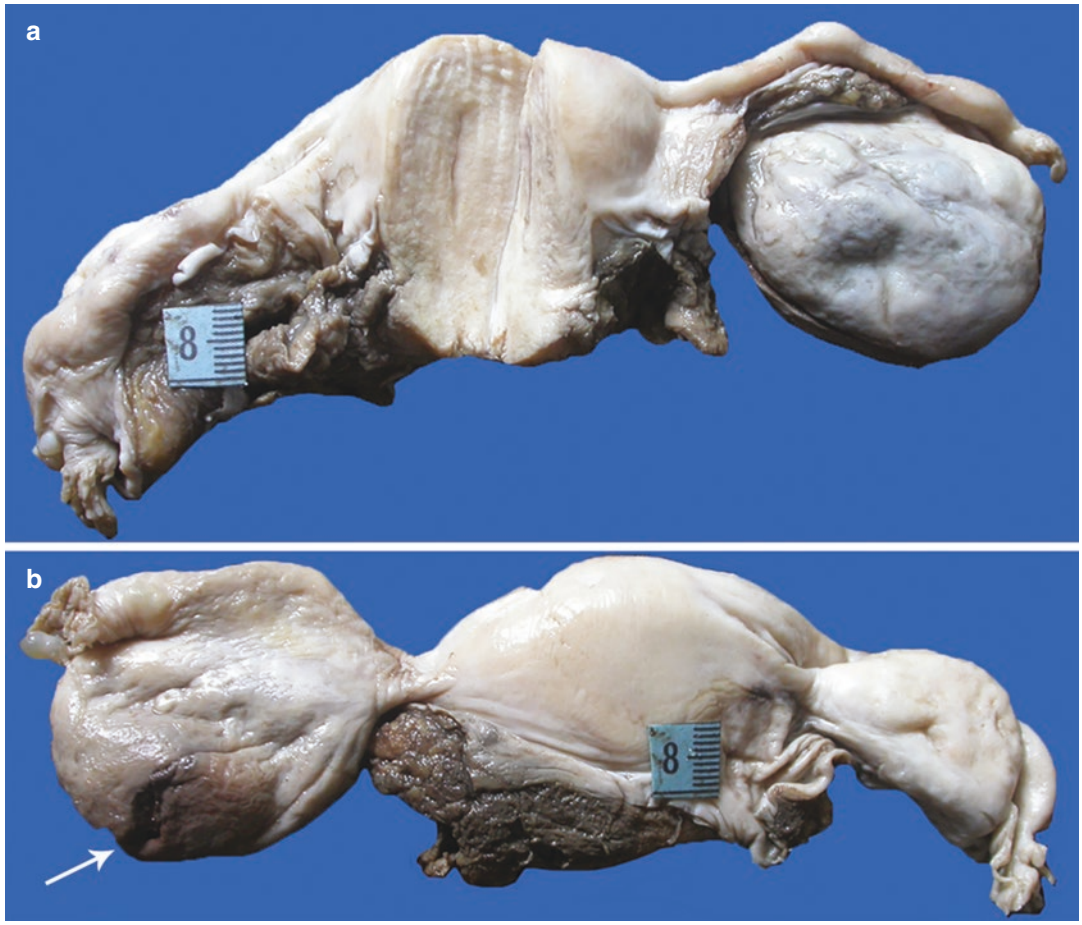

Fig. 6.3 (**a**) Anterior and (**b**) Posterior aspects of the uterus and its adnexae. The right ovary was enlarged, cystic, and hemorrhagic with a rent on its posterior surface (arrow)

appeared to be directly fused to the leaflets. All the 3 commissures of the aortic valve were fused (Fig. 6.2b). The cusps appeared normal, but on histology showed features of healed valvulitis. The dilated left atrium also showed hypertrophy and extensive interstitial fibrosis (Fig. 6.2c). Apart from chronic passive venous congestion, the lungs did not show features of pulmonary hypertension.

The surprise finding was the cause for the hemoperitoneum. The left ovary was enlarged (5 × 3 cm) with a congested external surface and a 1 cm rupture on the posteroinferior aspect (Fig. 6.3). This complication was produced by a hemorrhagic follicular cyst (Fig. 6.4). The uterine endometrium was in its proliferative phase. There was around 800 mL of fluid blood with blood clots in the lower abdominal cavity and the pelvis with patchy fibrinous exudates of the intestines. Other organs were normal.

Cause of Death: Hypovolemic shock due to hemoperitoneum following ruptured ovarian follicular cyst.

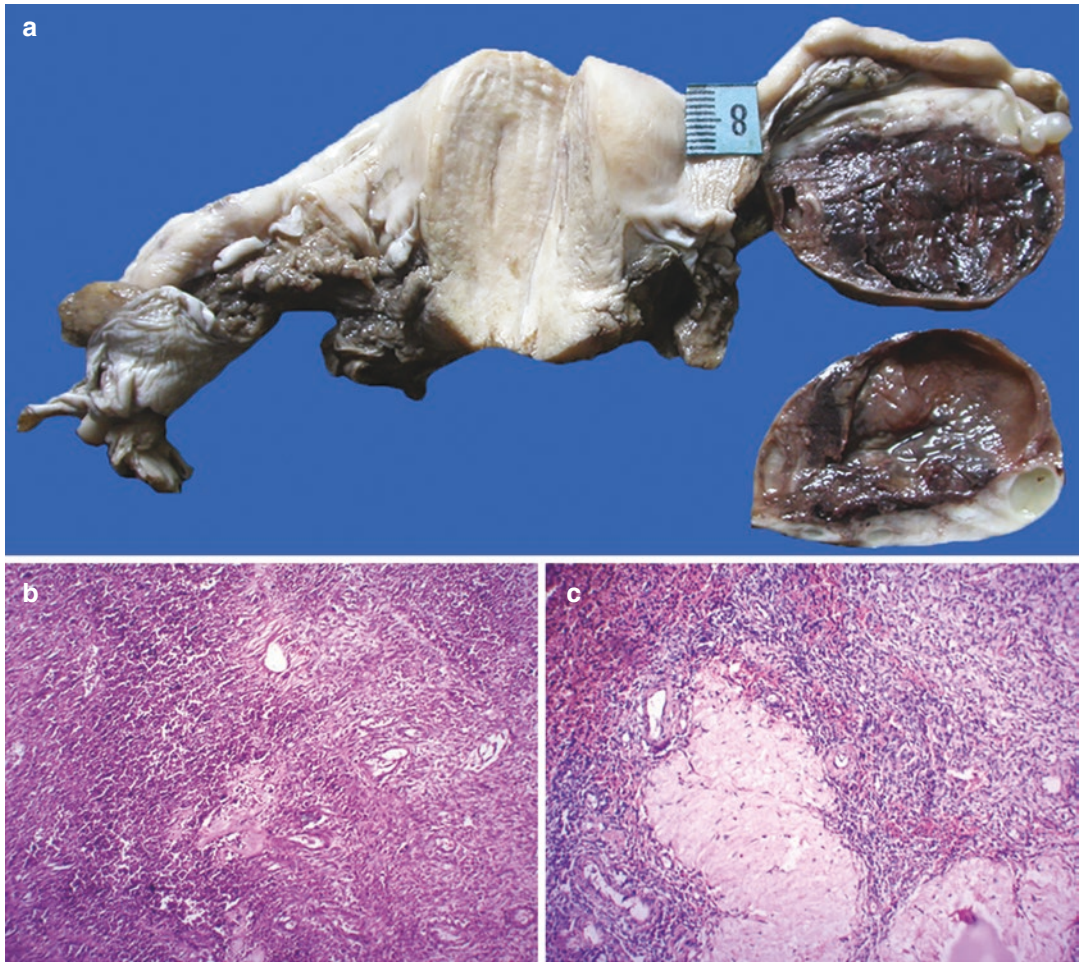

Fig. 6.4 (**a**) The opened out right ovary with a hemorrhagic cyst; (**b**) Most of the cyst wall was disrupted by hemorrhage which had involved the ovarian stroma (H&E × 250) and was also seen around the (**c**) Corpus albicans (H&E × 250)

6.3 Discussion

The medical management of rheumatic MS is mainly directed towards prevention of further attacks of acute rheumatic fever, alleviation of left ventricular dysfunction, prevention of infective endocarditis, and reduction of thromboembolic episodes. The deceased, who had well-established disease at the age of the 6 years, would fall in the category of 'juvenile' MS, a term coined by Roy et al in 1963. The disease, unfortunately, progressed to severe stenosis, which could not have been managed by medications alone and hence she also underwent the BMV at the age of 14 years. BMV is considered as the best option in such cases, which entails a transseptal puncture and passage of balloon through the interatrial septum with inflation across the stenotic valve (See Chap. 16). The intermediate and long-term results often depend on the morphology of the stenotic valves.

The mortality in this case was related to the anticoagulant therapy administered for her thromboembolic episode, which manifested as right-sided hemiparesis. The sources of the bland emboli in a setting of MS are thrombi located

mainly in the left atrial appendage; some are present as mural left atrial thrombi. Apart from stasis of blood, an important predisposing factor is development of atrial fibrillation, which itself is related to left atrial chamber dilatation and importantly to histomorphological changes in the chamber and its appendage, designated as "fibrotic atrial cardiomyopathy" as noted in the present case. Oral anticoagulant therapy is the standard treatment for well-established thrombi as well as a prophylactic measure, for which warfarin is the most commonly used oral anticoagulant. But, the therapy has an inherent risk of significant bleeding due to its widely variable dose requirement, narrow therapeutic window, drug and dietary interactions, and genetic variations in its metabolism. Hence, regular blood monitoring and dose adjustment are necessary to maintain the INR within the target therapeutic range (usually between 2 and 3) to prevent complications. An INR of >3 often results in bleeding, while an INR <2 leads to a thrombogenic tendency. Rupture of ovarian cyst causing hemoperitoneum is a rare but serious complication of chronic anticoagulation therapy. Most of them are due to ruptured corpus luteum as they are hypervascular. In a large case series of 46 patients by Jamal et al on corpus luteum rupture, almost 50% patients were on anticoagulation therapy, and among those, 77% patients presented with hemoperitoneum. However, hemoperitoneum due to follicular cyst rupture with anticoagulation therapy is not reported in the literature. Patients with hemoperitoneum due to ovarian cyst rupture commonly present with complaints of sudden abdominal pain, anemia, and signs of peritonitis. These signs and symptoms are also seen in cases of ruptured ectopic gestation, acute appendicitis, and acute salpingitis in women of reproductive age group. Hence, accurate diagnosis by imaging is important for management, as warfarin-related toxicity can be treated conservatively by transfusion of fresh frozen plasma, withholding, and subsequent readjustment of the dose as per INR. Thus, in all valvular heart disease patients with atrial fibrillation who are on oral anticoagulants, careful monitoring by regular follow-up and a high clinical suspicion in patients presenting with acute abdomen are most important for prevention and accurate diagnosis of this rare but life-threatening complication.

Further Reading

Hirsh BJ, Copeland-Halperin RS, Halperin JL. Fibrotic atrial cardiomyopathy, atrial fibrillation, and thromboembolism. J Am Coll Cardiol. 2015;65:2239–51.

Jamal A, Mesdaghinia S. Ruptured corpus luteum cysts and anticoagulant therapy. Int J Gynecol Obstet. 2002;76:319–20.

John B, Lau CP. Atrial fibrillation in valvular heart disease. Card Electrophysiol Clin. 2021;13:113–22.

Ozturk M, Ipekci A, Kiyak SK, Akdeniz YS, Aydin Y, Ikizceli I, et al. Bleeding complications in warfarin-treated patients admitted to the emergency department. J Clin Med Res. 2019;11:106–13.

Palacious IF. Percutaneous mitral balloon valvuloplasty–state of the art. Mini-invasive Surg. 2020;4:73.

Roy SB, Bhatia ML, Lazaro EJ, Ramalingaswami V. Juvenile mitral stenosis in India. Lancet. 1963;2:1193–6.

Russell EA, Walsh WF, Costello B, McLellan AJA, Brown A, Reid CM, et al. Medical management of rheumatic heart disease: a systematic review of the evidence. Cardiol Rev. 2018;26:187–95.

Rheumatic Mitral Stenosis with Sickling Crisis

7

Tejaswini Waghmare and Pradeep Vaideeswar

7.1 Clinical History

A 38-year-old woman, with a ward stay of 13 h, presented with progressive shortness of breath for the past 1 month, and fever, cough, mucoid expectoration, and palpitation since 10 days. She had exertional dyspnea for the past 2 years and a past history of a cerebrovascular accident; however, there were no reports available of the diagnosis or treatment. An echocardiography performed a month before the current admission had revealed chronic rheumatic heart disease (RHD) with severe mitral stenosis (MS, area of 0.7 cm^2), mild mitral/aortic regurgitation, severe tricuspid regurgitation, and severe pulmonary hypertension.

On examination, the pulse rate was 114 per minute and blood pressure 100/70 mmHg. Bilateral crepitations and diastolic murmur were heard on auscultation. The clinical diagnosis was rheumatic MS with lower respiratory tract infection. Apart from mild anemia (hemoglobin 12.4 g/dL), other routine hematological and biochemical investigations were normal. A repeat echocardiography showed similar features, but also picked up moderate aortic stenosis. She was given lasix infusion with antibiotics. Since there was marginal response to medical therapy, a decision to perform an emergency balloon mitral valvotomy was taken. She had cardiac arrest after the first inflation and could not be revived.

7.2 Autopsy Findings

A partial autopsy had been performed in this case. The heart was moderately enlarged (weight 370 g, Fig. 7.1a). There was marked enlargement of the right-sided chambers and moderate enlargement of the left atrium. The pulmonary trunk was larger than aorta. Fresh and organizing fibrinous exudates were present over the right atrium and its appendage. The interatrial septum in the midportion of the oval fossa showed a ragged transversely placed septostomy opening, 0.7 cm in length. It was of similar dimensions on the left atrial aspect. The valvotomy procedure had not produced the expected results, with continued marked commissural fusion and severe orificeal stenosis; the posteromedial commissure was superficially split (Fig. 7.1b). The postero-

T. Waghmare
Department of Pathology, Seth Gordhandas Sunderdas Medical College and King Edward Memorial Hospital, Mumbai, India

P. Vaideeswar (✉)
Department of Pathology (Cardiovascular and Thoracic Division), Seth Gordhandas Sunderdas Medical College and King Edward Memorial Hospital, Mumbai, India

P. Vaideeswar (ed.), *Tropical Cardiovascular Pathology*,
https://doi.org/10.1007/978-981-19-3720-0_7

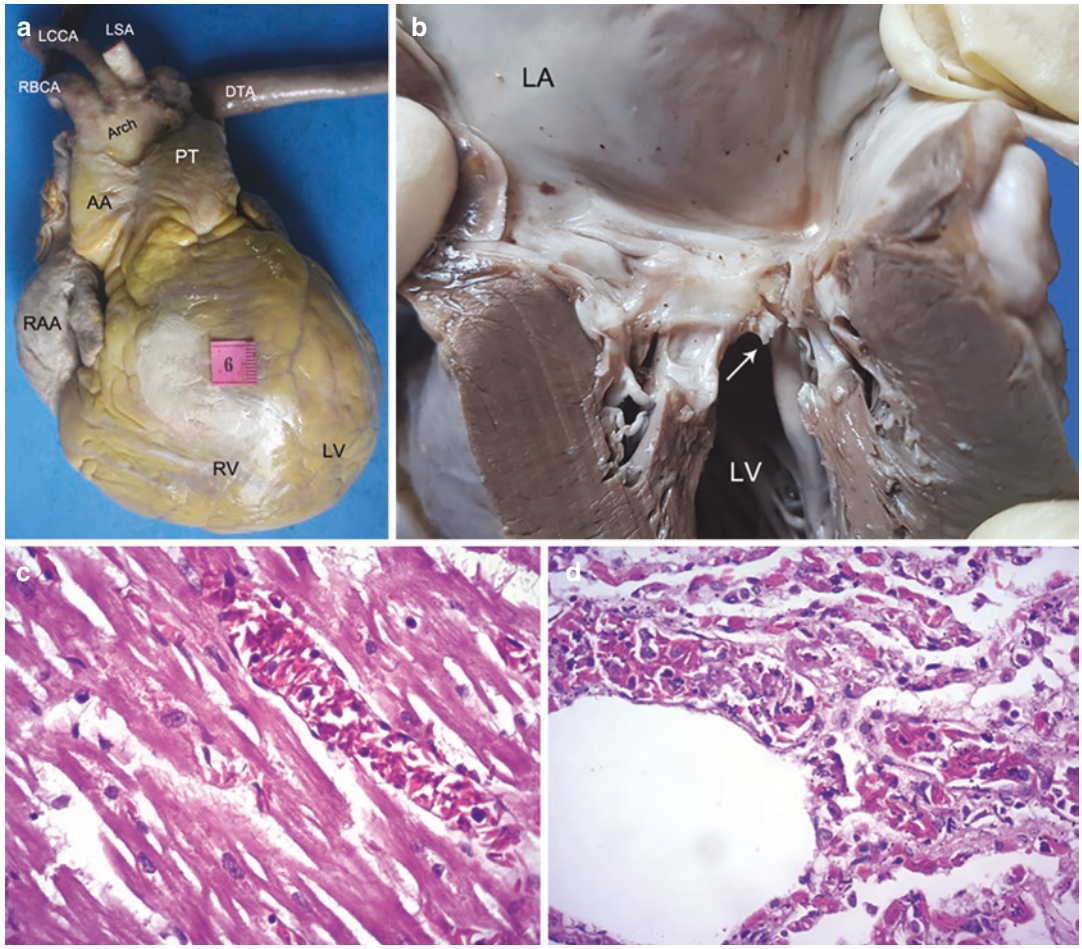

Fig. 7.1 (**a**) Moderate cardiomegaly. The apex is formed by both ventricles. Note a milk patch over anterior surface of right ventricle RV and pulmonary trunk PT, as large as the ascending aorta AA; (**b**) Severe mitral stenosis with superficial split (arrow) in the fused posteromedial commissure (*LA* left atrium, *LCCA* left common carotid artery, *LSA* left subclavian artery, *LV* left ventricle, *RBCA* right brachiocephalic artery, *RAA* right atrial appendage); Sickled RBCs in the vasculature of the (**c**) heart and (**d**) lungs (H&E × 400)

medial commissure was also heavily calcified with a calcific spur connecting it to the interventricular septum, as seen from the ventricular aspect. The chordae were markedly fused and the thickened leaflets appeared to be directly connected to the papillary muscles. There would have been mild aortic stenosis produced by marked fusion of the commissure between the right and left coronary cusps; there was mild cuspal thickening. The tricuspid and pulmonary valves were normal. Mild to moderate hypertrophy was present in the right-sided chambers and left atrium, with small foci of interstitial scarring.

The other findings included brown induration of the lungs with features of venous hypertension and cardiac cirrhosis of the liver (weight 1.2 kg). The spleen weighed 180 g and appeared normal (Fig. 7.2a). The most startling findings were the presence of sickled red cells in the heart, lungs (Fig. 7.1c, d), liver, kidneys, spleen (Fig. 7.2c, d), and bone marrow.

Cause of Death: Vaso-occlusive sickling crisis with severe rheumatic mitral stenosis.

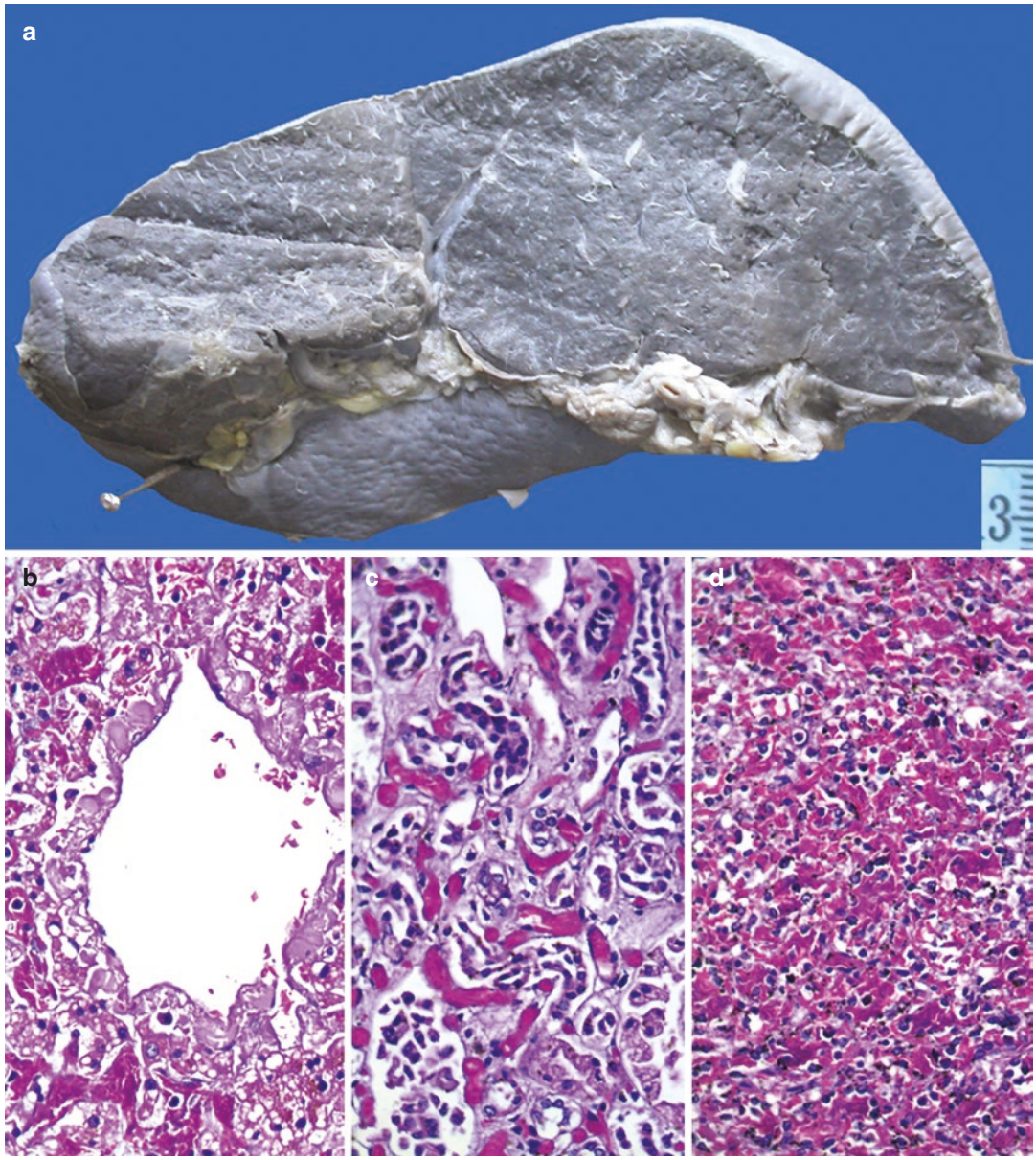

Fig. 7.2 (**a**) Spleen with a normal cut surface; Sickled red cells in the (**b**) Central veins and dilated sinusoids of the liver, (**c**) Vasa recta of the renal medulla and (**d**) Sinusoids of the red pulp of the spleen (H&E × 400)

7.3 Discussion

This young woman sustained a cardiac arrest during the well-established BMV procedure for rheumatic MS, and a restricted autopsy revealed the concomitant presence of widespread sickling of the RBCs. RHD (see Chap. 5) is an important cause of heart disease in India, a nation that is also estimated to have the second highest burden of sickle-cell disease (SCD). SCD, a prototypic hereditary hemolytic anemia, is characterized by the presence of HbS formed due to substitution of a hydrophilic glutamic acid residue in the sixth position of the β-globin chain by a hydrophobic

valine residue. It encompasses the homozygous inheritance HbSS, that is also termed as sickle-cell anemia (SCA), and a combination of HbS with other β-globin chain mutations and β-thalassemia. A common characteristic for all the conditions under SCD is a tendency for polymerization of deoxygenated HbS, initiated and/or potentiated by hypoxia, dehydration, acidosis, infection, or other unidentified factors. Through a sequence of events (nucleation, closure, growth, and final alignment), the HbS polymers form long fibers or tactoids leading to RBC rigidity and distortion and the formation of the characteristic sickle cells. The repeated process of sickling and unsickling of the RBCs results in a chronic hemolytic anemia, but can also predispose the individual to vaso-occlusive, hemolytic, and/or aplastic crises.

The current case demonstrated vaso-occlusive crisis, where the vasculature in various organs retrieved in the partial autopsy showed conglomeration of sickled erythrocytes. The effects are not only produced by mechanical occlusion of the blood vessels, but also by ensuing hyperviscosity, endothelial damage, and procoagulant/proinflammatory state. In this patient, the hemoglobin was within the normal range, and the spleen was also of normal size. This may be explained on the basis of benign phenotype of the homozygous state wherein the red cells are protected due to high levels of fetal hemoglobin, concurrent α-thalassemia, β-globin gene haplotypes and other gene polymorphisms, or the presence of sickle-cell trait (heterozygous state). In all these settings, sickling can occur under stressful conditions and be responsible for morbidity and mortality. In this patient, since red cell pathology was not suspected either clinically or at autopsy, testing for abnormal hemoglobin was not done.

Cardiovascular complications are mainly described in cases of SCD and are seen as left ventricular diastolic dysfunction related to microvascular occlusion and consequent ischemic scarring, dysrhythmias and sudden death, and pulmonary vascular complications in the form of acute chest syndrome and pulmonary hypertension. Our patient was a known case of RHD with severe MS. The myocardial scarring was noted in only perivascular regions in our case, a feature which typically occurs due to healing of an episode of acute rheumatic fever (ARF). The coexistence of RHD and SCD, though rare, is known and few studies have also suggested increased prevalence of RHD in cases of SCA. Some of the reasons postulated include damage to the vascular endothelium and moderate to severe immunosuppression produced by SCA, which make these individuals susceptible to the autoimmune response as seen in ARF.

Further Reading

Helvaci MR, Davran R, Abyad A, Pocock L. What a high prevalence of rheumatic heart disease in sickle cell patients. World Fam Med. 2020;18:74–9.

Hockham C, Bhatt S, Colah R, Mukherjee MB, Penman BS, Gupta S, et al. The spatial epidemiology of sickle-cell anaemia in India. Sci Rep. 2018;8:17685.

Italia K, Kangne H, Shanmukaiah C, Nadkarni AH, Ghosh K, Coah RB. Variable phenotypes of sickle cell disease in India with the Arab-Indian haplotype. Br J Haematol. 2015;168:156–9.

Naik RP, Haywood C Jr. Sickle cell trait diagnosis: clinical and social implications. Hematology Am Soc Hematol Educ Program. 2015;1:160–7.

Negi PC, Sondhi S, Asotra S, Mahajan K, Mehta A. Current status of rheumatic heart disease in India. Indian Heart J. 2019;71:85–90.

Novelli EM, Gladwin MT. Crises in sickle cell disease. Chest. 2016;149:1082–93.

Sundd P, Gladwin MT, Novelli EM. Pathophysiology of sickle cell disease. Annu Rev Pathol. 2019;14:263–92.

Vaideeswar P, Singh H, Singaravel S. Concurrent rheumatic mitral stenosis with sickling hemoglobinopathy. Indian Heart J Cardiovasc Case Rep. 2017;1:119–21.

8 Rheumatic Heart Disease and Prosthetic Valvular Thrombosis

Supreet P. Marathe and Pradeep Vaideeswar

8.1 Clinical History

A 35-year-old female was admitted with chief complaints of dyspnea for a week with associated orthopnea and paroxysmal nocturnal dyspnea for the past 3 days. She had undergone mitral valve replacement at the age of 19 years for severe rheumatic mitral stenosis and was on regular warfarin therapy that was poorly monitored. On examination, her general condition was poor with tachycardia (130/min) and hypotension (90/70 mmHg). Both the heart sounds were heard, but a click was not appreciated. There were bilateral crepitations. Routine laboratory investigations revealed anemia (hemoglobin 9 g/dL), neutrophilic leukocytosis (16,200/cmm), and a prolonged prothrombin time of 22.7 s (control of 13 s, INR 1.9). Sinus tachycardia with anterolateral myocardial infarction and a choked prosthetic mitral valve with severe pulmonary hypertension (60 mmHg) were noted on ECG and echocardiography, respectively. She was given ventilator support and started on diuretics, inotropes, and anticoagulants. Her condition remained poor and she expired after 13 h.

8.2 Autopsy Findings

The heart (280 g) was moderately enlarged with focal adherence of the layers of the pericardium. Milk patches were present over the right atrium and posterior surface of the left ventricle. Sutures buried in fibrous tissue were seen over the atria and ascending aorta. The right-sided chambers and the left atrium were moderately enlarged with mild myocardial hypertrophy. The entire mitral valve (including the papillary muscles) had been excised and replaced by a mechanical uni-leaflet valve. It showed restricted mobility due to a layer of firm pale brown to red-brown fresh thrombotic material over both atrial (Fig. 8.1a) and ventricular (Fig. 8.1b) aspects. The thrombus was histologically bland (Fig. 8.1c, d). Microscopy of the left ventricle revealed the presence of multiple healing and healed microinfarcts that corresponded to the foci of congestion and glistening grey-white areas seen on transverse sections; thrombotic occlusion of the epicardial or intramural coronary arteries was not seen in the samples taken. The lung and the liver showed features of chronic passive venous congestion; there were no changes of pulmonary hypertension.

Cause of Death: Prosthetic Valvular Thrombosis.

S. P. Marathe
Faculty of Medicine, Queensland Children's Hospital, University of Queensland, Brisbane, Australia

P. Vaideeswar (✉)
Department of Pathology (Cardiovascular and Thoracic Division), Seth Gordhandas Sunderdas Medical College and King Edward Memorial Hospital, Mumbai, India

P. Vaideeswar (ed.), *Tropical Cardiovascular Pathology*,
https://doi.org/10.1007/978-981-19-3720-0_8

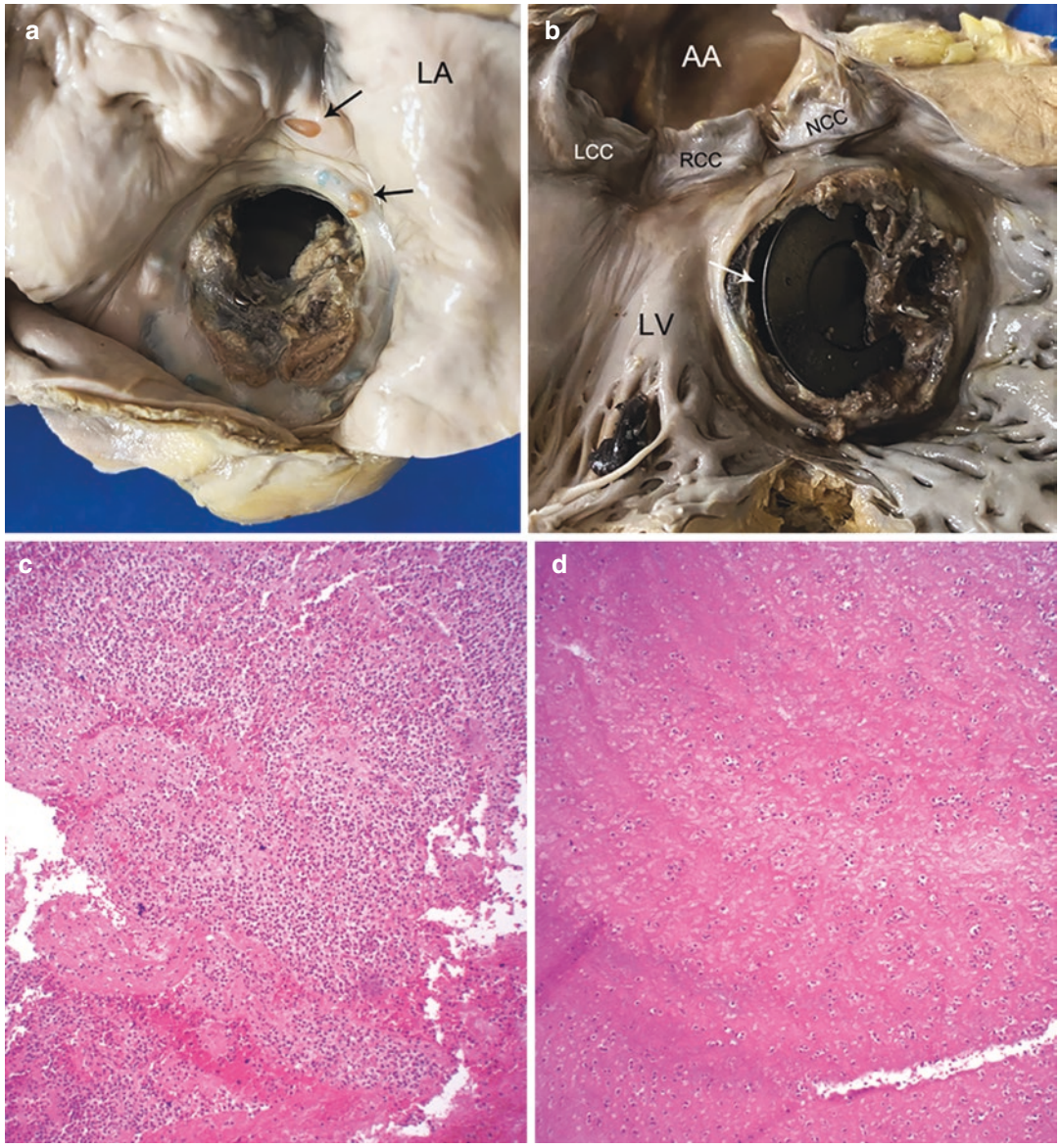

Fig. 8.1 (**a**) The uni-leaflet disc valve over one half is completely covered by a layer of friable thrombus. The ring is well-endothelialized. Foci of calcification (arrows) are seen over the ring and left atrial LA endocardium; (**b**) The valve is 'stuck' leaving a crescentic effective orifice (arrow). Thrombotic material over nearly half of the circumference of the prosthetic valve (*AA* ascending aorta, *LCC* left coronary cusp, *LV* left ventricle, *NCC* noncoronary cusp, *RCC* right coronary cusp); (**c**) The superficial aspect showed collections of leukocytes with underlying fibrin, while (**d**) layers of fibrin and platelets were present in the deeper portion of the thrombus (H&E × 200)

8.3 Discussion

India has an enormous load of rheumatic heart disease, which predominantly involves the mitral and aortic valves (See Chaps. 5 and 9). Unfortunately, most patients often present in the later stages when the disease process as well as valve pathology is significantly advanced. These valves are not amenable to repair and such patients often have to undergo valve replace-

ments, even at a younger age. Surgical valve replacement, using either mechanical or bioprosthetic valves, is an acceptable and standard mode of therapy. The choice of valve depends on a variety of factors including age, cost, patient selection, physical activity, presence of comorbidities, compliance with anticoagulation, and likelihood of future pregnancy. The flip side of the valve replacements is the ushering of prosthetic valve-related disease and consequent dysfunction in the form of valve degeneration, fibrous pannus overgrowth, and para-valvular leaks, and to the more life-threatening complications of thrombosis and endocarditis.

Prosthetic devices and materials implanted within the cardiovascular system are potentially thrombogenic and hence formation of thrombi is a norm. Such thrombi formed at the early stage of implantation are useful in endothelialization and reactive fibrosis, which strengthen the annular attachments of the prosthetic valves. On the other hand, prosthetic valvular thrombosis (PVT) is a pathological phenomenon, which induces valvular dysfunction and/or systemic thromboembolism. In general, mechanical valves are more thrombogenic (an annual rate of 0.1–5.7%) than bioprosthetic valves; the incidence is likely to be higher in developing countries. Also the valves in the mitral position are more likely to thrombose than those in the aortic position; highest incidence is seen for valves in the tricuspid position.

Popular bi-leaflet mechanical valves used in our setup include St Jude™ (St Jude Medical, St Paul, Minnesota, USA) and On-X™(On-X Life Technologies, Austin, Texas, USA). The indigenously manufactured uni-leaflet TTK Chitra valve from the Sri Chitra Institute is also popular. Ball and cage (no longer used) and uni-leaflet valves are more predisposed to thrombosis as compared to bi-leaflet disc valves. The prosthetic valve used in this patient was of the uni-leaflet type and the fatal thrombosis occurred almost 14 years after replacement. The thrombi initially form at the hinge points, restricting the mobility, and then extend around the annulus and/or towards the orifice. The mechanisms under the Virchow's triad are also applicable to PVT and include prosthetic surface factors, flow-related factors, and hemostatic (common and esoteric) factors. Most important and common cause is suboptimal anticoagulation, which would have also played a role in this instance; other important factors include left ventricular dysfunction, atrial fibrillation, and valvular malposition.

The clinical presentation of PVT can be variable depending on the degree as well as duration of obstruction. Acute thrombosis has a more dramatic presentation in the form of relatively sudden onset cardiac failure, pulmonary edema, arrhythmias, and cardiovascular collapse. Subacute or chronic thrombosis has a more subtle presentation in the form of progressive dyspnea. PVT also has a high risk of systemic thromboembolism and stroke, which can be the presenting symptom. Clinical history often reveals noncompliance with anticoagulation or subtherapeutic INR. A classic physical finding is absence or attenuation of the 'mechanical valve click'. Noninvasive modalities are enough to diagnose PVT including transesophageal echocardiography which reveals increased gradients across the valve with or without regurgitation, reduced effective valve area, lack of movement of one or both leaflets, and thrombus. Fluoroscopy is a useful noninvasive adjunct for diagnosis of mechanical PVT as it shows lack or decreased movement of valve leaflets.

Management of PVT in most situations is an emergency. Systemic anticoagulation is started in the form of intravenous heparin. After evaluating comorbidities and ruling out contraindications, thrombolytic therapy is often commenced (streptokinase, urokinase, or recombinant tissue plasminogen activator). This usually only works in acute PVT and is unlikely to prove completely successful for subacute or chronic PVT. However, it can prevent progression of the process and allow some clinical stabilization. This is followed by surgical rescue which involves explantation of the thrombosed prosthesis with implantation of a new valve. In rare situations of acute PVT, removal of thrombus without replacement of the valve is sufficient. Though initial anticoagulation was initiated, this patient succumbed as she also had features of acute coronary syndrome, an uncommon incident in a setting of PVT.

Further Reading

Choudhary SK, Talwar S, Airan B. Choice of prosthetic valve in a developing country. Heart Asia. 2016;8:65–72.

Dangas GD, Weitz JI, Giustino G, Makkar R, Mehran R. Prosthetic heart valve thrombosis. J Am Coll Cardiol. 2016;68:2670–89.

Gündüz S, Kalçık M, Gürsoy MO, Güner A, Özkan M. Diagnosis, treatment and management of prosthetic valve thrombosis: the key considerations. Expert Rev Med Devices. 2020;17:209–21.

Krishnan S. Prosthetic heart valve thrombosis: diagnosis and newer thrombolytic regimes. J Pract Cardiovasc Sci. 2016;2:7–12.

Lacey MJ, Raza S, Rehman H, Puri R, Bhatt DL, Kalra A. Coronary embolism: a systematic review. Cardiovasc Revasc Med. 2020;21:367–74.

Nishimura RA, Otto CM, Bonow RO, Carabello BA, Erwin JP, Guyton RA, et al. 2014 AHA/AC guideline for the management of patients with valvular heart disease: executive summary: a report of the American College of Cardiology/American Heart Association task force on practice guidelines. Circulation. 2014;129:2440–92.

9 Dominant Rheumatic Aortic Stenosis

Pawan Daga and Pradeep Vaideeswar

9.1 Clinical History

A 32-year-old unemployed male presented with progressive dyspnea associated with episodes of vomiting and disorientation since a day. He was a smoker and chronic alcoholic for the past 10 years with an alcoholic binge before the onset of the aforementioned symptoms. There was also a history of surgery for fracture of the right neck of femur a few years ago. On examination, the general condition was poor with a pulse rate of 96 per minute and blood pressure of 80/60 mmHg. He was disoriented with reference to time and place and also could not recognize his close relatives. There was mild icterus, and a systolic murmur was heard on chest auscultation, raising the suspicion of aortic stenosis. Apart from hyponatremia (Sodium 121 mEq/L), mild hyperbilirubinemia (total 2.2 mg/dL, direct 1.6 mg/dL), and metabolic acidosis, the other investigations were normal. Despite appropriate therapy, he expired within 6 h of admission.

9.2 Autopsy Findings

A complete autopsy had been performed. There was marked enlargement of the heart (weight 410 g) with marked enlargement and hypertrophy of the left ventricle (Fig. 9.1a). The transverse section showed severe hypertrophy with bulge of the interventricular septum on to the right side with visible small foci and streaks of grey-white fibrosis (Fig. 9.1b). The right coronary artery was dominant and all epicardial arteries were patent. The great arteries had a normal relationship. The ascending aorta was larger than the pulmonary trunk. The ascending aorta was opened out by cuts through its anterior and posterior walls to reveal marked valvular aortic

P. Daga
Seth Gordhandas Sunderdas Medical College and King Edward Memorial Hospital, Mumbai, India

P. Vaideeswar (✉)
Department of Pathology (Cardiovascular and Thoracic Division), Seth Gordhandas Sunderdas Medical College and King Edward Memorial Hospital, Mumbai, India

P. Vaideeswar (ed.), *Tropical Cardiovascular Pathology*,
https://doi.org/10.1007/978-981-19-3720-0_9

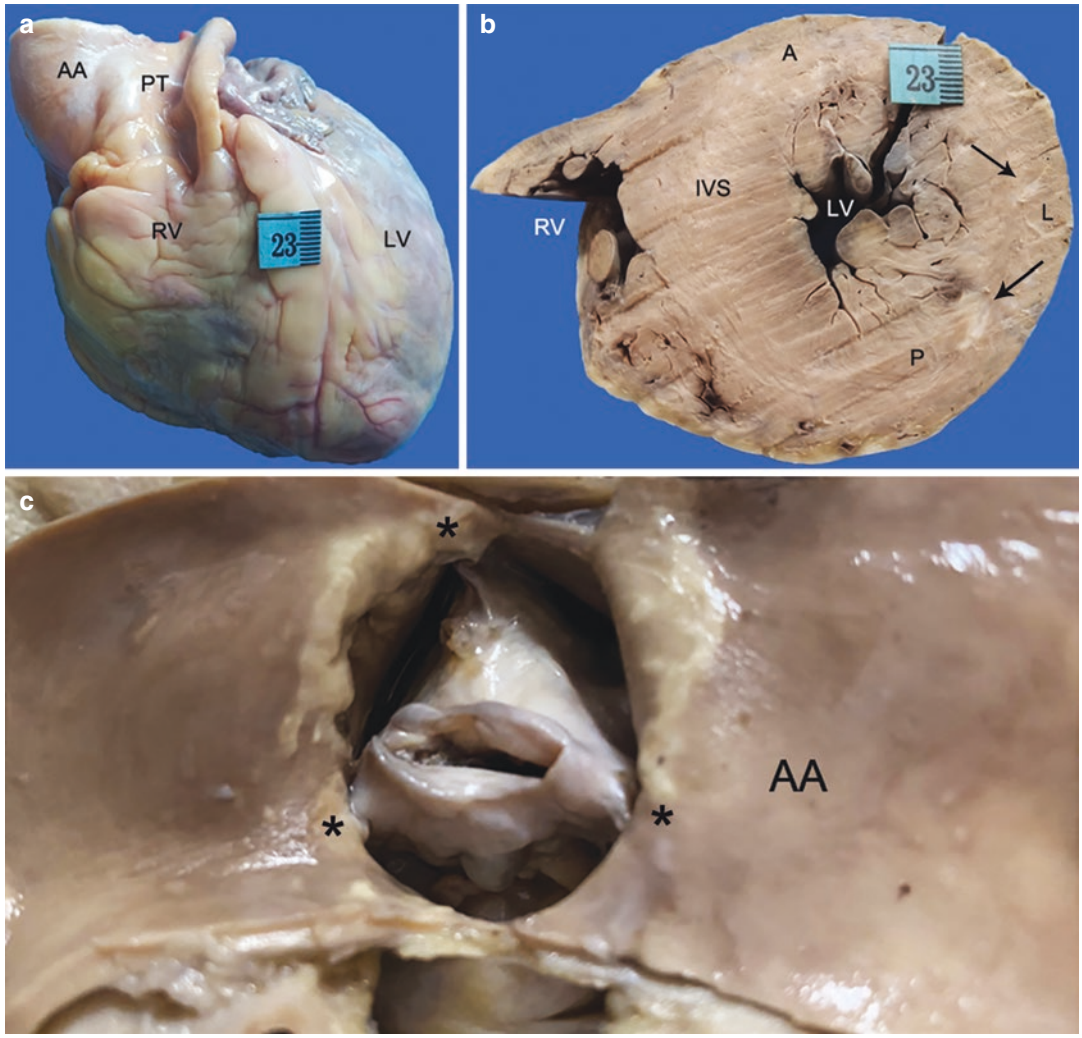

Fig. 9.1 (**a**) Marked cardiomegaly produced by left ventricular LV hypertrophy; (**b**) Hypertrophied LV myocardium with prominence of the papillary muscles and trabeculae. Note small foci of scarring (arrows); (**c**) Opened out ascending aorta AA reveals severe stenosis. All fused commissures * are at the same level. (*A* anterior wall, *IVS* interventricular septum, *L* lateral wall, *P* posterior wall, *PT* pulmonary trunk, *RV* right ventricle)

stenosis (AS, Fig. 9.1c). All the 3 commissures were present at the same level, but were extensively fused with a central slit like narrow orifice (0.8 cm across, Fig. 9.2a). All the cusps were markedly thickened with calcification and rolling out of the free margins (Figs. 9.2b and 9.3). Surprisingly, the mitral valve appeared minimally involved (Fig. 9.4). There was mild thickening of both leaflets with fusion of the posteromedial commissure and associated chordal thickening; histology revealed chronic healed mitral valvulitis (Fig. 9.4). Other organ findings included chronic passive venous congestion of liver and lungs with extensive pulmonary edema.

Cause of Death: Severe Rheumatic AS.

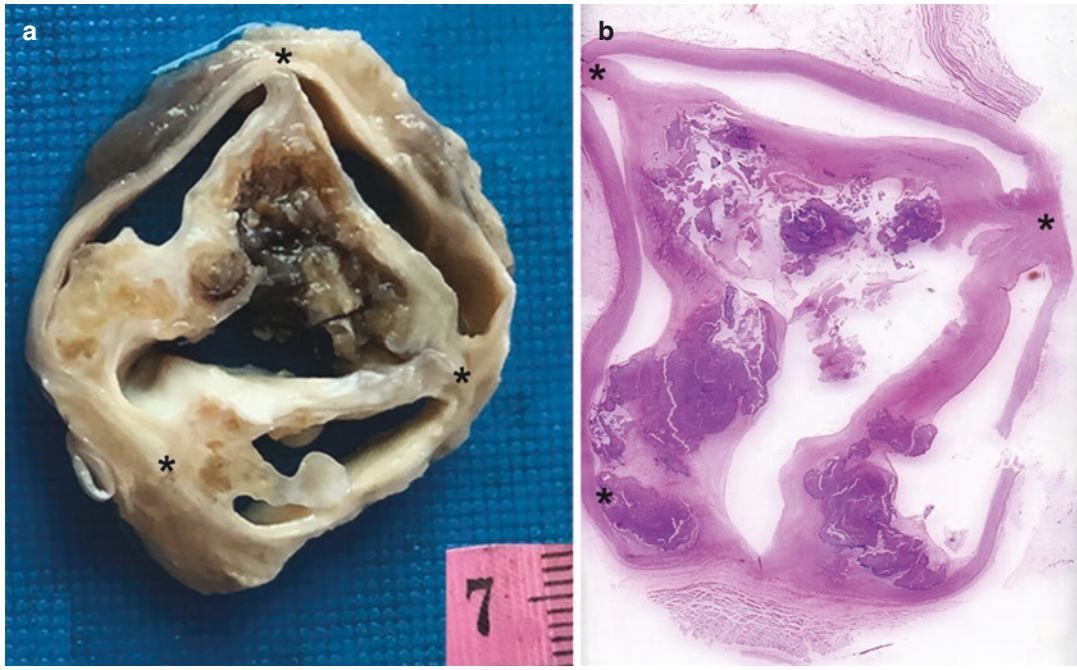

Fig. 9.2 (**a**) The aortic valve has been cross-sectioned after decalcification; (**b**) Scan of the whole mount section shows commissural fusion and cuspal thickening with calcification (H&E). * represents the commissures

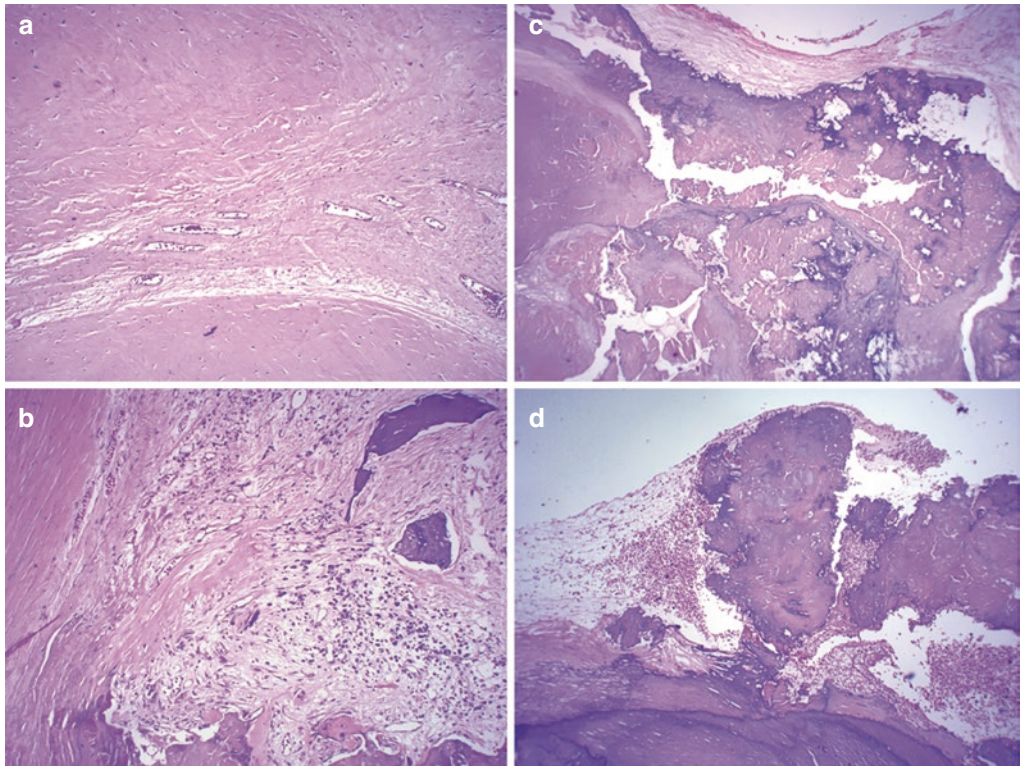

Fig. 9.3 (**a**) Cuspal fibrosis; (**b**) Intra-cuspal calcification with surrounding inflammation; (**c**) The calcification reaches up to the cuspal surface; (**d**) The calcific nodule ulcerates through the surface (H&E × 250)

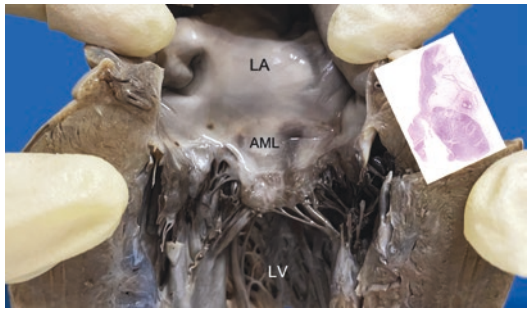

Fig. 9.4 The mitral valve shows mild changes in all the valvular components. Inset shows the section taken, stained by H&E

9.3 Discussion

In this young patient, severe AS had produced rapid deterioration of the left ventricular dysfunction. Traditionally, AS is classified with reference to the level of obstruction as subvalvular, valvular, and supravalvular. By and large, valvular AS represents the most common type of valvular heart disease in the developed countries, where it is related to age-related calcification of the normal aortic valve (AV) (See Chap. 12) or calcification of congenitally malformed AVs (See Chaps. 13 and 14). It is often associated with other valvular diseases, which may be of the same or another etiology. However, in the middle—and low-income countries, chronic rheumatic heart disease (RHD) remains the most common cause of AS, where it is always associated with concomitant rheumatic mitral valve disease (stenosis and/or regurgitation) or aortic regurgitation (AR). It should also be noted that the incidence of rheumatic AS is superseded by rheumatic MS and in the majority of RHD patients (75%), isolated mitral stenosis (MS) is seen. 'Clinically' isolated AS (as seen in our case) due to RHD is an uncommon finding, with a prevalence of less than 2%. If such cases are encountered at autopsy, it would be necessary to inspect the MV carefully for subtle changes and subject the valve for histopathology to demonstrate the chronic changes of rheumatic valvulitis (fibrosis and neovascularization).

Like MS, AS also begins with commissural fusion, which may uniformly affect all 3 commissures, as seen in the present case. At times, there may be severe involvement of one of the commissures, which may give a pseudo-bicuspid appearance. The cusps become thickened and retracted. In due course of time, calcification occurs, which typically involves the free margins and often placed towards the commissural aspects. These changes make an AV functionally stenotic as well as regurgitant in most cases. Slowly progressing AS leads to LV outflow tract obstruction, which is initially compensated with myocardial hypertrophy. This helps in maintaining cardiac output until excessive hypertrophy and decreased compliance lead to diastolic failure. Increased LV pressures are transmitted to left atrium (LA) which causes LA dilatation and predisposes an individual to atrial fibrillation, chronic pulmonary congestion, and venous hypertension. These pathophysiological adaptations are further modified by the presence of proximal valvular lesions. Due to the ability of the heart to maintain cardiac output with mild to moderate AS, patients may remain asymptomatic for many years. However, once the valve orifice is <1 cm^2, they become symptomatic reflecting exhaustion of compensatory mechanisms of the heart. Patients with rheumatic AS become symptomatic earlier in life (akin to those with AS produced by congenital deformed valves), and the mortality dramatically increases; without intervention, the average lifespan is only 2–3 years. The classic triad of symptoms (in the order of appearance) consists of dyspnea on exertion, chest pain, and syncope. In the later stages of the disease, symptoms of LV failure and right ventricular (RV) failure secondary to pulmonary hypertension set in. Occasionally, some asymptomatic patients with severe AS do die suddenly with an estimated risk of 0.5–1.0% per year, as noted in the index case.

Further Reading

1. Ancona R, Pinto SC. Epidemiology of aortic valve stenosis (AS) and of aortic valve incompetence (AI): is the prevalence of AS/AI similar in different parts of the world? J Cardiol Pract. 2020;18:10–2.
2. Carabello BA. Introduction to aortic stenosis. Circ Res. 2013;113:179–85.

3. Manjunath CN, Srinivas P, Ravindranath KS, Dhanalakshmi C. Incidence and patterns of valvular heart disease in a tertiary care high-volume cardiac center: a single center experience. Indian Heart J. 2014;66:320–6.
4. Sahu AK, Sagar P, Khanna R, Kumar S, Tewari S, Kapoor A, et al. Etiology and distribution of isolated aortic stenosis in Indian patients–a study from a large tertiary care hospital in North India. Indian Heart J. 2020;72:272–7.
5. Unger P, Tribouilloy C. Aortic stenosis with other concomitant valvular disease aortic regurgitation, mitral regurgitation, mitral stenosis, or tricuspid regurgitation. Cardiol Clin. 2020;38:33–46.

Part IV

Valvular Heart Disease: Non-Rheumatic

10 Mitral Valvular Prolapse and Sudden Cardiac Death

Shashank Tyagi, Manoj Parchake, and Pradeep Vaideeswar

10.1 Clinical History

A 34-year-old woman had a late night syncopal attack and could not be revived. The body was referred for a medicolegal autopsy.

10.2 Autopsy Findings

There was mild cardiomegaly (weight 310 g) with mild left ventricular enlargement (Fig. 10.1a). The striking discovery was an abnormality of the mitral valve, which had all the characteristic gross features of a valvular prolapse (Fig. 10.1b). There was no chordal rupture. The histopathology revealed disruption of the normal layered micro-architecture by increased proteoglycans in the valve substance (Fig. 10.1c) with classic mitral annular disjunction (Fig. 10.2). The myocardium of the left ventricle showed multiple small foci of scarring in the posterior and lateral walls (Fig. 10.3) and also in the posterior papillary muscles. The lungs showed extensive edema with focal hemorrhage. There was incidental lymphocytic thyroiditis. All other organs were normal.

Cause of Death: Mitral valvular prolapse and 'arrhythmogenic' sudden cardiac death.

S. Tyagi
Department of Forensic Medicine and Toxicology, Lady Hardinge Medical College and Associated SSK and KSC Hospitals Connaught Place, New Delhi, India

M. Parchake
Department of Forensic Medicine and Toxicology, Seth Gordhandas Sunderdas Medical College and King Edward Memorial Hospital, Mumbai, India

P. Vaideeswar (✉)
Department of Pathology (Cardiovascular and Thoracic Division), Seth Gordhandas Sunderdas Medical College and King Edward Memorial Hospital, Mumbai, India

P. Vaideeswar (ed.), *Tropical Cardiovascular Pathology*,
https://doi.org/10.1007/978-981-19-3720-0_10

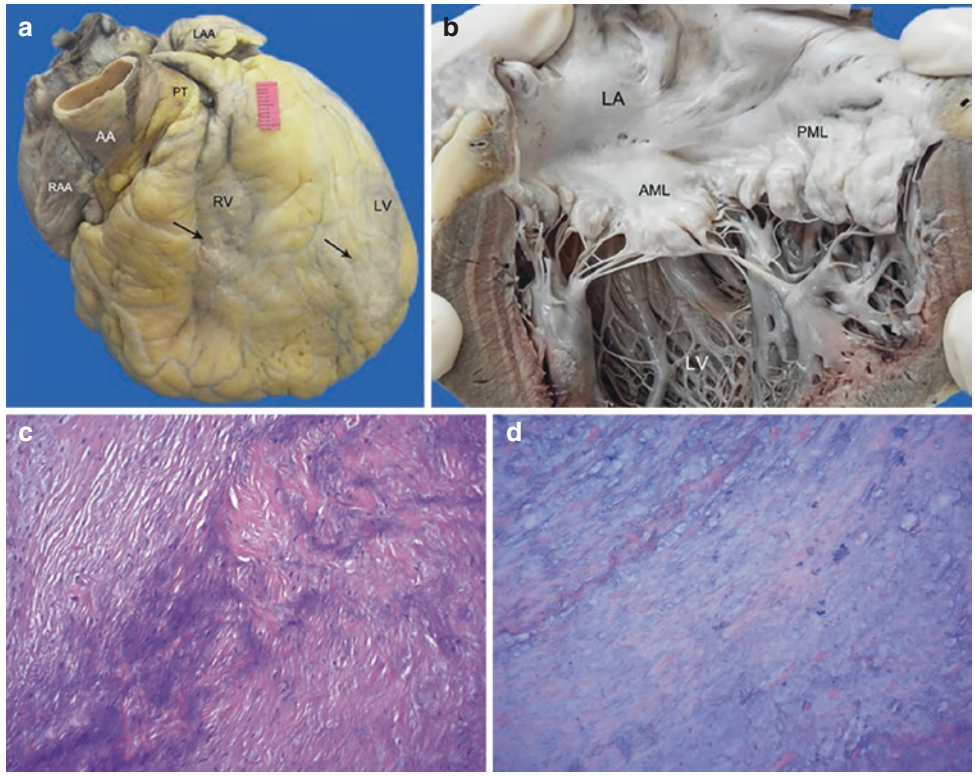

Fig. 10.1 (**a**) Mild cardiomegaly with milk patches over the epicardial surface of right RV and left LV ventricles (arrows); (**b**) The mitral valve with glistening and moist appearance of both the anterior AML and posterior PML leaflets with prominent inter-chordal hooding (*AA* ascending aorta, *LA* left atrium, *LAA* left atrial appendage, *PT* pulmonary trunk, *RAA* right atrial appendage); (**c**) Leaflet showing increased basophilic ground substance substance (H&E × 100); (**d**) stained light blue (Alcian blue × 100)

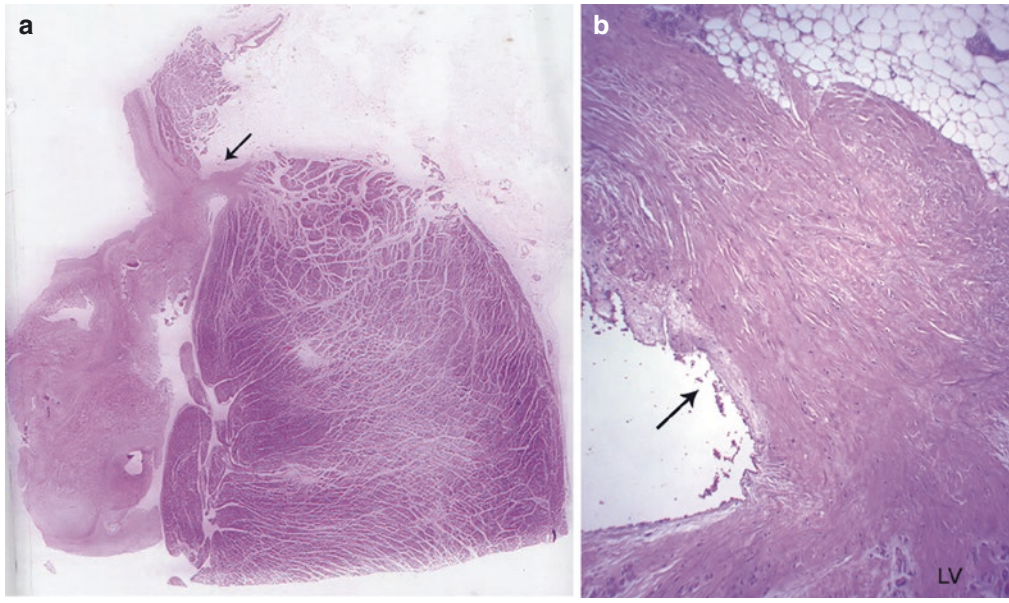

Fig. 10.2 Mitral annular disjunction (arrow) showing curtain-like separation of the left ventricular LV summit from the left atrial-mitral annular junction, (**a**) Scanned slide stained by H&E and (**b**) H&E × 100

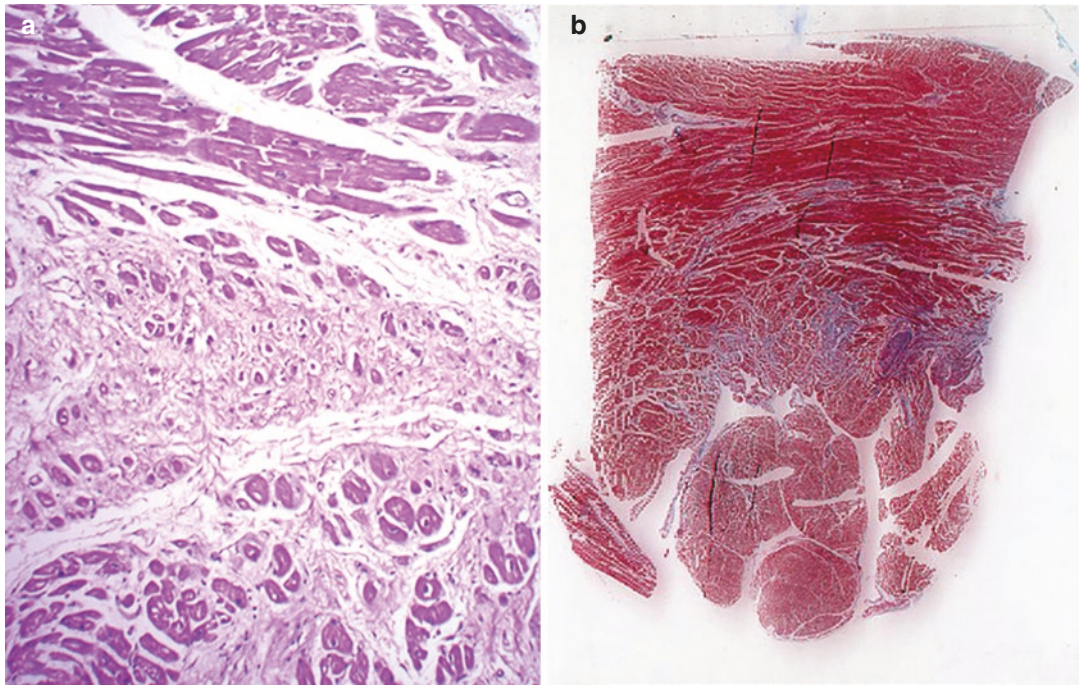

Fig. 10.3 (**a**) Fibrous tissue surrounding individual or groups of cardiomyocytes; (**b**) Scanned slide of a section from the posterolateral wall of the left ventricle showing fibrosis (stained green) prominently located in the subendocardial region (Masson trichrome)

10.3 Discussion

A previously asymptomatic young woman had sudden death (SD), which is defined as "*a natural, unexpected fatal event occurring within one hour from the onset of symptoms in an apparently healthy subject or in one whose disease was not so severe as to predict an abrupt outcome*". If the sudden demise is unwitnessed, SD refers to "*the death of an individual within 24h after being seen alive and in a normal state of health*". The term is also extended to include "*sudden, rapid and fatal deterioration in patients who have had a diagnosed stable chronic condition, or who have an illness, which would not be expected to cause death*". Most of the cases of SD are caused by cardiovascular disorders (sudden cardiac death, SCD), particularly ischemic heart disease (see Part VI) which accounts for over 80% of the cases in adults across all ages. Nonischemic myocardial disorders (see Part VII) and valvular diseases, though uncommon, are responsible for SCD in individuals below the age of 40 years. SCD in this young patient was caused by mitral valvular prolapse (MVP).

MVP is the most common example of myxoid mitral valvular disease and is the most frequent cause of mitral regurgitation (MR) in the developed world. It is characterized by a systolic displacement of one or both mitral leaflets above the mitral annular plane into the left atrium. When the displacement is >2 mm and when the leaflet thickness is >5 mm, the condition is referred to as the classic type; in the non-classic type, the leaflet thickness is <5 mm, but more than the normal thickness of 1–2 mm. MVP has a prevalence of 2–3% and can occur in syndromic (secondary) or non-syndromic (primary) settings. The syndromic type, best exemplified by the Marfan syndrome, is associated with other cardiac and extra-cardiac manifestations. Some cases of primary MVP are seen in the elderly and result from an acquired loss of collagen, elastin, and proteoglycans (fibroelastic deficiency). Another type of primary MVP that is seen in

young persons, especially women (like the present case), is associated with increased proteoglycans in the valvular spongiosa (Barlow's disease). It too occurs in isolation and the genetic basis (autosomal dominant in most cases) for this type is yet to be clearly elucidated; the setting can be sporadic or familial.

The morphological changes will vary depending on the degree of proteoglycan accumulation that leads to leaflet thickening/ chordal elongation/chordal rupture and can involve both leaflets, one leaflet, or parts of the leaflet. This is followed thereafter by mitral annular dilatation and patients present with chronic mitral regurgitation (MR). There is ensuing congestive cardiac failure and a predisposition to infective endocarditis (see Part V). Some patients also develop ST-T wave changes with ventricular ectopy which can lead to life-threatening tachyarrhythmias and SCD.

The prevalence of such cases of 'arrhythmogenic' or 'malignant' MVP in the SCD victims is 2.4% and they usually have bi-leaflet disease with moderate MR. Important substrates for the development of arrhythmias are left ventricular hypertrophy/fibrosis and MAD. Myocardial fibrosis is mainly seen in the basal and mid-inferolateral parts of the left ventricle and the papillary muscles. MAD refers to separation of the left atrial wall-MV junction from the LV free wall so that there is a curtain-like appearance at the posterior annulus. Endocardial 'frictional' fibrosis that develops between the chordae tendineae can also be additional substrates. The trigger is mainly the mechanical stretching of the cardiomyocytes, though there may be a role played by autonomic dysfunction.

Further Reading

Althunayyan A, Petersen SE, Lloyd G, Bhattacharyya S. Mitral valve prolapse. Expert Rev Cardiovasc Ther. 2019;17:43–51.

Basso C, Burke M, Fornes P, Gallagher PJ, Henriques de Gouveia R, Sheppard M, et al. Guidelines for autopsy investigation of sudden cardiac death. Virchows Arch. 2008;452:11–8.

Basso C, Iliceto S, Thiene G, Marra MP. Mitral valve prolapse, ventricular arrhythmias, and sudden death. Circulation. 2019;140:952–64.

Boudoulas KD, Pitsis AA, Mazzaferri EL, Gumina RJ, Triposkiadis F, Boudoulas H. Floppy mitral valve/ mitral valve prolapse: a complex entity with multiple genotypes and phenotypes. Prog Cardiovasc Dis. 2020;63:308–26.

Enriquez-Sarano M. Mitral annular disjunction: the forgotten component of myxomatous mitral valve disease. JACC Cardiovasc Imaging. 2017;10:1434–6.

Kitkungvan D, Nabi F, Kim RJ, Bonow RO, Khan MA, Xu J, et al. Myocardial fibrosis in patients with primary mitral regurgitation with and without prolapse. J Am Coll Cardiol. 2018;72:823–34.

Miller MA, Dukkipati SR, Turagam M, Liao SL, Adams DH, Reddy VY. Arrhythmic mitral valve prolapse. J Am Coll Cardiol. 2018;72:2904–14.

Wong CX, Brown A, Lau DH, Chugh SS, Albert CM, Kalman JM, et al. Epidemiology of sudden cardiac death: global and regional perspectives. Heart Lung Circ. 2019;28:6–14.

11 Congenital Valvular Mitral Stenosis

Pradeep Vaideeswar and Girish Sabnis

11.1 Clinical History

A 33-year-old male, admitted in severe respiratory distress, expired within 40 min of admission. He was symptomatic for a week with sudden-onset shortness of breath and atypical chest pain. There had been an admission in a private hospital, where a diagnosis of large ventricular septal defect (VSD) with Eisenmengerization was made. Due to financial constraints, he was discharged against medical advice.

11.2 Autopsy Findings

There was marked enlargement of the heart (weight 420 g, Fig. 11.1) with marked enlargement of the right (RV) and moderate enlargement of the left (LV) ventricles. The apex was formed by both the ventricles and was flattened. There was also mild to moderate dilatation and hypertrophy of the atrial chambers. The great arterial relationship was normal, but the pulmonary trunk was dilated and larger than aorta. There was no coarctation, but a probe patent ductus arteriosus was present, measuring 1 cm in length. The pulmonary trunk and its dilated branches showed intimal thickening with few atheromatous plaques. A large 1.5 × 1 cm VSD was present between the 2 limbs of the septal band below the anteroseptal commissure of the tricuspid valve on the right side (Fig. 11.2a), and below the right

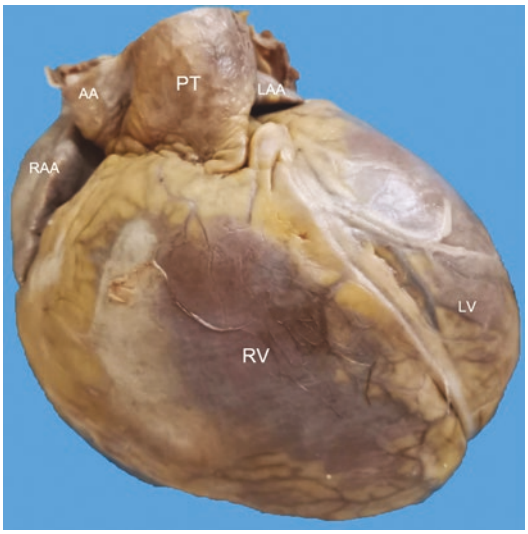

Fig. 11.1 Marked cardiomegaly. The apex is formed by both the enlarged ventricles. The pulmonary PT is dilated (*AA* ascending aorta, *LAA* left atrial appendage, *LV* left ventricle, *RAA* right atrial appendage, *RV* right ventricle)

P. Vaideeswar (✉)
Department of Pathology (Cardiovascular and Thoracic Division), Seth Gordhandas Sunderdas Medical College and King Edward Memorial Hospital, Mumbai, India

G. Sabnis
Dr KK Datey Department of Cardiology, Seth Gordhandas Sunderdas Medical College and King Edward Memorial Hospital, Mumbai, India

P. Vaideeswar (ed.), *Tropical Cardiovascular Pathology*,
https://doi.org/10.1007/978-981-19-3720-0_11

coronary cusp of the aortic valve on the left side (Fig. 11.2b). Accessory valvular tissue was present on the right aspect, which could have produced some degree of restriction to the left-to-right shunt (Fig. 11.2b). The septal and anterior leaflets adjoining their commissure were thickened, focally calcified with chordal thickening (Fig. 11.2a). There was marked RV and mild

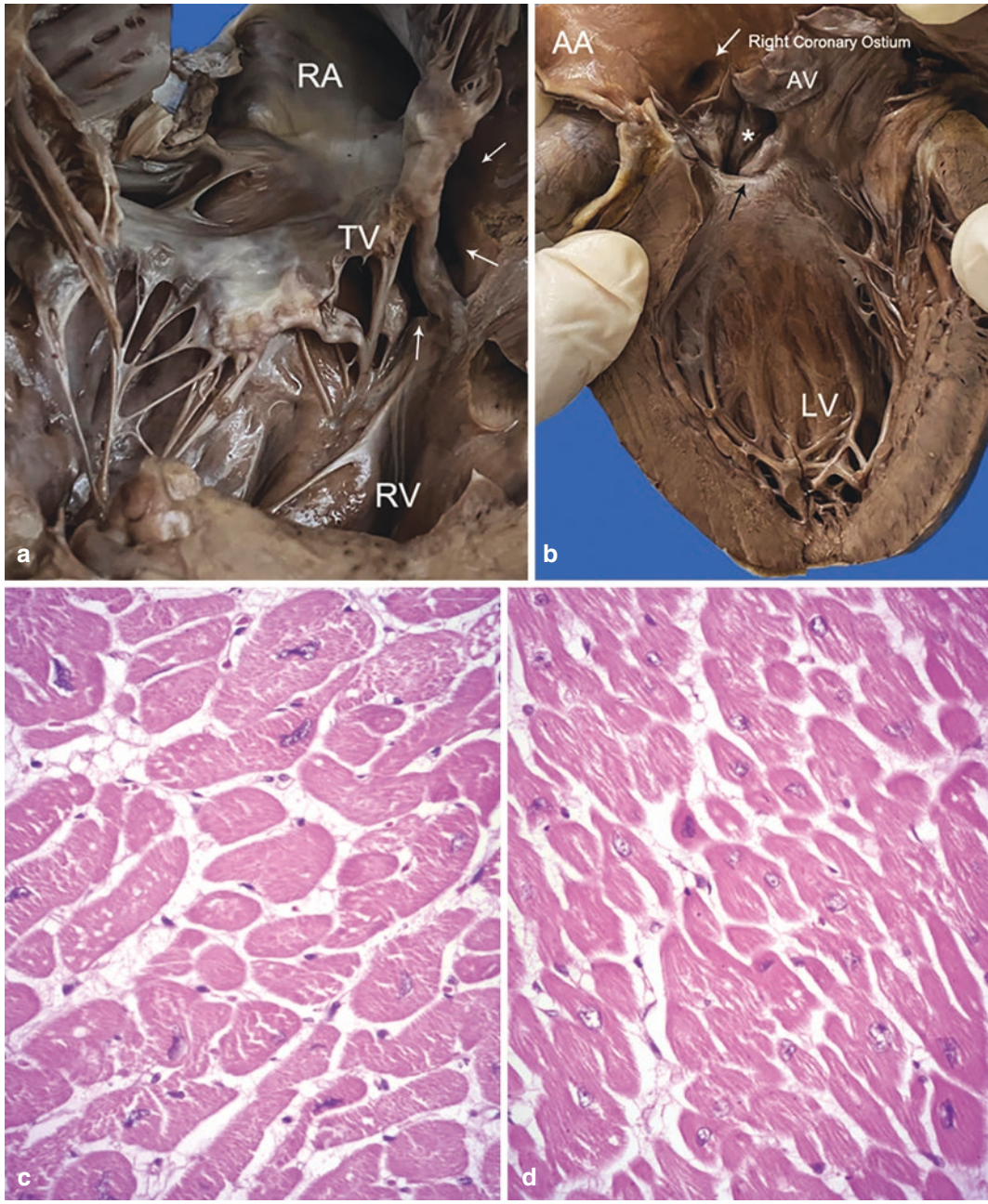

Fig. 11.2 Perimembranous ventricular septal defect as seen from the (**a**) right (white arrows) and (**b**) left side (black arrow). The tricuspid valve TV leaflets are thickened and focally calcified. Accessory valvular tissue * is seen at the site of the defect on the left side (*AA* ascending aorta, *AV* aortic valve, *LV* left ventricle, *RA* right atrium, *RV* right ventricle); Hypertrophy of (**c**) right and (**d**) left ventricle (H&E × 400). Note the larger size of the cardiomyocytes in the right ventricle

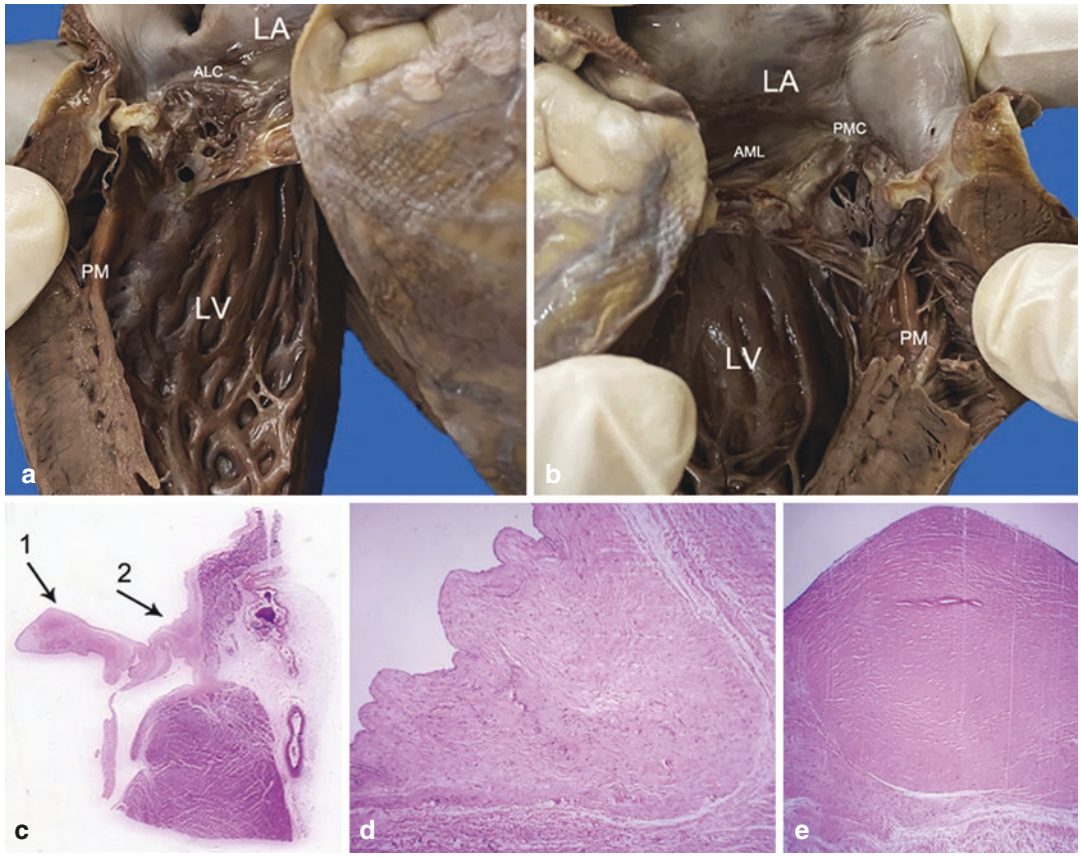

Fig. 11.3 Congenital mitral stenosis. Chordae tendineae attached to the (**a**) anterolateral commissure ALC and (**b**) posteromedial commissure PMC appear directly attached to left ventricular LV endocardium. Two slender papillary muscles appear to be directly attached to the leaflets; (**c**) Scanned image of the H & E stained section of the posterior mitral leaflet, which is thickened; Mounds of hyalinized fibrosis on the flow surface depicted in (**d**) area 2, which is at the left atrial-mitral annular junction and (**e**) area 1, which is at the line of closure (H & E × 100)

LV hypertrophy (Fig. 11.2c, d). An incidental finding was congenital mitral stenosis (MS). There was moderate commissural fusion with moderate leaflet thickening. The tendinous cords were hardly formed. A 'netted' curtain and a 'membranous' curtain connected the anterolateral and posteromedial commissures, respectively, directly to the left ventricular endocardium (Fig. 11.3). Two slender papillary muscles were also present and appeared directly attached to the leaflets. The lungs revealed only mild medial hypertrophy of the arteries. Other organs were normal.

Cause of Death: Congenital mitral stenosis with perimembranous VSD.

11.3 Discussion

The unexpected finding in this case was the typical congenital mitral stenosis (C-MS), which is an example of congenital obstruction to left ventricular inflow tract. Apart from C-MS, the obstruction can be located at/near the junction of pulmonary vein and left atrium or within the left atrium (cor triatriatum). In general, congenital mitral valve anomalies are uncommon entities and the incidence of stenosing lesions has been estimated at 0.6% of necropsy cases of congenital heart disease and 0.21–0.42% of clinical cases. It is important to note that C-MS involves

the annulus, the zone immediately above and contiguous with the annulus, the leaflets, and the subvalvular apparatus usually in combination and in varying severity. Moreover, it is typically associated with other congenital cardiac malformations (particularly obstructive like Shone's complex), which may mask or get masked by C-MS.

Ruckman and Van Praagh proposed a simple classification based on pathologic findings of autopsied specimens of C-MS, in which 4 categories were described: (1) Typical MS with thickened leaflets, short and thickened chordae tendineae, obliteration of interchordal spaces, underdevelopment of papillary muscles, and reduction of interpapillary distance (as seen in the present case); (2) Hypoplastic MS, where all components are miniaturized and which is almost always associated with a hypoplastic left heart syndrome; (3) Supramitral (supravalvular) ring with a nearly circumferential continuous or discontinuous endocardial fibrous ridge at or above the mitral annulus but distal to the opening of the left atrial appendage; and (4) Parachute mitral valve, where thick and short chordae are attached to a single papillary muscle (typically the posterior). The physiologic consequences of C-MS are analogous to acquired MS (See Chap. 5).

Any narrowing in the pulmonary circulation produces a reduction in pulmonary blood flow and pulmonary to systemic blood flow ratio in a posttricuspid shunt. The group of patients with VSD and mitral valve disease had high measured pulmonary vascular resistance (PVR) and low pulmonary blood flow on evaluation and had a significant immediate postoperative fall in PVR and pulmonary artery pressure. The absence of irreversible pulmonary vascular disease (as seen on histology in the case presented) may be due to the protective effect of C-MS. This can be explained as if we are taking Ohm's Law into action, i.e., $V = IR$, where V is pressure gradient across the pulmonary circulation, I indicates pulmonary blood flow, and R the pulmonary vascular resistance. Elevated left atrial pressure due to C-MS here acts as a resistance in series to the pulmonary blood flow, which was the natural mechanism that prevented significant left-to-right shunt and consequent irreversible pulmonary vascular changes. Additionally, the restriction of the left-to-right shunt produced by accessory valvular tissue might have played a secondary role. Lung pathology showing only mild to medial hypertrophy points against a significant Eisenmenger physiology. This hemodynamic situation is similar to pulmonary vascular disease observed in pure mitral valve disease which is reversible in most cases. Increased flow, rather than pressure, is the important factor in producing changes in pulmonary vascular disease associated with congenital heart disease and therefore in deciding the prognosis. Although an incidental finding, C-MS appears to be the central pathophysiologic mechanism leading to the terminal event in our case.

Further Reading

Agarwal S, Airan B, Chowdhary UK, Choudhary SK, Sharma R, Bhan A, et al. Ventricular septal defect and congenital mitral valve disease: long-term results of corrective surgery. Indian Heart J. 2002;54:67–73.

Hollman A, Hamed M. Mitral valve disease with ventricular septal defect. Br Heart J. 1965;27:274–85.

Maskatia SA. Congenital anomalies of the mitral valve. Congenit Heart Dis. 2011;6:77–82.

Ruckman RN, Van Praagh R. Anatomic types of congenital mitral stenosis: report of 49 autopsy cases with consideration of diagnosis and surgical implications. Am J Cardiol. 1978;42:592–601.

Senile Calcific Aortic Stenosis

12

Pradeep Vaideeswar and Sagar Kulat

12.1 Clinical History

A 72-year-old woman, with a past history of hypertension and ischemic heart disease, developed sudden onset of shortness of breath and was admitted in an unconscious state. The peripheral pulses were not felt and the blood pressure was not recordable. She expired despite resuscitative measures within an hour.

12.2 Autopsy Findings

There was moderate cardiomegaly (380 g). The apex, pointing to the left, was rounded and formed by a moderately enlarged left ventricle (Fig. 12.1a). The right coronary artery had a dominant circulation; all the coronaries showed multifocal atherosclerosis with short segments of critical stenosis. No thrombi were present. The

P. Vaideeswar (✉)
Department of Pathology (Cardiovascular and Thoracic Division), Seth Gordhandas Sunderdas Medical College and King Edward Memorial Hospital, Mumbai, India

S. Kulat
Director, Rudhira Diagnostics, Ahmednagar, India

P. Vaideeswar (ed.), *Tropical Cardiovascular Pathology*,
https://doi.org/10.1007/978-981-19-3720-0_12

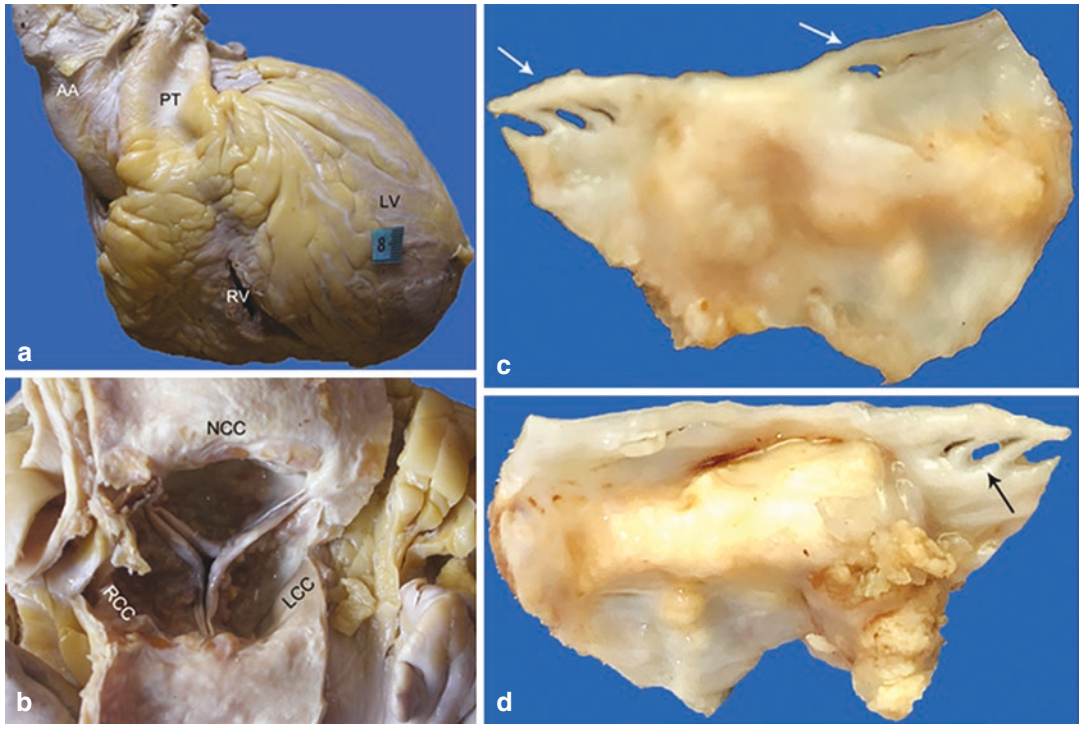

Fig. 12.1 (**a**) Rounded apex formed by an enlarged left ventricle LV; (**b**) The atherosclerotic ascending aorta has been opened out to show calcific nodules within the sinuses-of-Valsalva.; (**c**) Flow and (**d**) Non-flow surface of one of the calcified cusps with few fenestrations (arrows). The photograph has been taken after decalcification and the tissue appears yellow

myocardium showed concentric hypertrophy; regional foci of fibrosis or softening were not present. The aortic annulus was of normal size. All the 3 cusps were mildly thickened with rounding and rolling of the free margins and showed the presence of large and small nodules of calcification (Fig. 12.1b) that were predominantly localized to the basal aspects of the non-flow surfaces (Fig. 12.1c, d). The calcification was located within the valve substance (Fig. 12.2a, b). Some of the larger nodules also extended to the surface to produce ulcerations (Fig. 12.2c); no thrombi were present. This would have led to moderate aortic stenosis (AS). Calcification was not present on the ventricular aspect of the mitral valve or over the interventricular septum. There was no commissural fusion.

Cause of Death: Critical Coronary Atherosclerosis and Acute Myocardial Ischemia.

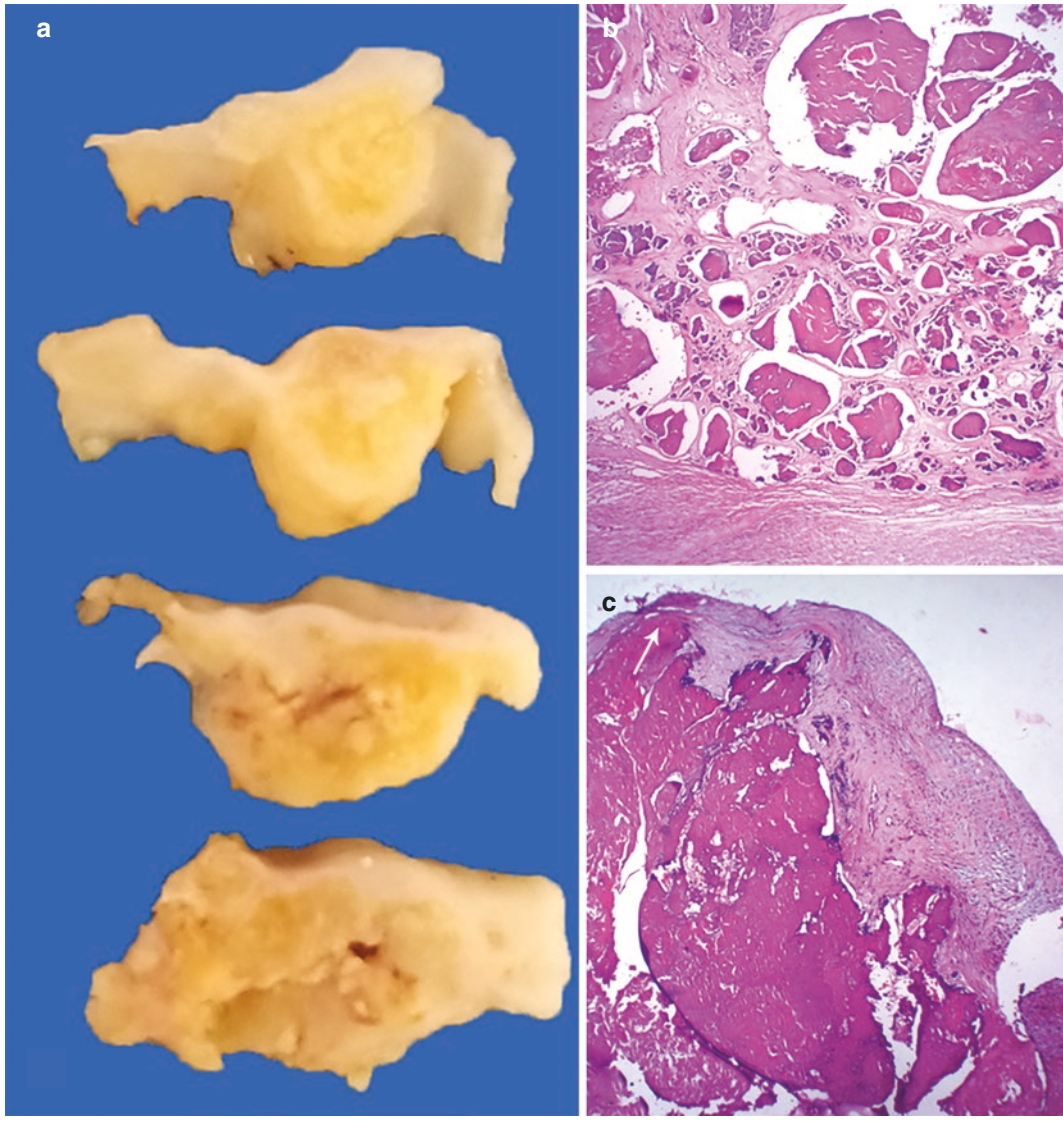

Fig. 12.2 (**a**) The cusp has been serially sectioned after the process of decalcification; (**b**) Calcification seen as irregular pinkish to purplish material (H&E × 200); (**c**) Calcification is seen to reach up to the surface (arrow) on the non-flow aspect of the cusp (H&E × 200)

12.3 Discussion

Aortic valve disease results in significant morbidity and mortality through all age groups and may be due to congenital, post-inflammatory, or 'degenerative' changes in the structure of the valve. With the decline in incidence of rheumatic heart disease in developed countries, most aortic valve surgery today (repair or replacement) is for noninflammatory causes and many such patients, especially adults who present clinically with AS. In the present case, a hypertensive lady in her seventh decade with diffuse critical coronary atherosclerosis, the autopsy also showed pres-

ence of nodular calcification of all the 3 cusps of the aortic valve. This is an example of an age-dependent calcific AS, which currently is the most prevalent form of stenosis across the world, especially in industrialized and high-income countries. It most commonly affects individuals above the age of 65 years with an almost equal sex distribution.

Aortic valvular sclerosis and calcific AS, which were thought to be separate entities, are now considered as two ends of the spectrum of the same disease process. In sclerosis, cuspal thickening and stiffening occur as a result of lipo-calcified deposits seen at the basal aspects of the semilunar cusps (the sites of maximal flexion) and at the lines of coaptation. This change, which involves the fibrosa layer, is devoid of any clinical dysfunction and is observed in about 30% of persons beyond 65 years of age and in almost 50% of individuals over the age of 85 years. In due course of time, depending on risk factors, the sclerosis can progress to calcareous masses that anchor the cusps to the annulus, leading to varying degrees of hemodynamically significant calcific AS. This affects 23% of those above 65 years of age and up to 12.4% of individuals greater than 75 years of age. There are specific features which differentiate calcification that develops over rheumatic affliction (See Chap. 9). There is no commissural fusion so that the valve remains triradiate (at least in the initial stages). The heaps of craggy calcification are ensconced within the sinuses-of-Valsalva towards the basal and non-flow aspect of the cusps. Furthermore, the free margins of the cusps are also initially uninvolved. The calcification can leave their valvular confines to extend onto the ventricular aspect of the mitral valve or over the interventricular septum. In patients with the latter, heart blocks can arise due to damage of the conducting tissue. The calcific deposits can ulcerate through the cusps and predispose to thrombosis, calcific/thromboemboli, and hemolytic anemia.

In the past, calcific AS was considered as an age-related and mechanical stress-related wear-and-tear disease and was termed as senile degenerative form of AS. However, it has now proved beyond doubt that it is indeed an active cell-mediated process. For optimal cuspal function and resistance to mechanical stress, the cuspal cells (valvular endothelial cells and valvular interstitial cells) and the extracellular matrix components (collagen, elastic, and proteoglycans) have a specific arrangement according to the blood flow, i.e., fibrosa on the non-flow aspect, ventricularis on the flow aspect, and spongiosa in the middle. Calcific AS is said to occur in 2 phases of initiation and propagation. The process is initiated by endothelial injury at the areas of maximal hemodynamic stress, accentuated by modifiable and non-modifiable risk factors that are usually attributed to the more common atherosclerosis. The injured endothelium is highly permeable with consequent lipid infiltration and deposition in the valvular interstitium. Lipid oxidation provokes chronic inflammatory cell infiltrate and there is formation of lipo-calcification and neoangiogenesis. Though our patient had both coronary atherosclerosis and calcific AS, all patients do not necessarily have a similar association, indicating that other pathways may also be involved. In the propagation phase, this initial 'atherosclerotic' process, through various molecular stimuli, leads to phenotypic switching of the valvular interstitial cells. With myofibroblastic and osteoblastic differentiation, there is increasing amounts of fibrosis, calcification, and eventually even osteo-chondromatous metaplasia (metaplastic calcification).

The pathophysiology of calcific AS is similar to the other causes of AS (See Chap. 9). Despite a mine of information regarding the pathogenesis, medical therapy is not yet available to prevent progression or reducing the mortality. Dramatic results are still offered by surgical or transcatheter aortic valve replacements. In the case presented, the stenosis appeared as an incidental finding and may have contributed indirectly to the mortality by adding on to the degree of hypertrophy produced by hypertension.

Further Reading

Fishbein GA, Fishbein MC. Pathology of the aortic valve: aortic valve stenosis/aortic regurgitation. Curr Cardiol Rep. 2019;21:81.

Galli D, Manuguerra R, Monaco R, Manotti L, Goldoni M, Becchi G, et al. Understanding the structural features of symptomatic calcific aortic valve stenosis: a broad-spectrum clinico-pathologic study in 236 consecutive surgical cases. Int J Cardiol. 2017;228:364–74.

Goody PR, Hosen MR, Christmann D, Niepmann ST, Zietzer A, Adam M, et al. Aortic valve stenosis: from basic mechanisms to novel therapeutic targets. Arterioscler Thromb Vasc Biol. 2020;40:885–900.

Lindman BR, Clavel MA, Mathieu P, et al. Calcific aortic stenosis. Nat Rev Dis Primers. 2016;2:16006.

Torre M, Hwang DH, Padera RF, Mitchell RN, Vandar Laan PA. Osseous and chondromatous metaplasia in calcific aortic valve stenosis. Cardiovasc Pathol. 2016;25:18–24.

Bicuspid Aortic Stenosis

13

Pradeep Vaideeswar

13.1 Clinical History

A 63-year-old lady had been diagnosed with degenerative aortic stenosis (AS) 2 years ago. There was associated mild regurgitation and the left ventricular ejection fraction was 65%. She had been advised surgery, but the patient and her relatives were unwilling for the procedure. She was on antihypertensives for the past 4 years. She was now admitted in a gasping state and expired within 30 min.

13.2 Autopsy Findings

The heart was markedly enlarged in size (460 g) with marked concentric left ventricular hypertrophy (Fig. 13.1a, b) and focal scarring. The ascending aorta was dilated (3.6 cm in diameter) and showed differential thickening of its walls. The anterolateral wall was papery thin, while the posteromedial wall was of normal thickness with a calcified atheroma (Fig. 13.1a). The transverse, the descending thoracic, and abdominal portions of the aorta were normal. The aortic valve was bicuspid (Fig. 13.1c, d) with a larger anterior and smaller posterior cusp. The anterior sinus-of-Valsalva showed low-lying calcified raphe, and the coronary ostia arose on either side of this ill-formed commissure. Calcific nodularity was present in both the cusps, but maximally over the raphe (Fig. 13.2). The coronary arteries were devoid of significant atherosclerosis. Sections from the thinned portion of the aorta revealed varying proportions of elastic tissue loss and fragmentation, loss of smooth muscle nuclei, and intralamellar increases in the mucoid extracellular matrix accumulation, which were summed up as moderate aortopathy (as per the *joint consensus statement from the Society for Cardiovascular Pathology and the Association for European Cardiovascular Pathology*). The lungs were edematous with additional features of chronic passive venous congestion. The kidneys and other organs were normal.

Cause of Death: Bicuspid aortic valve (BAV) with severe stenosis.

P. Vaideeswar (✉)
Department of Pathology (Cardiovascular and Thoracic Division), Seth Gordhandas Sunderdas Medical College and King Edward Memorial Hospital, Mumbai, India

P. Vaideeswar (ed.), *Tropical Cardiovascular Pathology*,
https://doi.org/10.1007/978-981-19-3720-0_13

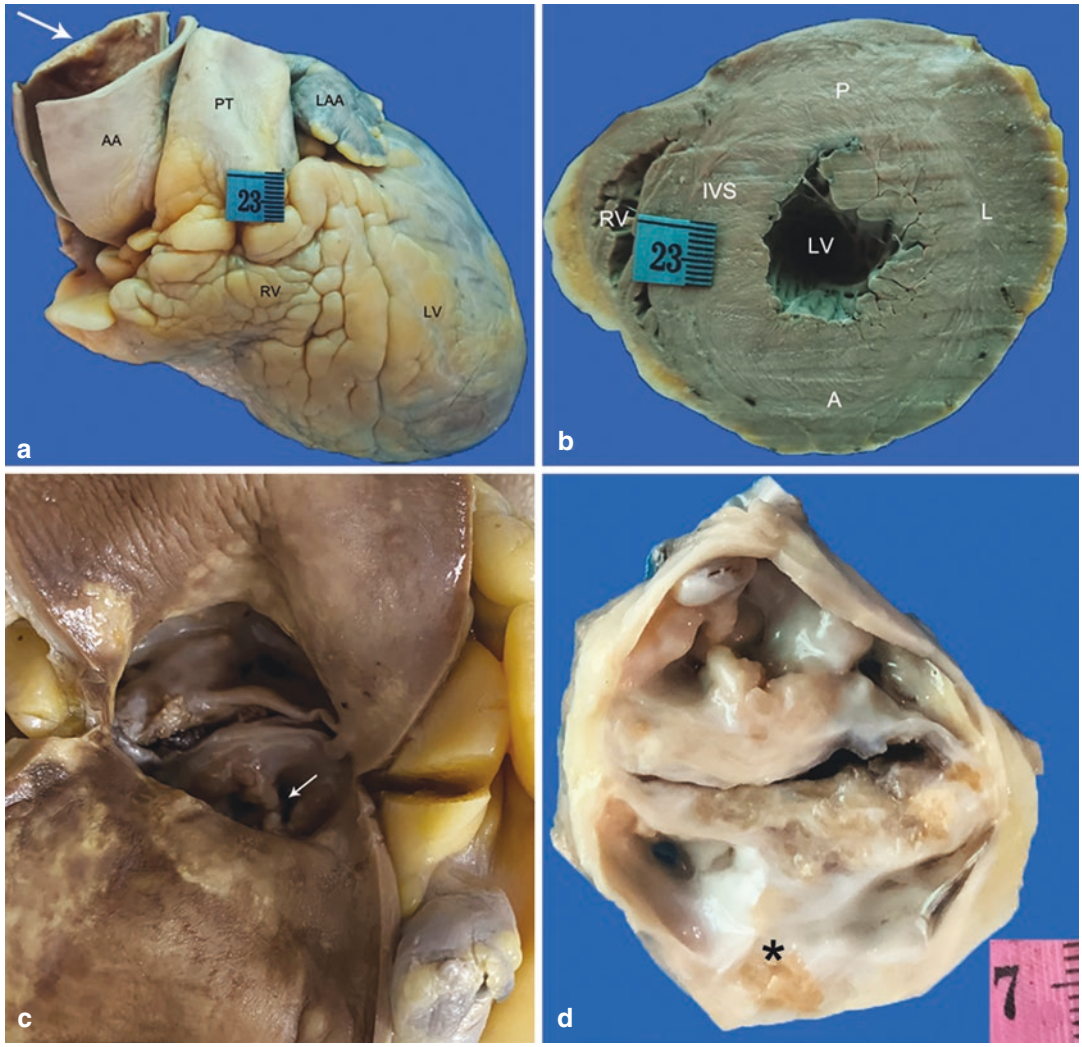

Fig. 13.1 (**a**) Marked cardiomegaly. Both great arteries are dilated; dilatation of the ascending aorta AA exceeds that of the pulmonary trunk PT. Arrow points to the atheroma in the posteromedial wall; (**b**) Marked concentric left ventricular LV hypertrophy with small cavity size and slit-like right ventricular RV chamber; (**c**) Calcified anterior-posterior type of bicuspid aortic valve with a low-set raphae in the anterior sinus (arrow); (**d**) Cross-section of the valve after decalcification showing prominent calcific nodularity at the site of the raphae * (*A* anterior wall, *L* lateral wall, *LAA* left atrial appendage, *IVS* interventricular septum, *P* posterior wall)

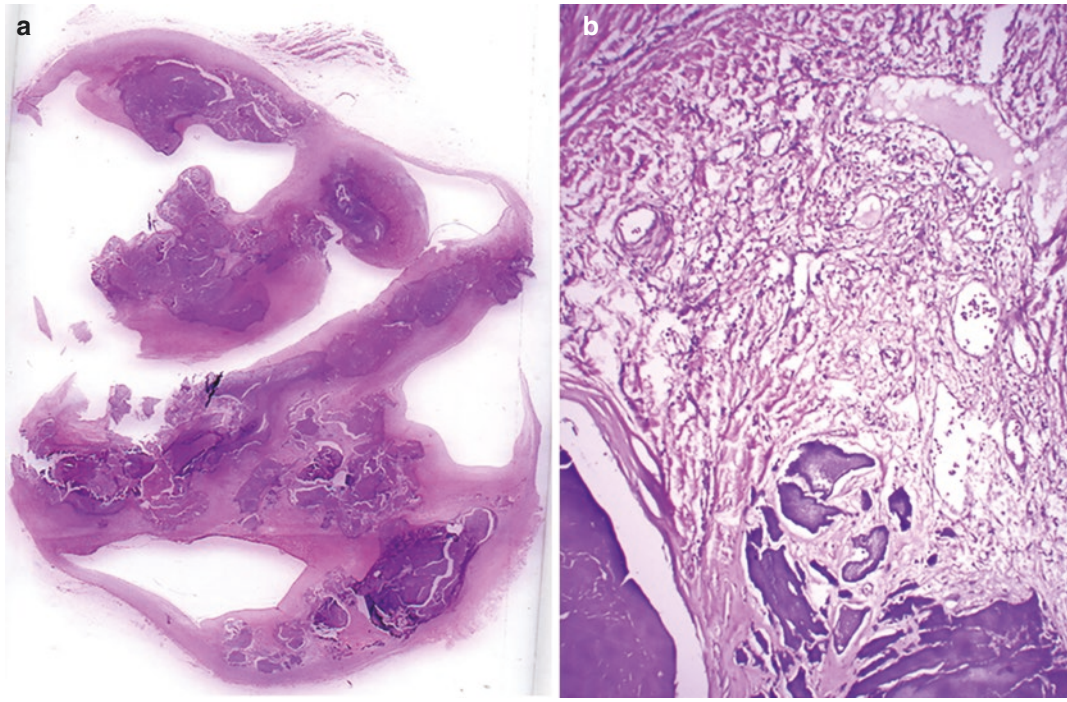

Fig. 13.2 (**a**) Image of the scanned H&E stained slide to cuspal calcification (stained blue) almost completely replacing the raphae *(**b**) Cuspal fibrosis, calcification, and focal neovascularization (H&E × 250)

13.3 Discussion

A clinical (and possibly an echocardiographic) diagnosis of AS due to 'degenerative' valvular disease (See Chap. 12) was found to be caused by heavy calcification of a BAV. It is the commonest congenital cardiac anomaly, where the AV is composed of 2 cusps, instead of the normal 3. It has an estimated prevalence of 1–2% of the population with a strong male predominance (male to female ratio of 3:1). BAV occurrence is sporadic or familial, where it is seen as an autosomal dominant disorder with low penetrance. It may also be associated with congenital cardiac malformations and other inherited chromosomal or connective tissue disorders.

Most often, the BAV comprises 2 unequal cusps, with the larger one having a central low-set raphe within the sinus-of-Valsalva. The raphe or the ill-formed commissure represents the site of fusion of the adjoining cusps during valvulogenesis and hence the larger conjoined cusp shows a notch at its free margin. In majority of the cases (74%, also seen in our case), the larger cusp is formed by the fusion of the right and left coronary cusps, which leads to the anterior-posterior subtype; the 2 coronary arteries arise from the sinus of the larger cusp on either side of the raphe. Embryologically, this type results from anomalous septation of the proximal portion of the cardiac outflow tract, caused by dysfunctional neural crest cells. In other individuals, the larger cusp is formed by fusion of the right and noncoronary cusps (24%) or by fusion of the left and noncoronary cusps (2%), both of which give rise to the left-right (laterolateral) subtype. The arteries would then arise in their respective right and left sinuses. This morphology arises from a defect that occurs before cardiac outflow tract septation on the basis of an exacerbated nitric oxide-dependent epithelial-to-mesenchymal transformation. Occasionally, the cusps are symmetrical and equal sized, devoid of raphe. This is the appearance of 'pure' BAV, which can also have anterior-posterior and left-right subtypes.

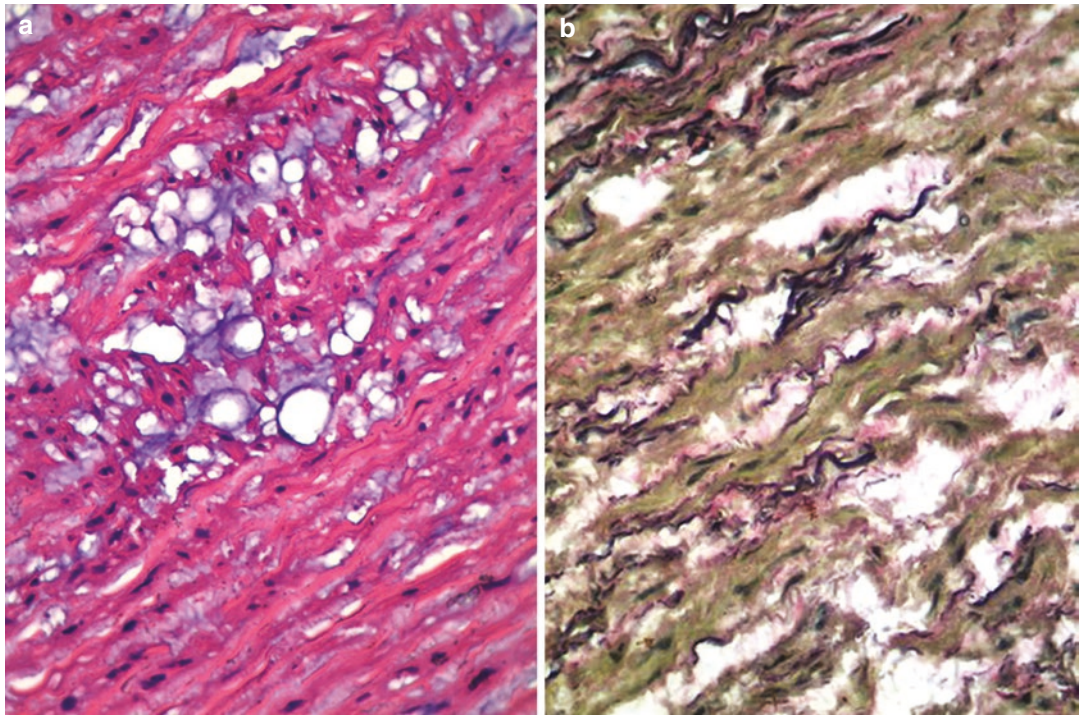

Fig. 13.3 (**a**) Increase in the basophilic mucoid extracellular material in the media confined to the lamellar units (H&E × 400); (**b**) Fragmentation and loss of elastic fibers in the media (Elastic van Gieson × 400)

There is substantial evidence that BAV is not just a disease of abnormal valvulogenesis and valvular function, but has effects exerted on to the aortic root and the thoracic aorta, which are not explained merely on the basis of altered hemodynamics. It is to be noted that irrespective of the cuspal placement, BAV is always morphologically stenotic (at least to begin with), but may be seen as incidental finding at autopsy as seemingly competent valves. However, in the majority of the cases, valvular dysfunction sets in by the third to fourth decades of life. The abnormally oriented orifices lead to abnormal flow pattern and turbulence, which in due course of time promotes valvular stenosis through fibrosis and calcification. Flow-induced annular dilatation with suboptimal coaptation, cuspal redundancy/prolapse, and/or cuspal destruction by infective endocarditis (See Part V) produces valvular incompetence. But, both dysfunctions can also coexist. Calcific stenosis remains the most common complication, with an incidence from 60 to 80% and is classically seen in the elderly population with BAV. Calcification is seen more commonly in the right-left form and usually begins at the raphe. The initiation and progression is through mechanisms similar to those in age-related calcific stenosis of a three-cuspid AV (See Chap. 12). Our patient was a hypertensive, and in all probability, the severe calcification would have obliterated the tell-tale features of BAV on imaging.

An additional finding, which in this case was incidental, was the presence of moderate degree of aortopathy restricted mainly to the anterolateral wall of the dilated ascending aorta. In this regard, it has been suggested that the BAV is a disease not only of the valve, but a disease of the aortic root and the aortic segment up to the ligamentum arteriosum. The abnormality manifests as aneurismal dilatations involving the aortic root, ascending aorta and arch in isolation or in combination (owing to their different embryological origins), and even acute aortic dissection. It has also been noted that the site and

degree of involvement may also depend on the type of BAV, e.g., the anterior-posterior type is associated with annulo-aortic ectasia and asymmetric dilatation of the ascending aorta, while isolated ascending aortic aneurysm is linked to the left-right type of BAV. The paucity of smooth muscle cells, loss and fragmentation of elastic fibers, and increased accumulation of proteoglycans are related to not only the flow-related hemodynamic stress, but also to genetic predisposition as well; mediation is through increase in the activity of matrix metalloproteinases and abnormalities in fibrillin-1 protein. Hence, the definitive treatment of BAV dysfunction by valve replacement is usually accompanied by aortic root repair and/or graft replacement of the tubular ascending aorta. It is also to be noted that the aortic changes are also prevalent (to the extent of 30%) in first degree relatives of BAV patients even with a normal three-cuspid aortic valves, which calls for screening of such individuals as well.

Further Reading

Halushka MK, Angelini A, Bartoloni G, Basso C, Batoroeva L, Bruneval P, et al. Consensus statement on surgical pathology of the aorta from the society for cardiovascular pathology and the association for european cardiovascular pathology: II. Noninflammatory degenerative diseases–nomenclature and diagnostic criteria. Cardiovasc Pathol. 2016;25:247–57.

Liu T, Xie M, Lv Q, Li Y, Fang L, Zhang L, et al. Bicuspid aortic valve: an update in morphology, genetics, biomarker, complications, imaging diagnosis and treatment. Front Physiol. 1921;2019:9.

Lo Presti F, Guzzardi DG, Bancone C, Fedak PWM, Corte AD. The science of BAV aortopathy. Prog Cardiovasc Dis. 2020;63:465–74.

Messner B, Bernhard D. Bicuspid aortic valve-associated aortopathy: where do we stand? J Mol Cell Cardiol. 2019;133:76–85.

Sakellaropoulos S, Mohammed M, Svab S, Lekaditi D, Sakellaropoulos P, Mitsis A. Causes, diagnosis, risk stratification and treatment of bicuspid aortic valve disease: an updated review. Cardiol Res. 2020;11:205–12.

Soto-Navarrete MT, López-Unzua MA, Durán AC, Fernández B. Embryonic development of bicuspid aortic valves. Prog Cardiovasc Dis. 2020;63:407–18.

14 Unicommissural Unicuspid Aortic Stenosis with Idiopathic Aortitis

Pradeep Vaideeswar

14.1 Clinical History

A 28-year-old male was admitted in a private nursing home for acute febrile illness with increasing shortness of breath and episodic chest pain. The routine hematological and biochemical tests were normal. The peripheral smear for malarial parasite and serology for hepatitis, dengue, leptospirosis, and HIV were negative. He was transferred to our center in a gasping condition and expired within 2 h.

14.2 Autopsy Findings

The heart weighed 452 g. There was moderate cardiomegaly due to marked enlargement of the left ventricle (Fig. 14.1a). A transverse section showed moderate concentric left ventricular hypertrophy (Fig. 14.1b). The aorta and pulmonary trunk had a normal relationship, but the ascending aorta (diameter of 3.8 cm) was twice the size of the pulmonary artery. The posterolateral aspect of the dilated aorta also showed a saccular bulge (5 × 4 cm, Fig. 14.1a) with a mulberry-like appearance. The aorta was opened out through cuts on its anterior and posterior walls to avoid the aneurysm. It showed a heavily calcified unicommissural, unicuspid aortic valve (UAV) with a small (0.8 cm) eccentric orifice that was oriented posteriorly (Fig. 14.2). The aneurismal wall was papery thin (Figs. 14.2a and 14.3a) and crackled due to focal calcification. Rest of the ascending aorta was firm in consistency and revealed characteristic features of aortopathy. But, the histology from the aneurismal area revealed occult idiopathic giant-cell arteritis. The arch and the descending portions of the aorta were normal. There was moderate left ventricular hypertrophy with foci of scarring and ischemia. Edema and focal bronchopneumonia were also present.

Cause of Death: Unicommissural unicuspid AV with severe calcific stenosis.

P. Vaideeswar (✉)
Department of Pathology (Cardiovascular and Thoracic Division), Seth Gordhandas Sunderdas Medical College and King Edward Memorial Hospital, Mumbai, India

P. Vaideeswar (ed.), *Tropical Cardiovascular Pathology*,
https://doi.org/10.1007/978-981-19-3720-0_14

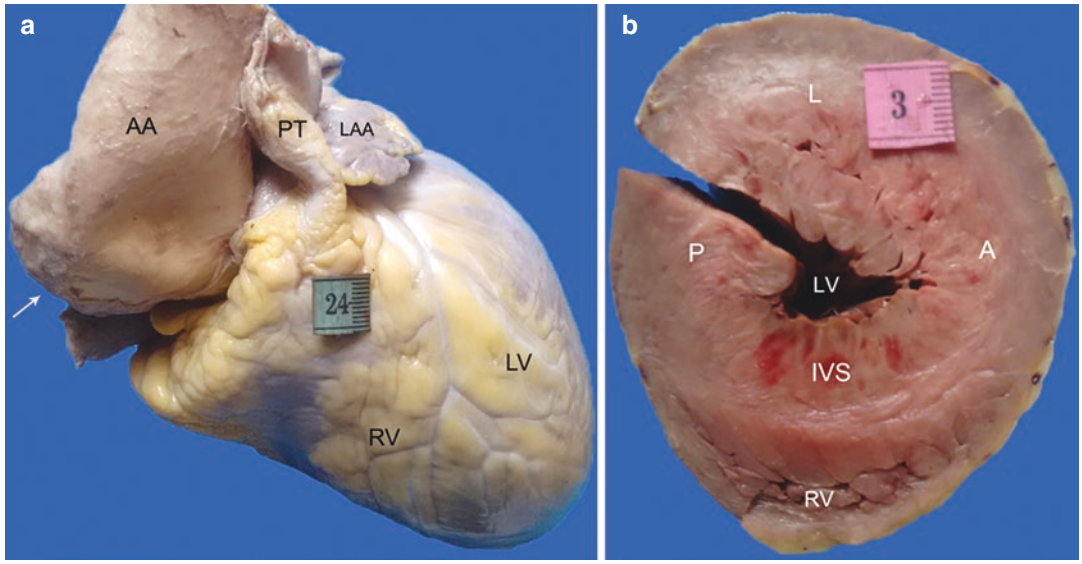

Fig. 14.1 (**a**) Moderate cardiomegaly. A dilated ascending aorta AA shows irregular outpouching (arrow) on the lateral aspect; (**b**) Concentric left ventricular LV hypertrophy (*A* anterior wall, *IVS* interventricular septum, *L* lateral wall, *LAA* left atrial appendage, *P* posterior wall, *PT* pulmonary trunk, *RV* right ventricle)

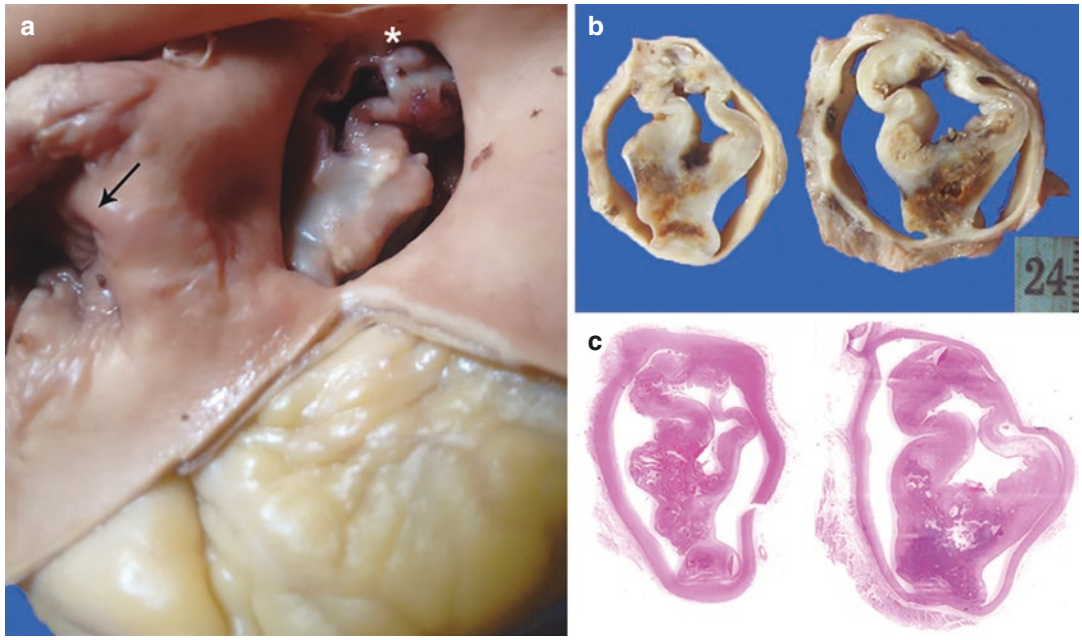

Fig. 14.2 (**a**) Opened out ascending aorta. It shows severe stenosis produced by a unicommissural * unicuspid aortic valve; (**b**) Serial slices of the decalcified valve and its corresponding (**c**) scanned H&E stained slide show extensive calcification. * represents the true commissure

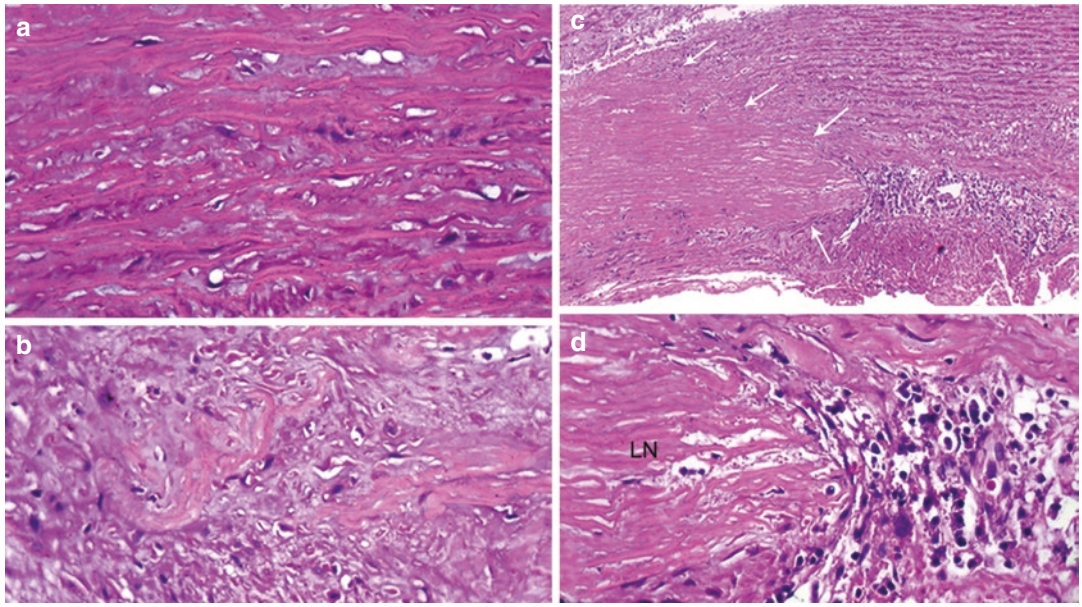

Fig. 14.3 Striking aortopathy—(**a**) Intralamellar increase of basophilic ground substance (H&E × 400) and (**b**) Fibrosis with separation and fragmentation of the elastic fibers, which appear as dark pink ribbons (H&E × 400); (**c**) A large focus of laminar necrosis (arrows) with surrounding inflammation. The entire necrotic zone shows loss of smooth muscle nuclei (H&E × 200); (**d**) Lymphocytes, plasma cells, macrophages, and occasional giant cells are seen to hug the laminar necrosis LN (H&E × 400)

14.3 Discussion

Apart from coronary artery disease, an important cause for chest pain in young adults is a dynamic or fixed obstruction to the left ventricular (LV) outflow. This is invariably induced by ischemia of hypertrophied LV myocardium, produced in this case by severe stenosis of UAV. Among the congenital malformations of the AV, UAV is a rare anomaly, predominantly seen in males with a male to female ratio of 4:1. It has an incidence of 0.02% in the general population to even as high as 22% for patients referred for AV surgery. This variation is explained by erroneous diagnosis of some cases as bicuspid AS (See Chap. 13) due to overlapping clinical presentation and imaging characteristics. Hence, postsurgery diagnosis by a cardiovascular pathologist is considered as the gold standard.

Two morphologic subtypes are described. The unicommissural valve has a single cusp that is attached circumferentially to the annulus, leading to a dome-shaped valve with a central pin-hole orifice, which results in significant stenosis in early childhood. Some of them are also associated with other congenital anomalies like ventricular septal defects, patent ductus arteriosus, aortic coarctation, and anomalous coronary arteries. Unicommissural valve, commonly seen in adults, has a single point of attachment to the aortic wall through a true commissure, leading to an eccentric, elliptical, and exclamation mark/U/tear drop-shaped orifice. In most cases, it is possible to identify the 2 ill-formed commissures or raphes. The distance between the true commissure and the raphes is nearly equal, while the cuspal tissue between the raphes is both smaller and thicker.

It is said that BAV and UAV represent the continuum of the same disease since they share similar underlying predisposition, demographics, and clinical presentation. However, a unicommissural UAV with a smaller orifice and an element of inherent incompetence predisposes the valve to early fibrosis and calcification leading to clinical manifestation of AS in the third to fifth decades of life, which is more common and more severe

when compared to age-matched bicuspid AS. Severe stenosis was present in this case too. As with BAV, the calcification is most severe at the raphes. Aortopathy (See Chap. 13) and ascending aortic dilatations/aneurysms also occur in UAV with a prevalence of 6–62%, a range higher as compared to BAV. Our patient too had extensive aortopathy that had led to diffuse ascending aortic dilatation, but the area of sacculations revealed active inflammation of the aortic wall—aortitis.

Aortitis refers to inflammation of the aorta, in particular the media with or without involvement of the intima and adventitia. The inflammatory response can be categorized into specific histopathological patterns of: granulomatous/giant-cell response, lymphoplasmacytic reaction, suppuration, or mixed inflammatory pattern. A predilection for the thoracic segments of the aorta is seen with the heterogeneous group of noninfectious aortitis, which would also require correlation of the pathological features with clinical, imaging, and laboratory parameters. In this background, many of the cases of noninfectious aortitis have an underlying rheumatologic basis (See Part IX) with development of aortic regurgitation, aneurysms, or dissections. However, a certain subset of patients (predominantly elderly women) with aortic aneurismal disease (to the extent of almost 70%) and pathological features of necrotizing/non-necrotizing, giant-cell/lymphoplasmacytic infiltrate do not have any evidence of systemic disease at the time of clinical presentation. This manifestation is termed as idiopathic, isolated or non-syndromic aortitis and is now considered as single-organ vasculitis. In the illustrated case, the necrotizing giant-cell inflammatory response involved only part of the aorta, which was otherwise affected by UAV-induced severe aortopathy. Such an association has not been reported so far. Other regions of the aorta or other arteries were also not involved and so, this would be an example of isolated aortitis, which may have manifested as a febrile illness in this young man. With an antemortem diagnosis, a regular follow-up of such patients with appropriate serological tests and imaging is advisable, as the current isolated aortitis may be the forerunner of a subclinical systemic vasculitis that could manifest subsequently.

Further Reading

Caspary L. Inflammatory diseases of the aorta. Vasa. 2016;45:17–29.

Cinar I, Wang H, Stone JR. Clinically isolated aortitis: pitfalls, progress, and possibilities. Cardiovasc Pathol. 2017;29:23–32.

Cozijnsen L, ter Borg EJ, Braam RL, Seldenrijk CA, Heijmen RH, Bouma BJ, et al. Ascending aortic aneurysm secondary to isolated noninfectious ascending aortitis. Clin Rheumatol. 2019;25:186–94.

Krepp JM, Roman MJ, Devereux RB, Bruce A, Prakash SK, Morris SA, et al. Bicuspid and unicuspid aortic valves: different phenotypes of the same disease? Insight from the gen TAC registry. Congenit Heart Dis. 2017;12:740–5.

Naito S, Sequeira-Gross T, Petersen J, Holst T, Reichenspurner H, Girdauskas E. Focus on a rare clinical entity: unicuspid aortic valve disease. Expert Rev Cardiovasc Ther. 2020;18:625–33.

Slostad BD, Witt CM, O'Leary PW, Maleszewski JJ, Scott SG, Dearani JA, et al. Unicuspid aortic valve: demographics, comorbidities, echocardiographic features, and long-term outcomes. Circulation. 2019;140:1853–5.

Stone JR, Bruneval P, Angelini A, Bartoloni G, Basso C, Batoroeva L, et al. Consensus statement on surgical pathology of the aorta from the Society for Cardiovascular Pathology and the Association for European Cardiovascular Pathology: I. inflammatory diseases. Cardiovasc Pathol. 2015;24:267–78.

Yuan SM, Lin H. Aortitis presenting as fever of unknown origin. Ann Thorac Cardiovasc Surg. 2018;24:279–87.

15 Mitral and Aortic Valvular Regurgitation Due To Rheumatoid Arthritis

Pradeep Vaideeswar

15.1 Clinical History

A 50-year-old female, a known case of rheumatoid arthritis (RA, rheumatoid factor 101 IU/mL, normal up to 20 IU/mL), was taking "Ayurvedic" preparations for her condition for the past 2 years. She now presented with generalized weakness, easy fatigability, palpitation, and edema feet for a month, followed by progressive dyspnea and orthopnea since the last 15 days. On examination, she was afebrile with a pulse rate of 96 per minute, blood pressure of 100/70 mmHg, and respiratory rate 42 per minute. There was raised jugular venous pressure. Mid-diastolic and early systolic murmurs with bilateral crepitations were heard on auscultation. The routine investigations revealed anemia (Hb 8.8 g/dL) and mild neutrophilia (total leukocyte count of 21,000/cmm); the biochemical investigations were within normal limits. Moderate mitral and aortic regurgitations were seen on 2-dimensional transthoracic echocardiography, while bilateral pulmonary ill-defined ground-glass opacities were present on high-resolution computed tomography. The clinical diagnosis was interstitial lung disease. She was treated with injectable antibiotics and steroids, but there was no improvement. She expired after 32 h of ward stay.

15.2 Autopsy Findings

At autopsy, there was moderate cardiomegaly (heart weight 320 g) with moderate biventricular enlargement (Fig. 15.1a). The great arteries had a normal relationship and the ascending aorta was larger than the pulmonary trunk. Apart from dilated right ventricular cavity, other right-sided structures were normal. The left atrium was normal. The left ventricular cavity was moderately dilated with patchy endocardial thickening and thinning of its wall (0.9 cm). Striking abnormalities were noted in the mitral (MV, Fig. 15.1b) and aortic (AV, Fig. 15.1c) valves. There was mild mitral annular dilatation. Both the commissures were mildly fused. The leaflets were grey-white, thick, and leathery. Few of the chordae attached to the anterior mitral leaflet were thickened and fused with each other, but there was no shortening. The aortic annulus was also mildly dilated with mild fusion of all commissures and moderate thickening of all 3 cusps. Jet lesion of aortic regurgitation was present in the subaortic region of the interventricular septum. On histology, both the mitral and aortic valves showed features of acute-on-chronic valvulitis. Characteristic find-

P. Vaideeswar (✉)
Department of Pathology (Cardiovascular and Thoracic Division), Seth Gordhandas Sunderdas Medical College and King Edward Memorial Hospital, Mumbai, India

P. Vaideeswar (ed.), *Tropical Cardiovascular Pathology*,
https://doi.org/10.1007/978-981-19-3720-0_15

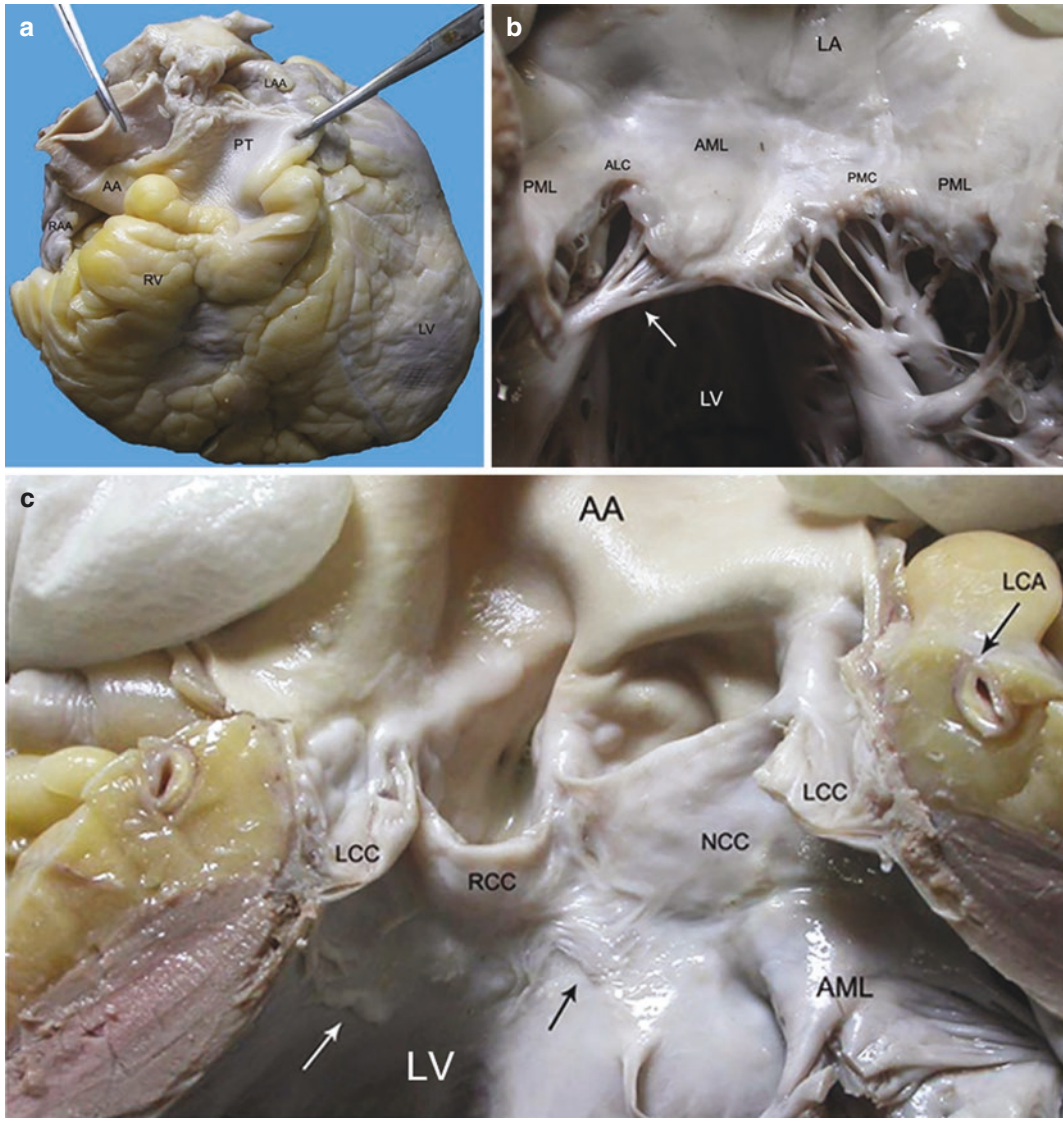

Fig. 15.1 (**a**) Biventricular enlargement. Note almost equal sizes of pulmonary trunk PT and ascending aorta AA; (**b**) There is mild mitral annular dilatation with commissural fusion and leaflet thickening. Few chordae are thickened and fused (arrow); (**c**) The aortic annulus is dilated with mild cuspal thickening. The right coronary cusp RCC also has rounding of its margin. Arrows point to jet lesions of aortic regurgitation. Note eccentric atheroma in the left circumflex artery LCA (*ALC* anterolateral commissure, *AML* anterior mitral leaflet, *LA* left atrium, *LAA* left atrial appendage, *LCC* left coronary cusp, *LV* left ventricle, *NCC* noncoronary cusp, *PMC* posteromedial commissure, *PML* posterior mitral leaflet, *RAA* right atrial appendage, *RV* right ventricle)

ings in these valves were the presence of small rheumatoid nodules, composed mainly of fibrinoid with palisaded histiocytic reaction and stromal fibrosis (Figs. 15.2 and 15.3). All coronary arteries were mildly atherosclerotic with no significant narrowing (Fig. 15.1c). The lungs showed capillaritis, interstitial pneumonitis, and diffuse alveolar damage. The liver showed centrizonal focal necrosis. Kidneys and other organs were normal.

Cause of Death: Congestive cardiac failure with diffuse alveolar damage.

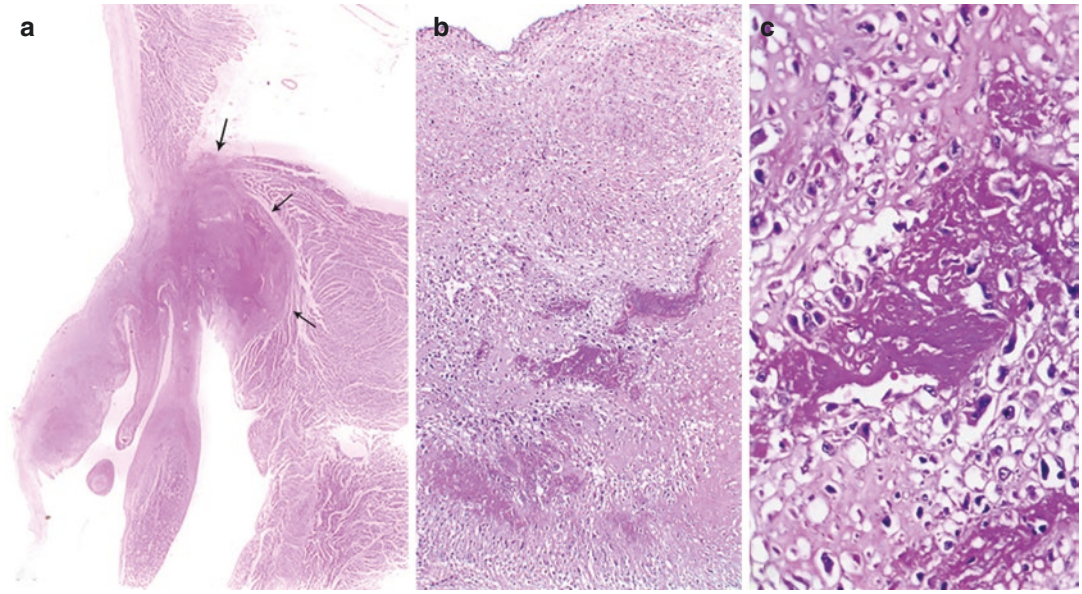

Fig. 15.2 (**a**) Scanned H&E stained slide of the mitral valve showing a nodule (arrows) at the annulus with thickening of the posterior leaflet; (**b**) Conglomerate of rheumatoid nodules with bright pink fibrinoid necroses (H&E × 200); (**c**) Palisaded histiocytes around the zone of necrosis (H&E × 400)

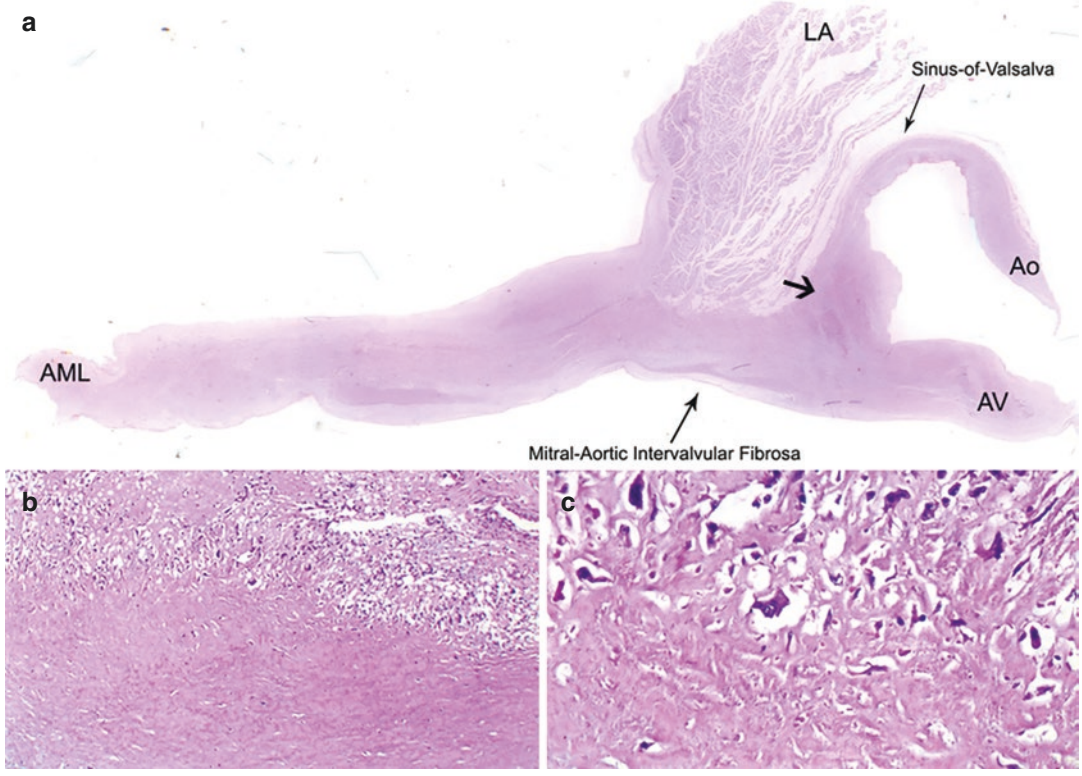

Fig. 15.3 (**a**) Scanned H&E stained slide at the mitral-aortic intervalvular fibrosa showing thickening of the anterior mitral leaflet and left coronary cusp. Fibrotic nodules (short arrow) present at the aortic annulus; Hyalinized nodules surrounded by irregular-shaped macrophages (**b**) (H&E × 200) and (**c**) (H&E × 400)

15.3 Discussion

Cardiopulmonary manifestations were responsible for morbidity and mortality, respectively, in this patient with a long-standing history of RA. RA is the most common example of a chronic autoimmune inflammatory disease, which produces symmetric polyarticular synovitis of the small joints of the hands and feet and subsequent destruction and distortion. In the developed world, the incidence ranges from 0.5% to 1.0%, while in India, the incidence is not exactly known but is said to be in the range of 0.28–0.7%. Though small joint arthritis is the most characteristic feature of RA, it is also associated with extra-articular involvement of several organs, especially the lungs and the heart. Since the treatment of RA entails prolonged medications, sometimes with immunosuppressives, there is a likelihood that some patients may resort to traditional medicine, as seen in this case, enhancing the chances of development of extra-articular manifestations. Lung involvement is seen in 60–80% of RA patients and is generally seen after about 5 years, though in a small proportion; it may even precede the joint involvement. All compartments of the lung parenchyma may be affected. Often an interstitial lung disease pattern is produced. In this case, diffuse alveolar damage (the cause of mortality) was present along with interstitial pneumonitis and capillaritis. The autopsy also revealed a concomitant cardiac disease in the form of left-sided valvular regurgitations.

In general, the causes of mitral regurgitation (MR) may be related to abnormalities of different components of the valve or may arise to left ventricular geometrical alterations. Similarly, aortic regurgitation (AR) arises not only due to valvular deformity, but is also produced by aortic root abnormalities secondary to left ventricular or aortic diseases. In this case, MR and AR were produced by smouldering valvulitis in a setting of RA. About 60% of patients with RA have some form of cardiovascular disease, which to a large extent is subclinical. However, it is the major contributor to mortality (35–50%) during the course of the disease. Important among them is ischemic heart disease due to coronary atherosclerosis initiated by the traditional risk factors and accelerated by chronic inflammation and cytokine activity. The aberrant immune response can also lead to cardiomyocyte hypertrophy and fibrosis with diastolic dysfunction, acute myocarditis, and reactive secondary amyloidosis, all of which are the nonischemic myocardial disorders of RA. Ischemic and nonischemic pathology can pave way for the development of arrhythmias and sudden death. Pericarditis (effusive or constrictive) is the most common cardiac manifestation of RA, but hardly produces any hemodynamic compromise. In the case presented, no changes were noted in the pericardium and myocardium; there was mild coronary atherosclerosis. Aortitis, another rare finding in RA, was also not present. The cardiac disease was seen in the form of combined mitral and aortic regurgitation.

Valvular disease is seen in about 30% of patients with RA, asymptomatic in the majority of the patients. MR is the most common form. The valvular dysfunction results from nonspecific inflammation that affects the annulus and leaflets, predisposing to subsequent fibrosis and calcification. In some cases, the chronic valvular changes are produced due to rheumatoid nodules (RN) that are often located at the annuli or the midportions of the leaflets or cusps. The nodules can also be seen within the myocardium and can localize within the atrioventricular node causing heart block in some patients with RA. RNs are the other common extra-articular manifestations of RA with pathogenetic mechanisms possibly unrelated to the synovitis. They commonly occur in the juxta-articular subcutaneous tissue, but can also occur at other sites, including the lungs and the heart. Palisading epithelioid histiocytes surrounding foci of necrobiosis and fibrin are typical histopathological features; fibrosis, granulation tissue, and lymphoplasmacytic infiltrate can also be present. In this case, multiple such nodules were located at the mitral and aortic annuli with prominent valvulitis. Nonbacterial thrombotic endocarditis can also develop over the affected valves; the thrombi and the nodules can serve as a nidus for infective endocarditis. Myocardial rheumatoid nodules and thrombi were not present in this case.

Further Reading

Bang S, Kim Y, Jang K, Paik SS, Shin SJ. Clinicopathologic features of rheumatoid nodules: a retrospective analysis. Clin Rheumatol. 2019;38:3041–8.

Buleu F, Sirbu E, Caraba A, Dragan S. Heart involvement in inflammatory rheumatic diseases: a systematic literature review. Medicina. 2019;55:249.

Choi JH, Park JE, Kim JY, Kang T. Non-bacterial thrombotic endocarditis in a patient with rheumatoid arthritis. Korean Circ J. 2016;46:425–8.

Esposito AJ, Chu SG, Madna R, Doyle TJ, Dellaripa PF. Thoracic manifestations of rheumatoid arthritis. Clin Chest Med. 2019;40:545–60.

Fishbein GA, Fishbein MC. Pathology of the aortic valve: aortic valve stenosis/aortic regurgitation. Curr Cardiol Rep. 2019;21:8.

Handa R, Rao URK, Lewis JFM, Rambhad G, Shiff S, Ghia CJ. Literature review of rheumatoid arthritis in India. Int J Rheum Dis. 2016;19:440–51.

Harb SC, Griffin BP. Mitral valve disease: a comprehensive review. Curr Cardiol Rep. 2017;19:73.

Sen D, González-Mayda M, Brasington RD Jr. Cardiovascular disease in rheumatoid arthritis. Rheum Dis Clin North Am. 2014;40:27–49.

Part V

Valvular Heart Disease: Verrucous Endocarditis

16 Infective Endocarditis Following Balloon Valvotomy for Rheumatic Mitral Stenosis

Pradeep Vaideeswar and Girish Sabnis

16.1 Clinical History

A 46-year-old lady underwent successful percutaneous balloon mitral valvotomy (BMV) for severe rheumatic mitral stenosis (MS) 6 weeks ago in a private health-care facility. A week after the procedure, she started getting spikes of high-grade fever and dry cough. She was readmitted to the same hospital, where the investigations showed a total leukocyte count (TLC) of 29,200/cmm with a leftward shift. Transthoracic echocardiography revealed well-relieved MS with mitral valve areas of 1.3 cm^2 and 1.4 cm^2 by planimetry and pressure half time, respectively, and a mean gradient of 8 mmHg. There were no vegetations. Blood cultures during a febrile episode grew *Pseudomonas aeruginosa* sensitive to piperacillin-tazobactam and amikacin. The fever responded to weight-adjusted doses of the above antibiotics, only to recur 3 weeks later. This was accompanied by acute monoparesis of the right upper extremity. A CT scan revealed a fresh nonhemorrhagic infarct in the left middle cerebral arterial territory. At this stage, 6 weeks post-BMV, the patient was transferred to our institute for further management.

On examination, the patient was looked sickly and poorly nourished with mild pallor and grade 1 clubbing. She had sinus tachycardia, blood pressure of 104/70 mmHg, and a normal jugular venous pressure. On auscultation, there was a short middiastolic murmur at the apex; the chest was clear. There was no hepatosplenomegaly. Her investigations on admission were as follows: hemoglobin 8.1 g/dL, TLC 18,000/cmm (86% neutrophils), platelet count of 3.2 lakhs/cmm, erythrocyte sedimentation rate 60 mm after 1 h, random blood glucose 115 mg/dL, serum creatinine 0.7 mg/dL, AST 16 U/L, and ALT 7 U/L. The HIV-ELISA was nonreactive; the C-reactive protein was elevated (180 U/mL, normal <5 U/mL). The ECG did not show atrial fibrillation. Transthoracic echocardiography revealed a successful valvotomy procedure, but there was a mass (1.5 × 1.0 cm) attached to the anterior mitral leaflet (AML, Fig. 16.1a). The diagnosis of the vegetation was confirmed on transesophageal echocardiography. The patient was empirically started on intravenous meropenem and amikacin. However, there was no improvement in the constitutional symptoms. Blood cultures again grew *P. aeruginosa*, which was now sensitive only to colistin, amikacin, netilmicin, and polymyxin B. A regimen of intravenous colistin with amikacin was initiated. However, she had a progressively downhill

P. Vaideeswar (✉)
Department of Pathology (Cardiovascular and Thoracic Division), Seth Gordhandas Sunderdas Medical College and King Edward Memorial Hospital, Mumbai, India

G. Sabnis
Dr KK Datey Department of Cardiology, Seth Gordhandas Sunderdas Medical College and King Edward Memorial Hospital, Mumbai, India

P. Vaideeswar (ed.), *Tropical Cardiovascular Pathology*,
https://doi.org/10.1007/978-981-19-3720-0_16

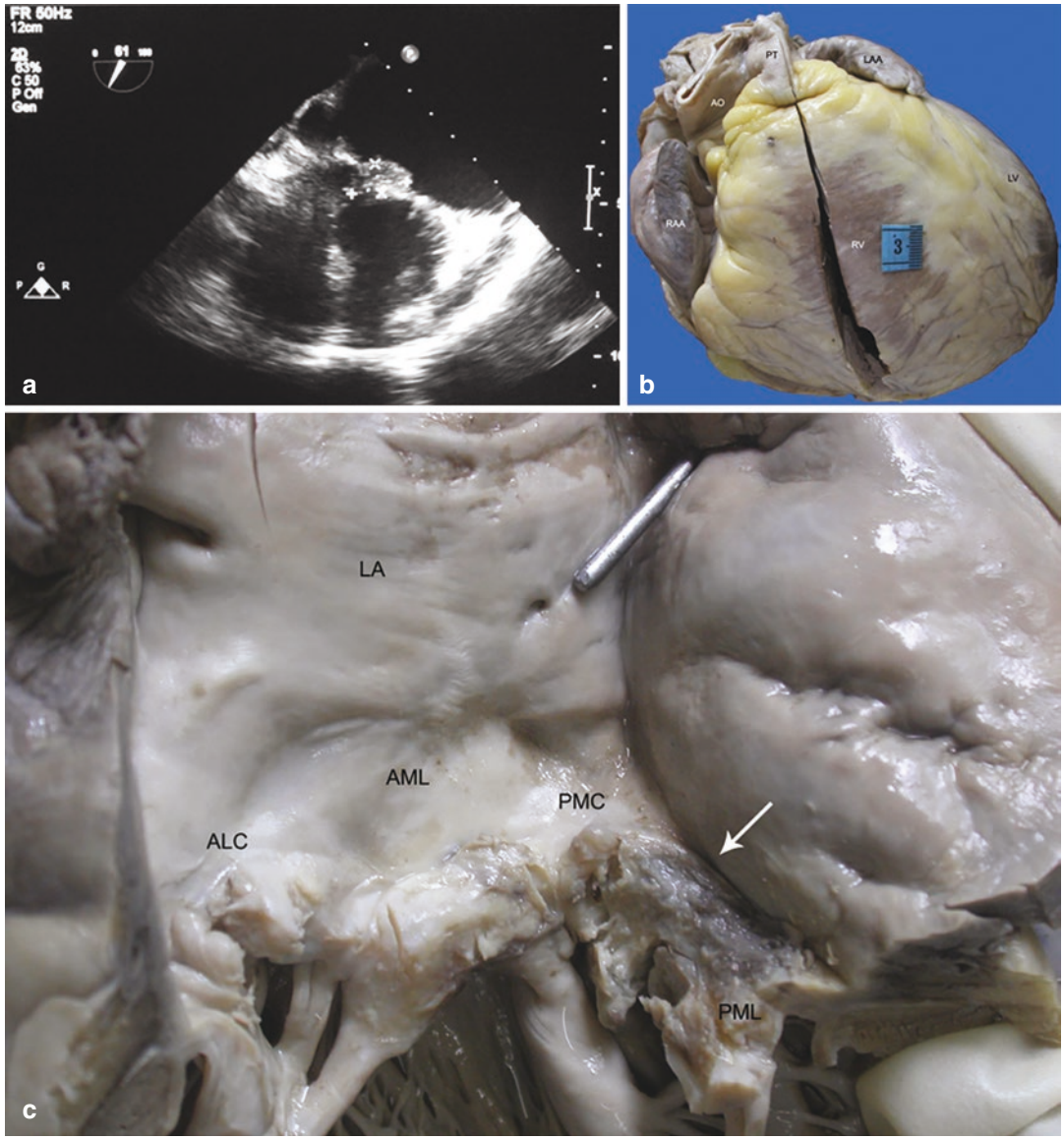

Fig. 16.1 (**a**) Vegetation attached to the anterior mitral leaflet; (**b**) Moderate enlargement of the right ventricle RV. The rounded apex is formed by both ventricles; (**c**) Mitral valve with characteristic features of rheumatic stenosis. A probe has been passed through the septostomy. BMV has produced a spilt of the anterolateral commissure ALC. The posteromedial commissure PMC and adjoining leaflets (arrow) are covered by flattened, firm and friable, pale brown vegetations (*AA* ascending aorta, *AML* anterior mitral leaflet, *LA* left atrium, *LAA* left atrial appendage, *LV* left ventricle, *PML* posterior mitral leaflet, *PT* pulmonary trunk, *RAA* right atrial appendage)

course, her leukocyte counts continued to rise (mean 24,300/cmm), and she succumbed 3 days later (8 days post-admission) to overwhelming sepsis.

16.2 Autopsy Findings

A restricted autopsy (partial chest and abdomen) was performed. The heart (300 g) was mildly enlarged in size with moderate enlargement of the right ventricle (Fig. 16.1b) and atria. The interatrial septum on the right atrial aspect showed a defect (0.8 × 0.5 cm) at the posterior aspect of the fossa ovalis (septostomy of BMV) with thickened irregular rim; on the left side, it appeared probe-patent (Fig. 16.1c). The mitral valve appeared stenosed (orifice measuring 1.4 × 0.8 cm) with a split at the anterolateral commissure. The posteromedial commissure continued to be fused and showed nodular calcification. Both the valve leaflets were markedly thickened with focal calcification. The medial aspect of the AML and the posterior leaflet were congested, rough, and irregular with red-brown granular thrombotic material over the flow surfaces (Fig. 16.1c). Basophilic bacterial colonies in a background of fibrin and neutrophils were present over healed mitral valvulitis (Fig. 16.2). There was mild subclinical involvement of the aortic valve (mild commissural fusion with slight prolapse of the noncoronary and right coronary cusps). No vegetations were seen. The left anterior descending artery showed 75% stenosis by a fibro-fatty atheroma. Focal micro-abscesses were seen in the myocardium. Other findings included bronchopneumonia with diffuse alveolar damage (Fig. 16.3a), and mild changes of pulmonary venous hypertension, neutrophils, and their precursors within dilated sinusoids of liver (Fig. 16.3b) and spleen, chronic tubule-interstitial nephritis, and splenic infarction (Fig. 16.3b).

Cause of Death: Septicemia due to Infective Endocarditis (IE).

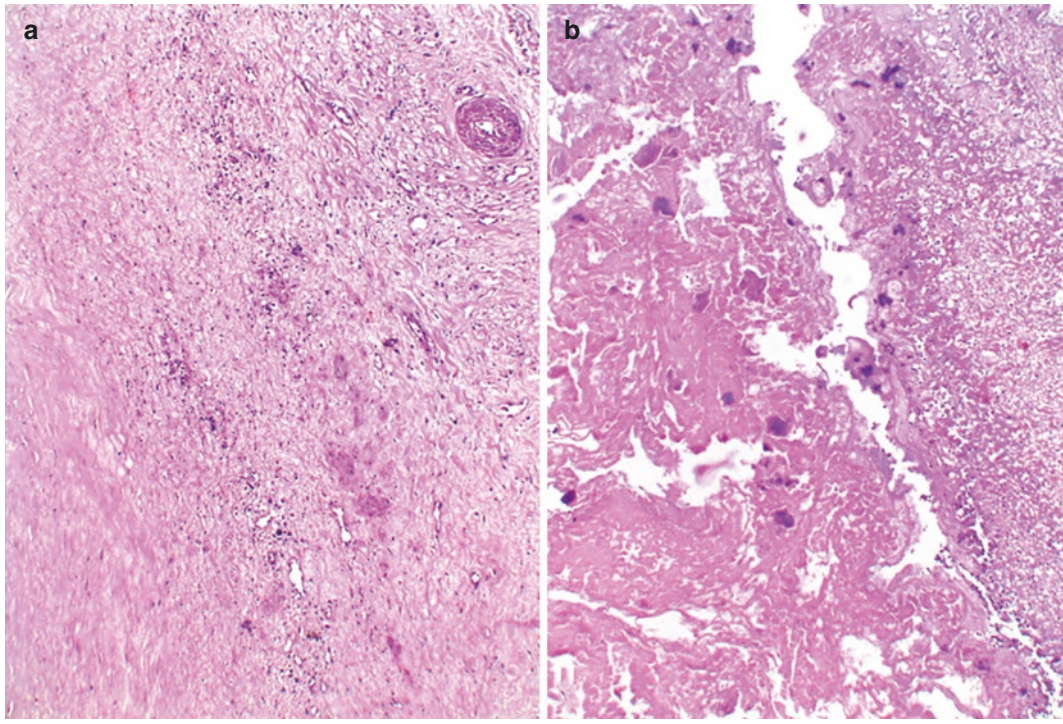

Fig. 16.2 (**a**) Mitral valve with fibrosis, vascularization, and focal inflammation; (**b**) Vegetation composed largely of fibrin with clusters of basophilic bacterial colonies (H&E × 200)

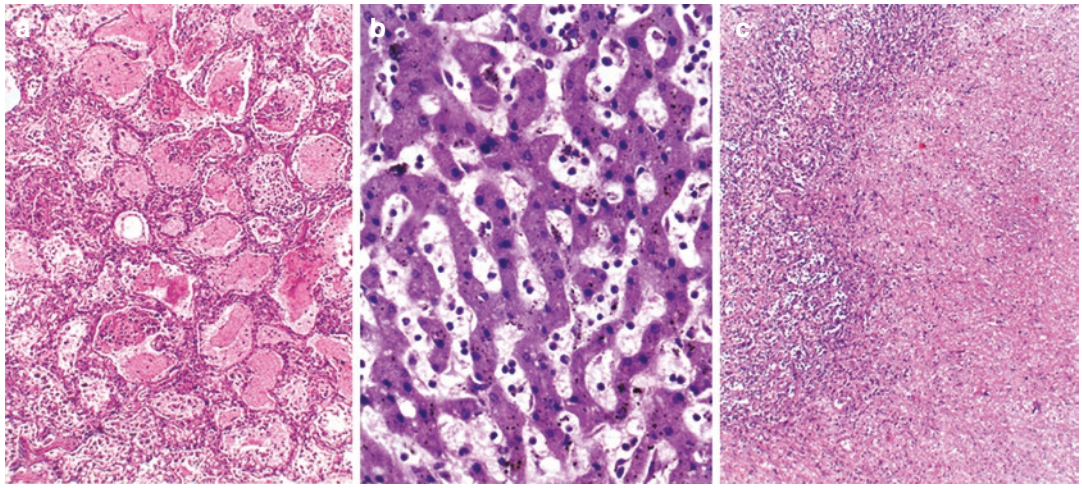

Fig. 16.3 (**a**) Pulmonary edema with hyaline membrane formations (H& × 200); (**b**) Dilated hepatic sinusoids containing neutrophils and their late precursors (H&E × 400); (**c**) Splenic infarction (H&E × 200)

16.3 Discussion

IE, a condition described 350 years ago, continues to instill a high degree of trepidation among the clinicians as it is still associated with debilitating morbidity and high mortality (25–30%); this is despite significant advances in the modes of diagnosis and therapy. It is an inflammation of the valvular or mural endocardium of the heart and endothelium of the large blood vessels induced by microorganisms, and this definition has been expanded to incorporate infections affecting prosthetic valves and other prosthetic devices/materials. Masses of septic thrombi or vegetations are finally formed at the site of infection. IE is an uncommon disease with an annual incidence of 3–10/100,000 of the population, particularly more frequent in males.

Formation of infective vegetation is a multistep process. It commences with endocardial or endothelial injury developing secondary to hemodynamic stress in a setting of acquired/congenital cardiac lesions or by mechanical trauma. The now abraded surface exposes the underlying extracellular matrix with ensuing deposition of fibrin and platelets and the formation of sterile thrombus. Under appropriate circumstances, a transient banal bacteremia allows initial adhesion and final colonization and proliferation of the microorganisms at the sites of injury. Involvement of the immune and hemostatic mechanisms allows deposition of larger amounts of fibrin. This 'immunothrombosis' forms a thick scaffold above the organisms, protecting them from phagocytosis and action of antibiotics. The underlying cardiovascular condition, the localizations of the vegetations, the overall status of the patient, the type and portal of entry of the offenders, and the temporal profile of onset lead to different categories of IE.

In the illustrated case, the patient developed acute left-sided IE over a mitral valve, which was deformed due to chronic rheumatic heart disease (RHD). In general, IE has a propensity to involve the left-sided valves and was often seen as untoward complication in acquired or congenital structural heart disease. In this context, chronic RHD was considered as the major risk factor, which unfortunately remains the most common predisposing factor in the developing world even today. The organisms implicated were the viridans group streptococci, released into the circulation during subtle cutaneous and oral, gastrointestinal or urogenital mucosal injury. In this case, the causative organism was *P. aeruginosa* and the IE was an example of health-care associated infection, which developed within a week of within a week of BMV (See Chap. 6).

BMV is now the procedure of choice in patients with severe rheumatic MS with a pliable mitral valve, despite the accompanying risk of minimal postprocedural regurgitation and left-to-right atrial shunting. In comparison to the more common serious complication of development of acute severe MR (incidence 3–8%), IE is a very rare event. Bacteremia occurs very infrequently during cardiac catheterization. The possible potentiating factors include prolonged procedure times, multiple catheter exchanges, and a possible reuse of single use disposable hardware. Apart from the existing deformity, the site of commissural fracture by balloon inflation could serve as a potential nidus for bacterial implantation, and the bacteria would have been directly transported to the left side via the septostomy opening. An aggressive pathogen, *P. aeruginosa,* was isolated, which is an organism causing right-sided endocarditis in intravenous drug abusers. In a review of *P. aeruginosa* IE without drug abuse, only 27 patients were reported in a span of 21 years, which was related to health-care in majority of the patients (74%) associated with relapse (explained on the basis of quick adaptive resistance to antipseudomonal agents), aggressive course, and high mortality (40%). As far as therapy is concerned, valve replacement remains the cornerstone of management of patients with fulminant sepsis not responding to antimicrobial treatment. Unfortunately, this was not possible in our patient due to rapid deterioration.

Further Reading

Banai S, Selitser V, Keren A, Benhorin J, Shitrit OB, Yalon S, Halperin E. Prospective study of bacteremia after cardiac catheterization. Am J Cardiol. 2003;92:1004–7.

Deshpande J, Vaideeswar P, Sivaraman A, Kulkarni H. Balloon mitral valvotomy: an autopsy study. Int J Cardiol. 1995;52:67–76.

Hu W, Wang X, Su G. Infective endocarditis complicated by embolic events: pathogenesis and predictors. Clin Cardiol. 2021;44:307–15.

Liesenborghs L, Meyers S, Vanassche T, Verhamme P. Coagulation: at the heart of infective endocarditis. J Thromb Haemost. 2020;18:995–1008.

Lin TI, Huang YF, Liu PY, Chou CN, Chen YS, Chen YY, et al. Pseudomonas aeruginosa infective endocarditis in patients who do not use intravenous drugs: analysis of risk factors and treatment outcomes. J Microbiol Immunol Infect. 2016;49:516–22.

Njuguna B, Gardner A, Karwa R, Delahaye F. Infective endocarditis in low- and middle-income countries. Cardiol Clin. 2017;35:153–63.

Palacious IF. Percutaneous mitral balloon valvuloplasty: state of the art. Mini Invas Surg. 2020;4:73.

Ramireddy S, Gudipatia S, Zervos M. Expect the unexpected: a rare case of Pseudomonas aeruginosa endocarditis. ID Cases. 2020;21:e00787.

Talha KM, DeSimone DC, Sohail MR, Baddour LM. Pathogen influence on epidemiology, diagnostic evaluation and management of infective endocarditis. Heart. 2020;106:1878–82.

Vincent LL, Otto CM. Infective endocarditis: update on epidemiology, outcomes, and management. Curr Cardiol Rep. 2018;20:86.

Infective Endocarditis of Normal Native Mitral Valve

17

Heena Desai and Pradeep Vaideeswar

17.1 Clinical History

A 22-year-old male was involved in a road traffic accident with trivial head injury. He was observed in a private hospital and discharged after 2 days; there was no fracture at any site. Five days later, he was readmitted in another hospital for moderate-grade fever with chills, headache, and right hemiparesis, where a diagnosis of pyogenic meningitis was made. Despite antibiotic therapy (details not available), he developed increasing respiratory distress and was transferred to our center for further management. He was admitted in an unconscious state with a pulse rate of 74 per minute and blood pressure of 90/60 mmHg. He was not responding to oral commands. The power and tendon reflexes were normal; plantars were down-going. The investigations have been compiled in Table 17.1. Intracranial tension-lowering agents and broad-spectrum antibiotics were administered, but he expired after 5 days.

Table 17.1 Investigations

Hematological	[a]Hemoglobin 6.8 g/dL [a]Total leukocyte count 18,050/cmm Differential count—Neutrophil predominant [a]Platelet count 1.64 lakhs/cmm
Biochemical—Routine	[a]Serum creatinine 1.45 mg/dL [a]Blood urea nitrogen 28 mg/dL [a]SGOT 72 U/L [a]SGPT 43.5 U/L [a]Sodium 149.3 mEq/L [a]Potassium 3.9 mEq/L [a]Chloride 132 mEq/L
Radiological	Ultrasonography: Mild right pleural effusion; splenic hypoechoic lesion Magnetic Resonance Imaging—Brain: Acute nonhemorrhagic infarct in left middle cerebral arterial territory and right thalamus
Others	Urine examination: Normal cerebrospinal fluid examination: Normal blood culture: Negative

[a]Mean values

17.2 Autopsy Findings

The heart was normal in size (230 g). There was a large (2.8 × 3.6 cm), friable, reddish brown vegetation at the posteromedial commissure, with extension into the adjoining leaflets and chordate tendineae; a small vegetation was also present over the posterior leaflet (Fig. 17.1a). Focal granularity was also present over the endocardium of the left atrial posterior wall (Fig. 17.1a). The vegetations (Fig. 17.2a) were composed of fresh throm-

H. Desai
Department of Pathology, Topiwala National Medical College and BYL Nair Charitable Hospital, Mumbai, India

P. Vaideeswar (✉)
Department of Pathology (Cardiovascular and Thoracic Division), Seth Gordhandas Sunderdas Medical College and King Edward Memorial Hospital, Mumbai, India

P. Vaideeswar (ed.), *Tropical Cardiovascular Pathology*,
https://doi.org/10.1007/978-981-19-3720-0_17

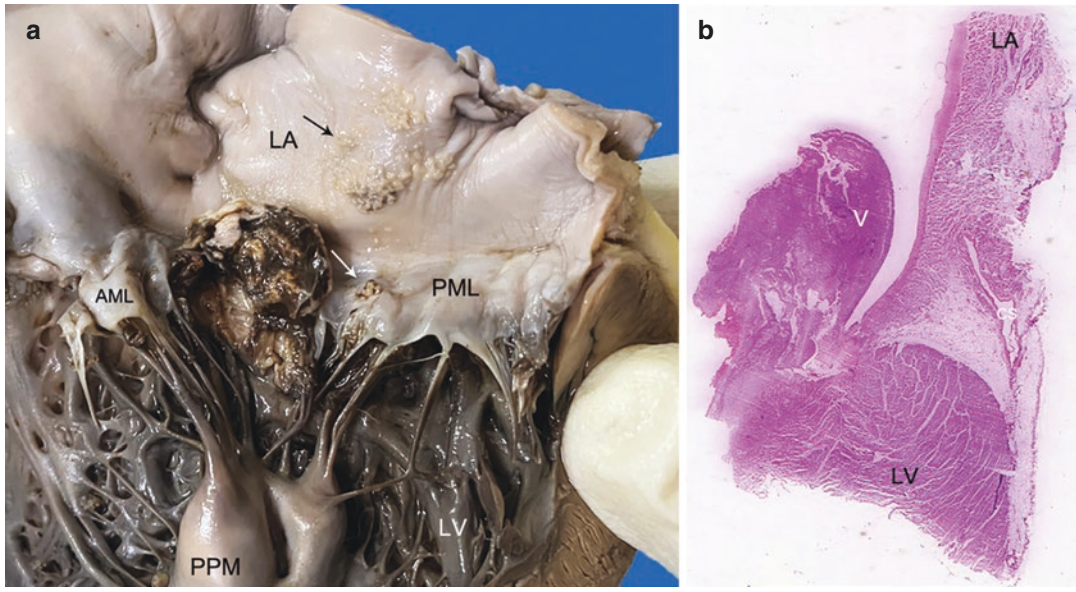

Fig. 17.1 (**a**) Large vegetation over the postero-medial commissure. Note smaller vegetation (white arrow) over the posterior leaflet and endocardial granularity (black arrow) of the left atrium LA (*AML* anterior mitral leaflet, *LV* left ventricle, *PML* posterior mitral leaflet, *PPM* posterior papillary muscle); (**b**) Scan of the section taken from the left ventricular LV inflow tract showing complete destruction of the valvular tissue by the large vegetation V (*CS* coronary sinus, *LA* left atrium)

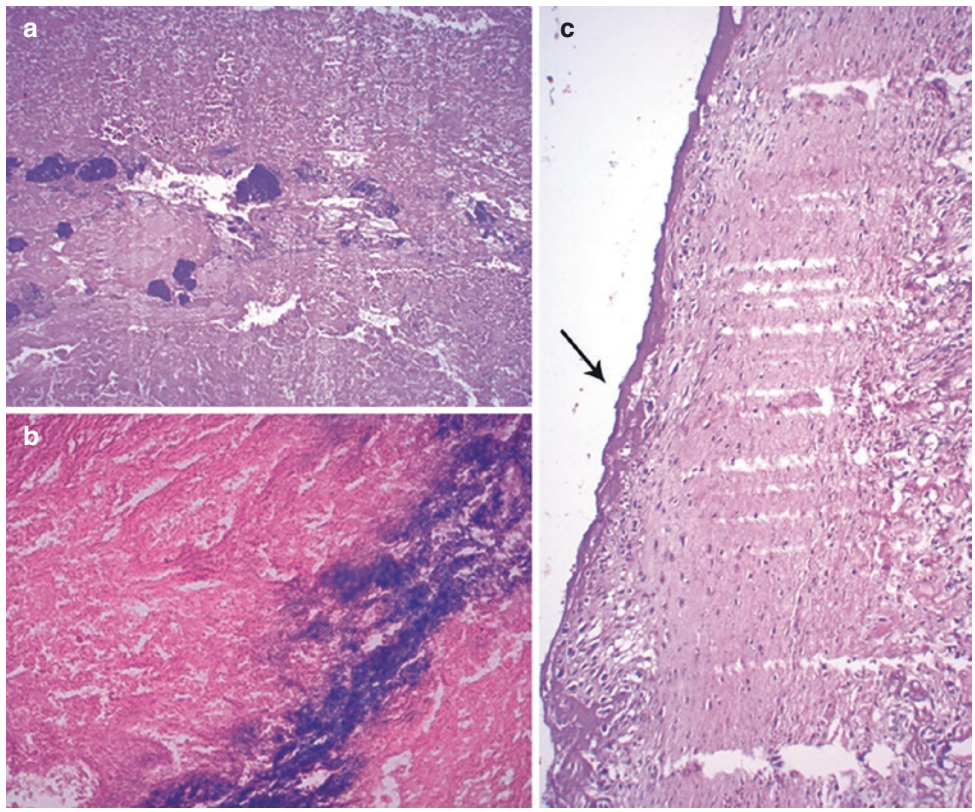

Fig. 17.2 (**a**) Basophilic granular bacterial colonies seen amidst fibrin and platelets (H&E × 100); (**b**) Gram-positive cocci (Modified Gram's stain × 400); (**c**) A layer of fibrin (arrow) lines the left atrial endocardium (H&E × 200)

bus, in which were embedded basophilic coarse Gram-positive bacterial colonies (Fig. 17.2b); the left atrial endocardial granularity was mainly composed by fresh fibrin with few inflammatory cells (Fig. 17.2c). There was no myocarditis or abscesses. The other autopsy findings were: left cerebral, splenic and bilateral renal infarctions with bilateral confluent bronchopneumonia, abscesses, and diffuse alveolar damage.

Cause of Death: Multiorgan failure due to Infective Endocarditis (IE).

17.3 Discussion

In this modern era, improvised diagnostic and therapeutic measures have failed to diminish the importance of IE (See Chap. 16) as a life-threatening condition, which reiterates the observation of Sir William Osler in 1885 ("Few diseases present greater difficulties in the way of diagnosis than malignant endocarditis, difficulties which in many cases are practically insurmountable") even today. Fortunately, it has an infrequent occurrence with a tendency to involve the left-sided valves (mitral valve, followed by aortic valve and followed by multivalvular disease). The infective friable vegetation is created by a series of complex interactions between the injured endocardial surface and the offending pathogen through local hemodynamics, microbial virulence, and host immune and hemostatic mechanisms. In most cases, the targets have been injured valvular or mural endocardia in rheumatic or nonrheumatic valvular heart diseases (depending on the geographic locations) and congenital cardiac anomalies. However, now there is an increasing trend of involvement of normal native valves, to the extent of 30% of the cases, as community acquired or health-care-associated IE (HCAIE), seen particularly in the developed countries but also poised to make an appearance in the low—and middle-income countries as well. HCAIE, often seen as a fallout of extensive diagnostic and/or therapeutic strategies, develops during the hospital stay (nosocomial) or is acquired from out-of-hospital health-care contact (non-nosocomial). This has introduced a distinct shift in the predisposing factors, patient demographics, and microbial spectrum of IE.

The young man in this case, with a history of hospitalization for head injury, developed IE of the normal mitral valve and mural left atrial endocardium and the histology revealed large numbers of Gram-positive cocci on special stain. The prevailing circumstances suggest the possibility of a non-nosocomial HCAIE. The common Gram-positive cocci producing left-sided IE are *Staphylococcus aureus* (*S. aureus)* viridians group streptococci, coagulase-negative *Staphylococcus* species, *Enterococcus* species, and other streptococcal species. Many among them are capable of infecting morphologically normal appearing valves or possess an inherent capacity of adherence to the endocardium or even platelets via certain specific cell wall proteins. The symptoms and signs of the patient in IE arise due to effects related to valvular and/or paravalvular destruction or local/systemic manifestations of vascular septic embolization, metastatic infection, and immunological phenomenon. The brief hospital stint, mitral valvular involvement, and extensive systemic embolization would probably suggest *S. aureus* as the etiologic agent. The blood culture was negative in the present case, a finding in 10–20% of the patients, and is explained by previous antibiotic therapy. Embolic phenomena are identified in almost half the patients with IE and a significant proportion among them (20–30%) develop neurological deficits, as was present in our case. They are related to large, globular, mobile vegetations, particularly located over the anterior mitral leaflet often caused by *S. aureus* in younger patients. Moreover, cerebrovascular embolic complications can also be seen on imaging even in those patients who do not have central nervous system symptoms. The embolic events may also involve other organs (kidneys and spleen in this case), but these are said to play a little role in the final outcome of the IE.

IE results in a heterogeneity of clinical presentations that range from nonspecific or constitutional symptoms (e.g. fever, malaise, dyspnea, arthralgia, or weight loss) in a relatively stable

patient to a more serious presentation of multiorgan failure or sepsis. Several 'text-book' features of IE may not always be seen and this could lead to delayed diagnosis and administration of appropriate therapy. Besides, the classic features of fever and cardiac murmur are present in 90% and 75% of patients, respectively. The diagnosis depends not only on detailed clinical assessment, but also leans heavily on microbiological investigations and imaging studies, which forms the basis of the modified Duke's criteria for definitive or possible diagnosis of IE. Thus, a multidisciplinary approach (IE heart team) involving the cardiologist, neurologist, microbiologist, infectious disease specialist, cardiovascular surgeon, and pathologist would be ideal for dealing with this ominous malady. IE was unfortunately not diagnosed in the case presented and hence a clinical suspicion and judgment would definitively prevail over the application of the Duke's criteria.

Further Reading

Ambrosioni J, Hernandez-Meneses M, Téllez A, Pericàs J, Falces C, Tolosana JM, et al. The changing epidemiology of infective endocarditis in the twenty-first century. Curr Infect Dis Rep. 2017;19:21.

Chambers HF, Bayer AS. Native valve infective endocarditis. N Engl J Med. 2020;383:567–76.

Hu W, Wang X, Su G. Infective endocarditis complicated by embolic events: pathogenesis and predictors. Clin Cardiol. 2021;44:307–15.

Hubers SA, DeSimone DC, Gersh BJ, Anavekar NS. Infective endocarditis: a contemporary review. Mayo Clin Proc. 2020;95:982–97.

Liesenborghs L, Meyers S, Vanassche T, Verhamme P. Coagulation: at the heart of infective endocarditis. J Thromb Haemost. 2020;18:995–1008.

Parra JA, Hernández L, Muñoz P, Blanco G, Rodríguez-Álvarez R, Vilar DR, et al. Detection of spleen, kidney and liver infarcts by abdominal computed tomography does not affect the outcome in patients with left-side infective endocarditis. Medicine. 2018;97:33.

Song JK. Infective endocarditis involving an apparently structurally normal valve: new epidemiological trend? Korean J Intern Med. 2015;30:434–42.

Sunil M, Hieu HQ, Singh RSA, Ponnampalavanar S, Siew KSW, Loch A. Evolving trends in IE in a developing country: a consequence of medical progress? Ann Clin Microbiol Antimicrob. 2019;18:43.

Vlasselaer AV, Rasmussen M, Nilsson J, Olaison L, Ragnarsson S. Native aortic versus mitral valve infective endocarditis: a nationwide registry. Open Heart. 2019;6(1):e000926.

Vogkou CT, Vlachogiannis NI, Palaiodimos L, Kousoulis AA. The causative agents in infective endocarditis: a systematic review comprising 33, 214 cases. Eur J Clin Microbiol Infect Dis. 2016;35:1227–45.

Wang A, Gaca JG, Chu VH. Management considerations in infective endocarditis: a review. JAMA. 2018;320:72–83.

18 Primary Botryomycotic Left-Sided Infective Endocarditis

Pradeep Vaideeswar and Sakshi Jain

18.1 Clinical History

A 65-year-old male, a known hypertensive and diabetic, presented with class II dyspnea with orthopnea and paroxysmal nocturnal dyspnea for the past 1 week. There had been no history of accompanying fever, cough, or pedal edema. On general examination, his pulse was 108 per minute and blood pressure was 150/90 mmHg. The heart sounds were well-heard. There were bilateral coarse crepitations. The clinical impression was heart failure and it was decided to treat him accordingly. But he sustained a sudden cardiac arrest and expired within 24 min of admission. No investigations had been performed.

18.2 Autopsy Findings

The heart was markedly enlarged in size (470 g) with moderate enlargement of all the chambers. There was mild increase in the epicardial fat with milk patches over the posterior surface of the right ventricle. The arch and the entire thoracoabdominal portion of the aorta showed multiple calcified and focally ulcerated atherosclerotic plaques; there were no thrombi. The right dominant coronary artery and all the other epicardial arteries were only mildly atherosclerotic with mild focal calcification. On opening the heart, the aortic annulus was dilated. The noncoronary and the left coronary (LCC) cusps were covered by friable, red brown vegetations, 1.0 × 0.8 × 0.8 cm and 1.5 × 1.5 × 1.0 cm, respectively (Fig. 18.1a). The LCC vegetation was associated with a small aneurismal outpouching at the intervalvular fibrosa as well as a little larger outpouching over the basal aspect of the anterior mitral leaflet (AML, Fig. 18.1a). The right coronary cusp showed rolling of its free margin (Fig. 18.1a) with fine granular fibrinous deposits. The aneurysm over the AML measured 2 cm across and on the flow surface was also covered by granular brown vegetations (Fig. 18.1b). The vegetations on histology (Fig. 18.2) showed large colonies of Gram-positive bacterial colonies surrounded by acellular thick bands of eosinophilic fibrinous material, which were in turn surrounded by neutrophils and other inflammatory cells. There was no myocarditis or abscess formation. The lungs revealed diffuse alveolar damage and edema. Other organs were normal; there were no changes of diabetic nephropathy.

Cause of Death: Left-sided infective endocarditis (IE) and congestive cardiac failure.

P. Vaideeswar (✉)
Department of Pathology (Cardiovascular and Thoracic Division), Seth Gordhandas Sunderdas Medical College and King Edward Memorial Hospital, Mumbai, India

S. Jain
Seth Gordhandas Sunderdas Medical College and King Edward Memorial Hospital, Mumbai, India

P. Vaideeswar (ed.), *Tropical Cardiovascular Pathology*,
https://doi.org/10.1007/978-981-19-3720-0_18

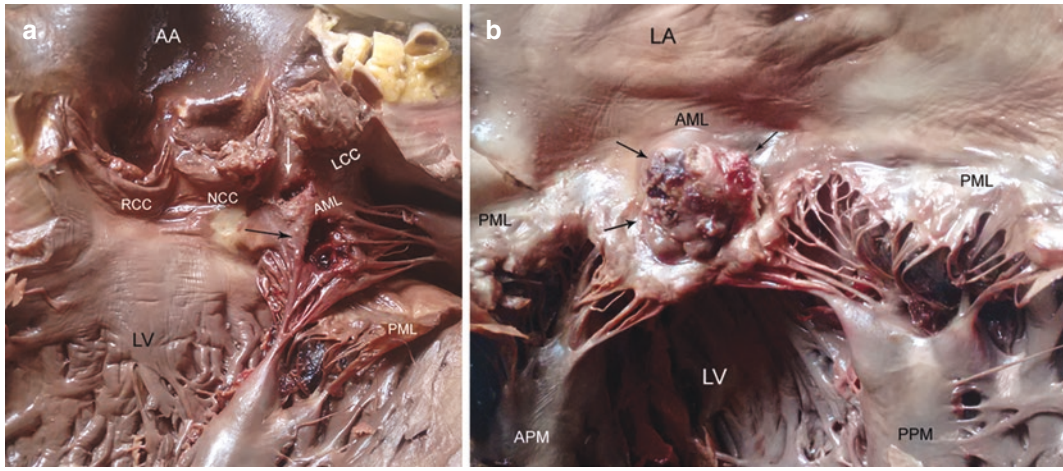

Fig. 18.1 (**a**) The left LCC and non-NCC coronary cusps are covered by firm and friable brown vegetations. Note openings of the aneurysm of the mitral-aortic intervalvular fibrosa (white arrow) and anterior mitral leaflet AML (black arrow). The free margin of the right coronary cusp RCC shows rolling indicating valvular incompetence; (**b**) Smaller vegetations (arrows) are also seen over the AML aneurysm (*AA* ascending aorta, *APM* anterior papillary muscle, *LA* left atrium, *LV* left ventricle, *PML* posterior mitral leaflet, *PPM* posterior papillary muscle)

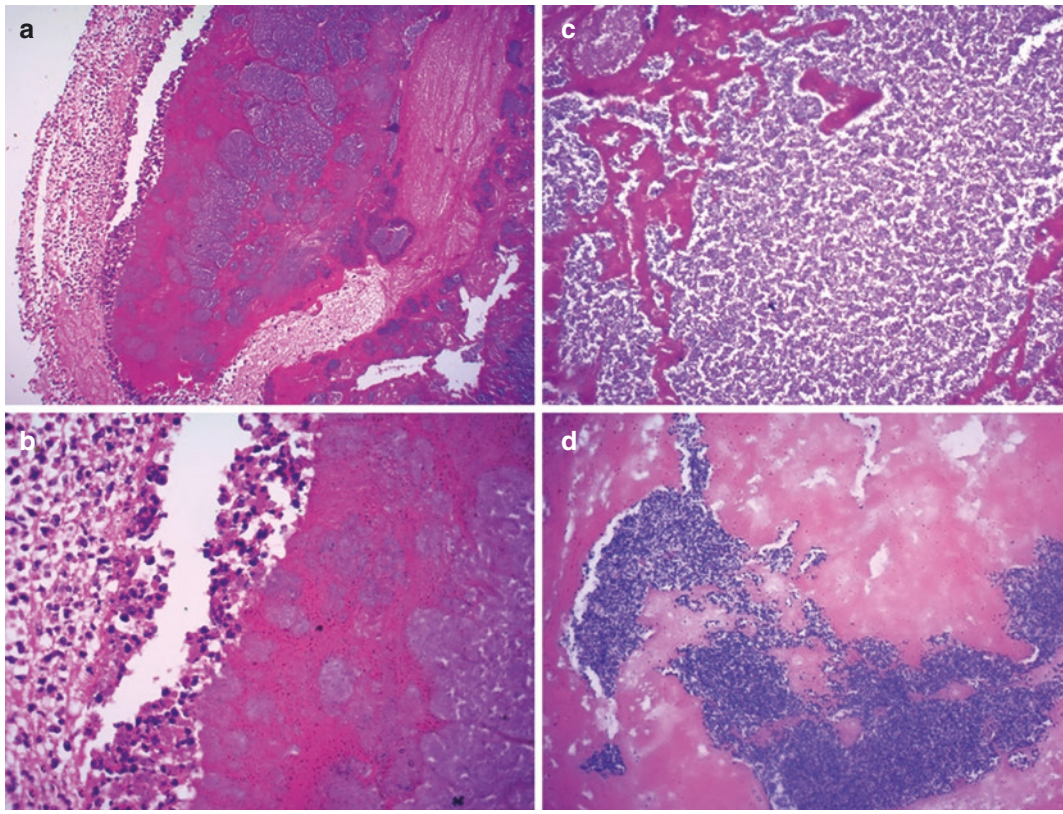

Fig. 18.2 Basophilic clumps of bacteria surrounded by a thick dark pink acellular material, the Splendore-Hoeppli phenomenon (**a**) H&E × 100 and (**b**) H&E × 200. The effect is like a bunch of grapes (*botryos*); (**c**) The bacteria are separated by bands of eosinophilic material (H&E × 400); (**d**) Gram-positive cocci (Modified Gram stain × 400)

18.3 Discussion

An elderly gentleman in his sixth decade with comorbid conditions, who presented with congestive cardiac failure to the emergency services department, was found to have IE of a normal aortic valve at autopsy. IE is notorious for its dreaded clinical course, which entails prolonged hospitalization and/or surgical intervention, and may also affect the quality of life at a later stage. Despite modern innovations in diagnostic methods and therapeutic measures, the incidence of IE refuses to abate. Modern medicine has, unfortunately, paved way for new avenues for disease occurrence, changing the risks factors, type of organisms involved, and hence the epidemiology. Currently, IE can no longer be viewed as an infection of the young or middle-aged afflicted by rheumatic or congenital heart diseases and caused by the host commensals. Furthermore, it cannot always be classified into the traditional acute or sub-acute forms. Instead, it is seen to increasingly affect older individuals with age-related valvular changes or life-style-related diseases. Advancing age is often associated with poor dentition, diabetes mellitus, renal dysfunction, blunted immunity, and cancer that require prolonged medications or hospitalizations. The organisms too are more virulent with increased antibiotic resistance. The classification systems are thus now directed to differentiate between native/prosthetic material IE and community-acquired/health-care-associated IE. Our patient was a chronic diabetic on irregular therapy; there was no history of any health-care contact in the near past. The oral cavity was not examined at autopsy.

The IE was left-sided but predominantly affected the aortic valve, which is the commonest normal native valve to be affected in IE and often associated with 'kiss' or satellite lesions over the mitral valve. This manifested in our patient as synchronous aneurysms of the mitral-aortic intervalvular fibrosa (an avascular fibrous curtain connecting the anterior mitral leaflet to the left half of the noncoronary cusp and adjacent one third of the left coronary cusp) and anterior mitral leaflet. The organisms isolated in the elderly IE patients are usually coagulase-negative staphylococci, enterococci, and *Streptococcus bovis*. Apart from blood cultures, the pathogens can also be identified by immunohistochemical staining and polymerase chain reactions in tissues. We could only identify the microbes within the vegetations as Gram-positive cocci. Very interestingly, the arrangement of the bacteria had a classic morphology of botryomycotic granules.

Botryomycosis is an example of a chronic pyogranulomatous inflammation caused by several bacterial genera, where the causative organisms form grape-like (*botryos*) aggregates and are in turn surrounded by a thick cuff of eosinophilic material, which simulates the grains formed in fungal mycetomas (*mycosis*). The material, Splendore-Hoeppli phenomenon, is composed of fibrin admixed with antigen-antibody complexes and tissue debris and effectively wards off further phagocytosis and destruction of the microbes. One also wonders if it can result in culture-negative IE. Among the 2 types, cutaneous botryomycosis (about 75% of the cases) is more common than the visceral type. The common organs affected in visceral botryomycosis are lungs, liver, and kidneys; other organs like the heart are more rarely affected. The involvement may be primary or secondary, when there is spread from an initial skin involvement. IE and myocardial abscesses are the cardiac manifestations; our case showed only IE (primary visceral disease) and hence possibly caused by endogenous bacteria. The causative organisms may be Gram-positive cocci such as *S. aureus*, coagulase-negative staphylococci, and *Streptococcus* species or Gram-negative bacilli like *Pseudomonas aeruginosa*, *Escherichia coli,* and *Proteus* species. The pathogenesis is still not clear, but immunological abnormalities related to low T-cell population and impaired neutrophil/macrophage function (as seen in diabetes mellitus) are implicated.

By and large, the clinical attributes of IE include an acute febrile illness with changing cardiac murmurs and features of systemic embolization, and hence the clinical diagnosis is based on the summation of multiple findings. It also has nonspecific, atypical, and variable presentations that could lead to delays or errors in diagnosis,

particularly in emergency situations and in the elderly population. The older patients tend to have nonspecific symptoms such as fatigue, malaise, anorexia, weight loss, and even confusion. Fever is usually absent. Development of heart failure, an important manifestation in them, is a consequence of valvular dysfunction that is more commonly associated with the more invasive aortic valvular IE, as compared to mitral valvular IE, which is more prone to embolic episodes. Though destruction of the aortic valve was not seen in the present case, the heart failure (seen in 70% of the cases with IE) can be explained on the basis of valvular incompetence leading to left ventricular decompensation. Nevertheless, even after diagnosis of IE, medical and surgical options may be limited due to attendant comorbidities.

Further Reading

Ambrosioni J, Hernandez-Meneses M, Téllez A, Pericàs J, Falces C, Tolosana JM, et al. The changing epidemiology of infective endocarditis in the twenty-first century. Curr Infect Dis Rep. 2017;19:21.

Bohbot Y, Peugnet F, Lieu A, Carbone A, Mouhat B, Philip M, et al. Characteristics and prognosis of patients with left-sided native bivalvular infective endocarditis. Can J Cardiol. 2021;37:292–9.

Gupta K, Das A, Radotra BD, Bhalla A. Cardiac botryomycosis: an autopsy report. J Clin Pathol. 2008;61:972–4.

Hubers SA, DeSimone DC, Gersh BJ, Anavekar NS. Infective endocarditis: a contemporary review. Mayo Clin Proc. 2020;95:982–97.

Long B, Koyfman A. Infectious endocarditis: an update for emergency clinicians. Am J Emerg Med. 2018;36:1686–92.

Padilla-Desgarennes C, Vázquez-González D, Bonifaz A. Botryomycosis. Clin Dermatol. 2012;30:397–402.

Ursi MP, Mangoni ED, Rajani R, Hancock J, Chambers JB, Prendergast B. Infective endocarditis in the elderly: diagnostic and treatment options. Drugs Aging. 2019;36:115–24.

Vlasselaer AV, Rasmussen M, Nilsson J, Olaison L, Ragnarsson S. Native aortic versus mitral valve infective endocarditis: a nationwide registry. Open Heart. 2019;6:e000926.

Yang E, Frazee BW. Infective endocarditis. Emerg Med Clin North Am. 2018;36:645–63.

19 Fungal Endocarditis of Normal Native Mitral Valve in a Renal Transplant Recipient

Gwendolyn Fernandes and Pradeep Vaideeswar

19.1 Clinical History

A 48-year-old renal transplant recipient presented in the 8th month after transplantation with: high-grade fever for 2 weeks, dry cough with breathlessness for 10 days, and slurring of speech and swaying while walking for the last 3 days. He was a known diabetic and hypertensive, which had led to chronic kidney disease. He was on maintenance hemodialysis for 6 years, before receiving a cadaveric donor transplant 1 year ago. Posttransplantation, the immediate graft function was good (baseline creatinine 1.6–1.7 mg/dL) and he was started on triple immunosuppression, comprising tacrolimus, mycophenolate mofetil, and prednisolone.

On examination, he was hemodynamically stable. There was pallor, slurred speech, and ataxic gait. The laboratory investigations revealed: Hb 8.7 g/dL, total leukocyte count 4320/cmm, absolute neutrophil count 1680/cmm, creatinine 1.75 mg/dL, and C-reactive protein level of 234.5 mg/L. Chest radiography showed midzonal haziness in the left lung. High-resolution computed tomography of the chest showed ill-defined, ground-glass, centrilobular, and nodular opacities, which was suspicious of fungal infection (Fig. 19.1a). Magnetic resonance imaging of the brain showed multiple peripheral ring-enhancing lesions in both cerebral hemispheres suggestive of invasive fungal infection (Fig. 19.1b). Bronchoalveolar lavage did not show any Gram stained organisms or acid-fast bacilli, but the galactomannan level was elevated (optical density index of more than 1.0), which suggested

G. Fernandes
Department of Pathology, Seth Gordhandas Sunderdas Medical College and King Edward Memorial Hospital, Mumbai, India

P. Vaideeswar (✉)
Department of Pathology (Cardiovascular and Thoracic Division), Seth Gordhandas Sunderdas Medical College and King Edward Memorial Hospital, Mumbai, India

P. Vaideeswar (ed.), *Tropical Cardiovascular Pathology*,
https://doi.org/10.1007/978-981-19-3720-0_19

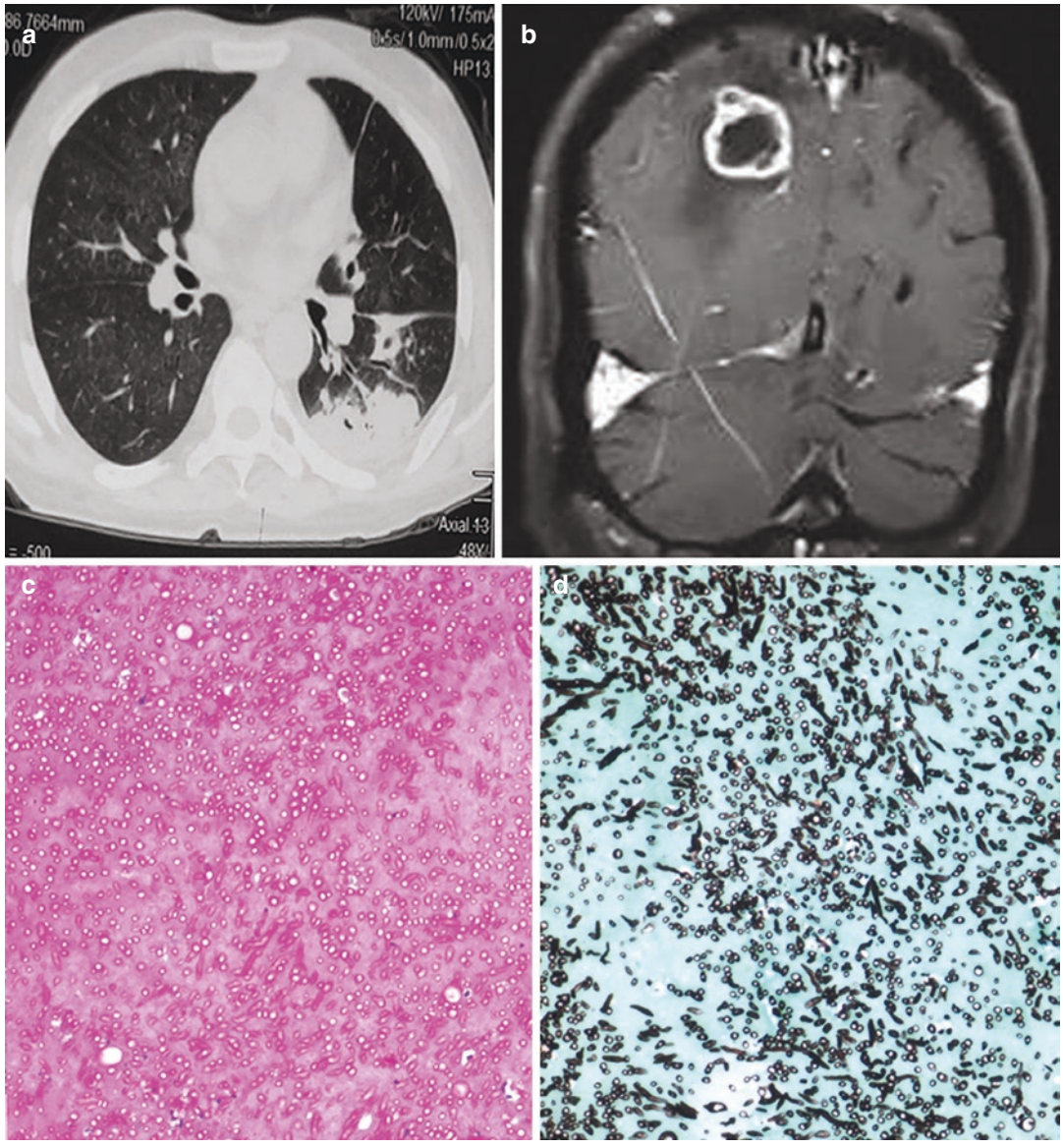

Fig. 19.1 (**a**) Arrow points to the ill-defined nodular opacities in the chest tomograms; (**b**) Magnetic resonance imaging, brain showing peripheral ring-enhancing lesions (arrow); histology of the embolectomy showing hyphal forms suggestive of *Aspergillus* species (**c**) H&E × 200 and (**d**) Gomori methenamine silver × 200

invasive pulmonary aspergillosis. Gene-Xpert molecular test for tuberculosis and cytomegalovirus load test were negative. The immunosuppression was reduced and the patient was started on antifungal drugs (voriconazole and itraconazole).

In the posttransplantation nineth month, the patient developed cough with expectoration and 1–2 cm sized nodules on his right eyebrow and left lateral malleolus. Microbiological analysis was suggestive of *Nocardia* species. The patient was treated with cotrimoxazole, which was later stopped in view of the leukopenia and minocycline was used. Three more nodules developed on his scalp and shin in spite of 3 weeks of treatment. The culture of one of the nodules revealed *Aspergillus nidulans*. The patient was then given liposomal amphotericin B and intravenous immunoglobulin. Then the patient developed swelling of the right elbow joint followed by the left knee joint. An ultrasonography of the joints showed localized fluid collections, which were conservatively managed. Repeat blood cultures were negative. The patient was treated with piperacillin-tazobactam, cotrimoxazole, and amphotericin B. In the 10th month posttransplantation, the patient developed vitreitis/endophthalmitis and intravitreal injections of voriconazole were given. Following this, there was no fever, breathlessness, or development of new skin nodules. The patient requested for a discharge. He discharged after a ward stay of two and half months on voriconazole and minocycline.

Three days later, the patient was readmitted with a 2-day history of anuria and pain in the right lower limb. The laboratory investigations showed hemoglobin 6.9 g/dL, total leukocyte count 17,120/cmm, platelets 90,000/cmm, creatinine 4 mg/dL, and prothrombin time 74.6 s (control 13.4 s). Doppler ultrasound examination showed complete thrombosis of the common iliac artery with no flow in the transplanted kidney (the renal artery of the transplanted kidney had been anastomosed to the right external iliac artery); there was no evidence of renal vein thrombosis. Right femoral artery embolectomy was done and was received as grey-brown tissue bits (2 × 0.5 cm and 1.6 × 1 cm) and showed fresh thrombi with septate fungal hyphae, suggestive of *Aspergillus* species (Fig. 19.1c, d); culture grew *Aspergillus fumigatus*. However, the patient continued to remain anuric with poor arterial flow in the transplanted kidney and hemodialysis was started; treatment with antifungals continued. A fortnight later, the patient developed thrombosis of the left radial artery along its entire course and had a rapid downhill course.

19.2 Autopsy Findings

The external examination showed a poorly nourished male with edema and dusky discoloration of the left upper limb. Few ulcers and papulo-nodular lesions (0.2–1.5 cm) were seen on the face (Fig. 19.2a) and neck. The heart (320 g) was mildly enlarged in size with moderate enlargement of the left ventricle. Transverse section through the midportion of the ventricular myocardium revealed mild concentric left ventricular (LV) hypertrophy with multiple small foci of congestion and a prominent hemorrhagic focus in the posterior papillary muscle (PPM). The right coronary artery had a dominant distribution; all the arteries were mildly atherosclerotic with no significant narrowing. Few ulcerated atherosclerotic plaques were seen in the arch and descending thoracic aorta. Examination of the right side of the heart showed a patent foramen ovale. Remarkable findings were seen on the left side. The left atrial (LA) endocardium at and above the posterior

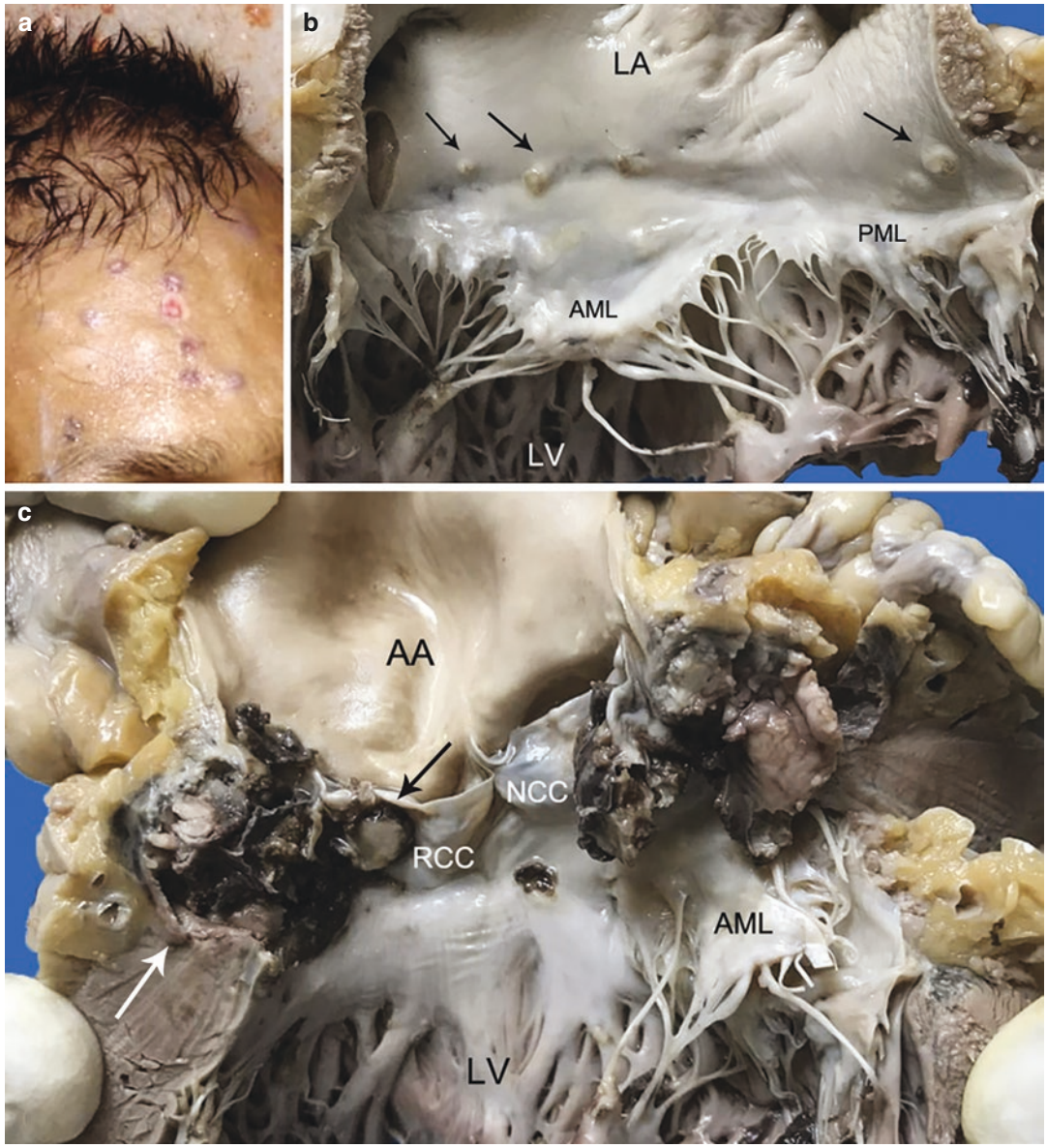

Fig. 19.2 (**a**) Small ulcers and papulo-nodular lesions on the forehead; (**b**) Left atrial LA endocardial granular papular lesions (arrows), situated above the mitral annulus; the valve itself is normal; (**c**) Large vegetation completely covering the left coronary cusp and producing a root abscess (white arrow). Flattened vegetation (black arrow) over the right coronary cusps RCC (*AA* ascending aorta, *AML* anterior mitral leaflet, *LV* left ventricle, *PML* posterior mitral leaflet)

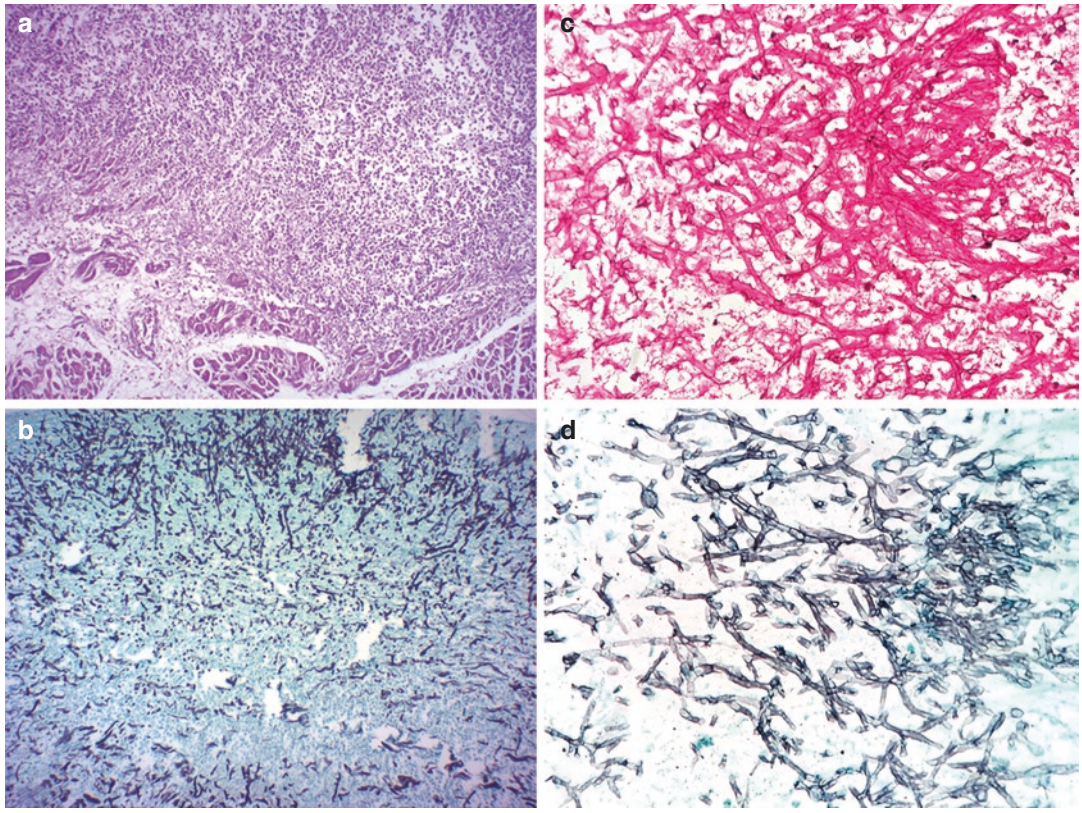

Fig. 19.3 (**a**) Left atrial mural endocarditis with large numbers of neutrophils (H&E × 200); (**b**) The Gomori methenamine silver GMS stain highlights the large number of fungal elements (× 200); The superficial aspect of the aortic valvular vegetation showed only a mass of hyphal forms (**c**) H&E × 400 and (**d**) GMS × 400

mitral annulus showed a cluster of soft papular lesions (Fig. 19.2b). The mitral valve leaflets were myxomatous, but did not show any vegetation. The left coronary cusp of the aortic valve (AV, Fig. 19.2c) was completely destroyed by large friable red-brown vegetation filling its sinus and eroding through the annulus into the subjacent myocardium to produce an annular abscess. Smaller plaque-like vegetation was present over the right coronary cusp. On histology, the papular lesions over the LA represented mural endocarditis with large colonies of septate slender fungal hyphae with fibrin and few neutrophils (Fig. 19.3a, b). The superficial aspect of the AV vegetation was entirely composed of hyphal tangles (Fig. 19.3c, d). There were fungal abscesses distributed all over the myocardium, including the PPM (Fig. 19.4) in the areas which had been macroscopically identified as congested foci. The ulceration of some of the atherosclerotic plaques had been produced by fungal panaortitis.

Multifocal fibro-caseous lesions were seen in the lungs; no infective pathology or diffuse alveolar damage was present. There was fungal meningitis with septic infarcts in the brain (Fig. 19.5a, b) and spleen, and fungal abscesses in the prostate. The native kidneys showed end-stage changes, while the transplanted kidney showed extensive cortical necroses (Fig. 19.5c) with few micro-abscesses.

Cause of Death: Fungal septicaemia.

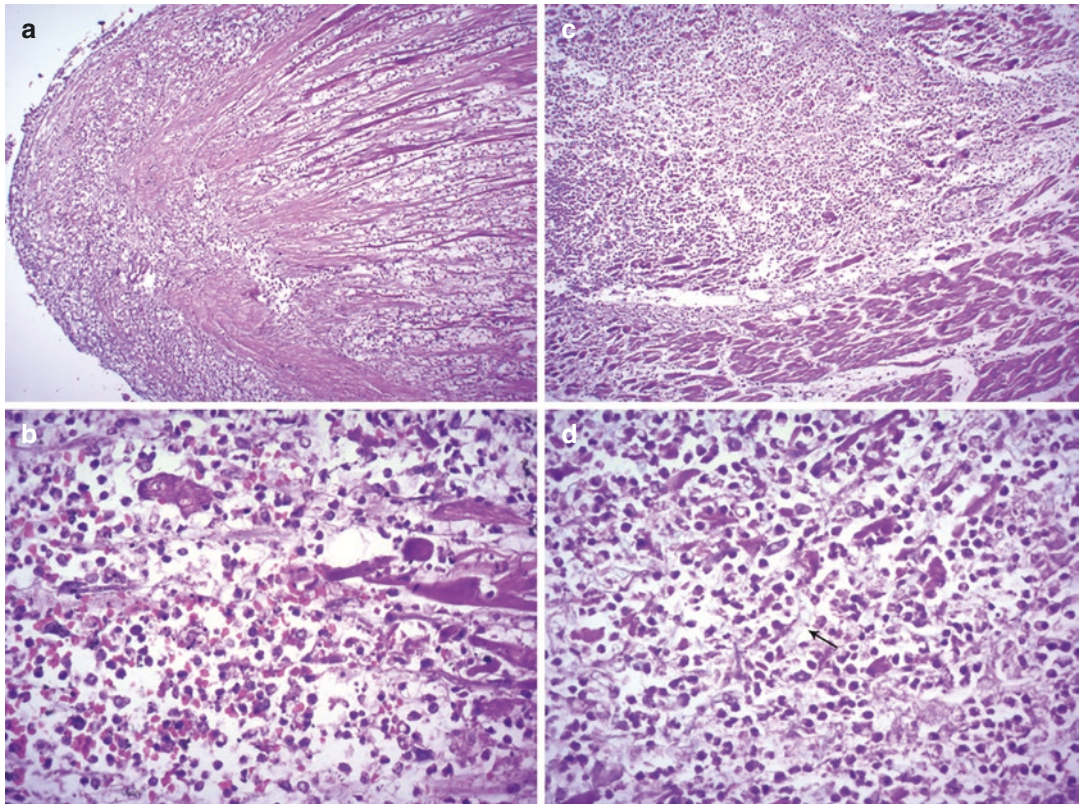

Fig. 19.4 Papillary muscle (**a**) Endocarditis (H&E × 200) and (**b**) Destruction with necrotic cardiomyocytes and abundant neutrophils (H&E × 400); Left ventricular myocardial abscess (**c**) H&E × 200, with (**d**) Swollen (arrow) septate hyphal forms (H&E × 400)

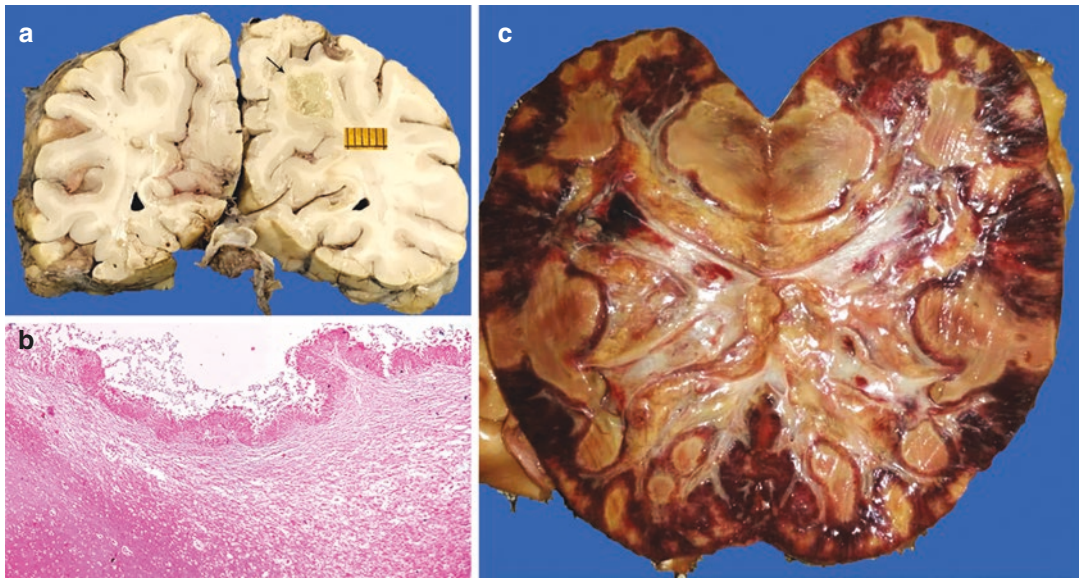

Fig. 19.5 (**a**) Coronal slice of the cerebral hemisphere with a focus of necrosis (arrow); (**b**) Focus of necrosis which is infiltrated by fungal hyphae (H&E × 200); (**c**) Bisected donor kidney revealing extensive cortical necroses

19.3 Discussion

Eight months posttransplant, this 45-year-old male patient developed multiorgan infection by both bacteria and fungi that progressively worsened despite appropriate therapeutic measures to culminate as a fatal disseminated fungal infection. The cause for the rapid dissemination was fungal infective endocarditis (FIE) and the organism was *A. fumigatus*. A severe opportunistic infection, FIE, constitutes about 1–10% of all cases of IE. It affects the native valvular or mural endocardium, vascular endothelium, prosthetic valves, and intracardiac or intravascular devices, producing bulky vegetations and invasive disease. It is a bane to the treating clinician due to difficulties in establishing the diagnosis and selecting appropriate treatment modalities, with resultant high mortality rate; many of the cases are diagnosed at autopsy, as seen in this case. The commonly identified fungal elements belong to the *Candida* (usually common in pediatric population) or *Aspergillus* (usually common in adults) species. FIE of native tissues is frequently seen in intravenous drug abusers, patients with prolonged hospital stay (where prolonged often broad-spectrum antibiotic therapy, central venous catheterization, and parenteral nutrition are necessary), extensive surgery, and immunocompromised/immunosuppressed states.

Solid-organ transplantation (SOT) is a well established option in patients suffering from end-organ damage and is frequently carried out in chronic kidney, hepatic, cardiac, and pulmonary diseases. Immunosuppressive therapy and frequent interventions render these patients susceptible to infections in general. Fungal infections account for 5% of all infections in renal transplant recipients, majority occurring within 180 days after transplantation. The agents may differ in different geographic locations. In North America, invasive candidiasis (little over 50%) was the most frequent, followed by invasive aspergillosis (about 20%), while in an Indian study, it was zygomycosis (about 30%) and aspergillosis (about 25%). The clinical course in this kidney transplant recipient showed a gamut of infections ranging from *Nocardia*, *Aspergillus nidulans,* and terminal *Aspergillus fumigatus*. At autopsy, no nocardiosis was identified in the lungs.

Among infections in SOT patients, IE constitutes 1–2% and most episodes are caused by bacteria (*S. aureus* in 60% of the cases). As compared to IE in the general population, in SOT patients there is a lower male predominance, involvement of younger patients, absence of any structural cardiac defects, and isolation of a wide range of organisms. The common sites for the vegetations are the mitral valve, mural endocardium, and aortic valve. Importantly, FIE is invariably caused by the *Aspergillus* species. *Aspergillus* is a ubiquitous, saprophytic fungus and an opportunistic pathogen in immunosuppressed individuals. Many of these patients develop invasive pulmonary aspergillosis. Major species of *Aspergillus* are *A. fumigatus*, *A. flavus*, *A. niger*, *A. terrus,* and *A. nidulans*; 2 among them were cultured in our case. *Aspergillus* has special affinity for blood vessels, and angioinvasion is an important characteristic of invasive aspergillosis, leading to ischemia, infarcts, and necrosis. Literature reveals that *Aspergillus* accounts for 24–28% of FIE, and 0.25–2.5% of all IE cases. Herein, the aortic valve was affected with an annular abscess and mural left atrial endocarditis, along with local (fungal abscesses in the myocardium) and systemic embolic dissemination. Surprisingly, the lungs were spared.

The clinical presentation of FIE is no different from bacterial IE, but aspergillus IE is frequently associated with absence of fever, hemorrhagic black cutaneous lesions, endophthalmitis, acute limb ischemia, and aortic root abscess or even aortic pseudoaneurysm, all of which were present

in the case presented. A high index of suspicion is the key for early diagnosis, which may be facilitated by utilization of nonculture based diagnostic tests such as detection of fungal antigens in body fluids, polymerase chain reactions, and next-generation sequencing. In general, FIE is a disease of high mortality (close to 50%); yet, timely administration of a combination of antifungal therapy and surgical intervention may salvage the patient.

Further Reading

Agmon IN, Goldberg E, Cohen E, Krause I. Infective endocarditis in the setting of renal transplantation: case report and review of the literature. Transpl Infect Dis. 2017;19:e12786.

Fishman JA. Infection in organ transplantation. Am J Transplant. 2017;17:856–79.

Gupta KL, Bagai S, Ramachandran R, Kumar V, Rathi M, Kohli HS, et al. Fungal infection in post-renal transplant patient: single-center experience. Indian J Pathol Microbiol. 2020;63:587–92.

Ioannou P, Papakitsou I, Kofteridis DP. Fungal endocarditis in transplant recipients: a systematic review. Mycoses. 2020;63:952–63.

Kabir V, Maertens J, Kuypers D. Fungal infections in solid organ transplantation: an update on diagnosis and treatment. Transplant Rev (Orlando). 2019;33:77–86.

Martínez-Sellés M, Valerio-Minero M, Fariñas MC, Rodríguez-Abella H, Rodríguez ML, de Alarcón A, et al. Infective endocarditis in patients with solid organ transplantation. A nationwide descriptive study. Eur J Intern Med. 2021;87:59–65.

Meshaal MS, Labib D, Said K, Hosny M, Hassan M, Abd Al Aziz S, et al. Aspergillus endocarditis: diagnostic criteria and predictors of outcome, a retrospective cohort study. PLoS One. 2018;13:e0201459.

Pasha AK, Lee JZ, Low SW, Desai H, Lee KS, Mohajer MA. Fungal endocarditis: update on diagnosis and management. Am J Med. 2016;129:1037–43.

Right-Sided Infective Endocarditis in a Child

20

Pragati Sathe and Pradeep Vaideeswar

20.1 Clinical History

A one and half year-old male child was admitted with rash and fever of 2 days duration. The child had a significant past history. He was diagnosed as a case of 'familial' Hirschsprung's disease at the age of 8 months. The infant had undergone of series of abdominal surgeries (laparoscopy-assisted transanal endo-rectal pull, gastrojejunostomy, and jejunal resection with end to side jejuno-jejunal anastomosis) in a span of 6 months with multiple blood transfusions, administration of broad spectrum antibiotics, and total parenteral nutrition.

During the current admission, the child was febrile and irritable, but in a fair general condition. The pulse rate was 110 beats per minute and respiratory rate was 28 per minute. On local examination, there was a generalized erythematous rash. There was associated peeling of the skin of fingers, perioral skin, and nape of the neck. The dermatology opinion was a viral exanthema or a drug-induced rash. Investigations revealed Hb 12.2 g/dL, total leukocyte count 15,200/cmm with neutrophilic predominance, and platelet count 85,000/cmm; biochemical estimations were within normal limits. The patient was treated with antipyretics, antihistaminics, and liquid paraffin for local application. Two days later, the chest roentgenogram showed bilateral pulmonary infiltrates and the platelet count dropped to 20,000/cmm. The child received antibiotics, nebulisation, mucolytics, and intravenous fluids. The condition worsened and he had to be intubated. He expired on the fourth day after admission.

P. Sathe
Department of Pathology, Seth Gordhandas Sunderdas Medical College and King Edward Memorial Hospital, Mumbai, India

P. Vaideeswar (✉)
Department of Pathology (Cardiovascular and Thoracic Division), Seth Gordhandas Sunderdas Medical College and King Edward Memorial Hospital, Mumbai, India

P. Vaideeswar (ed.), *Tropical Cardiovascular Pathology*,
https://doi.org/10.1007/978-981-19-3720-0_20

20.2 Autopsy Findings

The heart was normal sized with a weight of 40 g. No exudates were seen on the epicardial surface. Firm yellowish green button-like vegetation 1 × 1 × 0.5 cm was present over the region of the anteroseptal commissure of the tricuspid valve (Fig. 20.1a, b), extending on to the adjacent leaflets and attached tendinous cords. No vegetations or mural thrombi were seen on the other valves or chambers, respectively. The vegetation was composed of fibrin, neutrophils, and large numbers of basophilic granular clumps, representing coccoid bacterial colonies (Fig. 20.1b); these were Gram-positive. There was associated destruction of the leaflet (Fig. 20.2a) with endocarditis (Fig. 20.2b) and microabscesses (Fig. 20.2c) in the subjacent

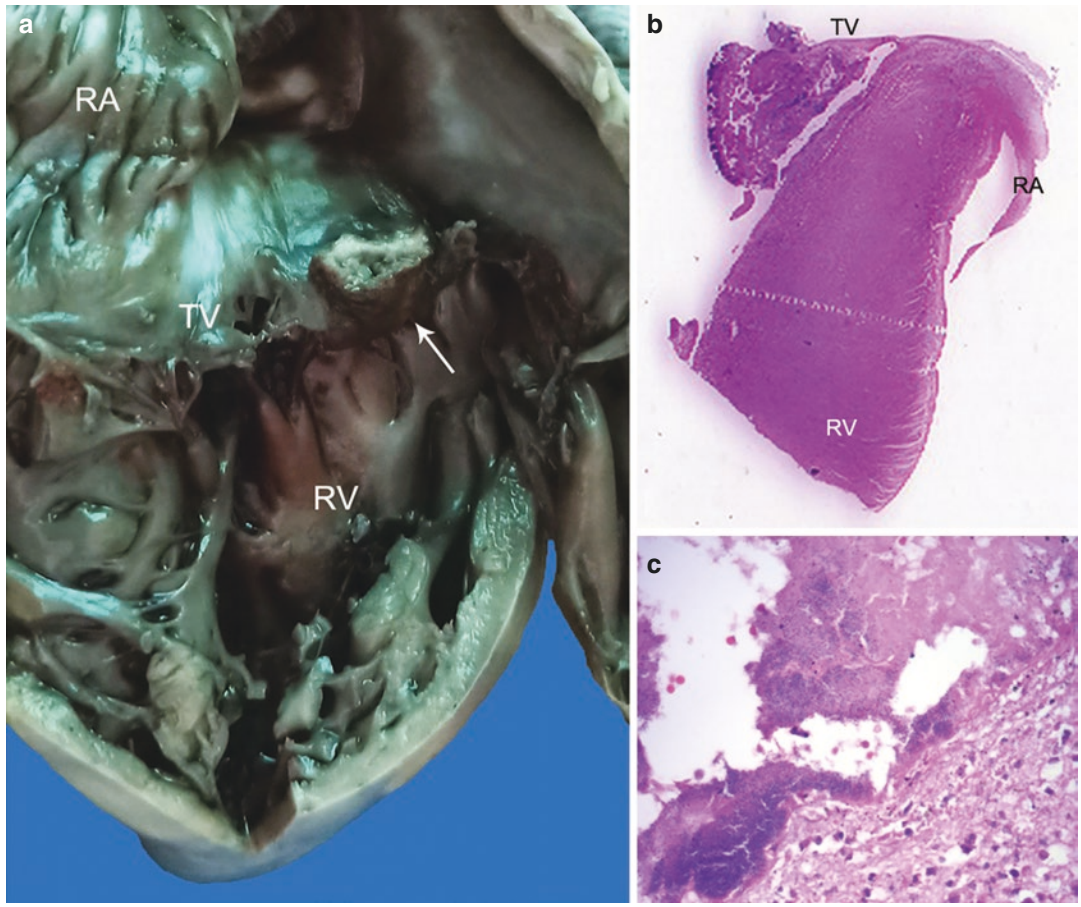

Fig. 20.1 (**a**) Extremely firm dark brown vegetation (arrow) stuck on the anteroseptal commissure; (**b**) Scanned slide (H&E) of the right-sided inflow tract showing destruction of the tricuspid valvular leaflet by vegetation (*RA* right atrium, *RV* right ventricle, *TV* tricuspid valve); (**c**) Basophilic blush produced by the bacterial colonies (H&E × 400)

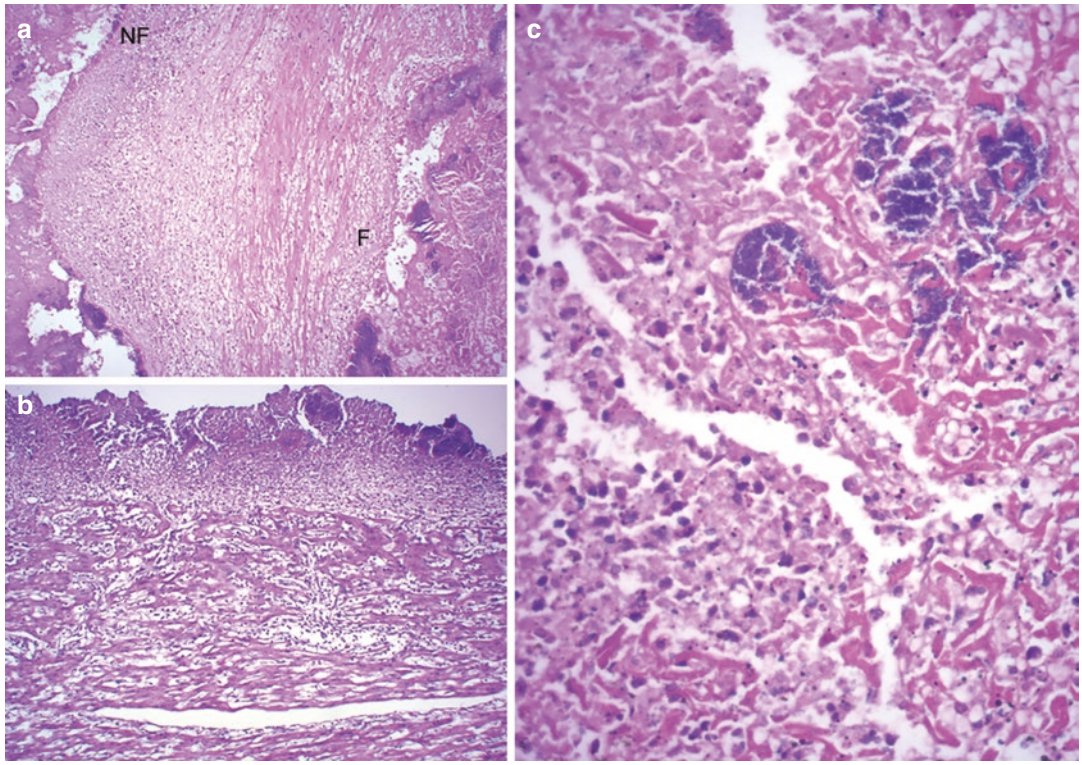

Fig. 20.2 (**a**) Flow F and non-flow NF surfaces of the septal tricuspid leaflet covered with fibrin. Bacterial colonies are seen on the flow surface (H&E × 200); (**b**) Mural endocarditis of the subjacent right ventricle (H&E × 200); (**c**) Micro-abscesses with bacterial colonies in the right ventricular myocardium (H&E × 400)

right ventricular myocardium. The inflammation, in all probability, had also extended into the AV node region. The septic emboli had produced focal necrotizing arteritis with formation of multiple abscesses in the lungs (Fig. 20.3). There was accompanying diffuse alveolar damage, focal hemorrhages, and suppurative pleuritis. Other organs were normal.

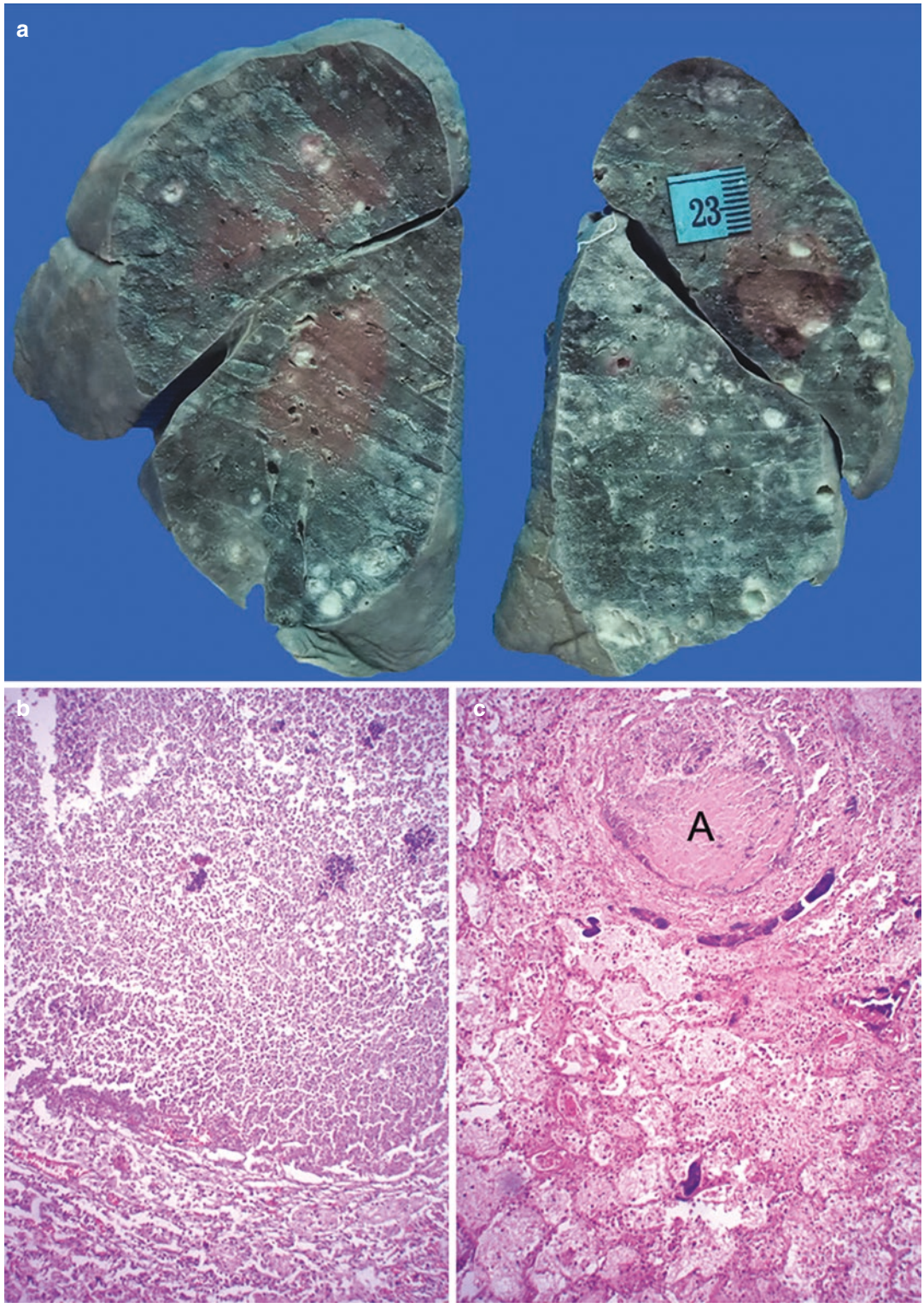

Fig. 20.3 (**a**) Cut surfaces of the both lungs showing intense congestion with multiple abscesses; (**b**) Lung abscess with neutrophils and bacterial colonies (H&E × 200); (**c**) An artery with septic thromboembolus. There is destruction of the arterial wall with focal hemorrhage. There is a cuff of bacteria around the artery (H&E × 200)

20.3 Discussion

This case presents 2 additional facets of infective endocarditis (IE)—involvement of the right side of the heart and its occurrence in a child. Right-sided IE (RSIE) forms a small fraction (5–10%) of all cases of IE, explained on the basis of lower hemodynamic stress on the right side, low oxygen saturation, and a lower prevalence of acquired valvular deformities. Moreover, RSIE has different risk factors, pathogens, clinical presentations, and management strategies. It can occur in isolation or in combination (approximately 13%) with left-sided IE (LSIE). Intravenous drug abusers, patients with implanted cardioverter defibrillators, and patients with congenital malformations (especially after corrective surgery) are more prone to the development of RSIE. But now a rising of RSIE is also seen with increasing use of intravascular catheters. Hence, apart from valvular involvement (tricuspid, pulmonary, or Eustachian valves), infective vegetations can also form over the mural endocardium over the right atrium and ventricle and the interventricular septum. Sepsis, alcoholism, immunodeficiency, and body piercing are the other predisposing factors. The commonest organisms are *S. aureus*, followed by coagulase-negative staphylococci and *Streptococcus* species.

Prolonged hospitalization, multiple gastrointestinal surgeries, and chronic parental nutrition predisposed our pediatric patient to RSIE, with vegetations localized to the tricuspid valve—the commonest site of involvement. The estimated annual incidence of pediatric IE (PIE) ranges from 3.3 per 100,000 per year among infants <1 year old to 0.3 to 0.8 per 100,000 per year in older children and adolescents. The trend of the risk factors is comparable to the adult population, except for a high proportion of congenital heart disease. *Candida* species should also be kept in mind as a possible causative organism particularly in neonates and infants. The organisms seen in our case were Gram-positive on histology; in view of the size of the vegetation, extensive pulmonary pathology and cutaneous manifestations would probably have been a virulent organism like *S. aureus*.

Diagnosis of RSIE is not easy as several features often associated with LSIE are not seen. The problems are accentuated in the absence of a preexisting cardiac condition. Dispersal of fragments of the infective vegetation from the right side of the heart into the pulmonary artery leads to septic pulmonary thromboembolism with subsequent lung consolidation and abscess formation. This occurs in almost 75% of the individuals. A combination of persistent fever and respiratory system involvement is a pointer to the likely presence of RSIE that should alert clinicians particularly when associated with risk factors for this lesion. Sometimes, there is accompanying microscopic hematuria, leading to the triad of a "tricuspid syndrome". Intracardiac invasive disease is seldom seen. Diagnosis of PIE faces similar hurdles as for adult IE (See Chaps. 17 and 18). Most of the cases of RSIE respond to appropriate antibiotic therapy, though surgical intervention may be required with larger vegetations, fungal etiology, or severe tricuspid regurgitation.

This was a rare case of isolated tricuspid valve IE without an underlying cardiac abnormality, complicated by multiple embolic pulmonary abscesses with myocardial micro-abscesses in the adjacent region. Diffuse alveolar damage and sepsis were the terminal events, though extension of the septic focus to the atrioventricular nodal region may have led to arrhythmias.

Further Reading

1. Chahoud J, Yakan AS, Saad H, Kanj SS. Right-sided infective endocarditis and pulmonary infiltrates. An update. Cardiol Rev. 2016;24:230–7.
2. Cox DA, Tani LY. Pediatric infective endocarditis: a clinical update. Pediatr Clin North Am. 2020;67:875–88.
3. Eleyan L, Khan AA, Musollari G, Chandiramani AS, Shaikh S, Salha A, et al. Infective endocarditis in paediatric population. Eur J Pediatr. 2021;180(10):3089–100. https://doi.org/10.1007/s00431-021-04062-7.
4. Shmueli H, Thomas F, Flint N, Setia G, Janjic A, Siegel RJ. Right-sided infective endocarditis 2020: challenges and updates in diagnosis and treatment. J Am Heart Assoc. 2020;9:e017293.
5. Yakut K, Ecevit Z, Tokel NK, Varan B, Ozkan M. Infective endocarditis in childhood: a single-center experience of 18 years. Braz J Cardiovasc Surg. 2020;36(2):172–82. https://doi.org/10.21470/1678-9741-2020-0035.

21 Isolated Pulmonary Valvular Infective Endocarditis in a Univentricular Heart

Heena Desai and Pradeep Vaideeswar

21.1 Clinical History

A 16-year-old adolescent was admitted with a history of low-grade fever on and off for the past 8 days and a symptomatic treatment was given. He was transferred to our institute with the development of altered sensorium. On examination, the general condition was poor with a pulse rate of 120 per minute and blood pressure of 100/70 mmHg. The patient was unconscious and was decerebrating. Examination of the chest revealed a pansystolic murmur and bilateral coarse crepitations. The clinical impression was of septic shock in a case of possibly a valvular heart disease. Investigations were as follows: Hb 15 g/dL, leukocytosis (total count of 19,200/cmm, predominant neutrophils with band forms), thrombocytopenia (count of 60,000/cmm), absent malarial parasites, random blood glucose 72 mg/dL, blood urea nitrogen 26.3 mg/dL, and creatinine 1.4 mg/dL. The ECG showed supraventricular tachycardia, right axis deviation, left ventricular hypertrophy, and inverted Q wave. He expired within 6 h of admission.

21.2 Autopsy Findings

In situ examination revealed abdominal *situs inversus* and broncho-atrial *situs* was *solitus*. In addition, there were 5 splenunculi. The heart was moderately enlarged in size (380 g) and the left-sided rounded apex was formed by a single ventricular chamber (Fig. 21.1). This impression was made since the interventricular septum was not delineated by the left anterior descending artery. The atria were present in their respective positions and had a normal external morphology. There was malposition of the great arteries—the larger ascending aorta was present anteriorly, while the smaller main pulmonary artery was seen as posterior trunk (Fig. 21.1). Below the aortic origin, there was a mound-like projection delineated on either side by coronary vessels (Fig. 21.1). The venous connections were normal.

The right and left atria had a normal internal morphology with the presence of patent foramen ovale. Both the atria lead to a common ventricular chamber through 2 separate atrioventricular valves (double inlet, Fig. 21.2a, b). Both these valves had morphology of the mitral valve, with 2 well-formed groups of papillary muscles, while the single ventricle had the morphology of the left

H. Desai
Department of Pathology, Topiwala National Medical College and BYL Nair Charitable Hospital, Mumbai, India

P. Vaideeswar (✉)
Department of Pathology (Cardiovascular and Thoracic Division), Seth Gordhandas Sunderdas Medical College and King Edward Memorial Hospital, Mumbai, India

P. Vaideeswar (ed.), *Tropical Cardiovascular Pathology*,
https://doi.org/10.1007/978-981-19-3720-0_21

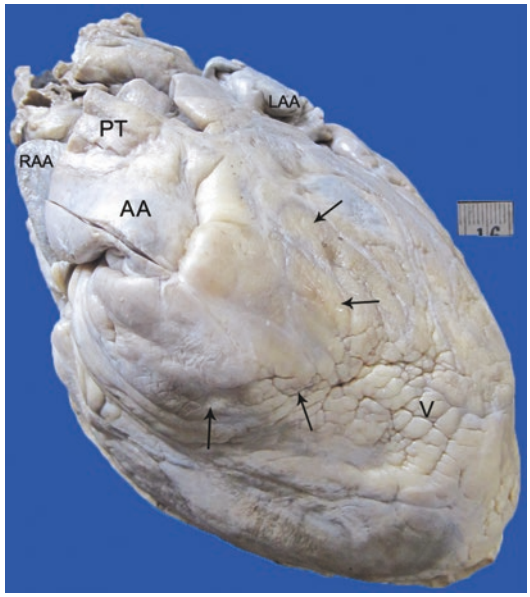

Fig. 21.1 Moderate cardiomegaly. The apex is formed by a single ventricular chamber V. The ascending aorta AA appeared to arise from a mound (arrows) and was anterior and to the left in comparison to the pulmonary trunk PT (*LAA* left atrial appendage, *RAA* right atrial appendage)

ventricle (thick compact portion and fine trabeculae carneae, Fig. 21.2). It was moderately enlarged with diffuse endocardial thickening and mild myocardial hypertrophy. The single ventricle appeared to lead directly to the pulmonary artery, below which was marked circumferential pearly white endocardial thickening—sub-pulmonic stenosis. (Fig. 21.3) The pulmonary annulus was normal in size with 3 cusps (2 anterior and 1 posterior). The free margin of the posterior cusp was covered by large friable red-brown vegetation. The vegetation showed presence of Gram-positive bacterial colonies on histology. The ascending aorta was connected via a small heavily trabeculated outlet chamber (resembling the right ventricular outflow tract) to the left ventricle through a ventricular septal defect (VSD). The valve was 3-cuspid with 1 anterior and 2 posterior cusps. Other autopsy findings included septic pulmonary thromboembolism with arteritis and embolic abscesses, bronchopneumonia, centrilobular hemorrhagic hepatocytic necroses, and renal/cerebral micro-abscesses.

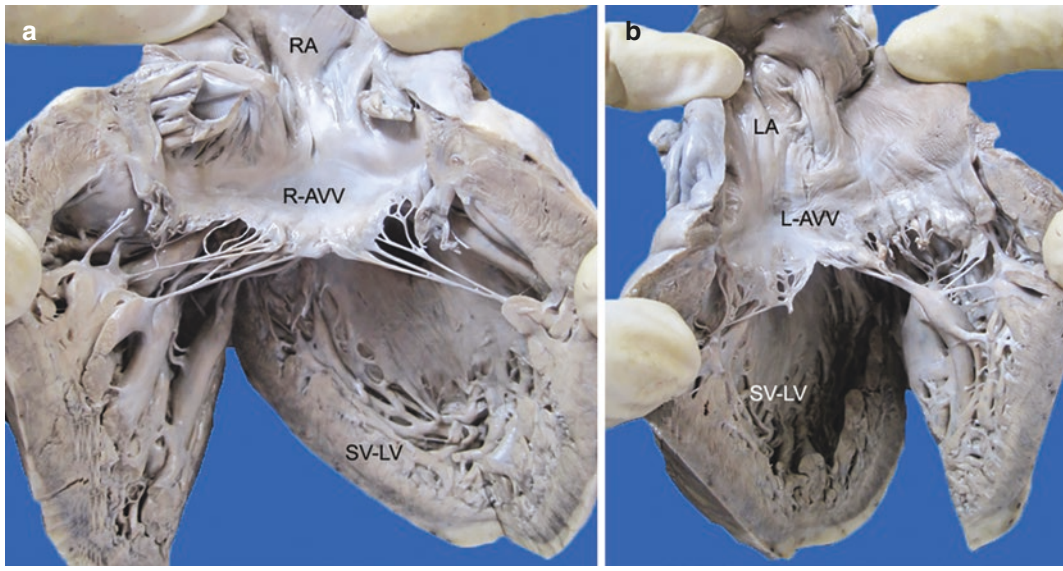

Fig. 21.2 (**a**) Right-sided inflow tract and (**b**) Left-sided inflow tract open into the single ventricle with left ventricular morphology S-LV. Note that both right R-AVV and left L-AVV atrio-ventricular valves resemble the mitral valve (*LA* left atrium, *RA* right atrium)

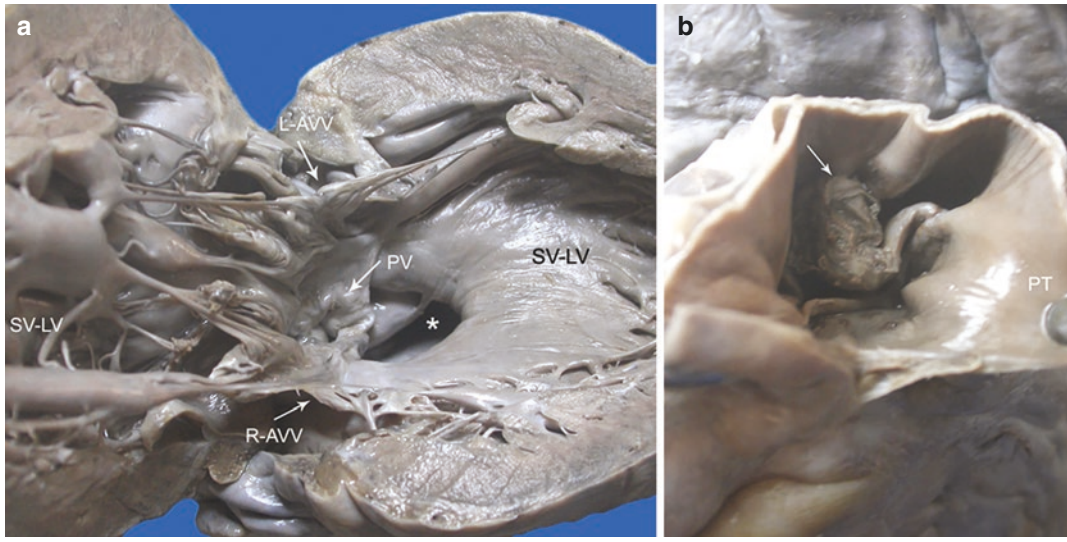

Fig. 21.3 (**a**) The specimen shows the outflow portion of the single ventricle S-LV. The outflow into the aorta is via a ventricular septal defect *. The pulmonary trunk arises directly from the S-LV. Corrugated endocardial thickening below the pulmonary valve PV produces sub-pulmonic stenosis (*L-AVV* left atrio-ventricular valve, *R-AVV* right atrio-ventricular valve); (**b**) Large reddish-brown vegetation (arrow) over the pulmonary valve (PT pulmonary trunk)

21.3 Discussion

In comparison to a 'high' frequency of left-sided infective endocarditis (IE, See Chaps. 16–19), IE of the right-sided heart valves (See Chap. 20) is rare with isolated involvement of the tricuspid valve with or without concomitant affection of the pulmonary valve (PV). Isolated PVIE, as seen in this report, is extremely uncommon and is observed in less than 2% of the patients with IE; a higher incidence may be seen at autopsy. The risk factors for PVIE are similar to those outlined for right-sided IE and include intravenous drug use, prolonged hospitalization, conditions associated with bacteremia, malnutrition, and immunodeficiency. An important cause in the pediatric population and young adults is congenital heart disease, with the proportion of infection increasing with repair of such defects. Hence, the IE can occur over native (normal or malformed) or prosthetic pulmonary valves. It is to be noted that almost 28% of cases of PVIE have no underlying predisposing factors. We have for the first time documented a case of IE affecting the PV in a case of double-inlet left ventricle. The single ventricle was seen as part of the heterotaxy syndrome with abnormal lateralization of the abdominal viscera. There was an incomplete right ventricle perched on the basal aspect of the dominant ventricle with ventriculo-arterial discordance. Though the PV in this case was morphologically normal, there was associated sub-pulmonic stenosis.

The vegetations can be small or bulky and friable and are typically found on the ventricular surface of the PV. Sometimes, extension of the vegetations onto the pulmonary trunk can occur. Varied organisms have been implicated as the etiological agents of PV endocarditis with the commonest ones being *S. aureus*, coagulase-negative staphylococci, and group B-streptococci. Blood culture was not performed in this patient; Gram-positive cocci were demonstrated on histology. Sterile blood cultures are frequently obtained and in such cases, transthoracic echocardiography or more sophisticated imaging techniques would play an important role. However, given the low incidence of PVIE and its presentation with fever and respiratory symptoms and signs, the diagnosis is a challenge for the physicians. Very often, the murmur of PV regurgitation is a late feature.

In this case, the sub-pulmonic stenosis with reduced flow across the PV would have reduced the magnitude of the regurgitant flow. The pansystolic murmur heard was due to the VSD. Apart from significant lung involvement due to septic pulmonary thromboembolism, the patient also had cerebral and renal micro-abscesses. PVIE usually follows a benign course and broad-spectrum antibiotics with supportive care have been successfully used. However, with antibiotic resistance, uncontrollable heart failure, obstruction of the infundibular chamber, and surgical intervention (pulmonary valvectomy or homograft use) become mandatory.

Further Reading

Cook AC, Anderson RH. The anatomy of hearts with double inlet ventricle. Cardiol Young. 2006;16(Suppl 1):22–6.

Edmond JJ, Eykyn SJ, Smith LD. Community acquired staphylococcal pulmonary valve endocarditis in non-drug users: case report and review of the literature. Heart. 2001;86:E17.

Fernández Guerrero ML, Álvarez B, Manzarbeitia F, Renedo G. Infective endocarditis at autopsy: a review of pathologic manifestations and clinical correlates. Medicine (Baltimore). 2012;91:152–64.

Fusco F, Scognamiglio G, Correra A, Merola A, Colonna D, Palma M, et al. Pulmonary valve endocarditis in adults with congenital heart disease: the role of echocardiography in a case series. Eur Heart J Case Rep. 2020;4:1–7.

Hamza N, Ortiz J, Bonomo RA. Isolated pulmonic valve infective endocarditis: a persistent challenge. Infection. 2004;32:170–5.

Khairy P, Poirier N, Mercier LA. Univentricular heart. Circulation. 2007;115:800–12.

Khosravi A, Rostami Z, Javanbakht M, Jafari NJ, Ghahroudi MS, Kalantar-Motamed MH. Pulmonary endarteritis and endocarditis complicated with septic embolism: a case report and review of the literature. BMC Infect Dis. 2020;20:212.

Lacalzada J, Enjuanes C, Izquierdo MM, Barragán Acea A, et al. Pulmonary valve infective endocarditis in an adult patient with severe congenital pulmonary stenosis and ostium secundum atrial septal defect. Cardiol Res Pract. 2010;2010:798956.

Pettersson GB, Hussain ST, Shrestha NK, Gordon S, et al. Infective endocarditis: an atlas of disease progression for describing, staging, coding, and understanding the pathology. J Thorac Cardiovasc Surg. 2014;147:1142–9.

Prieto-Arévalo R, Muñoz P, Cuerpo G, Marí-Hualde A, Castelo-Corral L, Navas-Elorza E, et al. Pulmonary infective endocarditis. JACC. 2019;73:2782–4.

Ramadan FB, Beanlands DS, Burwash IG. Isolated pulmonic valve endocarditis in healthy hearts: a case report and review of the literature. Can J Cardiol. 2000;16:1282–8.

Shmueli H, Thomas F, Flint N, Setia G, et al. Right-sided infective endocarditis 2020: challenges and updates in diagnosis and treatment. J Am Heart Assoc. 2020;9:e017293.

Vaideeswar P, Jawale RM, Tullu M. Isolated infective endocarditis of the pulmonary valve: an autopsy analysis of nine cases. Cardiovasc Pathol. 2009;18:231–5.

22 Nonbacterial Thrombotic Endocarditis and Occult Lung Adenocarcinoma

Pradeep Vaideeswar

22.1 Clinical History

A middle-aged lady woman was admitted with complaints of fever associated with chills and slurring of speech followed by altered sensorium since 2–3 days. The patient was apparently asymptomatic 2 months back when her complaints started in the form of acute chest pain associated with excessive perspiration. She had been admitted in a private hospital, where thrombolytic therapy was instituted for an inferior wall myocardial infarction. Later after her discharge, she developed gradual swelling of her right lower limb with severe calf pain, blackish discoloration of digits of both upper and lower limbs, and dry cough with exertional dyspnea. She underwent pericardial tapping in private nursing home, where a diagnosis of tuberculosis was made and antituberculous treatment was started. She also complained of sudden onset dimness of vision 15 days back for which no treatment was sought.

On examination, the patient was febrile (39° C) with pulse rate of 110/min (right radial artery—regular and of good volume) and blood pressure of 150/90 mmHg. Detailed examination revealed cold extremities, digital gangrene, pitting edema and weak peripheral pulses in both lower limbs, reduced air entry in both basal zones, and left hemiplegia with facial palsy. Routine hematological investigations showed moderate anemia (Hb 8.6 g%), neutrophilia (25,900/cmm), thrombocytopenia (40,000/cmm) and <1% index of *P. vivax*. Arterial and venous Doppler revealed thrombosis of most veins in the lower limbs and right distal anterior tibial artery, while recent nonhemorrhagic infarct right parietal lobe with hemorrhagic transformation of bilateral parietooccipital lobe infarcts and subarachnoid hemorrhage along right parietal convexity were seen on CT scan.

The patient was started on injectable artesunate and doxycycline, and in view of altered sensorium and neck stiffness, was also given injection ceftriaxone. She was also started on cerebral decongestants, injectable heparin and a pulse therapy of injectable methylprednisolone. The patient could not be shifted to intensive care unit due to shortage of beds. Her condition deteriorated; her sensorium dropped from 10/15–7/15 over next 24 h so she was intubated to protect her airways. In the next 24 h, she further deteriorated, sensorium dropped to 3/15, with features of severe raised intracranial tension and coning. Within next 24 h, her pulses were not palpable and she succumbed on the third day of her admission.

P. Vaideeswar (✉)
Department of Pathology (Cardiovascular and Thoracic Division), Seth Gordhandas Sunderdas Medical College and King Edward Memorial Hospital, Mumbai, India

P. Vaideeswar (ed.), *Tropical Cardiovascular Pathology*,
https://doi.org/10.1007/978-981-19-3720-0_22

22.2 Autopsy Findings

The heart was mildly enlarged in size (300 g). There was mild to moderate thickening of both layers of the pericardium with dense adhesions (Fig. 22.1a) and focal gray-white nodularity. There was also a loculated effusion around the region of the right atrial appendage with inspissated hemorrhagic material. There was mild dilatation of both the ventricular chambers and the presence of yellowish-white mottling in the left ventricular myocardium on the transverse slices. In addition, both the left-sided valves (Fig. 22.1b, c) showed the presence of multiple firm friable large pale brown vegetations (less than 0.5 cm) that were located at the lines of closure. The gross and the histological features (Fig. 22.2a, b) were characteristic of the bland nonbacterial thrombotic endocarditis (NBTE). These friable vegetations had embolized through the coronary arteries to produce multifocal healing and healed infarcts in both ventricles (Fig. 22.2c, d). There was systemic embolization in the form of multifocal hemorrhagic fresh and organizing infarcts in cerebral hemispheres with few fibrin thrombi in leptomeningeal arteries and small infarcts in the kidneys and spleen.

Sections of the right atrium and its appendage showed fresh and organizing fibrinous exudates, in which were present clusters of pleomorphic malignant epithelial cells (Fig. 22.3). The source of the pericardial metastases was a peripheral adenocarcinoma in the right lower lobe. It was seen as an area of pleural puckering in the apical segment of the right lower lobe, below which there was an ill-defined gray-white firm parenchyma (Fig. 22.4a). Though a focal lepidic pattern was present, much of the tumor showed clusters of cells within the alveolar spaces with cellular pleomorphism and abundant necroses (Fig. 22.4b, c). The lungs also showed pulmonary arterial thrombosis with fresh hemorrhagic infarction (Fig. 22.5a, b), and focal lymphatic permeation (Fig. 22.5c, d). Metastases were also seen in the hilar and para-aortic lymph nodes and the liver.

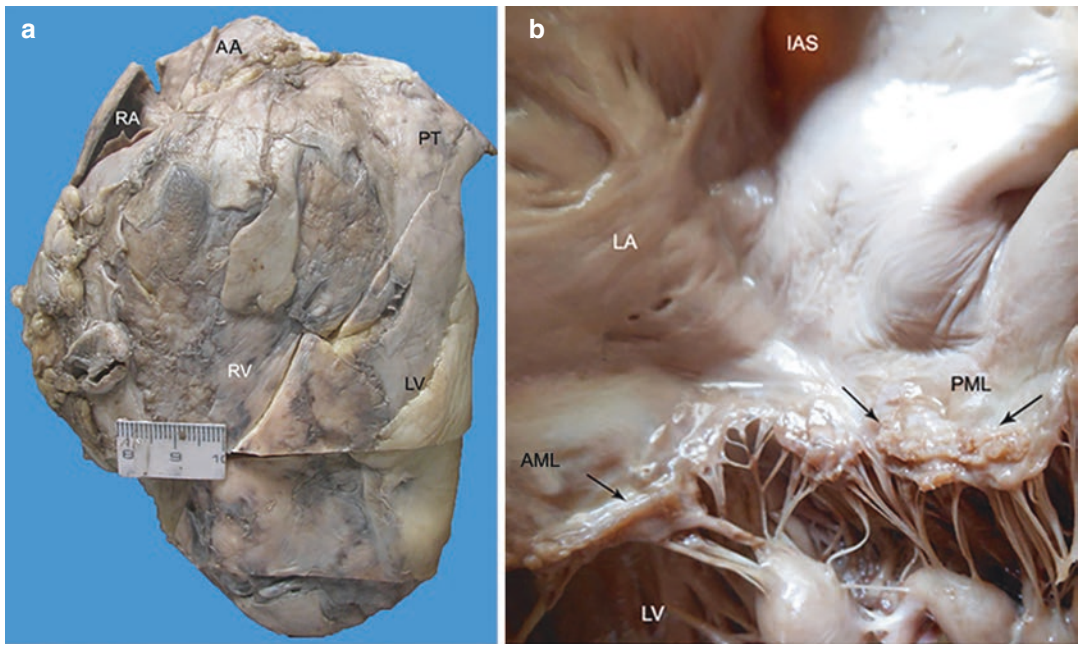

Fig. 22.1 (**a**) Dense adhesions between the parietal and visceral layers of the pericardium; Multiple warty friable light brown vegetations over (**b**) the lines of closure of the mitral valvular leaflets and (**c**) central nodules of the aortic valvular cusps (*AA* ascending aorta, *AML* anterior mitral leaflet, *IAS* interatrial septum, *LA* left atrium, *LCC* left coronary cusp, *LV* left ventricle, *MV* mitral valve, *NCC* noncoronary cusp, *PML* posterior mitral leaflet, *PT* pulmonary trunk, *RA* right atrium, *RCC* right coronary cusp, *RV* right ventricle)

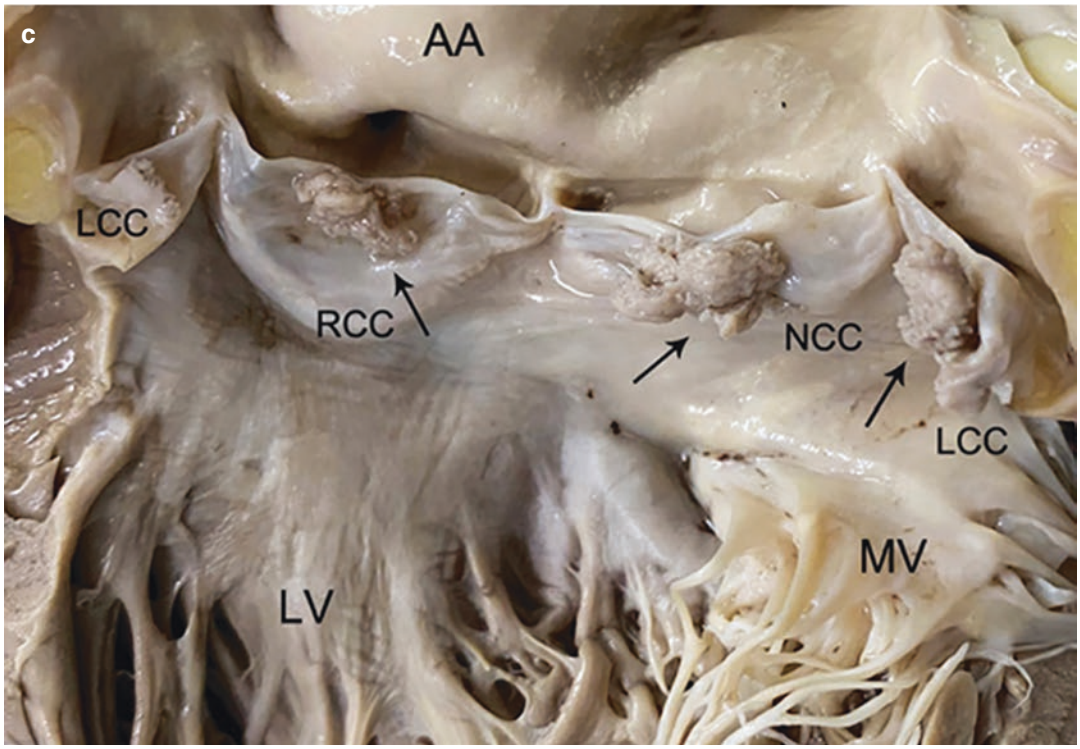

Fig 22.1 (continued)

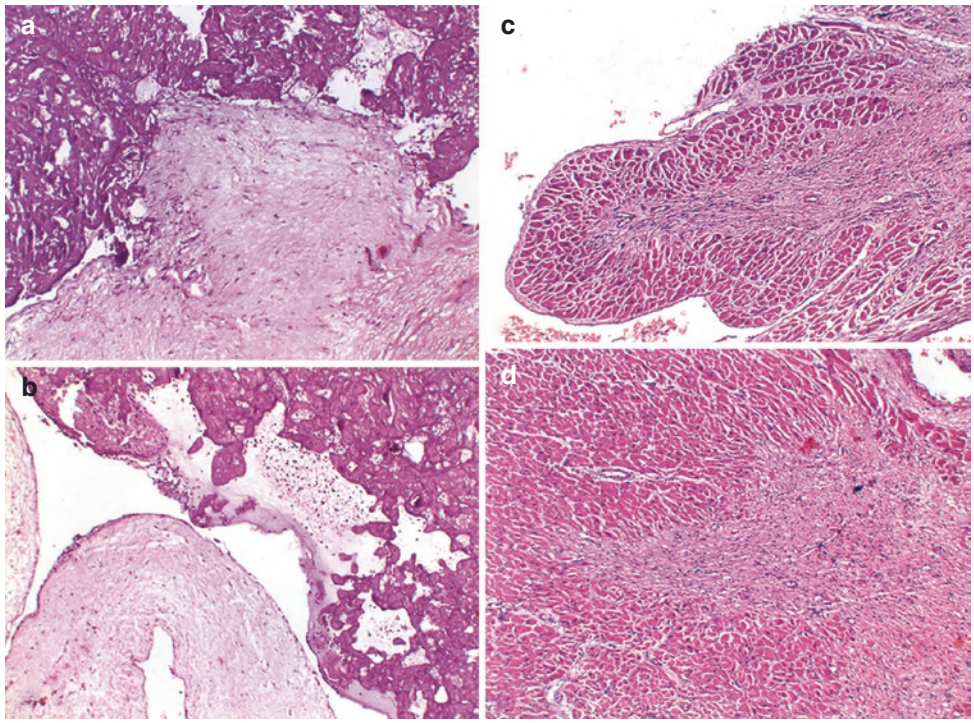

Fig. 22.2 Chunky bland deposits of fibrin and platelets over the flow surfaces of the (**a**) mitral leaflet and (**b**) aortic cusp; Healing foci of myocardial infarctions in the (**c**) right and (**d**) left ventricles, composed of vascularized fibrous tissue (H&E × 200)

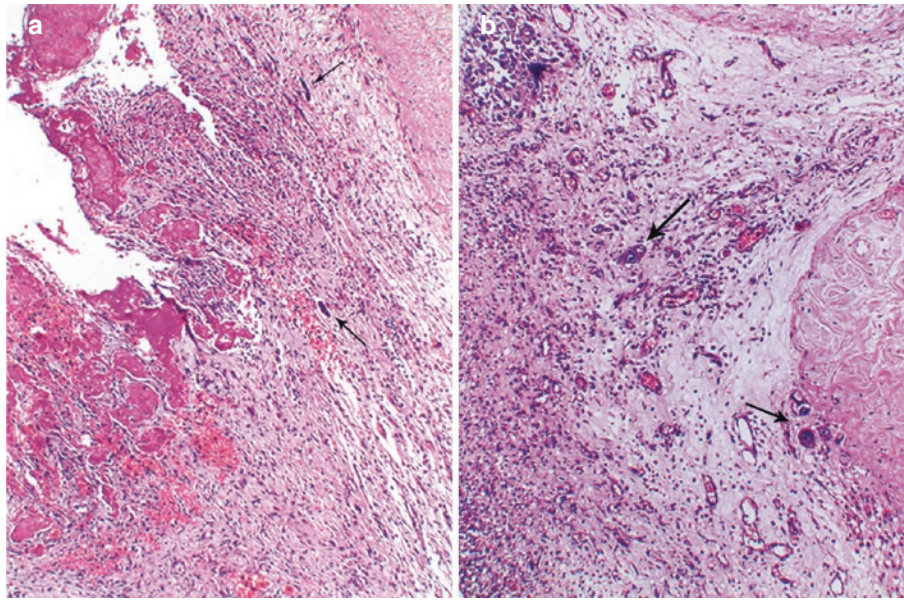

Fig. 22.3 (**a**) Fresh and organizing fibrinous exudate over the right atrial appendage showing spindle-shaped pleomorphic cells (arrows) amidst inflammatory cells (H&E × 100); (**b**) Singly dispersed uninucleate and binucleate cancer cells seen in the exudates at the right atrioventricular junction (H&E × 200)

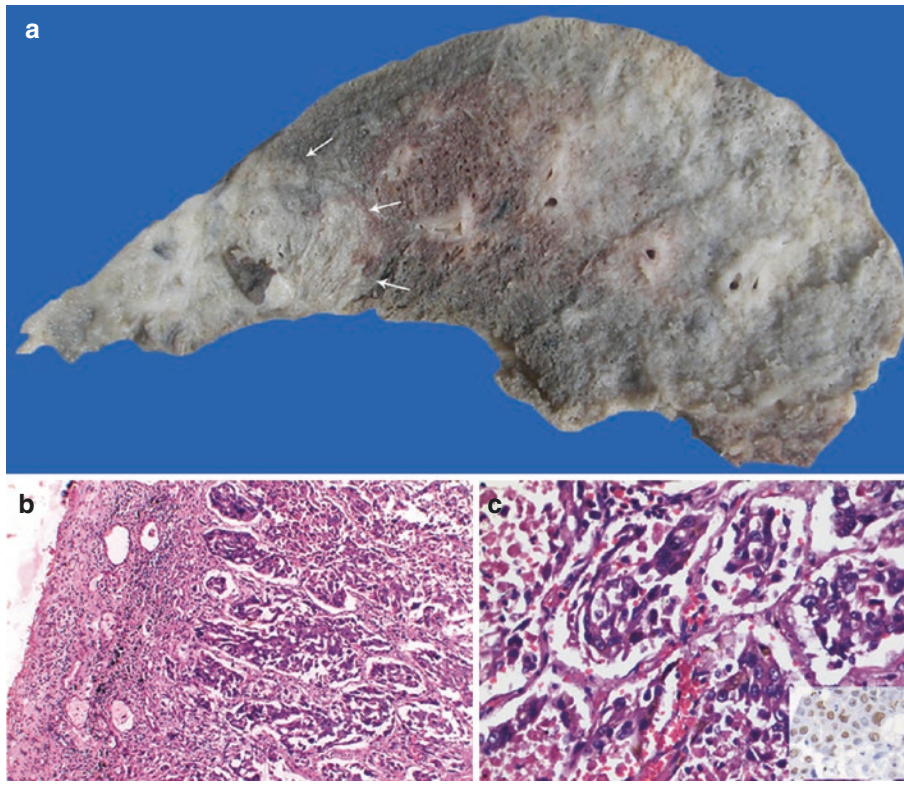

Fig. 22.4 (**a**) Subpleural gray-white consolidation (delineated by arrows) in the apical segment of the right lower lobe; (**b**) The pleura shows fibrotic thickening, inflammation, and vascularization. All the alveoli are filled with tumor cells with focal necrosis (H&E × 200); (**c**) Clusters of pleomorphic cells were present in the alveolar spaces (H&E × 400). Inset shows immunohistochemical nuclear positivity for thyroid transcription factor 1 (× 400)

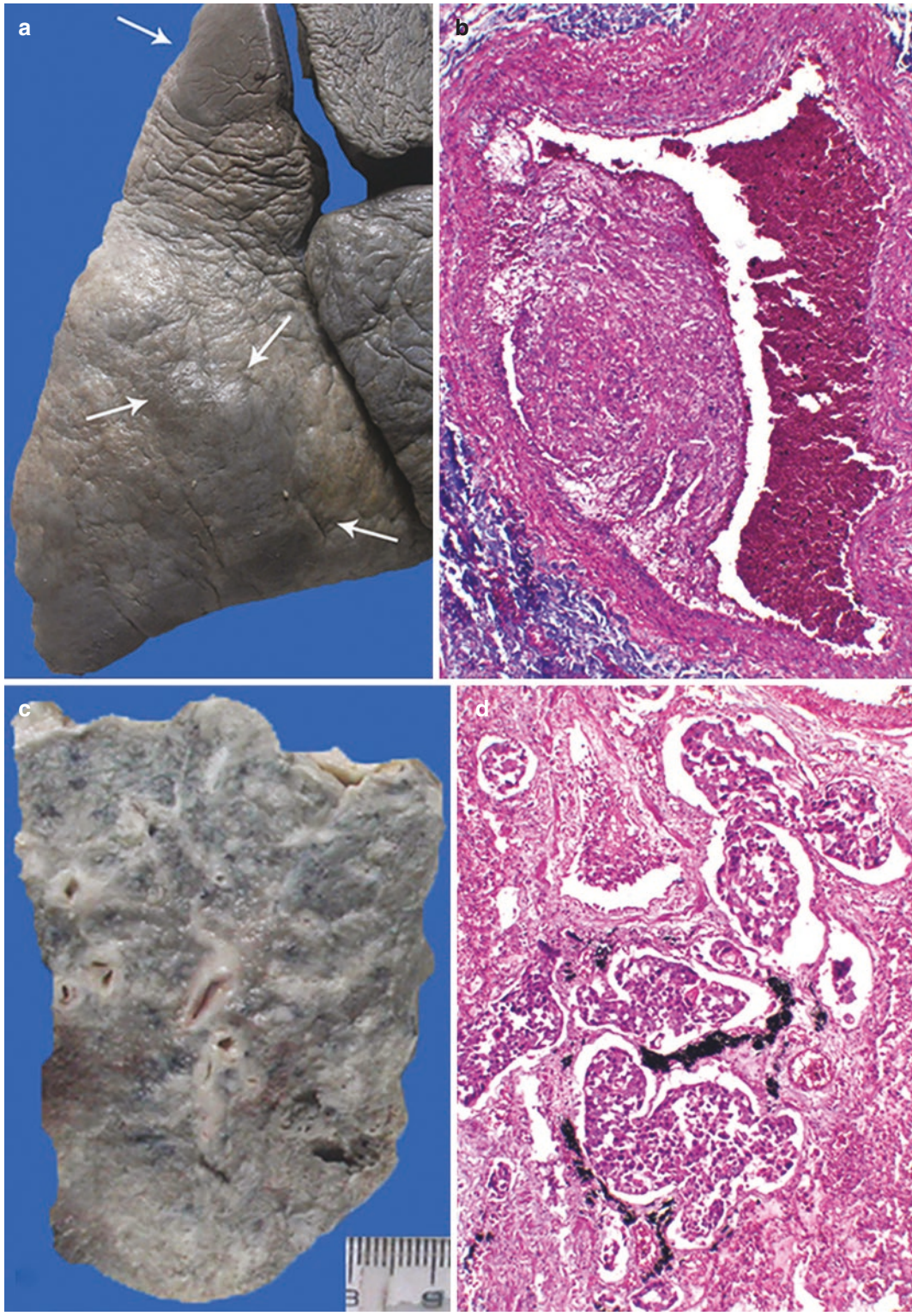

Fig. 22.5 (**a**) Subpleural wedge-shaped hemorrhagic infarcts (arrows) produced by (**b**) thrombotic narrowing of the muscular pulmonary arteries (H&E × 400); (**c**) Undue gray-white prominence of the lobular septa and broncho-vascular connective tissue produced by (**d**) lymphatic embolization—lymphangitis carcinomatosis (H&E × 400)

22.3 Discussion

Hypercoagulability was seen as a paraneoplastic phenomenon, induced by an occult adenocarcinoma of the lung. This 45-year-old woman presented not only with arteriovenous thrombosis, but also with multiple mulberry-like light-brown friable deposits of sterile fibrin and platelet clumps at the coaptation edges of her normal left-sided valves. This pathology had been variously designated in the past as thromboendocarditis and terminal, cachctic, or marantic endocarditis before the term NBTE was coined by Gross and Friedberg in 1936. Like infective endocarditis, NBTE too has a predilection for the left side of the heart and affects normal or damaged valvular or mural endocardium, including the chordae tendineae. In more than half the patients, the vegetations are multiple and <0.3 cm in size with involvement of a single valve (mitral valve being the commonest site). Later, there may be fibrosis and valvular dysfunction.

NBTE affects patients from the fourth to eighth decades of life with an equal sex distribution. It is often an autopsy diagnosis with an approximate incidence of 1.2% (range of 0.3–9.3%). However, this may not represent the true incidence as the vegetations, though small, have a remarkable tendency to embolize and the remnants (if any) will not be grossly visible. Besides, there is also inadequate histological evaluation of the valves at autopsy, particularly if they are normal. The pathogenetic mechanism operating in NBTE is damage (often subtle) to the valvular endocardium with prevailing hypercoagulability. The valvular injury can occur due to inherent natural hemodynamic stress, circulating inflammatory cytokines or immune complexes and iatrogenic trauma. Such vegetations are well-documented in several autoimmune disorders (e.g., primary antiphospholipid antibody syndrome and systemic lupus erythematosus—See Chap. 23), acquired and inherited coagulation defects (e.g., disseminated intravascular coagulation and protein C and S deficiencies), and inflammatory states (e.g., tuberculosis and sepsis). An important cause is covert or overt underlying cancer.

After antiphospholipid antibody syndrome (primary or secondary), cancer-related hypercoagulability is the next common etiology for cases of acquired thrombophilia. The pathophysiology is complex and multifactorial, depending on the type of malignancy; most often, the tumors are mucin-secreting adenocarcinomas, which may be pancreatico-biliary, gastrointestinal, or pulmonary in origin. The basic mechanism is an imbalance between the coagulation and fibrinolytic system produced by molecules released by the cancer cells themselves or through their interaction with the endothelial cells, leukocytes, and platelets. This may manifest merely as abnormalities in the coagulation profile or more ominously as thrombotic episodes, which can also precede the diagnosis of malignancy. They include venous thrombosis (most common), disseminated intravascular coagulation, thrombotic microangiopathy, arterial thrombosis, and NBTE, which were indeed the manifestations in this patient.

The malignancy in this case was pulmonary adenocarcinoma. The malignant epithelial cells formed clusters within the alveolar spaces, the so-called intra-alveolar variant with abundant necroses. In addition, features of pulmonary tumor thrombotic microangiopathy and lymphangitis carcinomatosis were also present. Also by the time NBTE is discovered, the patients tend to have disseminated cancers; our patient showed metastases in the pericardium, liver, and mediastinal, hilar, and para-aortic lymph nodes. A clinical clue to the presence of NBTE is not valvular dysfunction, but the occurrence of systemic embolization. This complication is seen in over 50% of patients and is unrelated to the size of the vegetations. Central nervous system is very commonly involved as seen in the case presented, though the initial clinical presentation began with coronary embolism. The digital gangrene can be explained by embolism, but arterial thrombosis, which was demonstrated, may also be the cause. Predictably, infarcts were also seen in the kidneys and spleen. The effects of NBTE can be, therefore, extremely detrimental and it can quickly worsen. It mandates adequate anticoagulant therapy and appropriate cancer therapy to improve possible survival.

Further Reading

Adams HP Jr. Cancer and cerebrovascular disease. Curr Neurol Neurosci Rep. 2019;19:73.

Cheung B, Shivkumar A, Ahmed AS. Embolic showering from non-bacterial thrombotic endocarditis and adenocarcinoma of the lung. Eur J Case Rep Intern Med. 2020;7(10):001798. https://doi.org/10.12890/2020_001798.

Hirsch E, Jagirdar J, Nazarullah A. Pulmonary adenocarcinoma, intra-alveolar variant: a rare entity mimicking desquamative interstitial pneumonia. Int J Surg Pathol. 2018;26:185–9.

Hurrell H, Roberts-Thomson R, Prendergast BD. Non-infective endocarditis. Heart. 2020;106:1023–9.

Liu J, Frishman WH. Nonbacterial thrombotic endocarditis: pathogenesis, diagnosis, and management. Cardiol Rev. 2016;24:244–7.

Patel MJ, Elzweig J. Non-bacterial thrombotic endocarditis: a rare presentation and literature review. BMJ Case Rep. 2020;13:e238585.

Sheth RA, Niekamp A, Quencer KB, Shamoun F, Knuttinen MG, Naidu S, et al. Thrombosis in cancer patients: etiology, incidence, and management. Cardiovasc Diagn Ther. 2017;7(Suppl 3):S178–85.

Libman-Sacks Endocarditis

23

Smita Divate and Pradeep Vaideeswar

23.1 Clinical History

A 35 years old woman presented with high grade fever and atypical chest pain. She had been diagnosed as a case of systemic lupus erythematosus (SLE) a year ago when she had complained of facial puffiness, joint swellings, oral ulcers, rash over chest and limbs, and alopecia. Her investigations in that period had revealed positivity for antinuclear antibodies and anti-double-stranded DNA antibodies, low C_3 and C_4 complement levels, and features of Type II b lupus nephritis on kidney biopsy. The anticardiolipin antibodies were within normal limits. She had been started on hydroxychloroquine, prednisolone, and lasix.

Her current investigations revealed hemoglobin ranging from 7.4 g/dL to 11.0 g/dL, total leukocyte count from 9000 to 11,300/cmm, differential leucocyte count of 78–80% neutrophils and 18–20% lymphocytes and adequate platelets, blood urea nitrogen 33 mg/dL, Serum creatinine 1.6 mg/dL, low C_3/C_4 levels, and hypoxia in arterial blood gases. *Streptococcus viridans* had been detected in a blood culture sample. Chest plain radiograph revealed bilateral pleural effusions with right basal consolidation. Along with the drugs for SLE, she was also started on multiple broad spectrum antibiotics and digoxin. However, her fever and chest pain persisted with development of tachypnea and edema feet. Also noted were increasing crepitations in the lung bases and a low ejection fraction. She continued to deteriorate and despite all measures died after 8 days of admission.

23.2 Autopsy Findings

There was moderate cardiomegaly (350 g) with moderate enlargement of the ventricles and mild enlargement of the atria. The remarkable feature was the presence of endocarditis of both Libman-sacks (LSE) and nonbacterial thrombotic (NBTE) types on the atrioventricular valves. Small nodular vegetations were on the under surfaces of the tricuspid valve leaflets at their annular attachments (Fig. 23.1a). The mitral valve (MV) leaflets also showed a chain of nodular vegetations close to their edges, along with the characteristic 'pocket lesions' on their non-flow surfaces (Fig. 23.1b). The 'pocket-lesions' or LSE (Fig. 23.1c, d) and the NBTE of MV revealed masses of hazy blue finely granular hematoxyphil body-like areas, which closely mimicked bacterial colonies within a background of fibrin and platelets.

S. Divate
Department of Pathology, Seth Gordhandas Sunderdas Medical College and King Edward Memorial Hospital, Mumbai, India

P. Vaideeswar (✉)
Department of Pathology (Cardiovascular and Thoracic Division), Seth Gordhandas Sunderdas Medical College and King Edward Memorial Hospital, Mumbai, India

P. Vaideeswar (ed.), *Tropical Cardiovascular Pathology*,
https://doi.org/10.1007/978-981-19-3720-0_23

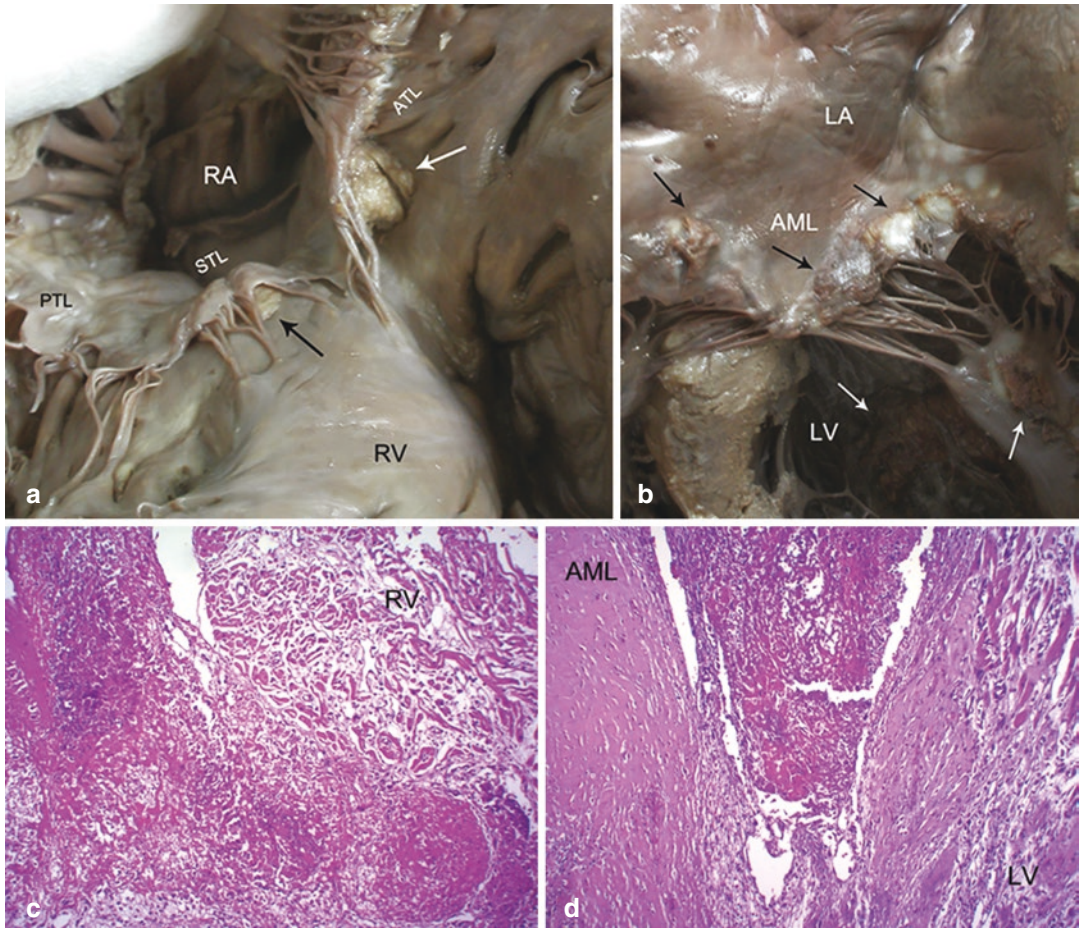

Fig. 23.1 (**a**) Thrombotic masses (arrows) between the non-flow surfaces of tricuspid valve leaflets and right ventricular RV endocardium—pocket lesions; (**b**) Nonbacterial thrombotic vegetations (black arrows) over the flow surfaces of the anterior mitral leaflet AML. Also note mural thrombi (white arrows) over papillary muscle and left ventricle LV (*ATL* anterior tricuspid leaflet, *LA* left atrium, *PTL* posterior tricuspid leaflet, *RA* right atrium *STL* septal tricuspid leaflet); Fibrin with patchy basophilic haze seen in the pocket lesions of (**c**) Tricuspid and (**d**) Mitral valves (H&E × 200)

Special stains for the microorganisms (modified Gram's and Gomori methenamine silver stains negative) were, however, negative.

The most prominent lesion was seen in the left ventricular chamber, which showed a large plaque-like mural thrombus that covered almost the entire endocardial surface of the posterior wall with extensions on to the septal (Fig. 23.2a) and anterior endocardial surfaces. Small thrombi were noted over the posterior papillary muscle, intertrabecular spaces of the right ventricle with a thrombotic plaque over the endocardium of the right atrium. The left ventricular mural thrombotic mass (Fig. 23.2b) as well as the other smaller mural thrombi appeared to have commenced in the subendocardial connective tissue and contained aggregates of cells undergoing karyolysis (Fig. 23.2c), forming characteristic hematoxyphil bodies that then merged into an eosinophilic fibrinous background. The left ventricular myocardium showed foci of fibrinoid necrosis of perivascular collagen that took on a lattice-like pattern and a focal perivascular proliferation of large mononuclear cells resembling Anitschkow cells. The intramural coronary arteries showed thrombotic occlusion associated with

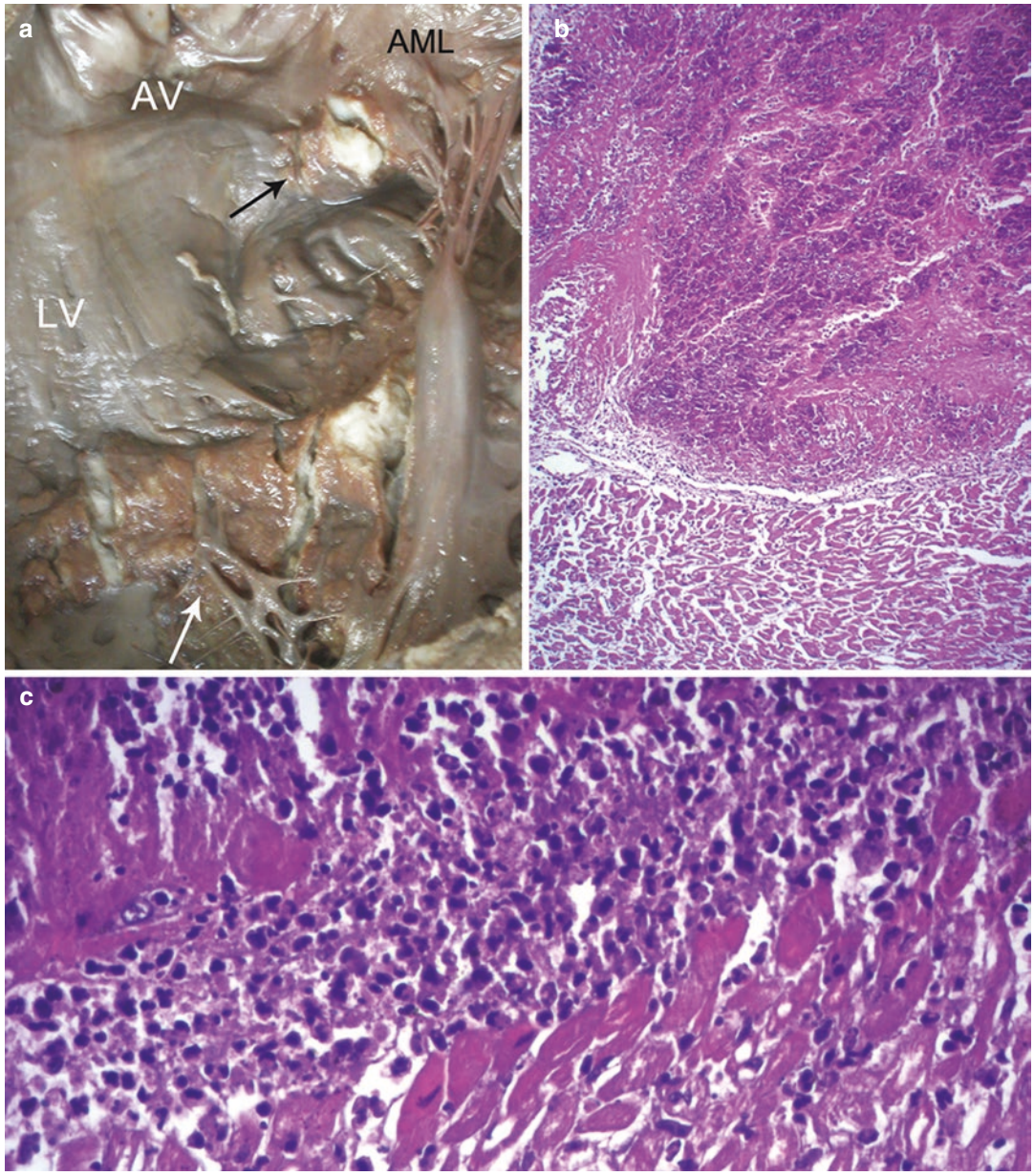

Fig. 23.2 (**a**) Band of thrombus over the posteroseptal wall of the left ventricle LV (*AML* anterior mitral leaflet, *AV* aortic valve); (**b**) The thrombus is predominantly composed of fibrin with strewn hematoxyphilic bodies (H&E × 200); (**c**) Tight mononuclear cell clusters in the subendocardial region of the left ventricle with overlying thrombus (H&E × 400)

myocytolysis and healing microinfarctions in the adjacent myocardium (Fig. 23.3a). The MV also showed active valvulitis with a prominent mononuclear cell infiltration (Fig. 23.3b). The aortic valve, coronary ostia, and all coronary arteries were normal.

Both lungs showed patchy congestion and focal bronchopneumonia. The kidneys were mildly swollen and revealed class IV lupus nephritis; glomerular thrombi and hematoxyphil bodies were seen in the background of mesangial proliferation. The liver, spleen, brain, and other

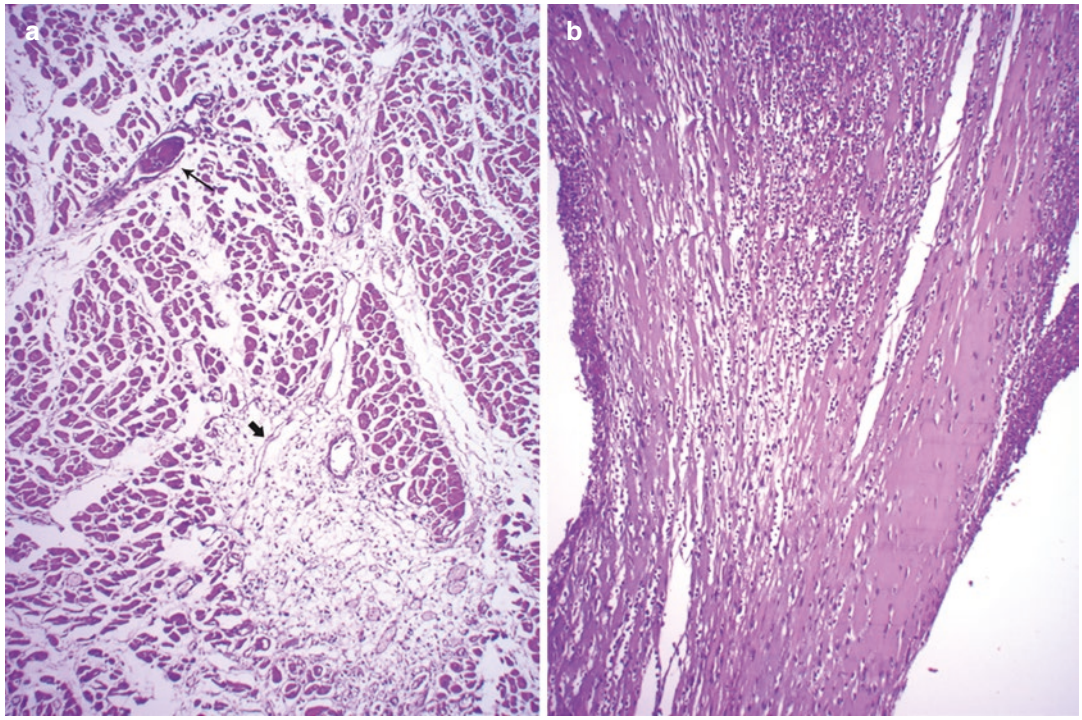

Fig. 23.3 (**a**) Intramural coronary artery occluded by fresh fibrin thrombus (thin arrow) with small focus of healing microinfarct (thick arrow, H&E × 200); (**b**) Acute mitral valvulitis with mixed inflammatory cell infiltrate (H&E × 200)

organs were unremarkable. No infarcts or abscesses were found in any of the organs.

Cause of Death: Libman-Sacks endocarditis with coronary thromboembolism and multifocal myocardial infarctions.

23.3 Discussion

Cardiac involvement is common in SLE with valvular involvement detected in over 50% cases on echocardiography. LSE is observed in 11–30% of patients with SLE. Clinically unrecognized lesions may be brought to light only at autopsy. LSE lesions were first described in 1924 as "atypical verrucous endocarditis" with valvular and mural components. While more commonly seen on either side of the valve leaflets, LSE may extend to the mural surfaces of the heart endocardium. Valvular lesions may form typical variable-sized thrombotic masses called "pocket lesions", on undersurfaces of leaflets necessitating lifting up of the valve to search for them. Such verrucae may extend along the chordae tendineae of the subvalvular apparatus and even within pockets between insertions of the chordae. Lesions of LSE are best distinguished from NBTE by virtue of smudgy blue necrobiotic mononuclear cells forming structures akin to hematoxyphil bodies that are characteristic of SLE. This feature was prominently noted in the present case. Verrucae of LSE have been described to have three zones: outer exudative, middle organizing, and inner neovascularization. However, extensive mural involvement as seen in the present case is extremely rare.

Pathogenesis of LSE appears to be primarily twofold: immunological and hypercoagulability-related. Immune complexes deposits detected in walls of small blood vessels are believed to play an important role in the pathogenesis of these lesions. Vegetations composed of platelet-fibrin thrombi and immune deposits as a consequence of autoimmunity-derived endothelial damage eventually lead to valvular fibrosis and thickening, deformity, and dysfunction. LSE in associa-

tion with the antiphospholipid antibody syndrome (APS) has been reported among the various causes of hypercoagulability in patients with SLE. Subsequently, other studies highlighted this association and gathered evidence for the pathogenetic role of antiphospholipid antibodies in LSE. It has also been reported that SLE patients with APS tend to have more severe LSE. In the present case, tests had been performed only for anticardiolipin antibodies. While these were negative, in view of lack of testing for other antiphospholipid antibodies, APS cannot be excluded with certainty. It is pertinent to state that glomerular thrombi noted in the index case add to the possibility of a hypercoagulable state.

While LSE may have limited clinical significance in many, yet it has been associated with thromboembolic phenomenon in 10–20% of cases, which could have explained the presence of intramural coronary arterial thrombi and multiple healing micro-infarctions. Echocardiography, both transthoracic and transesophageal, help in diagnosis of LSE. Aggressive lupus therapy and long-term anticoagulation is used in the management of this disorder.

Further Reading

Buleu F, Sirbu E, Caraba A, Dragan S. Heart involvement in inflammatory rheumatic diseases: a systematic literature review. Medicina (Kaunas). 2019;65:249.

Kato T, Takama N, Harada T, Koitabashi N, Murakami M, Abe T, et al. Nonbacterial thrombotic endocarditis—a rare case of acute Libman-Sack's endocarditis complicated by multiple cerebral infarcts: case report and literature review. CASE (Phila). 2020;4:507–11.

Lee JL, Naguwa SM, Cheema GS, Gershwin ME. Revisiting Libman-Sack's endocarditis: a historical review and update. Clin Rev Allergy Immunol. 2009;36:126–30.

Miner JJ, Kim AHJ. Cardiac manifestations of systemic lupus erythematosus. Rheum Dis Clin North Am. 2014;40:51–60.

Prasad M, Hermann J, Gabriel SE, Weyand CM, Mulvagh S, Mankad R, et al. Cardiorheumatology: cardiac involvement in systemic rheumatic disease. Nat Rev Cardiol. 2015;12:168–76.

Part VI

Ischemic Myocardial Disorders

Acute Myocardial Infarction in the Young

24

Shashank Tyagi, Pradeep Vaideeswar, and Girish Tasgaonkar

24.1 Clinical History

A 27-year-old man was admitted in the Emergency Services Department for a period of 3 h. He had intermittent retrosternal chest pain and developed cardiac arrest on arrival. After appropriate resuscitative measures, the patient was reverted back to sinus rhythm. The patient was a chronic smoker and alcoholic; a family history of ischemic heart disease (an elder brother alive and on treatment) was present. Lipid profile performed in the recent past was within normal limits. His routine hematological and biochemical parameters during the current admission had been normal; troponin T was elevated (19 ng/L; reference value 10–15 ng/L). The ECG revealed elevated ST segment in leads V_2 to V_5 (Fig. 24.1). Subsequently, he developed ventricular tachycardia and cardiac arrest, and he could not be revived.

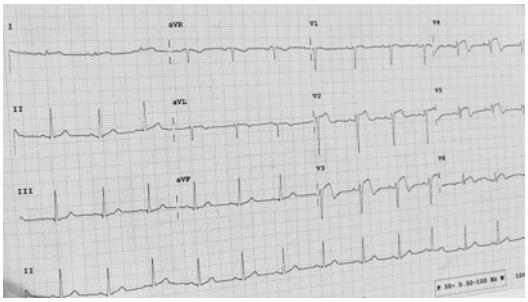

Fig. 24.1 The ECG tracing showing elevated ST segment

24.2 Autopsy Findings

The heart (230 g) was mildly enlarged in size with mild left ventricular enlargement (Fig. 24.2a). The right coronary artery had a dominant distribution. The left anterior descending (LAD) artery right from its origin for a length of 1.2 cm was critically narrowed by an eccentric pale yellow plaque; the lumen was occluded by granular pale brown thrombus (Fig. 24.2b). On histology, the plaque was fibro-fatty (equal proportions of fibrous and lipid material, Fig. 24.2c). The fibrous cap was cellular with a slight depression, over which was adherent fresh fibrin thrombus (Figs. 24.2c and 24.3a). The lipid content was in the form of foamy macrophages with admixed inflammatory cells (Fig. 24.3b, c) and cholesterol clefts; the latter had incited focal

S. Tyagi
Department of Forensic Medicine and Toxicology, Lady Hardinge Medical College and Associated SSK and KSC Hospitals, New Delhi, India

P. Vaideeswar (✉)
Department of Pathology (Cardiovascular and Thoracic Division), Seth Gordhandas Sunderdas Medical College and King Edward Memorial Hospital, Mumbai, India

G. Tasgaonkar
Department of Forensic Medicine and Toxicology, Seth Gordhandas Sunderdas Medical College and King Edward Memorial Hospital, Mumbai, India

P. Vaideeswar (ed.), *Tropical Cardiovascular Pathology*,
https://doi.org/10.1007/978-981-19-3720-0_24

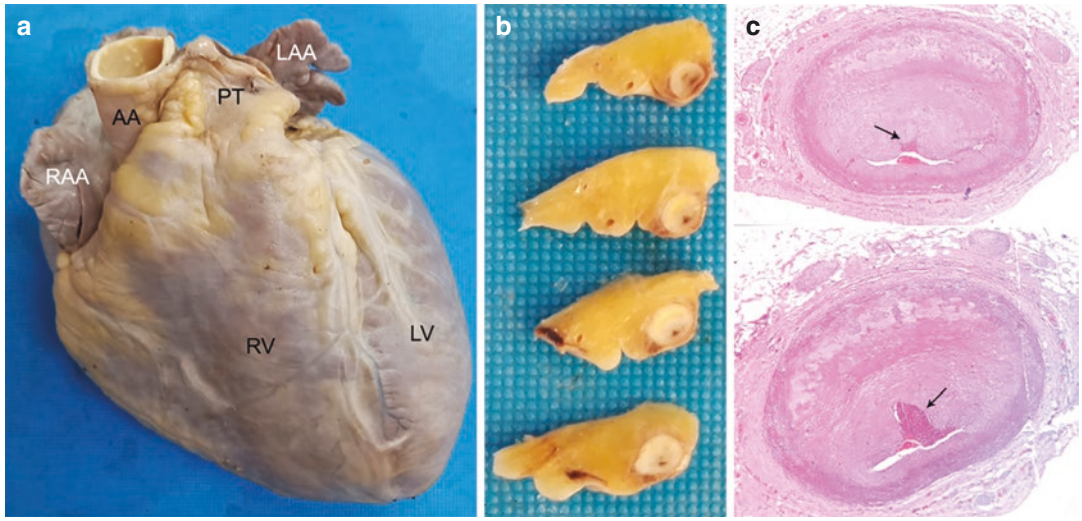

Fig. 24.2 (**a**) Mild cardiomegaly (*AA* ascending aorta, *LAA* left atrial appendage, *LV* left ventricle, *PT* pulmonary trunk, *RAA* right atrial appendage, *RV* right ventricle); (**b**) Serial cross-sections of the proximal left anterior descending artery (LAD) showing critical stenosis by a fibro-fatty plaque with luminal occlusion by brown thrombus; (**c**) Scanned H&E section of the LAD showing fibro-fatty plaque with adherent thrombus (arrows)

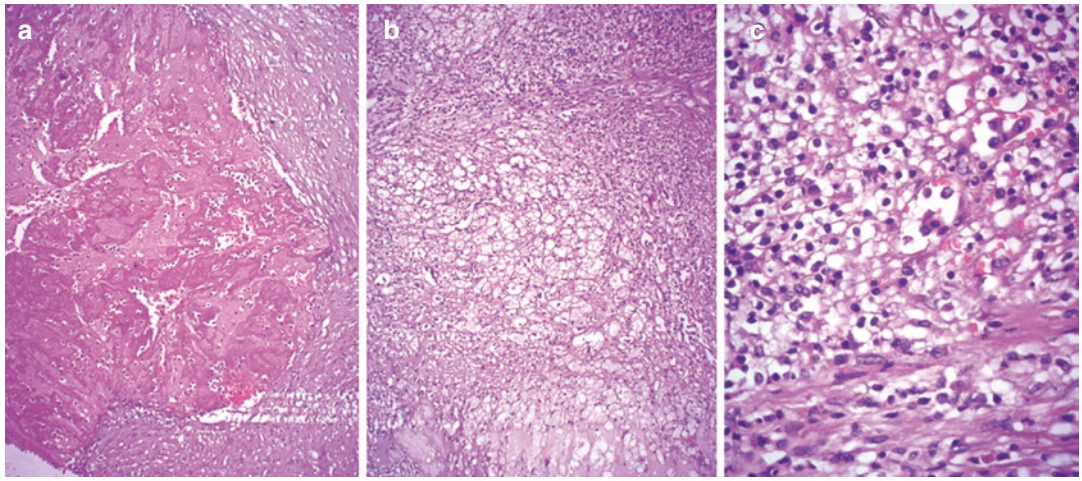

Fig. 24.3 (**a**) Adherence of fresh thrombus in an indentation in the fibrous cap (H&E × 400); Clusters of foam cells along with lymphocytes and histiocytes (**b**) H&E × 250 and (**c**) H&E × 400

granulomatous reaction. There was multifocal disruption of the internal elastic lamina, medial thinning, and adventitial fibrosis with mononuclear cell aggregates. The other arteries had hardly any changes.

The thrombotic occlusion had led to a fresh transmural infarction involving the anterior and septal walls, extending from the base to the apical regions (Fig. 24.4). Adherent fresh thrombi were also present over the endocardium of the anterior free wall. In addition, the smaller epicardial arteries were also occluded by organized and recanalized thrombi. Subendocardial foci of healed infarction were also present in the LAD territory, including the right ventricle. The lungs were edematous; other organs were normal. There was no hepatic steatosis.

Cause of Death: Acute myocardial infarction.

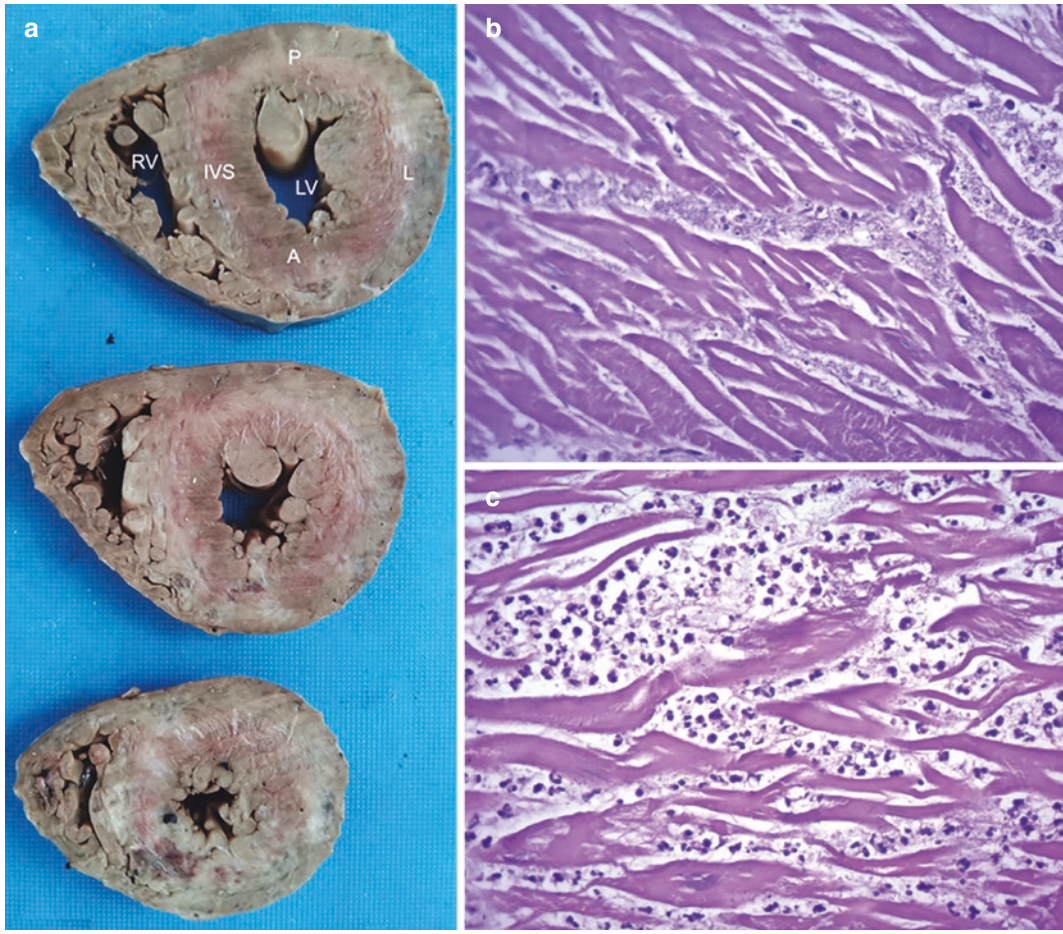

Fig. 24.4 (**a**) Transverse slices through the ventricles showing pallor, pale yellowish discoloration, and congestion in the anterior wall A of left ventricle LV and interventricular septum IVS (*L* lateral wall, *P* posterior wall); (**b**) Coagulative necroses of myofibers (H&E × 400); (**c**) Necrotic cardiomyocytes separated by edematous interstitium infiltrated by neutrophils (H&E × 400)

24.3 Discussion

The case illustrated draws attention to the occurrence of acute myocardial infarction (AMI) in a young male smoker with critical and complicated coronary atherosclerosis. Overall globally, there has been an increasing prevalence of cardiovascular disease, but the highest burden is seen in most of the South-East Asian countries, particularly India. The major contributor to the morbidity and mortality is coronary artery disease (CAD), with a prevalence ranging from 1.4 to 12.6% in India. It not only affects the elderly population, but is increasingly seen to occur in young individuals, with an incidence of symptomatic CAD (including myocardial infarction) in 3% of the young population. However, the prevalence (5–10%) may not be accurate as many such persons may remain asymptomatic and there is also a variability of the age cutoffs. While some studies have used a cutoff of 55 years, most of the studies consider patients below the age of 45 years as young. Our patient was only 29 years old.

AMI is a life-threatening condition that occurs following the ischemia-induced myocardial necrosis. The incidence of AMI has seen a declining trend over years due to advancements in the

healthcare facilities that enable early diagnosis and spontaneous treatment. However, developing countries have persistently higher AMI hospitalizations as compared to the developed ones. It is classified into 5 types depending on the pathophysiology and clinical settings into those resulting from (1) Atherosclerotic CAD (Type 1), (2) Supply–demand mismatch, not related to atherosclerotic complications (Type 2), (3) Sudden unexpected death with features of myocardial ischemia (Type 3), (4) Coronary arterial interventions (Type 4), or (5) Coronary arterial surgery (Type 5). Our case falls in the first category.

Generally, the conventional risk factors outlined for atherosclerosis in the older populations are smoking, hypertension, diabetes mellitus, obesity, and hyperlipidemia. These are typically seen even in the younger population as well and majority of them have at least 1 traditional risk factor, of which the commonest is history of smoking. Polymorphisms of genes coding for molecules involved in the lipid metabolism [most importantly lipoprotein (a)] leading to dyslipidemia, altered dietary habits, acute phase reactants, platelet aggregability, microorganisms, endocrinal disorders, collagen vascular disorders, and chronic alcoholic consumption are examples of nontraditional factors. Acute coronary incidents can be triggered by circadian variations in sympathetic responses, vascular reactivity, physical inactivity, sleep deprivation, air pollution as well as physical and emotional stress. A combination of these factors can lead to 'malignant' CAD. Our patient was a smoker and chronic alcoholic and also had a strong family history, which is a very important risk factor for young CAD and a strong predictor for future coronary events. Surprisingly, his lipid profile had been normal.

Atherosclerosis has been identified since the beginning of time, and it has progressed from a degenerative and proliferative intimal disease to a chronic inflammatory reaction to multifactorial endothelial injury. It leads primarily to formation of intimal plaques, which in the epicardial coronary arterial tree can be simply classified as fibrous, fibro-fatty, or fatty plaques and they can cause varying degrees of luminal stenosis. Fibrous plaques, as the name suggests, are mainly composed of fibro-cellular tissue in a background of collagen and proteoglycans. A core of lipid may be seen towards the basal aspect of the plaque. A large core of lipid that occupies most of the plaque is the characteristic of a fatty plaque. A thin fibrous cap separates it from the lumen (hence the term 'thin-cap atheroma'). Equal proportion of fibro-cellular and lipid is present in a fibro-fatty plaque. All the 3 may show calcification and varying degrees of inflammatory cell infiltrate. Thrombotic occlusion is the most common complication of coronary atherosclerosis, resulting in acute coronary syndromes. Inflammation-driven reduced synthesis or augmented degradation leads to fracture or rupture of the fibrous cap in a fatty plaque. On the other hand, in fibrous and/or fibro-fatty plaques, the thrombus develops over denuded endothelium induced by inflammatory cytokines, a process referred to as plaque erosion. In this case, a critically stenosed (>75% narrowing) LAD artery showed erosion of fibro-fatty plaque and formation of an occlusive thrombus. Other major epicardial arteries were hardly atherosclerotic. This is the usual finding in young patients who tend to develop single vessel disease that in majority of the cases affects the LAD artery. The ultimate result was acute myocardial infarction. It has also been observed that such 'premature' atheromas, despite their stenotic severity, seldom lead to clinical features; the first clinical manifestation is often sudden cardiac death. We also noted that smaller epicardial branches also showed organized and recanalized thrombi indicating that this patient may have had symptoms, which were unfortunately ignored.

Further Reading

Aggarwal A, Srivastava S, Velmurugan M. Newer perspectives of coronary artery disease in young. World J Cardiol. 2016;8:728–34.

Ahmed ST, Rehman H, Akeroyd JM, Alam M, Shah T, Kalra A, et al. Premature coronary heart disease in South Asians: burden and determinants. Curr Atheroscler Rep. 2018;20:6.

Buja LM, Zehr B, Lelenwa L, Ogechukwu E, Zhao B, Dasgupta A, et al. Clinicopathological complexity in the application of the universal definition of myocardial infarction. Cardiovasc Pathol. 2020;44:107153.

Dalal J, Hiremath MS, Das MK, Desai DM, Chopra VK, Biswas AD. Vascular disease in young Indians (20-40 years): role of ischemic heart disease. J Clin Diagn Res. 2016;10:OE01–5.

Rao M, Xavier D, Devi P, Sigamani A, Faruqui A, Gupta R, et al. Prevalence, treatments and outcomes of coronary artery disease in Indians: a systematic review. Indian Heart J. 2015;62:302–10.

Vaideeswar P, Tyagi S, Singaravel S. Pathology of atherosclerotic coronary artery disease in the young Indian population. Forensic Sci Res. 2019;16:241–6.

Acute Mitral Regurgitation in Acute Myocardial Infarction

25

Pradeep Vaideeswar

25.1 Clinical History

A 62-year-old male, a fisherman by occupation, chronic tobacco chewer, non-diabetic, and non-hypertensive, was admitted to a private healthcare facility for 15-day complaints of chest pain and dyspnea on exertion. An ECG was suggestive of inferior wall acute myocardial infarction (AMI), while an echocardiography performed revealed an impaired left ventricular dysfunction (ejection fraction of 30%), severe hypokinesia to akinesia of basal and middle portions of inferior, and lateral and septal walls of left ventricle (LV). There was Grade 3 mitral regurgitation (MR) and mild to moderate pulmonary hypertension. The patient was given warfarin for 5 days, and since there was no significant improvement, he was referred to our tertiary care center.

On examination, he was conscious with a pulse rate of 80 per minute, respiratory rate of 28 per minute, and blood pressure of 100/70 mmHg. There was pedal edema and bilateral crepitations. The heart sounds were normal. Apart from anemia (hemoglobin of 11.7 g/dL), the routine hematological and biochemical (including blood glucose and lipid profile) investigations were normal. A repeat EKG revealed sinus rhythm, prolonged QT interval, and an inferior wall infarct. A Color Doppler showed ischemic heart disease (IHD) with severe MR. On the third day of admission, the blood urea nitrogen was 28 mg/dL (reference value 7–20 mg/dL) and serum creatinine was 1.9 mg/dL (reference value 0.5–1.1 mg/dL). On the seventh day of the ward stay, a stent was deployed in the right coronary artery. However, his condition continued to remain poor with worsening of his azotemia, development of ventilator-associated pneumonia, and hypernatremia (158 mEq/L, reference value 135–145 mEq/L). He expired after 11 days of ward stay.

25.2 Autopsy Findings

The heart was moderately enlarged in size and weighed 330 g. There was moderate enlargement of the LV. The epicardial adipose tissue was mildly increased with milk patches over the anterior and posterior surfaces of the right ventricle. A dusky discoloration was observed in the entire posterior wall of the LV which was

P. Vaideeswar (✉)
Department of Pathology (Cardiovascular and Thoracic Division), Seth Gordhandas Sunderdas Medical College and King Edward Memorial Hospital, Mumbai, India

P. Vaideeswar (ed.), *Tropical Cardiovascular Pathology*,
https://doi.org/10.1007/978-981-19-3720-0_25

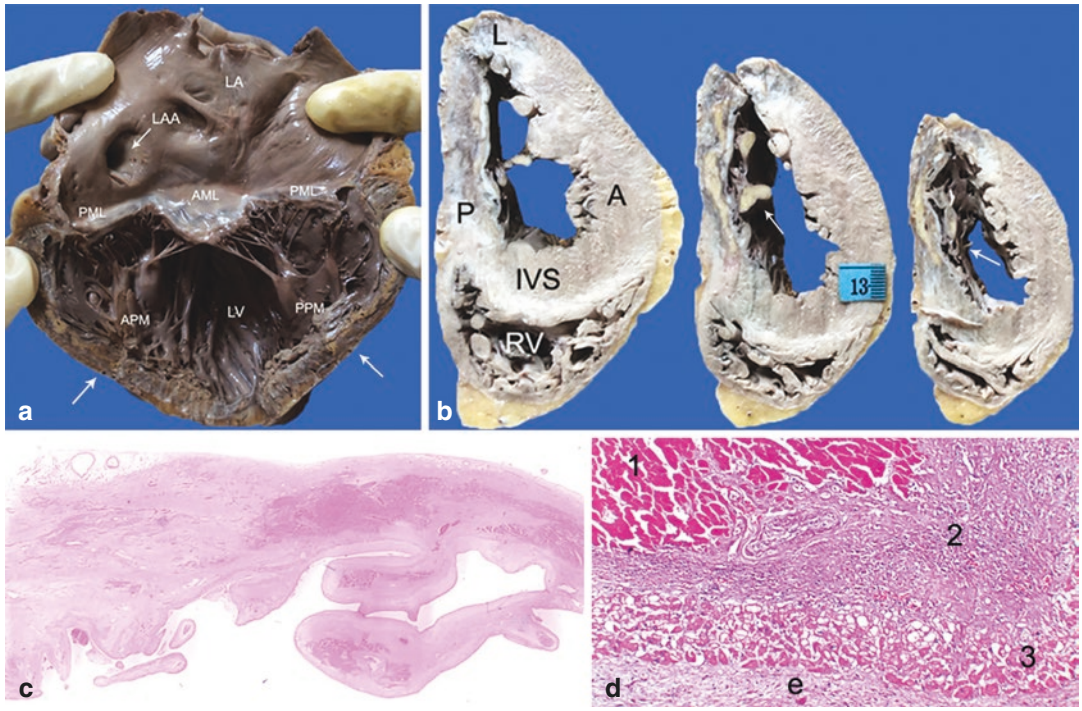

Fig. 25.1 (**a**) Dilated left atrium LA and ventricle LV. There is thinning and yellowish discoloration of the myocardium involving the entire length of the LV (arrows); (**b**) Serial transverse slices show pale yellow areas in the myocardium rimmed by zones of congestion. The posterior group of papillary muscles (PPM, arrows) shows similar changes (*A* anterior wall, *AML* anterior mitral leaflet, *APM* anterior papillary muscle, *IVS* interventricular septum, *LAA* left atrial appendage, *L* lateral wall, *P* posterior wall, *PML* posterior mitral leaflet); (**c**) Scanned H&E stained slide showing thinning of the posterior wall with extreme attenuation of the posterior papillary muscle bellies; (**d**) Histology showing (1) Coagulative necroses, (2) Granulation tissue, (3) Myocytolyses of the subendocardial cardiomyocytes, below which lies a thickened endocardium (H&E × 400)

produced by a transmural fresh infarction that extended from the base to the apex (Fig. 25.1a). The myocardium was thinned out particularly in the middle-third with a deep yellow color and broad zones of hyperemia (Fig. 25.1b). The infarction also involved the posterior group of papillary muscles, which were flattened and pale yellow (Fig. 25.1b, c). Small subendocardial foci of grey-white scarring were also present in the same region. The sections on microscopy showed features of both fresh and healing infarction (Fig. 25.1d). Such foci were also present in the subendocardial aspect of the interventricular septum. Fresh and healing microinfarcts were also present in the posterior wall of right ventricle.

The right coronary artery was dominant. The proximal part of the artery could be transversely cut with difficulty due to the luminal stent (Fig. 25.2a). However, beyond the stent, the artery continued to show critical atheromatous stenosis with fresh occlusive thrombus (Fig. 25.2b). On histology, the plaque was eccentric and fibrous with a small core of cholesterol clefts and collections of foamy macrophages. The thrombus was fresh with organization/recanalization (Fig. 25.3) at its site of attachment with the fibro-hyalinized cap. The other epicardial arteries showed only mild atherosclerosis. Other autopsy findings included extensive pulmonary edema, acute passive venous congestion of the liver with focal hepatocytic necrosis, and diffuse renal tubular damage.

Cause of Death: Acute myocardial infarction with acute ischemic mitral regurgitation and cardiac failure.

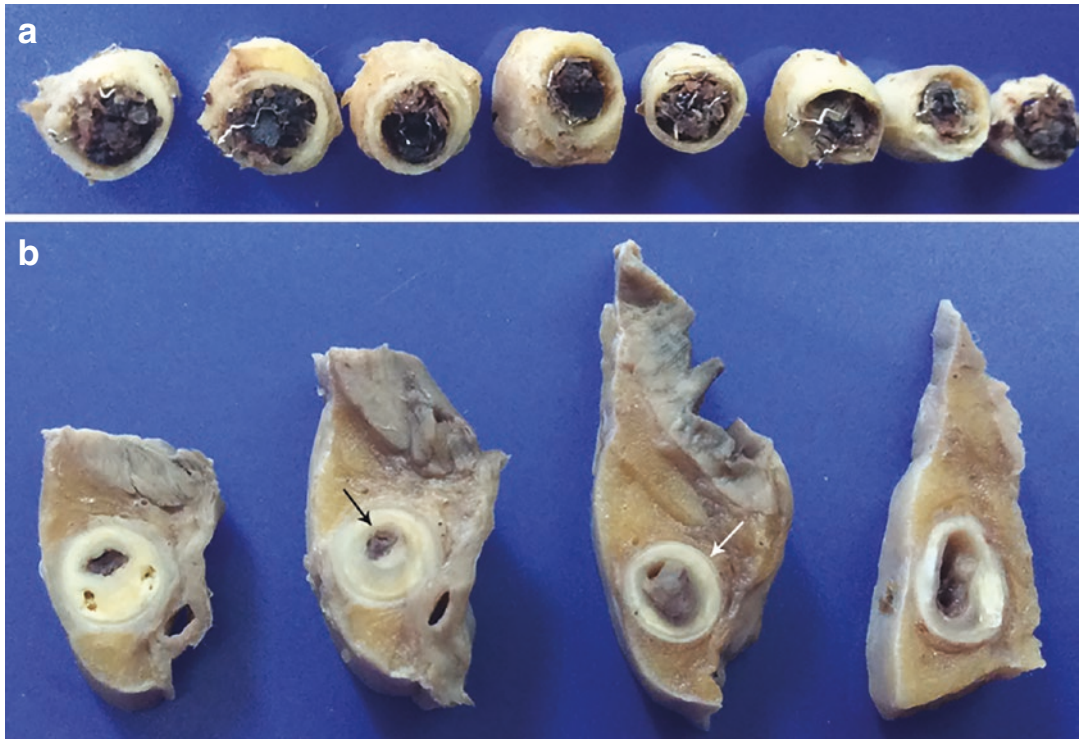

Fig. 25.2 (**a**) Stent deployed in the right coronary artery; (**b**) Distal portion of the same artery with eccentric atheroma and luminal occlusive thrombus

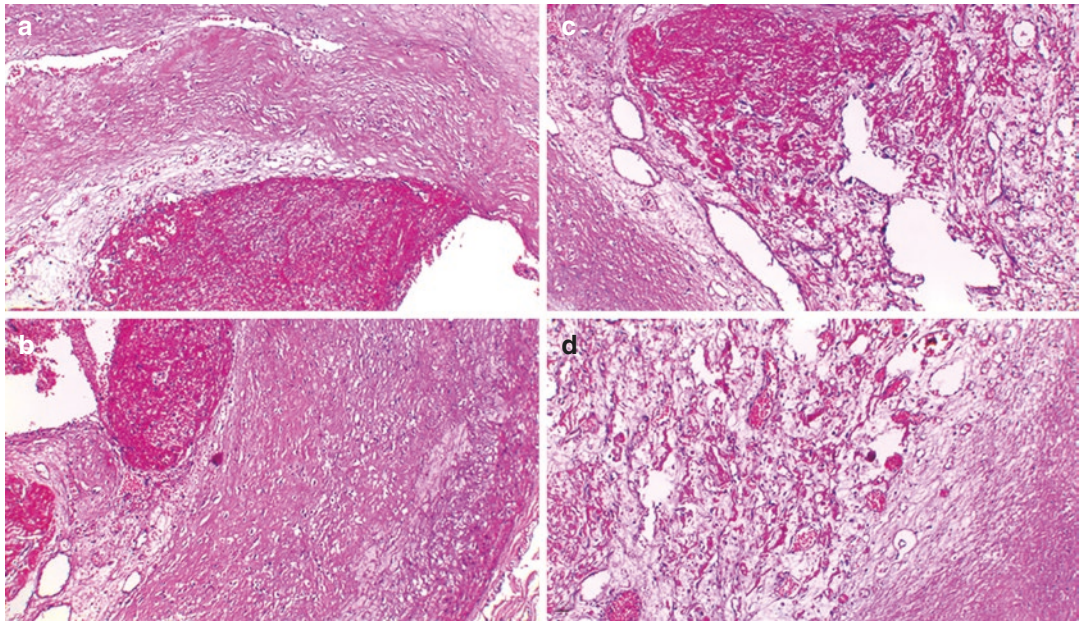

Fig. 25.3 Panels (**a**), (**b**), (**c**), and (**d**) show different histological profiles of the thrombus in the distal right coronary artery, fresh to organizing/recanalizing (H&E × 200)

25.3 Discussion

In the reported case, a substantial left ventricular myocardial loss had led to acute MR (AMR), which had progressed from a moderate degree to a severe degree in a fortnight. Depending on the mitral valvular pathology, AMR can be categorized as primary or secondary. Acute primary MR results from a structural inflammatory or noninflammatory destructive lesions affecting the mitral valve and/or its subvalvular apparatus, while in secondary (also referred to as functional) MR, the valve structure is preserved and the incompetence is a consequence of left ventricular dysfunction. Basically, the regurgitation develops from an imbalance between the closing and tethering forces on the mitral valve.

In the context of AMI, the AMR occurs with 2–7 days (median duration of hours). Torrential MR results from ruptured papillary muscles (often the posterior group) that are seen in <5% of patients. In about half of the patients (predominantly males) with AMI, AMR develops due to left ventricular myocardial damage (the secondary or functional component) and/or papillary muscle injury (the primary or structural component). This MR is of mild to moderate degree, transient, asymptomatic, and hence well-tolerated. Extensive damage particularly of the posteroinferior walls causes pronounced reduction in the LV contractility with reduction in the closing forces, while displacement of the papillary muscles produced by the ensuing LV dilatation leads to increased tethering forces. Such a pathology leads to severe AMR, which is a medical emergency as patients often present with decompensated cardiac failure (as evidenced by the clinical history in our patient). The effect of these forces is more pronounced on the posterior mitral leaflet, leading to an asymmetric type of tethering, incomplete coaptation, and hence an eccentric regurgitant jet. The imbalance is further accentuated with ischemic damage to the posterior papillary muscle (PPM) group. This group is more vulnerable to ischemia as they are usually supplied only by the posterior descending artery. In this patient, the acute infarction involved a large portion of the LV with involvement of all the bellies of the PPM. The increase in the dimensions of the leaflets and the chordae tendineae is achieved by 'uncrimping' of the collagen bundles. The process is self-perpetuating as the MR leads to further ventricular enlargement, annular dilatation, and increased interpapillary muscle distance; the final outcome is chronic MR with activation of biohumoral mechanisms mediated predominantly through tumor growth factor-β. Prognosis for ischemic AMR remains poor, with a mortality rate of 75% at 24 h and 95% at 2 weeks if left untreated. Such patients would benefit from revascularization procedure that is coupled with MV repair or replacement.

Further Reading

Calafiore AM, Totaro A, Testa N, Sacra C, Castellano G, Guarracini S, et al. The secret life of the mitral valve. J Card Surg. 2021;36:247–59.

Montrief T, Davis WT, Koyfman A, Long B. Mechanical, inflammatory, and embolic complications of myocardial infarction: an emergency medicine review. Am J Emerg Med. 2019;37:1175–83.

Nonaka DF, Fox AA. Ischemic mitral regurgitation: repair, replacement or nothing. Semin Cardiothorac Vasc Anesth. 2019;23:11–9.

Varma PK, Krishna N, Jose RL, Madkaiker AN. Ischemic mitral regurgitation. Ann Card Anaesth. 2017;20:432–9.

Vinciguerra M, Grigioni F, Romiti S, Benfari G, Rose D, Spadaccio C, et al. Ischemic mitral regurgitation: a multifaceted syndrome with evolving therapies. Biomedicine. 2021;9:447.

Watanabe N. Acute mitral regurgitation. Heart. 2019;105:671–7.

26 Acute Myocardial Infarction with Left Ventricular Free Wall Rupture

Ayushi Gupta, Girish Tasgaonkar, and Pradeep Vaideeswar

26.1 Clinical History

A 70-year-old non-hypertensive and non-diabetic woman presented with breathlessness and chest pain along with pain and swelling over the left shoulder for the past 2 days. There was a past history of cerebrovascular accident. She was admitted in a private nursing home with a clinical diagnosis of acute exacerbation of asthma and was transferred to our center for ventilator support. On examination, her general condition was poor with tachycardia and hypotension. There was a fracture of the proximal humerus with dislocation. The ECG was suggestive of inferior wall myocardial infarction with atrioventricular dissociation. She was treated with temporary pacing, antiplatelet agents, heparin, and dopamine and was mechanically ventilated. She had a sudden deterioration and expired with 19 h of admission.

A. Gupta
Seth Gordhandas Sunderdas Medical College and King Edward Memorial Hospital, Mumbai, India

G. Tasgaonkar
Department of Forensic Medicine and Toxicology, Seth Gordhandas Sunderdas Medical College and King Edward Memorial Hospital, Mumbai, India

P. Vaideeswar (✉)
Department of Pathology (Cardiovascular and Thoracic Division), Seth Gordhandas Sunderdas Medical College and King Edward Memorial Hospital, Mumbai, India

26.2 Autopsy Findings

A restricted autopsy (partial chest) was done. *In-situ* examination of the thoracic viscera revealed distension of the pericardial sac. It contained about 100 mL of hemorrhagic fluid with blood clots that weighed 600 g (Fig. 26.1a). The heart was normal in size (290 g). The right coronary artery had a dominant distribution and showed 0.2 cm segment of critical stenosis before its descent as the posterior descending artery. This had resulted in a transmural infarction over the posterior wall seen as faintly yellowish discoloration with congestion as seen from the epicardial surface. Over the discolored area was present an irregular vertically oriented tear (1.5 × 0.5 cm, Fig. 26.1b) at the midportion of the posterior wall of the left ventricle, which was responsible for the hemopericardium, cardiac tamponade, and sudden deterioration. Serial transverse sections showed thinning and pale yellow coloration of the basal region of the posterior wall with a regular, straight tract at the junction of the infarct with the viable myocardium (Figs. 26.1c, 26.2 and 26.3). There was also involvement of the adjoining posterior one third of the interventricular septum. These regions showed coagulative necroses of the myofibers with prominent interstitial edema and patchy intense neutrophilic infiltration. The

P. Vaideeswar (ed.), *Tropical Cardiovascular Pathology*,
https://doi.org/10.1007/978-981-19-3720-0_26

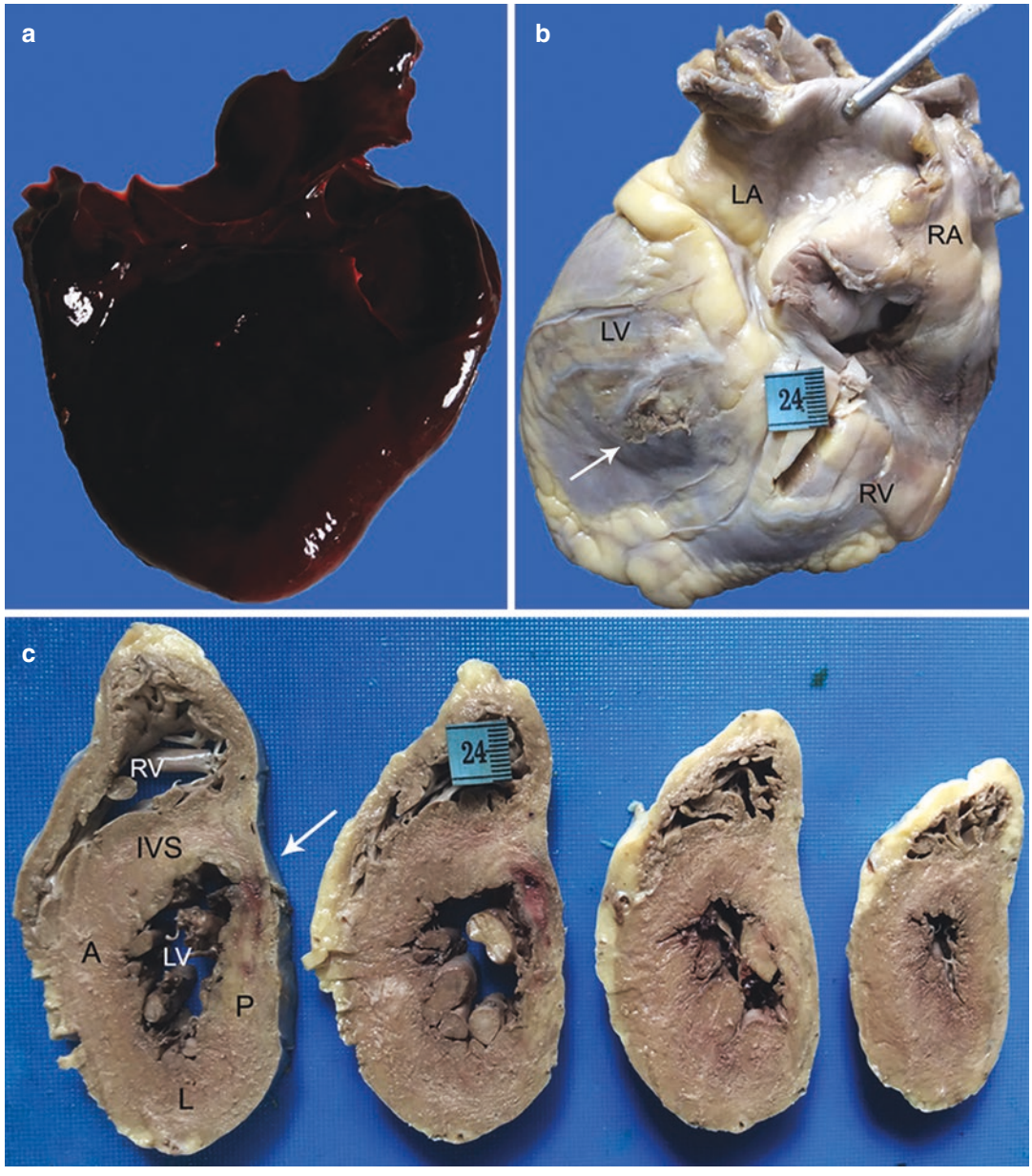

Fig. 26.1 (**a**) Large blood clot which was seen to cover the posterior aspect of the heart; (**b**) Ragged tear (arrow) over the midportion of the posterior wall of the left ventricle LV, surrounded by epicardial congestion; (**c**) Straight tract present at the junction of the fresh infarct in the posterior P wall with normal appearing interventricular septum IVS (*A* anterior wall, *L* lateral wall, *LA* left atrium, *RA* right atrium, *RV* right ventricle)

posterior papillary muscle also showed foci of necrotic fibers. The right coronary artery which was responsible for this catastrophe showed a thin-cap atheroma (fatty atheroma, See Chap. 24) with overlying occlusive fresh thrombus. Other organ findings included pulmonary edema, centrilobular emphysema, hepatic centrivenular hemorrhagic necroses, and patchy acute renal tubular necrosis.

Cause of Death: Left-ventricular free wall rupture (LVFWR), hemopericardium, and cardiac tamponade.

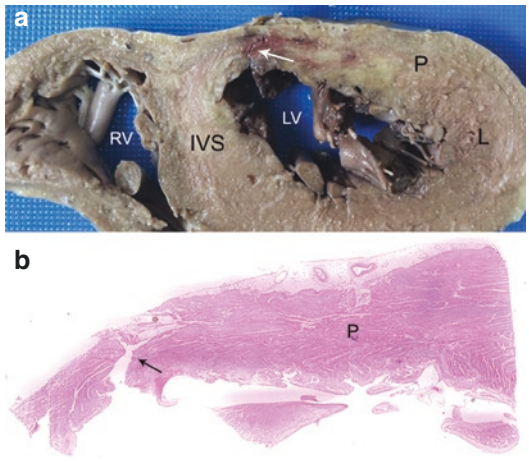

Fig. 26.2 Regular tract within the posterior wall P seen as (**a**) Close-up (white arrow) on gross inspection (*L* lateral wall, *LV* left ventricle, *IVS* interventricular septum, *RV* right ventricle) and on (**b**) Scanned H&E section (black arrow)

26.3 Discussion

Apart from ischemic mitral regurgitation, another important and lethal mechanical complication of acute myocardial infarction (AMI) is myocardial rupture, with an overall incidence of 2.3%. The ruptures may occur in the left ventricular free wall, papillary muscles and/or interventricular septum; increased application of prompt percutaneous interventions and thrombolytic therapy would decrease or have decreased this incidence to about 1.7%. The major risk factors for the rupture can be broadly attributed either to the patient or the infarct characteristics. The patient-related factors are an older age (typically >70 years), female gender, smoking or tobacco use, hypertension, obesity (with increased epicardial adipose tissue), sedentary lifestyle, and delayed admission after onset of symptoms of AMI. There

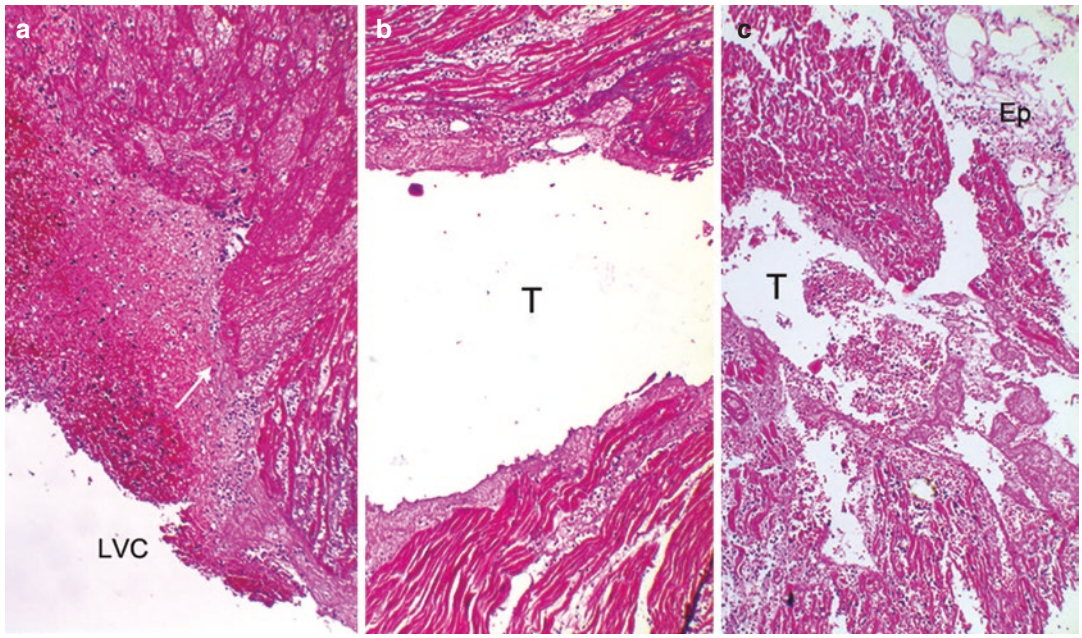

Fig. 26.3 (**a**) Tear (arrow) on the endocardial surface (*LVC* left ventricular cavity), partially sealed by fibrin; (**b**) Tract T in the midmyocardial region; (**c**) Tract T opening on to the epicardial Ep surface. Note that the tract is flanked on either side by coagulative necrotic myofibers with neutrophils (H&E × 200)

is often a lower frequency of diabetes mellitus in these patients. The acute infarction is generally smaller (as compared with those that cause cardiogenic shock) and transmural and is usually seen as the first manifestation of ischemic heart disease (IHD); the latter feature suggests that these patients have not yet developed a good collateral supply. Our patient was 70 years of age and did not have hypertension or diabetes. She also did not have regional fibrosis of the left ventricle, indicating that this had been the first episode of infarction. But she did have a past history of cerebrovascular accident and almost synchronous left-sided chest pain and shoulder pain due to humeral fracture. Osteoporosis is common among the elderly and postmenopausal women and it can lead to fractures from trivial trauma. Indeed, few studies have shown a link osteoporosis and IHD with raised C-reactive protein and inflammatory cytokines.

Basically, LVFWR (as do the other ruptures) commences with an endocardial tear. Very often, the tears are vertically oriented as they result from stretching of the damaged myocardium. They are situated at the midventricular level or at the junction of the interventricular septum to the free walls and are seen over the anterior or lateral walls, explained by the increased frequency of involvement of left coronary arterial system in IHD. Moreover, they may be present in the midportion of the AMI or at the junction of the viable and nonviable myocardium. The infarct in this case was almost 4 days old and revealed coagulative necrosis and fairly intense neutrophilic infiltrate, which would have rendered softening of the myocardium. This is the timing of most cases of ruptures and is termed as "late", as opposed to "early" ruptures that present within 24 h consequent to interstitial edema. In this setting, reperfusion injury may also be a contributing factor. The tear leads to formation of an intramyocardial tract, which can take the straight path of least resistance (simple tract) or may adopt a meandering course within the myocardium (complex tract). The endocardial tear was present at the posterior wall AMI/interventricular septal interface, and the tract was simple in the heart that was examined. Unfortunately, the lady presented finally with complete, acute LWFWR, or a blowout lesion causing a rapid chain of events of hemopericardium, cardiac tamponade, and death. In a minority of the cases, the through-and-through rupture is limited by pericardial adhesions or diaphragmatic support for posteroinferior wall infarcts, leading to LV pseudoaneurysms. This may also be a feature of narrow tracts. In few others, the rupture is incomplete leading to intramyocardial dissecting hematomas. Myocardial rupture still remains a major and catastrophic event (5–24% postinfarction deaths) and early diagnosis and treatment with prior education regarding proactive, healthy, and preventive measures in high-risk groups may confer a high survival rate.

Further Reading

Matteucci M, Fina D, Jiritano F, Meani P, Blankesteijn WM, Raffa GM, et al. Treatment strategies for post-infarction left ventricular free-wall rupture. Eur Heart J Acute Cardiovasc Care. 2019;8:379–87.

Montrief T, Davis WT, Koyfman A, Long B. Mechanical, inflammatory, and embolic complications of myocardial infarction: an emergency medicine review. Am J Emerg Med. 2019;37:1175–83.

Paccou J, D'Agnelo S, Rhodes A, Curtis EM, Raisi-Estabragh Z, Edwards M, et al. Prior fragility fracture and risk of incident ischaemic cardiovascular events: results from UK biobank. Osteoporos Int. 2018;29:1321–8.

Roberts WC, Burksa KH, Ko JM, Filardo G, Guileyardo JM. Commonalities of cardiac rupture (left ventricular free wall or ventricular septum or papillary muscle) during acute myocardial infarction secondary to atherosclerotic coronary artery disease. Am J Cardiol. 2015;115:125–40.

Vaideeswar P, Chaudhari JP, Butany J. Mechanical complications of myocardial infarction. Diagn Histopathol. 2013;19:13–9.

Acute Hemorrhagic Myocardial Infarction

27

Swati Kolhe, Pranita Zare, and Pradeep Vaideeswar

27.1 Clinical History

A 63-year-old woman, chronic tobacco chewer and hypertensive (since 8 years and on regular therapy), was admitted in the Emergency Services Department at 0825 h with severe chest pain that had been present since 0500 h. On general examination, the general condition was fair with pulse rate of 80 per minute, blood pressure 110/70 mmHg, and respiratory rate of 22 per minute. Both heart sounds were heard; there was no murmur. Investigations revealed hemoglobin 9.1 g/dL, creatinine 1.9 mg/dL, cholesterol 248 mg/dL, and low-density lipoprotein 203.4 mg/dL; other hematological, hepatic, renal, and other lipid parameters were normal. An ECG revealed acute myocardial infarction (AMI) of the anterior wall and she was immediately thrombolyzed with streptokinase (2 h and 15 min after chest pain), which was followed by antiplatelet drugs, heparin, and statins. Following thrombolysis, the chest pain was relieved, but the patient complained of mild back pain. Transthoracic echocardiography performed on the following day revealed ejection fraction of 35% and thrombus at the left ventricular apex. On the second day of admission, the prothrombin time was 18.1 s (international normalized ratio of i.51) and the creatinine level rose to 2.4 mg/dL. There were 15–20 pus cells and 4–5 RBCs in the urine and an ultrasound showed 4 mm calculus at the lower pole of the left kidney. A clinical diagnosis of urinary tract infection with acute kidney injury was made. A week later she developed multiple ecchymotic patches and a large hematoma (8 × 5 × 4 cm) over dorsum of right hand; no intervention was performed and heparin/antiplatelet drugs were continued. During this period, there was decline of her hemoglobin value to 7.7 g/dL, while the creatinine value continued to remain high. On the 10th day of admission, the patient complained of abdominal pain and a computed tomographic scan revealed 18.3 × 10 × 8.6 cm left-sided retroperitoneal hematoma, anterior to the psoas muscle. In view of this development, the anticoagulation was stopped; however, there was rapid deterioration and the patient succumbed.

27.2 Autopsy Findings

A complete autopsy was performed. There was pallor and ecchymotic patches over the anterior chest wall and right forearm with a hematoma over the dorsum of the right hand (Fig. 27.1a).

S. Kolhe
Department of Pathology, Seth Gordhandas Sunderdas Medical College and King Edward Memorial Hospital, Mumbai, India

P. Zare · P. Vaideeswar (✉)
Department of Pathology (Cardiovascular and Thoracic Division), Seth Gordhandas Sunderdas Medical College and King Edward Memorial Hospital, Mumbai, India

P. Vaideeswar (ed.), *Tropical Cardiovascular Pathology*,
https://doi.org/10.1007/978-981-19-3720-0_27

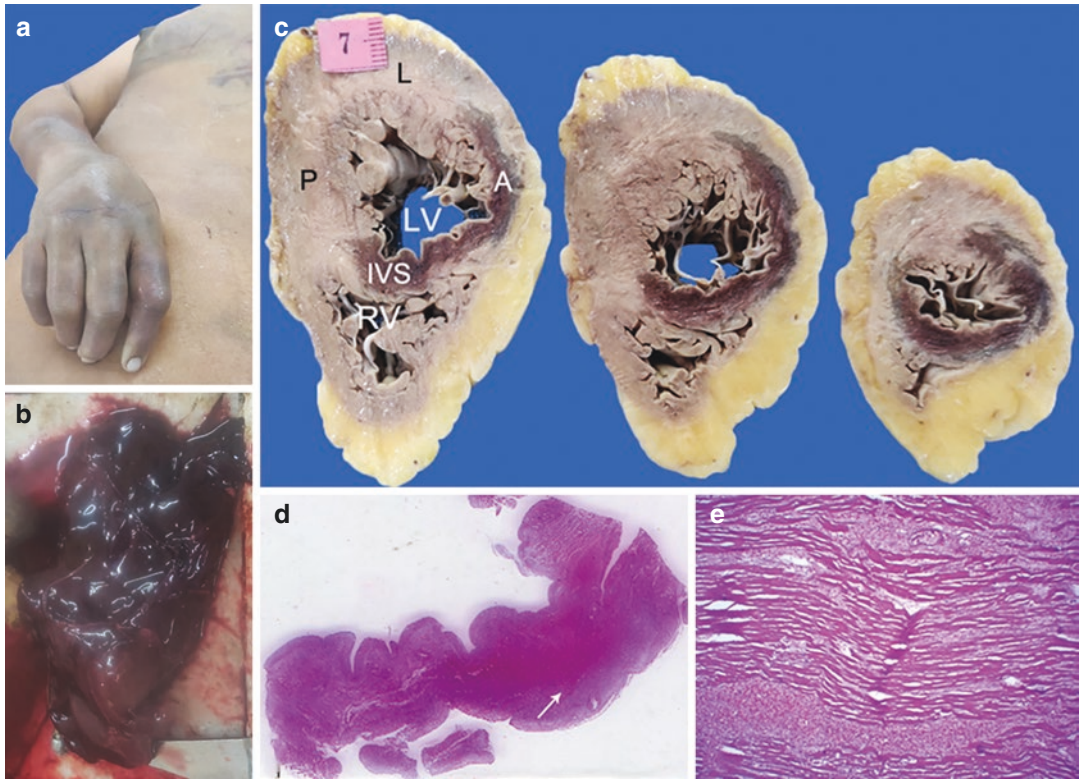

Fig. 27.1 (**a**) Ecchymosis over the anterior chest wall and right forearm with hematoma over the dorsum of the right hand; (**b**) Large blood clot retrieved from the retroperitoneal region; (**c**) Bread-loafed myocardium showing the presence of a transmural hemorrhagic infarction over the anterior wall A and anterior two-thirds of the interventricular septum IVS (L lateral wall, LV left ventricle, P posterior wall, RV right ventricle); (**d**) Scanned section of the interventricular septum showing the focus of hemorrhage (arrow); (**e**) Necrotic cardiomyocytes widely separated by interstitial edema and large numbers of red blood cells. Note paucity of neutrophils (H & E × 200)

In-situ examinations of the thoracic and abdominal cavities were normal. A very large retroperitoneal hematoma (RPH) was noted on the left paravertebral gutter. The heart was mildly enlarged (300 g) with mild enlargement of left ventricle (LV). Transverse section through both the ventricles displayed thinning and transmural hemorrhagic discoloration of the anterior wall and anterior two thirds of interventricular septum extending from the base to apex (Fig. 27.1b). Towards the apical region, the infarct was almost circumferential; there was no apical thrombus. The zone of the hemorrhagic infarct was wider in the septal wall (Fig. 27.1c). In the center of the affected myocardium, there were necrotic fibers, which were widely separated by extensive hemorrhage (Fig. 27.1d) and interstitial edema devoid of neutrophils. These areas were surrounded by exuberant granulation tissue extending towards the subepicardial and subendocardial regions. Remnants of thrombi were also not seen despite adequate sampling, even at the apex. The right ventricular wall also showed small areas of healing infarction (Fig. 27.2a).

The right coronary artery was dominant. The left anterior descending artery from its origin for a length of 0.4 cm showed 50% luminal narrowing by an eccentric atheroma; thrombotic occlusion was not present. However, on histology, a recanalized thrombus superimposed on eccentric fibro-fatty atheroma was noted. There were 2 lumens. The smaller channel still contained adherent fibrinous material (Fig. 27.2b), and both lumens were bordered by foamy and hemosiderin-laden macrophages (Fig. 27.2c); Focal calcification and basal collections of cholesterol clefts

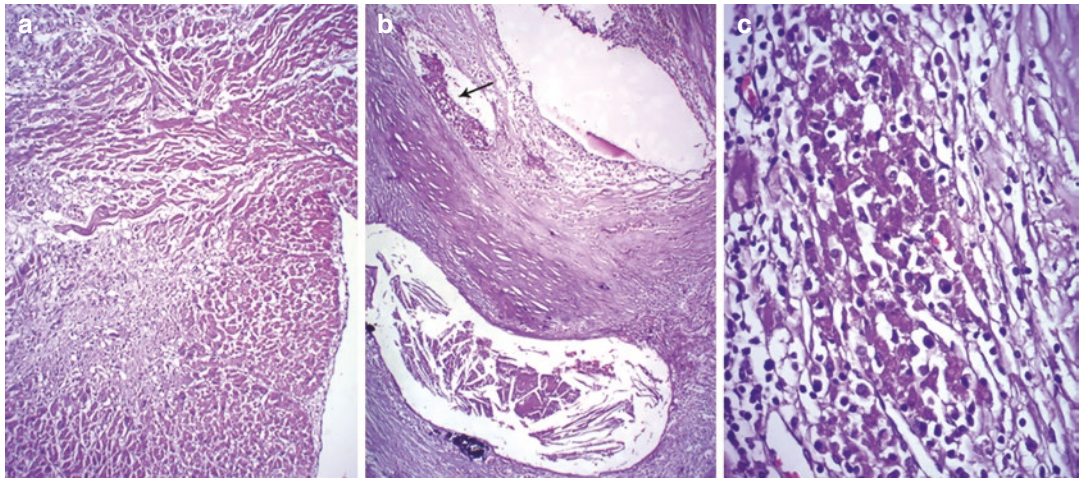

Fig. 27.2 (**a**) The subendocardial region of the right ventricle showing myocardial replacement by granulation tissue (H&E × 400); (**b**) The stenosed left anterior descending artery showing 2 lumens, the smaller of which still had adherent fibrin thrombus (H&E × 100); (**c**) Collections of hemosiderophages (H&E × 400)

and inflammation were also present. The lungs were edematous with a focus of fresh hemorrhage in the medial segment of the right upper lobe. The kidneys showed nephrosclerotic features with nephrolithiasis.

Cause of Death: Retroperitoneal hematoma and hypovolemic shock.

27.3 Discussion

This case illustrates the development of unfortunate events following reperfusion procedure for AMI in a woman in her sixth decade of life. AMI (See Chaps. 24–26) remains an important cause of morbidity and mortality worldwide. To improve survival and future quality of life, reperfusion techniques have been devised to decrease the size of ischemic myocardial injury and reverse morphological changes that develop in the ischemic cardiomyocytes. Reperfusion, through thrombolysis (e.g., streptokinase therapy used in the current case) and/or percutaneous coronary interventions, restores the blood flow beyond the coronary occlusion, but has to be achieved within 20 min ("time is muscle") for complete regional myocardial salvage. This has the most favorable outcome. If the procedure is performed in about 4 h of the infarction (critical period), there is recovery of some part of the myocardium. Beyond the critical period, the reperfusion results in unfavorable outcomes due to development of reperfusion injury in the form of microvascular obstruction or the no-flow phenomenon.

Ischemia alters the endothelial integrity, leading to increased microvasculature permeability. Due to proximal coronary occlusion and absent blood flow, no hemorrhage occurs in the edematous interstitium in the region of the AMI. Following delayed reperfusion, the no-flow occurs due to endothelial swelling, intraluminal protrusions and cytoplasmic blebs, distal embolization of the thrombotic material or atheromatous debris, extrinsic compression of the microvasculature by swelling of the cardiomyocytes and interstitial edema, neutrophil-platelet aggregates, and preexisting microvascular dysfunction (for example in diabetes mellitus). The reperfusion leads to generation of oxidative stress, inflammatory cytokines, and other cell-damaging molecules leading to reperfusion arrhythmias and myocardial stunning. Besides, it can also lead to exuberant extravasation of the red cells from the leaky capillaries with the formation of a hemorrhagic infarction. The intramyocardial hemorrhage occurs in almost 60% of the patients and has been earlier described in

many autopsy studies. It is now well-characterized on cardiac magnetic resonance imaging, which also brings out the characteristic zonation as seen on histopathology. The hemorrhage enhances the size of the infarction and can lead to additional complications such as acute myocardial ruptures (See Chap. 26). Though hemorrhagic infarction was seen in our case, the cause of death was related to the anticoagulant therapy.

Our patient developed 2 episodes of pain. The first episode was a backache that was present during the streptokinase infusion, which is an infrequent phenomenon with a still elusive etiopathogenesis. This usually ceases on completion or in some cases suspension of the thrombolytic therapy. The abdominal pain, which developed subsequently after 10 days of thrombolysis, occurred because of a large RPH with associated decrease in the hemoglobin and was preceded by cutaneous ecchymosis and hematoma. In retrospect, it is possible that the backache could have been an early sign of the RPH that caused abdominal pain when it reached a larger size. The bleeding in the soft tissues was the major complication of anticoagulant therapy; heparin was used in this case. The RPH (incidence of about 0.1%) most often caused blunt abdominal trauma or medical interventions. Therapeutic anticoagulation results in spontaneous RPH, seen in about 0.6–6.6% of such patients, who are often elderly women. Heparin is excreted by the kidneys and hence, compromised renal function is an additional risk factor for heparin-induced bleeding. Our patient had a high creatinine value throughout her ward stay related to her hypertensive nephropathy. The case reiterates that timely restoration of myocardial reperfusion is needed to reestablish the balance between myocardial oxygen demand and supply. Furthermore, recognition of RPH, which usually requires conservative management, is also imperative to avoid a devastating consequence.

Further Reading

Betgem RP, de Waard GA, Nijveldt R, Beek AM, Escaned J, van Royen N. Intramyocardial haemorrhage after acute myocardial infarction. Nat Rev Cardiol. 2015;12:156–67.

Frank A, Bonney M, Bonney S, Weitzel L, Koeppen M, Eckle T. Myocardial ischemia reperfusion injury—from basic science to clinical bedside. Semin Cardiothorac Vasc Anesth. 2012;16:123–32.

Maruyama T, Abe M, Furukawa T, Kobayashi S, Yoshida Y, Noda H, et al. Retroperitoneal hematoma in a patient with advanced chronic kidney disease receiving warfarin therapy. Intern Med. 2016;55:1153–8.

Neri M, Riezzo I, Pascale N, Pomara C, Turillazzi E. Ischemia/reperfusion injury following acute myocardial infarction: a critical issue for clinicians and forensic pathologists. Mediators Inflamm. 2017;2017:7018393.

Wang G, Yang HJ, Kali A, Cokic I, Tang R, Xie G, et al. Influence of myocardial hemorrhage on staging of reperfused myocardial infarctions with T2 cardiac magnetic resonance imaging: insights into the dependence on infarction type with ex vivo validation. JACC Cardiovasc Imaging. 2019;12:693–703.

Warren MH, Bhattacharya B, Maung AA, Davis KA. Contemporary management of spontaneous retroperitoneal and rectus sheath hematomas. Am J Surg. 2020;219:707–10.

28 Healed Myocardial Infarction with Left Ventricular Mural Thrombus

Pradeep Vaideeswar

28.1 Clinical History

A 32-year-old male (ex-smoker and ex-alcoholic) was transferred from a private nursing home (on request from the relatives) to our center with complaints of severe abdominal pain and associated nausea since the last 8 days. He was on insulin therapy for his diabetes mellitus and had sustained a myocardial infarction 4 years ago. A CT angiography performed had revealed a large thrombus in the left ventricle, occlusion of the distal superior mesenteric artery, and bilateral renal infarcts. On examination, he was in poor general condition with a pulse rate of 135/min and blood pressure of 140/80 mmHg. There was generalized abdominal tenderness with guarding. With a clinical diagnosis of small bowel gangrene, an emergency exploratory laparotomy was carried out. There was extensive gangrenous change of the small intestine, beginning 32 cm distal to the duodenojejunal junction to 40 cm proximal to the ileocecal junction. About 42 cm of the midportion of the jejunoileal loops were viable. A resection and anastomosis was carried out. Unfortunately, reexploration was attempted twice for anastomotic leaks. His condition continued to deteriorate and the patient expired after 10 days of admission. The investigations have been tabulated (Table 28.1).

Table 28.1 Investigations

Hematological	[a]Hemoglobin 9.1 g/dL [a]Total leukocyte count 12,200/cmm [a]Differential count—Neutrophil predominant [a]Platelet count 1.70 lakhs/cmm
Biochemical—Routine	[a]Blood glucose 216 mg/dL [a]Serum creatinine 3.1 mg/dL [a]Blood urea nitrogen 32 mg/dL [a]SGOT 30 U/L [a]SGPT 14 U/L [a]Total proteins 6.1 g/dL [a]Albumin 2.3 g/dL [a]Globulin 3.8 g/dL [a]Total bilirubin 3.7 mg/dL [a]Direct bilirubin 2.7 mg/dL [a]Sodium 135 mEq/L [a]Potassium 3.8 mEq/L [a]Chloride 113 mEq/L

[a]Mean values

P. Vaideeswar (✉)
Department of Pathology (Cardiovascular and Thoracic Division), Seth Gordhandas Sunderdas Medical College and King Edward Memorial Hospital, Mumbai, India

P. Vaideeswar (ed.), *Tropical Cardiovascular Pathology*,
https://doi.org/10.1007/978-981-19-3720-0_28

28.2 Autopsy Findings

The heart was mildly enlarged (230 g) with moderate enlargement of the left ventricle (Fig. 28.1a). There was mild patchy opacification of the epicardium with an oval milk patch over the anterior aspect of the apex (Fig. 28.1a). The descending aorta showed only mild atherosclerosis, devoid of complications (Fig. 28.1b). The dominant right coronary artery and the left main/circumflex arteries were devoid of significant atherosclerosis. However, the left anterior descending artery right from its origin for a length of 2 cm showed luminal occlusion by recanalized/organized pale brown gelatinous thrombus (Fig. 28.2). A large healed transmural infarct occurring as a consequence was noted in the anterior wall and anterior two-thirds of the interventricular septum from the mid-third to the apex. The endocardium overlying the healed infarct was exceedingly thickened and pearly-white with a large organizing thrombus occupying most of the ventricle topped by fresh thrombus towards the basal aspect (Fig. 28.3). Transmural scarring was also present in the posterolateral region. The thrombosis had resulted in infarcts in the kidneys and spleen and had been responsible for extensive small intestinal gangrene. Thromboemboli were also seen in the arterial radicles in the gastric wall and mesentery. There was also early acute pancreatitis.

Cause of Death: Multiorgan failure in a case of mural left ventricular thrombus with thromboembolism.

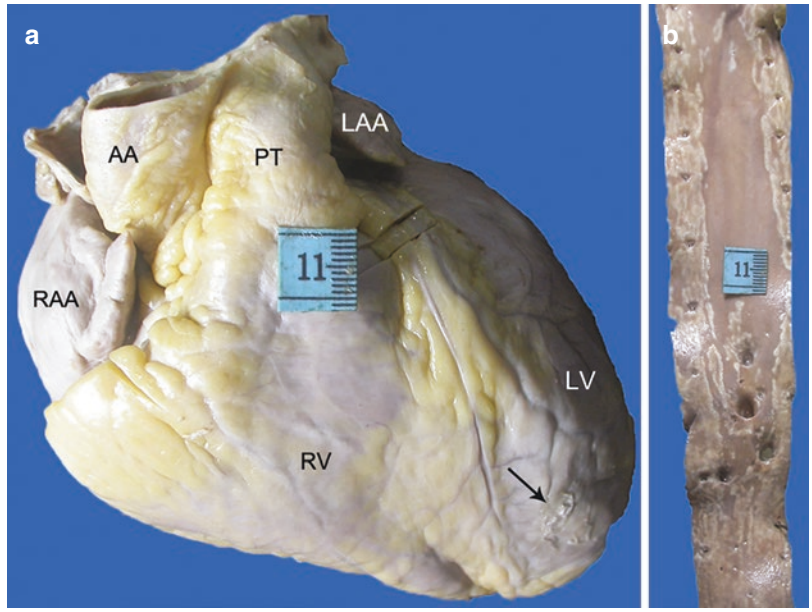

Fig. 28.1 (**a**) Moderate cardiomegaly with enlarged left ventricle LV. Milk patch (arrow) is present over the apex (*AA* ascending aorta, *LAA* left atrial appendage, *PT* pulmonary trunk, *RAA* right atrial appendage, *RV* right ventricle); (**b**) Opened out descending aorta mainly showing fatty streaks and plaques

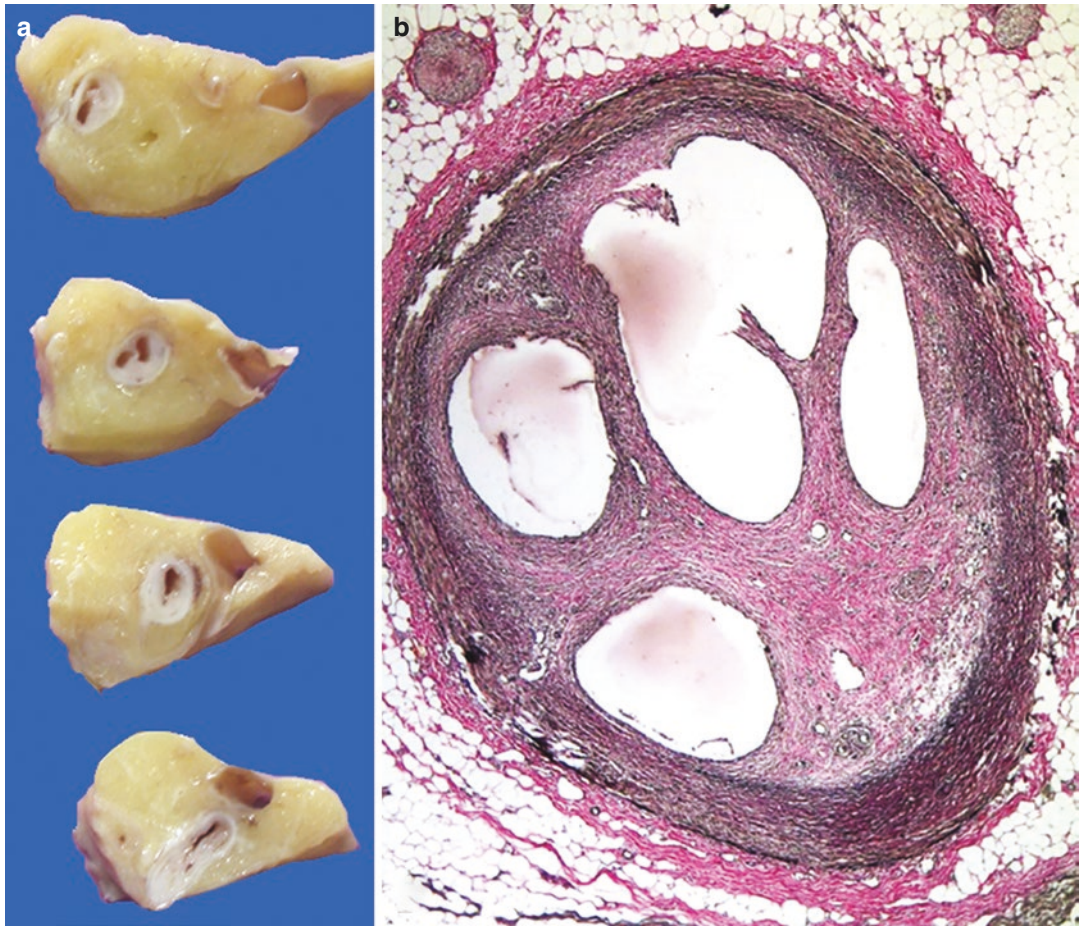

Fig. 28.2 (**a**) Serial cross-sections of the left anterior descending artery showing multiple sieve-like openings produced by (**b**) Recanalizing thrombus (Elastic van Gieson × 100)

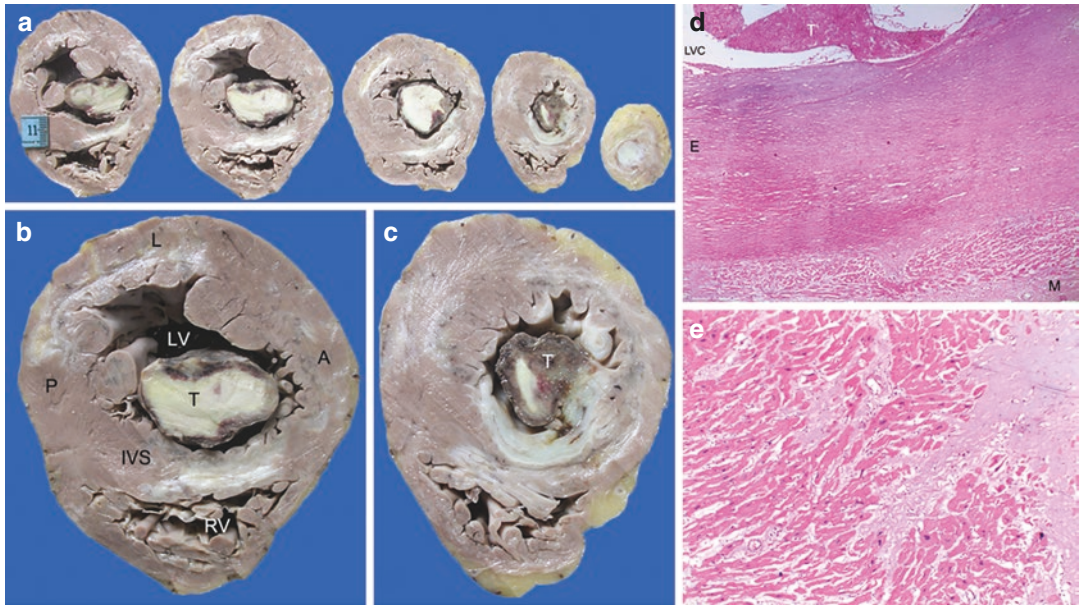

Fig. 28.3 (**a**) The entire left ventricular cavity is filled with a pale yellow thrombus topped by friable red-brown material; (**b**) Mid-portion shows the presence of transmural scarring in the anterior interventricular septum IVS with focal scarring in the posterior P and lateral L walls. Smaller scars are seen in the anterior A wall (*LV* left ventricle, *RV* right ventricle); (**c**) Towards the apical aspect, the thrombus T is red brown and adherent to an exceedingly thick endocardium; (**d**) Thrombus T over a markedly thick and fibrotic endocardium E (M myocardium, H&E × 200); (**e**) Replacement fibrosis in the myocardium (H&E × 200)

28.3 Discussion

A young man, smoker and diabetic (traditional risk factors of atherosclerosis, See Chap. 24), had developed myocardial infarction at the age of 28 years. After 4 years, he presented with manifestations of acute mesenteric ischemia that necessitated extensive small intestinal surgical resection, and renal/splenic infarctions were identified at autopsy. The etiological basis for this multiorgan involvement was embolism from a large left ventricular protruding thrombus, which is an example of a life-threatening mechanical complication of myocardial infarction (See Chaps. 25 and 26). The incidence of left ventricular thrombi (LVT), which can complicate both acute and healed infarcts, has been drastically reduced by timely use of reperfusion techniques and appropriate antithrombotic agents. But, it still stands at a wide range of 2–15%, explainable on the time lag after myocardial infarction of and the modalities used for, the detection of LVT.

The Virchow's triad comprising endothelial injury, blood stasis, and hypercoagulability continues to be used to explain the pathogenetic mechanisms for arteriovenous thrombosis. These factors also contribute to the development of LVT. For healed myocardial infarction (as observed in the present case) with an element of heart failure and/or postinfarct left ventricular aneurysms, blood stasis plays the most important role and results from myocardial motion abnormalities and reduced ejection fraction. This results in 'late' thrombus formation. The same substrate would also be present with acute infarctions, but in addition the major roles are played by endocardial injury particularly with transmural infarction and ensuing protracted pro-inflammatory and pro-thrombotic milieu. Such 'early' thrombi may develop as early as in 24 h, but in most cases are seen within 2 weeks of the acute episode.

The abnormal flow kinetics in the region of myocardial dysfunction causes chiefly apical sta-

sis, irrespective of the site of infarction; the apex remains the most common site of thrombus. The thrombi can be flat and plastered to the endocardium—mural type or can grow to protrude into the ventricular chamber—protruding type. Recognizing these mass lesions through appropriate imaging techniques is very important because of the worrisome complication of systemic thromboembolism. Cardiac magnetic resonance imaging is considered as the gold standard, but from the practical point of view, a well performed transthoracic echocardiography would suffice. The embolic phenomenon usually occurs after 3–4 months and invariably affects the central nervous system; the thrombi are of the protruding type. The thrombi of smaller sizes undergo fibrinolyses. It has also been observed that patients with persistent thrombi for a prolonged duration do not show embolic episodes since they can organize and sometimes form calcific masses. Therapy with anticoagulants and thrombolytic drugs with periodic imaging are the usual modalities of therapy. In some cases, surgical thrombectomy may also be performed. In the present case, a very large thrombotic mass was noted after 4 years of the myocardial infarction, and it was partially organized with superficial deposits of fresh thrombi. Moreover, it was clinically diagnosed after the patient had developed mesenteric ischemia, which is most often caused by occlusion of the superior mesenteric artery by thromboembolus of cardiac origin. This was the clinical scenario in the index case and it entailed extensive small bowel resection. He also had infarcts of the kidneys and spleen, and in such cases, the outcome tends to be poor.

Further Reading

Barbieri A, Mantovani F, Bursi F, Faggiano A, Boriani G, Faggiano P. Optimal use of echocardiography in management of thrombosis after acute anterior myocardial infarction. Echocardiography. 2020;37:1287–95.

Cruz Rodriguez JB, Okajima K, Greenberg BH. Management of left ventricular thrombus: a narrative review. Ann Transl Med. 2021;9:520.

Gnanapandithan K, Feuerstadt P. Mesenteric ischemia. Curr Gastroenterol Rep. 2020;22:17.

Habash F, Vallurupalli S. Challenges in management of left ventricular thrombus. Ther Adv Cardiovasc Dis. 2017;11:203–13.

Massussi M, Scotti A, Lip GYH, Proietti R. Left ventricular thrombosis: new perspectives on an old problem. Eur Heart J Cardiovasc Pharmacother. 2021;7:158–67.

Coronary Stent Infection

29

Saranya Singaravel and Pradeep Vaideeswar

29.1 Clinical History

A 72-year-old non-diabetic, non-hypertensive male presented with angina, dyspnea, and diaphoresis. He was diagnosed with acute coronary syndrome due to critical stenosis of the right coronary artery (RCA). He underwent percutaneous transluminal right coronary angioplasty with balloon dilatation and stenting using a sirolimus-eluting cobalt-chromium stent (Vactaflex). Postprocedure, the patient continued to remain symptomatic; a transfemoral thrombus aspiration was performed on postprocedure days 6 and 8. As there was no improvement, the patient was transferred to our institute in poor general condition with the femoral sheath in situ. A diagnosis of restenosis of the stent was rendered and the patient was managed conservatively. The patient expired 12 h after admission.

29.2 Autopsy Findings

At autopsy, the heart was normal in size (260 g). Transverse cuts through both ventricles (Fig. 29.1) showed grey-white areas of fibrosis with superadded areas of congestion in the posterior one-third of the interventricular septum, and the posterior walls of the right and left ventricles (Fig. 29.2a, b). Microscopically, sections from the posterior one-third of the interventricular septum, and the posterior wall of the right and left ventricles showed hypereosinophilia of the cardiomyocytes, with loss of nuclei and striations, edema, hemorrhage, and neutrophilic infiltration of the interstitium (Fig. 29.2c). This placed the time of myocardial infarction to 1–3 days after occurrence of obstruction of the coronary artery, indicating that the infarction occurred after the angioplasty. The stent from

S. Singaravel
Soleil Diagnostics, Mumbai, India

P. Vaideeswar (✉)
Department of Pathology (Cardiovascular and Thoracic Division), Seth Gordhandas Sunderdas Medical College and King Edward Memorial Hospital, Mumbai, India

P. Vaideeswar (ed.), *Tropical Cardiovascular Pathology*,
https://doi.org/10.1007/978-981-19-3720-0_29

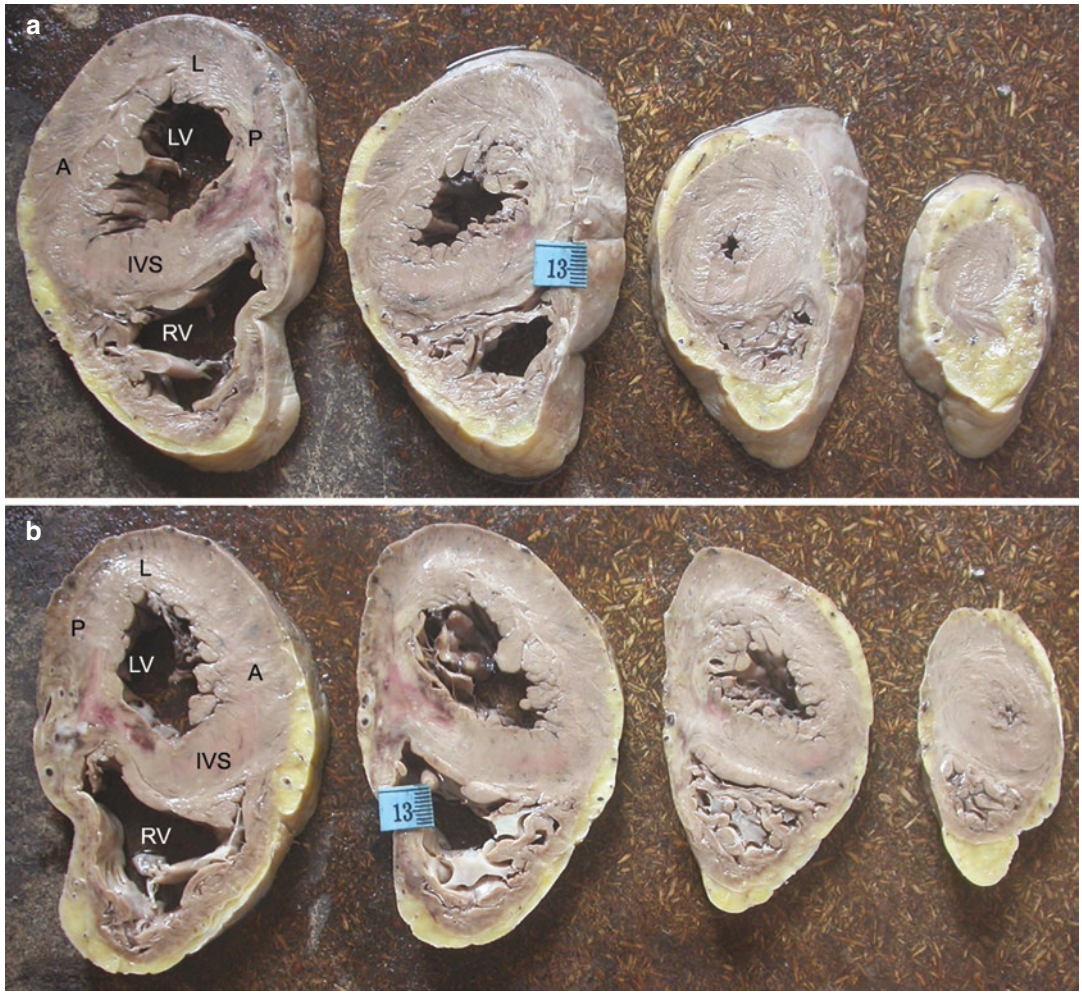

Fig. 29.1 (**a**) and (**b**) show serial cross sections of the ventricles from the base to the apex (*A* anterior wall, *IVS* interventricular septum, *L* lateral wall, *LV* left ventricle, *P* posterior wall, *RV* right ventricle)

the RCA was gently eased out and it showed adherent red-brown thrombotic material and blood clots (Fig. 29.3a). Serial sections through the RCA showed luminal brownish, friable, thrombotic material, and ectasia of the vessel with perivascular congestion (Fig. 29.3a). Section from the artery (Fig. 29.3b) showed the imprint of the stent (Fig. 29.3c–f), endoluminal thrombus formation, suppurative transmural arteritis, periarteritis (Fig. 29.4), and vascular wall ectasia. Sections from the distal radicles of the right coronary artery showed similar arteritic features (Fig. 29.5). The other coronary arteries were unremarkable. Special stains for organisms (per-iodic acid Schiff, Gomori methenamine silver, and modified Gram stains) were noncontributory.

Cause of Death: Coronary stent infection with suppurative arteritis and acute myocardial infarction.

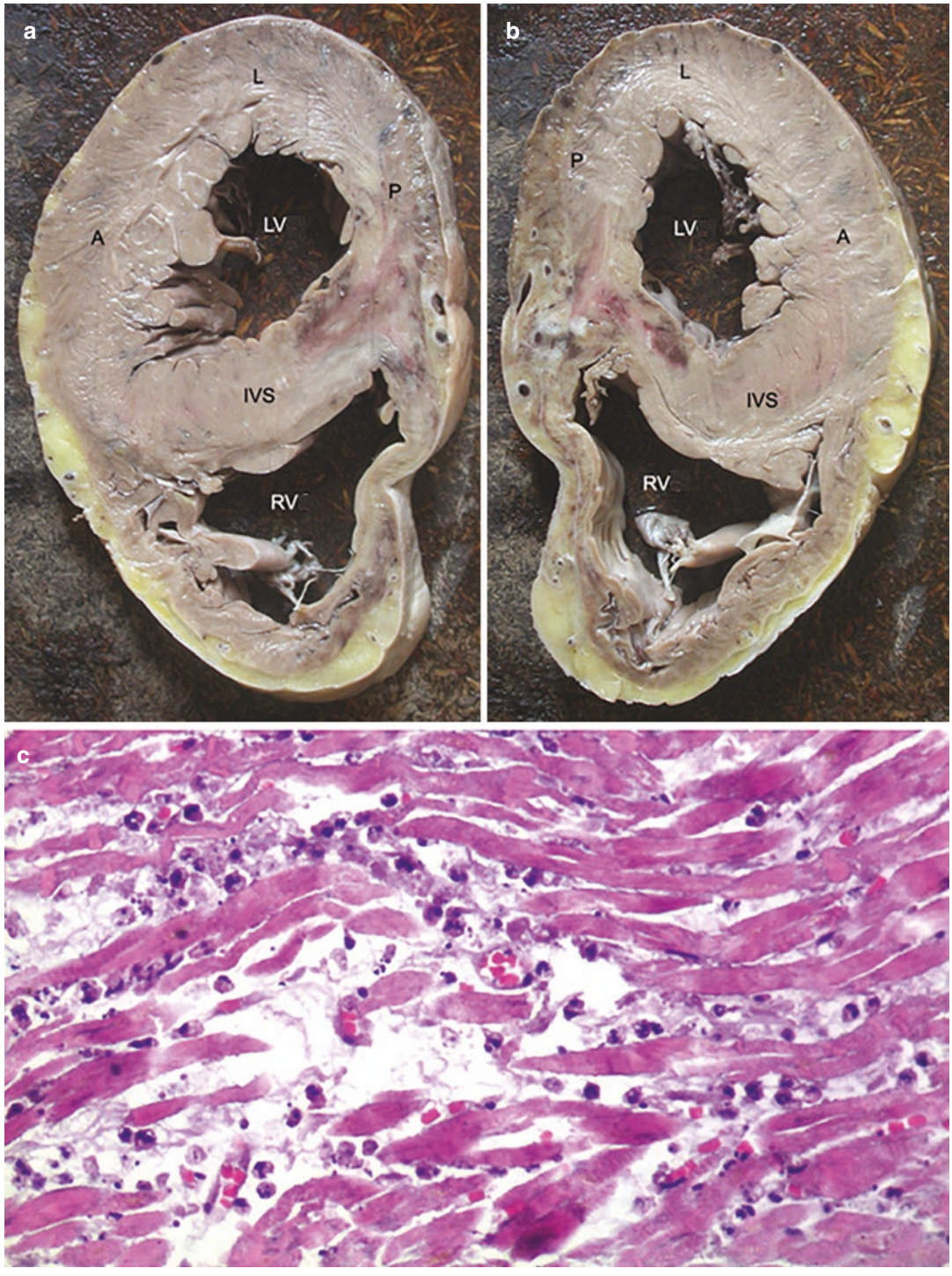

Fig. 29.2 (**a**) and (**b**) show transmural yellowish foci surrounded by hyperemic zones in the basal aspects of the posterior walls of right (RV) and left LV ventricles and posterior one third of the interventricular septum IVS (*A* anterior wall, *L* lateral wall, *P* posterior wall); (**c**) Wall of the right ventricle showing interstitial edema, coagulative necroses, and patchy neutrophilic infiltration (H&E × 400)

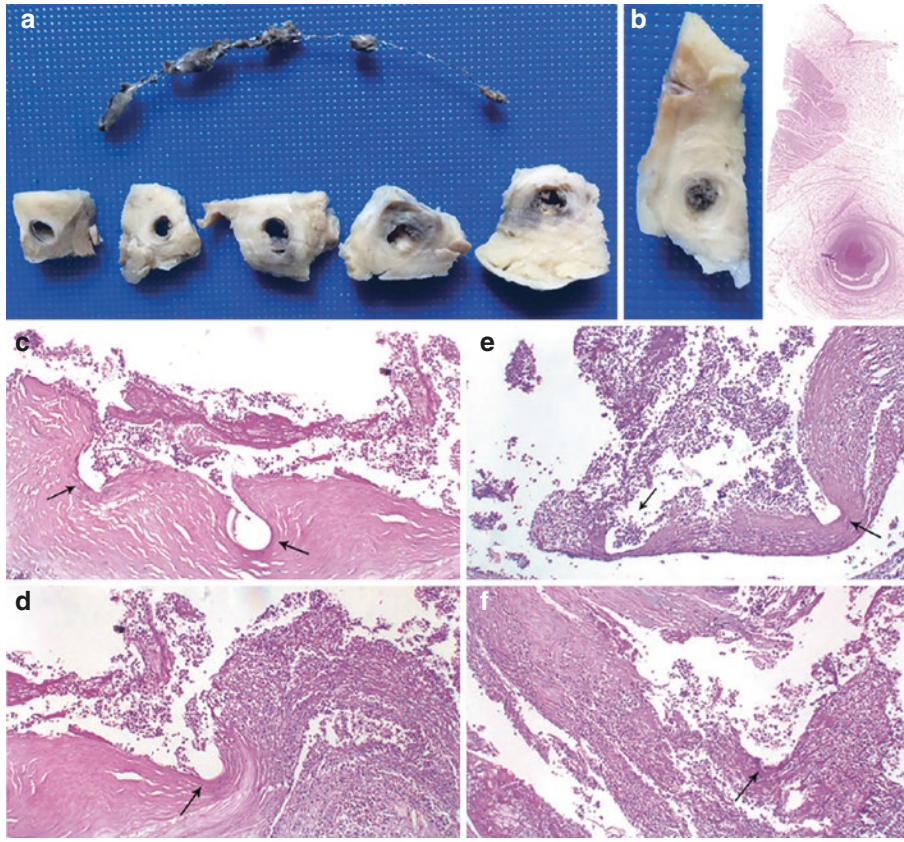

Fig. 29.3 (**a**) Stent covered with thrombi and blood clots. The right coronary artery (RCA) has been serially cross-sectioned; (**b**) Gross and scanned slide of the RCA (H&E); (**c**), (**d**), (**e**) and (**f**) All show imprints of the deployed stent (arrows) and necroses of the wall (H&E × 250)

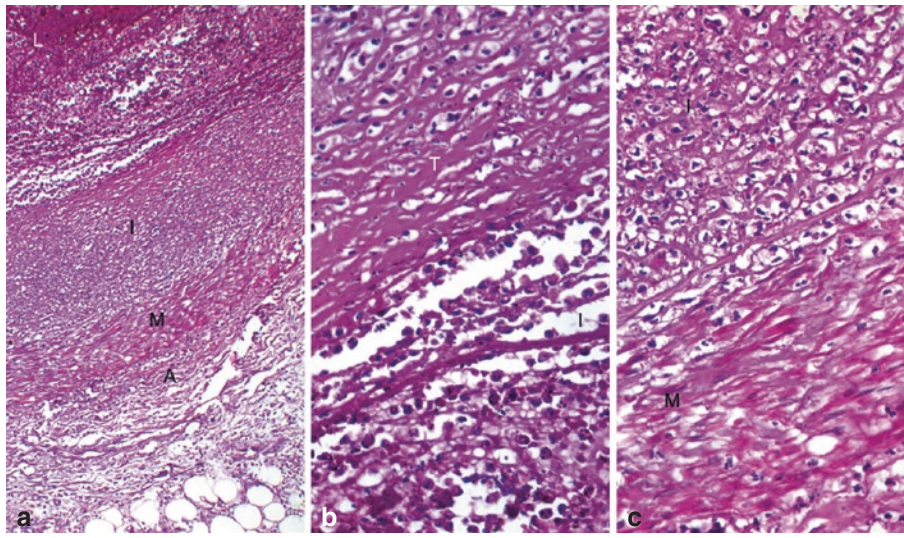

Fig. 29.4 (**a**) Lumen L is filled with thrombi admixed with blood clots. There is an intimal I fibrous plaque. The adventitial A and peri-adventitial tissue has neutrophils (H&E × 250); (**b**) The superficial aspect of the intima I is infiltrated by many neutrophils with overlying fresh thrombus T (H&E × 400); (**c**) The intimal plaque is inflamed. The internal elastic lamina (arrows) is intact. The media M also shows neutrophils towards the luminal aspect (H&E × 400)

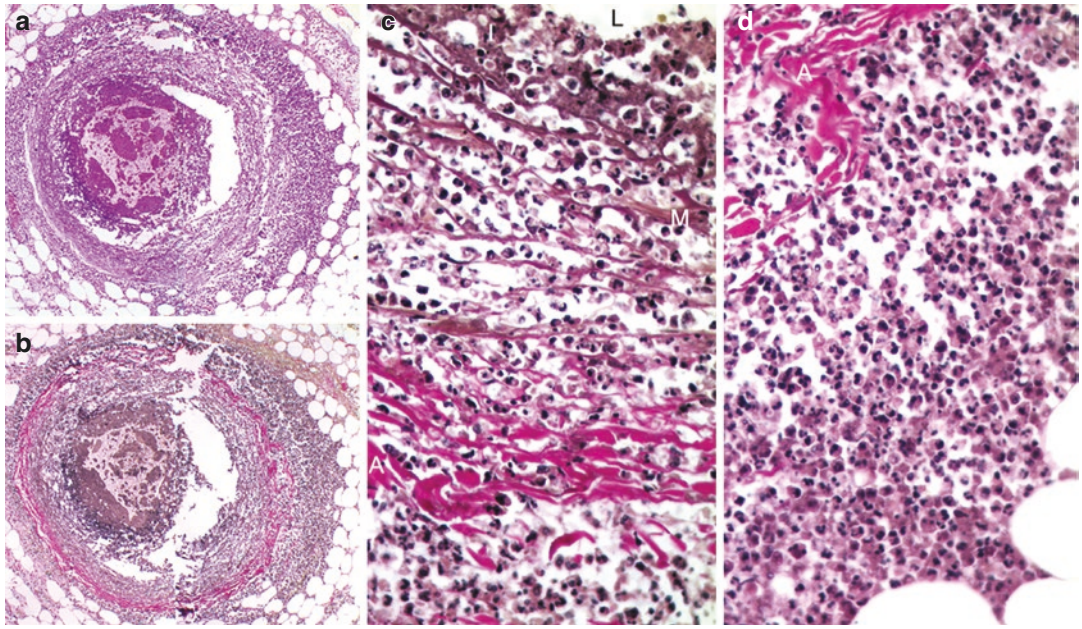

Fig. 29.5 Epicardial coronary arterial radical stained by (**a**) H&E (×100) and (**b**) elastic van Gieson stain (×100); Necrotizing arteritis with (**c**) involvement of the intima I, media M and adventitia A (elastic van Gieson × 400) and (**d**) spillover of neutrophils in the peri-adventitial region (elastic van Gieson × 400)

29.3 Discussion

Percutaneous coronary intervention (PCI), first introduced by the German radiologist Andreas Roland Grüntzig in 1977, has revolutionized the care of patients with atherosclerotic coronary artery disease. Balloon angioplasty is the most commonly performed intervention, in which a long, thin catheter with a small balloon on its tip is inserted to the site of blockage. The balloon is inflated, flattening or compressing the atherosclerotic plaque against the arterial wall. The procedure is followed by the insertion of a stent, a tubular endoluminal prosthetic device, which acts as a scaffold to stabilize the intimal flaps and restores the blood flow. Stents made entirely of metal and devoid of coatings are referred to as *bare metal* stents. Acute complications include postimplantation stent migration, traumatic disruption of the vascular walls, and thrombotic occlusion of the main artery and its branch arteries. Importantly, these stents have been implicated in the induction of neointimal hyperplasia, neoatherosclerosis, and restenosis that are seen as late complications. To counter this problem, stents are impregnated with a polymer matrix and drugs such as paclitaxel or sirolimus (*drug-eluting* stents or DES). Polymer embolization followed by a granulomatous or hypersensitivity response is known to occur with DES; however, newer biodegradable and reabsorbable stents are designed to overcome many of these problems.

The pathologist may encounter stents explanted due to a complication or in situ in an explanted heart or at autopsy. A detailed clinical history can offer insights into the number and location of the stents present. In the case of excessively calcified arteries, palpation may not be sufficient to localize the stents. In such cases, the heart should be X-rayed to determine the exact location of the stent. Rupture of the vessel wall should be ruled out on external examination. Longitudinal and transverse sections are both needed in order to study both the vascular lumen and the interface of the stent with the native vessel wall. The vessel with the stent in situ can be opened longitudinally with scissors; however, this can produce severe artifacts. Where facilities for elastic embedding and sectioning or electro-

chemical dissolution of the stent exist, these methods are preferred and allow study of the entire vascular segment.

Stent-related infection and thrombosis are exceedingly rare complications, with alarmingly high complications; such infections can occur as early or late complication. The proposed pathophysiology for stent-related infection following a percutaneous procedure is poor preparation of the puncture site with the stent itself acting as a vector and a nidus for bacterial adherence and colonization. The most commonly implicated microorganism is *Staphylococcus aureus*, a skin commensal. Inflammation of the vascular wall may be followed by complications such as pseudoaneurysm formation as seen in the present case, necrosis, or rupture of the vessel. Conflicting views exist about drug-eluting stents which are designed to prevent neointimal growth and restenosis. Some authors argue that the suppression of tissue response to injury may predispose to infection while others highlight the antimicrobial properties of these stents. The risk factors for infection may also be patient-related (age, immunosuppression, bacteremia, or other comorbidities), stent-related (local immunosuppression), procedure-related (lack of aseptic precautions and antibiotic prophylaxis), or postprocedural factors (coincident infections and repeat punctures). It has been proposed that the possibility of stent-related infection should be entertained in cases where a stent has been placed in the preceding 4 weeks, a history of multiple repeat procedures through the same arterial sheath, bacteremia, unexplained pyrexia, leukocytosis, acute coronary syndrome, or cardiac imaging suggestive of persistent inflammation. Stent-related infections due to rapidly growing *Mycobacteria* are being increasingly reported in the developing world. Inadequate infection control measures and reuse of single use devices including angioplasty balloon catheters due to financial constraints have been implicated. Concerns have also been voiced regarding the decreased antibiotic susceptibility of these isolates and the possible lack of therapeutic options for such cases in the future.

Further Reading

Elieson M, Mixon T, Carpenter J. Coronary stent infections: a case report and literature review. Tex Heart Inst J. 2012;39:884–9.

Nakamura K, Keating JH, Edelman ER. Pathology of endovascular stents. Interv Cardiol Clin. 2016;5:391–403.

Rippstein P, Black MK, Boivin M, Veinot JP, Ma X, Chen Y, Human P, Zilla P, O'Brien ER. Comparison of processing and sectioning methodologies for arteries containing metallic stents. J Histochem Cytochem. 2006;54:673–81.

Sanchez OD, Sakakura K, Otsuka F, Yahagi K, Virmani R, Joner M. Coronary stent evolution: from pathology to clinic. EMJ Int Cardiol. 2014;1:107–16.

Soman R, Gupta N, Suthar M, Sunavala A, Shetty A, Rodrigues C. Intravascular stent-related endocarditis due to rapidly growing mycobacteria: a new problem in the developing world. J Assoc Physicians India. 2015;63:18–21.

Torii S, Jinnouchi H, Sakamoto A, Kutyna M, Cornelissen A, Kuntz S, Guo L, Mori H, Harari E, Paek KH, Fernandez R, Chahal D, Romero ME, Kolodgie FD, Gupta A, Virmani R, Finn AV. Drug-eluting coronary stents: insights from preclinical and pathology studies. Nat Rev Cardiol. 2020;17:37–51.

30 Intramural Coronary Arterial Thrombosis and Myocardial Ischemia

Pradeep Vaideeswar, Jayashri Chaudhari, and Smita Divate

30.1 Clinical History

A 15-year-old healthy adolescent presented to the Emergency Services department with altered sensorium. On examination, her general condition was poor with heart rate of 108 per minute and blood pressure of 80/60 mmHg. Her investigations were as follows: hemoglobin 11.5 g/dL, total leukocyte count 6600/cmm with 66% neutrophils, platelet count 2.4 lakhs/cmm, total bilirubin of 1.6 mg/dL (direct of 0.3 mg/dL), SGOT 94 U/L, SGPT 16 U/L, total proteins 6.7 g/dL (albumin 3.4 g/dL). She expired within 6 h of admission.

30.2 Autopsy Findings

The heart (190 g) was mildly enlarged with mild biventricular dilatation. A transverse section revealed pale myocardium with multiple foci of congestion, which were more prominent over the left ventricle (Fig. 30.1). On histopathology, these foci revealed occlusive thrombi in many of

P. Vaideeswar (✉)
Department of Pathology (Cardiovascular and Thoracic Division), Seth Gordhandas Sunderdas Medical College and King Edward Memorial Hospital, Mumbai, India

J. Chaudhari
Department of Pathology, Hindu Hriday Samrat Balasaheb Thackeray Medical College, Mumbai, India

S. Divate
Department of Pathology, Seth Gordhandas Sunderdas Medical College and King Edward Memorial Hospital, Mumbai, India

P. Vaideeswar (ed.), *Tropical Cardiovascular Pathology*,
https://doi.org/10.1007/978-981-19-3720-0_30

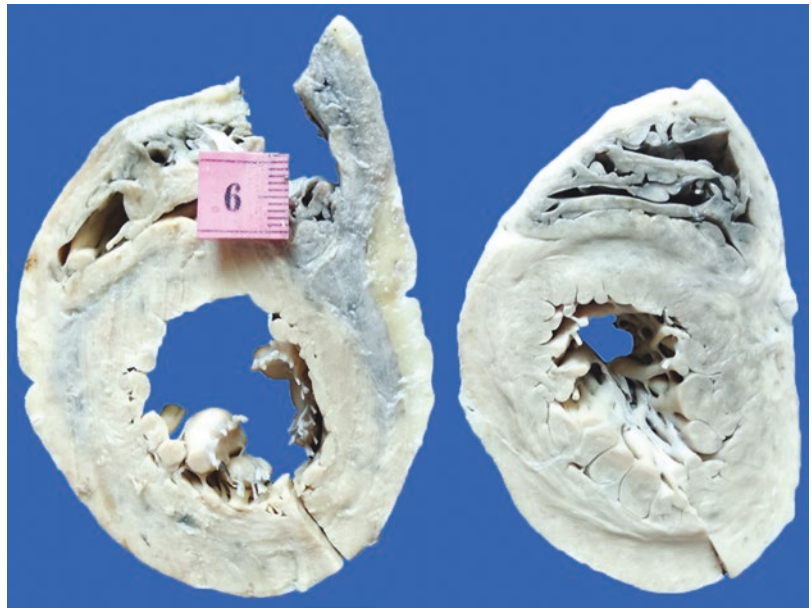

Fig. 30.1 Serial transverse slices of the myocardium reveal pallor and presence of small foci of congestion

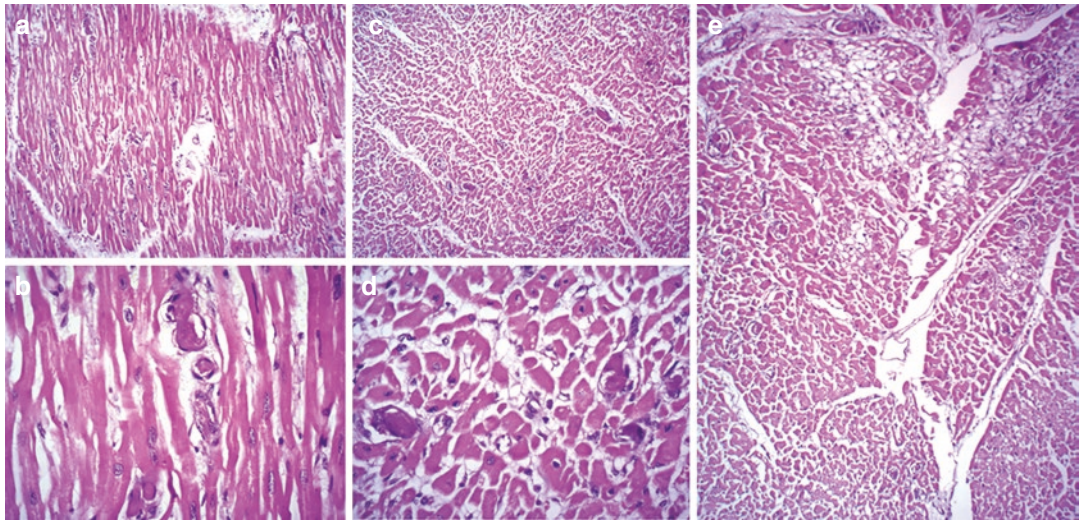

Fig. 30.2 Occlusive fresh thrombi in the intramural coronary arterioles, seen amidst longitudinally (**a**) H&E × 250, (**b**) H&E × 400 and transversely (**c**) H&E × 250, (**d**) H&E × 400 sectioned myofibers; (**e**) Small areas of necrosis, myofiber fragmentation, and cytoplasmic vacuolation (H&E × 250)

the intramural coronary arteries (Fig. 30.2a–d) that had led to multiple fresh and healing microinfarcts (Fig. 30.2e). In addition, there was widespread thrombotic microangiopathy that involved most of the other organs (Fig. 30.3); there was renal cortical necrosis as well.

Cause of Death: Multiorgan failure due to disseminated microvascular thrombosis.

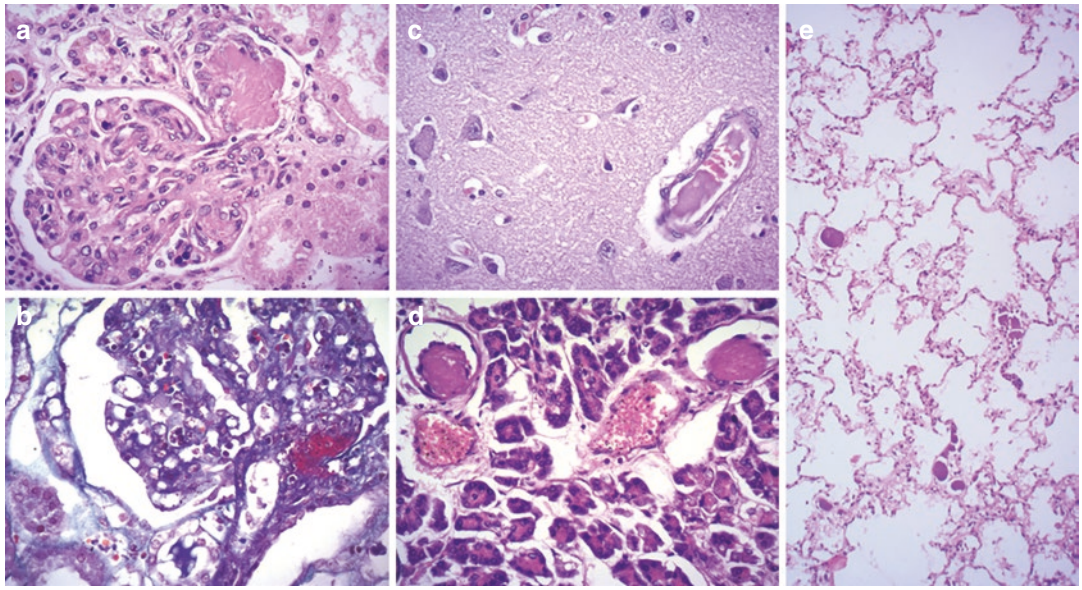

Fig. 30.3 Occlusive thrombus in the glomerular arteriole (**a**) H&E × 400 and (**b**) Putt's fibrin × 400; Arterial and arteriolar thrombi in the (**c**) Cerebral cortex (H&E × 400), (**d**) Pancreas (H&E × 400) and (**e**) Lungs (H&E × 250)

30.3 Discussion

Sudden, unexpected death occurred in this young patient, in whom widespread microvascular fibrin thrombi were identified at autopsy, particularly affecting the heart, lungs, kidneys, and brain. Traditionally, such small-vessel thrombi are described in 2 important conditions—disseminated intravascular coagulation (DIC) and thrombotic microangiopathy (TMA). In the presented clinical scenario, there were no predisposing factors for the development of DIC. Furthermore, there was absence of concomitant bleeding tendency. Hence, the likely diagnosis would be TMA, which encompasses a triad of microangiopathic hemolytic anemia, thrombocytopenia, and microvascular thrombi leading to organ ischemia. Evidence of hemolytic anemia is indicated by the presence of schistocytes (fragmented RBCs) in the peripheral smear, reticulocytosis, indirect hyperbilirubinemia, elevated levels of lactate dehydrogenase, and reduced levels of haptoglobin. Our patient had mild anemia and elevated indirect bilirubin of 1.3 mg/dL. However, neither schistocytes nor polychromatic cells had been observed in the peripheral smear and the platelet count (2.4 lakhs/cmm) was in the normal range (1.5–4.5 lakhs/cmm) in this patient. A possible explanation for the latter feature may be that her normal count before the illness could have been on the higher side of the normal range. A 25% decrease of the platelet count is also sufficient to indicate increased platelet consumption. The microvascular thrombi were seen only at autopsy.

The common clinicopathological features of TMA are shared by diverse group of conditions, which have different pathophysiological mechanisms and specific therapy (the common therapy being initial plasma exchange). There is often interplay of the coagulation factors, complement proteins, and platelets. The common and most important cause for TMA in the pediatric population is the typical or classic hemolytic uremic syndrome (HUS) caused by shiga toxin producing *Escherichia coli*, which damages the endothelium and has a propensity to involve the kidneys. Though the condition is largely self-limited, some patients (about 15–18%) can develop chronic kidney disease; cardiac and neurological involvement is seen in the more severe cases. Another TMA, which rarely occurs in this group, is thrombotic thrombocytopenic purpura,

where there is inherited or acquired and immune-mediated reduction in the levels (<10 IU/dL) of a metalloproteinase ADAMTS13 and frequent neurological symptoms and/or deficits. The reduced activity results in formation and accumulation of ultra-large von Willebrand factor multimers and disseminated microvascular platelet-rich thrombi. Hence, stool examination for detection of the shiga toxin and ADAMST13 assay are the specific preliminary laboratory investigations, which are to be performed whenever there is a clinical suspicion and investigational clues pointing to a diagnosis of TMA. Classic HUS was easily ruled out in the present case, as the patient did not have diarrhea or any other gastrointestinal symptoms in the recent past. Also, there was no other focus of infection in the patient, such as pneumonia which could lead to other infection-induced HUS. Some patients manifest with atypical HUS or secondary HUS. Atypical HUS is characterized by inherited or acquired (autoantibody-mediated) defects in the complement system or in the proteins that regulate complement deposition/activation on cell surfaces, particularly endothelium. On other hand, secondary HUS occurs with diverse disorders with varied mechanisms and includes pregnancy, autoimmune disorders, underlying cancers, infections, drugs, etc.

Another strong possibility that can be considered in this case is antiphospholipid antibody syndrome (APLS), which is an autoimmune thromboinflammatory disorder. It is recognized by presence of at least one clinical and laboratory criteria (Sapporo criteria). The clinical criteria include pregnancy morbidity ("obstetric" APLS, not applicable in our case) or clinical evidence of arteriovenous thrombosis ("thrombotic" APLS), while the laboratory criteria include presence of antiphospholipid antibody (lupus anticoagulant, anticardiolipin antibodies, or anti-β_2-glycoprotein I antibodies) that are detected on 2 occasions 12 weeks apart. When such features occur in isolation, it is referred to as primary APLS. Secondary APLS, which is more common, is seen in association with other autoimmune disorders, especially systemic lupus erythematosus. A more alarming presentation with a high fatality rate, designated as catastrophic APLS (CAPS), is characterized by abrupt and brisk microvascular thrombosis (minimum of 3 organ systems) within a short period of time (usually < than week) and has a prevalence of <1% of all APLS cases. It is important to note that APLS in the pediatric patient (our patient was 15 years old) is rare, occurring in about 3% of patients before the age of 15 years and is often underdiagnosed. Clinical characteristics of CAPS appeared to have been fulfilled in our patient and there were multiorgan thrombi (a criterion for CAPS), but antibody estimations were not available. CAPS is often the first manifestation of APLS, as noted in close to 90% of the affected children. Infection has been identified as a major trigger for CAPS. Though our patient had multisystem thrombosis, there was no preceding history of infection, and no infection was noted even at autopsy. Interestingly, schistocytes have been observed to be fewer in the peripheral smear in CAPS and have been reported in only 14%–16% of patients with CAPS. Schistocytes were not seen in the present case. Severe thrombocytopenia is also not common in CAPS.

In general, both adult and pediatric patients with TMA present with renal dysfunction. But some have more prominent extrarenal manifestations affecting the cardiovascular and central nervous systems and lungs. In the index case, microthrombi were seen in many organs and apart from thrombi, the kidneys did not show features of lupus. In the early phase, symptoms are produced due to myocardial ischemia or infarction largely related to intramural coronary arterial involvement, as identified in this case. This case emphasizes the importance of TMA as diagnosis in a child with abrupt onset of multiorgan dysfunction in a setting of infection. This would entail a detailed clinical examination and relevant investigations to assess clinical or subclinical multiorgan dysfunction and performance of laboratory tests to identify the cause of TMA. Early diagnosis and appropriate management are crucial for patient survival and prevent chronic organ dysfunction.

Further Reading

Appel GB. Thrombotic microangiopathies: similar presentations, different therapies. Cleve Clin J Med. 2017;84:114–30.

Arnold DM, Patriquin CJ, Nazy I. Thrombotic microangiopathies: a general approach to diagnosis and management. CMAJ. 2017;189:E153–9.

Blasco M, Guillen E, Quintana LF, Garcia-Herrera A, Pineiro G, Poch E, et al. Thrombotic microangiopathies assessment: mind the complement. Clin Kidney J. 2021;14:1055–66.

Hofer J, Rosales A, Fischer C, Giner T. Extra-renal manifestations of complement-mediated thrombotic microangiopathies. Front Pediatr. 2014;2:97.

Joly BS, Zheng L, Veyradier A. Understanding thrombotic microangiopathies in children. Intensive Care Med. 2018;44:1536–8.

Madison JA, Zuo Y, Knight JS. Pediatric antiphospholipid syndrome. Eur J Rheumatol. 2020;7(Suppl 1):S3–S12.

Masias C, Vasu S, Cataland SR. None of the above: thrombotic microangiopathy beyond TTP and HUS. Blood. 2017;129:2857–63.

Nayer A, Ortega LM. Catastrophic antiphospholipid syndrome: a clinical review. J Nephropathol. 2014;3:9–17.

Anomalous Coronary Artery Origin and Sudden Cardiac Death

31

Swati Kolhe, Pranita Zare, and Pradeep Vaideeswar

31.1 Clinical History

A 36-year-old male complained of sudden choking and breathlessness during his mid-morning break while having snacks. He was a wire line operator by profession working at an offshore oil rig. He was resuscitated and air-lifted to a nearby hospital, but declared dead on arrival.

31.2 Autopsy Findings

A medicolegal autopsy had been performed elsewhere and slices of organs were referred to our institute for histopathology. Only the basal part of the heart was received. There was mild dilatation of the ventricular chambers with a normal brown discoloration of the myocardium. The aortic annulus was mildly dilated; the semilunar cusps were normal. Few fatty streaks were noted in the ascending aorta. The remarkable finding was the origin of both the coronary ostia from the left anterior sinus-of-Valsalva (SOV). The left coronary arterial ostium was present within the mid-portion of the sinus below the sinutubular junction, while the right coronary arterial opening was present in the same sinus, but close to the commissure between the two anterior cusps (Fig. 31.1a). The right coronary artery, which was dominant, coursed between the ascending aorta and the pulmonary trunk (Fig. 31.1b). Distally, it had a normal course in the right atrioventricular groove. On histology, the coronary artery was partly incorporated in the outer wall of the ascending aorta with smooth muscle continuity (Figs. 31.1c, d and 31.2a). In addition, there was significant fibrosis of the arterial media (Fig. 31.2b) with presence of elastic fibers (Fig. 31.2c). The intima was normal. There was no evidence of myocardial ischemia or infarction. There was extensive pulmonary edema and mild hepatic steatosis. Other organs were normal.

S. Kolhe
Department of Pathology, Seth Gordhandas Sunderdas Medical College and King Edward Memorial Hospital, Mumbai, India

P. Zare · P. Vaideeswar (✉)
Department of Pathology (Cardiovascular and Thoracic Division), Seth Gordhandas Sunderdas Medical College and King Edward Memorial Hospital, Mumbai, India

P. Vaideeswar (ed.), *Tropical Cardiovascular Pathology*,
https://doi.org/10.1007/978-981-19-3720-0_31

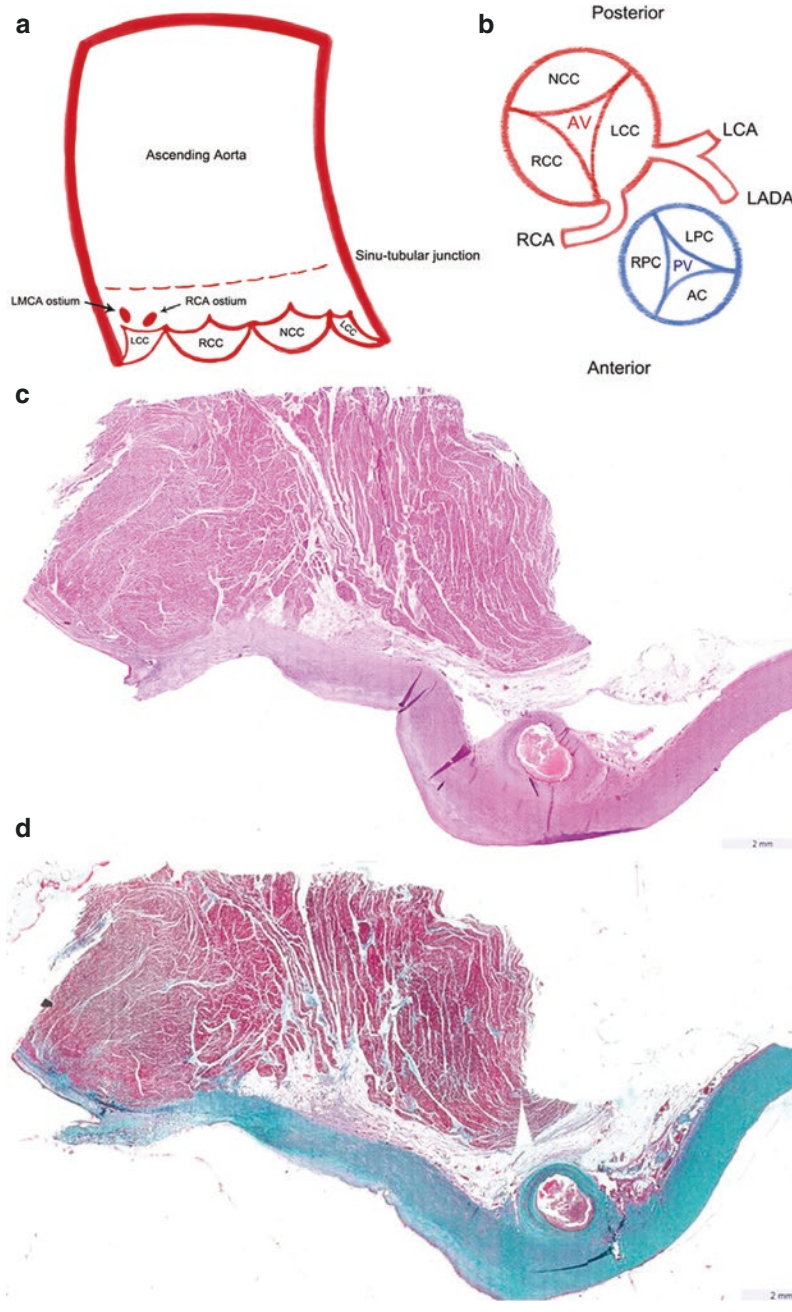

Fig. 31.1 (**a**) Diagrammatic representation of the right coronary arterial RCA ostium arising close to the commissure between the right RCC and left LCC coronary cusps; (**b**) Diagrammatic representation of the right coronary artery RCA between the ascending aorta and pulmonary trunk PT (*AC* anterior cusp, *AV* aortic valve, *LADA* left anterior descending artery, *LCA* left circumflex artery, *LMCA* left main coronary artery, *LPC* left posterior cusp, *NCC* noncoronary cusp, *PV* pulmonary valve, *RPC* right posterior cusp); Scanned images of the right coronary artery partly incorporated within the aortic wall (**c**) H&E and (**d**) Masson trichrome

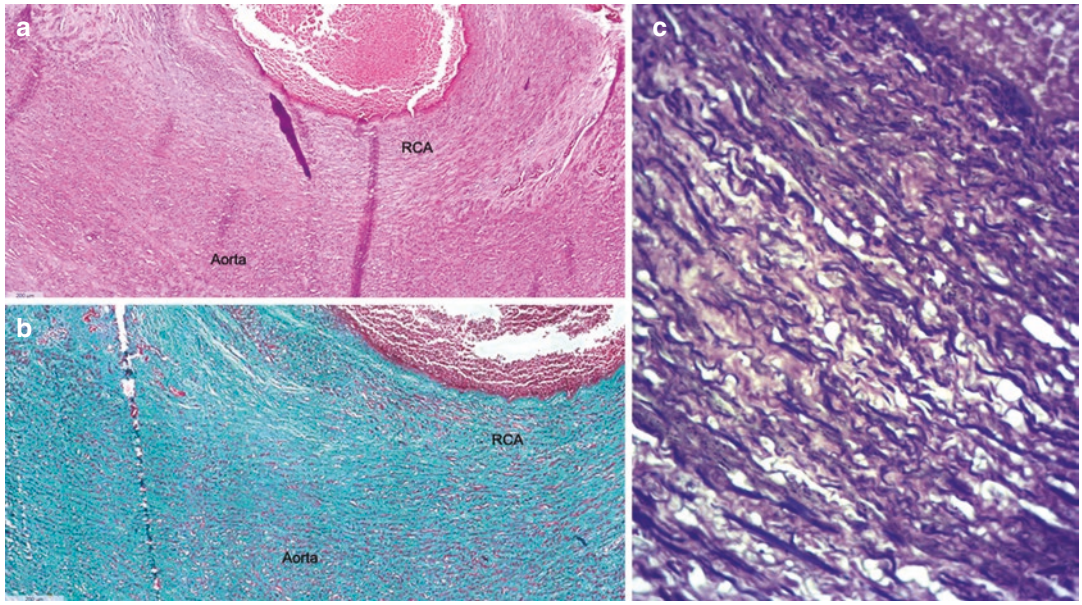

Fig. 31.2 (**a**) Merging of the media of the right coronary artery RCA and the ascending aorta (H&E × 200); (**b**) Prominent collagenization of the RCA (Masson's trichrome × 200); (**c**) Black elastic fibers are seen in the right coronary artery (Elastic van Gieson × 400)

31.3 Discussion

This case represents one of the several congenital anomalies of the coronary arteries, where there is an anomalous origin and/or courses of the epicardial coronary arteries. Though such lesions are uncommon, they are capable of producing sudden cardiac death (second most common cause), particularly in the young sportspersons and individuals with regular exercise routines. The anomalies can be classified into hemodynamically significant and insignificant lesions. Hemodynamically significant anomalies are usually always characterized by decreased myocardial perfusion, while the insignificant anomalies are not associated with major clinical events. However, there is a group of congenital anomalies where individuals are capable of leading a normal life, but can manifest with sudden-onset critical ischemic events. This occurs in an example of anomalous aortic origin of the coronary arteries (AAOCA).

Normally the right and left coronary ostia are placed in center of the anterior right and left SOV below the sinutubular ridge (See Chap. 1). The anomalous origin pertains to the number, location, and size of the coronary ostia and subsequent course of the coronary arteries. Of particular importance is the origin of the artery from the opposite or contralateral SOV, which has a prevalence of 0.26% in the general population; right coronary artery (RCA) is more affected (0.23%) as compared to the left main coronary artery (0.03%). Furthermore, after this origin, the artery can adopt different pathways to terminate into its normal course. The artery may be prepulmonic, interarterial, retro-aortic, transseptal, or retro-cardiac. In this case, we have described an anomalous origin of the RCA from the left SOV, close to the commissure between the two anterior cusps and coursed between the 2 great arteries. The interarterial course is considered as the malignant variant due to increased risk of sudden death. The pathogenetic mechanism can be explained on a 'two-tier' concept, which includes the fixed and dynamic components of obstruction of the ostium and/or the artery. The fixed component includes the presence of a slit-like ostium and proximal arterial narrowing; the former was present in the index case. The dynamic component is contrib-

uted by an acute take-off angle or compression of the coronary artery between the dilated ascending aorta and pulmonary trunk especially during vigorous exertion. The lumen would be further compromised when the interarterial course is also associated with mural incorporation of the RCA (intramural course) within the outer thirds of the aortic media, as was depicted in this case.

The clinical spectrum commonly seen is either sudden death (very often the first manifestation) or features related to myocardial ischemia such as chest discomfort or pain, syncope, and arrhythmias. Though they are often exertion-related, the trigger for sudden death is not always clear as some patients have died in their sleep or at rest, which was the clinical scenario in our case where the patient experienced chest discomfort while having snacks. In addition, some patients can remain asymptomatic. Nevertheless, a better understanding of the mechanisms of ischemia, early diagnosis with imaging, and preventive measures can help to identify and reduce the risk of fatal arrhythmias to avoid sudden death. The diagnosis is based on assessment of the coronary arteries by various imaging modalities like transthoracic echocardiography, multislice computed tomography (CT) scan, and coronary angiography (CT or magnetic resonance). It would also be important to identify presence of myocardial scarring due to past episodes of ischemia as these scars are also arrhythmogenic. Surgical correction is needed in all symptomatic patients and those carrying risks for sudden death especially in the malignant variants. An unroofing procedure, direct reimplantation of the anomalous RCA, or coronary bypass are the preferred surgical methods.

Further Reading

Bigler MR, Ashraf A, Seiler C, Praz F, Ueki Y, Windecker S, et al. Hemodynamic relevance of anomalous coronary arteries originating from the opposite sinus of Valsalva-in search of the evidence. Front Cardiovasc Med. 2021;7:591326.

Cubero A, Crespo A, Hamzeh G. Anomalous origin of right coronary artery from left coronary sinus—13 cases treated with the reimplantation technique. World J Pediatr Congenit Heart Surg. 2017;8:315–20.

Molossi S, Martínez-Bravo LE, Mery CM. Anomalous aortic origin of a coronary artery. Methodist Debakey Cardiovasc J. 2019;15:111–21.

Villa ADM, Sammut E, Nair A, Rajani R, Bonamini R, Chiribiri A. Coronary artery anomalies overview: the normal and the abnormal. World J Radiol. 2016;8:537–55.

Young ML, McLeary M, Chan KC. Acquired and congenital coronary artery abnormalities. Cardiol Young. 2017;27(Suppl 1):S31–5.

Extensive Myocardial Scarring in a Neonate

32

Pragati Sathe and Pradeep Vaideeswar

32.1 Clinical History

A male child had a near-term normal vaginal delivery (birth weight 2264 g) in a private healthcare facility. He was admitted to the neonatal intensive care unit at our institute for respiratory distress. An antenatal fetal echocardiography had revealed a possibility of mitral atresia with dilated right ventricle, a small ventricular septal defect, and mild pericardial effusion. On examination, the general condition was poor with heart and respiratory rates of 150 and 60 per minute, respectively. There was generalized anasarca with tense ascites, scrotal, and penile edema. The neonate died within 1 h of admission.

32.2 Autopsy Findings

A complete autopsy was performed. The heart when observed *in-situ* had an almost horizontal orientation in the chest; this was also seen when the heart and lungs were kept in normal anatomical position (Fig. 32.1a). There was diffuse epicardial fibrosis. The right ventricle (RV) had a peculiar configuration. It appeared dumb-bell-shaped with a small right and large left 'out-pouchings', between which arose the pulmonary trunk (Fig. 32.1a). The right-sided chamber communicated with the pulmonary artery, while the chamber towards the left was a muscle bound accessory chamber (Fig. 32.1a). Obvious whitish discoloration was seen in the RV myocardium and the interventricular septum (IVS, Fig. 32.1b). The IVS was intact; there was no mitral atresia. The left ventricular chamber was dilated with pale, focally thinned out myocardium. The endocardia of both ventricles were pearly white with obliteration of the trabeculae. The venous connections, coronary arterial origins, and distributions were normal. On histology, the myocardium showed transmural and circumferential replacement by vascularized fibrosis with multiple foci of calcifications (Fig. 32.1c–e) in the areas supplied by the left coronary arterial system. There was also varying degrees of epicardial fibrosis and calcification. Apart from vascular congestion, other organs did not show any significant pathology. The umbilical cord was also normal.

Cause of Death: Extensive myocardial scarring and cardiac failure.

P. Sathe
Department of Pathology, Seth Gordhandas Sunderdas Medical College and King Edward Memorial Hospital, Mumbai, India

P. Vaideeswar (✉)
Department of Pathology (Cardiovascular and Thoracic Division), Seth Gordhandas Sunderdas Medical College and King Edward Memorial Hospital, Mumbai, India

P. Vaideeswar (ed.), *Tropical Cardiovascular Pathology*,
https://doi.org/10.1007/978-981-19-3720-0_32

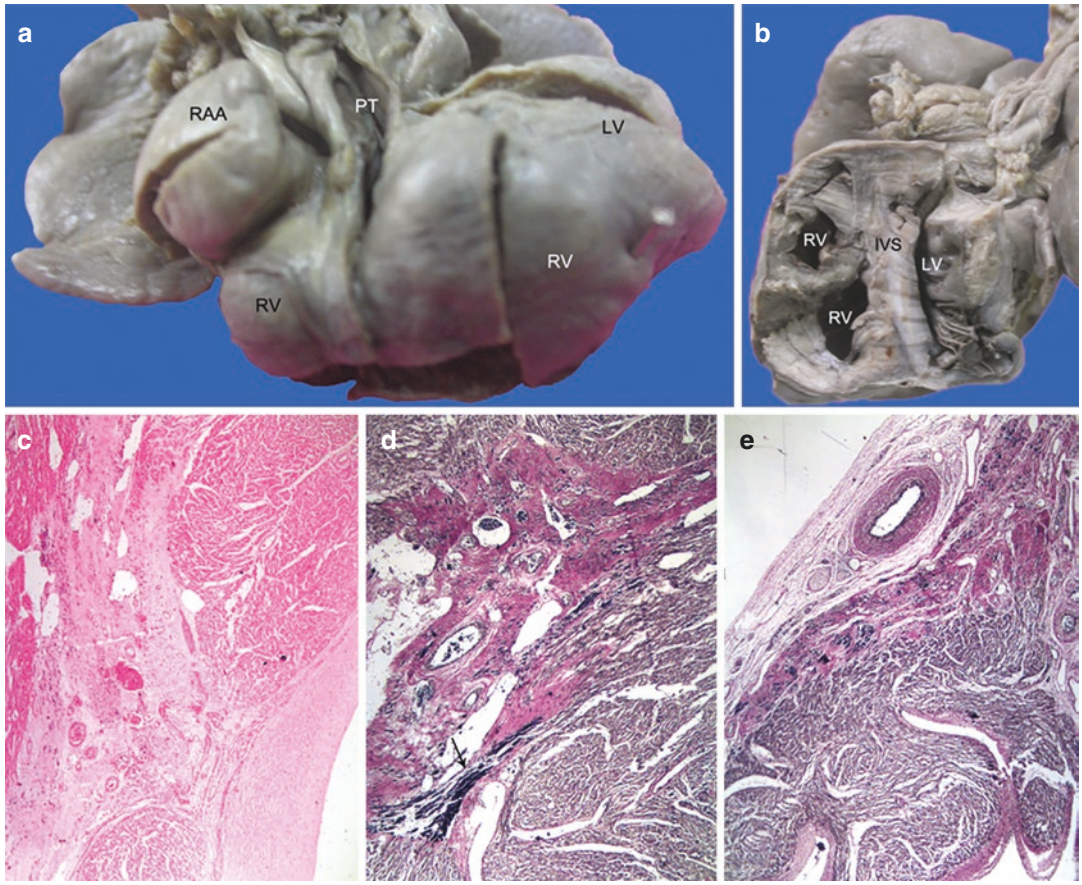

Fig. 32.1 (**a**) Horizontal placement of the heart with enlarged right ventricle RV. The pulmonary trunk PT arises between the 2 RV 'outpouchings'; (**b**) The transverse section shows division of the RV chamber by an anomalous muscle band. The RV, left ventricle LV, and interventricular septum IVS show pale white myocardium; Transmural fibrosis of the left ventricle (**c**) H&E × 100 and (**d**) Elastic van Gieson × 100. The granular dark deposits (arrow) represent dystrophic calcification; (**e**) Fibrosis in the right ventricle. The epicardial coronary artery is normal (Elastic van Gieson × 100)

32.3 Discussion

Extensive transmural fibrosis with calcification predominantly seen in the left ventricle of a 2-day male child had resulted in a nonimmune hydrops fetalis, arising due to left ventricular failure. The pattern of involvement suggested that this injury had an ischemic basis and occurred in intrauterine life. Myocardial infarction (MI, healed or otherwise) is an extremely uncommon condition to be diagnosed in the pediatric population in general and neonatal period in particular, where it forms a differential diagnosis for cardiac dysfunction due to neonatal myocardial disorders. Owing to its rarity and diagnostic challenges, the true prevalence and incidence is not exactly known; there is often a female predominance.

Most often, the MI is seen in association with congenital and structural heart diseases, which most often involve anomalies of the coronary arteries and include abnormalities in the origin, course, or structure of the epicardial coronary arteries. There have been also instances where coronary thromboembolism had occurred due to thrombosis of the umbilical vein or ductus venosus. In this case, such thrombi or emboli were not documented. Apart from these causes, the throm-

bogenicity and chances of coronary *in-situ* thrombosis are increased with prematurity, polycythemia (heightened by placental insufficiency, maternal hypertension, twin-to-twin, or maternal-fetal transfusion), and rare inherited thrombophilic disorders. Inflammatory and noninflammatory myocardial disorders can also predispose the neonates to MI. In another group of patients, the MI develops after cardiac surgery. It can also be unrelated to any cardiovascular pathology and is seen with perinatal asphyxia, congenital diaphragmatic hernia, intrauterine infection, neonatal sepsis, pregnancy-related disorders, or certain drugs. In few others, it may truly remain idiopathic. In this case, the mother had an uneventful pregnancy. No thrombi or emboli were documented on histopathology. It may be possible that the abnormal outpouching of the accessory chamber of the right ventricle could have led to compression of the left coronary artery.

In contrast to adults, adolescents, and older children, the presentation of MI in neonates, infants, and young children will not be clear and is often subtle and vague. Crying, pallor, cyanosis, respiratory distress, vomiting, feeding difficulties, hypotension, arrhythmias, or frank cardiac failure may be present, depending on the degree of myocardial injury. But the diagnosis can also be missed when it is superimposed on the more common neonatal problems like sepsis or respiratory distress syndrome. The clinical suspicion (if any) is usually confirmed on the basis of ECG changes, elevated biomarkers of cardiac injury, and abnormalities on cardiac imaging. It is to be noted that the biomarkers can be elevated in neonates (particularly preterm) and also in myocarditis, which can then lead to MI by virtue of coronary thrombosis or vasospasm and intramural coronary arteritis. In the index case, the child was admitted for only a few hours and the diagnosis of MI was made only at autopsy. The mainstay of the treatment of neonatal MI rests mainly on cardiovascular and respiratory support with thrombolysis or coronary artery intervention if required. In some cases, the myocardial function reverts to near normal, indicating the regenerative ability of the neonatal myocardium.

Further Reading

Aljohani OA, Perry JC, El-Sabrout HR, Hegde SR, Silva Sepulveda JA, Catanzarite VA, et al. Neonatal myocardial infarction: a retrospective study and literature review. Prog Pediatr Cardiol. 2019;55:101171. https://doi.org/10.1016/j.ppedcard.2019.101171.

Bansal MM. Myocardial disorders in the neonate. Neo Rev. 2018;19:e402–9.

Haubner BJ, Schneider J, Schweigmann U, Schuetz T, Dichtl W, Velik-Salchner C, et al. Functional recovery of a human neonatal heart after severe myocardial infarction. Circ Res. 2016;118:216–21.

Martínez MR, González ER, Parra-Llorca A, Torres MV, Carrascosa MA. Myocardial infarction in neonates: a diagnostic and therapeutic challenge. Case Rep Pediatr. 2019;2019:7203407.

Papneja K, Chan AK, Mondal TK, Paes B. Myocardial infarction in neonates: a review of an entity with significant morbidity and mortality. Pediatr Cardiol. 2017;38:427–41.

Part VII

Non-Ischemic Myocardial Disorders

33 Acute Lymphocytic Myocarditis and Sudden Cardiac Death

Ketan Ingle, Girish Tasgaonkar, and Pradeep Vaideeswar

33.1 Clinical History

An adolescent male, aged 15 years, had episodes of low-grade fever for the past few weeks. He was diagnosed as 'jaundice' and administered traditional medicines. During his sleep, he suddenly became restless with shaking of his arms and legs. He was rushed to our tertiary-care center, but declared dead on arrival.

33.2 Autopsy Findings

The heart (170 g) appeared normal on gross examination (hence no gross photographs were taken). The myocardium was extensively sampled and many of the sections revealed a normal histology (Fig. 33.1). However, two sections taken from the ventricular myocardium revealed features of acute lymphocytic myocarditis affecting the subepicardial regions of the left ventricular myocardium. The involvement was patchy and was composed of cardiomyocyte destruction and accompanying varying degrees

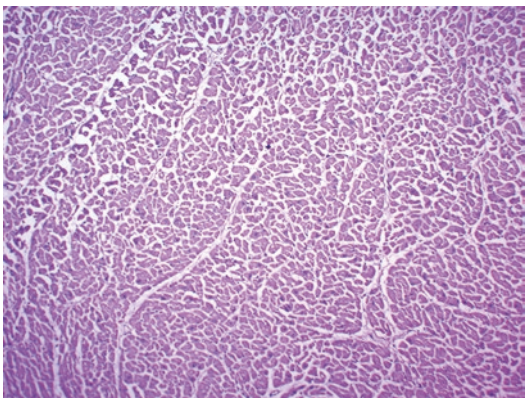

Fig. 33.1 Normal myocardial histology seen in the many sections taken (H&E × 200)

K. Ingle
Department of Pathology, Seth Gordhandas Sunderdas Medical College and King Edward Memorial Hospital, Mumbai, India

G. Tasgaonkar
Department of Forensic Medicine and Toxicology, Seth Gordhandas Sunderdas Medical College and King Edward Memorial Hospital, Mumbai, India

P. Vaideeswar (✉)
Department of Pathology (Cardiovascular and Thoracic Division), Seth Gordhandas Sunderdas Medical College and King Edward Memorial Hospital, Mumbai, India

P. Vaideeswar (ed.), *Tropical Cardiovascular Pathology*,
https://doi.org/10.1007/978-981-19-3720-0_33

of lympho-histiocytic infiltration (Fig. 33.2). No inflammation was seen in the interventricular septum. Sprinkling of inflammatory cells was seen in the right ventricle. Fine foci of scarring were also present. Surprisingly, an extraordinary degree of inflammation and destruction was present around the region of the atrioventricular (AV) node (Fig. 33.3a, b). The inflammatory cells were represented mainly by macrophages (Fig. 33.3c) and T-lymphocytes (Fig. 33.3d); B-lymphocytes were not present (Fig. 33.3e). Other findings included pulmonary edema and mild sinusoidal congestion in the liver.

Cause of Death: Sudden cardiac death due to acute lymphocytic myocarditis.

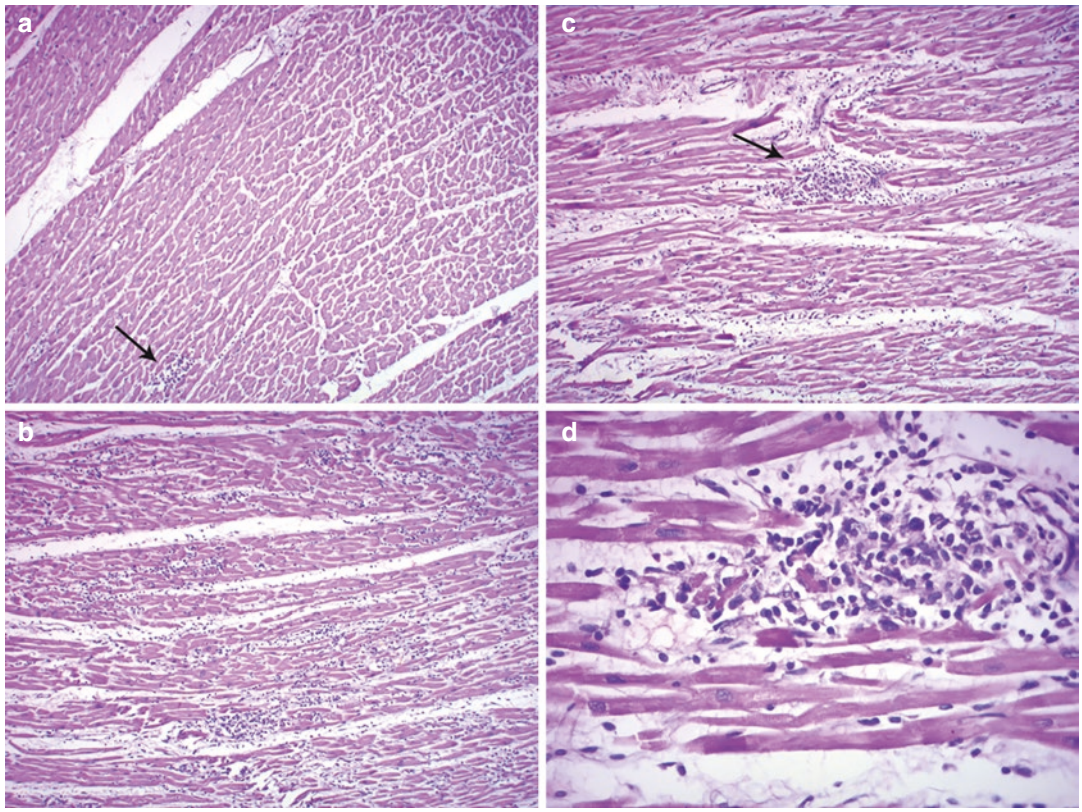

Fig. 33.2 (**a**) Myocardium showing a small focus (arrow) of mononuclear cell infiltration (H&E × 200); (**b**) Easily identifiable multifocal collections of inflammatory cells (H&E × 200); (**c**) Cellular aggregates (arrow) and infiltrates (H&E × 200); (**d**) The aggregate shows collections of macrophages and lymphocytes with destruction of the adjacent cardiomyocytes (H&E × 400)

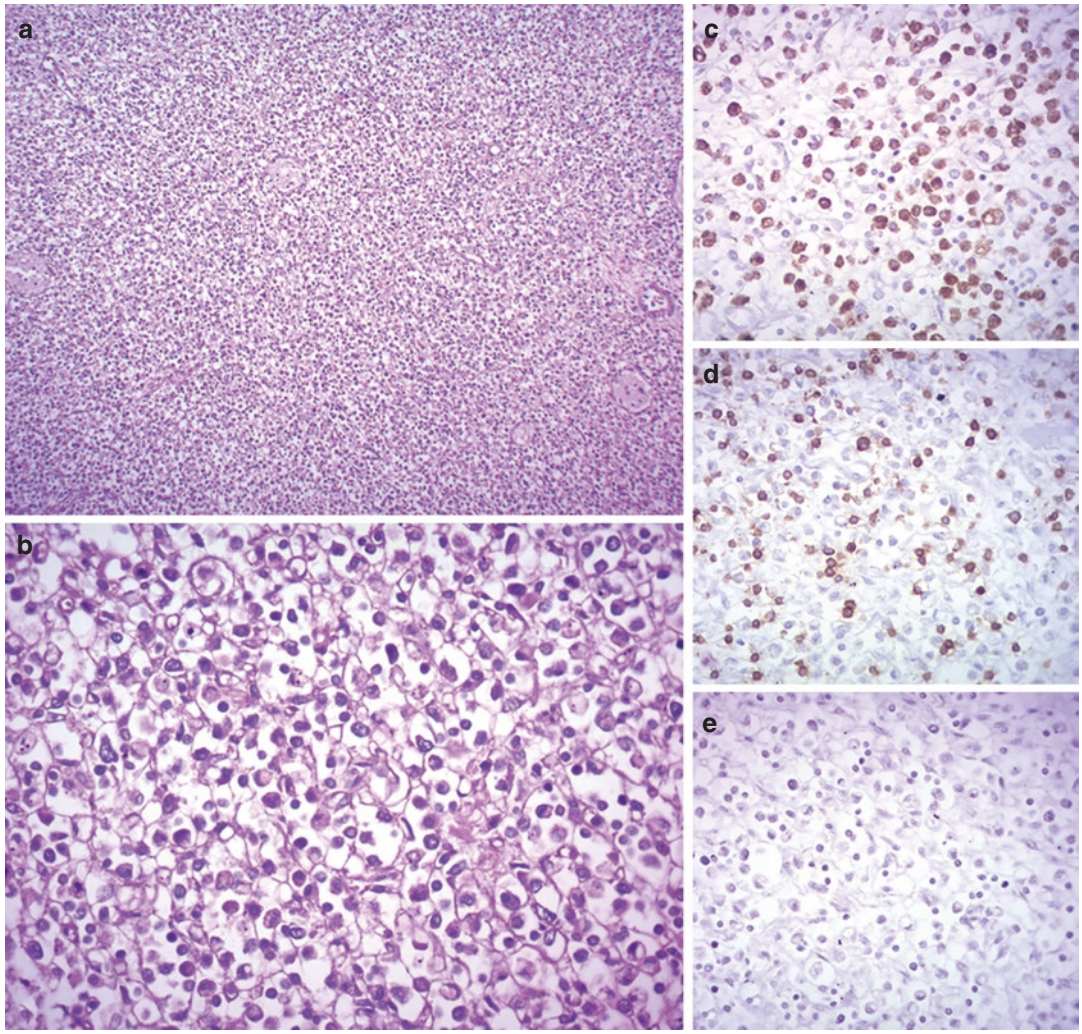

Fig. 33.3 Sea of inflammatory cells seen around the region of the atrioventricular node. The myocytes are hardly visible—(**a**) H&E × 200 and (**b**) H&E × 400; (**c**) Macrophages with positive CD 68 immunostaining (× 400); (**d**) T lymphocytes with positive CD 3 immunostaining (× 400); (**e**) CD 23 was negative, indicating absence of B lymphocytes (× 400)

33.3 Discussion

The heart in this adolescent showed patchy but dense lympho-histiocytic infiltration and associated cardiomyocytic destruction in the absence of ischemia, which are the defining features of myocarditis. The 'prescribed' number of inflammatory cells is at least 14 infiltrating leukocytes/mm^2 with up to 4 monocytes/mm^2 and at least 7 CD3+ T lymphocytes/mm^2. The condition, sometimes referred to as inflammatory cardiomyopathy, has an estimated incidence of 10–22 per 100,000 persons per year, though the true incidence of myocarditis is difficult to measure. Majority of the cases occur in the pediatric population, but it is identified as the third leading

cause of cardiovascular deaths, after coronary artery disease (See Chaps. 24 and 28) and hypertrophic cardiomyopathy (See Chap. 43) in young adult males (median age of presentation being 42 years). The myocarditis, occurring through infective and noninfective causes (such as autoimmune processes or toxic agents), can elicit varying types and degrees of leukocytic responses ranging from neutrophils to granulomatous or giant cell responses. Among the etiologic agents, viruses represent the most common cause (approximately 90% of inflammation caused by infective agents) and produce the characteristic lymphocytic myocarditis, as seen in this case.

A large number of viruses have been implicated in the causation of lymphocytic myocarditis, and in such cases, the condition is diagnosed not only on routine histopathological examination but also with immunological and immunohistochemical criteria. Furthermore, due to different mechanisms of cardiac injury, it may be possible to distinguish between virus-induced cytopathic effects and virus-associated inflammatory responses. Cardiotropic viruses such as enterovirus (Coxsackie A and B, and echovirus) or adenovirus have been shown to infect the cardiomyocytes through specific transmembrane coxsackievirus and adenovirus receptor to produce direct cytopathic effects. Elaboration of pro-inflammatory cytokines with myocardial damage is produced by endothelial injury that occurs on the entry of vasculotropic viruses such as parvovirus B19. However, the mechanisms of lymphotropic viruses (human herpesvirus 6, Epstein–Barr virus, and cytomegalovirus) and certain other viruses (human immunodeficiency virus, hepatitis C virus, influenza A/B viruses, and viruses from the Coronaviridae family) are not yet clearly defined and have been postulated to be the result of autoimmune phenomenon. Direct or indirect viral injury initiates the first phase (1–7 days), which is characterized by innate immune responses. This is followed by the second phase that can last from 1 to 4 weeks, where there is activation of the adaptive immunity, targeting the viruses or their products. There is also an element of autoimmunity due to release of intracellular or surface antigens of the injured cardiomyocytes with generation of autoreactive T cells and autoantibodies. Finally, in the third phase, there is clearing of the virus, a process that can last for months or years. In some individuals, there is ineffective or delayed clearing where persistent inflammation provokes fibrosis and remodeling leading to dilated cardiomyopathy (See Chap. 41).

Depending on the type of virus and the degree of inflammation elicited, viral myocarditis can result in protean manifestations, ranging from an asymptomatic presentation to rapidly progressive syndromes. Often there are prodromal manifestations in the form of fever, malaise, fatigability, and gastrointestinal symptoms (abdominal pain, nausea, vomiting, loss of appetite, or diarrhea - simulating the anicteric phase of acute hepatitis). Patients with clinically stable acute myocarditis usually present with chest pain, dyspnea, palpitation, syncope, and have mild to moderate left ventricular dysfunction. In pediatric patients with palpitation, syncope and arrhythmias do not necessarily have a depressed systolic function. Apart from the routine ECG and echocardiography, such cases are diagnosed on the basis of sophisticated imaging techniques (such as cardiac magnetic resonance imaging) and elevated cardiac biomarkers that are useful for prompt institution of appropriate supportive therapy. Endomyocardial biopsy may prove useful in identifying the viral genome and guiding a tailored therapy. However, immunohistochemical stains or facilities for detection of the specific viruses are not available in most of our institutions. A subset of patients has clinically unstable disease (fulminant myocarditis), presenting as cardiogenic shock due to global ventricular dysfunction that often requires mechanical circulatory support. The clinical presentation may also be reflected in the gross appearance of the heart at autopsy. In many of the cases, as seen in this patient too, the hearts appear normal. In few others, there may be biventricular dilatation with myocardial pallor, flabbiness, and/or congested mottling.

Our patient had low-grade fever, which was diagnosed as jaundice, but there was no icterus at autopsy and features of hepatitis were not seen on histopathology. There were apparently no cardiac symptoms and unfortunately he had sudden cardiac death (SCD), which can be the first clinical manifestation of acute myocarditis. Around 12% cases of SCD are caused by acute myocarditis in patients younger than 40 years of age. The inflammation renders the myocardium arrhythmogenic due to ion-channel dysfunction and alteration of intracellular signaling, leading to ventricular tachyarrhythmias in the form of ventricular tachycardia and fibrillation. In our opinion, in the present case, if the AV node had not been involved, the myocardial inflammation in the rest of the myocardium would possibly have resulted in a clinically stable disease. In all probability, the SCD in this case was due to atrioventricular block consequent to very extensive inflammation and destruction at the region of the AV node.

Further Reading

Ali-Ahmed F, Dalgaard F, Al-Khatib SM. Sudden cardiac death in patients with myocarditis: evaluation, risk stratification, and management. Am Heart J. 2020;220:29–40.

Kiamanesh O, Toma M. The state of the heart biopsy: a clinical review. CJC Open. 2020;3:524–31.

Lasrado N, Reddy J. An overview of the immune mechanisms of viral myocarditis. Med Virol. 2020;30:e2131.

Olejniczak M, Schwartz M, Webber E, Shaffer A, Perry TE. Viral myocarditis—incidence, diagnosis and management. J Cardiothorac Vasc Anesth. 2020;34:1591–601.

Putschoegl A, Auerbach S. Diagnosis, evaluation, and treatment of myocarditis in children. Pediatr Clin North Am. 2020;67:855–74.

Tschöpe C, Ammirati E, Bozkurt B, Caforio ALP, Cooper LT, Felix SB, et al. Myocarditis and inflammatory cardiomyopathy: current evidence and future directions. Nat Rev Cardiol. 2021;18:169–93.

Acute Leptospiral Myocarditis

34

Rachana Binayke, Heena Desai,
Pradeep Vaideeswar, and Smita Divate

34.1 Clinical History

High-grade fever with chills, increasing shortness of breath, and myalgia for the past 4 days were the presenting symptoms in a 20-year-old male, admitted for duration of 4 h in early monsoon. The general condition was poor with tachycardia (heart rate 118 per minute) and hypotension (blood pressure 70/50 mmHg) and bilateral coarse crepitations. There was no jaundice or oliguria. The clinical diagnosis was acute febrile illness with acute respiratory distress syndrome. Investigations revealed pancytopenia (hemoglobin 10.6 g/dL, total leukocyte count of 2600/cmm, platelet count of 20,000/cmm) and normal biochemical profile. Serological tests for malaria, dengue, and leptospirosis had been negative. He was put on inotropic support.

34.2 Autopsy Findings

The heart was mildly enlarged in size (240 g). Multiple petechial hemorrhages were present over the epicardial surface. The cross-sections showed biventricular dilatation with small foci of congestion/petechiae from the basal region to the apex (Fig. 34.1). Petechiae were also noted

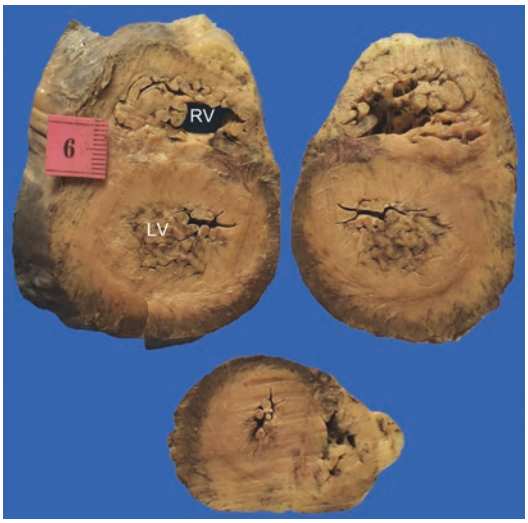

Fig. 34.1 The transverse slices of the myocardium reveal foci of congestion and petechial hemorrhages (*LV* left ventricle, *RV* right ventricle)

R. Binayke
Department of Pathology, Grant Government Medical College and JJ Group of Hospitals, Mumbai, India

H. Desai
Department of Pathology, Topiwala National Medical College and BYL Nair Charitable Hospital, Mumbai, India

P. Vaideeswar (✉)
Department of Pathology (Cardiovascular and Thoracic Division), Seth Gordhandas Sunderdas Medical College and King Edward Memorial Hospital, Mumbai, India

S. Divate
Department of Pathology, Seth Gordhandas Sunderdas Medical College and King Edward Memorial Hospital, Mumbai, India

P. Vaideeswar (ed.), *Tropical Cardiovascular Pathology*,
https://doi.org/10.1007/978-981-19-3720-0_34

over the endocardium. Microscopy revealed extensive interstitial edema, patchy but prominent foci of myocarditis (Fig. 34.2a, b), and focal hemorrhages (Fig. 34.2c). There was focal endocarditis (Fig. 34.2d) with fresh adherent thrombi. The cardiomyocyte destruction was accompanied by lymphocytes, histiocytes, and few plasma cells. Some perivascular aggregates bore a striking resemblance to Aschoff bodies of acute rheumatic fever (Fig. 34.3a, b). The coronary arteries revealed intimitis (Fig. 34.3c). Other findings included extensive intrapulmonary hemorrhage and acute tubulointerstitial nephritis.

Cause of Death: Massive intrapulmonary hemorrhage.

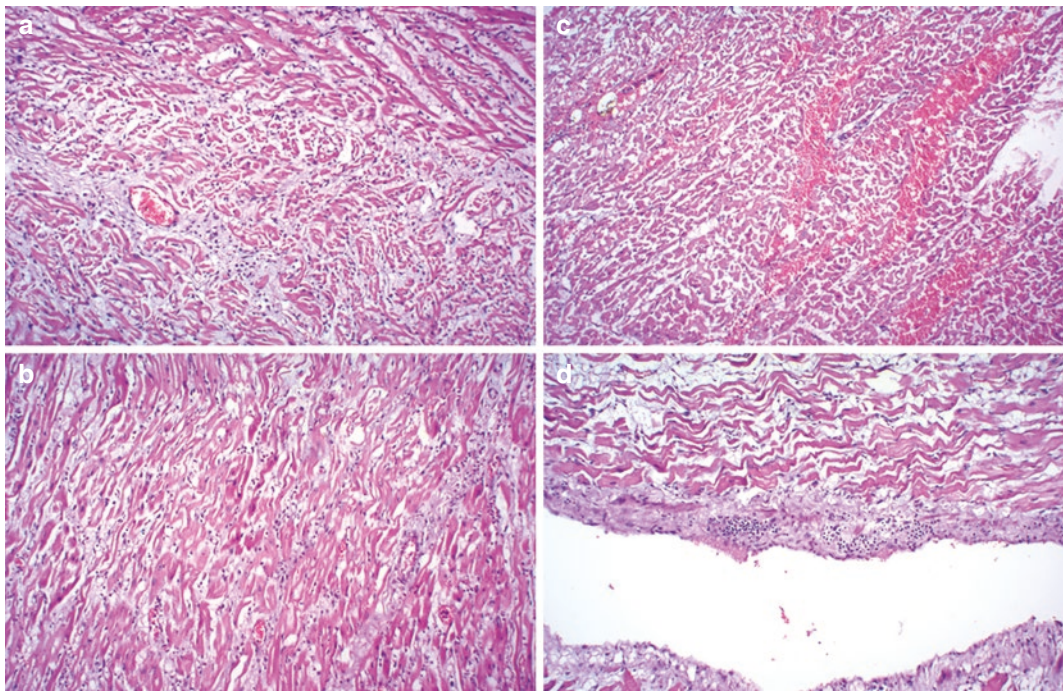

Fig. 34.2 Interstitial myocarditis present in the (**a**) Right and (**b**) Left ventricles; (**c**) Presence of petechial hemorrhages; (**d**) Inflammatory cells are also present in the thickened endocardium (H&E × 200)

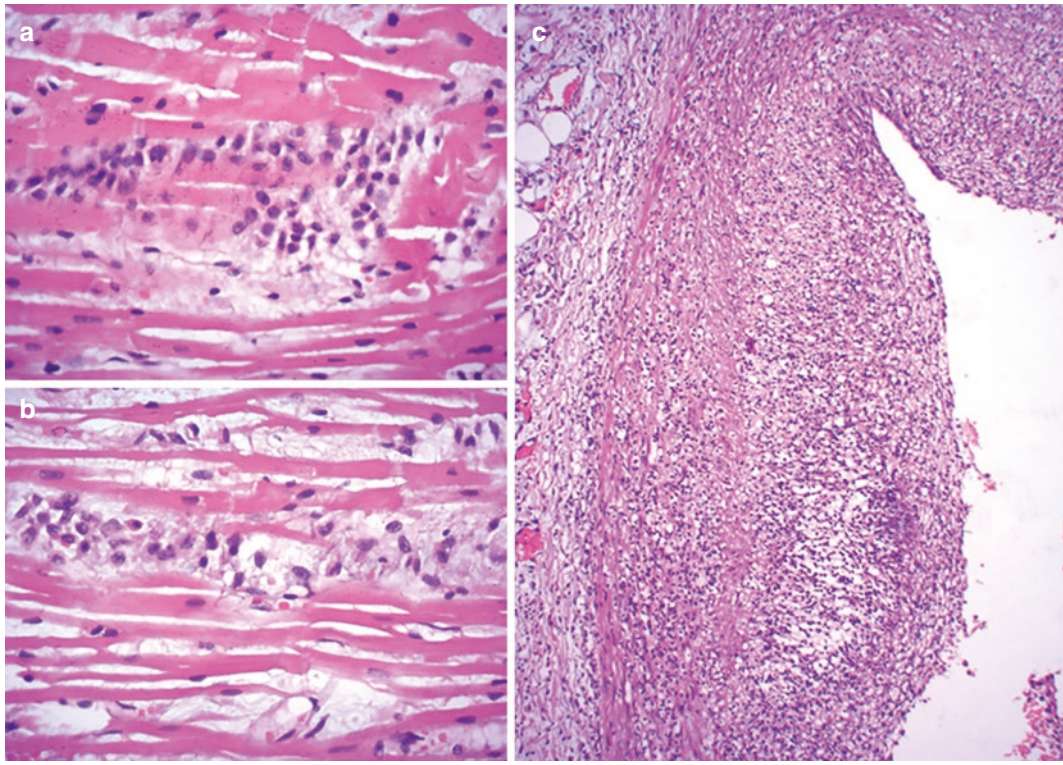

Fig. 34.3 Predominant histiocytic aggregates in the interstitium resembling Aschoff bodies are seen in (**a**) and (**b**) (H&E × 400). (**c**) There is expansion of the intima of the left anterior descending artery due to loose collections of inflammatory cells (H&E × 200)

34.3 Discussion

Acute undifferentiated febrile illness (AUFI) is defined as acute onset of fever (fever more than 38 °C lasting for less than 2 weeks), devoid of evidence of organ or system specific etiology. In the developing world and particularly in the tropical countries, many conditions with significant morbidity and mortality are included in the differential diagnoses of AUFI. Limited resources and the great diversity of the etiologies of AUFI are stumbling blocks to early diagnosis and treatment and therefore, clinical decision-making plays a major role in resource-poor settings. Development of high-grade fever with thrombocytopenia and the autopsy triad of severe intrapulmonary hemorrhage, acute tubulointerstitial nephritis, and interstitial myocarditis were highly suggestive of leptospirosis. A zoonotic disease caused by *Leptospira interrogans* that belongs to the family of *Leptospiraceae*, leptospirosis has an incidence of 10–100/100,000 persons in the tropical and subtropical countries. Transmission to humans occurs through water contaminated by urine of carrier animals (especially rodents) and the organisms enter through abraded skin or mucous membranes. The environment becomes conducive for disease transmission when there is monsoon-related flooding, which explains the occurrence of outbreaks not only in the rural regions, but also in flood-prone urban settings and constitutes a major public health problem.

After an incubation period of 7–14 days, the infection runs a biphasic course characterized by an initial acute septicemic phase lasting about a week and followed by an immune phase. Majority

of the infected individuals, to the extent of almost 90%, are either asymptomatic or develop self-limited febrile illness with associated headache and myalgia (the anicteric phase). Unfortunately, 5–10% of patients manifest with multisystemic damage such as the Weil's syndrome that is characterized by jaundice (icteric phase), splenomegaly, and renal manifestations. Our patient had acute tubuleinterstitial nephritis, but did not have jaundice or any other liver dysfunction, and developed bilateral diffuse pulmonary hemorrhage, which is increasingly seen in our country. This too is an example of a severe but atypical presentation of leptospirosis. The ensuing respiratory distress masked the cardiovascular manifestations.

Endothelial damage in all probability explains the development of the cardiac manifestations that are mediated by leptospiral cellular toxins, immune complex deposition, and antiphospholipid antibodies. There may also be direct injury to the cardiomyocytes. Autopsy studies have demonstrated a number of alterations such as interstitial edema, moderate to severe predominantly interstitial lympho-histiocytic myocarditis along with peri-vascular histiocytic clusters mimicking Aschoff bodies. These can be accompanied by pericarditis, mural or valvular endocarditis, intimitis of the coronary arteries, and/or the thoracic segments of the aorta and petechial hemorrhages (related to thrombocytopenia). The severity of myocardial inflammation is much more in the right ventricle. Most of these features were seen in the case presented. The outcome is myocardial systolic dysfunction, reminiscent of a similar manifestation in sepsis syndrome, and is often accompanied by myocardial infarction-like ECG changes and rise in the cardiac injury markers. Some patients also develop cardiogenic shock. Furthermore, involvement of the conduction system can also be present leading to arrhythmias. Such an involvement can be identified clinically in a variable proportion of patients, usually seen after a week's illness; in some cases, they can also occur early.

Early diagnosis of leptospirosis and its cardiac complication is not easy. Majority of the patients present with nondescript symptoms such as low-grade or high-grade fever, general malaise, headache, and myalgia, which may be seen in other monsoon-related illnesses such as malaria and dengue. These infections are also known to coexist. An epidemiology-based approach used by the clinician is likely to result in inappropriate antibiotic use at very early stages of infection, which tend to interfere with evolution of the illness process, mask symptomatology, and to some extent, even alter confirmatory diagnostics. Most of the rapid diagnostic tests for leptospirosis are usually based on serology, which may depend on background seroprevalence, time of appearance of antibodies, occurrence of cross-reacting antibodies, and antibiotic-therapy-related dampening of antibody responses. Besides, the positivity occurs in the latter part of the illness and definitive diagnosis requires demonstration of a fourfold rise in antibody titers. Although antigen-based or polymerase chain reaction-based diagnostics have been introduced to overcome these problems, their availability and affordability is limited. Imaging studies for the diagnosis of myocarditis is difficult as many patients require ventilator support. Levels of cardiac biomarkers are useful clues for cardiac involvement, but do not predict the degree of myocardial damage. More importantly, there is multiorgan involvement, which further hinders the diagnosis. Nevertheless, rapid and accurate identification would facilitate the use of inotropic support and fluids so as to reduce the morbidity and mortality. Long-term follow-up studies to determine the susceptibility of patients to eventual development of left ventricular dysfunction and cardiomyopathy are also warranted.

Further Reading

Chakurkar G, Vaideeswar P, Pandit SP, Divate SA. Cardiovascular lesions in leptospirosis: an autopsy study. J Infect. 2008;56:197–203.

Iglezias SD, Abreu PAE, Kanamura C, Magaldi AJ, Seguro AC, De Brito T. Immunohistochemical detection of Lp25 and LipL32 proteins in skeletal and car-

diac muscles of fatal human leptospirosis. Rev Inst Med Trop Sao Paulo. 2020;62:e85.

Jayathilaka PGNS, Mendis ASV, Perera MHMTS, Damsiri HMT, Gunaratne AVC, Agampodi SB. An outbreak of leptospirosis with predominant cardiac involvement: a case series. BMC Infect Dis. 2019;19:265.

Mathew A, Shanks M, Punnoose E, Fischer L, Koshy G, Potluri R, et al. Cardiac involvement in critically ill patients with leptospirosis: a prospective study using myocardial deformation imaging. Eur Heart J Acute Cardiovasc Care. 2020;9:975–83.

Salkade HP, Divate SA, Deshpande JR, Kawishwar V, Chaturvedi R, Kandalkar BM, et al. A study of autopsy findings in 62 cases of leptospirosis in a metropolitan city in India. J Postgrad Med. 2005;51:169–73.

Shah K, Amonkar GP, Kamat RN, Deshpande JR. Cardiac findings in leptospirosis. J Clin Pathol. 2010;63:119–23.

Cardiac Toxoplasmosis

35

Heena Desai and Pradeep Vaideeswar

35.1 Clinical History

A 55-year unemployed male presented with altered sensorium. There had been a history of acute onset of giddiness 3 days prior, which was followed by moderate grade fever, 5–6 episodes of vomiting, and 2–3 episodes of loose motions for 2 days. On examination, he was afebrile with pulse and respiratory rates of 84 and 22 per minute, respectively. The blood pressure was 120/84 mmHg. He was comatose with Glasgow coma scale of 9 (e2m5v2, 9/15) and features of raised intracranial pressure. The patient was moving all the limbs. A fundus examination was reported as grade 1 hypertensive retinopathy. Routine hematological and biochemical investigations were normal; the human immune deficiency status was negative. With a provisional diagnosis of meningitis, he underwent a cerebrospinal fluid (CSF) analysis and computed tomographic (CT) scan. The CSF was clear and colorless with proteins of 50 mg/dL, sugar of 29 mg/dL, and 2 neutrophils and 14 lymphocytes/cmm. India ink preparation did not reveal cryptococci. No organisms were seen on either Gram's or Ziehl-Neelsen staining. The CT scan revealed only few lacunar infarcts in the right lentiform nucleus and internal capsule.

The patient was administered mannitol and injection ceftriaxone; injection acyclovir was added after the CSF report for a possible viral meningitis or meningoencephalitis. But his neurological status gradually deteriorated and this was associated with spikes of moderate fever. On the third day of admission, he developed bleeding per rectum, a surgical evaluation of which revealed prolapsed thrombosed piles. The next day, the patient developed sudden respiratory distress, was intubated and ventilated. On the fifth day, he had a cardiorespiratory arrest and expired.

35.2 Autopsy Findings

A complete autopsy was performed. The leptomeninges appeared a little hazy over both temporoparietal regions. Coronal slices of the brain were normal. The heart weighed 270 g and was of normal size. All chambers and valves were normal, but transverse sections through both ventricles showed few congested areas. The coronary arteries were patent; the coronary circulation was right dominant. The thoracoabdominal aorta showed a fusiform atherosclerotic aneurysm for a length of 6 cm, extending up to the level of the

H. Desai
Department of Pathology, Topiwala National Medical College and BYL Nair Charitable Hospital, Mumbai, India

P. Vaideeswar (✉)
Department of Pathology (Cardiovascular and Thoracic Division), Seth Gordhandas Sunderdas Medical College and King Edward Memorial Hospital, Mumbai, India

P. Vaideeswar (ed.), *Tropical Cardiovascular Pathology*,
https://doi.org/10.1007/978-981-19-3720-0_35

renal ostia. The lungs were edematous with oozing of frothy hemorrhagic fluid. The right lobe of the liver had two (0.5 × 0.3 cam and 0.3 × 0.2 cm) well-circumscribed, firm yellowish nodules on the anterior surface, 1.5 cm from the lateral border and 4 cm from the inferior border. Apart from these findings, other organs appeared normal.

On histology, the seemingly normal appearing cerebral slices revealed small multifocal necroses of the superficial cortical parenchyma with moderate mononuclear cell infiltrate and prominent peri-vasculitis. There was also spill-over of the inflammation into the subarachnoid space. These changes were accompanied by small, rounded, fuzzy amphophilic structures with basophilic dots within them. They represented the tissue cysts of the parasite *Toxoplasma gondii* (*T. gondii*) with the dots representing the bradyzoites. Similar but smaller areas were seen in the midbrain. Surprisingly, the congested areas in the myocardium revealed large multifocal destruction of the myofibers with extremely heavy lympho-histiocytic infiltration (Fig. 35.1a, b) and few neutrophils. Some of the cardiomyocytes were expanded to accommodate the toxoplasmal cysts (Fig. 35.1a, c). In some foci, the pseudocysts had ruptured eliciting heavy inflammatory response (Fig. 35.1a, d). There would have been significant left ventricular dysfunction that led to prominent pulmonary edema noted at autopsy and sudden-onset respiratory distress that proved fatal. Sections of the liver revealed conglomerates of necroses walled off by thick fibrous tissue, surrounded by aggregates of mononuclear cells.

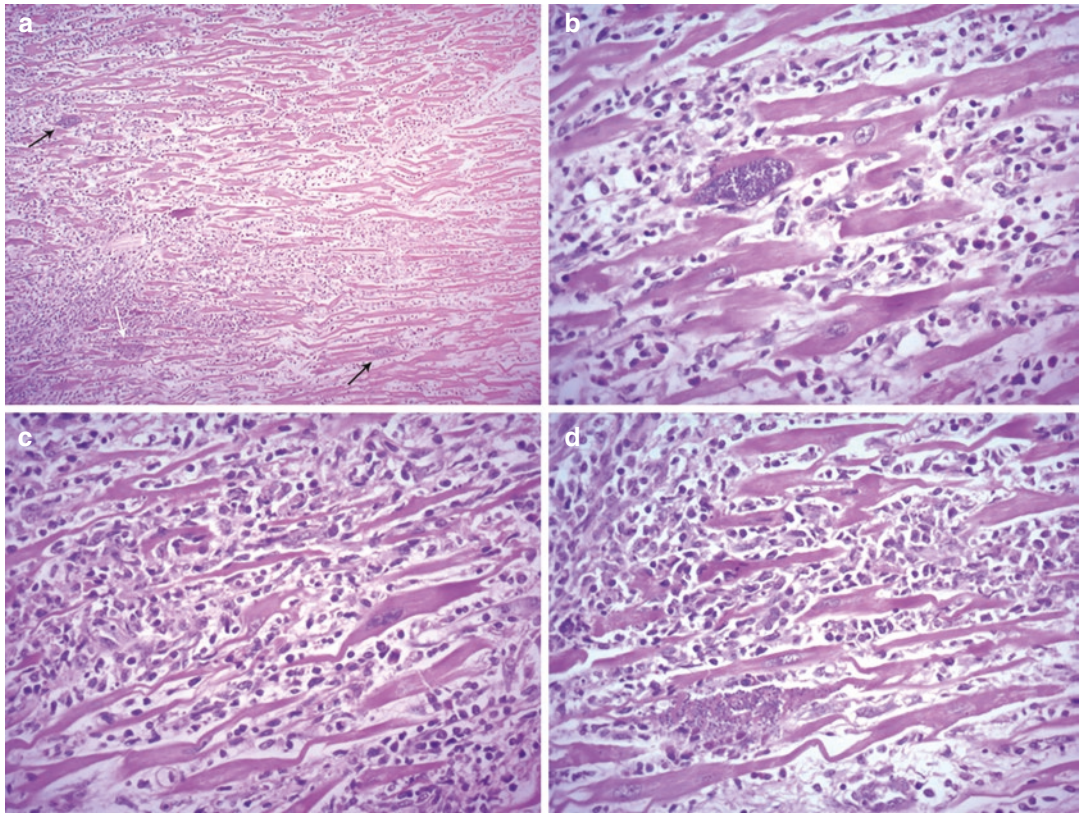

Fig. 35.1 (**a**) Acute myocarditis with destruction of the cardiomyocytes. Bluish structures (black and white arrows) are seen in some of them (H&E × 200); (**b**) The destruction is accompanied by extensive lympho-histiocytic infiltrate in the interstitium (H&E × 400); (**c**) A cardiomyocyte with an intracytoplasmic cyst (black arrows in **a**), which contains a number of bluish bradyzoites (H&E × 400); (**d**) Ruptured cyst (white arrow in **a**) with release of the bradyzoites into the interstitium (H&E × 400)

Rest of the parenchyma showed focal sinusoidal dilatation with small foci of necroses. No organisms were identified in the liver and other organs.

35.3 Discussion

Meningoencephalitis and lymphocytic myocarditis were the manifestations produced by the obligate intracellular protozoal parasite, *T. gondii*. This organism infects nearly half the world population, particularly in the tropical and subtropical developing nations with hot humid climates. The parasite exists in 3 forms: *oocysts*, *tachyzoites,* and *bradyzoites*. Most of the adult toxoplasmal infection occurs due to ingestion of water or food, contaminated by the *oocysts*, which are excreted in the feces of the definitive hosts belonging to the family Felidae. The most common member of this family is the domestic cat that explains the extensive prevalence of toxoplasmosis. *Tachyzoites* represent the intracellular proliferative forms that develop in the intestines of the intermediate hosts following the ingestion of the oocysts with subsequent lymphatic dispersal and frequent localization to muscle and neural tissues (acute phase of infection). This form explains the occurrence of congenital toxoplasmosis, where there is direct transplacental passage of the parasite from the mother to the developing fetus and also rare examples of transfusion-related infections. The host mounts cell-mediated and antibody-mediated immune responses, which convert the tachyzoites into *bradyzoites*; the latter reside in tissue cysts, most often involving the muscle. Hence, consumption of uncooked or undercooked meat (very frequent), and in some cases, organ transplantation serves as additional modes of transmission. It is to be noted that *T. gondii* remains viable in the tissue cysts with slow replication, which constitutes the chronic phase of infection. However, continued activation of T-lymphocytes and macrophages with elaboration of cytokines leads to dormancy and prevents reactivation and reinfection.

The clinical manifestation depends on the immune status of the host. In the majority of immunocompetent hosts, the infection is entirely asymptomatic, while around 10% of the individuals develop self-limited disease, manifesting with fever, headache, and/or lymphadenopathy and mimicking infectious mononucleosis. But in immunocompromised or immunosuppressed patients such as those with acquired immune deficiency syndrome or transplant recipients, decreased immune responses lead to rupture of the tissue cysts and transformation of bradyzoites to tachyzoites. This leads to widespread infection and multiorgan involvement, particularly meningoencephalitis and lymphocytic myocarditis. Our patient had both these features, but was immunocompetent, which is indeed unusual.

Lymphocytic myocarditis is the chief feature of cardiac toxoplasmosis; pericarditis, pericardial effusions, and constrictive pericarditis are distinctly uncommon. Apart from the constitutional features and symptoms related to central nervous system (CNS) involvement, myocardial inflammation can remain asymptomatic or subclinical. Symptoms such as chest pain, dyspnea, or palpitation may be attributed to concomitant pulmonary involvement or can be masked by the more prominent CNS symptoms, which happened in this case. The more severe cases can present with progressive left ventricular dysfunction, congestive heart failure or cardiogenic shock, arrhythmias, and atrioventricular or bundle branch blocks. In some cases, there is abrupt deterioration leading to sudden cardiac death, as can be seen with more common viral myocarditis (See Chap. 33). In general, myocarditis has always remained a diagnostic challenge because of the diversity in the presentation and varying etiology. Apart from use of ECG, imaging techniques, or biomarkers to diagnose the myocarditis, serological testing is usually employed for detecting active toxoplasmosis. This requires demonstration of rising antibody titers. Confirmation is achieved by endomyocardial biopsy. This may not be performed if the myocarditis is subclinical. Besides, the tissue cysts are most frequently localized in the left ventricle, which is not easily sampled. Hence, most often toxoplasmal myocarditis remains a postmortem diagnosis.

Further Reading

Amonkar GP, Desai HM, Sharma D. Cardiac toxoplasmosis and pneumocystis pneumonia: a fatal co-infection. IHJ Cardiovasc Case Rep. 2017;1:169–71.

England JH, Bailin SS, Gehlhausen JR, Rubin DH. Toxoplasmosis: the heart of the diagnosis. Open Forum Infect Dis. 2018;6:ofy338.

Gonzalez AJC, Matos IV, Revoredo VM. Acute toxoplasmosis complicated with myopericarditis and possible encephalitis in an immunocompetent patient. ID Cases. 2020;20:e00772.

Hidron A, Vogenthaler N, Santos-Preciado JI, Rodrigues-Morales AJ, Franco-Paredes C, Rassi A Jr. Cardiac involvement with parasitic infections. Clin Microbiol Rev. 2010;23:324–49.

Nunes MC, Guimaraes Junior MH, Diamantino AC, Gelape CL, Ferrari TC. Cardiac manifestations of parasitic diseases. Heart. 2017;103:651–8.

Zhou Z, Lopez HIAO, Perez GE, Burgos LM, Farina JM, Saldarriaga C, et al. Toxoplasmosis and the heart. Curr Probl Cardiol. 2021;46:100741.

Aspergillous Myocardial Absceses

36

Pradeep Vaideeswar

36.1 Clinical History

A 38-year-old male, nondiabetic and nonhypertensive, had been admitted in 3 private health-care facilities in the past 9 days for a left gluteal abscess. It had developed within a day of an intramuscular injection for an unspecified febrile illness. On the first day of the third admission (that lasted for 7 days), he had gone debridement of a large wound, which had now formed in the gluteal region. He developed acute renal failure and was put on hemodialysis. He was then shifted to our tertiary-care center due to financial constraints.

On examination, he was afebrile, conscious, and well-oriented with reference to time and place. The pulse was 110 per minute and blood pressure was 106/90 mmHg. At this point of time, there was no fever. There was a large wound 20 × 15 cm over the left gluteal region; the wound floor showed muscle, which was partly obscured by purulent exudates. There was an extension 15 × 5 cm over the lower back, which was also covered with purulent material. The investigations have been tabulated (Table 36.1). On the

Table 36.1 Investigations

Hematological	[a]Hemoglobin 6.8 g/dL [a]Total leukocyte count 17,550/cmm Differential count—Neutrophil predominant, with band forms, metamyelocytes and metamyelocytes and cytoplasmic toxic granules [a]Platelet count 3.15 lakhs/cmm
Biochemical—Routine	[a]Random blood glucose 90 mg/dL [a]Serum creatinine 4.1 mg/dL [a]Blood urea nitrogen 57.9 mg/dL [a]SGOT 201.1 U/L [a]SGPT 80 U/L [a]Total bilirubin 0.7 mg/dL [a]Sodium 134 mEq/L [a]Potassium 4.1 mEq/L [a]Chloride 116 mEq/L
Radiological	Chest computed tomography—Bilateral pleural effusions with basal consolidations
Others	Urine examination: Proteinuria 1+, pus cells 50–60 per high power field Wound culture: *Acinetobacter* species Blood culture: Negative

[a]Mean values

P. Vaideeswar (✉)
Department of Pathology (Cardiovascular and Thoracic Division), Seth Gordhandas Sunderdas Medical College and King Edward Memorial Hospital, Mumbai, India

P. Vaideeswar (ed.), *Tropical Cardiovascular Pathology*,
https://doi.org/10.1007/978-981-19-3720-0_36

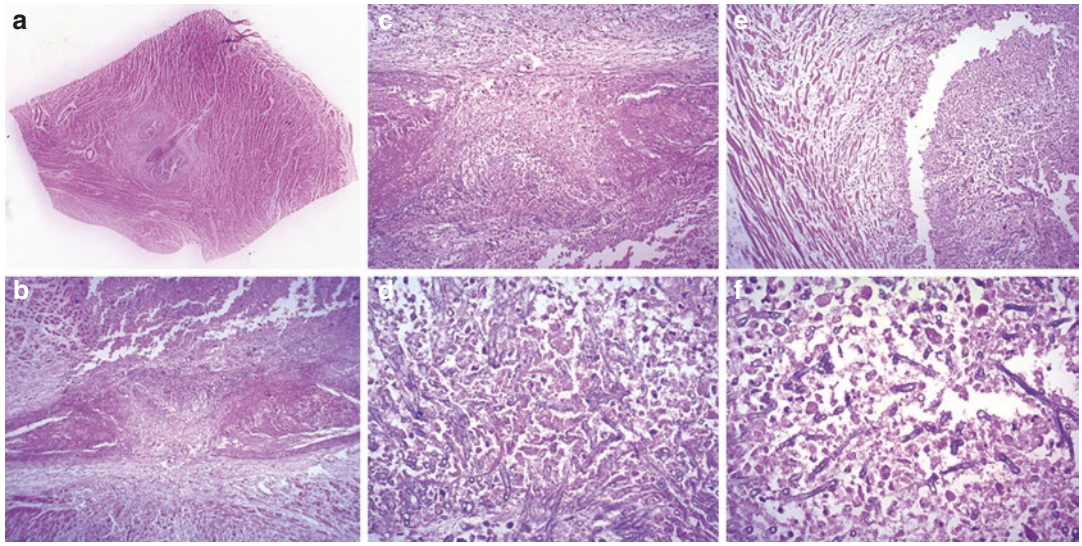

Fig. 36.1 (**a**) Scanned section of the left ventricular free wall showing a central area of breakdown; (**b**) Intramural coronary arteritis flanked on either side by abscesses (H&E × 100); (**c**) The lumens are occluded by fresh fibrin thrombi with associated necroses of their walls (H&E × 250); (**d**) Necrotic wall infiltrated by septate, slender, basophilic hyphal forms (H&E × 400); (**e**) A fairly circumscribed area of myocardial abscess formation (H&E × 250); (**f**) Fungal elements admixed with neutrophils (H&E × 400)

second day of admission, another extensive debridement was performed under general anesthesia. He was administered intravenous broad-spectrum antibiotics and was on hemodialysis. But the patient did not improve and developed altered sensorium and anuria. There was gradual deterioration and he expired 9 days after the operation.

36.2 Autopsy Findings

A complete autopsy was performed on a thin built male. The debrided wound was still covered with dirty slough and suppurative exudates. The heart was of normal size and weighed 240 g. All the chambers, valves, and coronary arteries were normal. Transverse slices of the ventricles, however, revealed multiple foci of congestion with breakdown of tissue in the left ventricular wall (Fig. 36.1a). On histology, these areas showed intramural coronary arterial radicles containing fresh fibrin thrombi with destruction of their walls and the presence of radiating lightly basophilic slender septate hyphal forms (Fig. 36.1b–d) resembling those of *Aspergillus* species (See Chap. 19). Surrounding such foci of necrotizing arteritis were many myocardial abscesses with hyphal filaments (Fig. 36.1e, f). Similar fungal micro-abscesses were also present in the brain (Fig. 36.2a–c). Surprisingly, the consolidated lung did not show any fungal elements even on the Gomori methenamine silver stain. Other findings were acute tubular necroses and pigment cast nephropathy (Fig. 36.2d) with focal micro-abscesses (no fungi seen) in the kidneys. Neutrophils were seen in the sinusoids of the liver and spleen.

Cause of Death: Septicemia with fungal myocardial and cerebral abscesses.

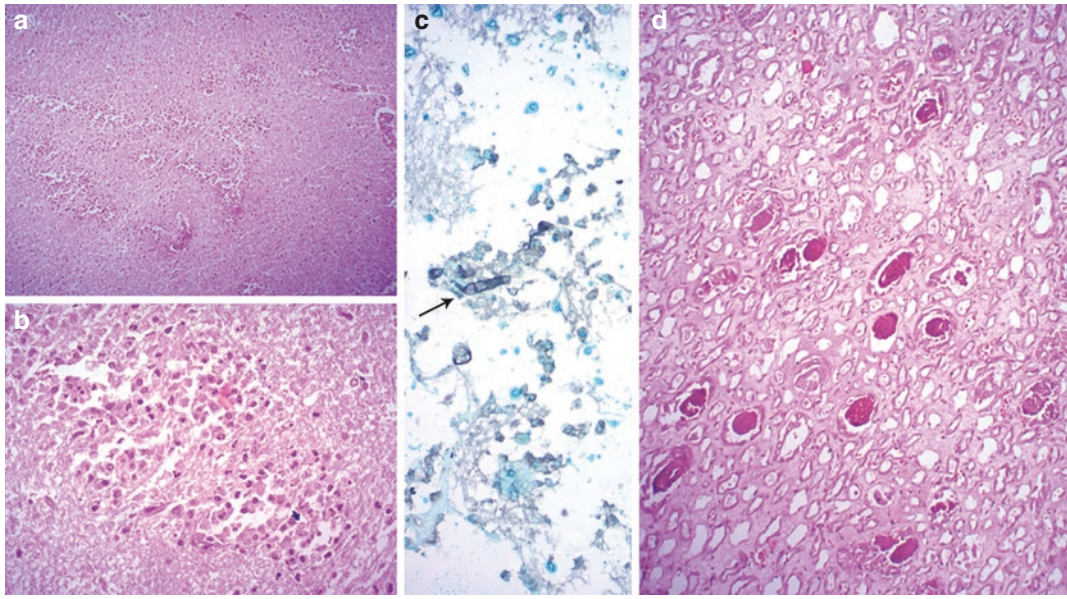

Fig. 36.2 Micro-abscesses seen in the cerebrum (**a**) H&E × 200 and (**b**) H&E × 400; (**c**) Scattered fungal hyphae (arrow) were present (Gomori methenamine silver × 400); (**d**) Presence of reddish-orange pigment cases in the collecting tubules (H&E × 250)

36.3 Discussion

A young immunocompetent man developed cardiac and cerebral necrotizing suppurative lesions following a large nonhealing wound over his left lower extremity. Such infective cardiac lesions form a diverse group of disorders, caused by a variety of microorganisms with involvement of one or more layers of the heart. Myocardial abscesses are found in about 0.18–1.52% of autopsies performed in adults and are very often caused by Gram-positive cocci especially *S. aureus*. In most instances, they are seen in patients with valvular or mural infective endocarditis (See Part V) either as a direct extension of the infection or through septic coronary arterial embolization. Very rarely, the softened and necrotic myocardium following an acute infarction and coronary arterial interventions (See Chap. 29) are contributing factors for abscess formation. Myocardial abscesses can also develop through dissemination from a distant septic focus or as a manifestation of sepsis, which was the mechanism in the case presented. The organism identified within the abscesses was a fungus, which had morphology of the *Aspergillus* species.

In general, unlike bacteria and viruses, fungi seldom produce infections in the immunocompetent hosts, except for superficial mycoses. Most of the invasive fungal diseases occur as opportunistic infections in individuals, whenever there is disruption of the immunological responses. The circumstances that permit penetration of immune barriers are immuno-deficient states, organ transplantation, hematological/non-hematological malignancies, administration of corticosteroids/antineoplastic drugs/prolonged broad-spectrum antibiotics, malnutrition, extensive surgery, critically ill immunocompetent patients, and contaminated devices. In such patients, diagnosis of fungal disease is not easy and requires a battery of tests, which include microbiological isolation, histopathological demonstration of tissue invasion, detection of fungal antigens, and even molecular analysis. Very often, the diagnosis is made or confirmed after postmortem examination. After *Candida* species, the organisms included in the genus *Aspergillus* are the next common fungi that are capable for producing dis-

seminated disease. The most common cardiovascular manifestation is infective endocarditis (See Chap. 19) and even with dissemination, the incidence of myocardial involvement is low, to the extent of 12%. These filamentous fungi are capable of producing saprophytic colonization, allergic reactions, and invasive disease depending on the host immunity. Since the spores of *Aspergillus* are ubiquitous and air-borne, pulmonary involvement is most frequent. In this case, however, the areas of bronchopneumonic consolidations failed to reveal the organisms even with special staining techniques, and very surprisingly, there were only myocardial and cerebral abscesses. This indicates that there would have been a hematogenous dissemination through the nonhealing wound. Even in and around the regions of the abscesses, the fungus showed the characteristic feature of angio-invasion with thrombotic occlusion of the intramural coronary arteries.

In most of the patients, the abscesses are scattered within the myocardium and clinical presentation would depend on the sizes and locations of the lesions. Few of these patients can remain asymptomatic, which is often the case with fungal dissemination. In some, the symptoms can be variable and vague, while others can present with conduction abnormalities, arrhythmias, valvular insufficiency (especially if the abscess is peri-valvular), congestive heart failure, myocardial rupture, or even sudden death. Clinical suspicion of fungal infection particularly in patients without obvious predisposing factors for such extensive, nonhealing wounds and the use of tissue biopsy and/or microbiological studies for fungi would have facilitated administration of appropriate antifungal therapy rather than broad-spectrum antibiotics. Unfortunately, material from the nonhealing wound was not sent for fungal cultures. Also, cardiac imaging would be useful for the detection of the life-threatening complication of fungal myocardial abscesses.

Further Reading

Albakri A. Fungal cardiomyopathy: a review and pooled analysis of pathophysiology, diagnosis and clinical management. Res Rev Insights. 2019;3:1–14.

Bullisa SS, Krywanczyka A, Haleb AJ. Aspergillosis myocarditis in the immunocompromised host. IDCases. 2019;17:e00567.

Gnat S, Łagowski D, Nowakiewicz A, Dylag M. A global view on fungal infections in humans and animals: opportunistic infections and microsporidioses. J Appl Microbiol. 2021;131(5):2095–113. https://doi.org/10.1111/jam.15084.

Kosmopoulos M, Frantzeskaki F, Dimopoulos G, Bulpa P, Van den Abeele A, Taccone FS, et al. Endomyocardial and pericardial aspergillosis in critically ill patients. Mycoses. 2017;60:576–80.

Murillo H, Restrepo CS, Marmol-Velez JA, Vargas D, Ocazionez D, Martinez-Jimenez S. Infectious diseases of the heart: pathophysiology, clinical and imaging overview. Radiographics. 2016;36:963–83.

Dual Mycosis of the Heart

37

Jayashri Chaudhari, Pradeep Vaideeswar, Shruti Mondkar, and Milind Tullu

37.1 Clinical History

A 1-year-old female child, residing in a slum, had been admitted in a small private healthcare facility with history of high grade, intermittent fever without chills or rash for 3 weeks, episodes of generalized tonic-clonic convulsions with increased respiratory activity for 12 days, followed by jaundice, melena, and swelling of the entire body for 7 days. Routine laboratory investigations revealed hemoglobin of 9.1 g/dL, total leukocyte count of 76,000/cmm (predominantly neutrophilic), elevated transaminases (plasma asparate aminotransferase, PAST/plasma alanine aminotransferase, PALT 112/118 U/L), and hyperbilirubinemia (total of 4.9 mg/dL and direct of 1.6 mg/dL). A computed tomographic scan of the brain had shown left middle cerebral artery territory infarct; cerebrospinal fluid examination had been normal. She had been given packed red cells, antimicrobials (piperacillin-tazobactum, vancomycin, and azithromycin), frusemide, phenobarbitone, and phenytoin.

Subsequently, she was referred to our tertiary-care center, where she was admitted for 9 days (last 7 days in the intensive care unit). On general examination, the patient was hemodynamically stable. The child was 8 kg and malnourished. The heart rate was 118 per minute and respiratory rate, 38 per minute. There was irritability, mild pallor, icterus, anasarca, a Foley's catheter in situ, and an erythematous ecchymotic patch on the right flank. On systemic examination, there were bilateral coarse crepitations and severe hepatosplenomegaly (liver 10 cm and spleen 7.5 cm). The hematological investigations revealed hemoglobin of 11 g/dL, mild neutrophilic leukocytosis (total count of 19,000/cmm), and adequate platelets

J. Chaudhari
Department of Pathology, Hriday Samrat Balasaheb Thackeray Medical College, Mumbai, India

P. Vaideeswar (✉)
Department of Pathology (Cardiovascular and Thoracic Division), Seth Gordhandas Sunderdas Medical College and King Edward Memorial Hospital, Mumbai, India

S. Mondkar · M. Tullu
Department of Pediatrics, Seth Gordhandas Sunderdas Medical College and King Edward Memorial Hospital, Mumbai, India
e-mail: milindtullu@kem.edu

P. Vaideeswar (ed.), *Tropical Cardiovascular Pathology*,
https://doi.org/10.1007/978-981-19-3720-0_37

(count of 5.6 lakhs/cmm). The peripheral smear showed large numbers of schistocytes and 8% nucleated RBCs; the reticulocyte count was 5.6%. These features were suggestive of a hemolytic anemia; sickling test was negative. Biochemical investigations showed increased levels of serum transaminases (PAST 146, PALT 120 U/L), serum lactate dehydrogenase (3463 IU/L), and serum creatinine (2.4 mL/dL). The coagulation profile was deranged—prothrombin time of 19 s (INR of 1.22) and activated partial thromboplastin time of 48 s. HIV status was negative. Routine urine examination showed many budding yeasts, but no pus cells. Sample collected for blood culture subsequently showed no growth. An ultrasonography confirmed the hepatosplenomegaly, while a computed tomographic scan of brain revealed left temporoparietal infarct with possible meningitis and vasculitis. The clinical impression was septicemia due to complicated pyogenic meningitis (as confirmed on cerebrospinal fluid examination) with disseminated intravascular coagulation and microangiopathic hemolytic anemia. In due course of time, the hemoglobin decreased from 11 g/dL to 5.4 g/dL and platelets from 5.6 lakhs to 40,000/cmm. She was treated with antibiotics (azithromycin, metronidazole, meropenem, and vancomycin), packed red cells, fresh frozen plasma, platelet concentrates, and mannitol. The patient's condition continued to worsen with development of hypotension, hypokalemia, and metabolic acidosis and she succumbed.

37.2 Autopsy Findings

A complete autopsy was performed. During the autopsy, a history of an initial consultation with a general practitioner with injection on the gluteal region was gathered from the relatives. Apart from the ecchymotic patch on the right flank (Fig. 37.1a), the skin on the but-

Fig. 37.1 (**a**) Ecchymotic patch on the right flank; (**b**) Greyish-white furry appearance on both the gluteal regions; (**c**) Cluster of pustules with reddish encrustations

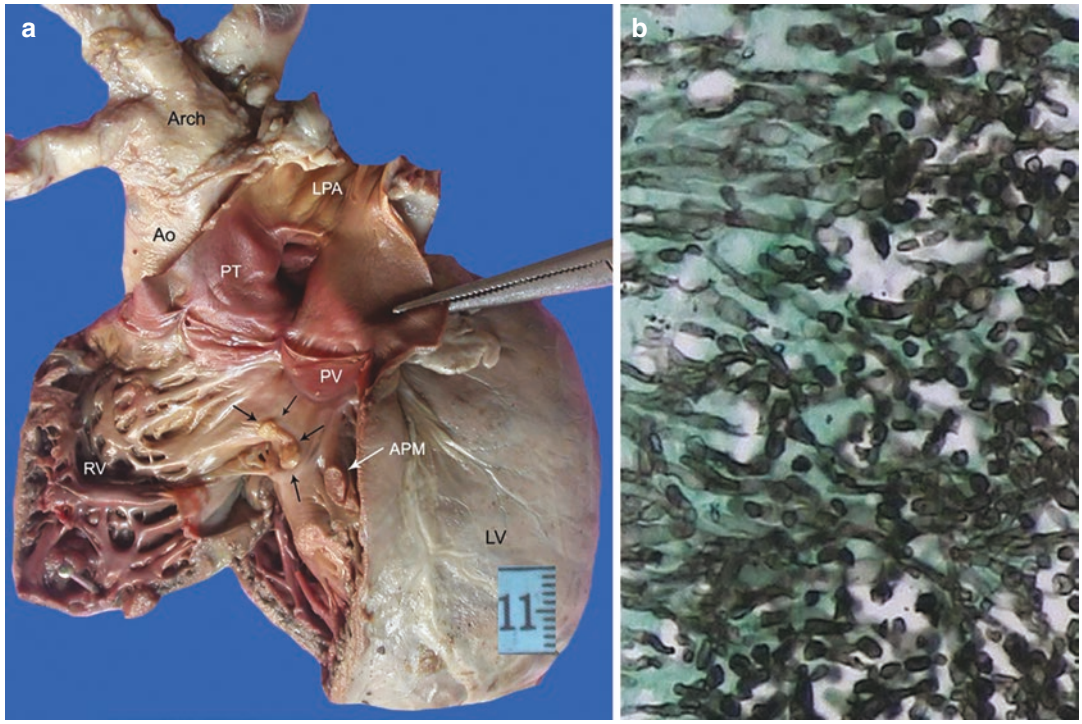

Fig. 37.2 (**a**) Opened out right ventricular RV outflow tract. Mural vegetation (black arrows) at the site of merging of the crista supraventricularis with the interventricular septum. The white arrow denotes the cut end of the anterior papillary muscle APM (*Ao* Ascending aorta, *LPA* left pulmonary artery, *LV* left ventricle, *PT* pulmonary trunk, *PV* pulmonary valve, *RA* right atrium); (**b**) Yeast and pseudohyphal forms suggestive of *Candida* species (Gomori methenamine silver × 400)

tocks also showed furry to granular white lesions (Fig. 37.1b) with multiple tiny pustules on the upper lateral aspect of the thigh, some of which were ulcerated (Fig. 37.1c). The heart was moderately enlarged in size (40 g) with moderate biventricular enlargement. The enlarged right ventricular cavity revealed plaque-like mural vegetation (Fig. 37.2a) over the crista supraventricularis, which on histology showed presence of yeasts and pseudohyphae that was suggestive of *Candida* species (Fig. 37.2b). There was a dusky discoloration of the endocardium over the dilated left ventricle. Transverse sections showed foci of pale red to yellowish foci with a flaky granularity in the intertrabecular spaces of both ventricles. These on histology corresponded to septic mural vegetations infiltrated by lightly basophilic slender septate hyphae, the morphology of which suggested *Aspergillus* hyphae (Fig. 37.3a–c). There was necrotizing arteritis of the intramural coronary arteries (Fig. 37.3d) and fungal myocarditis (Fig. 37.3e). Fungal elements were also noted in the suppurative inflammation over the visceral pericardium. Additional findings at autopsy included aspergillous meningoencephalitis with hemorrhagic infarcts (Fig. 37.4a, b), angioinvasive pulmonary aspergillosis, and aspergillous gastritis (Fig. 37.4c, d), along with candidial acute pyelonephritis and cystitis.

Cause of Death: Disseminated fungemia.

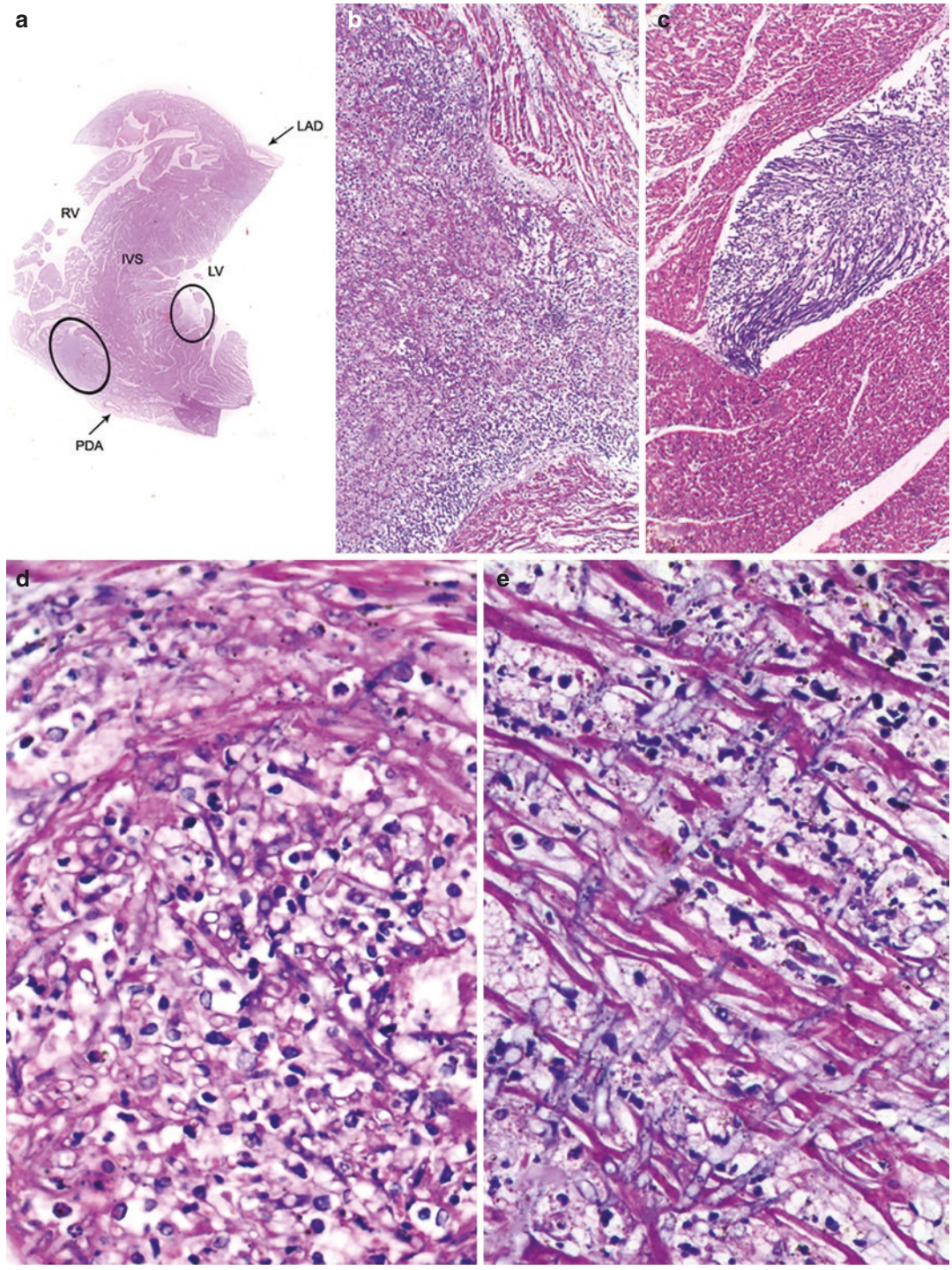

Fig. 37.3 (**a**) Scanner view of section of the interventricular septum IVS and adjoining ventricular free walls (*LAD* left anterior descending artery, *LV* left ventricle, *PDA* posterior descending artery, *RV* right ventricle). The circled areas on the right and left side of the IVS show mural fungal endocarditis in the intertrabecular spaces of the (**b**) right ventricle (H&E × 100) and (**c**) left ventricle (H&E × 100); (**d**) Fungal hyphae within the lumen of an intramural coronary artery (H&E × 400) (**e**) Fungal myocarditis showing necroses of the myofibers and interstitial neutrophilic infiltrate with abundant nuclear debris overrun by fungal hyphae (H&E × 400)

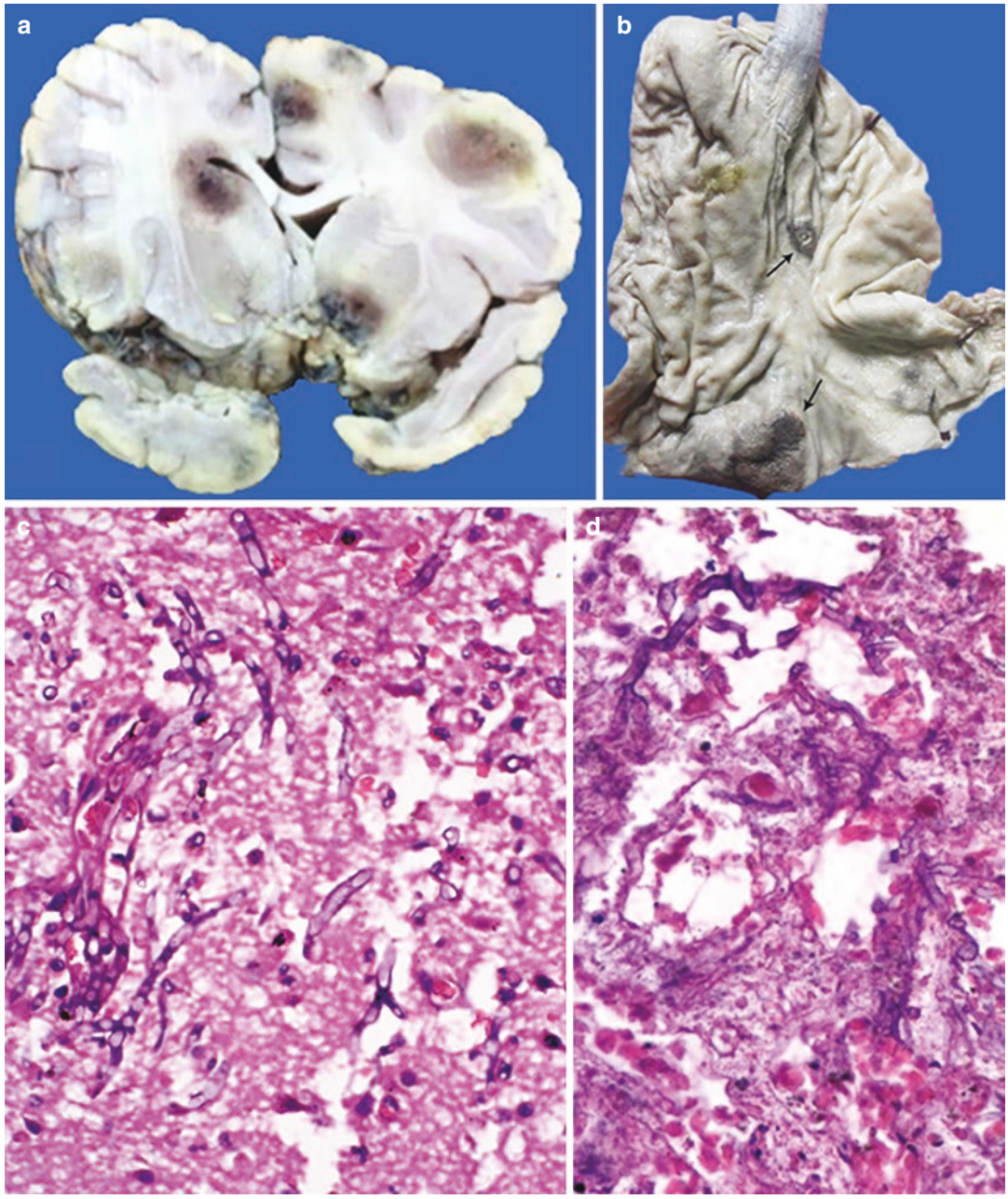

Fig. 37.4 (**a**) Coronal slice showing hemorrhagic infarcts; (**b**) Hyphal elements infiltrating the cerebral parenchyma (H&E × 400); (**c**) Opened out stomach with presence of ulcers with hemorrhagic rims; (**d**) Septate hyphae present in the mucosa with epithelial ulceration (H&E × 400)

37.3 Discussion

This is a report in a child of a rare occurrence of double (dual or mixed) mycotic infection, which was not suspected clinically but detected at autopsy. In the past few decades, the incidence of invasive opportunistic fungal infections is rising, not only among the adults, but also in the pediatric population. *Candida* and *Aspergillus* species are the most common causes of invasive fungal disease in neonates, infants, children, and adolescents. The risk factors are usually related to immunosuppressed states such as those with cancer, solid organ, or hematopoietic stem cell transplantations with their associated immunomodulatory therapy and immunocompromised conditions like primary or acquired immunodeficiencies. In these groups, invasive mycosis has an incidence between 5 and 25%. Another important group of patients are those who are admitted in the intensive care units. They are critically ill with prolonged hospital admissions and often receive ventilator support, prolonged broad-spectrum antibiotics, and invasive interventions. The fungal infection results due to disruption of the anatomical or physiological barriers, which can also be seen in patients with traumatic injuries, burns, or major surgeries. These circumstances would allow colonization of the endogenous commensals like the *Candida* species or entry of the exogenous filamentous fungi like the *Aspergillus* species in the form of spores. The usual portals of entry are the upper aerodigestive tract, the gastrointestinal tract, and skin and the organisms are disseminated by the hematogenous route to the tissues of one or more organs. In this patient, there were multiple pustules in the region of the gluteal injection, which may have been the possible site of entry. Also, there was a furry white rash on bilateral gluteal regions, predominantly around the clefts indicating diaper rash, which in 15–20% of the cases is caused by *Candida* species.

The *Candida* species continue to remain the leading cause of invasive disease in the pediatric population and are caused by both the *albicans* and non-*albicans* groups often depending on certain predisposing factors. Invasive candidiasis manifests as candidemia, disseminated candidiasis, or single organ infection; the most frequently affected organs are lungs, liver, kidney, and brain. When heart is involved, there is usually infective endocarditis. The mortality ranges from 20 to 30%. The next common fungus is *Aspergillus*, which is the leading cause for invasive mold infection. The main sites of infection are the lungs and the central nervous system, where lesions develop secondary to the angioinvasive properties of the hyphal forms. Involvement of the skin, gastrointestinal tract, and the heart is said to be uncommon, though cutaneous lesions are presumed to be more common in children. The mortality ranges from 10 to 20%. However, when one considers the concept of polymicrobial infection, the mixing can occur between kingdoms, genera, species, strains, and even substrains. Though this may be true for bacteremia and bacterial infections, fungal infections are usually considered monomicrobial disease. In this case, there was a double mycotic infection. Invasive candidiasis manifested as right-sided endocarditis and acute pyelonephritis/cystitis, while *Aspergillus* produced pancarditis, angioinvasive lung lesions, meningoencephalitis, and acute gastritis. Another interesting feature in this case was microangiopathic hemolytic anemia. The mechanism is similar to that seen with disseminated intravascular coagulation; the RBCs rupture due to extensive angioinvasion.

Diagnosis of fungal infection in children is very difficult as the clinical manifestations would vary depending on the overall immune status. Besides, the symptoms and signs may be nonspecific, develop during disease progression, and may be even minimal despite dissemination. Hence, a presumptive diagnosis should be made on the basis of the settings, which are congenial for the development of invasive fungal disease. A confirmation can be made with sophisticated imaging, fungal biomarkers, and molecular detection tests. Despite early detection, therapy is also challenging attributed to varying pharmacokinetics of the antifungal drugs in children.

Further Reading

Grigg A, Clouston D. Disseminated fungal infection and early onset microangiopathy after allogeneic bone marrow transplantation. Bone Marrow Transplant. 1995;15:795–7.

Jensen J, Munoz P, Guinea J, Rodriguez-Creixems M, Pelaez T, Bouza E. Mixed fungemia: incidence, risk factors, and mortality in a general hospital. Clin Infect Dis. 2007;44:e109–14.

Katragkou A, Fisher BT, Groll AH, Roilides E, Walsh TJ. Diagnostic imaging and invasive fungal diseases in children. J Pediatric Infect Dis Soc. 2017;6(S1):S22–31.

King J, Pana ZD, Lehrnbecher T, Steinbach WJ, Warris A. Recognition and clinical presentation of invasive fungal disease in neonates and children. J Pediatric Infect Dis Soc. 2017;6(S1):S12–21.

Pana ZD, Roilides E, Warris A, Groll AH, Zaoutis T. Epidemiology of invasive fungal disease in children. J Pediatric Infect Dis Soc. 2017;6(S1):S3–S11.

Tuberculous Myocarditis

38

Gayathri Amonkar and Pradeep Vaideeswar

38.1 Clinical History

Hypertension was detected in a young woman when she developed a cerebrovascular accident at the age of 38 years. She recovered and was on antihypertensives. Two years later, she developed sudden-onset headache followed by altered sensorium and was admitted in our emergency services department. The general condition was poor, the pulse rate was 76 per minute, and blood pressure was 170/100 mmHg. She was unconscious with nonreacting pupils and downgoing plantar reflexes. Rest of the systemic examination had been normal. Her routine hematological and biochemical investigations had been normal. The ECG (Fig. 38.1) showed abnormal inferior Q waves, borderline T wave abnormality, borderline prolonged QT interval, and baseline wander in leads V1, V3 and V4, while intraventricular hemorrhage was seen on computed tomographic scan. She was given antihypertensives, anticonvulsants, and intracranial tension lowering agents and antibiotics, but expired after 12 h.

G. Amonkar
Department of Pathology, Topiwala National Medical College and BYL Nair Charitable Hospital, Mumbai, India

P. Vaideeswar (✉)
Department of Pathology (Cardiovascular and Thoracic Division), Seth Gordhandas Sunderdas Medical College and King Edward Memorial Hospital, Mumbai, India

P. Vaideeswar (ed.), *Tropical Cardiovascular Pathology*,
https://doi.org/10.1007/978-981-19-3720-0_38

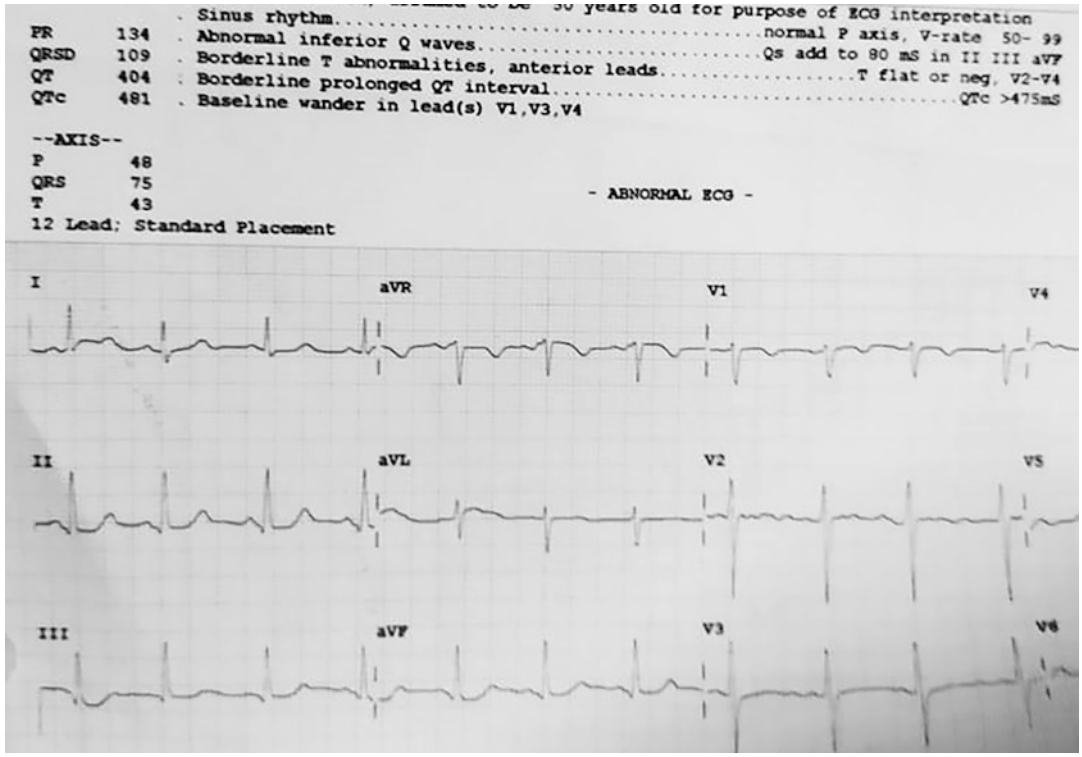

Fig. 38.1 Abnormal ECG tracing

38.2 Autopsy Findings

The heart (290 g) was moderately enlarged and globular due to biventricular enlargement. The heart also felt a little flabby and transverse sections revealed biventricular dilatation with myocardial thinning and few pale yellowish white areas in the subepicardial region (Fig. 38.2a). On histology, most of the sections of the right and left ventricular myocardial revealed caseating epithelioid granulomas in the interstitium (Fig. 38.2b, c); confluence of granulomas had produced the opalescent subepicardial foci (Fig. 38.2d, e). Lymphocytic myocarditis-like areas (Fig. 38.3a) were seen in the other parts of the myocardium with associated endocardial inflammation and fibrosis (Fig. 38.3a, b). All coronary arteries were patent. Rest of the chambers and valves were normal. Other findings were hypertensive intraventricular hemorrhage, Hashimoto's thyroiditis, mediastinal tuberculous lymphadenitis, pulmonary edema with bronchopneumonia, hepatic steatosis, and acute renal tubular necroses.

Cause of Death: Raised intracranial pressure due to intraventricular hemorrhage.

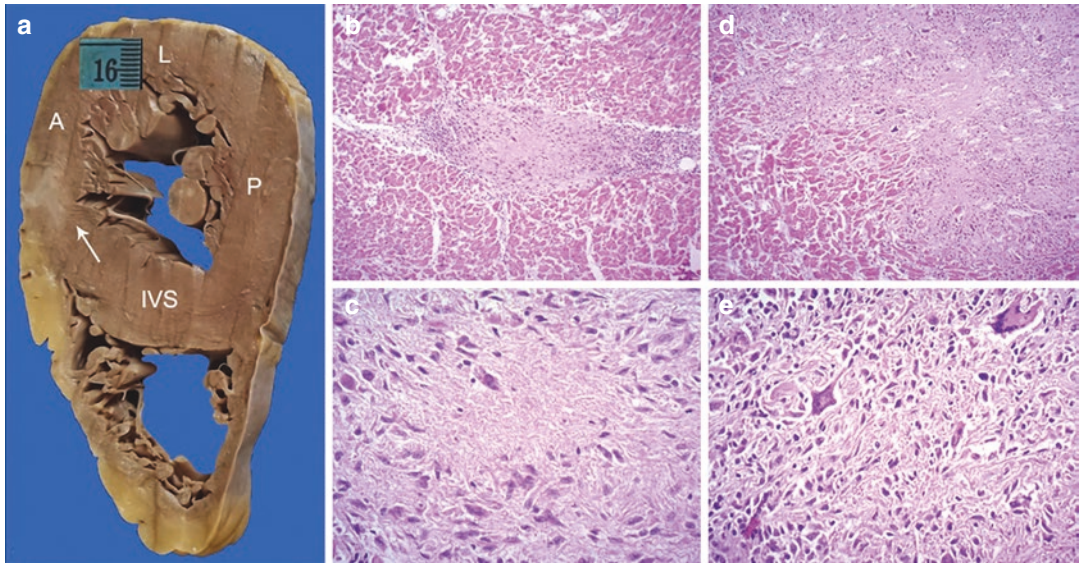

Fig. 38.2 (**a**) The transverse section forming the mid-portion of the ventricles shows a subepicardial irregular pale grey appearance of the myocardium. The interstitium shows a large caseating granuloma amidst the myofiber groups (**b**) H&E × 200 and (**c**) H&E × 400; The subepicardial focus was composed of confluent granulomas (**d**) H&E × 200 and (**e**) H&E × 400

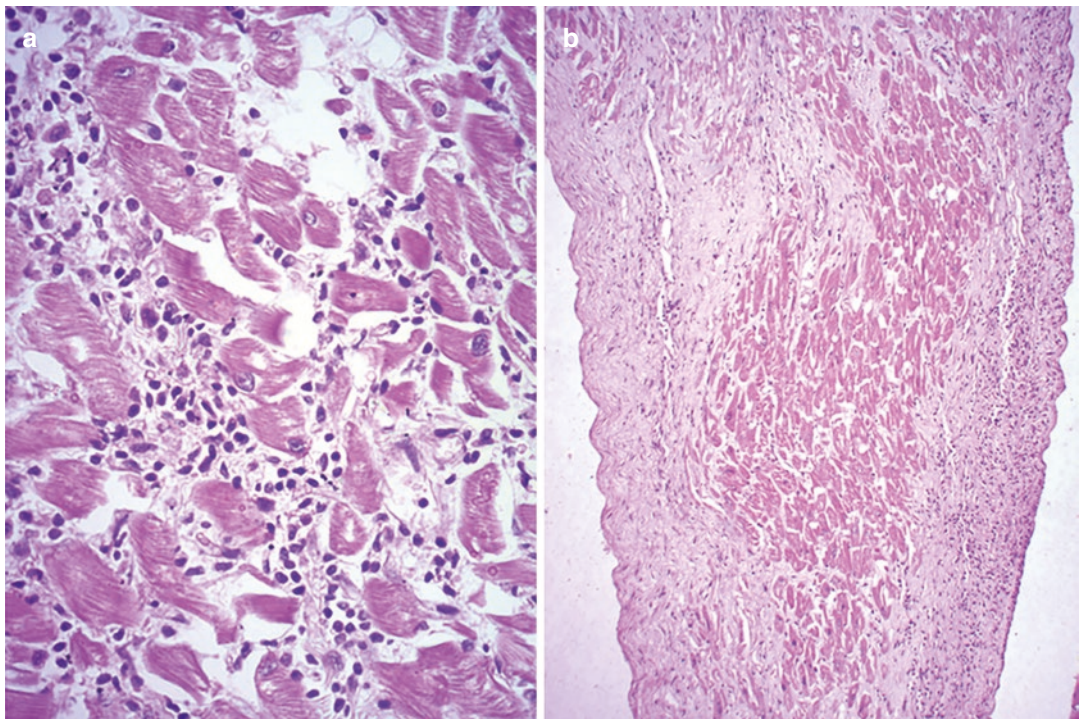

Fig. 38.3 (**a**) Dense lymphocytic clusters were seen in the interstitium (H&E × 400); (**b**) The endocardium over the trabecula was thickened with focal lymphocytic infiltration (H&E × 200)

38.3 Discussion

The ECG abnormalities recorded in this young woman were produced by tuberculous myocarditis, which is an uncommon manifestation of cardiovascular tuberculosis. Tuberculosis, which is still a major health problem in several countries, is generally said to spare the thyroid, heart, pancreas, and skeletal muscle. However, the heart is involved in around 1–2% of patients with tuberculosis and is primarily a disease of the pericardium (See Chap. 2). Affliction of the other layers of the heart (myocardium and endocardium), coronary arteries (See Chap. 66), or aorta (See Chap. 65) is exceedingly rare. The reported prevalence of tuberculous myocarditis ranges from 0.14 to 2% and affects the young population (<45 years of age), especially men. Many such patients have weak immune status produced by diseases, age, and even prevailing poor socioeconomic conditions. Active myocardial contraction and generation of lactic acid are said to be the factors for relative sparing of the myocardium. The inflammation generally occurs in conjunction with pericardial disease or may be associated with pulmonary or extrapulmonary tuberculous foci through retrograde lymphatic spread, hematogenous dissemination, or direct extension. Isolated myocardial disease is distinctly unusual. Though the right-sided chambers are collectively said to be the most vulnerable due to their proximity to the right-sided mediastinal lymph nodes (most frequently involved by tuberculosis), the left ventricle is commonly affected. Involvement of the mediastinal lymph nodes was present in the case presented; there was no active inflammation in any other organ at autopsy. Much of the granulomatous inflammation was present in the left ventricular myocardium.

Morphologically, the myocardial lesions may be nodular, miliary, or of the diffuse infiltrative type. The nodular pattern is the most common form, where the myocardium shows small or large (‘pea to egg’ sized) granulomatous reaction with caseation necrosis; the largest nodules (tuberculoma) are described in the right atrium. This is followed by the miliary lesions that usually develop in the context of miliary tuberculosis. The rarest is the diffuse pattern that is characterized by interstitial infiltration of lymphocytes and giant cells. Certain stringent criteria had been introduced for the diagnosis of tuberculous myocarditis, which included major [positive polymerase chain reaction (PCR), positive myocardial culture, or demonstration of acid-fast bacilli in the myocardial tissues] and minor [myocardial granulomas, myocardial imaging abnormalities, and involvement of extracardiac tissues] criteria. Diagnosis of myocardial tuberculosis is justified if there is presence of 2 or more major criteria or a major and 2 or more minor criteria. It should be noted that confirmatory tests, including the PCR, can often be inconclusive or may also not be available at all centers due to technical restraints and financial constraints. Hence, presence of the characteristic caseating granulomas in the myocardium should be considered as a major criterion. The acid-fast staining did not demonstrate mycobacteria in the myocardium, but was seen in the tuberculous lymphadenitis. Many patients, despite extensive involvement, can remain asymptomatic and the disease is diagnosed at autopsy, particularly with sudden death. Others present with arrhythmias (atrial fibrillation, paroxysmal ventricular tachycardia or long QT syndrome), atrioventricular block, valvular dysfunction, right-sided inflow or outflow tract obstructions, and congestive cardiac failure; the latter is seen with diffuse involvement and has decreased left ventricular ejection fraction. Magnetic resonance imaging is useful to recognize these lesions and should be coupled with other investigative procedures for confirmation of tuberculosis. Antituberculous, antiarrhythmic, and antifailure drugs result in significant amelioration. Though rare, one must be aware of this unusual presentation of tuberculosis, particularly in young patients with unexplained ECG abnormalities or cardiac failure, and making an early diagnosis will improve the prognosis and reduce mortality.

Further Reading

Al-Jahdali F, Al-Harbi A, Baharoon S, Al-Gamdi M, Jahdali H. Tuberculous myocarditis is not always fatal: report of three confirmed cases with uneventful outcome. Int J Mycobacteriol. 2017;6:111–5.

Kumar S, Bhutani N, Kataria SP, Sen R. Tuberculous myocarditis on autopsy: a rare underdiagnosed entity. Cardiovasc Pathol. 2018;37:5–7.

Langara B, Georgieva S, Khan WA, Bhatia P, Abdelaziz M. Sudden cardiac death in a young man. Breathe (Sheff). 2015;11:67–70.

López-López JP, Posada-Martínez EL, Saldarriaga C, Wyss F, Ponte-Negretti CI, Alexander B, et al. Tuberculosis and the heart. J Am Heart Assoc. 2021;10:e019435.

Michira BN, Alkizim FO, Matheka DM. Patterns and clinical manifestations of tuberculous myocarditis: a systematic review of cases. Pan Afr Med J. 2015;21:118.

Isolated Cardiac Sarcoidosis

39

Manoj Parchake, Shashank Tyagi,
and Pradeep Vaideeswar

39.1 Clinical Presentation

A body of a 38-year-old male was brought to our tertiary-care center for a medicolegal autopsy. He was found unconscious at a railway station.

39.2 Autopsy Findings

At autopsy, there was marked cardiomegaly (heart weight of 380 g) with extreme left and moderate right ventricular enlargements. All epicardial coronary arteries were patent. Bread-loafing of the ventricles showed an extraordinary degree of endocardial thickening towards the basal aspect with flattening and complete fibrosis of the trabeculae carneae, prominently affecting those of the right ventricle (Fig. 39.1a, b). The basal interventricular septum for a length of 2.5 cm in the posterior aspect had a width of 0.6 cm with a transmural, translucent fibrous replacement (Fig. 39.1a, b). The anterolateral free wall also showed thinning with similar grey-white tissue involving the subepicardial region. Focal epicardial and endocardial granularity were also noted. The histology from the affected portions showed classic features of sarcoidosis. There was extensive fibrosis and hyalinosis with multiple noncaseating granulomas (Figs. 39.2 and 39.3). Many of the giant cells showed asteroid bodies (Fig. 39.2a and b) in their cytoplasm. Surprisingly, the lungs, mediastinal lymph nodes, liver, kidneys, and spleen failed to show such granulomatous inflammation.

Cause of Death: Isolated cardiac sarcoidosis and sudden cardiac death (SCD).

M. Parchake
Department of Forensic Medicine and Toxicology, Seth Gordhandas Sunderdas Medical College and King Edward Memorial Hospital, Mumbai, India

S. Tyagi
Department of Forensic Medicine and Toxicology, Lady Hardinge Medical College and Associated SSK and KSC Hospitals, New Delhi, India

P. Vaideeswar (✉)
Department of Pathology (Cardiovascular and Thoracic Division), Seth Gordhandas Sunderdas Medical College and King Edward Memorial Hospital, Mumbai, India

P. Vaideeswar (ed.), *Tropical Cardiovascular Pathology*,
https://doi.org/10.1007/978-981-19-3720-0_39

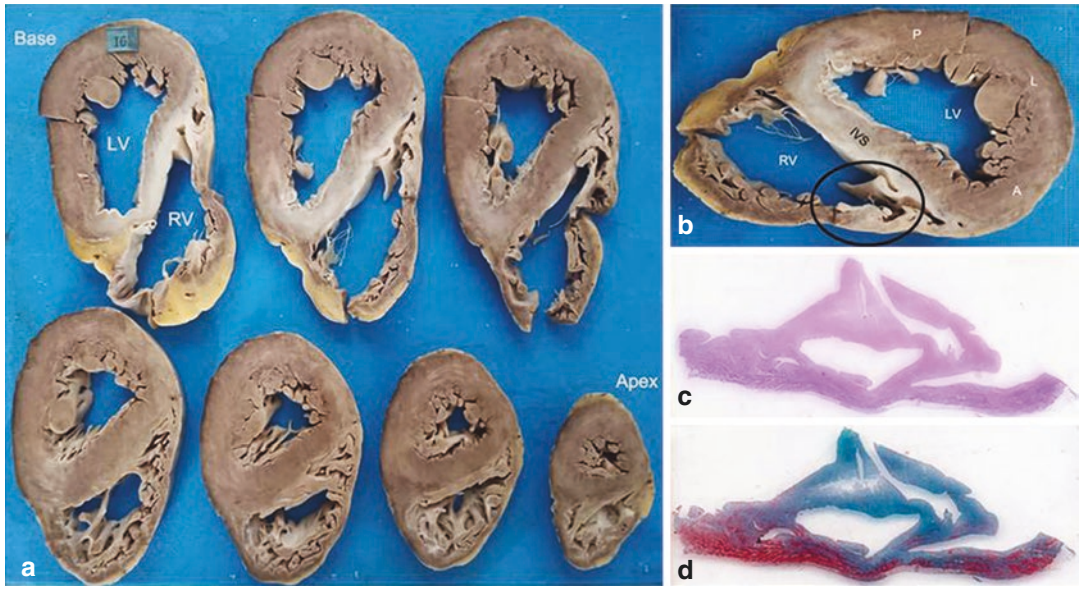

Fig. 39.1 (**a**) Serial transverse sections showing prominent involvement of the basal portions of the interventricular septum, part of the posterior wall, and anterior aspect of the right ventricle RV, as compared to the apical third. There is associated dilatation of the ventricular chambers; (**b**) Close-up of one of the basal slices with transmural fibrosis of the septum IVS, part of the posterior wall P and anterior wall of RV (*A* anterior wall, *L* lateral wall, *LV* left ventricle); Scanned slide of section of the circled area in image B as stained by (**c**) H&E and (**d**) Masson's trichrome, which reveals extensive fibrosis

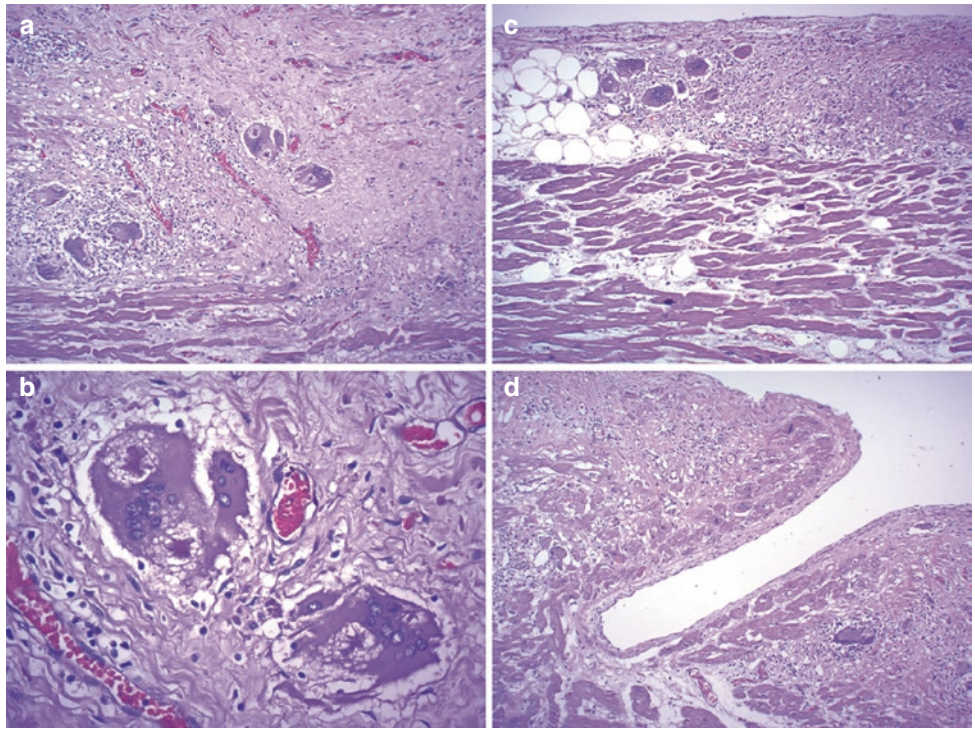

Fig. 39.2 (**a**) Noncaseating granulomatous inflammation in the right ventricle along with extensive interstitial fibrosis (H&E × 200); (**b**) Giant cells with cytoplasmic asteroid bodies (H&E × 400); Similar granulomas seen (**c**) over the epicardial and (**d**) endocardial aspects of the heart (H&E × 200)

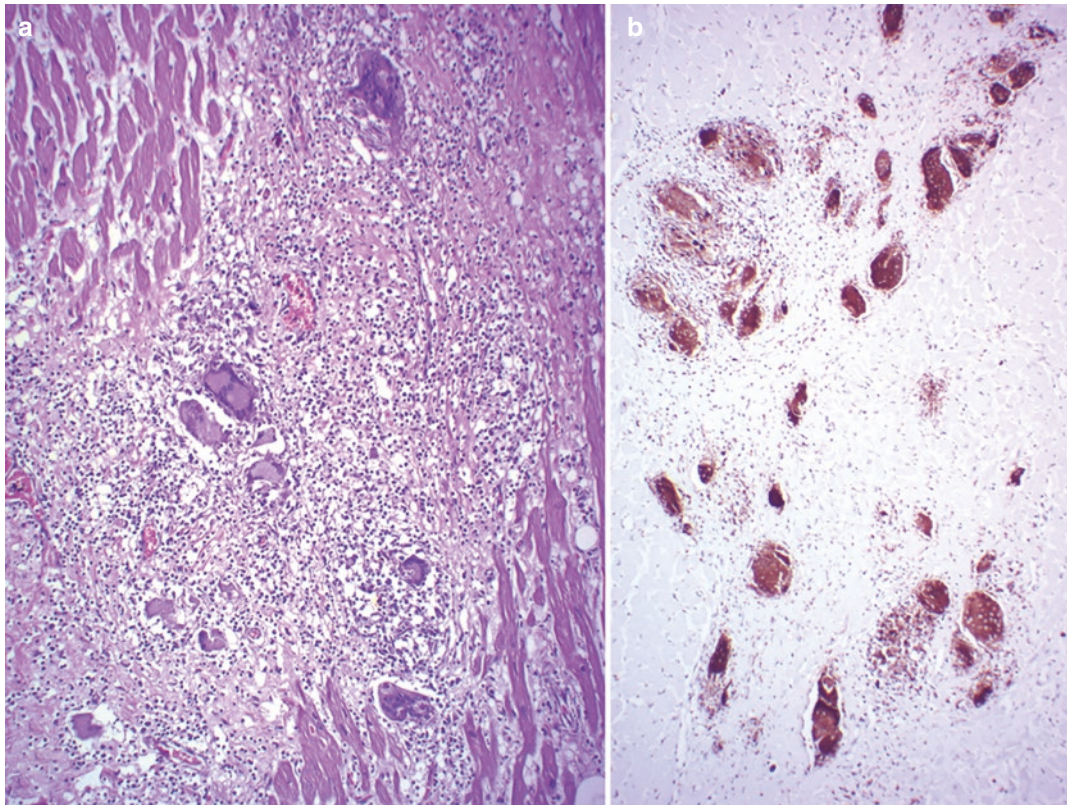

Fig. 39.3 (**a**) Granulomas in the left ventricle (H&E × 200); (**b**) The giant cells and other histiocytes show strong immune-histochemical cytoplasmic positivity for CD 68 (×200)

39.3 Discussion

A diagnosis of cardiac sarcoidosis (CS) was made in this case based on the documentation of characteristic non-necrotizing granulomatous inflammation with associated extensive myocardial scarring. This involvement is an example of the so-called infiltrative (or deposition) cardiomyopathy, where there is progressive myocardial stiffening with relaxation abnormalities and contractile dysfunction due to interstitial or intracellular accumulation of substances or cells (Also see Chaps. 48–51). As yet the trigger/s for sarcoidosis still remains elusive, but the antigen results in a systemic granulomatous response in genetically predisposed individuals affecting all ages and ethnic backgrounds. The global prevalence ranges from 4.7 to 64 in 100,000 with predominance in women. The mean age of presentation is 48 years, while a second peak of onset is seen especially in women over 50 years of age. The males who are affected are younger than their female counterparts. Although the disease may affect any organ, the lungs and mediastinal lymph nodes are most commonly affected. CS is said to occur more commonly in males and the current incidence (5–27%) is likely to increase as a result of better awareness and innovative imaging techniques. The regular use of these sophisticated sensitive imaging would also mean that there would be a decrease in isolated subtype of CS (cardiac involvement without pulmonary or extrapulmonary manifestations) as subtle, subclinical involvement of the noncardiac tissues would be picked up. In the index case, the heart was the sole organ to be affected as all other organs such as the lungs, liver, spleen, and lymph nodes failed to reveal granulomas despite exten-

sive sampling. Some studies have highlighted that patients, who had isolated CS to begin with, develop systemic disease on follow-up.

The inflammation in CS is patchy and occurs through successive stages of edema, granulomatous response, and finally post-inflammatory scarring. Though all the 3 layers of the heart are involved, the ventricular myocardium is the most favored site and is responsible for most of the clinical manifestations, which also depends on the extent of the lesions. It usually affects the basal portions of the heart and the order of frequency is the left ventricular free wall, interventricular septum, and right ventricle. In the very early phase of the disease, the granulomas are seen in the summit of the interventricular septum and may be composed merely of loose clusters of macrophages and lymphocytes. With progression, well-formed 'tight' granulomas are present with epithelioid and giant cells; in few areas only clusters of giant cells may be identified. Such granulomas in due course of time coalesce to form grey-white to tan-yellow lesions often located in the subepicardial or mid-myocardial regions. Some granulomas may show central fibrinoid necrosis, and here, it is important to rule out infective causes (mycobacterial or fungal) through special stains. Further advancement of the inflammatory process leads to a fibrous encasement of the granulomas with eventual predominant regional fibrosis (appearing as grey-white opaque to translucent areas) with or without lymphocytic aggregates.

The clinical presentation of CS would depend on 3 factors—the degree of inflammatory activity, the extent of ventricular scarring, and the location of fibro-inflammatory process. The cardinal manifestations of CS are conduction abnormalities and arrhythmias. It appears to a disease of the electrical conduction system of the heart and is part of the ocular-cardiac-cutaneous- central nervous system phenotype of sarcoidosis. Common are atrioventricular and sometimes bundle branch blocks, which should raise a suspicion of CS particularly when it develops in young patients. Scarring is the usual substrate for the development of tachyarrhythmias, which take the form of premature ventricular contractions, ventricular tachycardia, or ventricular fibrillation. These are responsible for the occurrence of SCD, which was seen in this case related to extensive post-inflammatory fibrosis. SCD can be the initial and only presentation in 40% of patients with CS. Sudden deaths can also be produced by atrial dysrhythmias and arrhythmias, resulting from a dominant right ventricular involvement that simulates arrhythmogenic cardiomyopathy (See Chap. 44). In about 20% of patients, the inflammation and ensuing fibrosis lead to congestive heart failure, mimicking dilated cardiomyopathy (See Chap. 41). Other infrequent presentations include formation of ventricular aneurysm, intracardiac mass lesions, valvular dysfunction due to papillary muscle involvement or primary valvular infiltration, acute coronary syndrome due to coronary vasculitis, and pericardial effusions or constrictive pericarditis. The diagnosis of CS not only rests on advanced imaging, but also on routine investigations like ECG, echocardiography, and estimations of biomarkers. Depending on the extent of disease, the treatment options include immunosuppressive, antiarrhythmic and heart failure medications, radio-frequency ablation, implantation of devices, and finally cardiac transplantation.

Further Reading

Mankad P, Mitchel B, Birnie D, Kron J. Cardiac sarcoidosis. Curr Cardiol Rep. 2019;21:152.

Masri SC, Bellumkonda L. Sarcoid heart disease: an update on diagnosis and management. Curr Cardiol Rep. 2020;22:177.

Okada DR, Bravo PE, Vita T, Agarwal V, Osborne MT, Taqueti VR, et al. Isolated cardiac sarcoidosis: a focused review of an under recognized entity. J Nucl Cardiol. 2018;25:1136–46.

Okada DR, Smith J, Derakhshan A, Gowani Z, Misra S, Berger RD, et al. Ventricular arrhythmias in cardiac sarcoidosis. Circulation. 2018;138:1253–64.

Pereira NL, Grogan M, Dec GW. Spectrum of restrictive and infiltrative cardiomyopathies: part 2 of a 2-part series. J Am Coll Cardiol. 2018;71:1149–66.

Serei VD, Fyfe B. The many faces of cardiac sarcoidosis. Am J Clin Pathol. 2020;153:294–302.

Tan JL, Fong HK, Birati EY, Han Y. Cardiac sarcoidosis. Am J Cardiol. 2019;123:513–22.

Giant Cell Myocarditis

40

Pradeep Vaideeswar and Ketan Ingle

40.1 Clinical History

A 48-year-male fell from the stairs after an episode of dizziness and was declared dead before admission. The deceased had been a diabetic for 6 years with associated ischemic heart disease for 3 years. He had undergone angioplasty 3 months ago, details of which had not been made available.

40.2 Autopsy Findings

The heart (460 g) was markedly enlarged with marked biventricular enlargement. A patchily opacified epicardial surface revealed multiple largely sessile polypoidal soft yellowish to pale brown projections all over (Fig. 40.1a, b); some had a short stalk. Serial cross-sections of the ventricles revealed multifocal thinning, scarring, and congestion in both ventricles (Fig. 40.1c). Similar areas were noted even in the territories not supplied by the stented left anterior descending artery. The epicardial plaques were found in relation to subepicardial foci of congestion or scarring. On histological examination, the ventricular myocardium showed classic features of giant-cell myocarditis (GCM, Fig. 40.2a–c), where foci of coagulative necroses bordered by giant cells, macrophages, lymphoplasmacytes, and eosinophils (acute phase) were present along with foci of granulation tissue (healing phase) and fibrosis (healed phase). The surprising finding was significant involvement of the epicardium, where mononuclear inflammation (devoid of giant cells or granulation tissue) formed projections capped by fibrinous exudates (Fig. 40.3a–c). There was mild coronary atherosclerosis, even in the stented segment; critical stenosis was not present. There was pulmonary edema; other organs were normal.

Cause of Death: Giant cell myocarditis.

P. Vaideeswar (✉)
Department of Pathology (Cardiovascular and Thoracic Division), Seth Gordhandas Sunderdas Medical College and King Edward Memorial Hospital, Mumbai, India

K. Ingle
Department of Pathology, Seth Gordhandas Sunderdas Medical College and King Edward Memorial Hospital, Mumbai, India

P. Vaideeswar (ed.), *Tropical Cardiovascular Pathology*,
https://doi.org/10.1007/978-981-19-3720-0_40

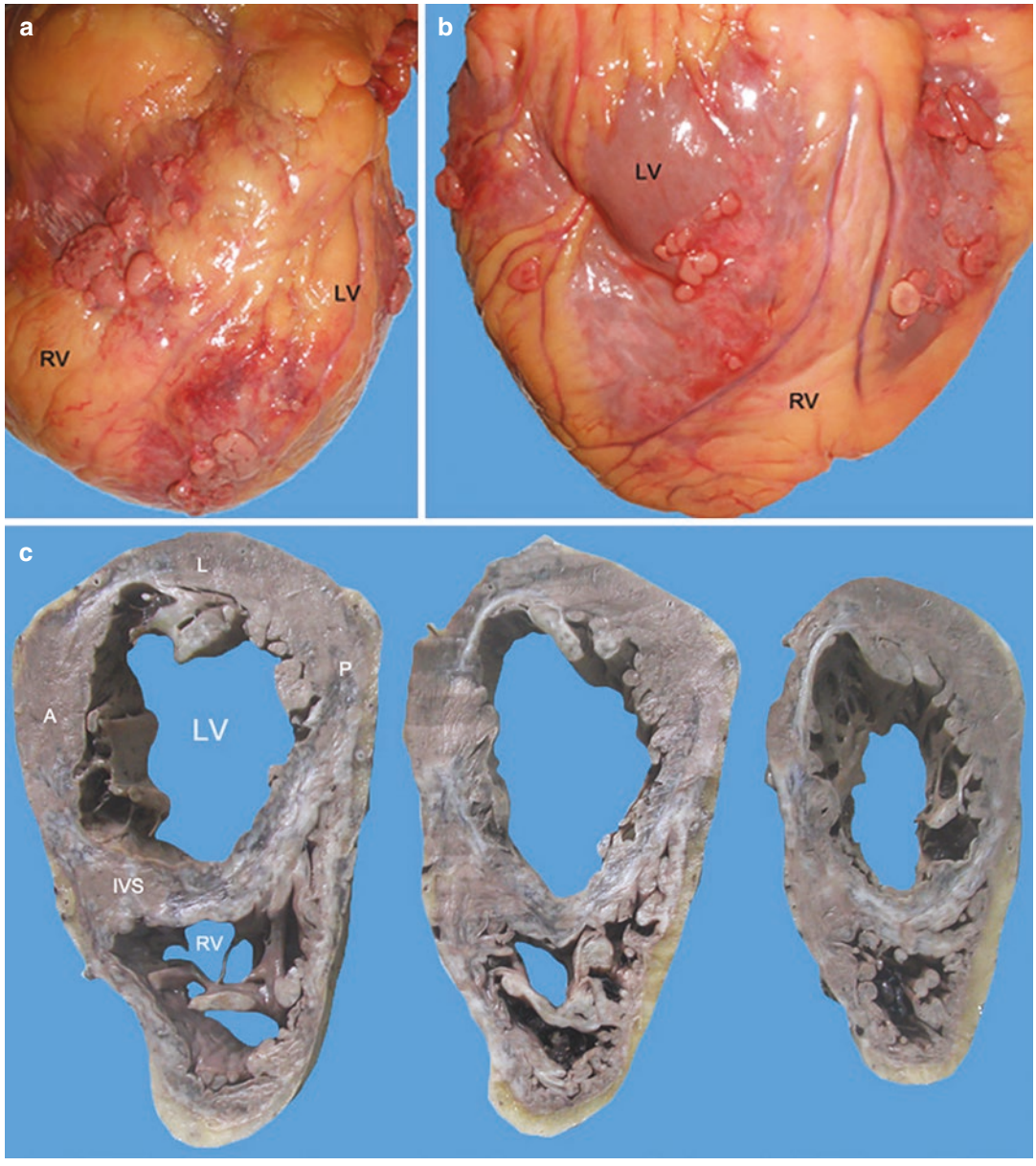

Fig. 40.1 Multiple soft sessile polypoidal "appendices epiploicae-like" projections seen on the (**a**) anterior and (**b**) posterior surfaces of an enlarged heart; (**c**) Serial cross-sections through the ventricles showing thinning of the walls with almost circumferential congestion and scarring (*LV* left ventricle, *RV* right ventricle)

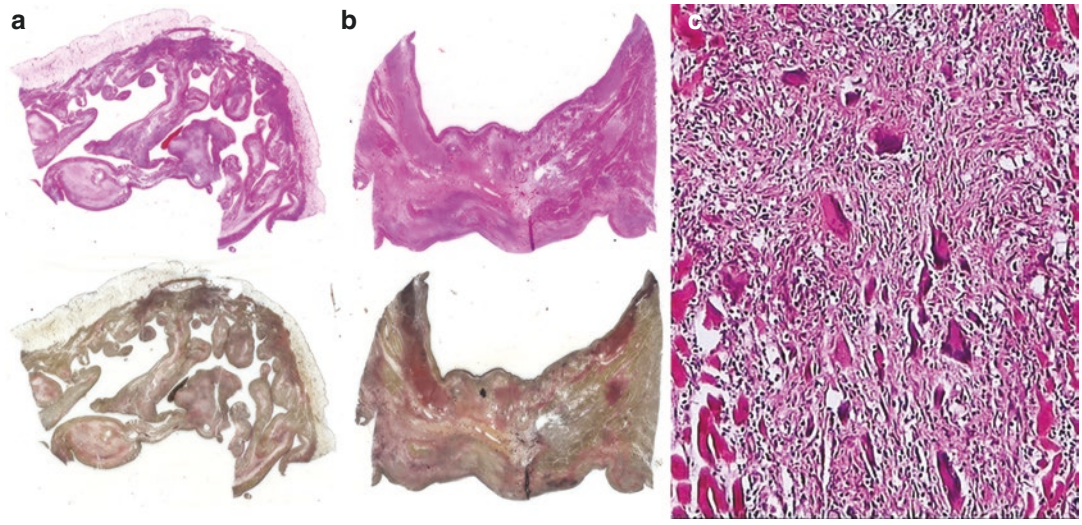

Fig. 40.2 Scans of the slides of the right ventricle and interventricular septum stained with (**a**) H&E and (**b**) elastic van Gieson, which highlights the degree of fibrosis; (**c**) Inflammatory reaction with prominent giant cells. Note absence of granulomas

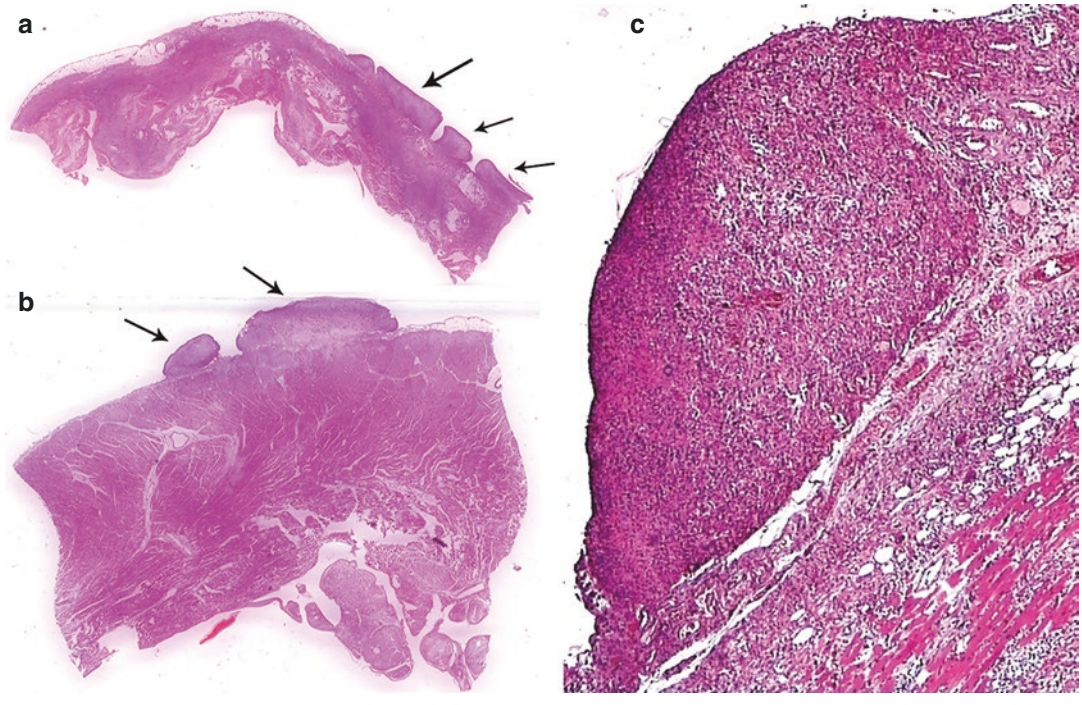

Fig. 40.3 Scans of the slides stained by H&E of (**a**) Right and (**b**) Left ventricle showing polypoidal projections (arrows); (**c**) The projections are entirely composed of coagulated fibrin with inflammatory cells

40.3 Discussion

The fulminant myocardial inflammatory process in this case is represented by a rare, potentially fatal nonischemic disorder designated as idiopathic GCM or simply labeled as GCM. The true incidence of this condition is unknown and also underestimated due to frequent rapid fatal outcome and lack of detailed cardiac evaluation at autopsy. Studies indicate an incidence ranging from 0.007 to 0.051% of the population. It usually affects the young to middle-aged population with no sex predilection and a median age of 42 years. The etiological basis continues to be an enigma, but its association with other immunological disorders (inflammatory bowel disease, Hashimoto's thyroiditis, pernicious anemia, and connective tissue disorders) or tumors (thymoma or lymphoma) seen in one-third of the patients with GCM suggests an autoimmune basis related to T-cell dysfunction.

The histopathological hallmark of GCM is the presence of multinucleated giant cells and aggregates of lymphocytes that form a cuff around small or large areas of coagulative necroses. The giant cells often have a similar contour of the surrounding cardiomyocytes and are also accompanied by abundant mixed inflammatory cells, particularly eosinophils. All these features characterize the acute phase of the inflammation, which can be identified on gross examination as diffuse or multifocal serpiginous or geographic foci of congestion. Immunohistochemistry for CD68 highlights the macrophages and giant cells, whereas CD3 can be used to denote T-lymphocyte infiltration. No well-defined granulomas are seen, which helps to distinguish GCM from tuberculous myocarditis (See Chap. 38) or sarcoidosis (See Chap. 39). Sometimes there may be large areas that might be indistinguishable from lymphocytic myocarditis, which can also have fulminant presentation. Depending on the degree of involvement, the heart can be enlarged with a flabby myocardial consistency. Granulation tissue and fibrosis represent the healing and healed phases, respectively. The present case also had novel finding of organized epicardial exudates, which simulated the appearance of appendices epiploicae of the colon. Such a finding has not been reported before.

Very often, GCM presents with rapidly progressive left heart failure and cardiogenic shock. Some patients may also have atrioventricular conduction abnormalities or ventricular arrhythmias. An acute coronary syndrome-like presentation has also been noted in a few cases and we wonder if our patient also had symptoms of acute myocardial infarction for which coronary stenting had been performed. Indolent manifestations akin to dilated cardiomyopathy or sudden death can also be present. Early diagnosis and differentiation from other forms of myocarditis is the key to the initiation of immunosuppressive therapy, which is known to improve the outcome along with mechanical circulatory support and management of heart failure and/or arrhythmias. But even with prompt therapy, some patients would require a cardiac transplantation. However, disease recurrence has been observed even in the transplanted hearts in 20–25% cases. By and large, the survival outcomes remain poor.

Further Reading

Bang V, Ganatra S, Shah SP, Dani SS, Neilan TG, Thavendiranathan P, et al. Management of patients with giant cell myocarditis. J Am Coll Cardiol. 2021;77:1122–34.

Liu S, Zheng L, Shen L, Wu L, Yao Y. Clinical identification and characteristic analysis of giant cell myocarditis in 12 cases. Front Cardiovasc Med. 2021;8:649094.

Vaideeswar P, Cooper L. Giant cell myocarditis: clinical and pathological disease characteristics in an Indian population. Cardiovasc Pathol. 2013;22:70–4.

Xu J, Brooks EG. Giant cell myocarditis: a brief review. Arch Pathol Lab Med. 2016;140:1429–34.

Ziegler JP, Batalis NI, Fulcher JW, Ward ME. Giant cell myocarditis causing sudden death in a patient with sarcoidosis. Autops Case Rep. 2020;10:e2020238.

Dilated Cardiomyopathy

41

Pradeep Vaideeswar

41.1 Clinical History

A 67-year-old male patient was referred by a private health-care facility, where he had been admitted with a diagnosis of ischemic bowel disease. The investigations performed in that hospital have been tabulated (Table 41.1). He was in very poor general condition with feeble pulsations and non-recordable blood pressure. He expired within 2 h.

Table 41.1 Investigations (Private health-care facility)

Hematological	Hemoglobin 15.1 g/dL Total leukocyte count 16,030/cmm Differential count—Neutrophil predominant Platelet count 2.2 lakhs/cmm
Coagulation profile	Prothrombin time 11.2 (Control 11.9, INR 0.98) D-Dimer 3642.9 (normal <500)
Biochemical—Routine	Random blood glucose 226 mg/dL Blood urea 38.52 Serum creatinine 2 mg/dL Total bilirubin 1.2 mg/dL SGOT/SGPT 145 / 45 U/L Total protein 6.1 g/dL Albumin 3.2 g/dL Serum cholesterol 165 mg/dL Sodium 129 mEq/L Potassium 5.12 mEq/L Chloride 92 mEq/L pH 7.3, pCO_2 32.6, pO_2 76 HbA_1C 5.3 Creatine phosphokinase-MB isoform 13.72 (normal 0.5–1 ng/mL) Troponin I 541.8 Procalcitonin 23.17
Serological	HBsAg negative HIV negative Anti-HCV negative
ECG	T-wave inversion in anterior leads; right bundle branch block
Imaging	Echocardiography: Left ventricular ejection fraction of 35% with global hypokinesia Ultrasonography: Enteritis and Prostatomegaly
Others	Urine examination: 20–25 pus cells, 280–300 RBCs

P. Vaideeswar (✉)
Department of Pathology (Cardiovascular and Thoracic Division), Seth Gordhandas Sunderdas Medical College and King Edward Memorial Hospital, Mumbai, India

P. Vaideeswar (ed.), *Tropical Cardiovascular Pathology*,
https://doi.org/10.1007/978-981-19-3720-0_41

41.2 Autopsy Findings

The heart (400 g) was moderately enlarged and globular in shape (Fig. 41.1) with the apex formed by both ventricles. There was marked enlargement of the left ventricle, while other chambers were moderately dilated. All coronary arteries were patent with minimal atherosclerosis. The left ventricular myocardium was thinned out and pale (Fig. 41.2a) with focal congestion. On histology, the left ventricular myocardium showed patchy but prominent interstitial and interfiber fibrosis with hypertrophy as well as attenuation of many groups of cardiomyocytes (Fig. 41.2b–d). Some of the intertrabecular spaces showed small deposits of thrombi. The intramural coronary arteries were normal. These features were highly suggestive of dilated cardiomyopathy (DCM). Other findings included centrilobular emphy-

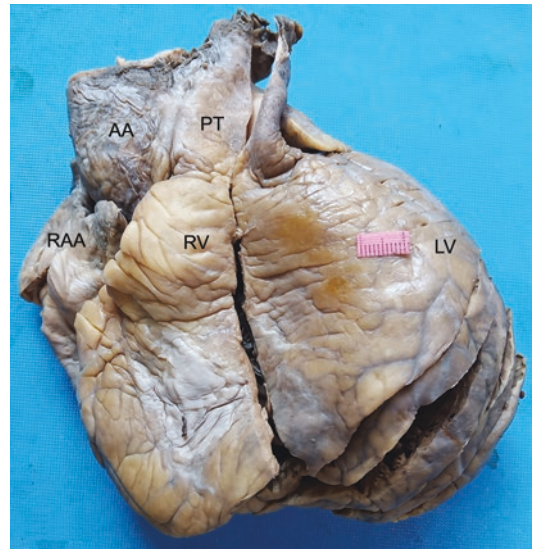

Fig. 41.1 Moderately enlarged heart with a globular shape

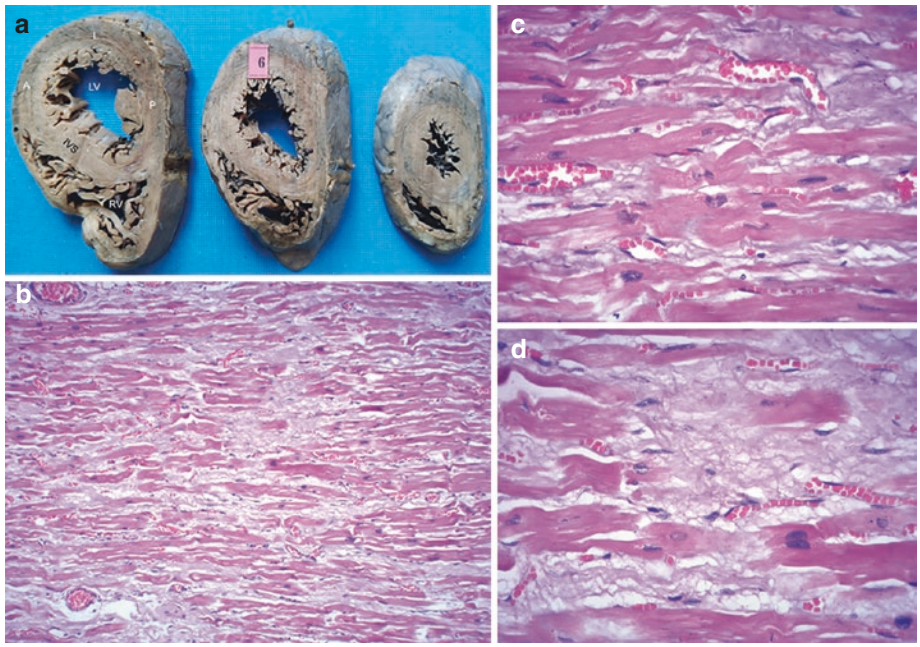

Fig. 41.2 (**a**) Transverse section through the ventricles shows dilated left ventricular LV cavity with pale appearing myocardium (*A* anterior wall, *IVS* interventricular septum, *L* lateral wall, *P* posterior wall, *RV* right ventricle); (**b**) The myocardium reveals prominent interfiber fibrosis (H&E × 200); (**c**) Mild and (**d**) Moderate degree of fibrosis, accompanied by hypertrophy of the cardiomyocytes. Note large hyperchromatic nuclei (H&E × 400)

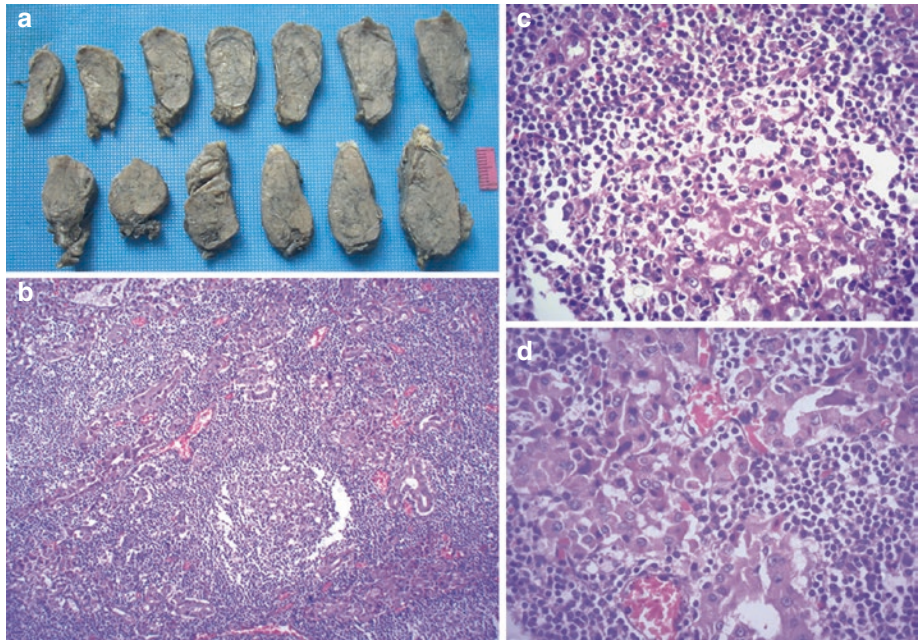

Fig. 41.3 (**a**) Both lobes of the thyroid were enlarged and showed pale, lobulated cut surface; (**b**) Lymphocytic infiltrate with formation of lymphoid follicles; (**c**) Formation of germinal centers (H&E × 400); (**d**) Focal prominent Hurthle cell or oncocytic metaplasia

sema and extensive small intestinal gangrene. There were no aortoarterial thrombi, but small-sized arteries with thrombotic occlusion were found in the mesentery. The thyroid gland was uniformly enlarged in size with a firm consistency and pale grey-white lobulated cut surface. These gross changes were produced by florid Hashimoto's thyroiditis that was noted on microscopy (Fig. 41.3).

Cause of Death: Extensive intestinal gangrene.

41.3 Discussion

Gross and histomorphological features of DCM were observed in the autopsy performed in an elderly male patient, who despite of his age had only minimal coronary atherosclerosis. DCM is one of the examples of cardiomyopathies, which are heterogeneous group of myocardial disorders associated with mechanical and/or electrical dysfunction which usually (but not invariably) exhibit inappropriate ventricular hypertrophy or dilatation. In most instances, there is overt or covert myocardial remodelling that occurs in the absence of ischemic, hypertensive, valvular, or congenital heart diseases and leads to development of heart failure or even sudden cardiac death. DCM encompasses a large complex group of nonischemic myocardial diseases, characterized by left ventricular or biventricular dilatation and reduced systolic ejection fraction of <45% in the absence of pressure or volume overload. A subset of patients may have contractile dysfunction without ventricular dilatation, which is designated as hypokinetic nondilated cardiomyopathy.

DCM is one of the commonest causes of heart failure with a prevalence varying from 1 in 20 to 1 in 2500 in the general population. This may not represent the true figure as some of the cases may be undiagnosed or underreported. DCM is commonly seen in males (male to female ratio of 3:1), occurring in the third to fourth decades of life. It is initiated by a variety of causes, which may be genetic or nongenetic. In about half the cases, the cause is not identified—idiopathic DCM and 35–50% of such patients are found to harbor

mutations in the sarcomeric and/or nonsarcomeric proteins, indicating a polygenetic basis. Other important conditions leading to DCM include infections (especially viral myocarditis, see Chap. 33), autoimmune disorders, metabolic diseases, and exposure to drugs or toxins. It is important to note that when more than 1 etiological factor is present simultaneously, it may potentiate the effects. Our patient had autoimmune thyroiditis that was not diagnosed. The autoimmune thyroiditis would have given rise to hypothyroidism, in which there is a decrease in the levels of the thyroid hormones and a consequent increase in the concentration of thyroid stimulating hormone. The prevalence of hypothyroidism in the developed world ranges from 2 to 6%, but in countries like India, the prevalence is around 11%. Though the effects of hypothyroidism are commonly seen in the form of atherosclerotic coronary artery disease (especially through dyslipidemia), the low levels of the thyroid hormones can also affect the myocardial contractility, eventually leading to the DCM phenotype.

Irrespective of the causes, DCM usually shows a globular configuration of the heart due to varying degrees of dilatation, prominently involving the left ventricle. There is associated myocardial thinning and pallor, and on histology, there is both hypertrophy and attenuation of the cardiomyocytes often with a moth-eaten appearance. An important feature is the presence of fibrosis, which is a characteristic of many myocardial disorders. The fibrosis can be replacement (as seen in healed myocardial infarction, see Chap. 28), reactive interstitial, or perivascular fibrosis (as seen in the healing of acute rheumatic fever, see Chap. 4). Interstitial fibrosis usually occurs without loss of the cardiomyocytes. In DCM, the stimulus for this type of remodelling is stretch of the ventricular chambers and often the fibrosis is observed in the mid-wall. The fibrosis results in separation of groups of myofibers and also separation of the individual cells from each other. All these features were seen in this case.

Most of the patients of DCM present with features of heart failure due to severe contractile dysfunction, indicating that there would have been a lengthy asymptomatic phase. Few others may present with arrhythmias (arrhythmogenic DCM), conduction blocks, sudden cardiac death, and thromboembolism; the last of these was the presentation in our case. The systolic dysfunction with dilatation is the most important pathogenetic mechanism for the development of mural thrombi in 1 or more chambers; the most frequent location is the left ventricle. There can also be a systemic hypercoagulable state, with increased circulating fibrinogen, d-dimer levels, increased systemic von Willebrand factor expression, and elevated concentrations of fibrinopeptide A and thrombin–antithrombin complexes. The thrombi predispose patients with DCM to systemic and/or pulmonary thromboembolism. Our patient had extensive intestinal gangrene, which was responsible for his death.

Further Reading

Ahmadi N, Ahmadi F, Sadiqi M, Ziemnicka K, Minczykowski A. Thyroid gland dysfunction and its effect on the cardiovascular system: a comprehensive review of the literature. Endokrynol Pol. 2020;71:466–78.

Eijgenraam TR, Silljé HHW, de Boer RA. Current understanding of fibrosis in genetic cardiomyopathies. Trends Cardiovasc Med. 2020;30:353–61.

Merlo M, Cannatà A, Gobbo M, Stolfo D, Elliott PM, Sinagra G. Evolving concepts in dilated cardiomyopathy. Eur J Heart Fail. 2018;20:228–39.

Razvi S, Jabbar A, Pingitore A, Danzi S, Biondi B, Klein I, et al. Thyroid hormones and cardiovascular function and diseases. J Am Coll Cardiol. 2018;71:1781–96.

Reichart D, Magnussen C, Zeller T, Blankenberg S. Dilated cardiomyopathy: from epidemiologic to genetic phenotypes. J Intern Med. 2019;286:362–72.

Schultheiss HP, Fairweather D, Caforio ALP, Escher F, Hershberger RE, Lipshultz SE, et al. Dilated cardiomyopathy. Nat Rev Dis Primers. 2019;5:32.

Wang J, Yang F, Wan K, Mui D, Han Y, Chen Y. Left ventricular midwall fibrosis as a predictor of sudden cardiac death in non-ischaemic dilated cardiomyopathy: a meta-analysis. ESC Heart Fail. 2020;7:2184–92.

42 Pheochromocytoma-Induced Cardiomyopathy

Pradeep Vaideeswar, Mrinal Sarwate, and Smita Divate

42.1 Clinical History

A 27-year-old woman underwent an emergency lower-segment Cesarean section for her third pregnancy at a private nursing home in view of pregnancy-induced hypertension with abruptio placentae. She had been on anti-hypertensives (Depin 10 mg, thrice a day) and her blood pressure recorded ranged from 130/80 to 90/60 mmHg. She was referred to the Emergency Services Department of our tertiary-care center on the 2nd day of the postpartum period with sudden onset of acute and progressive shortness of breath with palpitation. On examination, the general condition was fair with a pulse rate of 104 per minute and blood pressure of 90/60 mmHg. There was tachypnea with a respiratory rate of 36 per minute. The heart sounds were normal. There were bilateral crepitations, but no murmurs. The abdomen was soft and the uterus was well-contracted. Blood investigations revealed mild anemia with hemoglobin of 10.9 % and neutrophilic leucocytosis (total WBC count of 27,800/cu mm). Routine biochemical investigations and coagulation profile were within normal limits. The ECG revealed tall T waves, absence of P waves, and ventricular rate of 120 per minute, suggesting possibility of atrioventricular node reentry tachycardia. A 2-dimensional echocardiography showed ejection fraction of 20% with left ventricular global hypokinesia suggestive of severe systolic dysfunction. The patient's condition deteriorated subsequently and she expired after 20 h of ward stay.

42.2 Autopsy Findings

A complete postmortem examination was performed. The heart weighed 270 g and was mildly enlarged with mild enlargement and hypertrophy of left ventricle. Transverse sections through the ventricles showed the usual brown color of the myocardium. The histology revealed patchy interstitial edema, focal cytoplasmic vacuolization, mild patchy interstitial lymphocytic infiltrate (Fig. 42.1a, b), increase in interstitial connective tissue and fine foci of scarring (Fig. 42.1c, d), and hypertrophy of fibers (Fig. 42.1b, d). These changes were more prominent in the left ventricle (Fig. 42.2a–d) with prominent peri-nuclear lipofuscin pigment deposition. All the changes appeared secondary

P. Vaideeswar (✉)
Department of Pathology (Cardiovascular and Thoracic Division), Seth Gordhandas Sunderdas Medical College and King Edward Memorial Hospital, Mumbai, India

M. Sarwate
PGY 3, Cleveland Clinic Foundation, Cleveland, OH, USA

S. Divate
Department of Pathology, Seth Gordhandas Sunderdas Medical College and King Edward Memorial Hospital, Mumbai, India

P. Vaideeswar (ed.), *Tropical Cardiovascular Pathology*,
https://doi.org/10.1007/978-981-19-3720-0_42

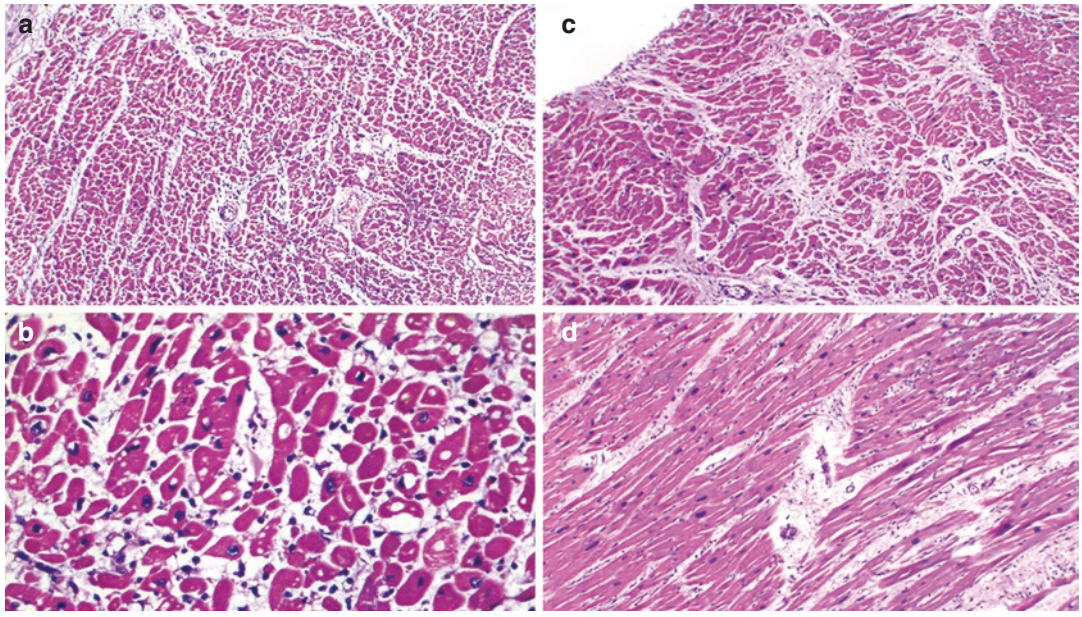

Fig. 42.1 (**a**) Patchy interstitial edema (H&E × 200); (**b**) Focal cytoplasmic vacuolization with features of hypertrophy (H&E × 400); (**c**) and (**d**) showing increased interstitial connective tissue (H&E × 200)

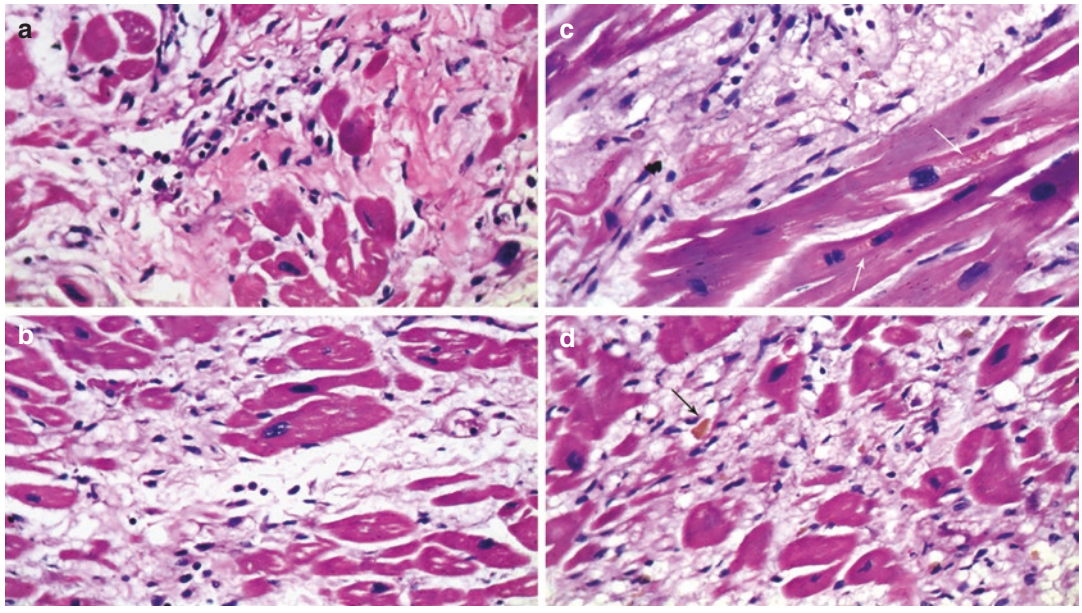

Fig. 42.2 (**a**) and (**b**) showing interstitial scarring with few lymphocytic infiltrates (H&E × 400); (**c**) Peri-nuclear lipofuscin deposition (arrows, H&E × 400); (**d**) Lipofuchsin (arrow) deposited in the interstitium, indicating cardiomyocyte loss (H&E × 400)

to a large 7 cm capsulated dark brown to tan-colored right adrenal pheochromocytoma (Fig. 42.3a, b), which showed the characteristic histomorphologic features of large polygonal cells set in a "zell-ballen" pattern (Fig. 42.4a, b). There was pulmonary edema and hepatic

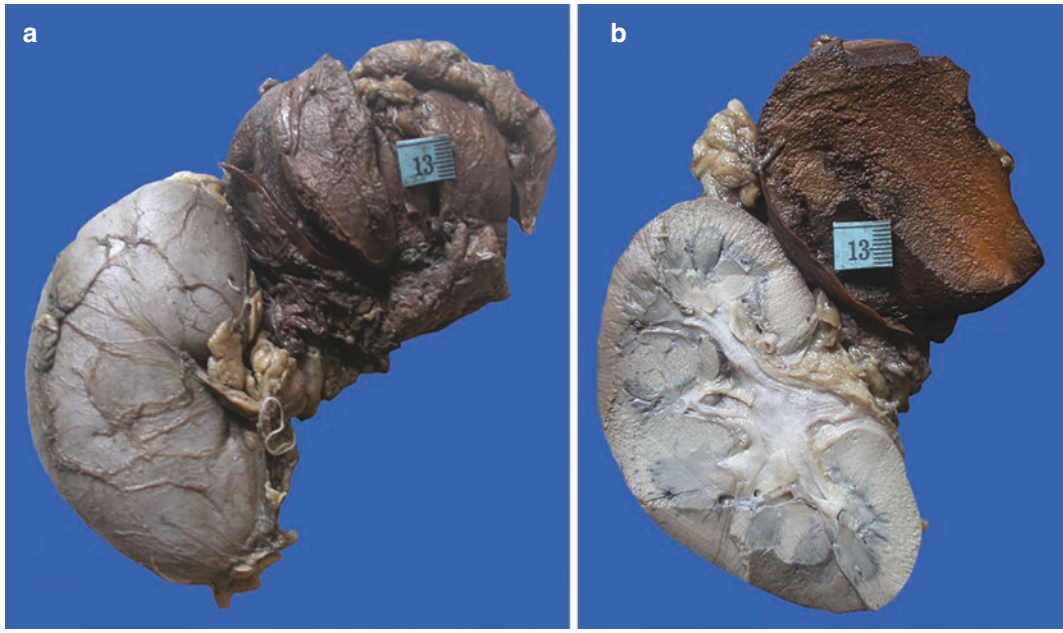

Fig. 42.3 Large right adrenal pheochromocytoma seen as (**a**) a dark encapsulated mass with (**b**) dark brownish-red cut surface

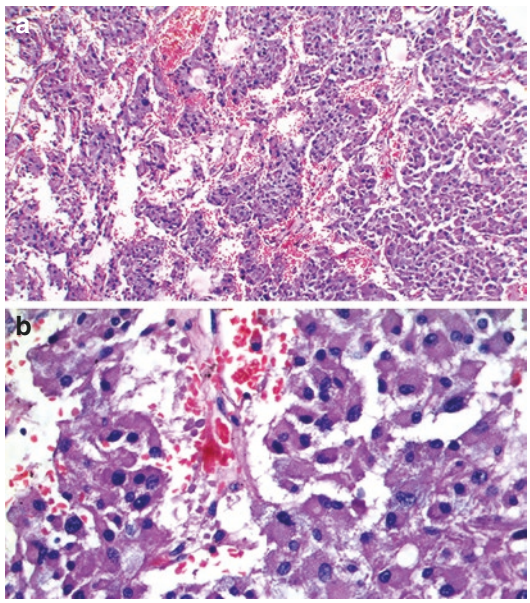

Fig. 42.4 Large polygonal cells with abundant granular eosinophilic cytoplasm arranged in the "zell-ballen" pattern (**a**) H&E × 200 and (**b**) H&E × 400

chronic passive venous congestion. All other organs were normal; uterine involutional changes were appropriate.

Cause of Death: Pheochromocytoma-induced Cardiomyopathy.

42.3 Discussion

Pregnancy is a physiological process associated with several reversible changes in the vital systems of the body in order to accommodate the fetus. Important alterations occur in the cardiovascular system, which include programmed dilatation and hypertrophy of the heart (particularly the left ventricle), increased stroke volume and cardiac output, fall in the peripheral vascular resistance and the arterial blood pressure, and expansion of plasma volume. It is easy to understand how these adaptations can prove deleterious in women with preexisting cardiovascular diseases. The physiological changes also entail health risks, when some women develop diseases unique to pregnancy in the form of hypertensive disorders and peripartum cardiomyopathy (PPCM). Elevation of blood pressure is seen in gestational hypertension and toxemias of pregnancy (preeclampsia and eclampsia), which are

differentiated on the basis of presence or absence of accompanying proteinuria and central nervous system manifestations. These features differentiate them from true chronic hypertension where an elevated blood pressure is present before the 20th week of pregnancy. PPCM is defined as an "idiopathic cardiomyopathy presenting with heart failure secondary to left ventricular systolic dysfunction (ejection fraction is nearly always reduced below 45%) towards the end of pregnancy or in the months following delivery, where no other cause of heart failure is found"; hypertensive disorders pose a risk for its development. We have reported death of a 27-year-old pregnant lady with pregnancy-induced hypertension and postpartum clinical features of PPCM, caused by an adrenal pheochromocytoma discovered at autopsy.

Pheochromocytoma is a neuroendocrine tumor of adrenal medulla, which secretes predominantly epinephrine and norepinephrine, along with small amounts of dopamine. Such tumors in pregnancy are extremely rare, with an estimated incidence of approximately 0.007%. The diagnosis is particularly important because undiagnosed and/or untreated pheochromocytoma has high maternal and fetal mortality, ranging from 15 to 50%. At the same time, it is to be noted that diagnosis is difficult as presenting symptoms of a pheochromocytoma can overlap with symptoms of hypertensive disorders of pregnancy. The diagnostic modalities of ultrasonography and radioisotope scanning used for diagnosis of pheochromocytoma are less helpful in pregnancy. There are some important, often subtle differences in the manifestation of hypertension. It may be either sustained or paroxysmal and there is paradoxical supine elevation of the pressure, despite a normal pressure measurement in the sitting or erect position. Associated features include nonresponsiveness to the usual antihypertensives, heat intolerance, palpitations, dyspnea, chest pain, and impaired glucose tolerance. The tumor can manifest at any time during pregnancy; the factors responsible are increased intraabdominal pressure, fetal movements, uterine contractions, process of delivery, an abdominal surgical intervention, and even general anesthesia. In addition, it can lead to uteroplacental insufficiency, abruptio placentae (as in this case) and intrauterine growth restriction, and postpartum pulmonary edema.

Pheochromocytoma has deleterious effects on the cardiovascular system during pregnancy, seen in the form of cardiogenic shock, angina pectoris, myocardial infarction, arrhythmias, and even CMP. Pheochromocytoma-induced CMP is related to direct toxic effect from norepinephrine and other oxidized products with consequent downregulation of beta receptors with reduction in myofibrils alfa-1—adrenergic receptor stimulation and increased inotropy, chronotropy, and afterload. Excess levels of catecholamines lead to coronary vasospasm, resulting in less blood flow to myocardium. They also increase the permeability of sarcoplasmic membrane to calcium ions leading to myocyte necrosis. Cardiomyopathy secondary to pheochromocytoma can be dilated (seen in this case), hypertrophic, or "inverted" Takotsubo-like. The clinical features of pheochromocytoma-induced CMP are similar to those of PPCM. The common symptoms described in literature include shortness of breath, chest pain, palpitations, along with signs of cardiac failure, ECG changes, and reduced ejection fraction on echocardiography. It is important to differentiate between them since the management differs. PPCM is treated with vasodilators, beta blockers, and diuretics, while pheochromocytoma-induced CMP requires both alfa- and beta-blockers and surgical removal of the tumor. A high index of clinical suspicion for this condition and early recognition of symptoms, prompt diagnosis, and treatment will help reduce the maternal and fetal morbidity and mortality associated with it.

Further Reading

Affinati AH, Auchus RJ. Endocrine causes of hypertension in pregnancy. Gland Surg. 2020;9:69–79.

Khatiwada S, Boro H, Farooqui FA, Alam S. Endocrine causes of heart failure: a clinical primer for cardiologists. Indian Heart J. 2021;73:14–21.

Langton K, Tufton N, Akker S, Deinum J, Eisenhofer G, Timmers HJLM, et al. Pregnancy and phaeochro-

mocytoma/paraganglioma: clinical clues affecting diagnosis and outcome—a systematic review. BJOG. 2021;128:1264–72.

Malik R, Kumar V. Hypertension in pregnancy. Adv Exp Med Biol. 2017;956:375–93.

Santos JRU, Brofferio A, Viana B, Pacak K. Catecholamine-induced cardiomyopathy in pheochromocytoma: how to manage a rare complication in a rare disease? Horm Metab Res. 2019;51:458–69.

Schaufelberger M. Cardiomyopathy and pregnancy. Heart. 2019;105:1543–51.

Sethi P, Peiris CD. A review of catecholamine associated cardiomyopathies and channelopathies. Cureus. 2020;12:e 6957.

Shams Y-H, Falhammar H. Cardiovascular manifestations and complications of pheochromocytomas and paragangliomas. J Clin Med. 2020;9:2435.

van der Weerd K, van Noord C, Loeve M, Knapen MFCM, Visser W, de Herder WW, et al. Pheochromocytoma in pregnancy: case series and review of literature. Eur J Endocrinol. 2017;177:R49–58.

Hypertrophic Cardiomyopathy

43

Pradeep Vaideeswar and Shashank Tyagi

43.1 Clinical History

An 18-year-old, without features of ill-health, suddenly developed dizziness followed by unconsciousness during a parade at 0530 h. She was declared dead on arrival. On enquiry, it was learnt that her father had also died suddenly at the age of 34 years.

43.2 Autopsy Findings

There was mild cardiomegaly (weight 240 g) with mild and moderate enlargement of both ventricular chambers (Fig. 43.1). All coronary arteries were patent with normal origins and courses. The transverse section revealed mild left ventricular hypertrophy with asymmetry involving the interventricular septum (1.8 cm) in the mid- and apical portions (Fig. 43.2a). On histology, the hypertrophy was accompanied by multifocal disarray of the myocytes with focal interstitial fibrosis (Fig. 43.2b, c). The intramural coronary arteries were normal. Larger areas of replacement fibrosis were not seen. The lungs and other organs were normal.

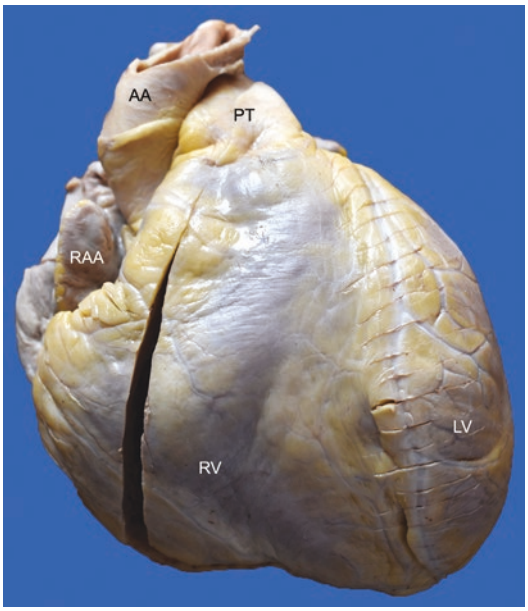

Fig. 43.1 Mild cardiomegaly with biventricular enlargement

Cause of Death: Hypertrophic cardiomyopathy.

P. Vaideeswar (✉)
Department of Pathology (Cardiovascular and Thoracic Division), Seth Gordhandas Sunderdas Medical College and King Edward Memorial Hospital, Mumbai, India

S. Tyagi
Department of Forensic Medicine and Toxicology, Lady Hardinge Medical College and Associated SSK and KSC Hospitals, New Delhi, India

P. Vaideeswar (ed.), *Tropical Cardiovascular Pathology*,
https://doi.org/10.1007/978-981-19-3720-0_43

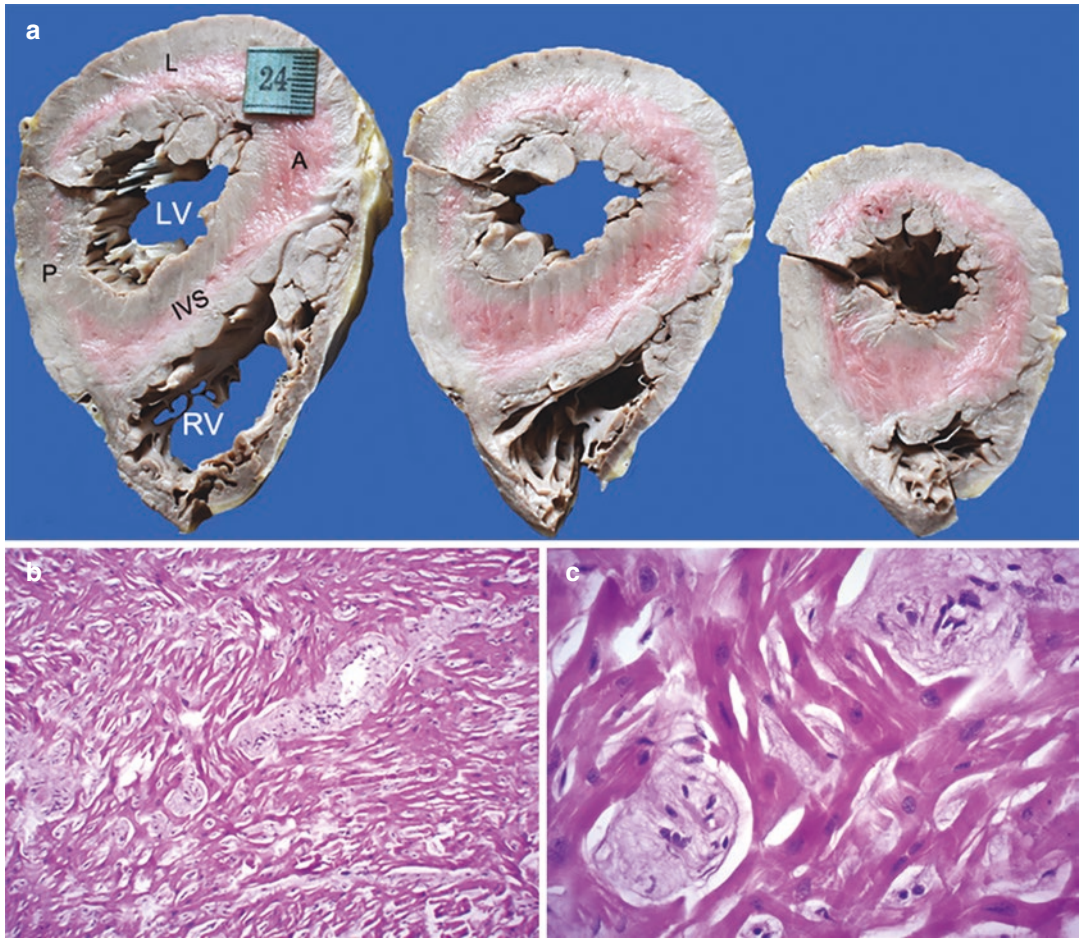

Fig. 43.2 (**a**) Asymmetric hypertrophy involving the interventricular septum IVS, well seen in the middle and apical sections (*A* anterior wall, *L* lateral wall, *LV* left ventricle, *P* posterior wall, *RV* right ventricle); (**b**) Multifocal disarray (H&E × 200); (**c**) Disarray accompanied by myocyte hypertrophy and interstitial fibrosis (H&E × 400)

43.3 Discussion

Left ventricular hypertrophy (LVH) and cardiomyocyte disarray were the main features seen in this young woman with sudden cardiac death (SCD) that occurred during mild exercise. LVH is often a common finding at autopsy in deaths related to cardiovascular diseases and is diagnosed when the thickness of the interventricular septum and the free wall are more than 1.5 cm and 1.4 cm, respectively. The hypertrophy may be concentric (increased myocardial thickness without cavity dilatation) or eccentric (cavity dilatation with decreased, normal, or increased myocardial thickness). In both types, the heart weights are increased beyond the prescribed normal for the local population, which ranges from 180 to 300 g in our autopsy (unpublished) data. The myocardium may exhibit the same degree of thickness in the free wall and the interventricular septum (symmetric hypertrophy) or the thickness may be variable (asymmetric hypertrophy). The hypertrophy is also reflected on histological analysis, wherein the cardiomyocytes are large in size (diameter of more than 15 μm) with large, hyperchromatic, and irregular nuclei. This is particularly useful when there is dilatation of the left ventricular cavity and consequent thinning of the myocardium. In this case, there was concentric and asymmetric hypertrophy, though the heart weight remained in the normal range.

From the point of view of the etiology, LVH is either physiological or pathological. Apart from pregnancy (See Chap. 42), physiological LVH also occurs in individuals when there is frequent strenuous exercise related to their fitness routine or participation in dynamic or endurance sport activities and these changes may be present to a lesser or greater extent even in adolescents. In majority of these individuals, the left ventricular remodeling ("athlete's" heart) leads to eccentric LVH, where the myocardial thickness seldom reaches a value above 1.5 cm. These changes may mimic the effects produced by other more serious cardiovascular disorders (pathological LVH), very often related pressure and/or volume overload, which were absent in this case. This young lady was part of an organization that imparts basic military training. But besides hypertrophy, the histology showed an additional important and prominent feature of myocardial disarray.

Myocardial disarray may be defined as "disorganized cardiomyocyte spatial distribution with loss of physiological fiber alignment and orientation", which may take up different patterns. The most easily identifiable pattern is arrangement of hypertrophied cells in the form of whirls, twirls, or tangles in a pin-wheel configuration with a central focus of connective tissue. When bundles of myofibers are arranged perpendicularly or obliquely to each other, it is referred to as the herring-bone pattern. This, when accompanied by collagenic fibrosis, can be recognized on gross appearance as it shows a whorled or fasciculated pattern reminiscent of uterine leiomyoma. Myofibrillar disorganization can also be recognized on ultrastructural examination. Myocardial disarray is considered as a pathognomonic feature of hypertrophic cardiomyopathy (HCM), but is also seen in primary restrictive cardiomyopathy and around areas of scarring; it even normally occurs around coronary vasculature, at junctions between the ventricles and within the trabeculae. Hence, the pathologist must be vigilant in diagnosing myocyte disarray until it is noticeable in areas away from these zones. Though the distribution of disarray is patchy, the interventricular septum is a favored site. The disarray may not be linked to the degree of hypertrophy degree. In view of LVH (thickness of >1.5 cm) disproportionate to the loading conditions and the amount of myocardial disarray (which can range from 5 to 20% of the myocardial samples) and the circumstances of death, a diagnosis of HCM was rendered in this patient. It must be borne in mind that some cases of HCM may have normal heart weights and ventricular wall thickness, but it may have significant microscopic myocyte disarray.

HCM is the most common heritable heart disease with a general population prevalence of about 1 in 500. The disorder is said to be devoid of gender, race, or geographic predilection and majority of the patients exhibit an autosomal dominant inheritance pattern. The LVH (with heart weights that may be 100–200% of normal) is caused mostly by mutations of the sarcomeric proteins. The protein products of such mutations result in an impairment of the calcium homeostasis and energy handling mechanisms which result in morphological features of hypertrophy, disarray, and fibrosis along with functional alterations in the form of diastolic impairment. In most of the patients, the hypertrophy is asymmetric and tends to affect the basal interventricular septum (ratio of the thickness of the septum to the free wall is $\geq$1.3/1.0), which explains the subaortic obstruction. Along with the ventricular remodeling, there is also genetically driven structural and functional abnormalities of the intramural coronary arteries that lead to myocardial ischemia and subsequent myocardial scarring. The morphological abnormalities include intimal hyperplasia, medial hypertrophy, and peri-vascular fibrosis. The coronary abnormalities and scarring were not identified in this case. Despite all these alterations, the clinical presentations of HCM are heterogeneous and depend on the type of mutation and the expressivity, genetic modifiers, and environmental factors. Hence, the disease can be diagnosed at all ages and at different stages (nonhypertrophic, classic phenotype, adverse remodeling, and finally an overt systolic dysfunction). Some patients have a stable disease with a normal life span, while others present with features of outflow obstruction, myocardial ischemia, heart failure, arrhythmias, mitral valvular regurgitation, thromboembolism, and apical aneurysms with an annual morality rate of about 1%. The most dramatic event is SCD.

The risk of SCD in patients with HCM is heightened in the presence of previous aborted cardiac death, development of ventricular tachycardia, family history of SCD, young age, past history of syncope, severe LVH > 30 mm, hypotensive response after exercise, outflow tract obstruction, systolic dysfunction, and presence of apical aneurysms of any size. The annual rate of SCD in these patients is about 2% and it increases to almost 6% in young athletes. In persons with cardiovascular disease, exercise is often a risk factor for SCD, especially young athletes who have a 2.5 times greater chance of sudden death than nonathletes. More than 90% of SCD occur at or shortly after an exercise session or competition, as exercise is believed to trigger ventricular tachyarrhythmia. Our patient had been participating in parade and had mild asymmetric LVH, mild interstitial scarring, and normal intramural coronary arteries. It is possible that extensive disarray, which may have been related to high-risk genotype, was responsible for SCD.

Further Reading

Basso C, Michaud K, d'Amati G, Banner J, Lucena J, Cunningham K, et al. Cardiac hypertrophy at autopsy. Virchows Arch. 2021;479:79–94.

Finocchiaro G, Sheikh N, Leone O, Westaby J, Mazzarotto F, Pantazis A, et al. Arrhythmogenic potential of myocardial disarray in hypertrophic cardiomyopathy: genetic basis, functional consequences and relation to sudden cardiac death. Europace. 2021;23:985–95.

Kitaoka H, Kubo T, Doi YL. Hypertrophic cardiomyopathy: a heterogeneous and lifelong disease in the real world. Circ J. 2020;84:1218–26.

Kogut J, Popjes ED. Hypertrophic cardiomyopathy 2020. Curr Cardiol Rep. 2020;22:154.

Maron BJ, Mackey-Bojack S, Facile E, Duncanson E, Rowin EJ, Maron MS. Hypertrophic cardiomyopathy and sudden death initially identified at autopsy. Am J Cardiol. 2020;127:139–41.

Musumeci B, Tini G, Russo D, Sclafani M, Cava F, Tropea A, et al. Left ventricular remodeling in hypertrophic cardiomyopathy: an overview of current knowledge. J Clin Med. 2021;10:1547.

Pieles GE, Stuart AG. The adolescent athlete's heart: a miniature adult or grown-up child? Clin Cardiol. 2020;43:852–62.

Arrhythmogenic Cardiomyopathy

44

Pradeep Vaideeswar

44.1 Clinical History

A 42-year-old male was referred to our center for persistent hypotension from a far-off rural private hospital. He had previously developed an acute febrile illness with vomiting and jaundice for 15 days and then had been admitted due to development of altered sensorium. He recovered with treatment (no details available) except for the hypotension. On examination, the patient was conscious and alert. The pulse was 80 per minute and the blood pressure was 70 mmHg systolic. There was mild icterus. Crepitations were heard on chest auscultation. The investigations were as follows: Hb 8.1 g/dL, total leukocyte count 25,500/cmm (81% neutrophils), platelet count 2 lakhs/cmm, random blood glucose 92 mg/dL, serum creatinine 1.8 mg/dL, total bilirubin 1.8 mg/dL, Na^+ 145 mEq/L, K^+ 3.2 mEq/L, and Ca^{2+} 10.1 mg/dL. The patient had a sudden cardiovascular collapse and expired within 2 h of admission.

44.2 Autopsy Findings

The heart was moderately enlarged in size (340 g) with moderate enlargement of the right atrium and marked enlargement of the right ventricle. The apex was pointing to the left and formed by both ventricles. There was a large amount of adipose tissue over both the anterior and posterior walls of the right ventricle (RV) with patchy epicardial thickening (Fig. 44.1). On opening, the right-sided tracts, the trabeculae of the RV (Fig. 44.2a), and the wall of the outflow tract were seen to be infiltrated by fat (Fig. 44.2b). This was very well seen on transverse slices, where the adipose tissue was also seen to infiltrate the anterior and posterior aspects of the interventricular septum and the anterior wall of the left ventricle (LV) also (Fig. 44.2c, d). The fat, on histology, was associated by multifocal areas of interstitial fibrosis (Fig. 44.3a–d).

Cause of Death: Arrhythmogenic cardiomyopathy (ACM) and sudden cardiac death.

P. Vaideeswar (✉)
Department of Pathology (Cardiovascular and Thoracic Division), Seth Gordhandas Sunderdas Medical College and King Edward Memorial Hospital, Mumbai, India

P. Vaideeswar (ed.), *Tropical Cardiovascular Pathology*,
https://doi.org/10.1007/978-981-19-3720-0_44

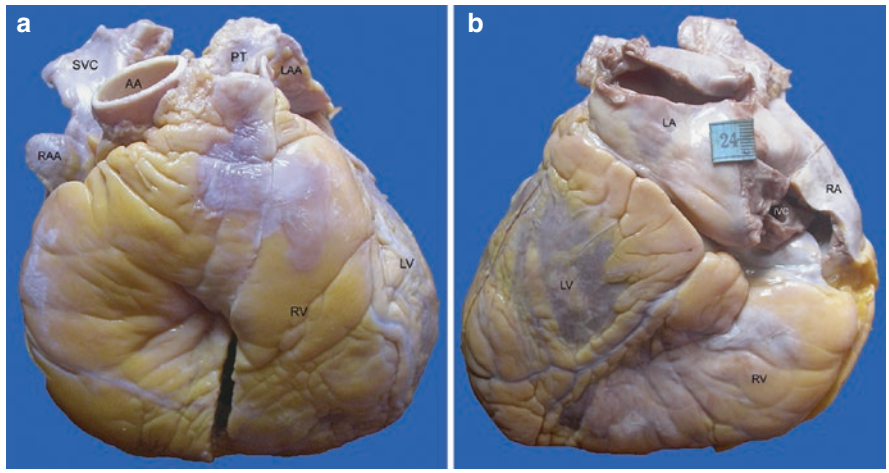

Fig. 44.1 Moderate cardiomegaly with marked right ventricular RV enlargement—(**a**) Anterior surface showing increased adipose tissue; (**b**) Adipose tissue and epicardial thickening over the entire posterior surface of RV (*AA* ascending aorta, *IVC* inferior vena cava, *LA* left atrium, *LAA* left atrial appendage, *LV* left ventricle, *PT* pulmonary trunk, *RA* right atrium, *RAA* right atrial appendage, *SVC* vena cava)

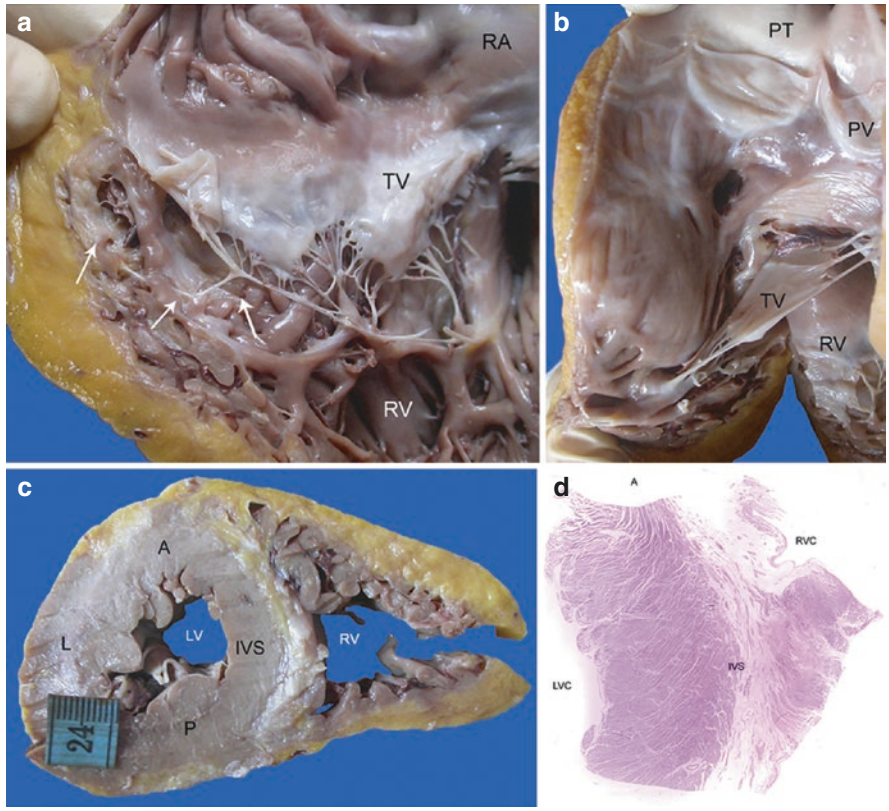

Fig. 44.2 (**a**) The free wall of the right ventricle RV is replaced completely by fat. The overlying epicardium is thickened and pale yellow in color (arrows); (**b**) Similarly in the outflow tract too, the myocardium is replaced by fat; (**c**) Transverse section through mid-portion of the ventricles also shows infiltration of the anterior wall A of the left ventricle LV and interventricular septum IVS (*L* lateral wall, *LVC* left ventricular cavity, *P* posterior wall, *PT* pulmonary trunk, *PV* pulmonary valve, *RA* right atrium, *TV* tricuspid valve); (**d**) Similar features seen in the scanned slide stained by H&E

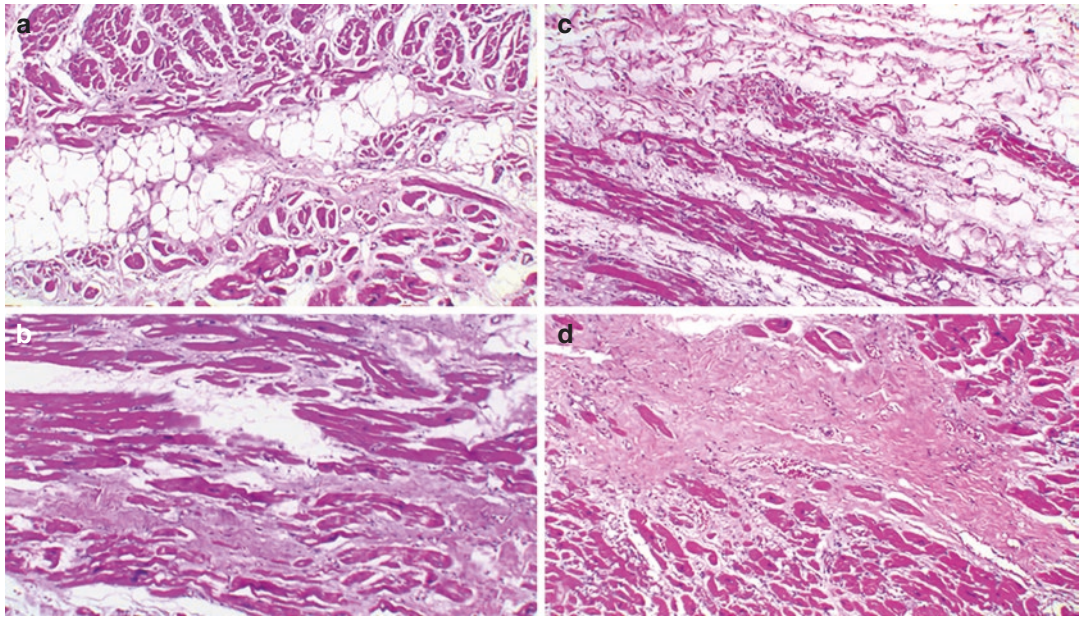

Fig. 44.3 Fibro-fatty replacement seen in the right ventricle (**a**) and (**b**) and left ventricle (**c**) and (**d**) (H&E × 200)

44.3 Discussion

The fibro-fatty infiltration of the RV and to some extent of the LV as well, in all probability, triggered a sudden arrhythmic death in this young patient. These clinicopathological features suggested the diagnosis of an ACM, which has been known by several synonyms in the past such as right ventricular dysplasia, right ventricular cardiomyopathy, or arrhythmogenic right ventricular dysplasia. The current term ACM was adopted for this genetically inherited nonischemic disorder since the myocardial fibrous or fibro-fatty replacement can affect not only the RV or both ventricles, but can also involve the LV exclusively. Though many cardiac disorders can lead to an arrhythmic death, the descriptive term 'arrhythmogenic' indicates the inherent capability of this disorder to induce ventricular arrhythmias even before the development of the morphological changes. The clinical manifestation begins usually between the second and fourth decades of life (with a male predominance, male to female ratio of 3:1) and is seldom seen before and beyond the age of 12 and 60 years, respectively. The estimated prevalence of ACM is from 1 in 2000 to 1 in 5000 with geographic variations.

Barring the autosomal recessive cardiocutaneous syndromes, majority of the cases of ACM are inherited as autosomal dominant disease with one or more pathogenic mutations in the genes coding for several desmosomal proteins. These finally lead to alterations in the intercalated disc protein complex, and hence, ACM is also referred to as intercalated disc or cell-junction disease. Currently, causal mutations in the non-desmosomal genes have also been implicated in some of the cases. About 40% of patients are still genetically undefined, and there is also incomplete penetrance and variable expressivity modified by environmental factors including exercise. The final outcome is a loss of cell adhesiveness leading to an electrical instability and mechanical damage to the cardiomyocytes with apoptosis. Alterations in cellular signaling lead to increased expression of the fibrogenic and adipogenic genes, with subsequent fibro-fatty myocardial remodeling; the latter begins in the subepicardial region with a variable extension towards the subendocardial region and transmural thinning. Depending on the type of mutation and the con-

comitant modifying factors, and the distribution of the fibro-fatty tissue, ACM can be classified into 3 types—isolated RV type (the classic type), isolated LV dominant, or biventricular disease (balanced, dominant-right, or dominant-left), which with reference to the Padua criteria (major and minor) have differences in the functional/structural assessment, tissue characterization, repolarization/depolarization abnormalities, arrhythmias, and family history. The RV involvement characteristically begins in the basal and inferior regions and later involves the free wall with extreme parchment-like thinning of the wall and formation of aneurysms; the apex is affected in only the late stages of the disease. In the LV, the fibro-fatty tissue is seen initially in the posterolateral region and then extends into the subepicardial and mid-myocardial regions of the free wall, but this is not associated with wall thinning or aneurismal outpouchings. When the interventricular septum is affected, the fibro-fatty tissue is distributed towards the RV aspect, as was seen in this case. The cardiomyocytes may also be hypertrophied with cytoplasmic vacuolation and dysmorphic nuclei. In addition, in many cases there is infiltration of T-lymphocytes, which may also play a role in the pathogenesis of the disease.

ACM progresses through 4 phases. In the preclinical or concealed phase, the heart does not show any identifiable structural abnormalities and the patients may remain asymptomatic or may show subtle ECG abnormalities. However, in these individuals, SCD remains an important manifestation, triggered by strenuous exercise (especially those engaged in athletic activities) and even day to-day stressful conditions. Such cases can be identified only on the basis of mutational analysis. Symptoms related to arrhythmias, particularly ventricular tachyarrhythmias, develop in the overt or symptomatic phase, which are associated with identifiable pathological features. In the subsequent phases with more pronounced involvement, the clinical presentation is related to RV or biventricular dysfunction. In these scenarios, SCD is prevented by implantation of intracardiac defibrillators and appropriate life style changes. The patient in this report would have been in the symptomatic phase with development of SCD, which was the first and only mode of presentation. The hypotension may be explained on the basis of RV systolic dysfunction leading to inadequate LV preload.

Further Reading

Bosman LP, te Riele ASJM. Arrhythmogenic right ventricular cardiomyopathy: a focused update on diagnosis and risk stratification. Heart. 2021;108(2):90–7.

Cadrin-Tourigny J, Bosman LP, Wang W, Tadros R, Bhonsale A, Bourfiss M. Sudden cardiac death prediction in arrhythmogenic right ventricular cardiomyopathy: a multinational collaboration. Circ Arrhythm Electrophysiol. 2021;14:e008509.

Corrado D, Marra MP, Zorzi A, Beffagna G, Cipriani A, De Lazzari M, et al. Diagnosis of arrhythmogenic cardiomyopathy: The Padua criteria. Int J Cardiol. 2020;319:106–14.

Costa S, Cerrone M, Saguner AM, Brunckhorst C, Delmar M, Duru F. Arrhythmogenic cardiomyopathy: an in-depth look at molecular mechanisms and clinical correlates. Trends Cardiovasc Med. 2020;29:S1050–738.

Gao S, Puthenvedu D, Lombardi R, Chen SN. Established and emerging mechanisms in the pathogenesis of arrhythmogenic cardiomyopathy: a multifaceted disease. Int J Mol Sci. 2020;21:6320.

Mattesi G, Zorzi A, Corrado D, Cipriani A. Natural history of arrhythmogenic cardiomyopathy. J Clin Med. 2020;9:878.

Neto JE, Tonet J, Frank R, Fontaine G. Arrhythmogenic right ventricular cardiomyopathy/dysplasia (ARVC/D): what we have learned after 40 years of the diagnosis of this clinical entity. Arq Bras Cardiol. 2019;112:91–103.

Restrictive Cardiomyopathy: Loeffler's Endo-Myocarditis

45

Pradeep Vaideeswar and Tejaswini Waghmare

45.1 Clinical History

The patient was a 19-year-old male student, who presented initially with a low-grade fever without any localizing symptoms for the past 10–12 days. This was followed by headache, weakness of both lower limbs (left > right) with urinary incontinence since 3 days, and weakness of both upper limbs a day later. He had no sensory complaints. There was no previous history of significant illness. Having maintained sensorium for the previous 10 days, he began to become progressively disoriented since a day. On admission to the hospital, the patient was afebrile, normotensive with mild pallor. He was drowsy, responding to oral commands. The pupils were reacting and bilaterally equal; the fundus was normal. His gag reflexes and extraocular movements were impaired. There were no signs of meningeal irritation. He was hypertonic, the power in right upper limb was 4/5, left upper was 3/5, right lower limb was 2/5, and left lower limb was 1/5. The reflexes in upper limbs were 3+ and lower limbs, 4+. Both plantars were extensors. Systemic examination revealed only mild tender splenomegaly.

Investigations revealed Hb 8.9 g/dL, total leukocyte count of 67,000 cells/cmm with 81% eosinophils (absolute count of 54,513 cells/cmm), platelet count 2.4 lakhs/cmm, creatinine 1.5 mg/dL, blood urea nitrogen 32 mg/dL, plasma aspartate aminotransferase 32 U/dL, plasma alanine aminotransferase 35 U/dL, alkaline phosphatase 44 U/dL, sodium 133 mEq/dL, potassium 4.3 mEq/dL, and chloride 128 mEq/dL. Urine analysis was within normal limits. The chest X-ray was normal; ECG showed ST depression and T wave inversion in leads V_2–V_6. The plain and contrast-enhanced magnetic resonance imaging (MRI) examination of the brain revealed abnormal signal intensity lesions in both cerebral hemispheres, suggesting infarcts (Fig. 45.1).

The patient was put on high dose steroids (methylprednisolone 1 g/day) for his weakness, but the general condition of the patient worsened over the next 12 h. He became extremely dyspneic (respiratory rate 44/min) and hypotensive (blood pressure 100/50 mmHg) with onset of high grade fever. He had developed bilateral coarse crepitations. His power had reduced and was 0/5 in all 4 limbs. In view of the respiratory distress, the patient was shifted to medical intensive care unit, intubated immediately, and put on ventilator. Injectable antibiotics (piperacillin and tazobactum) along with acyclovir and artesunate were administered. A repeat chest X-Ray revealed infil-

P. Vaideeswar (✉)
Department of Pathology (Cardiovascular and Thoracic Division), Seth Gordhandas Sunderdas Medical College and King Edward Memorial Hospital, Mumbai, India

T. Waghmare
Department of Pathology, Seth Gordhandas Sunderdas Medical College and King Edward Memorial Hospital, Mumbai, India

P. Vaideeswar (ed.), *Tropical Cardiovascular Pathology*,
https://doi.org/10.1007/978-981-19-3720-0_45

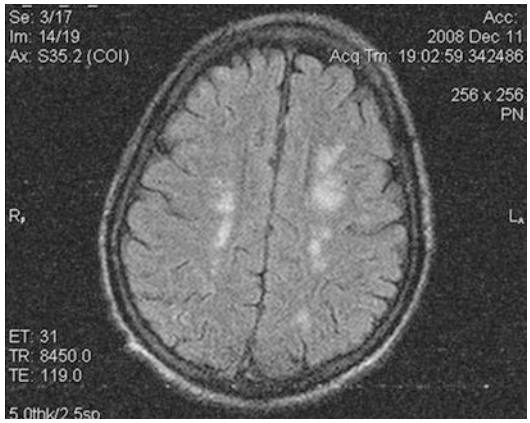

Fig. 45.1 MRI showing abnormal signal intensity lesions in both cerebral hemispheres

trates in right lower and middle lobes. A complete hemogram of patient was done on the third day, which revealed a total leukocyte count of 45,200/cmm with 70% eosinophils and an absolute count of 31,640/cmm. In view of the altered sensorium, the cerebrospinal fluid was examined; it was normal. Blood culture did not grow any organism. In spite of high dose steroids, the patient's weakness did not improve and he continued to remain febrile. The antibiotics were stepped up; meropenem and teicoplanin were started. A hematology reference was taken and BCR/ABL test from peripheral blood was advised. However, due to financial condition of the family, test was deferred. The patient was started on imatinib. By the 5th day, the patient deteriorated. He had become hypotensive and his urinary output had dropped. The patient required high dose noradrenaline. He went into acute respiratory distress syndrome and expired on the 8th day of admission.

45.2 Autopsy Findings

The heart was markedly enlarged in size (350 g) with marked biventricular enlargement. There was diffuse opacification of the visceral layer of the pericardium, but pericardial effusion was not present. Both the ventricular chambers were moderately enlarged with mild to moderate diffuse endocardial thickening. Major part of the ventricular cavities was occupied by extremely firm pale red brown to yellow 'fleshy' thrombus (Fig. 45.2a–d). In the right ventricle, it had produced obliteration of the apex with entrapment of the papillary muscles of the tricuspid valve. The thrombus extended on the anterior and posterior free walls, reaching up to the tricuspid annulus. It had also extended on to the right ventricular outflow tract and was around 2.5 cm away from the pulmonary valvular annulus. In the left ventricle, the thrombus had 'engulfed' the papillary muscles and plastered down the posterior mitral leaflet, extending right up to the mitral annulus (Fig. 45.3a). On the outflow tract, it extended in part to the mid-portion of the left coronary cusp of the aortic valve (Fig. 45.3b, d). The arterial annuli were dilated and the cusps were normal. The right atrium also showed a thrombus over the anterior rim of the fossa ovalis (probably related to the intravenous catheter).

On histopathology, the ventricles showed similar features. The thick layer of fresh thrombus (rich in eosinophils along with other leukocytes) was attached to the endocardium, which showed mild to moderate loose fibrocellular edematous thickening and dense infiltration by large numbers of eosinophils and histocytes (Fig. 45.4). The subendocardial tissue was also edematous and inflamed, sending in edematous fibrous tentacles (rich in eosinophils) into the underlying myocardium. The subendocardial and mid-myocardial regions also showed eosinophilic myocarditis (Fig. 45.5a) and intramural coronary thromboembolism (Fig. 45.5b) with multifocal fresh infarction (Fig. 45.5c). These thrombi had also produced pulmonary and systemic thromboembolism (brain and spleen, Fig. 45.6a). There was eosinophilic pneumonia (Fig. 45.6b) with diffuse alveolar damage. The vasculature in many organs showed eosinophils (Fig. 45.6c), while the bone marrow was also rich in eosinophils and its precursors. Acute tubular necroses and occasional thromboemboli (Fig. 45.6d) were present in the kidneys.

Cause of Death: Loeffler's endo-myocarditis with systemic thromboembolism and eosinophilic pneumonia.

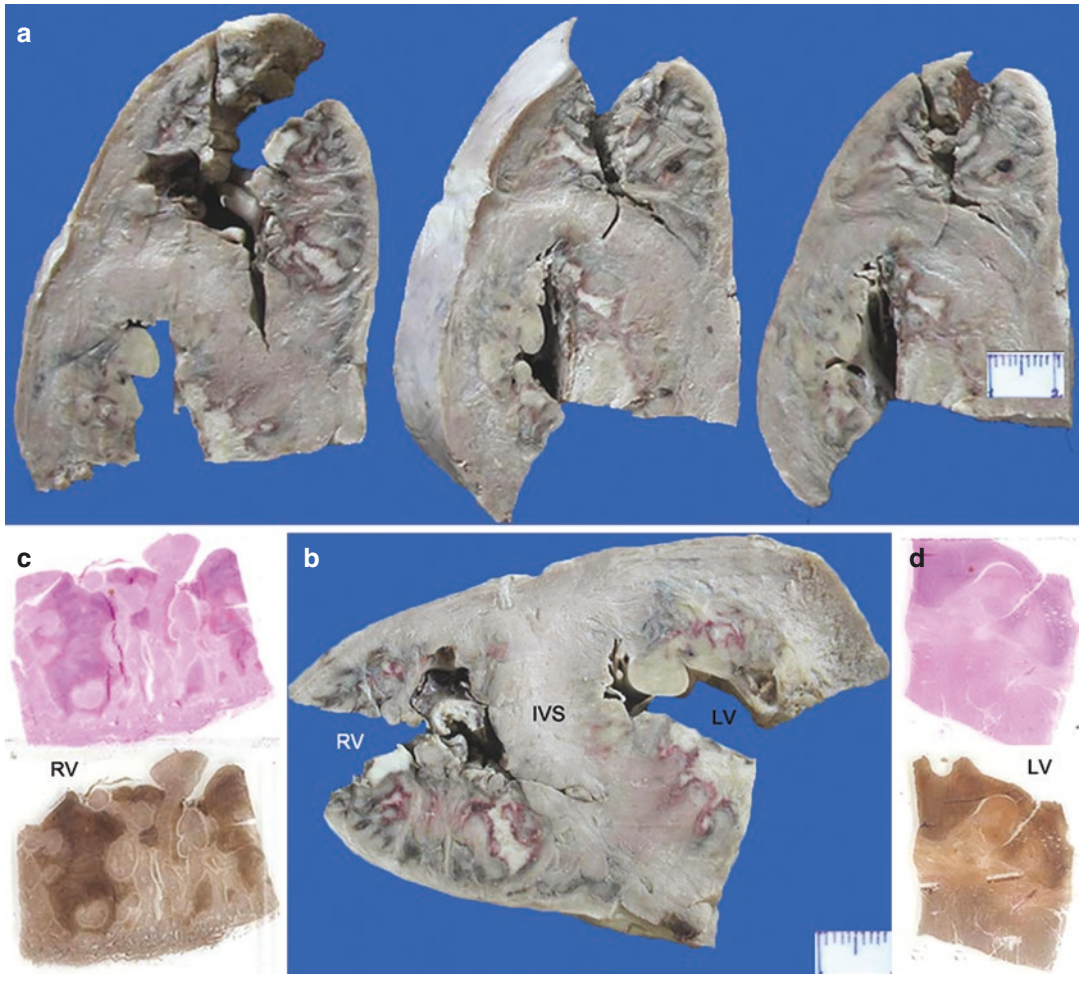

Fig. 45.2 (**a**) Serial transverse slices of the ventricular myocardium and (**b**) transverse slice from the mid-portion shows the presence of large mural thrombi that have obliterated the intertrabecular spaces; Scanned slides stained by H&E and elastic van Gieson of the (**c**) Right ventricle RV and (**d**) Left ventricle LV showing features similar to the gross findings

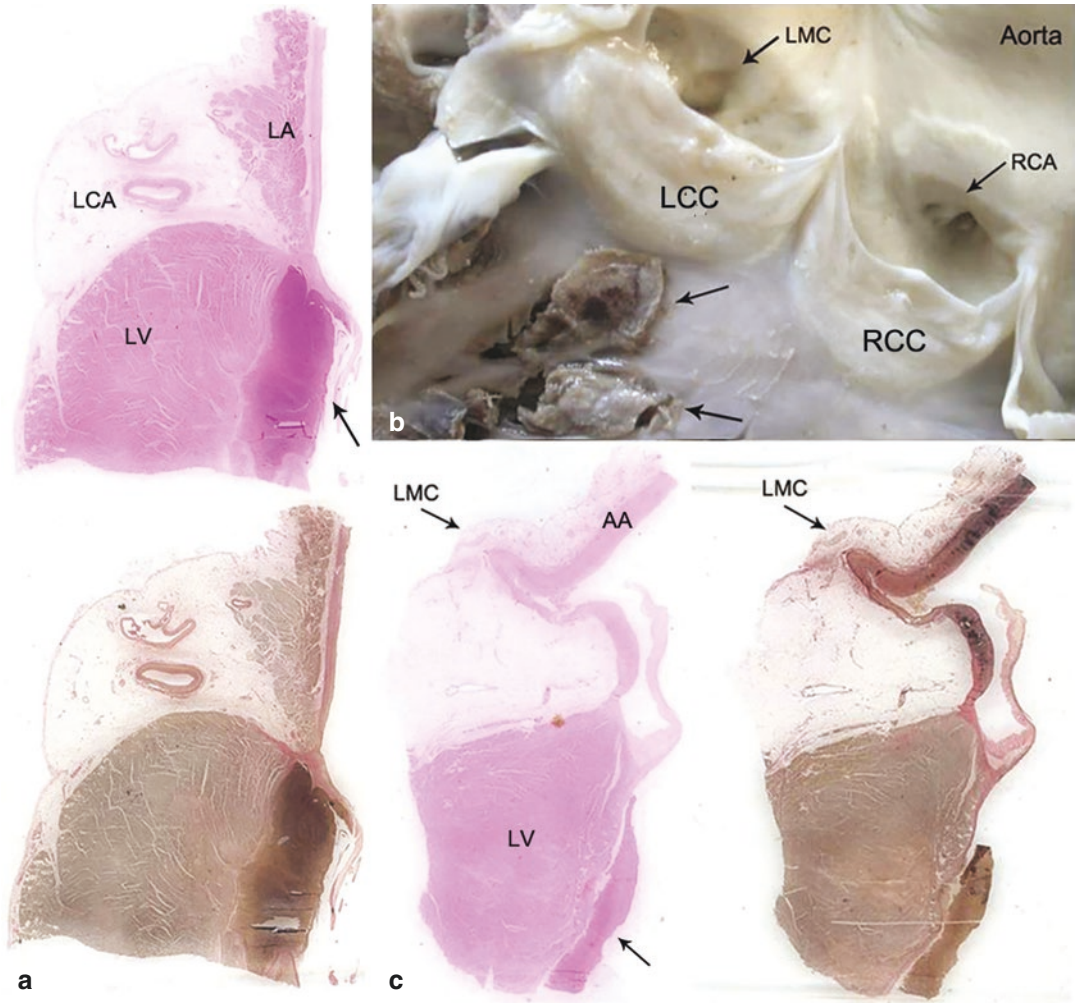

Fig. 45.3 (**a**) Scanned slides stained by H&E and elastic van Gieson through left ventricular inflow tract showing thrombus (arrow) reaching up to the mitral annulus; (**b**) Thrombus (arrows) in the left ventricular outflow tract extending up to the attachment of the left coronary cusp LCC; (**c**) Scanned slides stained by H&E and elastic van Gieson through left ventricular outflow tract showing thrombus (arrow) reaching up to the aortic annulus (*LA* left atrium, *LCA* left circumflex artery, *LMC* left main coronary artery, *LV* left ventricle, *RCA* right coronary artery, *RCC* right coronary artery cusp)

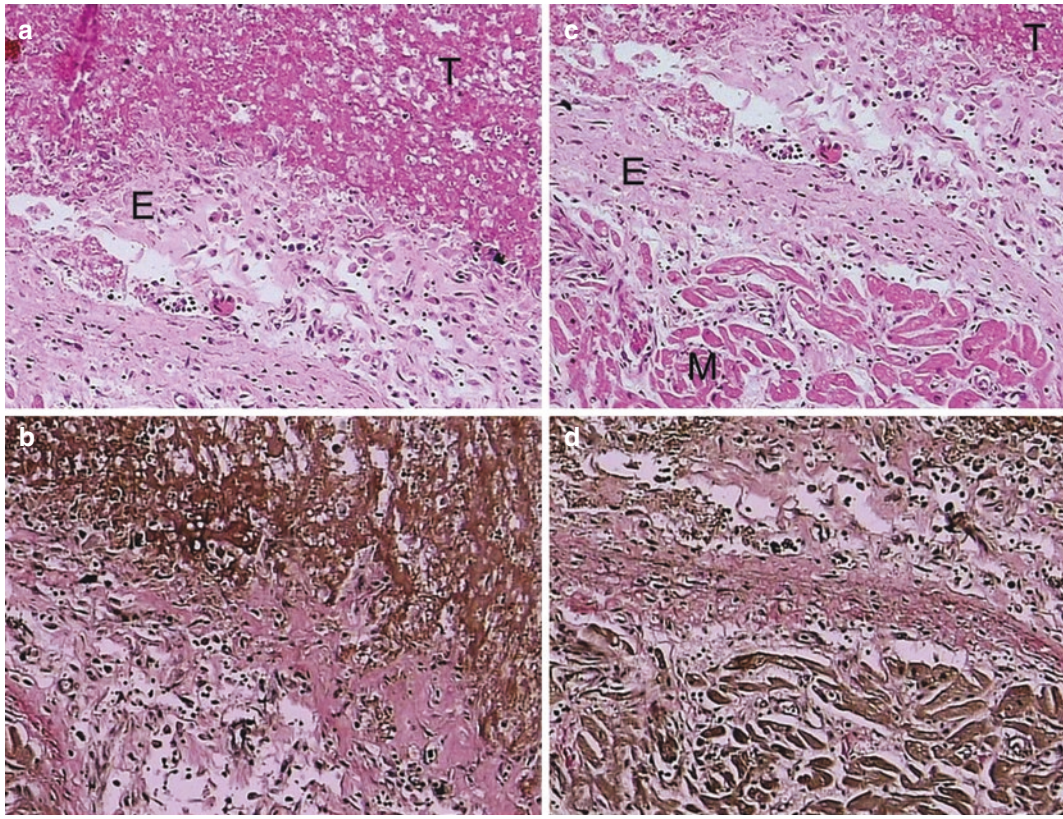

Fig. 45.4 Right ventricle (**a**) stained by H&E (× 200), (**b**) elastic van Gieson (× 200) and Left ventricle (**c**) stained by H&E (× 200), (**d**) elastic van Gieson (× 200) showing thrombus T adherent to the inflamed and edematous endocardium E (M myocardium)

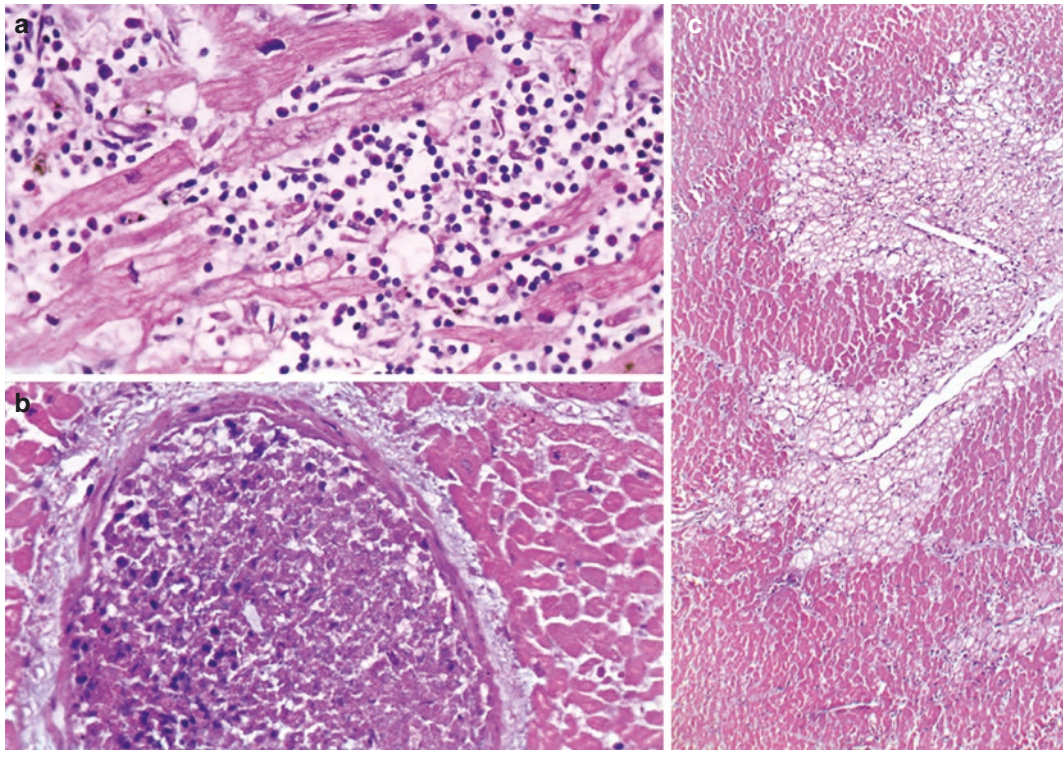

Fig. 45.5 (**a**) Eosinophilic myocarditis (H&E × 400); (**b**) Intramural coronary artery occluded by fresh thromboembolus (H&E × 400); (**c**) Coagulative necroses of cardiomyocytes with extensive myocytolyses in the sub-endocardial region (H&E × 200)

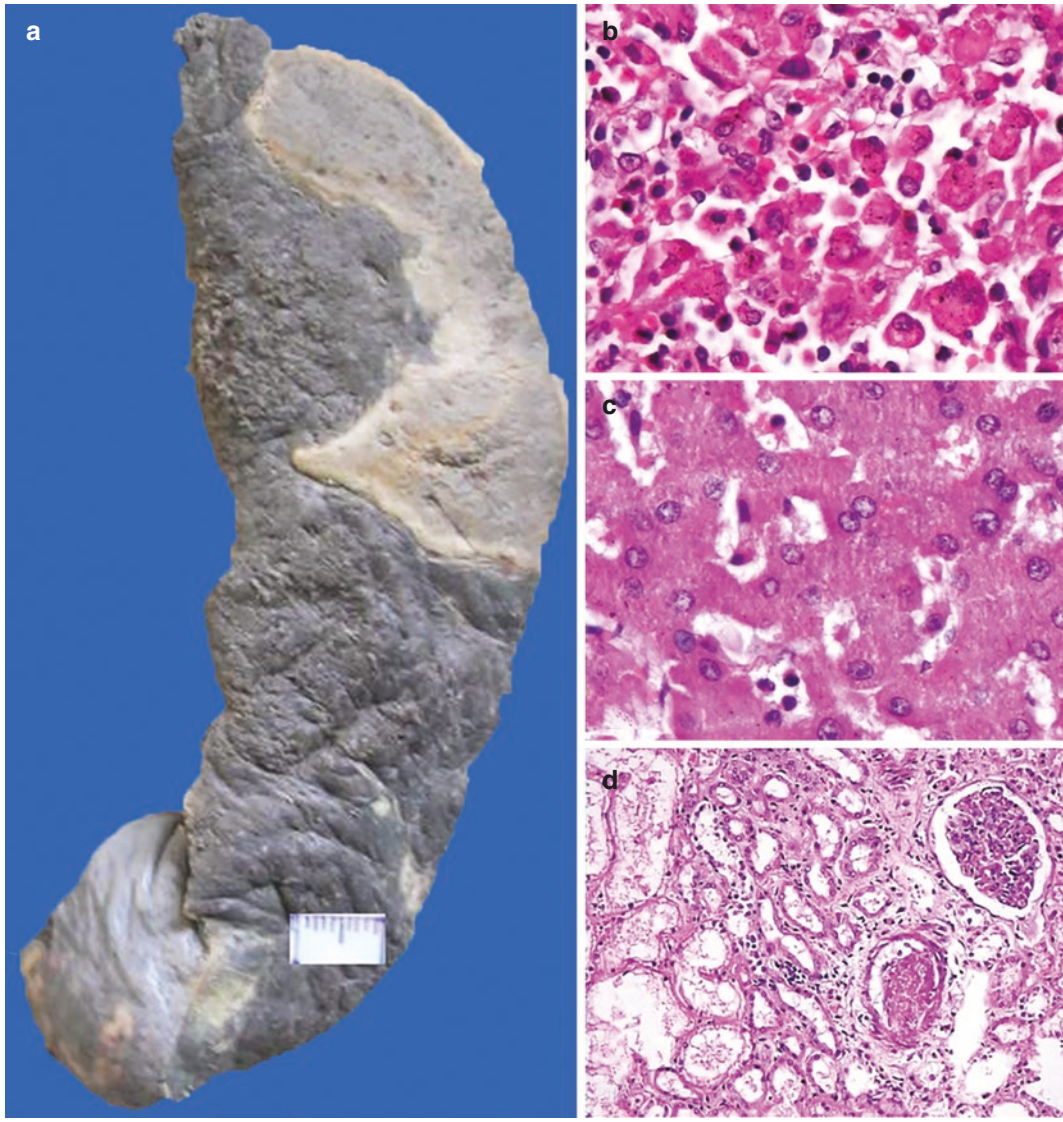

Fig. 45.6 (**a**) Splenic infarct; (**b**) The alveoli in the lungs were filled with large number of macrophages and eosinophils (H&E × 400); (**c**) Hepatic sinusoids with few eosinophils; (**d**) Renal tubular damage with thromboembolus in an artery (H&E × 200)

45.3 Discussion

The heart in this young adult male was characterized by an extraordinary degree of biventricular fibrosis of the endocardium and myocardium in a background of peripheral blood and tissue eosinophilia. Blood hyper-eosinophilia refers to documented eosinophil counts of more than 1500 per mL on at least 2 separate occasions with a minimum time interval of 4 weeks, while tissue eosinophilia includes a count of more than 20% in the bone marrow, histological confirmation of eosinophils in the tissues, or immunohistochemical demonstration of eosinophil products in the tissues examined. In the tissues, the eosinophils are known to release a repertoire of pro-inflammatory and prothrombotic mediators and cytokines that are capable of altering the local

milieu through angiogenesis and fibrosis. Besides the tissue remodeling, some of the eosinophil products such as eosinophil cationic protein, eosinophil major basic proteins, eosinophil peroxidase, and eosinophil-derived neurotoxin exhibit cytotoxic effects and lead to organ damage. This evolves into the hyper-eosinophilic syndrome (HES), as seen in this case.

HES is an uncommon entity with an age-adjusted incidence rate of 0.036 cases per 100,000 person years, more often affecting the males (male to female ratio of 9:1) between 20 and 50 years of age. Both hyper-eosinophilia and HES can be categorized into 3 types—Primary: related to myeloproliferative disorders or proliferation of aberrant T-cells, Secondary: that develops as a paraneoplastic syndrome or as a reaction to allergic/infective conditions, and Idiopathic: where a cause is not found despite detailed investigations. Our patient was not thoroughly investigated due to financial constraints, but a secondary cause could be ruled out on the basis of the history and the autopsy findings. The effects of organ damage are commonly encountered in the skin, heart, lungs, gastrointestinal tract, and nervous system. The heart is affected in 35–50% of patients with HES, where it assumes a life-threatening manifestation (aptly represented by the current case) conventionally referred to as Loeffler's endo-myocarditis (LEM).

LEM progresses in 3 stages, which may not always be sequential and can be overlapping. Biventricular involvement is seen in 50% of the cases, while isolated left ventricular and right ventricular affection occur in 40% and 10% of the cases, respectively. In the necrotic stage, the eosinophils infiltrate the endocardium and the variable thickness of the subendocardial myocardium and the patients are generally asymptomatic. In rare instances, there is diffuse infiltration—acute eosinophilic myocarditis that results in an enlarged, heavy, and flabby heart. Myocyte necroses, coronary arteritis, and pericardial involvement may be accompanying features and these individuals present with cardiac failure or even tamponade. Mural thrombi develop initially in the ventricular apices in the thrombotic stage. Later, there may be extension to the basal portions of the inflow tracts, often entrapping the papillary muscles, chordae tendineae, and leaflets of the atrioventricular valves. Such patients are at a risk for embolization and development of secondary valvular regurgitation. Thick white plaque-like endocardial thickening with distinct borders and rolled edges are seen in the inflow tracts in the fibrotic stage. This then leads to an uncommon cardiomyopathy (CMP)—restrictive CMP (RCM) that shows increased ventricular stiffness, impaired diastolic filling, and normal systolic function, leading often to right heart failure. Sudden death can also occur in some cases. In this patient, there was telescoping of the thrombotic and fibrotic stages and clinical manifestations developed mainly as result of systemic thromboembolism. A further contributor to the morbidity was eosinophilic pneumonia with diffuse alveolar damage.

Cardiac involvement in hyper-eosinophilia, as depicted, carries a poor prognosis and significant mortality. It requires prompt diagnosis and treatment, depending on the stage of the disease. Multimodality imaging is extremely useful and may at times be combined with an endo-myocardial biopsy. If diagnosed early, immunosuppressive therapy to decrease the eosinophil count (corticosteroids, tyrosine kinase inhibitors, and other cytotoxic medications) can be beneficial. Presence of mural thrombi, as seen in this patient, would also entail anticoagulation.

Further Reading

Bondue A, Carpentier C, Roufosse F. Hypereosinophilic syndrome: considerations for the cardiologist. Heart. 2021;108(3):164–71.

Kariyanna PT, Hossain NA, Onkaramurthy NJ, Jayarangaiah A, Hossain NA, Jayarangaiah A, et al. Hypereosinophilia and Löffler's endocarditis: a systematic review. Am J Med Case Rep. 2021;9:241–8.

Kiani R, Naghavi B, Amin A, Sadeghpour A, Zahedmehr A, Firouzi A, et al. Central nervous system and cardiac involvement in the hypereosinophilic syndrome: a case report. Immunol Invest. 2021;50:356–62.

Polito MV, Hagendorff A, Citro R, Prota C, Silverio A, De Angelis E. Loeffler's endocarditis: an integrated multimodality approach. J Am Soc Echocardiogr. 2020;33:1427–41.

Salih M, Ibrahim R, Tirunagiri D, Al-ani H, Ananthasubramaniam K. Loeffler's endocarditis and hypereosinophilic syndrome. Cardiol Rev. 2021;29:150–5.

Valent P, Degenfeld-Schonburg L, Sadovnik I, Horny HP, Arock M, Simon HS, et al. Eosinophils and eosinophil-associated disorders: immunological, clinical, and molecular complexity. Semin Immunopathol. 2021;43:423–38.

46 Endomyocardial Fibrosis as an Incidental Autopsy Finding

Pradeep Vaideeswar and Pranita Zare

46.1 Clinical History

A 58-year-old postmenopausal lady had been on regular medications for atrial fibrillation for the past 5 years. She was admitted to a private nursing home with 3-day complaints of pain in the abdomen with loose motions. The abdominal pain was continuous, moderate grade, nonradiating, not relieved by any medication, and was located in the epigastric and umbilical regions. A computed tomography performed revealed subacute small intestinal obstruction with minimal bilateral pleural effusions. She was transferred to our tertiary center on inotropic support for persistent hypotension. On examination, the general condition was poor with a pulse rate of 130 per minute and blood pressure of 70/40 mmHg. The abdomen was distended and tender. Her routine hematological and biochemical investigations had been normal. The inotropic drugs were continued but there was no significant response and she succumbed 7 h after admission.

P. Vaideeswar (✉) · P. Zare
Department of Pathology (Cardiovascular and Thoracic Division), Seth Gordhandas Sunderdas Medical College and King Edward Memorial Hospital, Mumbai, India

46.2 Autopsy Findings

The heart was moderately enlarged in size and weighed 390 g. The inferior border was entirely flattened (Fig. 46.1a) with a left-sided protuberance formed by the left ventricular apex, leading to a 'boot' shaped appearance. Both atria were moderately enlarged in size with a distinct puckering of the right ventricular apex (Fig. 46.1a, b). There was marked grey-white endocardial thickening over the anterior and posterior free walls (Fig. 46.1b) that had produced flattening of the trabeculae carneae with attenuation and plastering of the posterior papillary muscles. The endocardial thickening stopped abruptly 2.4 cm below the pulmonary valve and had produced obliteration of the apical portion of the right ventricular cavity (Fig. 46.1b). On histopathology, there was hyalinized collagenic thickening of the endocardium (Fig. 46.1c, d). At the endo-myocardial interface, there were foci of vascularization and delicate fibrous tentacles were also seen to infiltrate the underlying muscle (Fig. 46.1e). The left ventricular apex was rendered shallow by the thickened endocardium, which also extended to involve the mid-portions of the ventricle as well (Fig. 46.2a). Similar changes

P. Vaideeswar (ed.), *Tropical Cardiovascular Pathology*,
https://doi.org/10.1007/978-981-19-3720-0_46

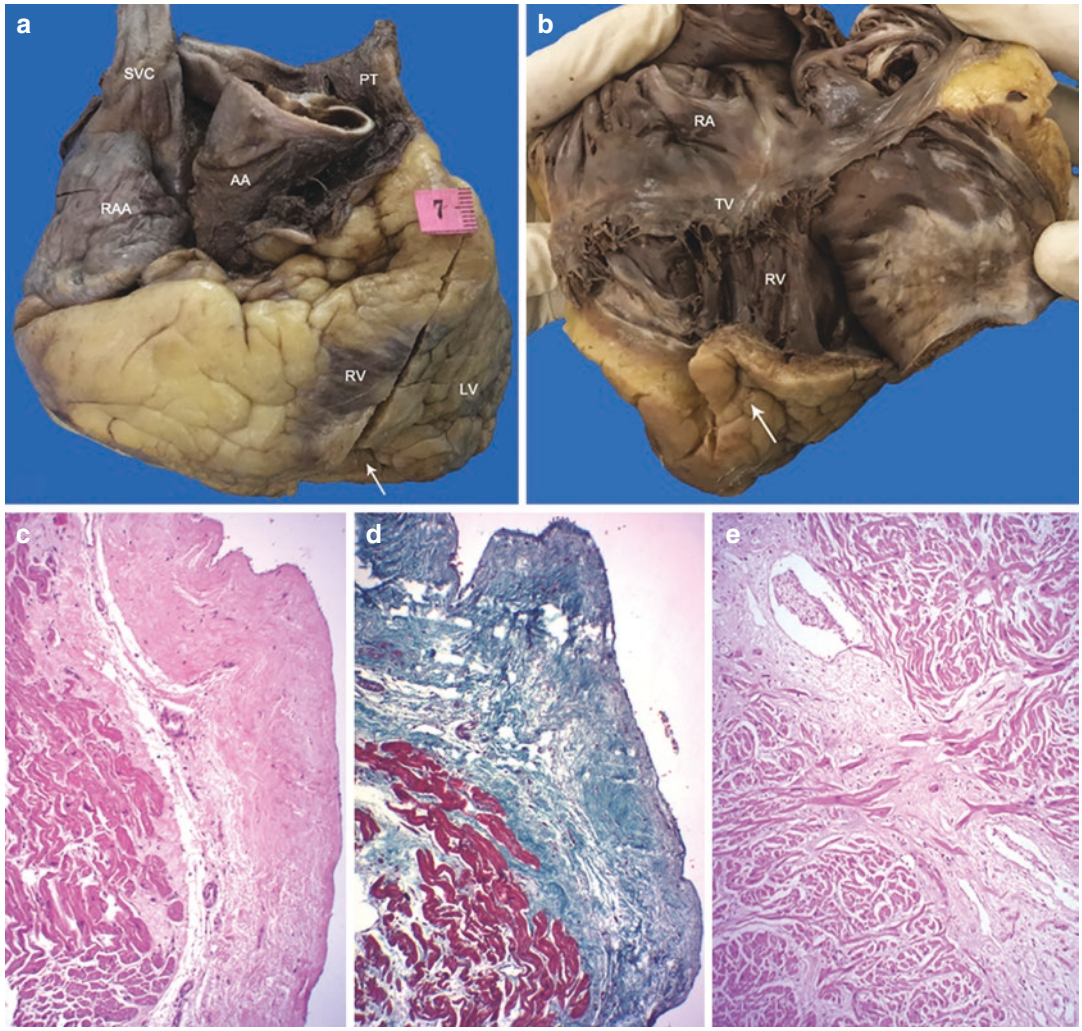

Fig. 46.1 (**a**) Flattened inferior border of the heart. Note moderate enlargement of the right atrium. The arrow points to the puckered right ventricular RV apex; (**b**) Leathery grey-white thickening of the endocardium with retraction (arrow) of the RV apex (*AA* ascending aorta, *LV* left ventricle, *PT* pulmonary trunk, *RA* right atrium, *RAA* right atrial appendage, *TV* tricuspid valve, *SVC* superior vena cava); Marked endocardial thickening that is stained (**c**) pale pink (H&E × 250) and (**d**) green (Masson's trichrome stain × 250); (**e**) Fibroblastic proliferation insinuates between groups of cardiomyocytes in the subendocardial region (H&E × 250)

were noted on the histology (Fig. 46.2b). In addition, focal surface thrombi were noted at places. Furthermore, chunks of fibrin surrounded by hyalinized collagen were also present (Fig. 46.2c). There was biatrial hypertrophy with extensive interstitial fibrosis and vacuolation of the myocytes (Fig. 46.3a). There were no eosinophils. Other findings at autopsy included small intestinal gangrene (Fig. 46.3b) and bilateral small renal infarcts.

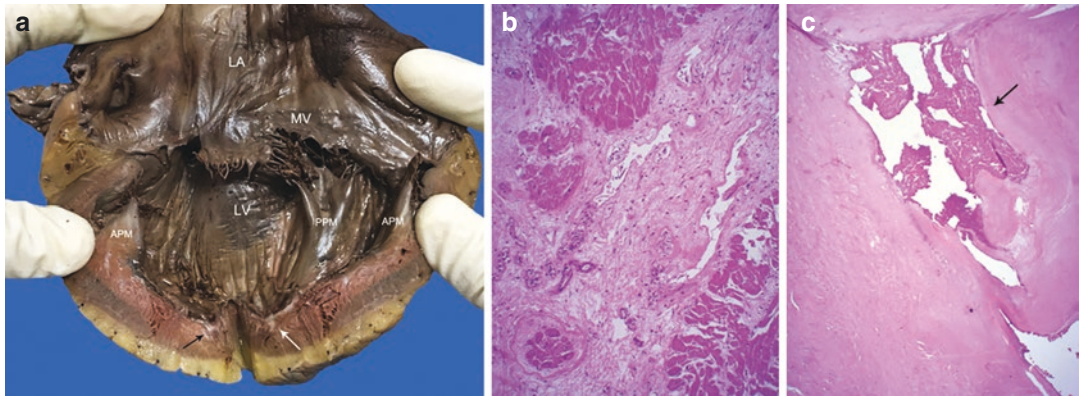

Fig. 46.2 (**a**) Opened out left ventricular LV inflow tract showing thickened endocardium which has obliterated the apex with fibrosis extension into the subendocardium (arrows). The bellies of the posterior papillary muscle PPM are also not seen distinctly (*APM* anterior papillary muscle, *LA* left atrium); (**b**) Fibrovascular tentacles intersect the bundles of cardiomyocytes (H&E × 250); (**c**) Chunks of fibrin (arrow) are incorporated within the endocardial fibrosis (H&E × 250)

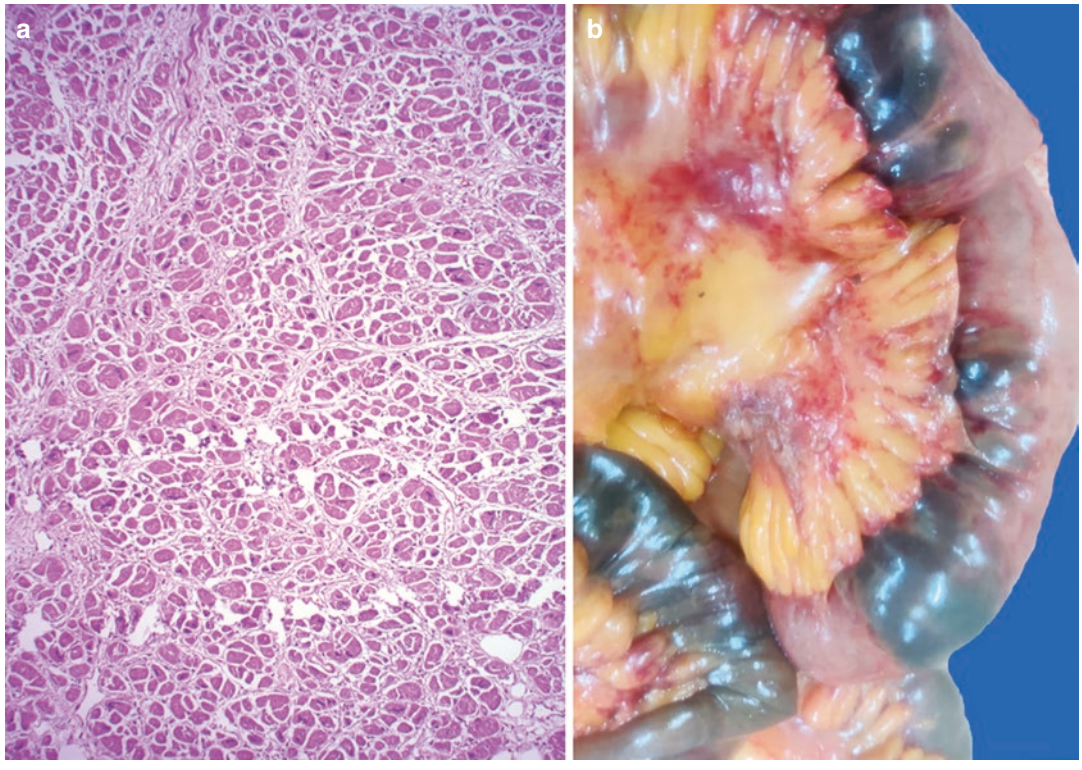

Fig. 46.3 (**a**) Left atrium with hypertrophy and prominent interstitial fibrosis (H&E × 250); (**b**) Focal dusky discoloration of the serosa of the ileum

46.3 Discussion

Marked endocardial fibrotic thickening affecting the apices and the inflow tracts with apical obliteration of both ventricles was seen as an incidental finding in this patient and would have produced stiffening of the chambers with restriction of diastolic filling. These functional features, not documented in life, are the hall marks of the uncommon restrictive cardiomyopathy (RCM), which forms 2–5% of the nonischemic myocardial disorders. Though some of the cases of RCM may be idiopathic (often with a genetic basis related to mutations affecting sarcomeric or nonsarcomeric proteins), most of the cases of RCM develop due to other diverse genetic and nongenetic causes (See Chaps. 47–50). Extensive endocardial pathology with concomitant involvement of the subjacent myocardium noted in this patient is the trait of endo-myocardial fibrosis (EMF), which is produced by 2 distinct clinicopathologic entities, Loeffler's endocarditis (See Chap. 45) and tropical EMF (T-EMF). Despite the similarities of pathologic findings in end-stage disease, these two entities differ in geographic, age, gender distribution, clinical presentation, and evolution.

T-EMF, also called as Davies disease, was endemic in equatorial Africa, South America, India, and other countries located near the equator (hence 'tropical'), where it was a relatively frequent cause of congestive heart failure. Now the incidence of this disease has reduced considerably due to improved socioeconomic conditions; the true prevalence is not known. In comparison to Loeffler's endo-myocarditis, the disease affects both men and women equally and is more common in children and young adults. Although individuals of any age can be affected, there is a bimodal distribution with peaks at 10 and 30 years. The focal or diffuse fibrosis tends to involve both the ventricles in 50% of the cases (as seen in this patient), while isolated left and right ventricular fibrosis is seen in about 40% and 10% of the patients, respectively. The early lesion appears to begin at the ventricular apex and appears gelatinous. In well established disease, the lesion resembles tenacious thick white paint, extending towards the atrioventricular valve with subsequent entrapment of the papillary muscles and the tendinous cords, and even plastering of the leaflets. Finally, the endocardium resembles a porcelain saucer and is sharply demarcated from the normal endocardium. There are 3 zones which can be identified on histology: an innermost layer of dense and loose collagen, then a layer of granulation tissue with mixed inflammatory infiltrate and proliferating vascular channels, which finally rests on groups of often vacuolated cardiomyocytes with enlarged atypical nuclei and focal interstitial scarring. Thrombi in different stages of organization may be also seen. Collagenous septa extend into the myocardium.

There are several hypotheses regarding the pathogenesis of T-EMF. Eosinophil participation in some cases is undeniable and such eosinophil-dependent disease is frequently encountered in parasitic infestations, particularly in the tropics. The eosinophil-independent causes include malnutrition, diets rich in some types of tubers, magnesium/vitamin D deficiency, increased levels of cerium, toxic agents, and autoimmune mechanisms with an element of genetic predisposition. The disease has an insidious onset, but a relentless course. Hence, in the beginning majority of the patients remain asymptomatic for prolonged periods of time. The clinical manifestations depend on which ventricle is affected: left-sided involvement is associated with pulmonary congestion, whereas predominantly right-sided disease may result in clinical symptoms suggestive of a constrictive pericarditis. Biventricular involvement, which is the most frequent, shows an additional finding of low cardiac output. This involvement may finally culminate in complications such as atrial arrhythmias, thromboembolism, and/or progressive atrioventricular regurgitation, leading to mortality. Our patient had atrial fibrillation (AF) and developed embolic intestinal gangrene. Patients with AF have the worst prognosis. There is no specific therapy available for T-EMF. Medical management with surgical intervention if required may lead to substantial symptomatic improvement, especially in patients with predominant left ventricular involvement.

Further Reading

Beaton A, Mocumbi AO. Diagnosis and management of endomyocardial fibrosis. Cardiol Clin. 2017;35:87–98.

Duraes AR, de Souza Lima Bitar Y, Roever L, Neto MG. Endomyocardial fibrosis: past, present, and future. Heart Fail Rev. 2020;25:725–30.

Grimaldi A, Mocumbi AO, Freers J, Lachaud M, Mirabel M, Ferreira B, et al. Tropical endomyocardial fibrosis: natural history, challenges, and perspectives. Circulation. 2016;133:2503–15.

Gupta PN, Kunju SM, Rajan B, Koshy AG, Vishwanathan S, George PS, Velappan P. Geographical variation in the clinical presentation of endomyocardial fibrosis in India? Indian Heart J. 2018;70:56–65.

Mbanze J, Cumbane B, Jive R, Mocumbi A. Challenges in addressing the knowledge gap on endomyocardial fibrosis through community-based studies. Cardiovasc Diagn Ther. 2020;10:279–88.

Mocumbi AO, Stothard JR, Correia-de-Sa P, Yacouab M. Endomyocardial fibrosis: an update after 70 years. Curr Cardiol Rep. 2019;21:148.

Scatularo CE, Posada Martínez EL, Saldarriaga C, Ballesteros OA, Baranchuk A, Liprandi AS, et al. Endomyocardiofibrosis: a systematic review. Curr Probl Cardiol. 2021;46:100784.

Vijayaraghavan G, Sivasankaran S. Tropical endomyocardial fibrosis in India: a vanishing disease! Indian J Med Res. 2012;136:729–38.

47 Cardiac Amyloidosis in an Octagenarian

Pradeep Vaideeswar, Girish Sabnis, and Dhiraj Kumar

47.1 Clinical History

An 80-year-old woman, suffering from hypertension (regular treatment with tablet Cilnidipine 10 mg daily for 2 years), presented to Emergency Room with complaints of recent onset worsening of long-standing dyspnea for 5 days prior to presentation. She was also suffering from diarrhea since past 2 days with edema feet and distension of abdomen. On examination, there was pallor and an irregular pulse, normal blood pressure, distended jugular veins, bilateral fine crepitations, and absent breath sounds in basal areas. Laboratory investigations showed mild anemia (hemoglobin 7.8 g/dL) and elevated serum creatinine of 3.2 mg/dL; other investigations had been normal. On ECG, the patient was found to have atrial fibrillation with low voltage complexes. The chest X-ray showed bilateral pleural effusions with a normal sized heart. Abdominal ultrasonography revealed mild ascites. On blood gas analysis, there was mixed respiratory and metabolic acidosis. The patient underwent decongestion using diuretics. However, on the second day of her admission, she had sudden cardiac arrest and could not be revived despite prolonged cardiopulmonary resuscitation.

47.2 Autopsy Findings

The heart was of normal size (weight 290 g). All chambers were of normal sizes. There were no mural thrombi or left ventricular hypertrophy. The myocardium appeared pale brown (Fig. 47.1a) with faintly discernible slightly glistening grey-white streaks, prominently seen in the subepicardial half. There was a focal fine endocardial granularity of the left atrium and thickening, nodularity, and pale yellow appearance of the free margin of the anterior mitral leaflet (Fig. 47.1b). The central nodules of all the cusps of the aortic valve also appeared prominent. The coronary circulation was right dominant. All coronaries showed focal calcific atherosclerosis.

On histology, the walls of the epicardial coronary arterial radicles (Fig. 47.1c) and the interstitium of the epicardial adipose tissue (Fig. 47.1d) showed the presence of irregular,

P. Vaideeswar (✉)
Department of Pathology (Cardiovascular and Thoracic Division), Seth Gordhandas Sunderdas Medical College and King Edward Memorial Hospital, Mumbai, India

G. Sabnis · D. Kumar
Dr KK Datey Department of Cardiology, Seth Gordhandas Sunderdas Medical College and King Edward Memorial Hospital, Mumbai, India

P. Vaideeswar (ed.), *Tropical Cardiovascular Pathology*,
https://doi.org/10.1007/978-981-19-3720-0_47

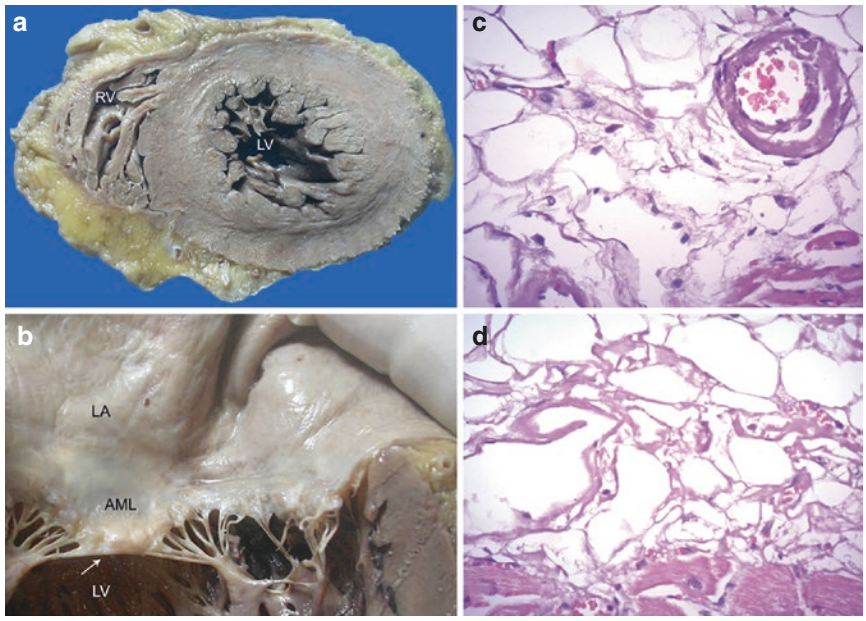

Fig. 47.1 (**a**) Transverse slice shows pale myocardium. There is an increase in the epicardial adipose tissue; (**b**) Granular texture of the left atrial LA endocardium. Note thickening and pale yellow color (arrow) of the free margin of the anterior mitral leaflet AML (*LV* left ventricle, *RV* right ventricle); (**c**) The wall of the epicardial coronary artery and (**d**) interstitium of the adipose tissue show deposition of acellular pink material (H&E × 400)

acellular, hyaline deposits. In the myocardium, the groups of cardiomyocytes were variably separated by similar irregular hyaline deposits with increased interstitial connective tissue (Fig. 47.2a, b), presence of healing and healed microinfarcts, and prominent myocytolysis in the subendocardial regions (Fig. 47.2c). Such deposits were also seen in the endocardium (Fig. 47.2d) and intramural coronary vessels (Fig. 47.3a). These accumulations were Congophilic and showed the characteristic apple-green birefringence (Fig. 47.3a, b). The mitral leaflets and aortic cusps also had similar amyloid deposits (Fig. 47.3c, d). There was widespread amyloid vasculopathy affecting all organs except the brain with prominent involvement of the kidneys and spleen (Figs. 47.4a–d and 47.5a, c). The bone marrow was normal.

Cause of Death: Cardiac amyloidosis.

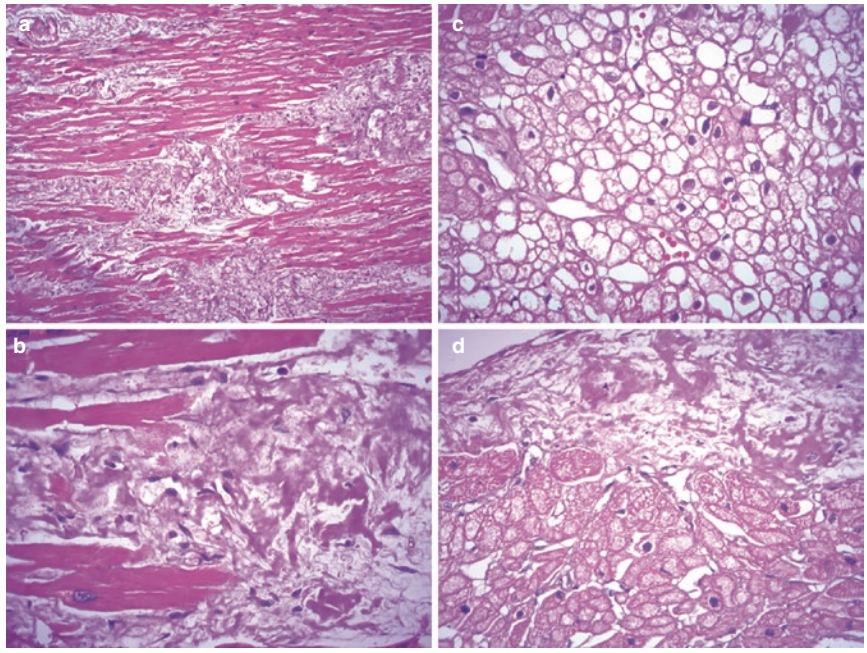

Fig. 47.2 Groups of cardiomyocytes separated by loose interstitial connective tissue that contains eosinophilic acellular material (**a**) H&E × 200 and (**b**) H&E × 400; (**c**) Pink thick shells surrounding the myocytolytic foci (H&E 400); (**d**) Irregular deposits in the thickened endocardium (H&E × 400)

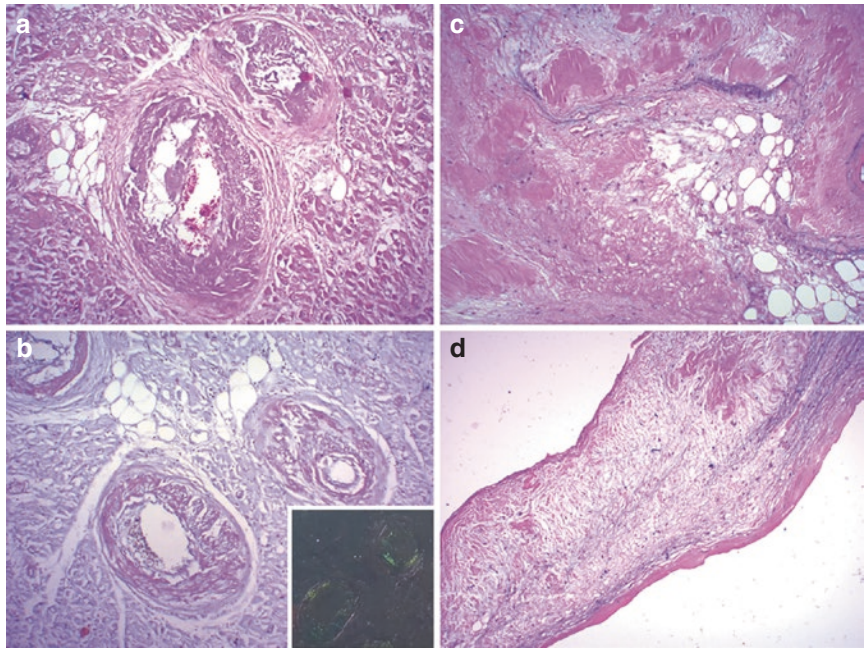

Fig. 47.3 (**a**) Deposits of acellular material in the intramural coronary vessels (H&E × 200), which were (**b**) strongly Congophilic (× 200). Inset reveals the apple green birefringence under polarized light; Similar deposits seen in the (**c**) mitral valve leaflet (H&E × 200) and (**d**) aortic valve cusps (H&E × 200)

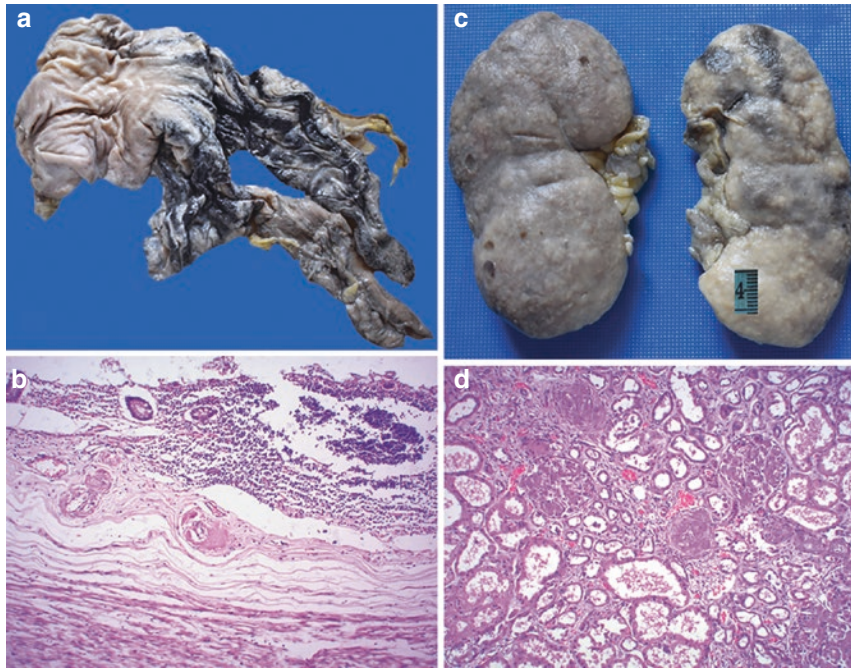

Fig. 47.4 (**a**) Gastric hemorrhages; (**b**) Vessel in the appendicular wall showing amyloid deposits; (**c**) The kidneys were small in size with a granular white appearance with congestion and retention cysts; (**d**) Extensive nodular deposits in the glomeruli (H&E × 200)

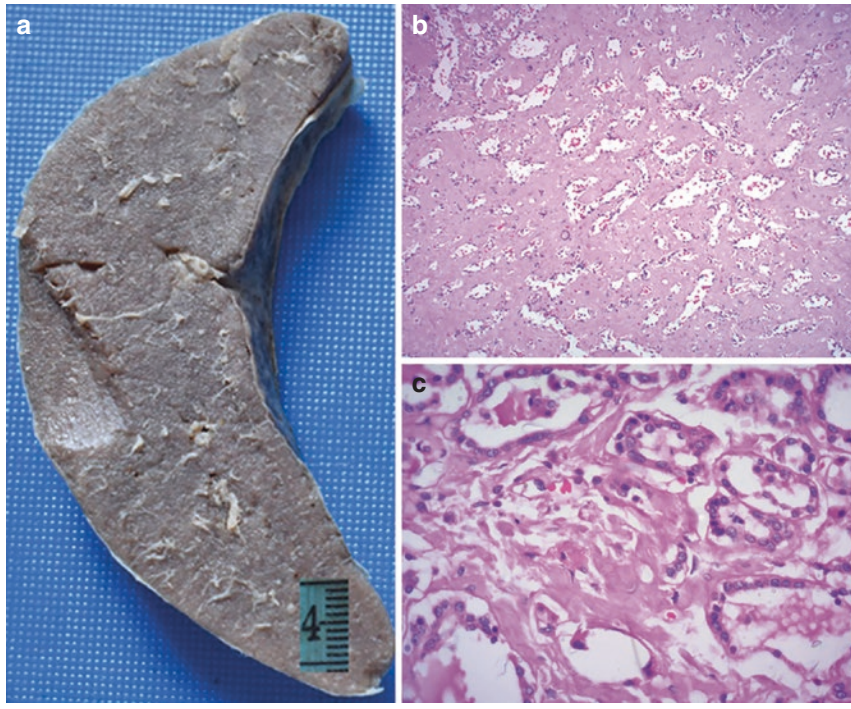

Fig. 47.5 (**a**) Cut surface of a normal sized spleen showed a typical waxy appearance—lardaceous spleen; (**b**) The red and white pulps of the spleen are completely replaced by amyloid (H&E × 200); (**c**) Amyloid deposits also seen in the thyroid (H&E × 400)

47.3 Discussion

As human lifespan increases, a significant proportion of people will reach their sixth, seventh, or even eighth decade of life. However, the geriatric population has multiple age-related comorbidities. Apart from coronary artery disease, they may also suffer from degenerative valvular diseases like calcific aortic stenosis (See Chap. 12) or regurgitation due to mitral annular calcification. In addition, there are other uncommon diseases such as systemic amyloidosis, which was detected at autopsy in this octogenarian; she presented with clinical features of biventricular failure due to extensive amyloid deposition in the heart. Amyloidosis is an example of a "conformational" disease, characterized by conversion of normal or mutant proteins into misfolded, fibrillar aggregates with deposition in the extracellular matrix of different tissues. Though more than 30 different precursor proteins are "amyloidogenic", the proteins (regardless of their chemical composition and function), when deposited as amyloid fibrils, have similar ultrastructural characteristics (nonbranching β-pleated structure), which also confer their avid binding to Congo red with apple-green birefringence on cross-polarized light, a histological hallmark. Though the deposition can occur in any tissue, some organs are preferentially affected, depending on the type of amyloid fibril and their interaction with other components of the extracellular matrix and the surrounding external milieu.

The epidemiologic data regarding the occurrence of amyloidosis are scarce owing to the large number of undiagnosed cases. It has an equal sex distribution and predominantly affects adults. In the majority of the cases, systemic disease results from misfolding of the immunoglobulin light chains (AL amyloidosis) related to abnormal proliferation of plasmacyte clone, transthyretin (ATTR amyloidosis), and amyloid associated protein (AA amyloidosis) related to chronic inflammatory states. In ATTR amyloidosis, the transthyretin is deposited as the wild-type (ATTRwt) or the mutated/variant (ATTRv) forms. The acquired forms are more frequent as compared to those which are inherited.

The overall estimated prevalence of cardiac amyloidosis is 6–10 per million populations with predominance of middle-aged or elderly individuals; much of the morbidity and mortality results from restrictive cardiomyopathy (See Chaps. 45 and 46) and heart failure with preserved ejection fraction. The heart is mainly affected by AL and ATTR amyloidoses; only minority of the patients have cardiac involvement in AA amyloidosis. In current scenario, the bone marrow was normal, which ruled out AL amyloidosis. On account of the age of the patient and the pattern of distribution, the most likely diagnosis is ATTRwt amyloidosis. It is produced by an intrinsic propensity of normal transthyretin (wild type) to misfold during senescence through unknown mechanisms, in all probability related to posttranslational protein modifications and inadequate clearance. This was formerly known as senile systemic amyloidosis and is identified at autopsy in around 25% of patients who are above the age of 80 years, especially males and often in association with calcific aortic stenosis (See Chap. 12). However, with a significant improvement in the imaging modalities, it is likely that the diagnosis of ATTRwt would increase, and in near future, it would be the most common type of cardiac amyloidosis.

An apparently disconnected array of clinical findings leads to description of cardiac amyloidosis as a 'great pretender' or 'hiding in plain sight'. The amyloid fibrils can get deposited in all layers of the heart, epicardial and/or intramural coronary arteries, and also the conduction system. The peri-cellular and/or nodular deposition of the amyloid in the myocardium causes increased thickness ("hypertrophy") and imparts a waxy or lardaceous appearance. These gross features were not very evident in the present case, though the myocardium did appear paler than usual. The amyloid fibrils lead to cellular damage through several cytotoxic pathways, leading to alterations in the cellular activities, subsequent myocardial remodeling, and interstitial fibrosis. This usually manifests in majority of the cases as restrictive cardiomyopathy with predominant signs of right

ventricular failure and presence of low-voltage ECG, as was seen in the present case. However, involvement of the kidneys, which was noted in this case, produces nephrotic syndrome and consequent proteinuria that also manifests with pedal edema and effusions. Though a normal blood pressure had been recorded in this hypertensive patient, hypotension develops due to low cardiac output and peripheral vasomotor dysfunction, which is related to amyloid vasculopathy. The vasculopathy can also lead to a clinical presentation of ischemic heart disease and to malabsorption and diarrhea, which was one of the presenting symptoms. Deposition of amyloid in the atria leads to myopathy and predisposes to mural thrombosis and atrial fibrillation. The patients can also develop various types of tachy- or brady-arrhythmias as a result of deposition in the conduction tissues. Though valves can also be involved, they seldom produce severe valvular dysfunction.

Diagnosis of cardiac amyloidosis requires a high index of suspicion and the presence of various cardiac and noncardiac symptomatic features often requires a multidisciplinary team. But it is now being increasingly recognized through newer developments in imaging techniques, particularly in early stages of the disease. Furthermore, correctly identifying the amyloid type is vital, as it has a major impact on prognosis and completely dictates different therapeutic options. Patients with ATTRwt amyloidosis are said to have a better prognosis as compared to those with light chain amyloid disease.

Further Reading

Adam RD, Coriu D, Jercan A, Bădeliţă S, Popescu BA, Damy T, et al. Progress and challenges in the treatment of cardiac amyloidosis: a review of the literature. ESC Heart Fail. 2021;8:2380–96.

Ash S, Shorer E, Ramgobin D, Vo M, Gibbons J, Golamari R. Cardiac amyloidosis: a review of current literature for the practicing physician. Clin Cardiol. 2021;44:322–31.

D'Aguanno V, Ralli M, Artico M, Russo FY, Scarpa A, Fiore M, et al. Systemic amyloidosis: a contemporary overview. Clin Rev Allergy Immunol. 2020;59:304–22.

Jamal F, Rosenzweig M. Amyloidosis with cardiac involvement: identification, characterization, and management. Curr Hematol Malig Rep. 2021;16:357–66.

Joury A, Gupta T, Krim SR. Cardiac amyloidosis: presentations, diagnostic work-up and collaborative approach for comprehensive clinical management. Curr Probl Cardiol. 2021;46:100910.

Khanna S, Lo P, Cho K, Subbiah R. Ventricular arrhythmias in cardiac amyloidosis: a review of current literature. Clin Med Insights Cardiol. 2020;14:117954680963055.

Kozak S, Ulbrich K, Migacz M, Szydło K, Mizia-Stec K, Holecki M. Cardiac amyloidosis: challenging diagnosis and unclear clinical picture. Medicina (Kaunas). 2021;57:450.

Isolated Fabry Cardiomyopathy

48

Pradeep Vaideeswar and Shobhana P. Pandit

48.1 Clinical History

A 27-year-old male suddenly collapsed while on a visit to see a hospitalized ailing relative. He was apparently healthy with no medical complaints.

48.2 Autopsy Findings

A medicolegal autopsy was performed. The heart was moderately enlarged in size (weight 415 g), slippery, and glistening with a distinct and uniform pale yellow discoloration (Fig. 48.1). There was moderate biventricular hypertrophy (right ventricle 0.8 cm and left ventricle 1.9 cm in all walls). The myocardium had a uniform pale yellow appearance. The cardiomyocytes were enlarged with abundant vacuolated cytoplasm and large hyperchromatic and even bizarre nuclei (Fig. 48.2a, b). The intervening connective tissue appeared almost scant in many areas. When the myocardial tissue was subjected to electron microscopy, the cytoplasm revealed classic 'zebra bodies" (Fig. 48.2c). All other organs were completely normal.

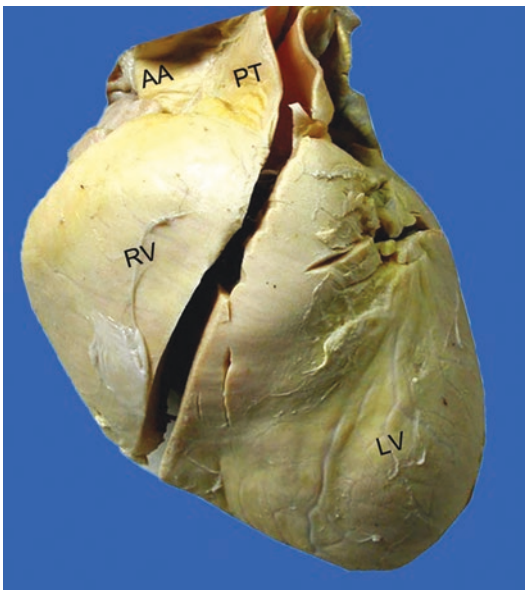

Fig. 48.1 Moderate cardiomegaly with a distinct yellow discoloration (*AA* ascending aorta, *LV* left ventricle, *PT* pulmonary trunk, *RV* right ventricle)

Cause of Death: Isolated Fabry Cardiomyopathy.

P. Vaideeswar (✉) · S. P. Pandit
Department of Pathology (Cardiovascular and Thoracic Division), Seth Gordhandas Sunderdas Medical College and King Edward Memorial Hospital, Mumbai, India

P. Vaideeswar (ed.), *Tropical Cardiovascular Pathology*,
https://doi.org/10.1007/978-981-19-3720-0_48

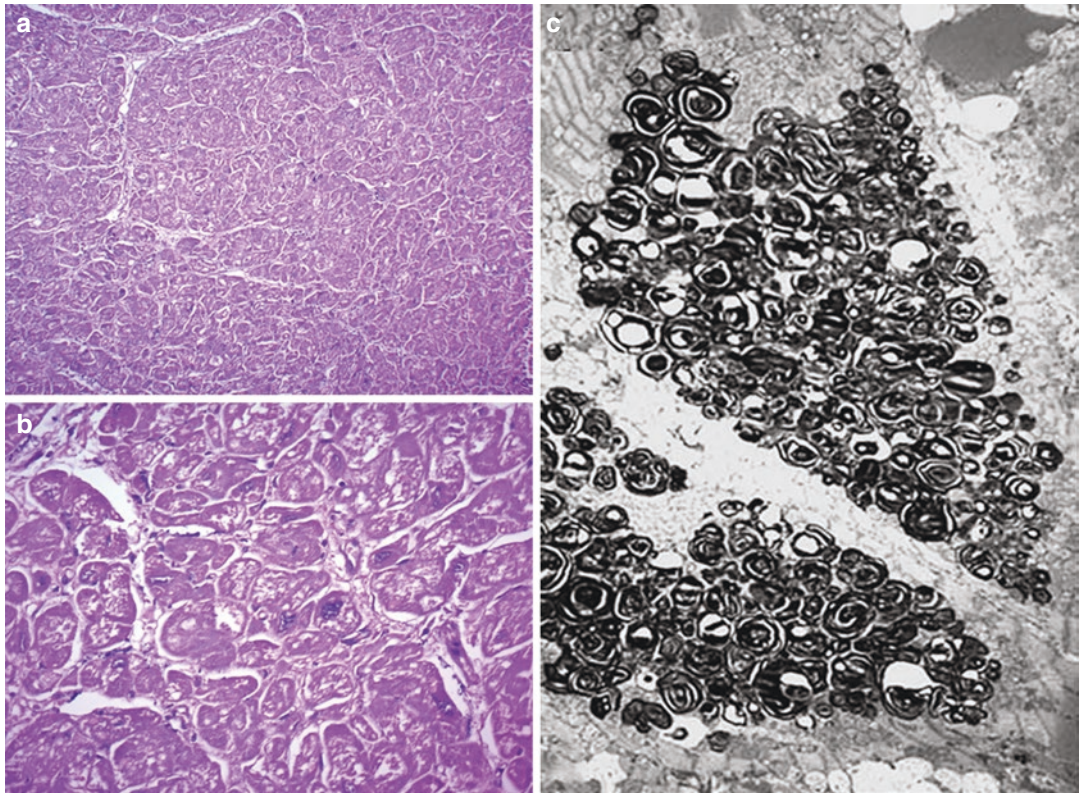

Fig. 48.2 (**a**) H&E × 200 and (**b**) H&E × 400 show hypertrophied cardiomyocytes with abundant vacuolated cytoplasm that imparts a lacework like pattern; (**c**) Electro-micrograph showing largely concentric lamellae (× 10,000)

48.3 Discussion

Biventricular hypertrophy with a yellowish discoloration of the myocardium and vacuolated cytoplasm of enlarged cardiomyocytes suggested a diagnosis of infiltrative cardiomyopathy (CMP). The presence of parallel lamellar "zebra" bodies on electron microscopy clinched the diagnosis of Fabry's disease (FD), which is now considered as the commonest example of lysosomal storage disease. The metabolic disorder, also known as Anderson-Fabry disease, results from mutations in the α-galactosidase A gene and is inherited as X-linked autosomal recessive condition. Consequently, there is absence or reduction of the activity of the enzyme α-galactosidase A, leading to accumulations of glyco-lipids (especially globotriaosylceramide and its deacylated form, globotriaosylsphingosine) in several tissues.

The commonly quoted incidence of FD in the range of 1 in 40,000 to 1 in 117,000 generally refers to the classic form, which is a multisystem disorder in which a variety of symptoms occur from childhood. This manifestation is severe in homozygous males with <1% enzyme activity, developing with nonsense/missense variants or premature stop codons. On the other hand, certain missense variants permit some degree of activity of α-galactosidase A, giving rise to the nonclassic form of the disease affecting males in the their fourth to sixth decades of life (late-onset phenotype). Both categories of patients sooner or later develop features of neurological, renal, and/or cardiac dysfunction. FD also occurs in heterozygous women who develop mild to severe disease, depending on the degree of inactivation of the X-chromosome. Interestingly, our patient had isolated involvement of the heart and such 'cardiac' variants are being increasingly recognized,

constituting 1% of the patients diagnosed with hypertrophic CMP (HCM) or unexplained left ventricular hypertrophy (LVH). Hence, there is likelihood of an underestimation of the incidence of FD. Ideally, all clinically diagnosed cases of FD should be subjected to enzymatic or genetic confirmation; this could not be done in this medicolegal autopsy where it was a surprise autopsy finding.

The accumulation of glyco-lipids in virtually all types of cells in the heart leads to progressive cardiac dysfunction, which has been termed as Fabry cardiomyopathy. The deposition not only produces alteration of cellular structure, but also results in functional impairment through disturbances in the energy generation, ion channel expressions, and endothelial function along with increased proapoptotic and pro-inflammatory signals. The outcome is compensatory hypertrophy, ischemia, and fibrosis. The LVH is usually concentric and depends on the degree of involvement of the cardiomyocytes. Sometimes, the hypertrophy can also be asymmetric along with disarray mimicking HCM. In the present case, the deposition was mainly present in the perinuclear without involvement of interstitium and intramural coronary vessels, indicating a recent onset of the disease. The deposits in the tissues are demonstrated by frozen sections, where they appear Sudanophilic, periodic acid-Schiff positive, and are strongly birefringent. The fibrosis is most commonly seen in the basal posterolateral region, affecting the mid-myocardial portion and may be rarely associated with aneurismal dilatations. The hypertrophy and fibrosis lead most commonly to manifestations of heart failure, while some patients develop arrhythmias or conduction defects, including sudden death, an unfortunate incident noted in our case. However, advanced imaging modalities and effective therapeutic options (enzyme-replacement treatment in particular) have played an important role in the diagnosis and prognosis of patients with FD. Therefore, young patients with unexplained LVH should be screened for FD to prevent disastrous consequences.

Further Reading

Azevedo O, Cordeiro F, Gago MF, Miltenberger-Miltenyi G, Ferreira C, Sousa N, et al. Fabry disease and the heart: a comprehensive review. Int J Mol Sci. 2021;22:4434.

Bernardes TP, Foresto RD, Kirsztajn GM. Fabry disease: genetics, pathology, and treatment. Rev Assoc Med Bras. 2020;66(Suppl 1):s10–6.

Hagège A, Réant P, Habib G, Damy T, Barone-Rochette G, Soulat G, et al. Fabry disease in cardiology practice: literature review and expert point of view. Arch Cardiovasc Dis. 2019;112:278–87.

Kok K, Zwiers KC, Boot RG, Overkleeft HS, Aerts JMFG, Artola M. Fabry disease: molecular basis, pathophysiology, diagnostics and potential therapeutic directions. Biomol Ther. 2021;11:271.

Nair V, Belanger EC, Veinot JP. Lysosomal storage disorders affecting the heart: a review. Cardiovasc Pathol. 2019;39:12–24.

Pieroni M, Moon JC, Arbustini E, Barriales-Villa R, Camporeale A, Vujkovac AC, et al. Cardiac involvement in Fabry disease. JACC review topic of the week. J Am Coll Cardiol. 2021;77:922–36.

Yim J, Yau O, Yeung DF, Tsang TSM. Fabry cardiomyopathy: current practice and future directions. Cell. 2021;10:1532.

49 Acute Myocardial Calcification: Sepsis-Related?

Pradeep Vaideeswar

49.1 Clinical History

A 66-year-old male, with a history of diabetes mellitus for 'many' years (on irregular therapy), was admitted for left lower limb cellulitis. The investigations have been tabulated (Table 49.1). An initial debridement of the wound was followed by a left below-knee amputation after 24 days, under the cover of insulin infusion and antibiotics. A day after operation, he developed sudden onset of severe shortness of breath and expired.

Table 49.1 Investigations

Investigations	
Hematological	Hemoglobin: 7.4 g/dL[a] Total WBC count: 29,550/cmm[a] (neutrophil predominant differential count) Platelet count: 1.6 lakhs/cmm[a] Normal coagulation profile
Biochemical	Plasma glucose: Mean 78.2 mg/dL[a] Blood urea nitrogen: 28.2 mg/dL[a] Creatinine: 2.75 mg/dL[a]
Others	HIV/HBsAg: Negative Pus swab cultures: *Pseudomonas* and *Klebsiella* species

[a]Mean values

P. Vaideeswar (✉)
Department of Pathology (Cardiovascular and Thoracic Division), Seth Gordhandas Sunderdas Medical College and King Edward Memorial Hospital, Mumbai, India

P. Vaideeswar (ed.), *Tropical Cardiovascular Pathology*,
https://doi.org/10.1007/978-981-19-3720-0_49

49.2 Autopsy Findings

The heart, at autopsy, showed very remarkable features. It was mildly enlarged in size and weighed 340 g. There was a distinct pale-yellow discoloration of the superficial myocardium affecting the middle and apical portions of the posterior wall of the left ventricle (Fig. 49.1a). Serial transverse sections of the ventricles revealed nontransmural, subepicardial, and mid-myocardial slightly glistening (almost wet paint-like in the fresh state), pale yellow firm areas (Fig. 49.1b). The yellow areas were easy to cut and present almost diffusely in the posterior, lateral, and septal walls (from the base to the apex) and focally in the mid-portion of the anterior wall. The apical third of the left ventricular cavity was obliterated by a shaggy reddish-brown thrombus (Fig. 49.1b). The right coronary artery had a dominant distribution; the arteries were patent with no significant atherosclerosis. To our surprise, the yellowish foci were seen to be composed of large groups of calcified, viable myofibers (Fig. 49.2a–c). Foci of coagulative necroses of the cardiomyocytes or foci of healed infarction were not present. No calcification was seen in the right ventricle. There was mural infective endocarditis (Fig. 49.2c). Other autopsy findings included pulmonary thromboembolism, diffuse alveolar damage, bronchopneumonia, mixed dust pneumoconiosis with centrilobular emphysema, and diabetic nephropathy. The parathyroids were normal.

Cause of Death: Pulmonary thromboembolism.

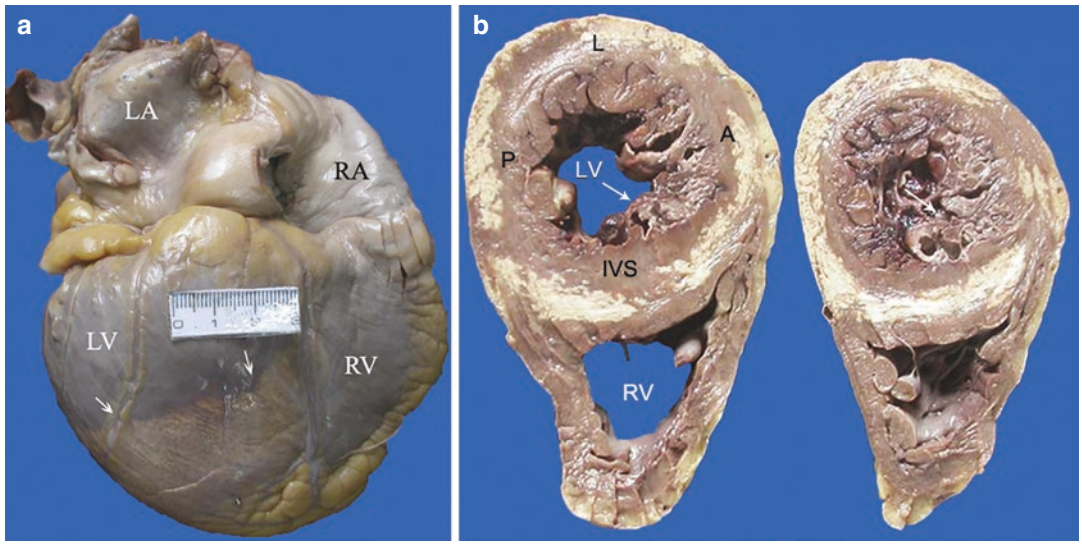

Fig. 49.1 (**a**) Posterior aspect of the heart showing a yellowish discoloration (arrows) in the mid- and apical portions; (**b**) The transverse slices showed the presence of yellowish discoloration in all the walls, prominently in the subepicardial regions. Mural to occlusive thrombus (arrows) were present in the apical one-third of the left ventricular LV cavity. Note that the calcification in the interventricular septum IVS is towards the LV aspect (*A* anterior wall, *L* lateral wall, *LA* left atrium, *P* posterior wall, *RA* right atrium, *RV* right ventricle)

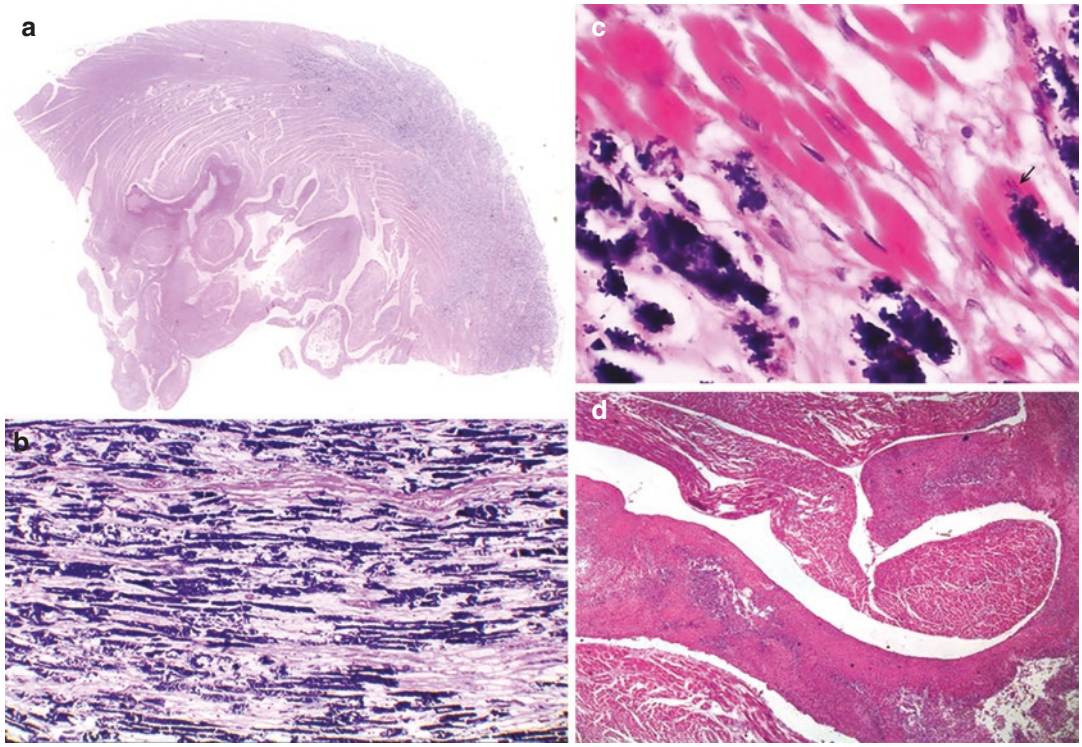

Fig. 49.2 (**a**) Scan of the section taken towards the apical one-third showing epicardial basophilic appearance and mural thrombus (H&E); (**b**) The entire section showed presence of calcification seen as granular basophilic material (H&E × 200); (**c**) Cytoplasmic calcific deposits. Note retention of the nuclei (arrow) in some of the cardiomyocytes (H&E × 400); (**d**) Mural endocarditis (H&E × 100)

49.3 Discussion

Calcification of viable cardiomyocytes affecting a wide area of the left ventricular myocardium, unrelated to coronary arterial distribution, was found in a setting of sepsis; there was no associated calcification of the pericardium or endocardium. The pathology in this case appeared to be of uncertain significance since echocardiography or other cardiac imaging modalities and estimations of cardiac biomarkers had not been performed. Pathological calcification is the abnormal deposition of insoluble calcium salts in tissues. The 2 forms of pathologic calcification are dystrophic, when calcium deposition occurs locally in the dying or dead tissues with normal serum levels of calcium, and metastatic calcification, which occurs in otherwise normal tissues, secondary to disturbances in calcium metabolism with ensuing hypercalcemia. Clinicians and pathologists also often encounter calcification in the cardiovascular system, occurring through similar mechanisms. As in other organs, in the heart too dystrophic calcification is more common than metastatic. This may affect one or more layers of the heart and assumes different morphologies and is known to occur rapidly from days to months after the insult. At a later stage, the differentiation between dystrophic and metastatic calcifications becomes blurred. When present, the calcific deposits may cause or accelerate cardiac dysfunction; hence, identification of these during life influences therapeutic options.

In the older age groups, the calcification is usually seen with healing of transmural myocardial infarcts, where the calcific deposits are distributed in a curvilinear fashion at the periphery of the infarcted zone. In present case, there was no previous history of ischemic heart disease. The autopsy too did not reveal regional scarring

and the epicardial coronary arteries were patent, devoid of significant atherosclerosis. In addition, in older patients there can be extension of calcification into the myocardium for varying degrees in patients with calcific aortic stenosis (where the calcification is of the metaplastic type, See Chap. 12) and mitral annular calcification. Such valvular involvement was not seen in this heart. Large calcific nodules with cardiac distortion through unexplained mechanisms have also been reported. In all such cases, the calcification with or without osseous metaplasia is predominantly identified in the myocardial interstitium. In the case presented, the calcium appeared to have been deposited in a short duration within the cytoplasm of many cardiomyocyte groups; there was preservation of their nuclei despite extensive cytoplasmic calcium. Furthermore, it occurred in a setting of sepsis, but devoid of myocarditis or micro-abscesses (See Chap. 36), though the heart showed mural infective endocarditis.

Sepsis is now defined as life-threatening organ dysfunction triggered by dysregulation of the host response to infection (particularly Gram-negative bacteria) and the lungs are the favored targets, manifesting as diffuse alveolar damage, as noted in this patient at autopsy. However, the circulating inflammatory cytokines can also induce transient cardiac dysfunction seen as left, right, or global systolic or diastolic dysfunctions, which has been referred to as septic cardiomyopathy (CMP) or sepsis-induced CMP. Current interest is focused on mitochondrial dysfunction caused by oxidative stress with resultant cardiac energy failure. But, there are other equally compelling mechanisms put forth to explain the sepsis-related myocardial calcification such as microvasculature derangement, circulating myocardial depressants and myofibrillar hypocontractility, apoptosis and autophagy, autonomic nervous system dysfunction, and importantly abnormal intracellular calcium homeostasis. Increased membrane permeability and endoplasmic reticulum stress during sepsis leads to excessive cytoplasmic accumulation of the calcium ions leading to this phenomenon; the cardiomyocytes show varying degrees of myocytolyses followed by necroses. In most cases, the calcification is exclusively left ventricular. In this case, apart from Gram-negative septicemia, an element of renal dysfunction due to diabetic nephropathy was present with a possibility of disturbance of calcium homeostasis and metastatic calcification, which have been a common scenario in the cases that have been previously reported. The mean duration of development of the calcification was 27 days. Though the condition appears uncommon, it is likely that it is underrecognized and there are increased chances of diagnosis of such a condition with sophisticated imaging modalities. Since there is often multiorgan failure in sepsis, its contribution to mortality is still unclear. In the present case, the cause of death was related to pulmonary thromboembolism and the patient did not apparently have symptoms and signs related to the calcification. Nevertheless, follow-up of sepsis survivor patients diagnosed with diffuse myocardial calcification would be important as some may develop restrictive cardiomyopathy or arrhythmias.

Further Reading

Ahmed T, Inayat F, Haq M, Ahmed T. Myocardial calcification secondary to toxic shock syndrome: a comparative review of 17 cases. BMJ Case Rep. 2019;12:e228054.

Hollenberg SM, Singer M. Pathophysiology of sepsis-induced cardiomyopathy. Nat Rev Cardiol. 2021;18:424–34.

Nance NW Jr, Crane GM, Halushka MK, Fishman EK, Zimmerman SL. Myocardial calcifications: pathophysiology, etiologies, differential diagnoses, and imaging findings. J Cardiovasc Comput Tomogr. 2015;9:58–67.

Ravikumara N, Sayed MA, Poonsupha CJ, Sehgala R, Shirke MM, Harky A. Septic cardiomyopathy: from basics to management choices. Curr Probl Cardiol. 2021;46:100767.

Torfs M, Salgado R, Van Herck P, Corthouts B, Robert D, Parizel PM. A curious case of acute myocardial calcifications. Circulation. 2016;133:e426–7.

Wang R, Xu Y, Fang Y, Wang C, Xue Y, Wang F, et al. Pathogenetic mechanisms of septic cardiomyopathy. J Cell Physiol. 2021;237(1):49–58.

50 Cardiac Involvement in Primary Hyper-Oxaluria

Pradeep Vaideeswar and Gwendolyn Fernandes

50.1 Clinical History

A 25-year-old male was diagnosed as chronic kidney end-stage disease consequent to bilateral nephrolithiasis. He was on bi-weekly maintenance hemodialysis, and later, bilateral nephrectomies were performed to avoid infection of a future graft. After 10 months, he received a live-related renal transplant and was given triple immunosuppression of tacrolimus, mycophenolate mofetil, and prednisolone. The immediate posttransplant graft function was good, but his serum creatinine levels rose from 1.1 mg/dL on the 5th posttransplant day to 2.6 mg/dL by the 4th posttransplant week. A biopsy of the transplant kidney was reported as acute rejection with crystals filling all tubular lumina. The graft rejection was treated with pulse methyl prednisolone and the tacrolimus dose was also stepped up. He was transferred to our institute on the 8th posttransplant week as there was no improvement in graft function (serum creatinine of 3.6 mg/dL). A review of the histopathology slides of the previous nephrectomies and graft biopsy showed extensive deposition of calcium oxalate crystals in the tubules, interstitium, blood vessels, and sclerosed glomeruli; there were no features of rejection. On further investigations, his urinary oxalate levels were found to be 124 mg/day (normal urine oxalate levels <45 mg/day) and a skin biopsy revealed oxalate crystals in dermal blood vessels. A retrospective diagnosis of primary hyper-oxaluria with recurrence in the renal allograft was made and the patient was treated with pyridoxine.

In the 9th posttransplant week, the patient developed fever, breathlessness, abdominal pain, tenderness over the site of the transplanted kidney, and necrotizing skin lesions of the lower limb. This was followed by an episode of generalized tonic-clonic seizure and left hemiplegia. Serum creatinine levels rose to 6.8 mg/dL. A chest radiograph was normal. Blood and urine cultures were negative. Computed tomography scans of the brain showed an infarct in the frontal lobe of the brain and an ultrasonography of the abdomen showed infarcts of the kidney. His condition kept worsening with the development of altered sensorium, metabolic acidosis, hypotension, and shock. He died 10 weeks after the renal transplantation.

50.2 Autopsy Findings

A complete autopsy was performed. The heart was mildly enlarged in size (weight 350 g) with mild concentric left ventricular hypertrophy and streaky fibrosis. All other chambers and

P. Vaideeswar (✉)
Department of Pathology (Cardiovascular and Thoracic Division), Seth Gordhandas Sunderdas Medical College and King Edward Memorial Hospital, Mumbai, India

G. Fernandes
Department of Pathology, Seth Gordhandas Sunderdas Medical College and King Edward Memorial Hospital, Mumbai, India

P. Vaideeswar (ed.), *Tropical Cardiovascular Pathology*,
https://doi.org/10.1007/978-981-19-3720-0_50

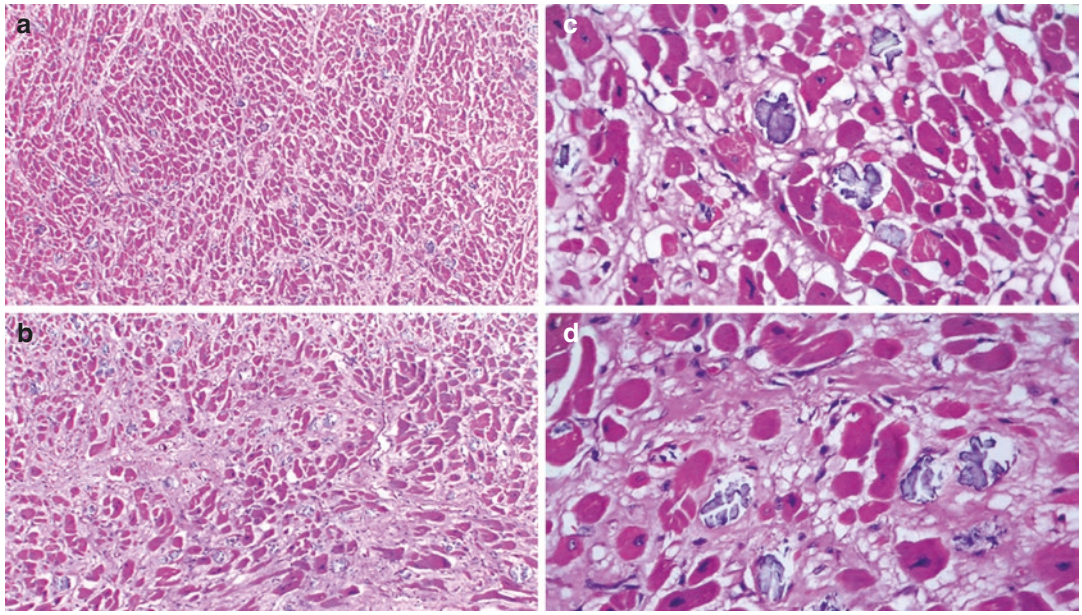

Fig. 50.1 Glassy, irregular, lightly basophilic calcium oxalate crystals are deposited in the myocardium with varying degrees of interstitial fibrosis—(**a**), (**b**) H&E × 200 and (**c**), (**d**) H&E × 400

valves were normal. The right coronary artery had a dominant distribution; there was hardly any atherosclerosis. But on histology, there was wide separation of the hypertrophied cardiomyocytes by very prominent interstitial and interfiber connective tissue with deposits of calcium oxalate crystals (Fig. 50.1a–d). The media of all the epicardial coronary arteries were distorted and even expanded by similar crystals (Fig. 50.2a, b). Similar crystals affected the vessels in most of the organs studied and were also found in the renal tubules (Fig. 50.2c, d). Additionally, there was disseminated zygomycosis producing acute infarcts in the brain, liver, spleen, transplanted kidney with invasive pulmonary mycosis, and small intestinal gangrene.

Cause of Death: Disseminated zygomycosis.

50.3 Discussion

Widespread tissue deposition of calcium oxalate crystals was a prominent feature in this autopsy, which indicated the presence of disordered oxalate metabolism. Such patients have hyper-oxaluria, where urinary excretion of oxalate exceeds 40–45 mg in 24 h, as compared to the normal range of 10–40 mg. The cause for the increased excretion may be primary or secondary. Primary hyper-oxalurias (PH) are a group of autosomal recessive disorders caused by deficiency of 3 hepatic oxalic acid metabolic enzymes, which are alanine-glyoxylate aminotransferase, glyoxylate reductase/hydroxypyruvate reductase, and 4-hydroxy-2-oxoglutarate; they result in types I, II, and III PHs, respectively. On the other hand, secondary hyperoxaluria results from increased intestinal absorption, excessive dietary intake of rich oxalate precursors (food or supplements), alterations in certain microbial intestinal flora and chronic renal dysfunction (unrelated to oxalate metabolism).

In view of the young age of the patient, the presence of bilateral nephrolithiasis, and end-stage renal disease, the likely diagnosis in this case is PH. This was a retrospective diagnosis in our case and hence enzyme levels were not done. Lack of specific enzymes results in accumulation of glyoxylate and overproduction of oxalate, which outstrips the renal capacity. There is then urolithiasis, renal damage, further reduction in oxalate, hyper-oxalemia (exceed-

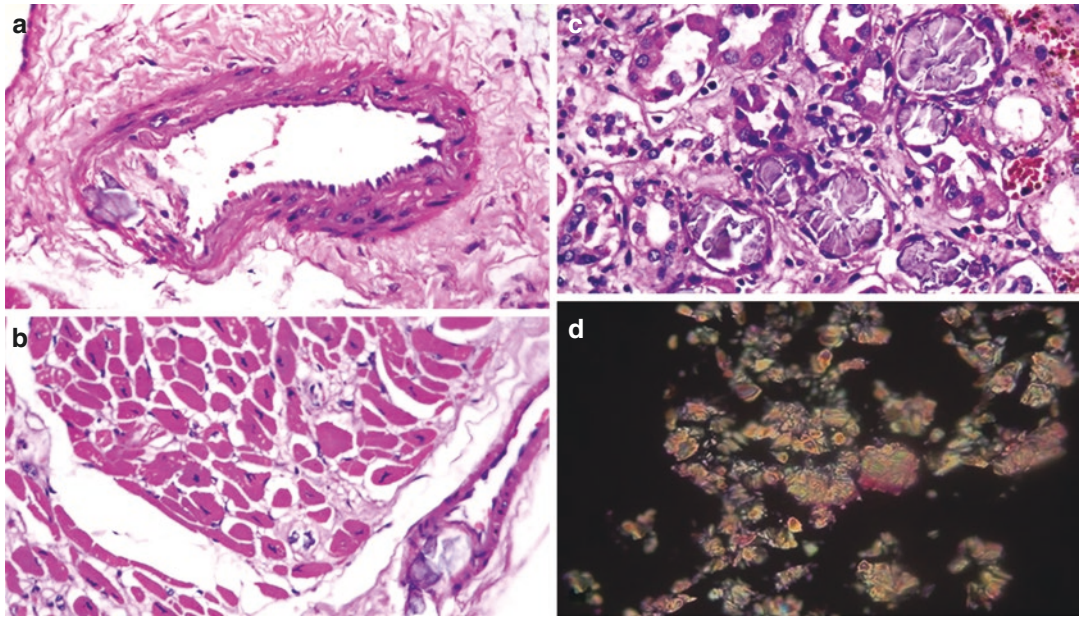

Fig. 50.2 Calcium oxalate crystals were seen in (**a**) epicardial and (**b**) intramural coronary arteries (H&E × 200); (**c**) Crystals occluding the tubular lumina of the donor kidney (H&E × 400); (**d**) Colorful appearance on polarizing microscopy (× 400)

ing the normal values of 30–45 μmol/L), and subsequent calcium oxalate deposition in various tissues. Majority of the patients have Type I PH (nearly 80%) with a prevalence of 1–3 per 100,000 live births. Since the primary mode of excretion of oxalate is through glomerular filtration, renal dysfunction is the common and the first manifestation of PH. With progressive decline in the renal function, nephrocalcinosis caused by calcium oxalate deposits in the kidneys is accompanied by similar deposits in various organs, particularly the musculoskeletal, cardiovascular, and peripheral nervous systems, including the retina and skin. The symptoms arising from extrarenal tissue depositions vary from patient to patient and this tissue accumulation may decrease the levels of plasma oxalate.

Though the exact incidence is not known, cardiac involvement may be seen in almost 70% of patients with PH. The crystals are deposited in the conduction tissue, coronary vessels, and myocardium, where they often elicit inflammatory and fibrogenic responses and produce increased wall thickness with effects similar to cardiac amyloidosis (See Chap. 47). The patients can manifest features related to restrictive cardiomyopathy, heart failure, conduction system blocks, tachy—or brady-arrhythmias, and rarely atrioventricular valvular regurgitations and even pulmonary hypertension. Hence, such an involvement is the major cause for mortality in these patients and calls for appropriate imaging modalities such as cardiac computed tomography or magnetic resonance imaging; these obviate the need of the invasive, but gold standard procedure of endo-myocardial biopsy. It is to be noted that coexisting hypertension can also produce cardiac abnormalities, especially left ventricular hypertrophy. Interstitial and interfibrillar fibrosis was seen prominently in our case. However, no cardiological investigations had been performed due to absence or masking of the cardiac symptoms by an overwhelming fungal infection that is frequently seen with kidney transplantation (See Chap. 19). Ideally, a liver or a combined liver/kidney transplant would have been the definitive therapy. The diagnosis of PH was unfortunately not made in the pretransplant workup, where the patient had received mainly renal replacement therapy with pyridoxine during the current admission.

Further Reading

Albakri A. Deposition diseases cardiomyopathy: a review and pooled analysis of pathophysiology, diagnosis and clinical management. Trends Res. 2019;2:1–2.

Bhasin B, Ürekli HM, Atta MG. Primary and secondary hyperoxaluria: understanding the enigma. World J Nephrol. 2015;4:235–44.

Mookadam F, Smith T, Jiamsripong P, Moustafa SE, Monico CG, Lieske JC, et al. Cardiac abnormalities in primary hyperoxaluria. Circ J. 2010;74:2403–9.

Sweet ME, Mestroni L, Taylor MRG. Genetic infiltrative cardiomyopathies. Heart Fail Clin. 2018;14:215–24.

Endocardial Fibroelastosis

51

Pragati Sathe and Pradeep Vaideeswar

51.1 Clinical History

A 3-day-old male child, admitted in respiratory distress, could not be salvaged. A lower segment Cesarean section had been performed in view of meconium aspiration. The birth weight was 2360 g. An antenatal ultrasonography had revealed the possibility of hypoplastic left heart syndrome (HLHS). On examination, the general condition was very poor with a heart rate of 148 per minute and respiratory rate of 88 per minute. The chest X-ray had shown bilateral opacities in the lower zones.

51.2 Autopsy Findings

The heart was mildly enlarged in size (weight 25 g). There was marked enlargement of the right atrium and ventricle; the apex was formed by the right ventricle (Fig. 51.1). The left ventricle (LV) was small in size and was bound by tortuous coronary arteries (Fig. 51.1). The great arteries had a normal relationship. The pulmonary trunk was larger than the aorta and a patent ductus arteriosus (0.8 cm in length), as large as the ascending aorta, was present at its usual site (Fig. 51.1). On open-

Fig. 51.1 Anterior surface showing an enlarged right ventricle RV forming the apex. Only a small part of the left ventricle LV is seen. Patent ductus PDA is present (*AA* ascending aorta, *DTA* descending thoracic aorta, *LAA* left atrial appendage, *PT* pulmonary trunk, *RAA* right atrial appendage)

P. Sathe
Department of Pathology, Seth Gordhandas Sunderdas Medical College and King Edward Memorial Hospital, Mumbai, India

P. Vaideeswar (✉)
Department of Pathology (Cardiovascular and Thoracic Division), Seth Gordhandas Sunderdas Medical College and King Edward Memorial Hospital, Mumbai, India

P. Vaideeswar (ed.), *Tropical Cardiovascular Pathology*,
https://doi.org/10.1007/978-981-19-3720-0_51

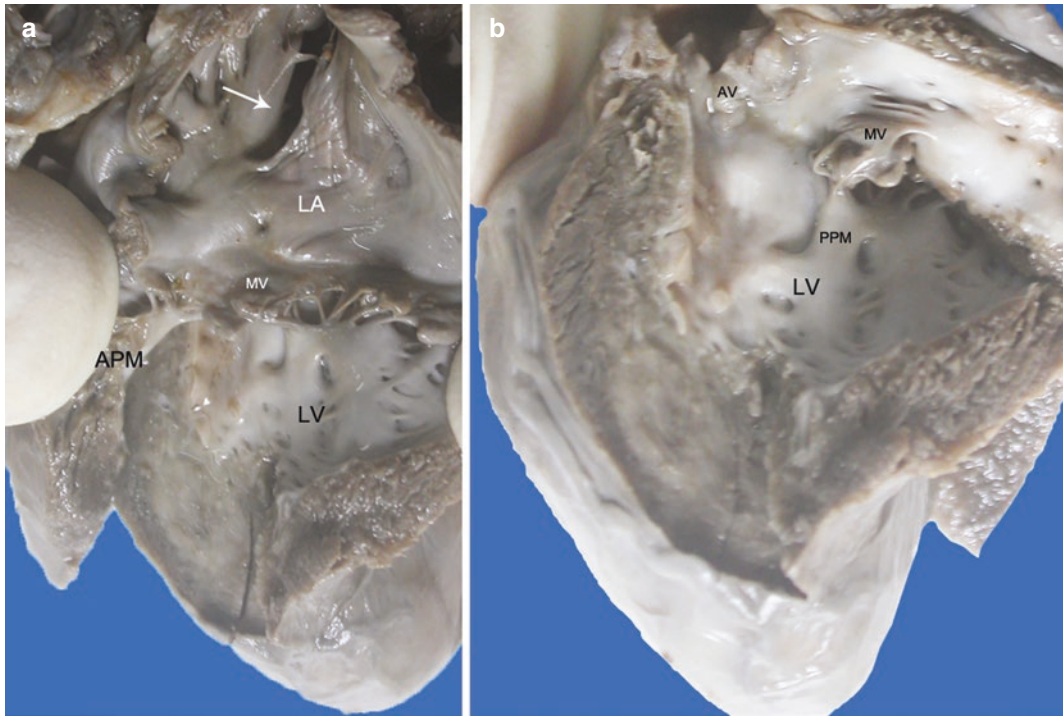

Fig. 51.2 Left ventricular LV (**a**) Inflow and (**b**) Outflow tracts showing small-sized cavity which is lined by very thick pearly white endocardium. The arrow points to the patent foramen ovale. Note attenuation and plastering of the posterior papillary muscle PPM and smoothening of the trabeculae (*APM* anterior papillary muscle, *AV* aortic valve, *LA* left atrium, *MV* mitral valve)

ing, the right-sided chambers were dilated and lined by normal endocardium. The fossa ovalis showed a patent foramen ovale (Fig. 51.2a). The LV cavity was small in size with marked pearly white thickening of the endocardium (Fig. 51.2a, b). It had produced smoothening of the trabeculae carneae and even plastering of the posterior papillary muscle of the mitral valve (Fig. 51.2a) with extension onto the outflow tract (Fig. 51.2b). The mitral annulus was dilated with mild dysplasia of its leaflets; there was a bicuspid aortic valve (anterior-posterior type, See Chap. 13). The coronary ostia arose from the larger anterior sinus on either side of the low-set raphe. Microscopically, the endocardium was composed of fibroelastotic tissue (Fig. 51.3a–c). The lungs showed focal meconium aspiration (Fig. 51.3d). Other organs were normal and devoid of any congenital anomaly.

Cause of Death: Endocardial fibroelastosis (EFE).

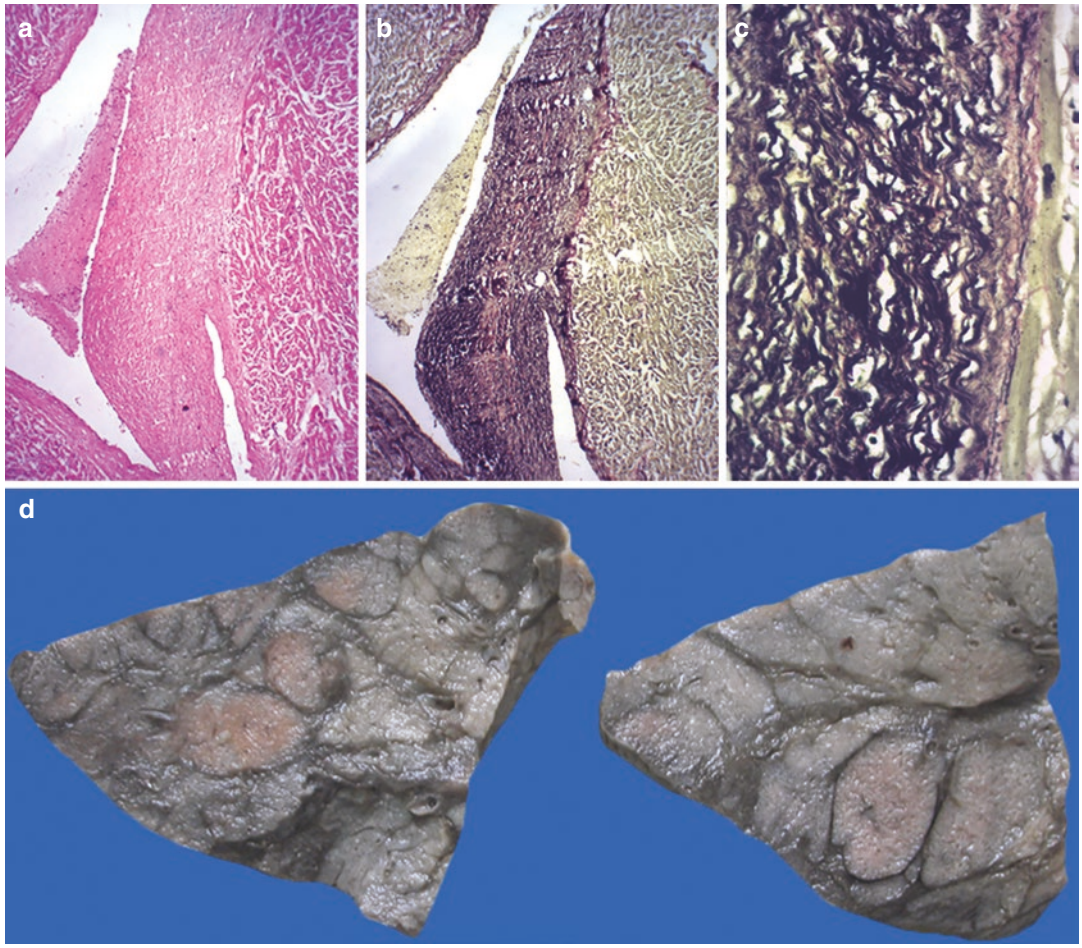

Fig. 51.3 (**a**) Left ventricle lined by very thick endocardium (H&E × 100); (**b**) Endocardium stained black and red (elastic van Gieson × 100); (**c**) Thick elastic fibers of varying lengths (elastic van Gieson × 400); (**d**) Meconium aspiration seen as faintly yellowish deposits in the lung parenchyma

51.3 Discussion

A prenatal diagnosis of HLHS was made in this 3-day-old neonate. However, at autopsy, there was no mitral atresia or congenital mitral stenosis, and the aortic valve was bicuspid. A remarkable finding was small sized, muscle bound left ventricle (LV), lined by exceedingly thick fibroelastotic endocardium. This pearly-white sugar icing-, porcelain- or cartilage-like endocardial thickening characterizes EFE, which is an uncommon disease of obscure etiology with an incidence at birth estimated at 1 in 5000. It occurs predominantly in children, often diagnosed between 3–6 months of age. It forms the commonest cause for restrictive cardiomyopathy (CMP) with a clinical presentation of unexplained heart failure or unexpected death. It can be diagnosed antenatally, and the earliest detection has been reported at 14 weeks of gestation. In a review of pediatric heart transplantations, evidence of EFE was found in one-fourth of the patients, suggesting that this condition may not be as uncommon as previously thought.

The categorization of EFE into primary and secondary subtypes depends on the presence or absence of associated congenital cardiac malformations. The associated structural heart diseases

include HLHS, congenital aortic stenosis, patent ductus arteriosus, coarctation of aorta, and anomalous origin of the left coronary artery from pulmonary artery. In those patients devoid of cardiac anomalies, genetic predispositions (mostly autosomal recessive), infections, nutritional deficiencies, transplacental passage of maternal antibodies, and hypoxia during cardiac development are suggested as the possible causes. However, few authors believe that all cases of EFE are secondary. The endocardial thickening is triggered by myocardial stress through aberrant endothelial to mesenchymal transition in the endocardium. Although the endocardium is thickened, the ventricular myocardium thickness is within the reference range and largely devoid of fibrosis. These features differentiate EFE from another form of restrictive CMP, i.e., endomyocardial fibrosis (See Chap. 46). Among the two pathological types of primary EFE, the dilated form is more common and can mimic the idiopathic dilated CMP. Dilated EFE is characterized by a markedly enlarged globular heart, mainly involving the LV and left atrium. There is diffuse endocardial thickening of the LV, which is most marked in the outflow tract. The less common contracted type of EFE is associated with a hypoplastic (as seen in the current case) or normal LV size. The right-sided chambers and left atrium, apart from enlargement or hypertrophy, hardly showed any endocardial sclerosis. The associated ASD could have contributed to the right-sided enlargement. Half the cases of EFE have a biventricular involvement; isolated LV or right ventricular thickening is seen in 40% and 10% cases, respectively. Papillary muscles and trabeculae carneae are flattened and partially incorporated in the fibrotic process, giving a smooth appearance to the cavity. They also exert traction on the chordae tendineae and valvular leaflets or cusps, leading to faulty leaflet apposition resulting in valvular mitral incompetence. Since it is a progressive lesion, there is a spectrum of endocardial changes ranging from microscopic thickening to gross changes. The endocardial fibrosis acts as a substrate for mural thrombosis, predisposing to systemic emboli.

The common presentation in infants and young children is with congestive heart failure as seen in the present case as well. Few reports also mention about the occurrence of conduction disturbances and arrhythmias such as first-degree heart block, atrial fibrillation, or tachycardia. In general, EFE and in particular the contracted form have a grave prognosis and the treatment is cardiac transplantation. If the condition is diagnosed before the need for cardiac transplantation, endocardial stripping is another method of treatment in these patients. When diagnosed antenatally, it is advisable to terminate the affected pregnancy.

Further Reading

Lurie PR. Changing concepts of endocardial fibroelastosis. Cardiol Young. 2010;20:115–23.

Reyes JA, Dipchand AI, Chiasson DA. Paediatric dilated cardiomyopathy with and without endocardial fibroelastosis: a pathological analysis of 89 explants. Cardiol Young. 2021:1–7. https://doi.org/10.1017/S1047951121003590.

Sana MK, Mahajan M. Endocardial fibroelastosis. In: Stat Pearls [Internet]. Treasure Island, FL: Stat Pearls; 2021.

Seki A, Patel S, Ashraf S, Perens G, Fishbein MC. Primary: an underappreciated cause of cardiomyopathy in children. Cardiovasc Pathol. 2013;22:345–50.

Weixler V, Hammer PE, Marx GR, Emani SM, del Nido PJ, Friehs I. Flow disturbances and progression of endocardial fibroelastosis: a case report. Cardiovasc Pathol. 2019;42:1–3.

Xu X, Friehs I, Zhong HT, Melnychenko I, Tampe B, Alnour F, et al. Endocardial fibroelastosis is caused by aberrant endothelial to mesenchymal transition. Circ Res. 2015;116:857–66.

Part VIII

Cardiac Tumors

52 Neonatal Multifocal Rhabdomyomas

Tejaswini Waghmare and Pradeep Vaideeswar

52.1 Clinical History

A 2-day-old male child was delivered by an emergent lower-segment Cesarean section in a 30-year-old woman with an antenatal diagnosis of oligohydramnios. The birth weight was 1.086 kg with the Apgar score of 6/10 at 1 min and 8/10 at 5 min. The baby was transferred to neonatal intensive care unit in view of very low birth weight. On examination, the vital parameters were stable. However, the baby had not passed urine for more than 24 h despite administration of lasix bolus. The hematological, biochemical, and radiographic investigations were normal. The neonate was found unresponsive on the 2nd day.

52.2 Autopsy Findings

A complete postmortem examination revealed remarkable findings in the heart; other organs were normal. The heart weighed 26 g and showed epicardial opacification with faint focal undulations on the surfaces of both ventricles. On opening the heart, there were multiple soft to firm, biventricular endocardial polypoidal projections (Fig. 52.1a). A cross section of the ventricles revealed glistening, pale-yellow nodules of varying sizes (Fig. 52.1b, c) with obliteration of the apices. All the nodules were composed of large distended cardiomyocytes with cytoplasmic vacuolations (Fig. 52.2a). Eosinophilic cytoplasmic strands radiated from the nucleus towards the periphery, giving rise to the characteristic "spider cell" (Fig. 52.2b). Some clusters were entirely microscopic while many of them also showed small foci of dystrophic calcification (Fig. 52.2b, c). Microscopic tumors, comprising small groups of large vacuolated cells, were also present. The brain and other organs were normal.

Cause of Death: Multifocal cardiac rhabdomyomas.

T. Waghmare
Department of Pathology, Seth Gordhandas Sunderdas Medical College and King Edward Memorial Hospital, Mumbai, India

P. Vaideeswar (✉)
Department of Pathology (Cardiovascular and Thoracic Division), Seth Gordhandas Sunderdas Medical College and King Edward Memorial Hospital, Mumbai, India

P. Vaideeswar (ed.), *Tropical Cardiovascular Pathology*,
https://doi.org/10.1007/978-981-19-3720-0_52

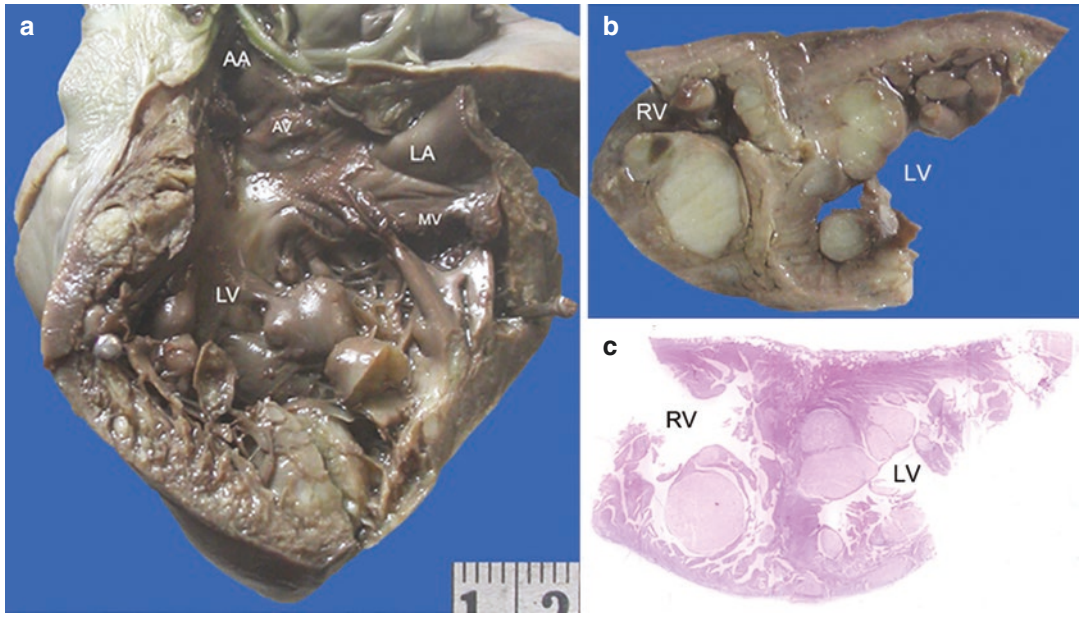

Fig. 52.1 (**a**) Left ventricular LV inflow and outflow tracts showing the presence of endocardial nodules that fill the middle and apical thirds of the ventricle; (**b**) Transverse section showing obliteration of the right ventricular RV apex with mural/endocardial nodules in the entire LV; (**c**) Scanned slide of the ventricles stained by H&E showing a similar appearance (*AA* ascending aorta, *AV* aortic valve, *LA* left atrium, *MV* mitral valve)

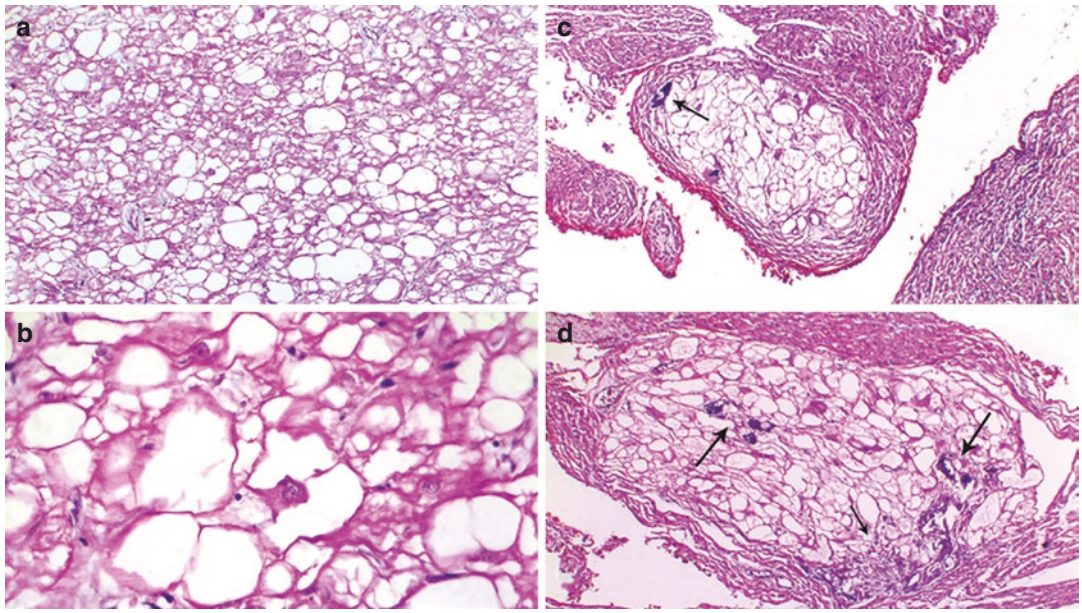

Fig. 52.2 (**a**) Vacuolated cardiomyocytes (H&E × 200); (**b**) Pathognomonic spider cell (H&E × 400); (**c**) and (**d**) showing peripheral and central areas of calcifications in small and large nodules (H&E × 200)

52.3 Discussion

Multifocal cardiac rhabdomyomas (CRMs) with partial obliteration of the ventricular cavities were presumably the cause for neonatal anuria (defined as failure to pass urine for 24 h) and sudden death. Such primary cardiac tumors are uncommon at all ages, and in the pediatric population (particularly neonates and infants), the estimated incidence is around 0.25%. With widespread use of echocardiography, cardiac tumors are being increasingly diagnosed not only postnatally, but also in fetal life during antenatal screening. Fortunately, most of them are benign, and rhabdomyomas are the most common histological subtype in fetal and neonatal age groups (with an incidence of almost 60%), followed by fibromas, teratomas, and myxomas.

CRMs are said to be the commonest (80–90%) and the initial manifestation of tuberous sclerosis complex (TSC), an autosomal dominant disorder, characterized by development of hamartomas/tumors in multiple organs (brain, retina, heart, and kidneys) and other associated nontumorous lesions. It is caused by mutations in 2 tumor suppressor genes, hamartin (TSC 1) and tuberin (TSC 2) that work in unison to inhibit cell proliferation. Over 50% of TSC patients develop CRMs. However, in this case, general examination at autopsy did not reveal any skin lesions and systemic examination showed absence of lesions in the brain, kidneys, and other organs. Analysis for TSC could not be performed due to financial constraints. It is possible that features of TSC would have appeared at a later stage had the neonate had survived.

In almost 90% of the patients, the CRMs are multiple, occurring in the ventricles and interventricular septum. Some can be isolated and occur at other sites including the atria and the even subepicardial regions forming exophytic masses. Tissue diagnosis is not necessary as the tumors are well-characterized by imaging techniques. An important feature of CRMs is their tendency for spontaneous regression, either partially or completely (therefore not requiring any treatment). In some cases, they remain asymptomatic and patients with TSC present due to central nervous system lesions. Manifestations related to CRMs would depend on the number, sizes, and locations of these tumors and can result in nonspecific heart murmurs on auscultation or serious complications like outflow tract obstructions, myocardial dysfunction with heart failure, and life-threatening arrhythmias with sudden death. It is to be noted that the tumors can act as accessory pathways in the generation of arrhythmias. Though the smaller tumors in our patient did show regression with calcification, the larger masses produced intracavitatory protrusions with obstructions to the blood flow. Surgery is recommended in cases where there are significant or intractable cardiac complications and in other cases medical management through rapamycin inhibitors (sirolimus or everolimus) is being advocated.

Further Reading

Chen J, Wang J, Sun H, Gu X, Hao X, Fu Y, et al. Fetal cardiac tumor: echocardiography, clinical outcome and genetic analysis in 53 cases. Ultrasound Obstet Gynecol. 2019;54:103–9.

Frudit P, Vitturi BK, Navarro FC, Rondelli I, Pozzan G. Multiple cardiac rhabdomyomas in tuberous sclerosis complex: case report and review of the literature. Autops Case Rep. 2019;9:e2019125.

Kwiatkowska J, Wałdoch A, Meyer-Szary J, Potaż P, Grzybiak M. Cardiac tumors in children: a 20-year review of clinical presentation, diagnostics and treatment. Adv Clin Exp Med. 2017;26:319–26.

Yuan S. Fetal primary cardiac tumors during perinatal period. Pediatr Neonatol. 2017;58:205–10.

53 Undifferentiated Pleomorphic Sarcoma Mimicking Left Atrial Myxoma

Pradeep Vaideeswar and Amey Rojekar

53.1 Clinical History

A 37-year-old male patient had been operated in a private health-care facility for a left atrial mass after 4 months history of progressive dyspnea, paroxysmal nocturnal dyspnea, and dry cough. The mass had occupied the entire left atrial cavity and was attached to the left atrial-left superior pulmonary vein junction. It measured 10 × 8 cm and was firm, lobulated, homogeneous gray-white (Fig. 53.1a–c), and was confined well within the limits of the heart. The CT scan had also revealed bilateral mild to moderate pleural effusions. The surgery was uneventful and a histopathology report of "consistent with clinical diagnosis of cardiac myxoma" was given.

Three months after the initial surgery, he had recurrence of the dyspnea with right hypochondriac pain and bilateral pedal edema, episodes of hemoptysis and syncope, and was referred to our tertiary-care center. The patient was conscious and well oriented in time. The pulse rate was 93 per minute and blood pressure was 86/58 mmHg. The external and systemic examinations suggested left ventricular inflow tract obstruction with congestive heart failure. He was posted for excision of recurrent left atrial myxoma and was treated with diuretics, antifailure drugs, and heparin. The investigations have been tabulated (Table 53.1). He had sudden cardiac arrest on the 6th day of admission.

P. Vaideeswar (✉)
Department of Pathology (Cardiovascular and Thoracic Division), Seth Gordhandas Sunderdas Medical College and King Edward Memorial Hospital, Mumbai, India

A. Rojekar
Department of Pathology, Seth Gordhandas Sunderdas Medical College and King Edward Memorial Hospital, Mumbai, India

P. Vaideeswar (ed.), *Tropical Cardiovascular Pathology*,
https://doi.org/10.1007/978-981-19-3720-0_53

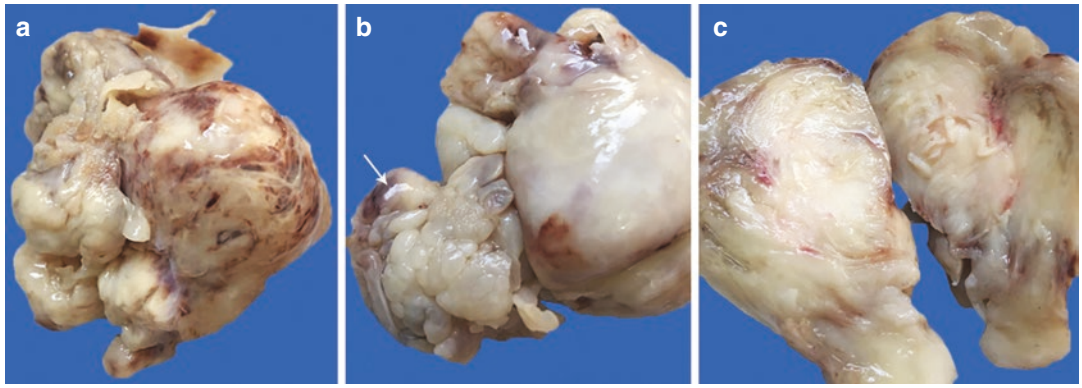

Fig. 53.1 Large, firm left atrial tumor—(**a**) External surface on the site of attachment and (**b**) on the luminal aspect. Note bulbous, papillary, finger-like projections (arrow); (**c**) Faintly lobulated glistening to opaque white cut surface

Table 53.1 Investigations

Hematological	[a]Hemoglobin 9.7 g/dL [a]Total leukocyte count 15,900/cmm Differential count—Neutrophil predominant [a]Platelet count 60,000/cmm
Biochemical—Routine	[a]Blood glucose 98 mg/dL [a]Serum creatinine 1.4 mg/dL [a]Blood urea nitrogen 57.4 mg/dL [a]Total bilirubin 2.18 mg/dL [a]Direct bilirubin 1.12 mg/dL [a]SGOT 2422.4 U/L [a]SGPT 1747.6 U/L [a]Total proteins 6.2 g/dL [a]Albumin 3.7 g/dL [a]Sodium 124.3 mEq/L [a]Potassium 4 mEq/L [a]Chloride 88.5 mEq/L
Imaging	Echocardiography: Recurrent left atrial myxoma with grade 1 mitral regurgitation, severe pulmonary hypertension, left ventricular grade 1 diastolic dysfunction
Others	ECG: Right bundle branch block Urine examination: Normal Pleural fluid: Transudate HIV: Negative

[a]Mean values

53.2 Autopsy Findings

The heart was markedly enlarged in size (550 g) with a dull epicardial surface. The apex was pointing to the left and formed by both ventricles. The left atrial appendage was not clearly delineated and was replaced by a firm, solid gray-white tumor (Fig. 53.2a). A large tumor mass (3 × 3 × 2.5 cm) protruded through the inferior vena caval opening (Fig. 53.2b), while both the left pulmonary venous lumens were obliterated by tumor. The heart was bisected longitudinally into 4 slices. They revealed: (1) Tumorous obliteration of the left atrial appendage (Fig. 53.2c); (2) A nodular mass 2.5 × 1.5 × 1.5 cm over the interventricular septum, 2.2 cm below the aortic valve (Fig. 53.2c); (3) Large firm yellowish white, glistening left atrial mass (8.5 × 3.5 × 3 cm, Fig. 53.2d), originating from the left pulmonary veins, which prolapsed through the mitral orifice into the left ventricular cavity; (4) A 0.8 cm tumor nodule over the posterior wall of the right atrium, and (5) Small tumor nodules within the superior vena cava. All these tumorous lesions showed short intersecting fascicles of short spindle-shaped cells in a collagenic (Fig. 53.3a–d) to focally myxoid background with pleomorphic nuclei and brisk mitoses (Fig. 53.4). The tumor cells were vimentin-positive (Fig. 53.4b inset) and were negative for smooth muscle actin, desmin, CD34, CD99, and S-100. The original histopathology slides, which were retrieved and reviewed, also showed a similar morphology. Other findings included brown induration of the lungs with a chronic abscess cavity in the postero-basal segment of the right lower lobe.

Cause of Death: Left atrial undifferentiated pleomorphic sarcoma.

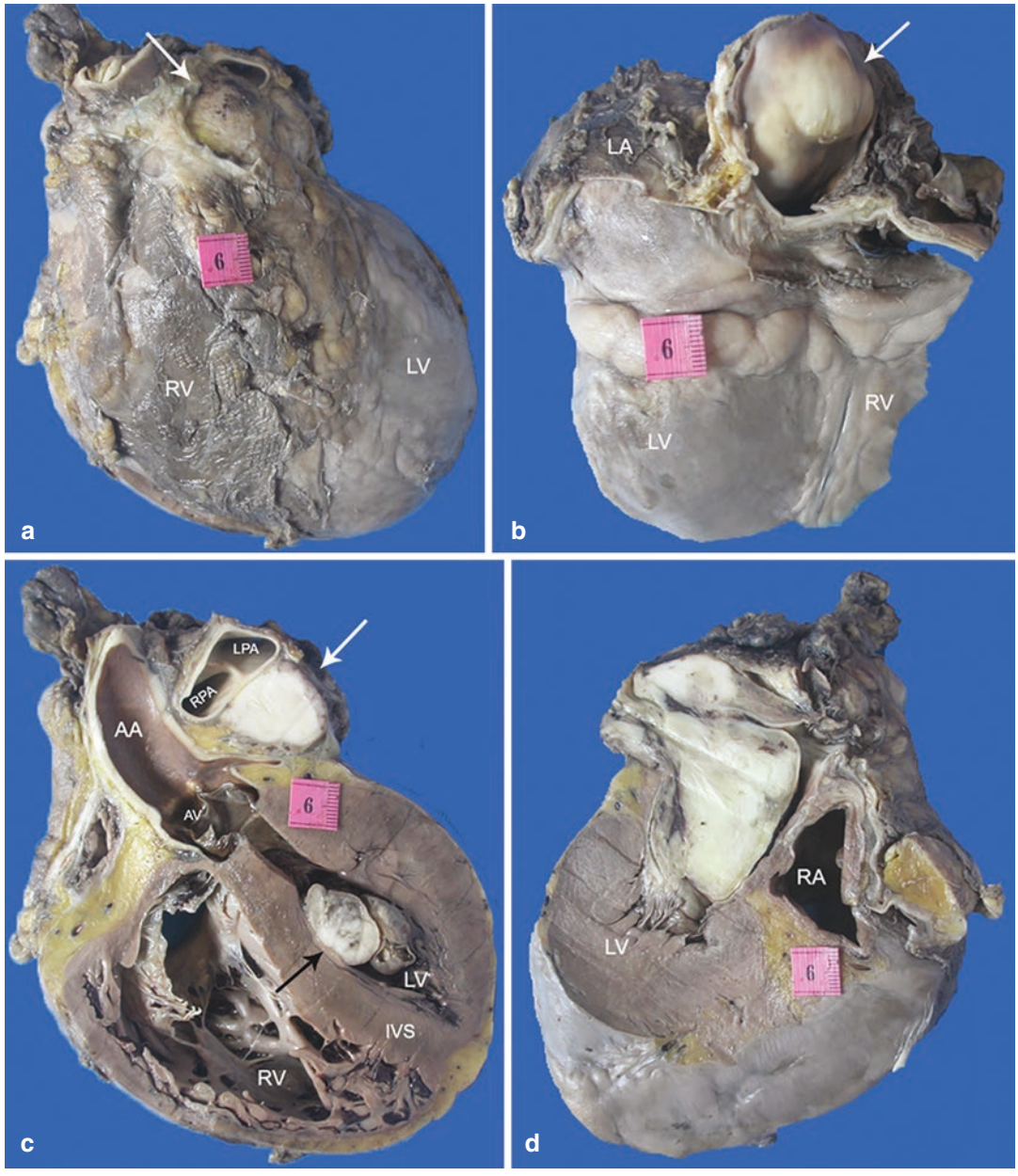

Fig. 53.2 (**a**) Anterior surface showing visceral pericardial thickening. A grey-white tumor replaces the crenellated left atrial appendage (arrow); (**b**) Protrusion of a large nodular tumor (arrow) through an enlarged opening of the inferior vena cava; (**c**) Obliteration of the left atrial appendageal lumen by tumor (white arrow). Sessile polypoidal lesion over the interventricular septum IVS (black arrow); (**d**) Tumor occupying the entire left atrial cavity (*AA* ascending aorta, *AV* aortic valve, *RA* right atrium, *RPA* right pulmonary artery, *RV* right ventricle, *LPA* left pulmonary artery, *LV* left ventricle)

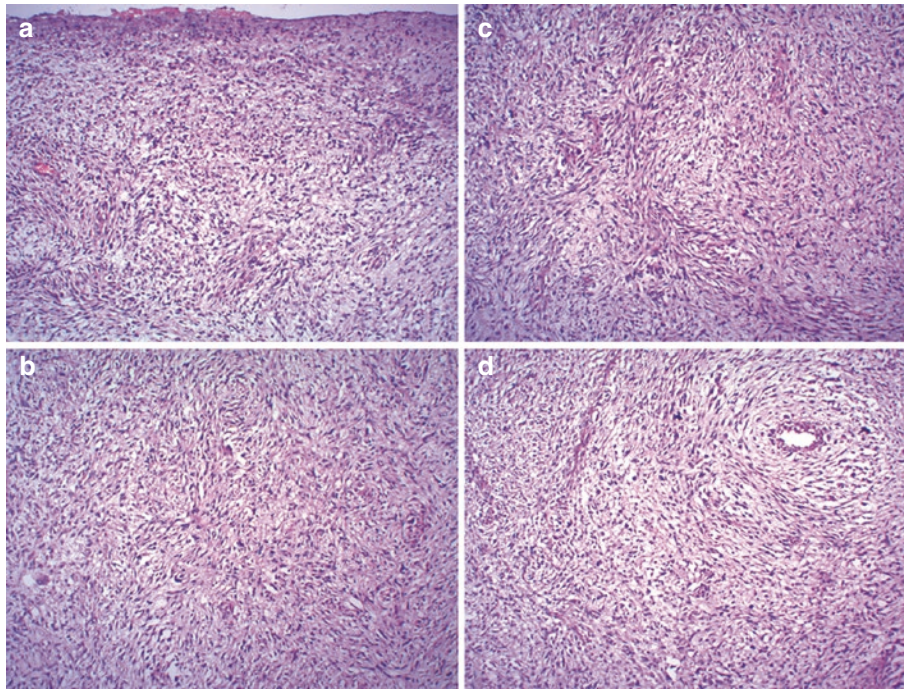

Fig. 53.3 (**a**)–(**c**): Pleomorphic spindle-shaped tumor cells in short fascicular and swirling patterns; (**d**) Presence of peri-vascular arrangement (H&E × 200)

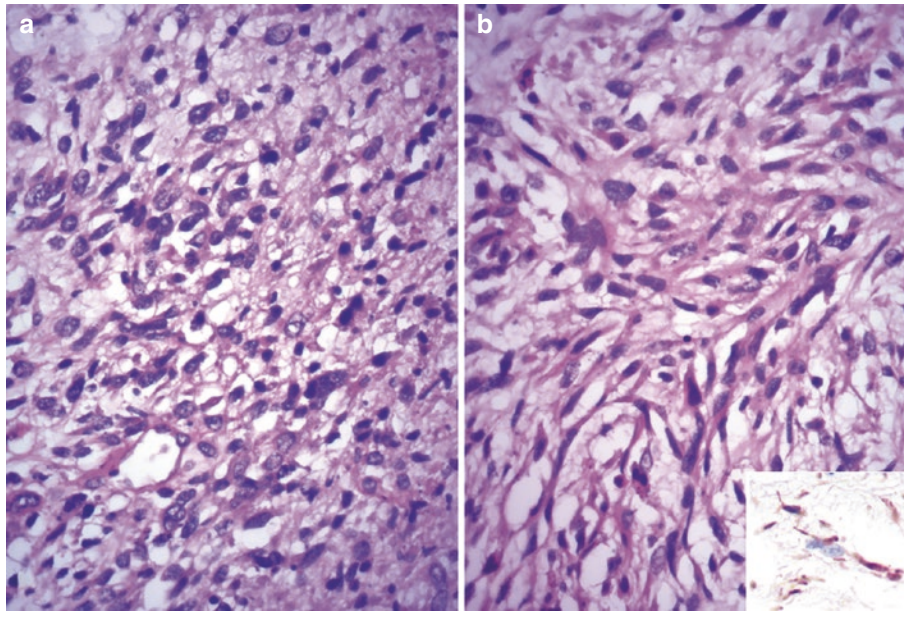

Fig. 53.4 (**a**) and (**b**) showing plump spindle-shaped to ovoid pleomorphic cells (H&E × 400). Inset shows immune-histochemical positivity for vimentin (× 400)

53.3 Discussion

A large, recurrent polypoidal, malignant mass lesion within the left atrial cavity in a young male was diagnosed as a primary cardiac sarcoma. About 25% of primary cardiac tumors are malignant, and sarcomas constitute the most common subtype, accounting for nearly 95% of primary heart cancers; remaining 5% are lymphomas and mesotheliomas. Cardiac sarcomas have an autopsy prevalence of 0.001%–0.03% and form 1% of all sarcomas. They usually occur in the third and fourth decades of life, especially in males and can be located in any part of the heart, but many occur in the right-sided structures. The full histomorphological spectrum of soft tissue sarcomas can occur in the heart, but the frequently encountered subtypes are angiosarcoma and undifferentiated pleomorphic sarcoma (UPS). The morphology in the present case—spindle-shaped pleomorphic tumor cells arranged in a predominant fascicular pattern, was reminiscent of intimal sarcoma. These mesenchymal tumors are most often diagnosed in the great arteries, where they are said to arise from the subendothelial cells of the arterial intima. When tumors in the heart show a similar morphology, the term UPS is preferred; only few cases are reported.

UPSs are often located in the left atrium and hence confused with cardiac myxomas, which are the commonest tumors in the left atrium. In contrast to the usual interatrial septal attachment of the myxomas, UPSs present as sessile or pedunculated polypoidal masses arising from wall of the atria or at the orifices of the pulmonary veins. The tumor in the present case was attached to the roof of the left atrium. The cut surface is uniform white to tan with a variegated appearance due to foci of hemorrhage or necrosis; gelatinous appearance (ascribed to myxomas) may be seen focally. Microscopically, UPS shows pleomorphic spindle cells arranged in variable patterns with focal myxoid stroma; mitotic activity is generally brisk. On immunohistochemistry, there is usually a lack of specific lineage with only vimentin positivity, as seen in our case. Besides a shared morphology with the intimal sarcomas, UPSs also exhibit a high prevalence of murine double minute 2 amplifications; this could not be performed in our case due to financial constraints.

The clinical presentation of cardiac sarcomas, in general, depends on the site, size, the rate of growth, and extent of invasion and not particularly on the histological features. Often, the patients remain asymptomatic for a prolonged duration of time before presenting with cardiac symptoms related to mechanical obstruction (as seen in our case) or conduction abnormalities. These may be accompanied by constitutional symptoms and even features due to distant metastases. Though the tumor recurred within months, it remained confined within the heart. Echocardiography is the initial and commonly used modality for the diagnosis; however, cardiac computed tomography and/or magnetic resonance imaging are essential preoperative investigations for the tumor size, location, and extent of invasion into surrounding normal tissue. Owing to the rarity of cardiac sarcomas, the mode of treatment is not standardized. Surgical resection is the main available option with adjuvant chemo-radio-therapy. There is also some role of cardiac autotransplantation and conventional cardiac transplantation in some cases. Nevertheless, the overall prognosis of UPS is very poor and median survival is less than 1 year due to highly invasive nature, high recurrence rate, and difficulty in obtaining clear surgical margin.

Further Reading

Burke A, Tavora F. The 2015 WHO classification of tumors of the heart and pericardium. J Thorac Oncol. 2016;11:441–52.

Durieux R, Tchana-Sato V, Lavigne J, Radermecker MA, Moonen M, Scagnol I. Recurrent cardiac intimal sarcoma misdiagnosed as a myxoma or malignant transformation of a cardiac myxoma? J Card Surg. 2021;36:357–62.

Hudzik B, Miszalski-Jamka K, Glowacki J, Lekston A, Gierlotka M, Zembala M, et al. Malignant tumors of the heart. Cancer Epidemiol. 2015;39:665–72.

Koelsche C, Benhamida JK, Kommoss FKF, Stichel D, Jones DTW, Pfister SM, Heilig CE, et al. Intimal sarcomas and undifferentiated cardiac sarcomas carry mutually exclusive MDM2, MDM4, and CDK6

amplifications and share a common DNA methylation signature. Mod Pathol. 2021;34(12):2122–9. https://doi.org/10.1038/s4379-021-00874-y.

Maleszewski JJ, Bois MC, Bois JP, Young PM, Stulak JM, Klarich KW. Neoplasia and the heart: pathological review of effects with clinical and radiological correlation. J Am Coll Cardiol. 2018;72:202–27.

Qin J, Li R, Ma F, Li H, Fang Z, Fei Y. Left atrial spindle cell sarcoma: a case report and literature review. Medicine. 2021;100:e24044.

Scicchitano P, Sergi MC, Cameli M, Miglioranza MH, Ciccone MM, Gentile M, et al. Primary soft tissue sarcoma of the heart: an emerging chapter in cardio-oncology. Biomedicine. 2021;9:774.

Torabi S, Rad AA, Vardanyan R, Lopuszko AT, Van den Eynde J, Zubarevich A, et al. Surgical and multimodality treatment of cardiac sarcomas: a systematic review and meta-analysis. J Card Surg. 2021;36:2476–85.

54 Intracardiac Metastases of Squamous Cell Carcinoma

Pradeep Vaideeswar, Anuja Kekatpure, Subhash Yadav, and Neha Lanke

54.1 Clinical History

The body of a 32-year-old man was referred to our institute for a medicolegal autopsy after he suddenly collapsed at the outpatient department of a tertiary cancer center, 3 days after his discharge from a year's admission in the same hospital. There was a short preceding history of vomiting and breathing difficulty. The patient, a chronic tobacco chewer, had been diagnosed with moderately differentiated squamous cell carcinoma of left buccal mucosa and upper gingivobuccal sulcus with extensive surgery and chemoradiation. Chest radiography, performed during the 9th month of admission, was normal.

P. Vaideeswar (✉)
Department of Pathology (Cardiovascular and Thoracic Division), Seth Gordhandas Sunderdas Medical College and King Edward Memorial Hospital, Mumbai, India

A. Kekatpure
AKMC Pathology Laboratory and Nurture Diagnostics, Nagpur, India

S. Yadav
Department of Pathology, Tata Memorial Hospital, Mumbai, India

N. Lanke
Department of Pathology, MGM Medical College, Aurangabad, India

54.2 Autopsy Findings

A complete autopsy was performed. The external examination showed extreme cachexia with a fistulous opening over the left zygoma. The heart (200 g) was normal in size. A bulge 3 × 2.5 cm was present over the anterior wall of the right ventricle, a little above the apex (Fig. 54.1a). The heart was cut as per the flow of blood and then longitudinally sliced. The apical portion of the right ventricle was obliterated by a smooth-surfaced 3 × 3 × 1.5 cm mass (Fig. 54.1b), attached to the anterior aspect of the interventricular septum. It was focally covered by fresh thrombi and had a homogeneous, pearly white cut surface. Similar metastatic nodules were seen in the lateral wall (Fig. 54.1b) and left ventricular apex, almost completely replacing the posterior papillary muscle (Fig. 54.1c). Sections from the tumor revealed a moderately differentiated squamous cell carcinoma. In addition, nodules were found all over the chest wall, diaphragm, pleurae, lungs, thyroid, adrenals, and omentum; many paratracheal and hilar lymph nodes were also replaced by tumor (Figs. 54.2 and 54.3).

Cause of Death: Intracardiac metastases of squamous cell carcinoma and sudden death.

P. Vaideeswar (ed.), *Tropical Cardiovascular Pathology*,
https://doi.org/10.1007/978-981-19-3720-0_54

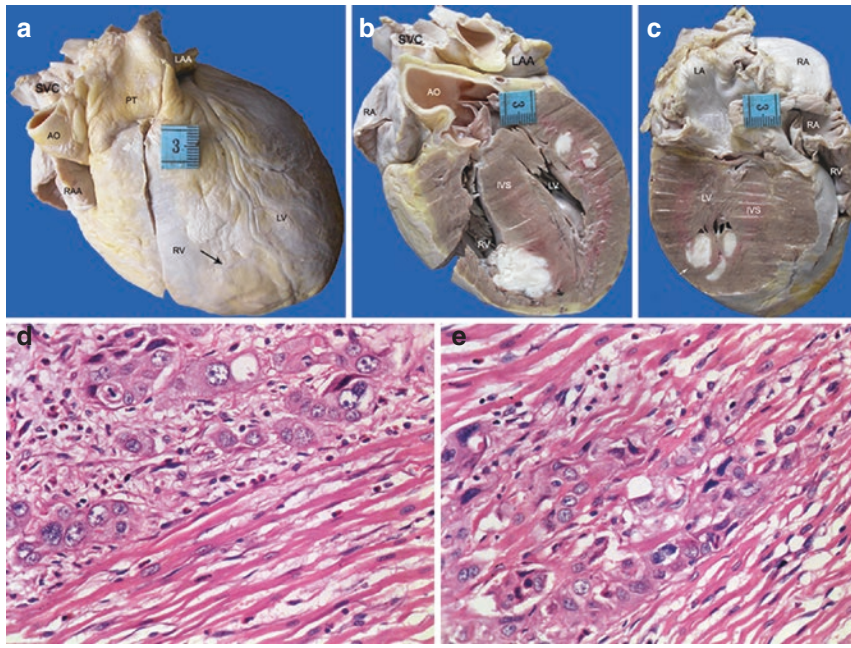

Fig. 54.1 (**a**) A bulge (arrow) is seen on the anterior aspect of the right ventricle RV; (**b**) The bisected heart on the anterior aspect shows tumor in the apical portion of RV and lateral wall of the left ventricle LV; (**c**) The posterior aspect of the longitudinal slice showing metastatic nodule (arrow), which has replaced the posterior papillary muscle (*AO* aorta, *IVS* interventricular septum, *LA* left atrium, *LAA* left atrial appendage, *PT* pulmonary trunk, *RA* right atrium, *RAA* right atrial appendage, *SVC* superior vena cava); (**d**) and (**e**): Myocardium infiltrated by metastatic squamous cell carcinoma (H&E × 400)

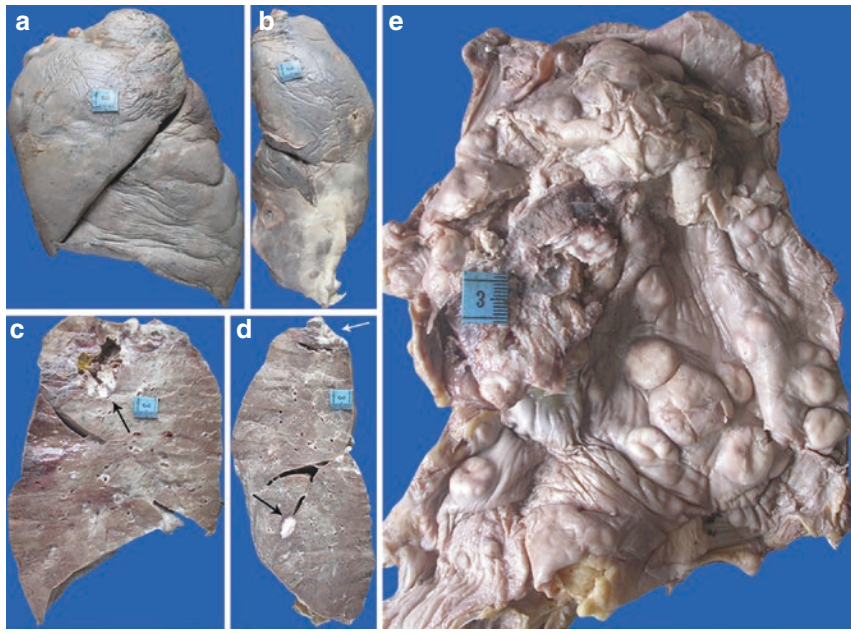

Fig. 54.2 Visceral pleural surfaces of the (**a**) left and (**b**) right lungs. The right lung is small in size with pleural thickening and opacification due to pleural effusion; Cut surfaces of the (**c**) left and (**d**) right lungs, showing parenchymal cavitatory and pleural metastases (arrows); (**e**) Nodules of varying sizes in the diaphragm

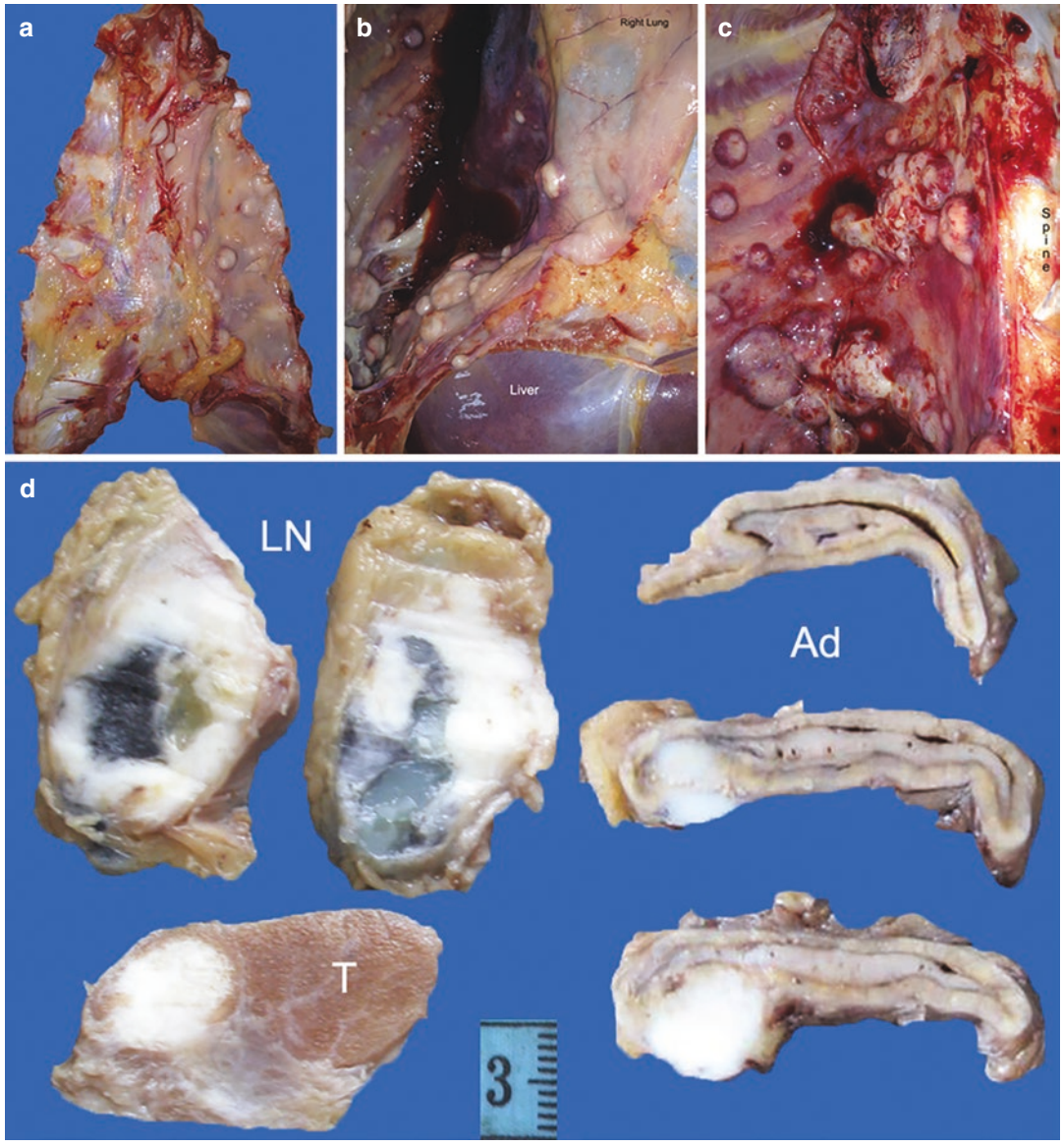

Fig. 54.3 Metastatic nodules over the (**a**) inner aspect of the sternum and (**b**) and (**c**) Inner aspects of the thoracic cavities over the parietal pleura; (**d**) Metastases in the paratracheal lymph nodes LN, thyroid T and adrenal glands Ad

54.3 Discussion

This young patient, despite extensive treatment, was found to have extensive dissemination of oral cancer (affecting the left gingivo-buccal mucosa), which remained clinically undiagnosed. The gingivo-buccal region is part of the oral cavity, which extends from the skin-vermilion junction of the lips to the junction of the hard and soft palate above, and to the circumvallate papillae below. Oral cancer is one of the most common forms of cancer in the Indian subcontinent and is very strongly related to smokeless tobacco. In most parts of India, it is a common practice among all classes of society to chew tobacco, often mixed with areca nut and other ingredients; this practice begins at an early age. Our young patient was chronic tobacco chewer, who developed moderately differentiated squamous cell carcinoma of the buccal

mucosa, and this is the commonest type of degree of differentiation and site, respectively. In general, the prevalence of distant metastases in head and neck cancers ranges from 0.9% to even more than 50%, which is paradoxically related to better locoregional control, as was seen in our case. Along with other organs, the metastasis was found in the ventricular myocardium.

Although secondary tumors involving the heart and pericardium are reported to be 20–30 times more frequent than primary neoplasms, they nevertheless are rare occurrences due to continuous strong myocardial contractions and high speed of blood within the heart. Most often, they occur in a setting of disseminated cancer, which can camouflage the cardiac involvement. Hence the incidence, ranging from 1.5 to 25%, is largely based on postmortem examinations. The cancer cells reach the heart through hematogenous (especially transvenous) or retrograde lymphatic spread, or even by direct extension. In about 75% of patients, the sources of metastases are carcinomas, followed by hematological malignancies, melanomas, malignant germ cell tumors, and sarcomas; these chiefly affect the pericardium, myocardium, and rarely the endocardium. The three most common carcinomas that invade the heart arise from the lung, breast, and esophagus due to their prevalence and/or their close proximity to the mediastinal structures. In general, cardiac involvement in cancers of the upper aerodigestive tract is distinctly unusual. They manifest as myocardial nodules with or without intracavitary projections.

Majority of the patients with cardiac metastases are asymptomatic, though at times the symptoms are overlooked or misinterpreted due to cancer recurrence or dissemination. Irrespective of the route employed, the pericardium is said to be the commonest site for tumor deposition. The effusion that ensues is slow-filling and loculated, delaying the diagnosis. On the other hand, myocardial or intracavitary metastases, if strategically located or of large size, can result in conduction disturbances, valvular stenosis, obstruction to coronary arterial flow, tumor/thromboembolism, or cardiac failure. The myocardial involvement is explained on the basis of retrograde lymphatic spread and is seen in the right and left ventricles in about 60% and 40%, respectively. Our patient had masses in both ventricles with almost complete replacement of the posterior papillary muscle. Sudden cardiac death was the sole and fatal clinical manifestation and the report highlights that there is always a possibility of cardiac metastases, even though a patient has no symptoms and culminates with disastrous complications at times. Despite availability of diagnostics investigative modalities such as transesophageal echocardiography or computed tomography, the prognosis in such cases is generally poor.

Further Reading

Andrianto A, Mulia EPB, Suwanto D, Rachmi DA, Yogiarto M. Case report: complete heart block as a manifestation of cardiac metastasis of oral cancer. F1000Res. 2020;9:1243.

Delabie P, Evrard D, Zouhry I, Ou P, Rouzet F, Benali K, et al. Squamous cell carcinoma of the tongue with cardiac metastasis on 18F-FDG PET/CT: a case report and literature review. Medicine. 2021;100(15):e25529.

Duband S, Paysant F, Scolan V, Forest F, Peoc'h M. Sudden death due to myocardial metastasis of lingual squamous cell carcinoma. Cardiovasc Pathol. 2011;20:242–3.

Martell K, Simpson R, Skarsgard D. Solitary myocardial metastasis from locoregionally controlled squamous cell carcinoma of the oral cavity. Cureus. 2016;8:e650.

Sarode G, Maniyar N, Sarode SC, Jafer M, Patil S, Awan KH. Epidemiologic aspects of oral cancer. Dis Mon. 2020;66:100988.

Cardiac Posttransplant Lymphoproliferative Disorder

55

Pradeep Vaideeswar, Gwendolyn Fernandes, and Pritam Khairkar

55.1 Clinical History

We describe a case of a 30-year-old male who had undergone a live-related renal transplantation procedure (father was the donor) 7 years ago for end-stage renal disease (exact etiology was not known). He was human immunodeficiency virus and hepatitis B surface antigen-negative. He had stable graft function and was on triple immunosuppression, comprising tacrolimus, mycophenolate mofetil, and prednisolone. After an uneventful 7 years posttransplant period, the patient was admitted in a private health-care facility with a 15-day history of grade 2 dyspnea on exertion and palpitation. Laboratory investigations were as follows: hemoglobin 12 g/dL, total leukocyte count 14.63 × 10^9/L (neutrophils 83%, lymphocytes 15%, eosinophils 2%), platelet count 278 × 10^9/L, serum creatinine 2.8 mg/dL, serum bilirubin 0.46 mg/dL, SGOT 234 U/L, SGPT 121 U/L, and serum LDH 4482 IU/L. He was evaluated and found to have moderate pericardial effusion, atrioventricular dissociation, and hyperkalemia. He underwent a permanent pacemaker implantation. The immunosuppressives were continued.

A fortnight after the pacemaker implantation, the patient rapidly developed left eye proptosis, cervical lymphadenopathy, nodule over the right forearm, penile swelling, and pain and lump in the abdomen. The patient was then admitted at our institute after nearly 2 months after his initial presentation for further management. His pulse was 98 beats/min and blood pressure was 150/80 mmHg. The laboratory investigations revealed Hb 12 g/dL, mild neutrophilia (total count of 14.63 × 10^9/L), normal platelet count, blood urea nitrogen 88.2 mmol/L, serum creatinine 2.8 mg/dL, serum bilirubin 0.46 mg/dL, plasma aspartate aminotransferase 121 U/L, plasma alanine aminotransferase 234 U/L, and serum lactate dehydrogenase 4482 IU/L. A whole body computed tomographic scan revealed bony erosions of left supraorbital ridge/left orbital roof and left temporoparietal bones, moderate pericardial effusion, 15 × 10 × 8.5 cm, ill-defined, invasive, hypodense mass in II, III, IV hepatic segments, nodular thickening of the greater omentum, and thickening of the penile shaft. The PET scan showed metabolically active disease involving the liver, multiple bones, subcutaneous tissues, and muscles. Sheets of dissociated atypical lymphoid cells were seen in biopsies of cervical lymph node and liver mass. A diagnosis of

P. Vaideeswar (✉)
Department of Pathology (Cardiovascular and Thoracic Division), Seth Gordhandas Sunderdas Medical College and King Edward Memorial Hospital, Mumbai, India

G. Fernandes
Department of Pathology, Seth Gordhandas Sunderdas Medical College and King Edward Memorial Hospital, Mumbai, India

P. Khairkar
Department of Pathology, Chhindwara Institute of Medical Sciences, Chhindwara, India

P. Vaideeswar (ed.), *Tropical Cardiovascular Pathology*,
https://doi.org/10.1007/978-981-19-3720-0_55

high-grade non-Hodgkin's lymphoma, B-cell type (CD 20 positive) was made; CD3 and Epstein-Barr virus (EBV) latent membrane protein−1 were negative. No such atypical lymphoid cells were seen in the cytological preparations of the aspirated serosanguineous pericardial fluid. A bone marrow aspiration and biopsy revealed normocellular marrow with trilineage hematopoiesis. The patient received injection hydrocortisone and lasix along with ceftriaxone, tacrolimus, azathioprine, cilnidipine, telmisartan, tramadol, febuxostat, and atorvastatin. During the course of treatment, he had repeated episodes of rapidly filling pericardial effusion, and he succumbed to the illness.

55.2 Autopsy Findings

A complete autopsy was performed. On general examination, right cervical region 8 × 2 cm mass, right forearm 2 × 2 cm mass, and prominent swelling of the penile shaft were noted. *In-situ* examination showed the presence of massive hemorrhagic pericardial effusion; no free fluid was seen in the pleural and peritoneal cavity. The connective tissue of the mediastinum appeared infiltrated by whitish tissue with adherence between the vascular structures, the tracheabronchial tree, and esophagus.

The heart was markedly enlarged in size and weighed 560 g. There was mild increase in the epicardial adipose tissue with patchy opacification and fibrinous exudate. Noticeable features were firm nodularity of the superior cavoatrial junction, nodular protrusions in the entire left atrioventricular groove and firm greyish white plaques over the posterior right atrioventricular groove (Fig. 55.1a, b), left atrium, pulmonary veins, left lateral border, and basal portion of the posterior left ventricular wall. The inner aspect of the parietal pericardium also showed few nodules. The heart was longitudinally bisected. There was extreme infiltration of the interatrial

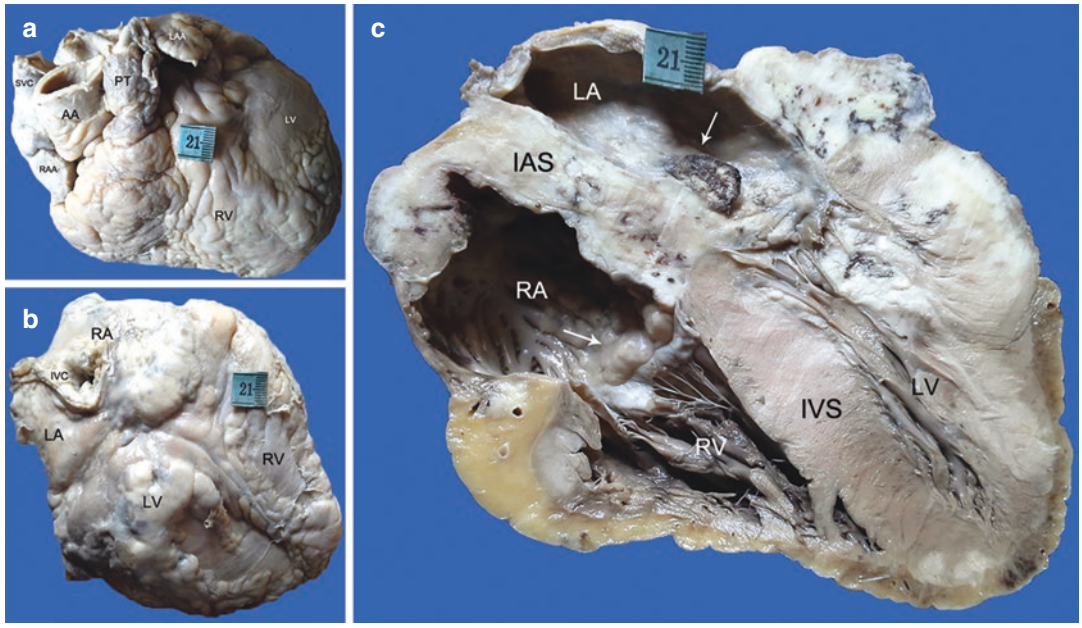

Fig. 55.1 Moderate cardiomegaly. (**a**) Anterior and (**b**) Posterior surfaces showing epicardial opacification and the presence of grey-white nodularity, prominently seen at the atrioventricular grooves; (**c**) Four-chamber view showing expansion of the interatrial septum IAS with fresh thrombus (arrow on left side), extension over the basal aspects of the tricuspid valve leaflets (arrow on right side), and replacement of the myocardium (*AA* ascending aorta, *IVC* inferior vena cava, *IVS* interventricular septum, *LA* left atrium, *LAA* left atrial appendage, *LV* left ventricle, *PT* pulmonary trunk, *RA* right atrium, *RAA* right atrial appendage, *RV* right ventricle, *SVC* superior vena cava)

septum (maximum thickness of 2 cm) with bulge and fresh thrombus over the left atrial aspect (Fig. 55.1c). The tumor appeared pale yellow to white and had also infiltrated the summit of the interventricular septum. There was also involvement of the right atrial free wall, the cavoatrial junctions, basal aspects of the leaflets of the atrioventricular valves, lateral basal aspect of right ventricle, lateral wall of the left ventricle, and adjoining papillary muscles (Fig. 55.1c). There was obliteration of the openings of the coronary sinus and left atrial appendage. The ascending aorta showed intimal thickening and wrinkling with adherent flattened fresh friable thrombi. Few atherosclerotic plaques were also seen in the arch and descending segments. The liver weighed 1.5 kg and showed a large, firm, grey-white mass of 10 × 6 cm (Fig. 55.2a) and fatty change in the surrounding liver. Both the native kidneys showed a grey-white fleshy tumor measuring 2 × 2 cm in their lower poles (Fig. 55.2b). The small and large intestines showed multiple grey-white fleshy, serosal nodules measuring 0.5–2 cm along the entire length. The transplanted kidney, brain, lung, thyroid, adrenals, and spleen were uninvolved. Histopathological examination of all tumor masses showed histomorphological features of a high grade non-Hodgkin's lymphoma, B cell type (Figs. 55.3, 55.4a, b and 55.5a) with a strong immunohistochemical positivity for leukocyte common antigen, and CD20; CD3, CD5, CD30, high-molecular weight cyto-keratin, and synaptophysin were negative. Such cells had infiltrated the pancreas, skeletal muscle, and retroperitoneal fat (Fig. 55.5b–d). A diagnosis of posttransplant diffuse large B-cell non-Hodgkin's lymphoma (DLBCL) was made. The lungs also showed diffuse alveolar damage and arterial thromboemboli.

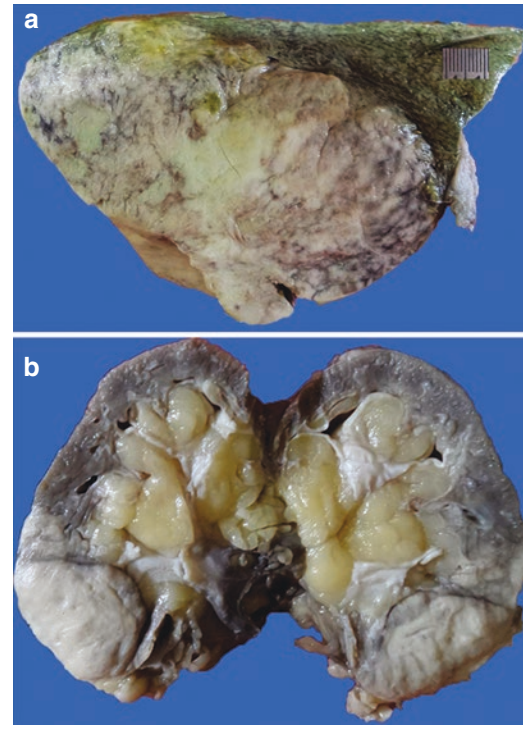

Fig. 55.2 (**a**) Liver showing a large, firm, greyish-white mass; (**b**) A 2 × 2 cm, firm greyish-white mass in the lower pole of one of the native kidneys

Cause of Death: Cardiac tamponade due to massive hemorrhagic pericardial effusion in a case of disseminated postrenal transplant DLBCL.

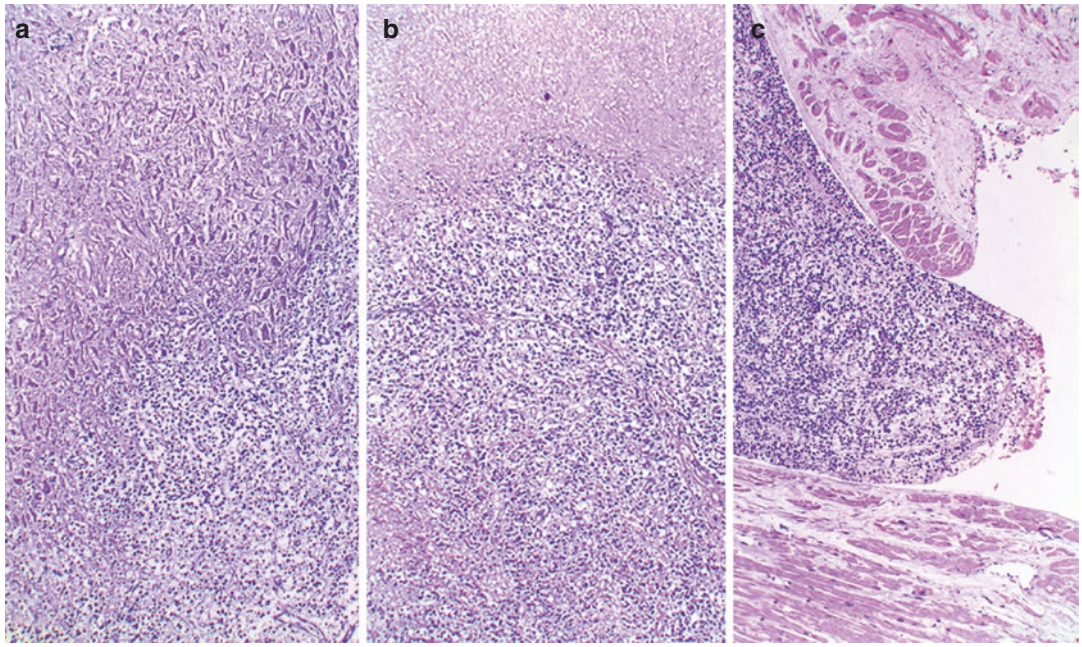

Fig. 55.3 Atypical lymphoid cells with (**a**) myocyte necroses and (**b**) tumor necrosis; (**c**) Mass of lymphoid cells insinuating into the intertrabecular space (H&E × 100)

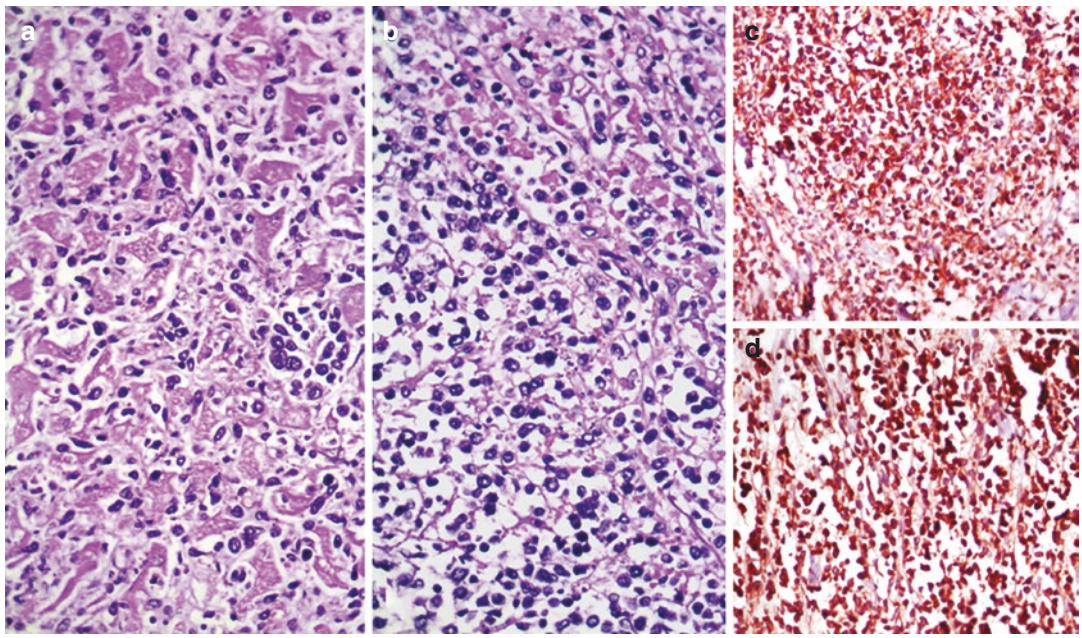

Fig. 55.4 Atypical large, pleomorphic lymphoid cells infiltrating the myocardium as (**a**) small clusters and (**b**) in sheets (H&E × 400); Positive immunohistochemistry for (**c**) Leukocyte common antigen and (**d**) CD 20 (× 400)

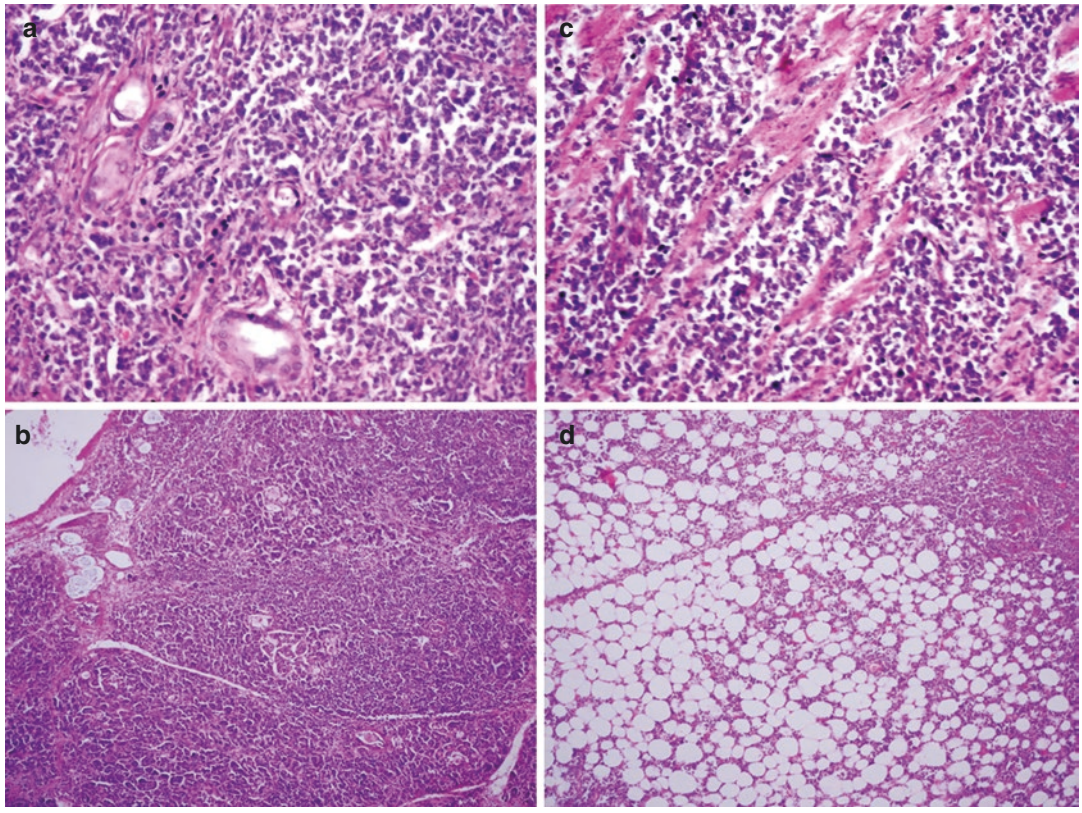

Fig. 55.5 The lymphoma cells in the (**a**) native kidney (H&E × 400), (**b**) pancreas (H&E × 200); (**c**) Skeletal muscle (H&E × 400) and (**d**) Retroperitoneal fat (H&E × 100)

55.3 Discussion

Synchronous to metachronous multiorgan lymphomatous proliferations were seen in a young renal transplant recipient in whom the procedure had been performed 7 years ago. Kidney transplantation is now a well-established procedure in patients with end-stage renal disease, and with judicious employment of appropriate immunosuppressives, there is a drastic improvement in the quality of life and long-term survival of the recipients. Unfortunately, apart from episodes of rejection, complications related to cardiovascular diseases and infections (See Chap. 19) also develop, leading to significant morbidity and mortality. Adding to the woes, the renal transplant recipients have a two to fourfold higher risk (as compared to the general population) of developing a posttransplant malignancy, which forms the third leading cause of death in these patients with an incidence of 2–31%. The etiopathogenesis is related not only to the traditional risk factors of malignant neoplasia, but is majorly due to an interplay between 4 important factors of chronic immunological stimulation, cancer-provoking antirejection drugs, oncogenic viruses, and donor-derived immune cell interactions. The multiorgan lymphoma, which occurred in our patient, is one of the components of a heterogeneous group of lymphoplasmacytic disorders ranging from indolent polyclonal reactive proliferations to aggressive monoclonal disease, designated as posttransplant lymphoproliferative disorder (PTLD).

PTLD occurs after both solid organ and hematopoietic stem cell transplantations with a lifelong incidence ranging from 2 to 20%. It is the most common disorder after skin cancer in adults with solid organ transplants. The key factors that determine the incidence and features of PTLD depend on the type of organ transplanted and the type of immunosuppressive therapy; particularly important is the triple drug immunosuppression that was administered in our patient. Kidney transplant recipients have the lowest risk of occurrence of 1–1.5%, as compared to other solid organ or stem transplantations. In most instances, the altered immunological milieu leads to uncontrolled B-cell proliferations, which have been categorized by the World Health Organization into 4 main groups—the nondestructive and polymorphic types both of which are basically polyclonal proliferations of different morphologies, and the monomorphic and Hodgkin-type of PTLDs that are essentially malignant. Our case had multifocal monomorphic PTLD, which represent the posttransplant counterparts of non-Hodgkin lymphomas (NHL) seen in immunocompetent patients. DLBCL is the most common type of NHL seen in these patients, accounting for almost 90% of the cases, though certain other types have also been described. Though PTLD can develop at any time after the transplant, they are identified within the first year in 60 to 80% of the recipients. Such early-onset PTLDs are usually donor derived, frequently EBV positive, and generally affect the graft with minimal extranodal involvement. Significant extranodal and EBV-negative host-derived PTLDs are seen as late-onset or very late-onset disease, after 2–10 and after more than 10 years, respectively. Some can also show the T-cell origin. Ours was an example of late-onset monomorphic PTLD, which was also EBV-negative and devoid of involvement of the transplanted kidney. Apart from multivisceral involvement, the interesting feature was involvement of the subcutaneous tissues and muscles and a large tumor burden in the heart.

Involvement of the heart is seen in 9–30% of the patients due to dissemination from nodal or extranodal lymphomas elsewhere in the body. Such secondary cardiac lymphomas develop as a result of direct invasion from mediastinal masses or through hematogenous/lymphatic dissemination. On the other hand, primary cardiac lymphomas (PCL) are extremely uncommon, forming 1.3–2% of all primary cardiac tumors and 0.5% of extranodal lymphomas. Though these tumors are diagnosed when there is sole involvement of the heart or pericardium, a diagnosis of PCL is permitted if the patient presents with dominant cardiac symptoms with bulk of the tumor in the heart, as was seen in this case. Nevertheless, they represent less than 5% of all lymphomas arising in immunosuppressed or immunocompromised patients. There are no significant differences in the gross features, imaging, and clinical presentation in primary and secondary lymphomas of the heart. Cardiac involvement by lymphoma is generally seen as firm, ill-defined, and infiltrative nodules in the cardiac chambers and/or the pericardium. There is predominant affection of the right-sided chambers, especially the right atrium and the epicardial surface that is associated with encasement of the basal structures and the right atrioventricular groove. The most common histological type is DLBCL, as also seen in the case presented. There was nodular as well as diffuse lymphomatous involvement of the pericardium, interatrial septum, summit of interventricular septum, basal aspects of atrioventricular valves and basal ventricular myocardium by the process. Such extensive cardiac infiltration has been seldom reported. Although routine transthoracic or transesophageal echocardiography can be used for initial identification, use of other imaging modalities (computed tomography or magnetic resonance imaging) allows enhanced evaluation.

This extensive involvement of the heart with infiltration of the atrioventricular conducting system led to atrioventricular dissociation, for which pacemaker implantation was performed in the initial stage of the lymphoma. Later, much of the morbidity and the unfortunate demise were due to repeated pericardial effusion and cardiac tamponade. Arrhythmias, conduction disturbances, and pericardial effusions are the common modes of presentation of cardiac lymphomas. They can also

present with features of obstruction and myocardial dysfunction, while some may have constitutional symptoms or can be even asymptomatic. But it is to be noted that transplant recipients with cardiac PTLD are more likely to have multivisceral involvement and dissemination and hence multiorgan dysfunction. Though our patient had initially presented with cardiac involvement, the clinical assessment and autopsy revealed dissemination to multiple sites. The donor kidney, lungs, thyroid, brain, adrenals, and spleen were uninvolved. The prognosis for patients with primary or secondary cardiac lymphomas is generally poor. It is often considered as a oncologic emergency and the therapy includes chemotherapy, which may be combined with radiation. In the setting of PTLD, reduction of immunosuppression may produce a dramatic reduction in the tumor burden or even complete remission in some cases.

Further Reading

Abbas F, Kossi ME, Shaheen IS, Sharma A, Halawa A. Post-transplantation lymphoproliferative disorders: current concepts and future therapeutic approaches. World J Transplant. 2020;10:29–46.

Aguilera N, Gru AA. Reexamining post-transplant lymphoproliferative disorders: newly recognized and enigmatic types. Semin Diagn Pathol. 2018;35:236–46.

Jeudy J, Kirsch J, Tavora F, Burke AP, Franks TJ, Mohammed TL, et al. Cardiac lymphoma: radiologic-pathologic correlation. Radiographics. 2012;32:1369–80.

Marcelis L, Tousseyn T. The tumor microenvironment in post-transplant lymphoproliferative disorders. Cancer Microenviron. 2019;12:3–16.

Miyazono A, Okamoto Y, Nagasako H, Hamasaki Y, Shishido S, Yoshioka T, et al. Multifocal Epstein-Barr virus-negative posttransplantation lymphoproliferative disorder treated with reduction of immunosuppression. Am J Kidney Dis. 2016;68:469–72.

Petrich A, Cho SI, Billett H. Primary cardiac lymphoma: an analysis of presentation, treatment, and outcome patterns. Cancer. 2011;117:581–9.

Rossi AP, Klein CL. Posttransplant malignancy. Surg Clin N Am. 2019;99:49–64.

Sen A, Callisen H, Libricz S, Patel B. Complications of solid organ transplantation cardiovascular, neurologic, renal, and gastrointestinal. Crit Care Clin. 2019;35:169–86.

Shareef MA, Eshaq AM, Alshawaf R, Alharthi E, Al Muslat AA, AbuDawas R, AlAmodi AA. Case study-based systematic review of literature on lymphomaassociated cardiac tamponade. Contemp Oncol (Pozn). 2021;25:57–63.

Zhao Y, Huang S, Ma C, Zhu H, Bo J. Clinical features of cardiac lymphoma: an analysis of 37 cases. J Int Med Res. 2021;49:1–13.

56 Leiomyosarcoma of the Inferior Vena Cava

Pradeep Vaideeswar

56.1 Clinical History

A 38-year-old woman presented with a three-week history of abdominal pain and low-grade fever with loss of weight and appetite. Physical examination and laboratory findings were within normal limits. She had no history of abdominal or pelvic surgery. An initial diagnosis of abdominal tuberculosis was made and antituberculous therapy was started in a private hospital. Eight days after the discharge, the patient was readmitted with breathlessness, abdominal distension, anasarca, and jaundice. She was referred to our hospital in view of possibly antituberculous therapy-induced hepatitis, accompanied by altered sensorium. On examination, the general condition was average with pulse rate of 96 per minute and blood pressure of 110/70 mmHg. She was responding poorly to oral commands. There was icterus, bilateral pedal edema, abdominal distension, and basal crepitations. Her investigations revealed Hb 12.5 g/dL, total leukocyte count 8450/cmm (84% neutrophils), platelet count 80,000/cmm, blood urea nitrogen 55 mg/dL, creatinine 1.2 mg/dL, SGOT/SGPT 431/288 U/dL, and alkaline phosphatase 94 U/dL. A color Doppler and computed tomographic (CT) scan of the abdomen (Fig. 56.1a, b) revealed dilatation and occlusion of the inferior vena cava (IVC) by possibly a thrombus, extending from proximal common iliac vein up to right atrium along with extension into right renal vein and right hepatic vein. Based on this report, a diagnosis of Budd-Chiari syndrome was entertained and the patient underwent thrombolytic therapy with streptokinase and maintained on warfarin. However, her dyspnea continued to progress and she died after 12 days of admission.

56.2 Autopsy Findings

A complete autopsy was performed. There was massive ascites (approximately 2 L of opalescent, amber-colored fluid). The IVC, from 2 cm below the openings of the renal veins and till its entry into the right atrium, was markedly dilated with a diameter of 3.1 cm, and in the region of the renal veins, it was covered by an irregular, firm, 6.1 × 3.5 × 2.8 cm mass (Fig. 56.1c). The dilatation was due to the presence of firm, grayish brown, slightly gelatinous tumor that had produced luminal obliteration; the cut surface was grey-white with focal hemorrhages (Fig. 56.2a).

P. Vaideeswar (✉)
Department of Pathology (Cardiovascular and Thoracic Division), Seth Gordhandas Sunderdas Medical College and King Edward Memorial Hospital, Mumbai, India

P. Vaideeswar (ed.), *Tropical Cardiovascular Pathology*,
https://doi.org/10.1007/978-981-19-3720-0_56

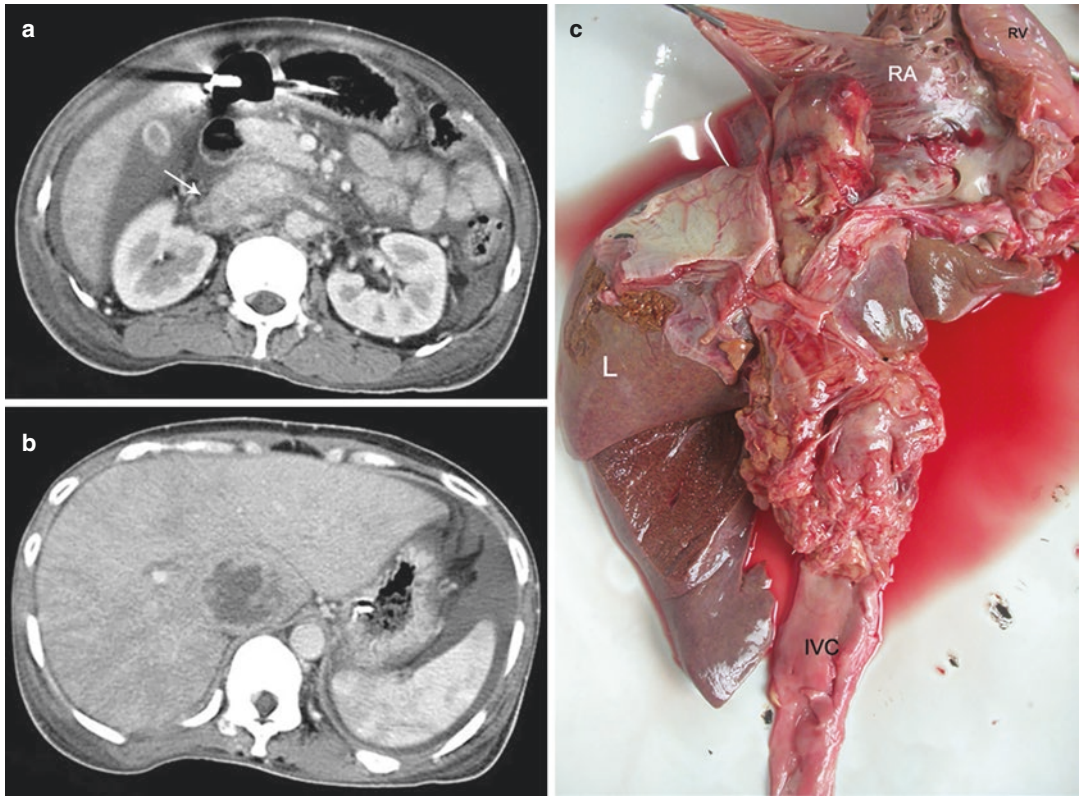

Fig. 56.1 CT scan of the abdomen showing mass lesion in the dilated inferior vena cava IVC—(**a**) Lesion at the region of the renal veins. Note extension (arrow) into the right renal vein; (**b**) Lesion in the hepatic portion of the vein; (**c**) Specimen in the fresh state showing a para-caval mass below the liver and extension of the IVC luminal lesion as a right atrial RA polypoidal mass (*RV* right ventricle)

At the infrarenal portion, the tumor had projected into the lumen as three to four blunt polypoidal projections. The tumor had extended into both renal veins, right more than the left as well as the right hepatic vein. Within the right atrium, the tumor had formed a large smooth-surfaced polypoidal lesion, which rested on the posterior tricuspid leaflet (Fig. 56.2a). No tumor was identified in other organs, especially in the genital tract. Microscopy revealed a pleomorphic tumor arising from the venous wall, composed of irregular fascicles of plump spindle-shaped (Fig. 56.2b) and multinucleate bizarre cells (Fig. 56.2c) embedded in loose fibromyxoid background. There were large areas of hemorrhage and necrosis, brisk mitoses, and a rich lymphoplasmacytic infiltrates and aggregates. The immunohistochemical profile (Fig. 56.2d) confirmed the diagnosis of leiomyosarcoma. The heart was normal and weighed 220 g. Other organs were normal; there were no pulmonary metastases.

Cause of Death: Congestive cardiac failure due to IVC leiomyosarcoma.

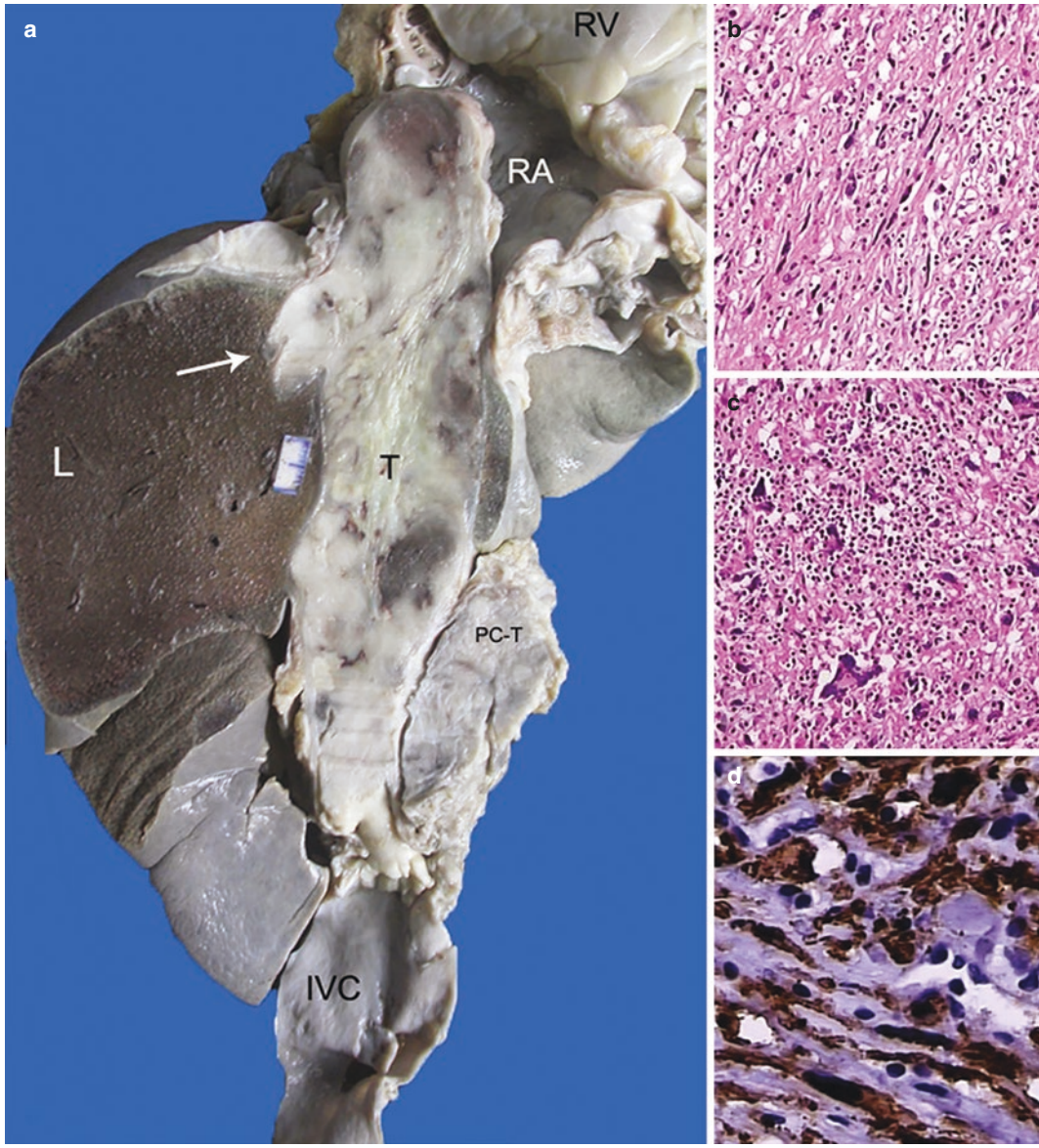

Fig. 56.2 (**a**) After formalin fixation, the tumor was longitudinally bisected to show luminal obliteration of the dilated inferior vena cava IVC lumen by a grey-white to pale yellow tumor, extension into the right hepatic vein (arrow) and right atrium RA (RV right ventricle). Foci of hemorrhage and necrosis are present; (**b**) and (**c**) The tumor is composed of pleomorphic spindle-shaped cells with bizarre multinucleated giant cells and sprinkling of lymphocytes in the background (H&E × 400); (**d**) On immunohistochemistry, the cells were positive for smooth muscle actin (× 400)

56.3 Discussion

Leiomyosarcoma (LMS), a malignant tumor that usually occurs in the soft tissues and certain viscera, was found to arise in the IVC with formation of both luminal and para-caval mass lesions. Only 2% of LMS have a vascular origin and venous origin is 5 times more common than arterial. Over 50% of these tumors affect the IVC, where they form 5–15% of primary retroperito-

neal sarcomas. A worldwide report of around 600 cases (mainly as case reports and isolated case studies) indicates the rarity of these lesions. Women in their sixth decades of life (median age of 54 years) are most commonly affected (male to female ratio of 1:4). The IVC LMS, which arises from the tunica media, can have an intraluminal (5%) growth or extra-luminal (62%) extension, and sometimes a combination of both growth patterns (33%). A combination was seen in our case, but the tumor was predominantly intra-luminal producing distension of the inferior caval vein. When the para-caval mass is of a sizable proportion, it would form a differential diagnosis for similar tumors which arise in the retroperitoneal soft tissues or from the kidney (the renal vein, capsule, or pelvis).

Despite the sarcomatous nature, the tumors are often slowly growing (allowing development of collateral venous drainage) with an insidious presentation and hence diagnosis is made at advanced stages of the malignancy. The clinical presentation depends on the location of the tumor and the classification is based on the relation with the renal and hepatic veins. Zone or segment I represents the growth of the tumor below the renal veins, i.e., infrarenal region, and these patients develop varying degrees of pedal edema and right lower abdominal, back, or flank pain. Tumors located between the renal and hepatic veins represent zone or segment II lesions (most frequent site of occurrence) and the patients present with upper quadrant abdominal pain, nephrotic syndrome, and sometimes even renovascular hypertension. Symptoms related to Budd-Chiari syndrome such as hepatomegaly, ascites, abdominal pain, and jaundice are seen in patients with suprahepatic location and variable right atrial extension, which is zone or segment III. The patient in this case had involvement of all 3 segments with a sizable extra-luminal growth and hence presented with multitude of symptoms. The intraatrial extension would have also induced right heart failure and exacerbated the features related to Budd-Chiari syndrome.

Imaging in the form of computed tomography and magnetic resonance imaging (MRI) is extremely useful in the diagnosis of IVC LMS, but biopsy may be necessary for a definitive diagnosis. A thrombus of the IVC is an important differential diagnosis. An important clue would have been lack of significant response to anticoagulant therapy (as seen in this case), and in these situations, gadolinium-enhanced MRI helps to distinguish between thrombus and tumor. Surgical resection is the mainstay of treatment with variable contribution with chemoradiotherapy. The prognosis depends on the location of the tumor, the pattern of growth, and differentiation. Involvement of the upper segment with right atrial extension, predominant intra-luminal growth, cellular pleomorphism, and severe hepatic dysfunction, many of which were seen in our patient, are associated with poor prognosis. It has also been shown recently that high expression of cytoplasmic β-catenin, insulin growth factor—1R, and Pten gene mutations is also associated with higher chances of metastases and recurrences.

Further Reading

Joung HS, Nooromid MJ, Eskandari MK, Wayne JD. Surgical approach, management, and oncologic outcomes of primary leiomyosarcoma of the inferior vena cava: an institutional case series. J Surg Oncol. 2020;122:1348–55.

Nabati M, Azizi S. Leiomyosarcoma of the inferior vena cava presenting as a cardiac mass. J Clin Ultrasound. 2018;46:430–3.

Rusu CB, Gorbatâi L, Szatmari L, Koren R, Bungărdean CI, Feciche BO, et al. Leiomyosarcoma of the inferior vena cava. Our experience and a review of the literature. Rom J Morphol Embryol. 2020;61:227–33.

Suneetha KP, Gudaganatti SB, Gayathri J. Rare case presentation of leiomyosarcoma as IVC thrombus. Indian J Surg Oncol. 2019;10:540–1.

Wang MX, Menias CO, Elsherif SB, Segaran N, Ganeshan D. Current update on IVC leiomyosarcoma. Abdom Radiol (NY). 2021;46:5284–96.

Part IX

Systemic Vascular Diseases

Supra-Cardiac Aortic Atherosclerosis

57

Swati Kolhe and Pradeep Vaideeswar

57.1 Clinical History

A 62-year-old chronic smoker and diabetic was admitted with complaints of sudden onset severe back pain and weakness of both lower limbs since morning. There was no history of fever, headache, convulsions, or trauma. On examination, his pulse rate was 88 beats per minute and blood pressure was 140/90 mmHg. The sensations, power, and reflexes were lost over both lower limbs. The clinical diagnosis was acute bilateral symmetrical flaccid paraparesis of lower limbs. The investigations have been tabulated (Table 57.1). He was treated with anticoagulants, steroids, and antiviral drugs, but he developed sudden-onset breathlessness and succumbed after 2 days of admission.

Table 57.1 Investigations

Hematological	Hemoglobin 15.4 g/dL Total leukocyte count 18,200/cmm Differential count—Neutrophil predominant platelet count 2.4 lakhs/cmm
Biochemical—Routine	Blood glucose 262 mg/dL Serum creatinine 1.4 mg/dL Blood urea nitrogen 70 mg/dL PAST 479 U/L PALT 376 U/L Sodium 124 mEq/L Potassium 3.0 mEq/L Chloride 90 mEq/L Cholesterol 318 mg/dL Triglycerides 382 mg/dL High-density lipoproteins 44 mg/dL Very low-density lipoproteins 76.4 mg/dL Low-density lipoproteins 204.7 mg/dL Cholesterol/high-density lipoprotein 7.23
Radiological	Computed tomography, brain: Mild generalized cerebral atrophy Magnetic resonance imaging, spine: Degenerative changes at L_4—L_5 and L_5—S_1 levels; posterior disc bulge at L_5—S_1
Others	ECG: Sinus tachycardia Cerebrospinal fluid examination: Normal

S. Kolhe
Department of Pathology, Seth Gordhandas Sunderdas Medical College and King Edward Memorial Hospital, Mumbai, India

P. Vaideeswar (✉)
Department of Pathology (Cardiovascular and Thoracic Division), Seth Gordhandas Sunderdas Medical College and King Edward Memorial Hospital, Mumbai, India

P. Vaideeswar (ed.), *Tropical Cardiovascular Pathology*,
https://doi.org/10.1007/978-981-19-3720-0_57

57.2 Autopsy Findings

A restricted autopsy (partial chest) had been performed. The heart was moderately enlarged and weighed 380 g. There was moderate left ventricular hypertrophy and diffuse calcific coronary atherosclerosis exhibiting multifocal 50% luminal narrowing. The available aorta showed multiple atherosclerotic plaques, some of which were calcified. The arch below the origin of left subclavian artery (LSA) and the adjoining proximal descending thoracic aorta showed a distinct bulge for a length of 4 cm (Fig. 57.1a). This mildly aneurismal atherosclerotic segment was covered with mural thrombus (Figs. 57.1b and 57.2a). There was propagation of the thrombus into the atherosclerotic LSA (Fig. 57.2b, c). The lung histology revealed occlusive arterial thromboemboli.

Cause of Death: Pulmonary thromboembolism (PTE).

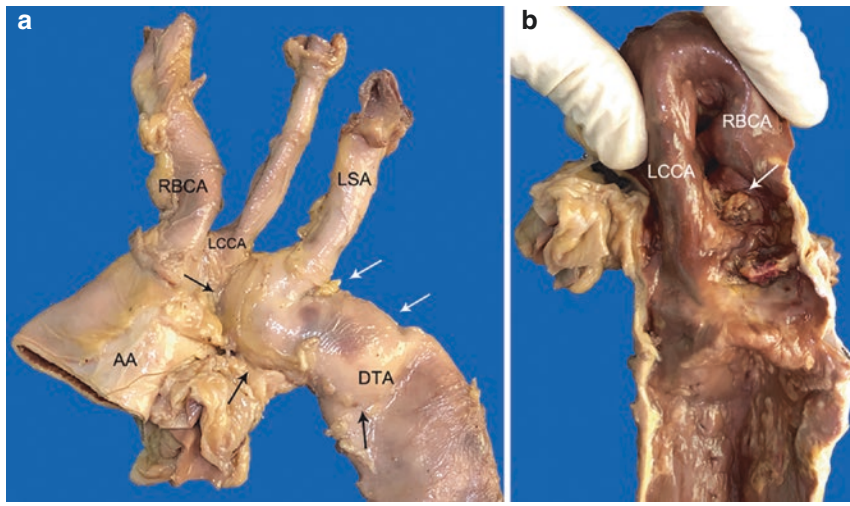

Fig. 57.1 (**a**) An aneurismal bulge (arrows) is present in the distal arch and proximal descending thoracic aorta DTA; (**b**) Opened out aorta showing an ulcerated atheroma covered with fresh thrombus (arrow) in the region of the aneurismal bulge obliterating the orifice of the left subclavian artery LSA (*AA* ascending aorta, *DTA* descending thoracic aorta, *LCCA* left common carotid artery, *RBCA* right brachiocephalic artery)

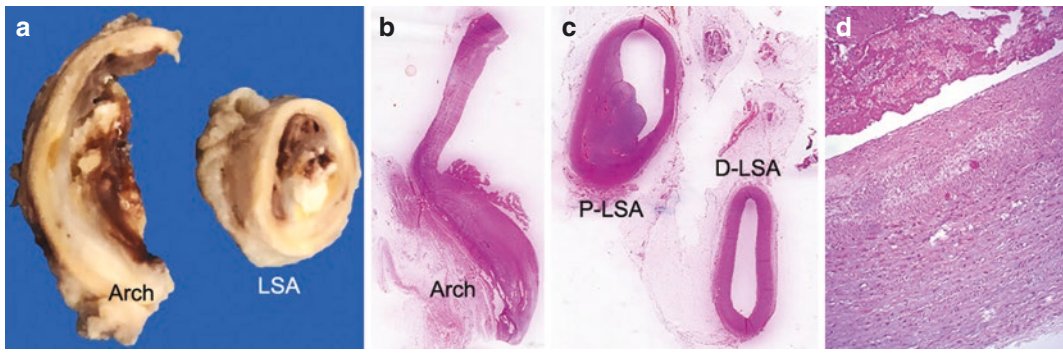

Fig. 57.2 (**a**) Section of the arch showing thrombus over the atherosclerotic plaque. Thrombus is also present in the lumen of the left subclavian artery LSA; (**b**) Scanned image stained by H&E of complicated plaque in the arch. The irregular surface is produced due to superimposed thrombus (H&E); (**c**) Scanned image stained by H&E. The proximal P-LSA is partly obstructed by atheroma and thrombus, while the distal D-LSA appears normal (H&E); (**d**) Fresh fibrin thrombus in the lumen of the LSA (H&E × 250)

57.3 Discussion

The presentation of acute flaccid paralysis of bilateral lower limbs with severe back pain, which appeared in all probability unrelated to the lumbosacral pathology, suggested ischemia of the spinal cord. In comparison to the brain, spinal cord ischemia is distinctly uncommon and the exact prevalence is still unknown. In adults, atherosclerosis is the main etiological factor; other important causes include aortic aneurismal disease and/or surgery, aortic dissections, and hypercoagulable states. The clinical manifestations would depend on the location and degree of obstruction of the supplying arterial system, and the ischemia is often invariably accompanied by back pain, present in over 70% of the cases. The clinical presentation in our case also suggested anterior spinal artery syndrome. Unfortunately, due to restricted autopsy, the thoracic part of the spinal cord could not be examined. The arterial system is supplied by the LSA, which at autopsy revealed atherothrombotic complication. This location is included under a unifying category referred to as supra-cardiac atherosclerosis (SCA).

SCA is a new term coined to include complicated atherosclerotic disease at the level of the aortic arch or in the carotid, vertebrobasilar, and intracranial arterial systems. It has been recently proposed to be an important cause of "embolic stroke of undetermined source"; traditionally these strokes were ascribed mainly to atrial fibrillation, atrial cardiomyopathy, valvular heart disease, or patent foramen ovale. In cases of SCA, the arterial lumen is reduced to less than 50% of its normal caliber due to atherosclerosis or its complications, especially intra-plaque hemorrhage or ulceration with overlying thrombosis. In our case, the lumen of the atherosclerotic LSA was further stenosed by extension of thrombus localized to the arch of aorta. Such an involvement is 4 times more common than right subclavian artery. Furthermore, these atherosclerotic plaques are usually associated with bland white thrombi, composed of fibrin and platelets, which have a high tendency to embolization but also have a better response to antiplatelet agents. Vulnerable plaques with high embolic risk can be readily identified by advanced and sophisticated imaging techniques to ensure prompt diagnosis and offer a guide to selection of optimal medical therapy. The present case highlights the importance of a high index of suspicion of an ischemic cause for acute flaccid paralysis and the need to rule out SCA as the etiological factor. The mortality was unrelated to SCA and was due to PTE, which is the third most common cause of death among cardiovascular diseases (See Chap. 68).

Further Reading

Di Tullio MR, Russo C, Jin Z, Sacco RL, Mohr JP, Homma S, et al. Aortic arch plaques and risk of recurrent stroke and death. Circulation. 2009;119:2376–82.

Ntaios G, Perlepe K, Lambrou D, Sirimarco G, Strambo D, Eskandari A, et al. Prevalence and overlap of potential embolic sources in patients with embolic stroke of undetermined source. J Am Heart Assoc. 2019;8:e012858.

Ntaios G, Wintermark M, Michel P. Supracardiac atherosclerosis in embolic stroke of undetermined source: the underestimated source. Eur Heart J. 2021;42:1789–96.

Sagris D, Georgiopoulos G, Leventis I, Pateras K, Pearce LA, Korompoki E, et al. Antithrombotic treatment in patients with stroke and supracardiac atherosclerosis. Neurology. 2020;95:e499–507.

Vargas MI, Gariani J, Sztajzel R, Barnaure-Nachbar I, Delattre BM, Lovblad KO, et al. Spinal cord ischemia: practical imaging tips, pearls, and pitfalls. Am J Neuroradiol. 2015;36:825–30.

58 Shaggy Aortic Syndrome, Penetrating Atherosclerotic Ulcer, and Rupture

Pradeep Vaideeswar and Pranita Zare

58.1 Clinical History

A 60-year-old male, admitted in a poor general condition, expired with 2 h of admission. He was hypotensive (blood pressure of 100/60 mmHg) with cold clammy skin and poorly felt peripheral pulses. He had been a hypertensive (blood pressure of 200/120 mmHg) on irregular therapy.

58.2 Autopsy Findings

The heart was mildly enlarged in size (340 g) with mild concentric left ventricular hypertrophy and mild diffuse atherosclerosis of all 3 epicardial coronary arteries. The entire aorta was aneurysmally dilated (circumferences ranging from 7.2 to 10.8 cm) and had a classic appearance of 'shaggy aorta'. The intima had multiple ulcerated atheromas of varying sizes; calcification was predominantly present in the infrarenal portion of the abdominal aorta. There was thickening of the wall with dense adherence of the thoracic descending segment to the left lung. In addition, the mid-portion of this segment showed a depression (Fig. 58.1a), which on cut section was seen to burrow through the aortic wall (Fig. 58.1b)—'penetrating atherosclerotic ulcer' (PAU) to rupture into the left lower lobe (Fig. 58.1c). The lobe was expanded with shiny, stretched pleura, very firm, and completely hemorrhagic. Other findings were centri-acinar emphysema and chronic pyelonephritis.

Cause of Death: Hypovolemic shock following rupture of PAU into left lung.

P. Vaideeswar (✉) · P. Zare
Department of Pathology (Cardiovascular and Thoracic Division), Seth Gordhandas Sunderdas Medical College and King Edward Memorial Hospital, Mumbai, India

P. Vaideeswar (ed.), *Tropical Cardiovascular Pathology*,
https://doi.org/10.1007/978-981-19-3720-0_58

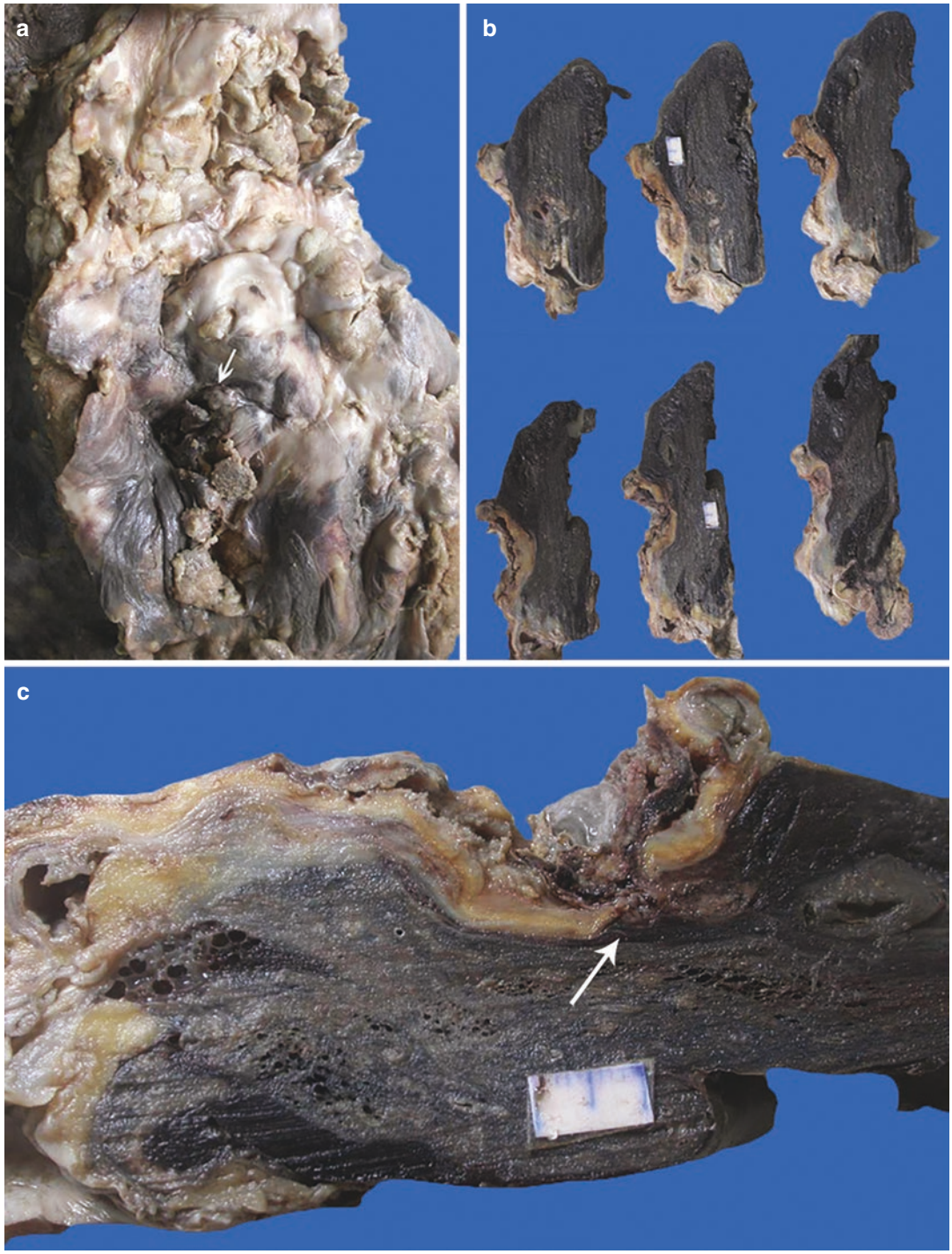

Fig. 58.1 (**a**) Dilated descending thoracic aortic segment with extensive complicated atherosclerosis—'shaggy aorta'. Note a depressed area (arrow) surrounded by thrombi and blood clots; (**b**) Serial slices showing dense adherence of the aorta to hemorrhagic lung parenchyma; (**c**) There is ulceration of the atheromatous plaque that has produced a transmural breach in the wall and formation of hemorrhagic tract (arrow) extending into the lung parenchyma

58.3 Discussion

The case draws attention to 3 interesting phenomena, namely 'shaggy aorta', PAU, and its rupture into the lung that were seen in an elderly patient with uncontrolled hypertension. Shaggy aorta is a descriptive term that has been used for atherosclerotic aortic segments, which show localized or diffuse irregularity and spiculations as visualized on computed tomographic (CT) angiogram. The shagginess is imparted by complications in the form of multifocal ulcerations, calcification, and/or overlying thrombi. Shaggy aorta is currently defined as "diffuse, irregularly shaped atherosclerotic change involving more than 75 % of the length of the aorta from the arch to the visceral segment with atheromatous plaque thickness of greater than 4 mm, as confirmed by contrast enhanced CT". Most of these patients are elderly, predominantly males with comorbid conditions like hypertension, diabetes mellitus, chronic obstructive pulmonary disease, coronary artery disease, peripheral vascular disease, and stroke. The extensive atheromatous degeneration is very often associated with cholesterol emboli or thromboemboli leading to 'shaggy aortic syndrome', a condition characterized by peripheral and visceral ischemia (not present in the current case). The mortality in this patient was due to PAU with extensive intrapulmonary hemorrhage, seen in the background of shaggy aorta.

PAU is one of the 3 common entities that are included under the term "acute aortic syndrome", which refers to a constellation of life-threatening aortic pathologies (especially involving thoracic aorta) mediated by alterations and subsequent disruption of the aortic wall layers; others include acute aortic dissection (See Chap. 61) and intramural hematoma. PAUs, as the name suggests, are caused by ulceration of the atherosclerotic plaque with extension and encroachment of the media that produces a mushroom-like silhouette on computed tomographic angiogram, which is the most common modality used for the diagnosis of this condition. They are typically seen in elderly individuals with uncontrolled hypertension and occur as unifocal or multifocal lesions in diffusely atherosclerotic and often aneurismal aortas, particularly in the mid-portion or distal third of the descending thoracic aorta, as seen in the present case. They are frequently asymptomatic and seldom manifest with luminal compromise and ischemic manifestations. However, large PAUs (diameter of 20 mm) with a depth greater than 10 mm are responsible for 2–7% of cases of AASs. Further extension towards the aortic adventitia leads to hematoma and pseudoaneurysm formation or even a devastating event of transmural aortic rupture, well-illustrated in this case; the rupture was into the left lung with extensive intrapulmonary hemorrhage. When symptomatic, PAUs demand either open or endovascular repair.

Further Reading

Bossone B, LaBounty TM, Eagle KA. Acute aortic syndromes: diagnosis and management, an update. Eur Heart J. 2018;39:739–49.

Dev R, Khorwal G, Darbari A. Demystifying penetrating atherosclerotic ulcer of aorta: unrealised tyrant of senile aortic changes. J Cardiovasc Thorac Res. 2021;13:1–14.

El Hassani I, Van Damme H, Creemers E, Boesmans E, Defraigne JO. Penetrating atherosclerosis aortic ulcer: a re-appraisal. Acta Chir Belg. 2017;117:1–7.

Hollier LH, Kazmier FJ, Ochsner J, Bowen JC, Proctor CD. "Shaggy" aorta syndrome with atheromatous embolization to visceral vessels. Ann Vasc Surg. 1991;5:439–44.

Hosaka A, Motoki M, Kato M, Sugai H, Okubo N. Quantification of aortic shagginess as a predictive factor of perioperative stroke and long-term prognosis after endovascular treatment of aortic arch disease. J Vasc Surg. 2019;69:15–23.

Serra R, Bracale UM, Jiritano F, Ielapi N, Licastro N, Provenzano M, et al. The shaggy aorta syndrome: an updated review. Ann Vasc Surg. 2021;70:528–41.

Atherosclerosis and Neutrophils

59

Pradeep Vaideeswar

59.1 Clinical History

A 65-year-old lady with a past history of diabetes mellitus on irregular therapy presented with left lower limb cellulitis. There had been a blackish discoloration with peeling of the skin and focal suppuration for a week. On examination, her vital parameters were within normal range, except for mild tachycardia (pulse rate of 95 per minute). Systemic examination also had been normal. The significant findings of investigations showed anemia (Hb 8.4 g/dL), leukocytosis (total leukocyte count of 27,400/cmm, 89% neutrophils), hyperglycemia (random blood sugar of 442 mg/dL) and azotemia (blood urea nitrogen of 55.5 mg/dL, serum creatinine of 3.2 mg/dL). She was treated with antibiotics and hypoglycemics and a below knee amputation was performed on the 2nd day of her admission. She had a cardiac arrest, 7 h after the operation and expired.

59.2 Autopsy Findings

The heart was mildly enlarged in size (260 g) with mild biventricular enlargement. On serial cross sections through the mid-portion of the heart, there were pale yellow, fresh mural thrombi that were restricted to the intertrabecular spaces of both the ventricles (Fig. 59.1a). In addition, there were 2 capsule-shaped fresh 'free-floating' thrombi in the right ventricular cavity (Fig. 59.1b). Apart from dilatation of the cavities and thinning of the walls, the myocardium did not show congestion or any other discoloration. On histology, the thrombi appeared bland (Fig. 59.1c) and were not associated with underlying septic myocarditis. There were mild myxomatous changes in the atrioventricular valves.

The left anterior descending artery showed diffuse calcific atherosclerosis, and 2.2 cm from its origin, it showed critical stenosis by an eccentric fatty atheroma for a length of 0.7 cm. Beyond this segment, the artery along with the dominant right coronary and left circumflex arteries showed only mild calcific atherosclerosis with no significant narrowing. The entire aorta showed scattered focally calcified atheromatous plaques. The eccentric plaque in the left anterior descending artery was composed of large numbers of foamy macrophages with basal collections of cholesterol clefts. In addition, there was diffuse and intense infiltration of neutrophils in the entire plaque (Figs. 59.1d and 59.2) with plenty of foamy macrophages (Fig. 59.2b). The internal elastic lamina was not seen at the site of plaque with thinning of the underlying media, which also showed destruction by neutrophils (Fig. 59.2c). There was mild adventitial fibrosis with mixed inflammatory cell infiltrate. In

P. Vaideeswar (✉)
Department of Pathology (Cardiovascular and Thoracic Division), Seth Gordhandas Sunderdas Medical College and King Edward Memorial Hospital, Mumbai, India

P. Vaideeswar (ed.), *Tropical Cardiovascular Pathology*,
https://doi.org/10.1007/978-981-19-3720-0_59

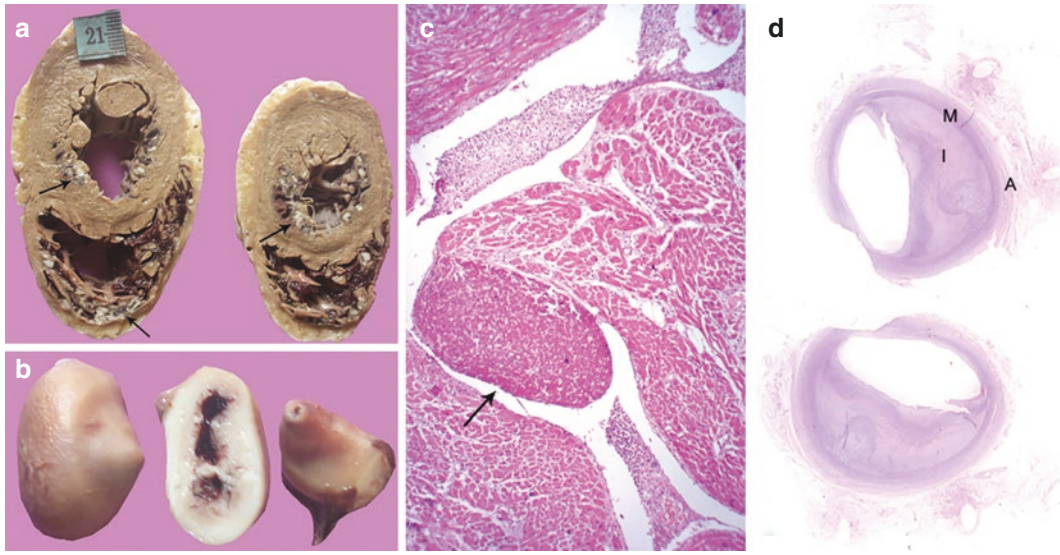

Fig. 59.1 (**a**) Transverse slices of the ventricles showing opaque white thrombi in the intertrabecular spaces of the right RV and left LV ventricles; some of them are shown with arrows; (**b**) Free-floating thrombi found in the right ventricle; (**c**) Bland thrombus (arrow) attached to the right ventricular endocardium (H&E × 250); (**d**) Scanned slide of the left anterior descending artery stained by H&E showing a distinct blue hue over the superficial aspect and core of an eccentric atheroma present in the intima I. There is 50% luminal narrowing (*A* adventitia, *M* media)

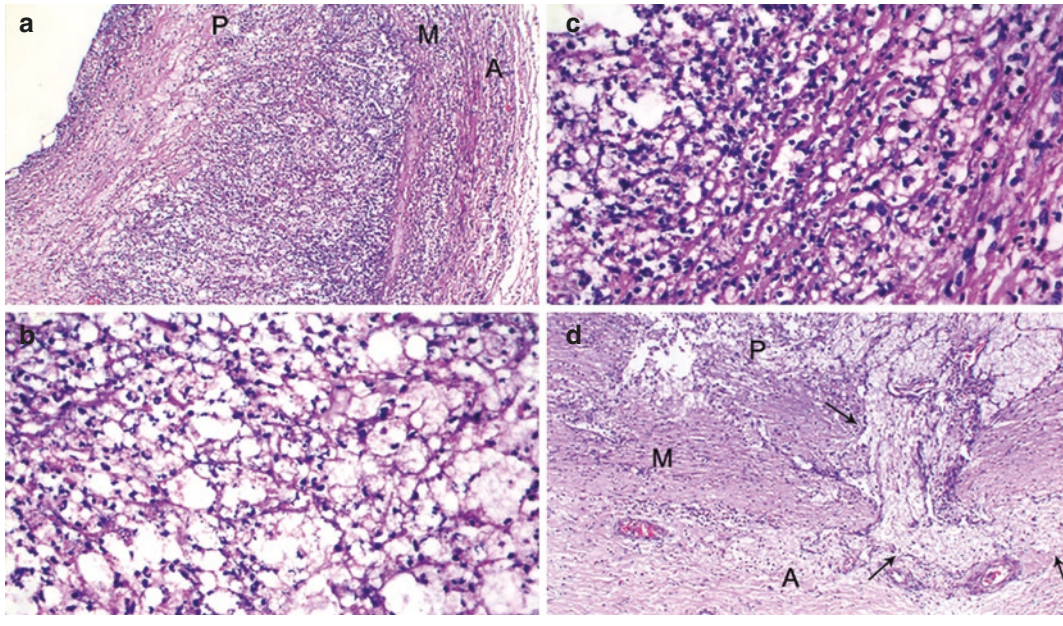

Fig. 59.2 (**a**) Infiltration of the intimal plaque P, media M, and adventitia A by neutrophils (H&E × 200); (**b**) Neutrophils admixed with large numbers of macrophages (H&E × 400); (**c**) Destruction of the media by neutrophils (H&E × 400); (**d**) Foam cells (arrows) migrating from the intimal plaque P through the media M into the adventitia (H&E × 200)

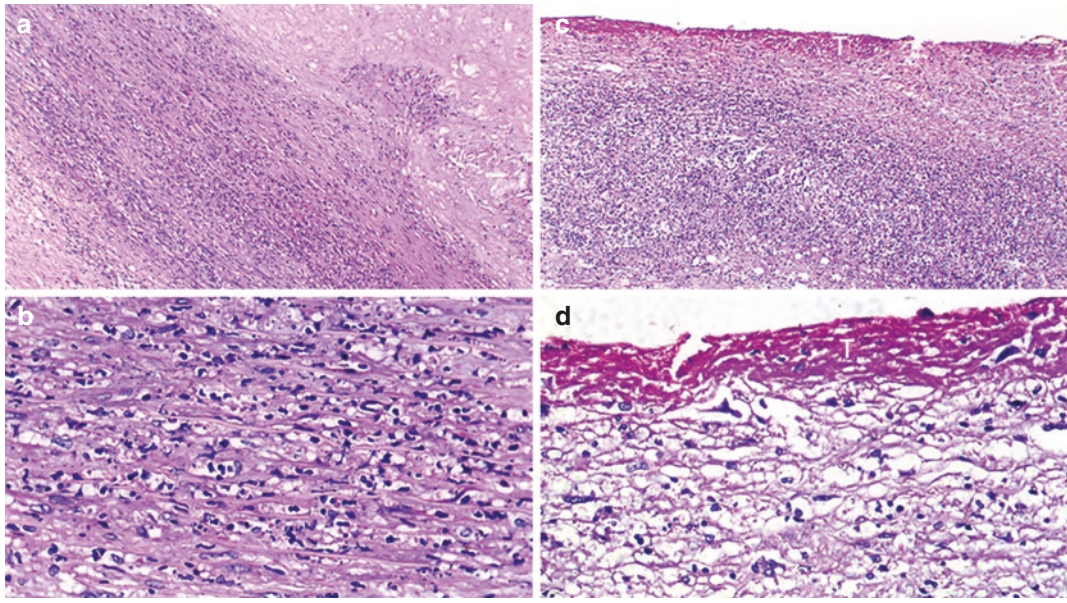

Fig. 59.3 Aortic media infiltrated by neutrophils—(**a**) H&E × 250) and (**b**) H&E × 400; (**c**) Superimposed thrombus T over an intimal plaque that is heavily infiltrated by neutrophils (H&E × 250); (**d**) Thrombus over the plaque, which is rich in foam cells (H&E × 400)

some areas, there appeared to be an active migration of foam cells into the adventitia to form small clusters (Fig. 59.2d). Similar features were seen in the aortic atheromatous plaques (Fig. 59.3a, b) with a thin layer of superimposed thrombi seen focally (Fig. 59.3c, d). The non-atherosclerotic regions of the aorta did not show such features. Few thromboemboli were seen in some of the intrapulmonary arteries; no bronchopneumonia, abscess, or hyaline membranes were identified. The kidneys revealed focal cortical necrosis with accompanying papillary necrosis. The sinusoids of the liver and spleen were infiltrated by neutrophils.

Cause of Death: Septicemia and acute coronary insufficiency.

59.3 Discussion

This case presentation highlights the exclusive accumulation of neutrophils within the coronary and aortic atherosclerotic plaques in a setting of septicemia. Atherosclerosis, primarily an intimal disease of the arteries of all sizes, is considered as a chronic inflammation that occurs in response to multifactorial endothelial injury. The process begins independent of race, gender, or environmental factors due to physiological hemodynamic stress, which explains its presence at certain anatomic sites such as the dependent portions of the body and at sites of natural eddy currents or arterial tortuosity. However, the age-related progression of these preclinical lesions and/or formation of fresh lesions at other sites, with accumulation of intracellular/extracellular lipid and collagenic/noncollagenic matrix, is related to the presence of risk factors.

The chief conductor of the atherosclerotic orchestra is undoubtedly the macrophage. Endothelial damage and dysfunction induced by shear forces, hyperlipidemia, pro-inflammatory cytokines, and even chronic stress facilitate the adhesion of circulating monocytes with subsequent transmigration and intimal accumulation as

foam cells. In the later stages, they contribute to the formation of the necrotic core, and through release of variety of molecules, lead to plaque destabilization. In the recent years, neutrophils—the first line of defense in infections, have also been shown to play an unobtrusive role (owing to their short life span) in the initiation, build-up, and complications of the atherosclerotic plaque. In general, there is an increase in the neutrophil count in response to the metabolic alterations associated with atherosclerosis, particularly hyperglycemia and dyslipidemia. The endothelial injury and activation of platelets recruit the neutrophils and potentiate the entry of the cells into the arterial wall with enhanced expression of the cytokines and adhesion molecules. During the phases of activation, transmigration, and tissue infiltration, there is release of various proteins and enzymes present within the azurophilic, specific, and tertiary granules, which play an important role in macrophage activation, plaque destabilization, and erosions of the fibrous caps. Another important mechanism that triggers the aforementioned phenomena is disintegration of the neutrophils and formation of neutrophil extracellular traps, which are aggregated complexes of DNA, histones, and several components of the neutrophil granules. In this case, there was an extraordinary degree of neutrophils within the plaques with abundant nuclear debris. There also appeared to be a "second wave" of macrophage migration and accumulation, which was focally seen to breach the media and extend into the adventitia. We feel that these findings could be related to circulating microbial endotoxins, which are known to affect the plaque stability in experimental studies.

Further Reading

Cochain C, Ait-Oufella H, Zernecke A. Neutrophils promote atherosclerotic plaque destabilization in a mouse model of endotoxinaemia. Cardiovasc Res. 2018;114:1573–4.

Döring Y, Drechsler M, Soehnlein O, Weber C. Neutrophils in atherosclerosis: from mice to man. Arterioscler Thromb Vasc Biol. 2015;35:288–95.

Franck G. Role of mechanical stress and neutrophils in the pathogenesis of plaque erosion. Atherosclerosis. 2021;318:60–9.

Hartwig H, Roig S, Daemen M, Lutgens E, Soehnlein O. Neutrophils in atherosclerosis: a brief overview. Hamostaseologie. 2015;35:121–7.

Klopf J, Brostjan C, Eilenberg W, Neumayer C. Neutrophil extracellular traps and their implications in cardiovascular and inflammatory disease. Int J Mol Sci. 2021;22:559.

Acute Aortic Dissection

60

Pradeep Vaideeswar, Girish Sabnis, Charan Lanjewar, and Sarit Kundu

60.1 Clinical History

A 55-year-old male was brought to the casualty with acute retro-sternal excruciating chest pain (radiating to medial aspect of left arm and back) and acute shortness of breath since 1 h. He was a chronic smoker and alcoholic. There was no history of hypertension or diabetes mellitus. The patient was diaphoretic with a pulse rate of 110 per minute, blood pressure of 108/90 mmHg, and respiratory rate of 24 per minute; he was hemodynamically stable. Since the ECG was suggestive of acute inferior wall myocardial infarction, it was decided to take up the patient for primary angioplasty. The baseline investigations were normal. He was given a loading dose of aspirin and clopidogrel and was shifted to the cardiac catheterization laboratory. About 20 min later, he developed excruciating pain in the right lower limb. Stenting of the left coronary was performed; however, his condition deteriorated and could be revived despite inotropic support.

60.2 Autopsy Findings

The moderately enlarged heart was kept with the entire aorta. The ascending aorta was larger than the pulmonary artery. Adventitial hemorrhage and a "crackling" consistency were present over the ascending aorta. The hemorrhage also extended into the adventitia of the pulmonary trunk and the anterior right and left atrioventricular grooves. These changes on the external aspect were produced by an acute aortic dissection (AAD), involving the entire aorta (Stanford type I), affecting the greater curvature of the descending aorta. There was a transverse intimal tear (Fig. 60.1a), 4 cm in length in the ascending segment, 3.2 cm above the aortic annulus. The aortic valve was devoid of any congeni-

P. Vaideeswar (✉)
Department of Pathology (Cardiovascular and Thoracic Division), Seth Gordhandas Sunderdas Medical College and King Edward Memorial Hospital, Mumbai, India

G. Sabnis · C. Lanjewar
Dr KK Datey Department of Cardiology, Seth Gordhandas Sunderdas Medical College and King Edward Memorial Hospital, Mumbai, India

S. Kundu
Seth Gordhandas Sunderdas Medical College and King Edward Memorial Hospital, Mumbai, India

P. Vaideeswar (ed.), *Tropical Cardiovascular Pathology*,
https://doi.org/10.1007/978-981-19-3720-0_60

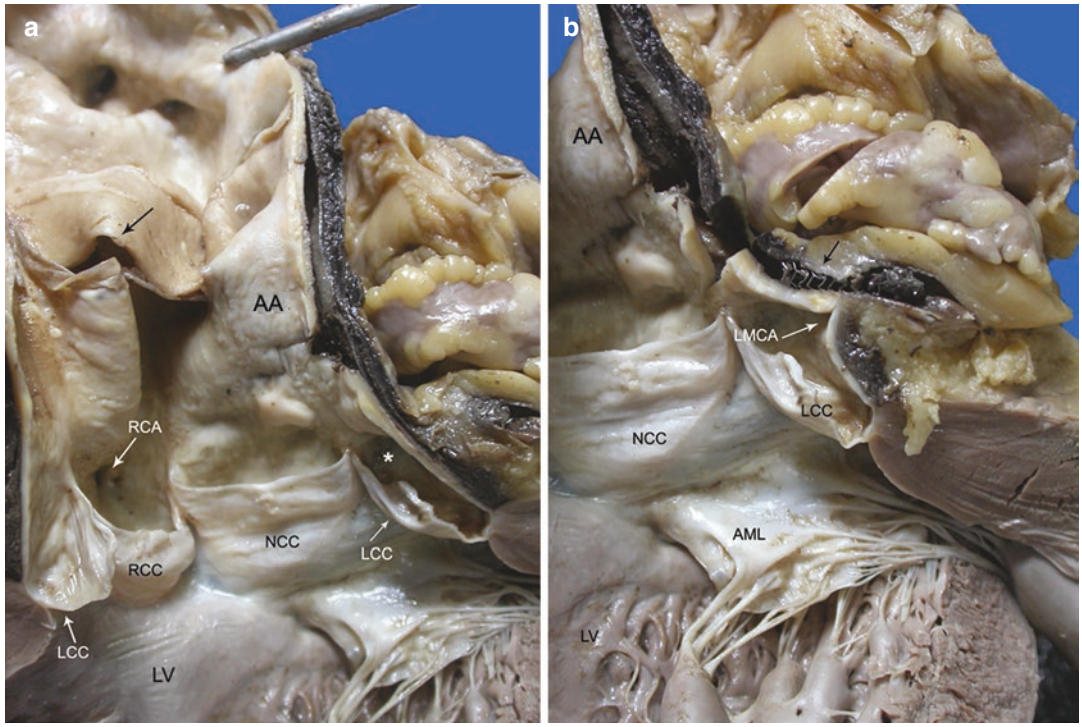

Fig. 60.1 (**a**) A transverse tear (white arrow) is seen in the intima of the ascending aorta AA, well above the sinutubular junction with presence of hemorrhage in the wall. * represents the ostium of the left main coronary artery LMCA, not visible in the image; (**b**) An additional cut reveals the presence of a stent (black arrow) in the false lumen of the dissected LMCA (*AML* anterior mitral leaflet, *LCC* left coronary cusp, *LV* left ventricle, *RCA* right coronary artery, *RCC* right coronary cusp, *NCC* coronary cusp)

tal anomalies. The ostium of the left coronary artery was narrowed and a stent was seen to be deployed into the false channel of the artery (Figs. 60.1b and 60.2a–c). The right coronary artery was surrounded by hemorrhagic epicardial fat (Fig. 60.1a); there was no dissection. There was extension of the dissection into the right brachiocephalic artery (0.8 cm), left common carotid artery (1.6 cm, Fig. 60.1a), left subclavian artery (1 cm), and also into the common iliac arteries. Features of acute myocardial infarction and aortopathy were not seen. There were pulmonary edema and smoking-related respiratory bronchiolitis.

Cause of Death: Acute myocardial ischemia following AAD.

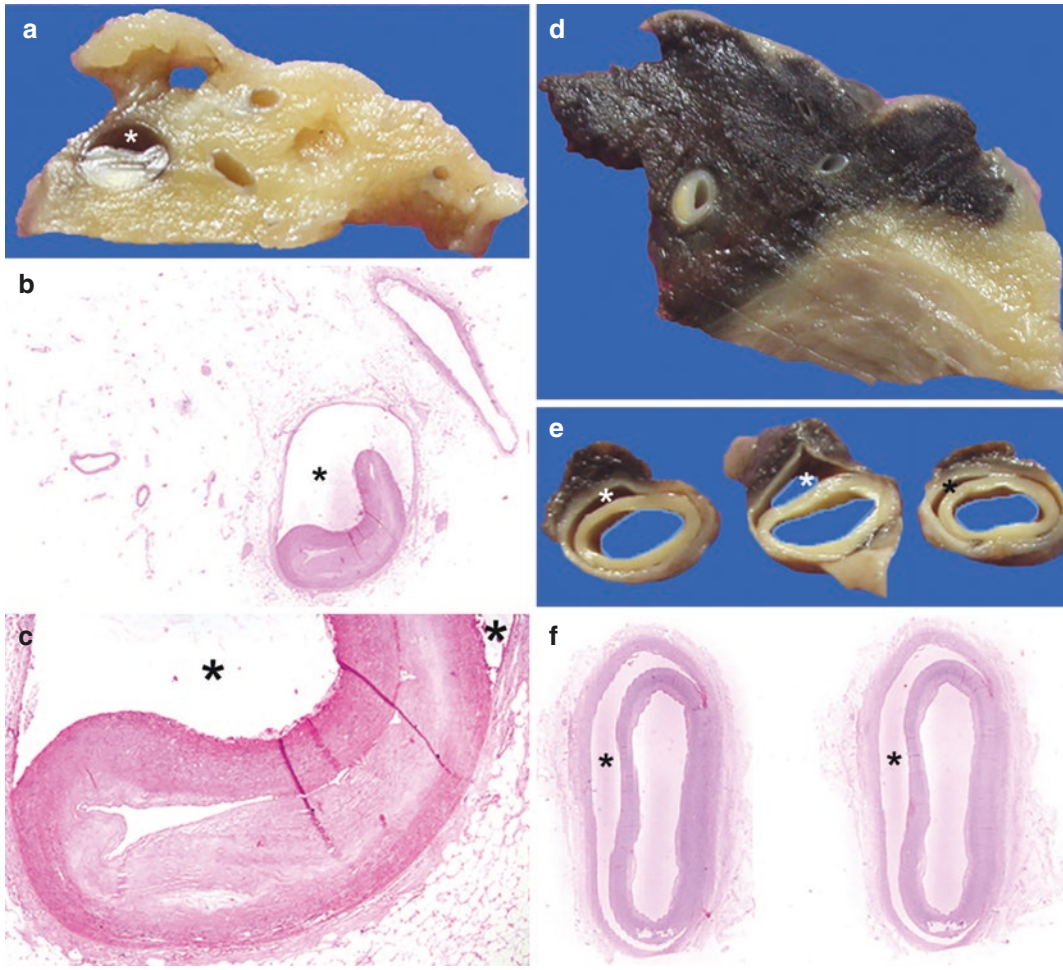

Fig. 60.2 Dissection seen in (**a**) the cut surface of the left anterior descending artery; (**b**) scanned H&E stained section, and (**c**) low power (H&E × 100) of the artery. Note eccentric non-critical plaque atheromatous plaque and slit-like true lumen; (**d**) the right coronary artery is surrounded by hemorrhagic epicardial fat; dissection of the left common carotid artery as seen in (**e**) serial slices and (**f**) scanned H&E stained section. * is in the false channel

60.3 Discussion

The differential diagnoses of acute severe chest pain in adults must include acute aortic syndrome (AAS) in addition to the more common acute coronary syndromes (see Chaps. 24–27) and pulmonary thrombo-embolism (see Chap. 68). AAS is a well-established term that includes 3 uncommon (3.5–6.0 per 100,000 patients/year), but devastating aortic disorders of acute aortic dissection (AAD), penetrating atherosclerotic ulcer (see Chap. 58), and intra-mural hematoma. The common binding factor for these lesions is the clinical presentation of aortic pain (with or without radiation), pulse deficits, blood pressure variations, and/or end-organ ischemia; the pain is caused by disruption of the media that develops often due to long-standing alterations in the aortic wall. In this instance, AAS was initiated by a transverse almost circumferential intimal tear in

the ascending aorta, which allowed the "high pressure" blood to enter and split the aortic media at the junction of its inner two-thirds and outer one-third. This is the defining feature of classic aortic dissection (AD) that is responsible for 85–95% of cases of AASs. It results in the formation of double-barreled aorta with its true lumen and a false channel within the wall; the latter may propagate within the wall for a variable distance taking an anterograde (most commonly) or a retrograde course. The propagation may re-enter the true lumen through another tear (intimal re-entry or exit tear) or may result in aortic rupture. With reference to the duration of symptoms, the ADs are hyper-acute (less than 24 h, as in the present case), acute (within 1 week), sub-acute (8–30 days), and chronic (for more than a month).

The estimated worldwide incidence of AAD is around 4.8 per 100,000 individuals per year, which may increase up to 30 in persons above the age of 65 years. However, the true incidence remains unknown as some cases would have had sudden cardiac death and may not have been necessarily autopsied. It occurs more often in males and has a chrono-biologic rhythm pattern with its more frequent occurrence during winter, in the early hours of the morning, and on Mondays! Conditions that increase the wall stress or induce abnormalities of the aortic media are the main causes of non-traumatic and non-iatrogenic AAD. Hypertension (often poorly controlled) is the major risk factor, seen in almost two-thirds of the patients with AAD; other factors include syndromic/non-syndromic genetic abnormalities, congenital aortic valvular abnormalities (see Chaps. 13 and 14), inflammatory diseases, smoking, and drugs like cocaine or amphetamines. In the non-inflammatory conditions, there are very often moderate to severe alterations in the aortic media (aortopathy, see Chap. 61) that permits the catastrophic disruption.

Aortic dissection is classified according to the extent of involvement. In the Stanford system, presence and absence of dissection of the ascending aorta constitute Type A and Type B dissections, respectively. Type A AAD is more frequent (60–70%, incidence rate of 1–3 per 100,000 individuals per year) and affects younger individuals, while Type B AAD has a rate of occurrence of 1.6 per 100,000 individuals per year, affecting the elderly hypertensive patients. The other classification was devised by DeBakey Type I where there is dissection of the ascending aorta with variable extension into the remaining segments; Type II with dissection limited to the ascending aorta; and Type III where there is involvement of the descending aorta distal to origin of the left subclavian artery with dissection in the thoracic (Type IIIa) or thoraco-abdominal (Type IIIb) segments. In the case presented, there was dissection of the entire aorta (Stanford Type A or DeBakey Type I). Our patient did not have hypertension. The only risk factor was smoking, and despite such extensive involvement, there were hardly any medial changes seen on histology. There was large intimal tear in the ascending aorta, which is seen in 65% cases of AAD. Such tears are located in the right lateral wall within 3 cm of the sinutubular junction. Tears in the descending aorta are present in close proximity to the ligamentum arteriosum (20% of the cases). Both areas are sites of greatest hydraulic stress. Arch (10%) and distal portions of the descending aorta (5%) are the less common sites for such tears.

Acute chest pain, which has been variously described as instantaneous, severe, sharp, stabbing, tearing, ripping, or lancinating (aortic pain) is the most common mode of presentation seen in almost 80–90% of the patients. Radiation of the pain to the neck indicates involvement of the ascending aorta, while radiation to the back or abdomen is suggestive of dissection in the descending aorta. But sometimes, the pain may be absent. Since the blood pressure in the false channel is high and constant, there is dynamic or static compression of the true lumen leading to malperfusion of the aortic branches, resulting in end-organ ischemia or infarction. This results in a variety of non-cardiac symptoms and signs. The cardiac complications include aortic insufficiency, myocardial dysfunction, and hemopericardium due to rupture within the pericardial cavity. There can also be an extravasation of blood onto the pulmonary arterial adventitia (pulmonary sheath hematoma) or within the wall (intra-mural hematoma) or even fistulous connections with features of right ventricular failure.

Our patient was an elderly male smoker at risk for atherosclerosis and had presented with typical angina and normal blood pressure. ECG also showed features of inferior wall myocardial infarction. The ischemic myocardial dysfunction is seen in 1–2% of patients with AAD and is caused by an extension of the dissection into the coronary artery or an ostial occlusion by the dissection flap, often affecting the right artery. Differentiating Stanford A AAD with coronary malperfusion from true ACS can be challenging and the misdiagnosis occurs to an extent of 40% in the emergency room. It is important to note that AAD is the most catastrophic event associated with a high early mortality rate of 1–2% per hour within the first few hours. Besides, misdiagnosis may lead to inappropriate administration of anticoagulant/thrombolytic therapy or even interventions, as seen in this patient. The only clue of AAD was the excruciating pain in the lower limb that manifested during per-cutaneous coronary intervention suggesting passage of catheter into the false lumen. This case demonstrates that AAD should always be considered as a differential diagnosis in patients presenting with acute chest pain. It is imperative to carefully evaluate clinical history (especially history of hypertension), chest pain characteristics, and risk factors in patients presenting with ST segment elevation. It must be a matter of habit to check the arterial pulses and blood pressure in all four limbs for possible difference. D-dimer level over 1600 ng/mL within the first 6 h of presentation favors aortic dissection and may be a useful tool in differentiating it from ACSs. Rapid identification and categorization of AAD are aided by imaging as the therapy and outcome relies on multi-disciplinary approach for the use of medical therapy and surgical and/or endo-vascular interventions.

Further Reading

Bossone E, Eagle KA. Epidemiology and management of aortic disease: aortic aneurysms and acute aortic syndromes. Nat Rev Cardiol. 2021;18:331–48.

Gouveia E, Melo R, Mourão M, Caldeira D, Alves M, Lopes A, Duarte A, et al. A systematic review and meta-analysis of the Incidence of acute aortic dissections in population-based studies. J Vasc Surg. 2022;75(2):709–20.

Grewal N, Velders BJJ, Gittenberger-de Groot AC, Poelmann R, Klautz RJM, Van Brakel TJ, et al. A systematic histopathologic evaluation of Type-A aortic dissections implies a uniform multiple-hit causation. J Cardiovasc Dev Dis. 2021;8:12.

Joannaa G, Felix S, Arnold VE. Acute aortic dissection: pathogenesis, risk factors and diagnosis. Swiss Med Wkly. 2017;147:w14489.

Morello F, Santoro M, Fargion AT, Grifoni S, Nazerian P. Diagnosis and management of acute aortic syndromes in the emergency department. Intern Emerg Med. 2021;16:171–81.

Noda K, Inoue Y, Matsuo J, Yokawa K, Uehara K, Sasaki H, et al. Type A aortic dissection with left coronary malperfusion. Gen Thorac Cardiovasc Surg. 2021;70(2):178–80. https://doi.org/10.1007/s11748-021-01728-9.

Rogers RK, Reece TB, Bonaca MP, Hess CN. Acute aortic syndromes. Cardiol Clin. 2021;39:495–503.

Sayed A, Munir M, Bahbah EI. Aortic dissection: a review of the pathophysiology, management and prospective advances. Curr Cardiol Rev. 2021;17:e230421186875.

Sherk WM, Khaja MS, Williams DM. Anatomy, pathology, and classification of aortic dissection. Tech Vasc Interv Radiol. 2021;24:100746.

Yadav R, Mughal H, Rimmer L, Bashir M. From ER to OR-Type A aortic dissection delay dilemma. J Card Surg. 2021;36:1056–61.

Ascending Aortic Aneurysm

61

Pradeep Vaideeswar

61.1 Clinical History

A 27-year-old female was admitted in the Emergency Services Department in a gasping state, and despite resuscitative measures, she expired within 2 h. The pulse rate had been 96 per minute and the systolic blood pressure was 90 mmHg. The clinical impression had been aortic regurgitation (AR) as ejection systolic and diastolic murmurs had been heard. Progressive dyspnea, palpitation, and episodic left-sided chest pain had been present for the past 4 months.

61.2 Autopsy Findings

A complete autopsy was performed. The patient was averagely built. There was moderate enlargement of the heart (weight 570 g) with moderate enlargement of the ventricles and right atrium, and mild enlargement of the left atrium. Diffuse epicardial opacification was present. A remarkable feature was the aneurismal dilatation (diameter of 7.4 cm) restricted to the ascending aorta (AA). The arch and the descending aorta were of normal sizes. The opened out left ventricular outflow tract revealed mild dilatation of the aortic root with separation of the commissures. The aortic valve had 3 semilunar cusps, which appeared slightly stretched and shortened accompanied by prominent central nodules and rolling of their free margins. This indicated the presence of chronic AR; the regurgitant jet had also produced a jet lesion in the subaortic region of the interventricular septum (Fig. 61.1). In sharp contrast to the mildly dilated aortic annulus, there was an aneurismal dilatation of the AA that had a slippery consistency, rugose intimal thickening, and thick gelatinous wall. The aneurysm abruptly tapered towards the junction between AA and arch of aorta. Moderate dilatation of the left ventricular cavity with moderate hypertrophy and patent foramen ovale (PFO) were also present.

The histology of the AA showed severe changes of aortopathy (Fig. 61.2) in the form of extensive fragmentation and paucity of the elastic fibers, intralamellar/translamellar increase of basophilic ground substance, and focal loss as well as haphazard proliferation of smooth muscle cells. This was accompanied by diffuse moderate to marked fibrocellular intimal thickening. There was no dissection; rest of the aorta was normal. Similar changes were also present in the pulmonary trunk. Apart from histomorphological features of hypertrophy, the left ventricle also showed ischemia of the cardiomyocytes with focal increases in the interstitial connective tissue. The other findings were chronic passive

P. Vaideeswar (✉)
Department of Pathology (Cardiovascular and Thoracic Division), Seth Gordhandas Sunderdas Medical College and King Edward Memorial Hospital, Mumbai, India

P. Vaideeswar (ed.), *Tropical Cardiovascular Pathology*,
https://doi.org/10.1007/978-981-19-3720-0_61

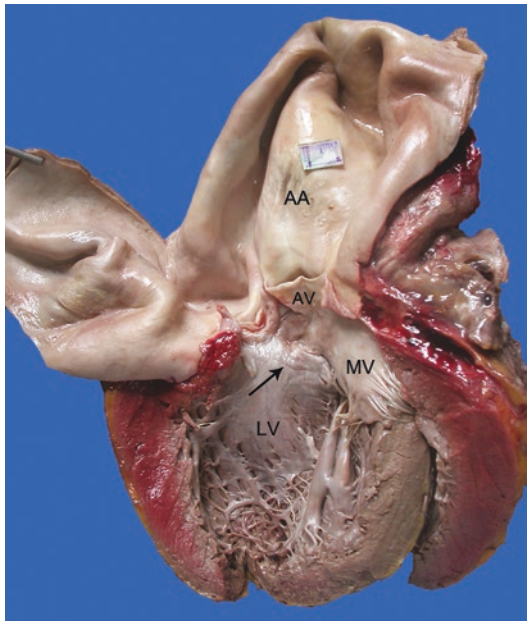

Fig. 61.1 Opened left ventricular LV outflow tract with dilated aortic annulus and jet lesion of aortic regurgitation (arrow). The ascending aorta AA is aneurismal with thick gelatinous walls (*AV* aortic valve, *MV* mitral valve)

venous congestion of the lungs/liver and congestive splenomegaly.

Cause of Death: Severe aortopathy, AA aneurysm, and AR.

61.3 Discussion

A large aneurysm exclusively restricted to the AA, unrelated to atherosclerosis or inflammation, was found at autopsy in a young woman. The underlying cause was an extensive "degeneration" of the aortic tunica media. Aneurysms, defined as localized arterial dilatation that exceeds 50% of the normal diameter at that site, can affect both the thoracic and abdominal segments of the aorta (usually diameter of more than 3 cm). The thoracic portion includes the aortic root, and ascending, transverse, and descending thoracic components. Since these segments differ in their embryological developments (neural crest/second heart field derivation for the aortic

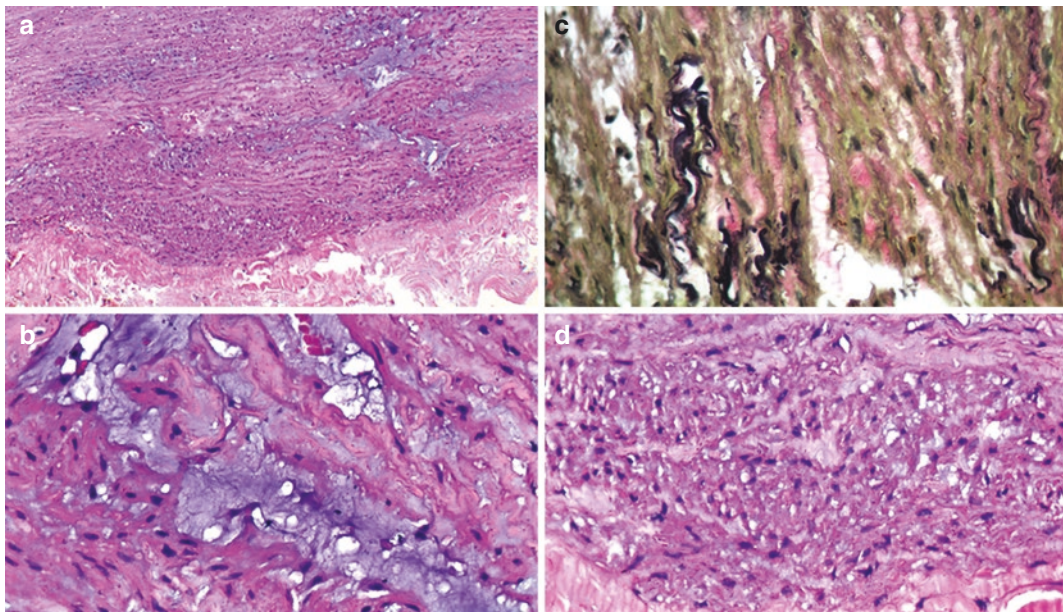

Fig. 61.2 Features of aortopathy—(**a**) Thickening of the wall due to increased basophilic ground substance and collagenization (H&E × 200); (**b**) The basophilic ground substance separates the elastic fibers and smooth muscle cells (H&E × 400); (**c**) There is paucity of elastic fibers with short stumps and fragmentation. Note accompanying collagenization (Elastic van Gieson × 400); (**d**) Irregular, nodular proliferation of the smooth muscle fibers (H&E × 400)

root, ascending aorta and arch of aorta, para-axial mesoderm for the descending aorta), there are striking differences in the mechanisms of aneurismal dilatations. The abdominal aortic aneurysms are more frequent and develop mostly in elderly individuals with prevailing cardiovascular risk factors; they are commonly located in the infrarenal region. However, thoracic aortic aneurysms (TAAs) are uncommon with an estimated incidence of 6–10 cases per 100,000 per year. The patients are younger and lack the traditional risk factors, and moreover, the pathogenesis is related usually to inherited alterations of the aortic media.

In general, the aortic media is composed of circumferentially arranged fenestrated elastic laminae, which enclose similarly arranged vascular smooth muscle cells and these are organized within a complex of mucopolysaccharides and collagen. This arrangement constitutes the lamellar unit (approximately 11 μm thick). Expectedly larger number of lamellar units and thicker media are seen in the thoracic aortic segments to withstand, accommodate, and transmit the pressure during left ventricular systole. The mechanical stimuli are transmitted from the endothelial cells to the smooth muscle cells by biochemical signals with subsequent cellular and noncellular modifications directed towards integrity and optimal function of the media. The ordered structure and function is perturbed by a range of mutations in genes that encode the extracellular matrix components, contractile proteins of the smooth myocytes, and proteins in the signalling pathways. These disturbances trigger a transition of the vascular smooth muscle from a "contractile" phenotype to a "synthetic" cell along with an upregulation of the proteolytic enzymes and/or downregulation of their inhibitors. It results in a constellation of changes, designated as 'aortopathy', which includes the eye-catching mucoid extracellular matrix accumulation (MEMA, previously called as cystic medionecrosis of Erdheim), elastic fiber fragmentation, loss, thinning and/or disorganization, loss of smooth muscle nuclei, smooth muscle disorganization, laminar collapse, and fibrosis. These features can be individually and subjectively graded with a final summation of the overall medial degeneration as mild, moderate, or severe. The effect manifests as aneurysms and/or aortic dissections (See Chap. 60)

Severe aortopathy (affecting more than 10 lamellar units), particularly involving the AA, was seen in our patient. These medial changes in young patients result from heritable disorders that are classified as syndromic and non-syndromic, depending on the presence or absence of extracardiac organ involvement. The syndromic variants include Turner's syndrome and connective tissue disorders like Marfan, Loeys-Dietz, and vascular Ehlers-Danlos syndromes. The non-syndromic forms may be familial (autosomal dominant) or sporadic (including the bicuspid aortic valve, See Chap. 13). Up to 80% of the cases are sporadic in nature. In this case, features of Turner's syndrome or other connective tissue disorders were not seen. The aortic valve had 3 cusps. Apart from the PFO, there were no other structural congenital anomalies. A family history could not be elicited. Genetic analyses could not be also performed due to lack of facilities.

Majority of the TAAs occur in the aortic root or AA (60%), followed by the descending thoracic aorta (30%) and arch of aorta (10%); in some patients, more than one component may be affected. The cellular modulation and maladaptive remodelling of the matrix produce a pear-shaped or fusiform dilatation of the wall; saccular morphology is not the usual feature. Following dilatation, with reference to the Laplace's law, there is increase in the wall stress, exacerbating the medial abnormalities and further dilatation, setting up a vicious circle. Unfortunately, despite the aneurysm, 95% remain asymptomatic since the dilatation is slow-paced (about 0.1 cm per year). The remaining patients develop symptoms related to AR or compression of the adjoining structures. Such symptomatic aneurysms should undergo evaluation by imaging techniques for surgical repair to prevent the most ominous complications of rupture, aortic dissection, or sudden death. The risk

of these complications is 6.5% and 14.1% for TAAs with diameters greater than 5.0 cm and 6.0 cm, respectively. The aneurysm in this deceased was 7.4 cm and was associated with myocardial ischemia. A diameter of 5.5 cm or more entails a prophylactic surgical excision in asymptomatic individuals. Since ruptures or dissections can occur with a lesser diameter, the aortic dimensions could be correlated with location, etiology, other risk factors, and other personalized parameters like age, sex, height, body size, and lifestyle.

Further Reading

Bossone E, Eagle KA. Epidemiology and management of aortic disease: aortic aneurysms and acute aortic syndromes. Nat Rev Cardiol. 2021;18:331–48.

Creamer TJ, Bramel EE, Mac Farlane EG. Insights on the pathogenesis of aneurysm through the study of hereditary aortopathies. Genes (Basel). 2021;12:183.

Halushka MK, Angelini A, Bartoloni G, Basso C, Batoroeva L, Bruneval P, et al. Consensus statement on surgical pathology of the aorta from the Society for Cardiovascular Pathology and the association for European cardiovascular pathology: II. Noninflammatory degenerative diseases—nomenclature and diagnostic criteria. Cardiovasc Pathol. 2016;25:247–57.

Huang T, Yang B. Heritable thoracic aortic aneurysms and dissections. Tech Vasc Interv Radiol. 2021;24:100747.

Iddawela S, Ravendren A, Harky A. Bio-chemo-mechanics of the thoracic aorta. Vasc Biol. 2021;3:R25–33.

Senser EM, Misra S, Henkin S. Thoracic aortic aneurysm: a clinical review. Cardiol Clin. 2021;39:505–15.

Thakker PD, Braverman AC. Cardiogenetics: genetic testing in the diagnosis and management of patients with aortic disease. Heart. 2021;107:619–26.

Yap ZJ, Sharif M, Bashir M. Is there an immunogenomic difference between thoracic and abdominal aortic aneurysms? J Card Surg. 2021;36:1520–30.

62 Long-Segment Aortic Thrombosis with Myoglobinuria and Acute Renal Failure

Pradeep Vaideeswar and Balaji Baste

62.1 Clinical History

A 42-year-old male was referred from a rural health center for complaints of backache, inability to stand, and incontinence of bowel and bladder for the past 2 days. There was no history of fever or trauma. On examination, the general condition was fair. The patient was conscious and well-oriented to time and space. The pulse rate was 90 per minute and the blood pressure was 148/80 mmHg. There was bilateral lower limb hypotonia with absent knee and ankle reflexes. The investigations were as follows: hemoglobin 15 g/dL, total leukocyte count 30,800/cmm (Neutrophil predominant—86%), platelet count 2 lakhs/cmm, blood glucose 171 mg/dL, blood urea nitrogen 51 mg/dL, creatinine 4.3 mg/dL, serum aspartate aminotransferase 585 U/L, serum alanine aminotransferase 1945 U/L, alkaline phosphatase 236 U/L, serum electrolytes—sodium 135 mEq/L, potassium 5 mEq/L, and chloride 96 mEq/L. The clinical diagnosis was paraparesis and acute renal failure of uncertain etiology. The patient had a rapid deterioration and expired within 45 min of his admission.

P. Vaideeswar (✉)
Department of Pathology (Cardiovascular and Thoracic Division), Seth Gordhandas Sunderdas Medical College and King Edward Memorial Hospital, Mumbai, India

B. Baste
Department of Pathology, Seth Gordhandas Sunderdas Medical College and King Edward Memorial Hospital, Mumbai, India

62.2 Autopsy Findings

The heart was mildly enlarged in size with a weight of 330 g. There was mild enlargement of both the ventricles. The transverse section through both ventricles showed the presence of mild concentric left ventricular hypertrophy along with yellowish-white to yellowish-brown mural thrombi in the ventricular cavities (Fig. 62.1a). The right coronary artery had a dominant distribution. The left anterior descending artery, right from its origin for a length of 2 cm, showed critical stenosis by a fibro-fatty plaque (Fig. 62.1b).

The ascending, transverse, and proximal 14 cm of the descending thoracic aortic segments were normal. The remaining portion of the distal thoracic segment and the entire abdominal portion were occluded by a fresh thrombus (Fig. 62.2a). The thrombus extended into the bifurcation and both the common iliac arteries; the right branch was occluded in its entire length (Fig. 62.2b). Surprisingly, the underlying aorta/arteries revealed only uncomplicated atherosclerotic plaques (Fig. 62.2c). The acute renal failure was related to extensive myoglobinuria with formation of large numbers of myoglobin casts (Fig. 62.3), which would have been related to ischemic rhabdomyolysis occurring in his lower limbs.

Cause of Death: Myoglobinuria and acute renal failure.

P. Vaideeswar (ed.), *Tropical Cardiovascular Pathology*,
https://doi.org/10.1007/978-981-19-3720-0_62

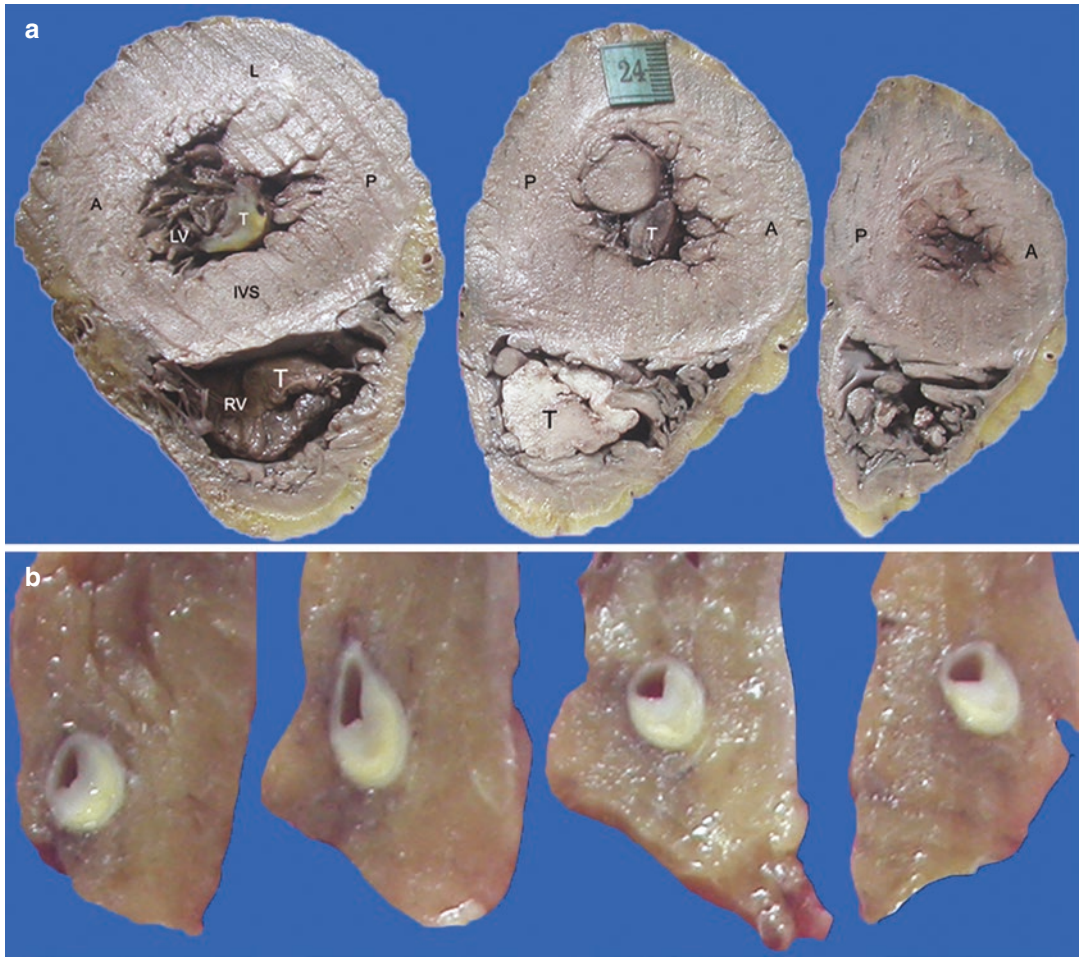

Fig. 62.1 (**a**) Mural thrombi T seen in both ventricles. There is mild left ventricular LV hypertrophy (*A* anterior wall, *IVS* interventricular septum, *L* lateral wall, *P* posterior wall, *RV* right ventricle); (**b**) Critical stenosis of the left anterior descending artery by fibro-fatty eccentric plaque

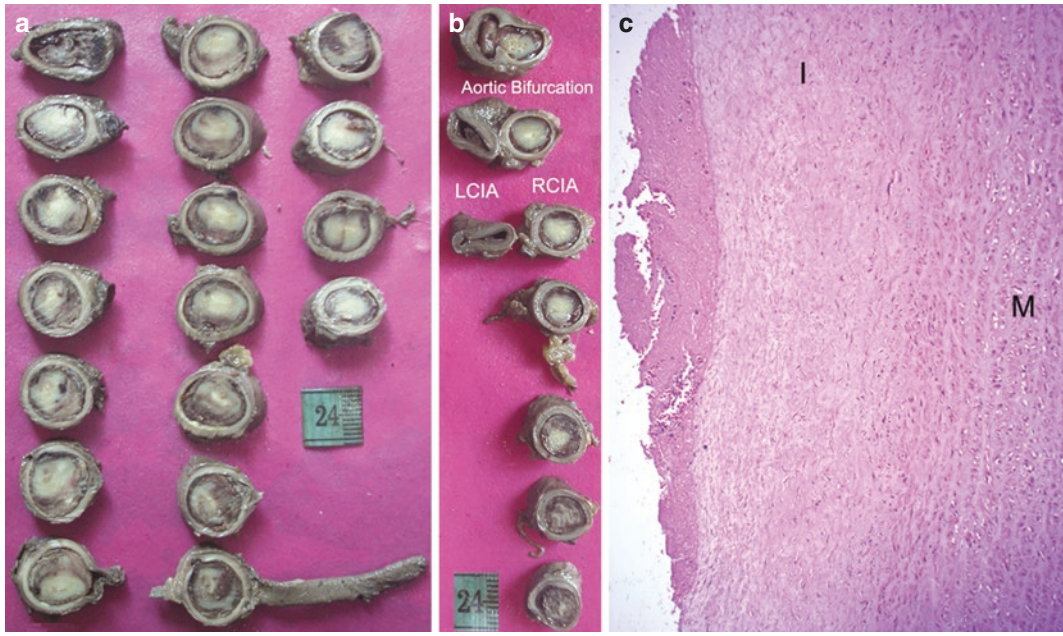

Fig. 62.2 (**a**) Occlusive thrombus in the distal descending thoracic and entire abdominal aorta; (**b**) The thrombus extends up to the bifurcation and involves the right common iliac artery RCIA (*LCIA* left common iliac artery); (**c**) Fresh thrombus is adherent to a fibrous intimal I plaque. The media M is normal

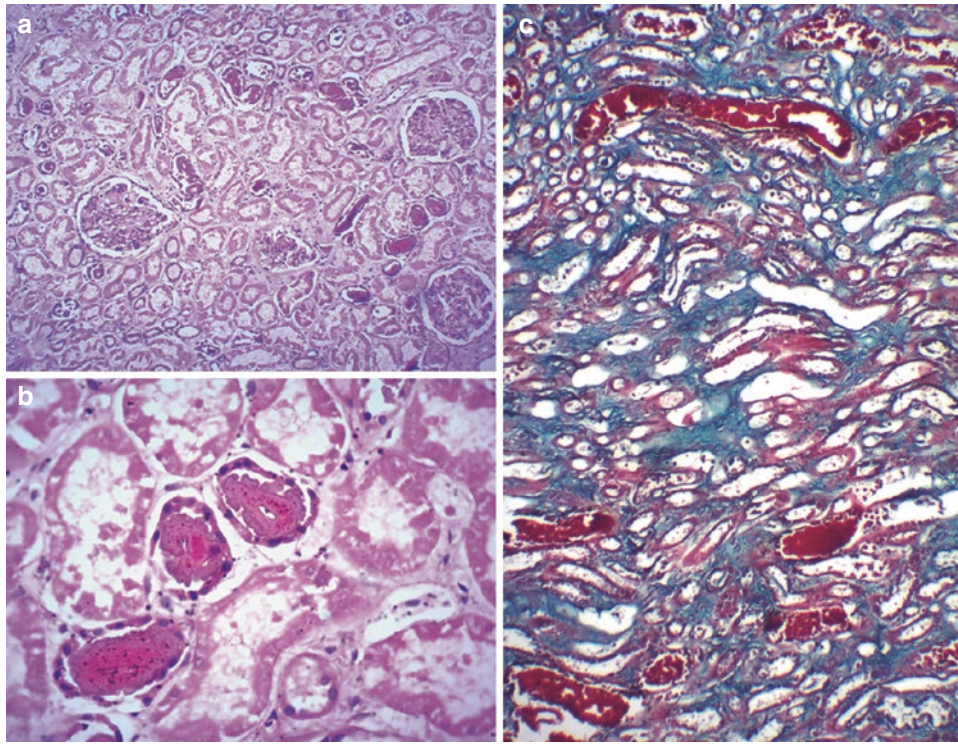

Fig. 62.3 Many of the tubules are filled with reddish brown material—myoglobin, (**a**) H&E × 200 and (**b**) H&E × 400. (**c**) The myoglobin casts appear bright red (Masson Trichrome × 200)

62.3 Discussion

Thrombogenicity stems from one or more of the causal factors involved in the Virchow's triad of endothelial injury, blood flow stasis, and hypercoagulability. The prevailing view is that venous and arterial thromboses are 2 distinct pathophysiological entities. Venous thrombosis is more common and has been related more to an activation of the clotting system often in a setting of stasis. Arterial thrombosis, on the other hand, has been most often associated with platelet activation, inflammation, and lipid interplay. Hence, most arterial thrombi develop as a sequel to erosion or rupture of an underlying atherosclerotic plaque. Besides, the arterial occlusion or obstruction can be a manifestation of embolization from intracardiac thrombi or thrombi from an atherosclerotic or aneurysmal aorta. Mural thrombi that form in the aorta in the absence of significant atherosclerosis or aneurysmal disease are uncommon with an autopsy incidence of 0.45%. In the case depicted too, there was no aneurysm and the atherosclerosis was minimal. The thrombus in the left ventricle also did not appear to be a likely source such as of an extensive long-segment aortic involvement and occlusion.

The non-atherosclerotic and non-aneurysmal aortic thrombosis in some instances are truly idiopathic or primary, but in other cases are associated with traditional risk factors (smoking, hypertension, diabetes mellitus, and dyslipidemia) and other infrequent hypercoagulable states such as thrombocytosis, polycythemia, collagen vascular disorders, antiphospholipid antibody syndrome, deficiencies of proteins C and S, cancers, use of oral contraceptives, steroid therapy, and drug abuse. Our patient also had biventricular mural thrombi, unassociated with ischemic or nonischemic myocardial pathology. He also had prominent coronary atherosclerosis, but unfortunately, the patient was not thoroughly investigated for traditional risk factors or other conditions that could have induced hypercoagulability. Besides, there were no signs of denudation of the atherosclerotic plaques, a phenomenon identified on histology of the excised aortic segments and which cannot be observed on imaging studies.

The clinical presentation depends on the location of the aortic thrombus and they are classified as Type I (ascending aorta and arch), Type II (descending aorta), Type III (suprarenal abdominal aorta), and Type IV (infrarenal abdominal aorta up to the bifurcation or beyond). The thrombus can be sessile or pedunculated and mural or occlusive. Most of the cases have involvement of the abdominal aorta and present with visceral or lower limb ischemia. Prompt recognition of these lesions by appropriate imaging techniques is important. Apart from anticoagulation, some patients would require endovascular intervention or even aortotomy and thrombectomy. Search for the underlying cause through laboratory studies is also important to prevent future catastrophe.

In the present case, there was involvement of the thoracoabdominal aorta with extension into the common iliac arteries (Leriche's syndrome) with lower limb weakness, which was misconstrued as paraparesis. The cause of the weakness was related to ischemic injury of the muscles of the lower limbs resulting in rhabdomyolysis. The duration of ischemia determines the degree of muscle damage; necroses sets from 2 to 6 h. Loss of about 100 g of skeletal muscle is sufficient to produce a classic triad of symptoms (not seen in all patients) of myalgia, muscle weakness, and passage of cola-colored urine. Apart from various intracellular metabolites and proteins (especially creatine phosphokinase), an important component that is released from injured muscle fibers is myoglobin, which is responsible for the discolored urine. Release of excessive amounts of myoglobin overwhelms the binding capacity of certain plasma proteins like haptoglobin and myoglobin is filtered through the glomeruli. However, myoglobin is toxic and leads to acute tubular damage with deposits of myoglobin casts (in combination with Tamm-Horsfall protein), as seen in this case. The cast formation is enhanced under an acidic environment. The tubular damage and obstructive casts with other factors such as arteriolar vasoconstriction and disseminated intravascular coagulation result in acute renal failure seen in 3–33% of the patients with rhabdomyolysis (clinically severe). Histopathological features of cardiac, pulmonary, or hepatic

involvement were not present. This myorenal syndrome is life-threatening (cause of death in this case) and entails renal replacement therapy.

Further Reading

Fayad ZY, Semaan E, Fahoum B, Briggs M, Tortolani A, D'Ayala M. Aortic mural thrombus in the normal or minimally atherosclerotic aorta. Ann Vasc Surg. 2013;27:282–90.

Gupta A, Thorson P, Penmatsa KR, Gupta P. Rhabdomyolysis: revisited. Ulster Med J. 2021;90:61–9.

Meyermann K, Trani J, Caputo FJ, Lombardi JV. Descending thoracic aortic mural thrombus presentation and treatment strategies. J Vasc Surg. 2017;66:931–6.

Nayak S, Jindal A. Myoglobinuria and acute kidney injury. J Integr Nephrol Androl. 2015;2(2):50–4.

Verma H, Meda N, Vora S, George RK, Tripathi RK. Contemporary management of symptomatic primary aortic mural thrombus. J Vasc Surg. 2014;60:1524–34.

Childhood Takayasu's Arteritis

63

Pradeep Vaideeswar

63.1 Clinical History

An 8-year-old male had several admissions to private hospitals from December onwards for high-grade fever associated with chills with a temporary response to symptomatic medication. He was admitted to our tertiary-care center with high-grade fever, neck rigidity, and mediastinal/axillary lymphadenopathy (fine-needle aspiration and biopsy reports of reactive lymphadenitis) in the month of May in the following year. He was discharged on antibiotics after 26 days. After 41 days, he was again admitted to our center in the month of July for recurrence of fever. Investigations during this admission revealed hypertension (blood pressure of 160/100 mmHg), mild global dyskinesia (ejection fraction of 50%), circumferential thickening of the arch of aorta and its major branches, and high grade left renal ostial stenosis. He was diagnosed with Takayasu's arteritis (TA) disease and discharged after a 9-day ward stay on anti-hypertensives and steroids. Unfortunately, he was admitted again in our center for the third time in the month of August (after 32 days) for decreased appetite, backache, abdominal pain, and vomiting. There were no visual or neurological complaints. On examination, he was conscious and afebrile with a heart rate of 102 per minute, respiratory rate of 38/min, and blood pressure of 110/74 mmHg. There was severe pallor and grade 2 clubbing; the left radial pulse was not palpable. Chest examination revealed a hyperdynamic apex and early systolic murmur. Other systemic examinations were normal. Apart from anemia (hemoglobin 6.8 g/dL), raised erythrocyte sedimentation rate (60 mm after 1 h), and elevated C-reactive protein (123 mg/L), rest of routine hematological/biochemical tests were normal. With the diagnosis of Takayasu disease, he was treated with antibiotics, anti-hypertensives, steroids, antituberculous drugs, packed red cells, and intravenous fluids. On day 2 of admission, he expired following a sudden-onset chest pain with hemodynamic collapse.

63.2 Autopsy Findings

The heart was kept with the aorta (180 g). The heart (Fig. 63.1a) was markedly enlarged in size with diffuse moderate thickening of the visceral epicardium. The apex was pointing to the left, slightly rounded and formed by both ventricles. There was moderate enlargement of the left ventricle and mild enlargement of the right ventricle. The great arteries had a normal relationship, but the aorta was almost twice the size of pulmonary trunk (Fig. 63.1a). The ascending, transverse, and the 9.0 cm of the descending portions of the aorta were dilated and slightly tortuous (Fig. 63.1a).

P. Vaideeswar (✉)
Department of Pathology (Cardiovascular and Thoracic Division), Seth Gordhandas Sunderdas Medical College and King Edward Memorial Hospital, Mumbai, India

P. Vaideeswar (ed.), *Tropical Cardiovascular Pathology*,
https://doi.org/10.1007/978-981-19-3720-0_63

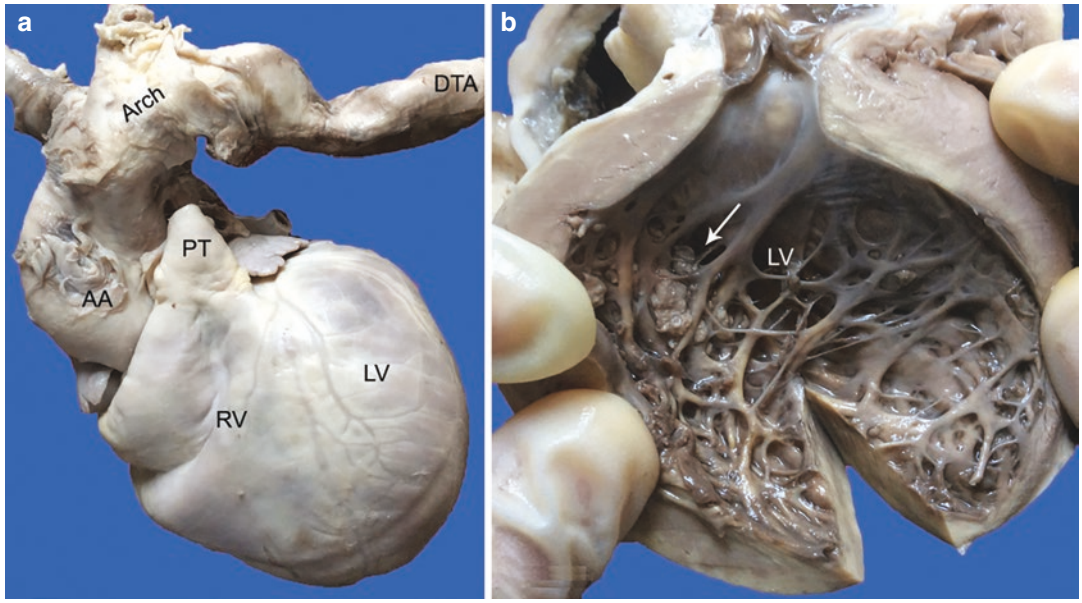

Fig. 63.1 (**a**) Moderate cardiomegaly with rounding of the apex and moderately enlarged left ventricle LV. Most of the thoracic portions of the aorta appear dilated, tortuous, and rigid; (**b**) The intertrabecular spaces of the hypertrophied LV are filled with fresh, friable thrombi (arrow). The myocardium appeared pale brown (*AA* ascending aorta, *DTA* descending thoracic aorta, *PT* pulmonary trunk, *RV* right ventricle)

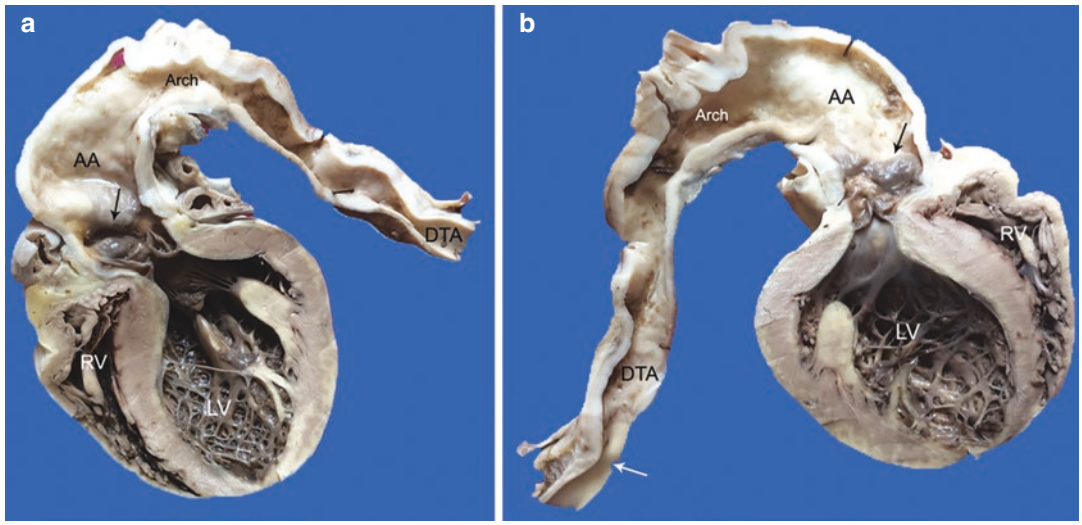

Fig. 63.2 (**a**) and (**b**) show the bisected halves of the heart. There is extreme thickening of the walls of the entire aorta, except for the distal portion of the descending thoracic aorta DTA (white arrow). Glistening plaques (black arrows) are prominently seen at the sinutubular junction obscuring the coronary ostia (*AA* ascending aorta, *LV* left ventricle, *RV* right ventricle)

The heart was longitudinally bisected. The left ventricle was moderately dilated with a pale-yellowish discoloration of the myocardium and the presence of multiple friable pale brown mural thrombi seen in the anterolateral free walls in the intertrabecular spaces (Fig. 63.1b). Glistening gray-white plaques were present around both the coronary ostia (Fig. 63.2). Except for the distal 1.5 cm of the descending thoracic aorta that was normal, the rest of the thoracic aortic segments

had an extremely firm consistency with marked pale yellow to grey-white thickening of their walls (Fig. 63.2). Similarly, the right brachiocephalic artery (1.0 cm), right common carotid artery (2.0 cm), right subclavian artery (1.0 cm), left common carotid artery (4.0 cm), and the left subclavian artery (1.0 cm) appeared enlarged, rigid with extreme grey-white thickening of their walls (Fig. 63.3a). The thickened descending thoracic aorta (Fig. 63.3b) had a short distal normal segment before its continuation of the abdominal aorta (Fig. 63.3c), which was thickened and narrowed for a length of 4.5 cm. The thickening stopped abruptly at the origin of the inferior mesenteric artery. The intima showed glistening plaques as well as multiple granular pale yellow to red brown thrombi (Fig. 63.3c) that simulated granular bacterial colonies on agar plates. The celiac and renal arterial ostia were narrowed; thrombus occluded the ostium of the superior mesenteric artery (SMA, Fig. 63.3c).

The histology revealed active-on-chronic aortitis and arteritis (Fig. 63.4) of all the arch arteries, right pulmonary artery, celiac, SMA, and bilateral renal arteries. Fresh thrombus over the intimal surface (Fig. 63.4a) and focal granulomatous inflammation (Fig. 63.4b, c) were also present. Ischemic changes in the myocardium in all the walls were seen (Fig. 63.5). Other organs were normal; there was no evidence of tuberculo-

Fig. 63.3 (**a**) Arch arteries and their branches showing varying degrees of wall thickening and luminal stenosis (*LCCA* left common carotid artery, *LSA* left subclavian artery, *RBCA* right brachiocephalic artery, *RCCA* right common carotid artery, *RSA* right subclavian artery); (**b**) Close-up of the descending thoracic aorta with wall thickening and diffuse luminal narrowing; (**c**) Thickened wall of the abdominal aorta with narrowing of the visceral arterial ostia. Thrombus also occludes the opening of the superior mesenteric artery (SMA). The aorta below the inferior mesenteric artery IMA abruptly transitions into normality. Mural thrombi are also present (*CA* celiac artery, *LRA* left renal artery, *RRA* right renal artery)

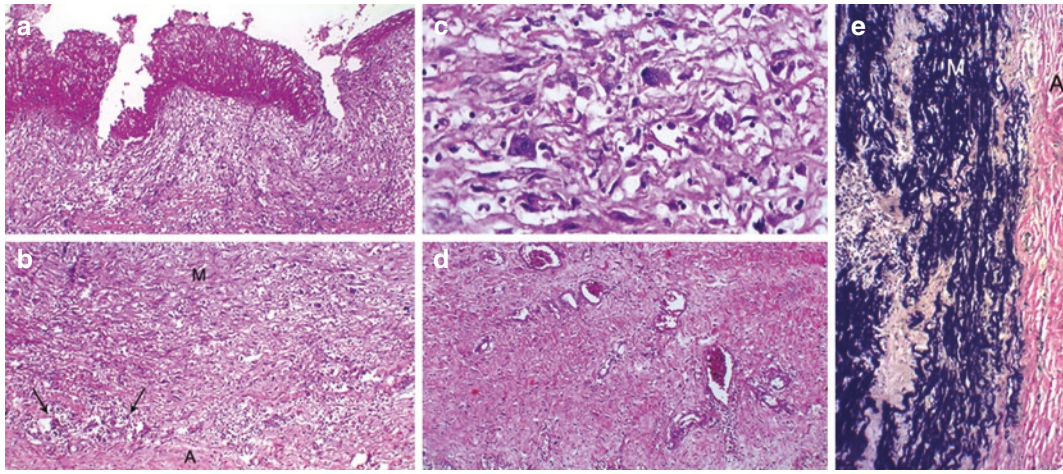

Fig. 63.4 Pan-arteritis of Takayasu's arteritis—(**a**) Intimal fibrocellular thickening and inflammation with overlying fresh fibrin thrombus (H&E × 250); (**b**) Destruction and inflammation of the media M. Note focal granulomatous inflammation (arrows) at the medioadventitial A junction (H&E × 250); (**c**) Clusters of giant cells and few lymphocytes splaying apart the smooth muscle and elastic fibers (H&E × 400); (**d**) Extensive adventitial fibrosis (H&E × 250); (**e**) Destruction of the elastic fibers and inflammation of the media M with adventitial A fibrosis (Elastic van Gieson × 250)

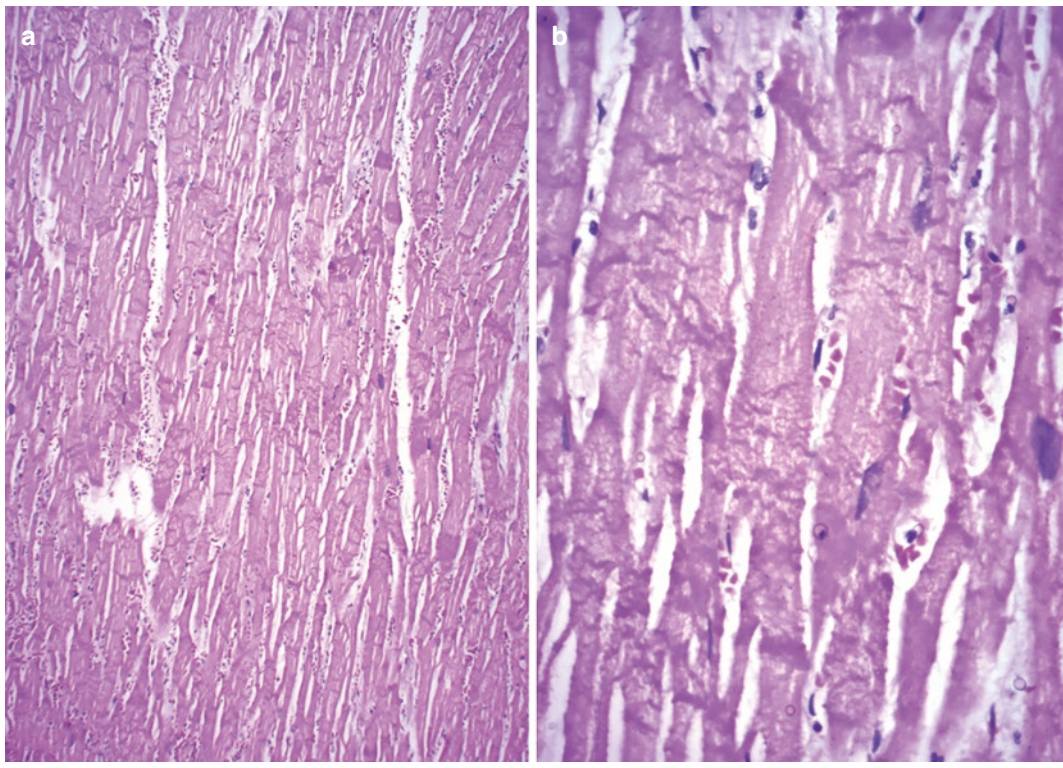

Fig. 63.5 Myocardial ischemia indicated by the presence of contraction band necrosis—(**a**) H&E × 250 and (**b**) H&E × 400

sis. Features of intestinal gangrene were also not present.

Cause of Death: Acute myocardial ischemia following coronary ostial stenosis in Takayasu arteritis (TA).

63.3 Discussion

Vasculitides represent a spectrum of diseases unified by the presence of inflammation and necroses of one or more layers of the wall and exhibit diverse etiopathogenesis, organ involvement, and clinical presentation. The widely accepted classification of vasculitis utilizes the vascular size, categorizing them as large, medium, or small-sized vasculitis with an overlap of involvement seen in some cases. In the above case, there was involvement of most of the aortic segments with inflammation seen in all the layers along with variable inflammatory extension into many of its major branches; there were no identifiable microorganisms. This aortitis, therefore, serves as an example of noninfectious large-vessel vasculitis (LVV). The pattern of involvement and the accompanying inflammatory response was highly suggestive of TA, which largely occurs in woman in the reproductive age groups (male-to-female ratio of 1:8) with a prevalence of 1.2–2.6 per 100,000 persons per year; it is more frequent in South-east Asian, and Indian subcontinents. About 30% of the cases occur in children (from infants to adolescents) where it forms the third common vasculitis (after Kawasaki disease and Henoch-Schonlein purpura) and the most common type of LVV. The male-to-female ratio in childhood TA (c-TA) is 1:2.

The etiopathogenesis of TA has not been well-delineated. Cell-mediated and humoral immunological responses are triggered by unknown but possibly infectious antigen (particularly tuberculosis in this part of the world) in a background of genetic susceptibility. The latter involves the genes of the human leukocyte antigen-B loci and those that code certain inflammatory cytokines and/or their receptors/regulators. Though all the layers are affected in TA (pan-arteritis), the initial site of the autoimmune response is at the medioadventitial junction, which then proceeds into 3 overlapping stages. In the active stage, there is mononuclear infiltration composed of macrophages and T-lymphocytes with destruction at the outer-thirds of the media, often accompanied by a granulomatous reaction, which was well seen in the current case. A characteristic finding is fragmentation of the elastic fibers and their phagocytosis ('elastophagia'). The chronic stage shows patchy inflammation with medial fibrosis and vascularization with reactive intimal fibrocellular proliferation, accumulation of mucopolysaccharides, and superadded mural thrombosis; there is frequently exuberant adventitial fibrosis with vasa vasora endarteritis. With healing, there is extensive fibrosis with or without calcification. Both active and chronic changes were observed in multiple aortic segments and their branches in this child.

The inflammatory aftermath manifests as luminal stenosis/occlusion and/or aneurysms. The site/s of involvement is utilized for the classification of TA—Type I (sole involvement of the aortic arch arteries), Type II (a: involvement of the ascending aorta, aortic arch, and its branches; b: involvement of the ascending aorta, aortic arch, and its branches, and descending thoracic aorta), Type III (involvement of the descending thoracic aorta, abdominal aorta, and/or renal arteries), type IV (involvement of the abdominal aorta and/or renal arteries), and type V (the combined features of Types IIb and IV, which was present in our patient). There may be concomitant affection of the coronary (denoted as C+) and/or pulmonary arteries (denoted as P+, See Chap. 73). Coronary osteitis was present; right pulmonary artery was affected.

The presentation in this pediatric patient highlights to a great extent the clinical manifestation (triphasic pattern) of TA. The first phase is the systemic or nonvascular period where the patients chiefly develop constitutional symptoms and in children, they include headache, fever, shortness of breath, weight loss, vomiting, and musculoskeletal features. Herein, TA masqueraded as fever of unknown origin and these febrile episodes with accompanying lymphadenopathy had

resulted in frequent hospitalizations. In the vasculitic stage, the nonspecific symptoms are associated with angiodynia or pain/tenderness over the vessels. It is known to be uncommon in c-TA and had not been noted in our case. But in a matter of few months, the disease had progressed to the late phase with ischemic organ dysfunction secondary to stenotic aortoarteriopathy and was also associated with constitutional symptoms. In many cases, however, diagnostic delay (4 times higher than adults with TA) can occur.

Organ-specific features are mainly related to the cardiovascular system, occurring in nearly 85% of c-TA, followed by neurological (20%) and gastrointestinal (10%) features; visual disturbances and renal/pulmonary parenchymal features are distinctly uncommon. Since there is a variation in the clinical expression of c-TA as compared to adults, the criteria for diagnosis adopted by the European League Against Rheumatism/Pediatric Rheumatology International Trials Organization/Pediatric Rheumatology European Society (EULAR/PRINTO/PRES) include demonstrable angiographic abnormalities with one of the 5 other features, i.e., pulse deficit or claudication, blood pressure discrepancy in the 4 limbs, bruits over the major arteries, hypertension, and evidence of elevated acute phase reactants. Hypertension and absence of peripheral pulses are known to be common in c-TA. Most of these features were evident in our case. Apart from features related to the cardiovascular symptoms, this child also had abdominal pain due to acute mesenteric ischemia. Though the SMA ostium was narrowed and there were mural thrombi in the abdominal aorta, small intestinal histopathology did not reveal ischemic changes. Most often, the mortality is related to cardiovascular complications in the form of myocarditis, myocardial ischemia or infarction, and aortic regurgitation, which can lead to heart failure. The cause of death in this case was myocardial ischemia related to coronary ostial stenosis and this may have been responsible for left ventricular dysfunction and formation of thrombi. Apart from symptomatic therapy, the usual drug options include steroids or other immunosuppressants; other aggressive medical modalities include interleukin-6 or tumor necrosis factor inhibitors. Vascular stenosis or occlusions may also demand radiological or surgical interventions. It should be borne in mind that the disease in childhood is often progressive, despite therapy and/or may be refractory to therapy with repeated flares. In the scenario of the present case, we wonder if use of nonsteroidal immunosuppressives would have changed the outcome.

Further Reading

Aeschlimann FA, Barra L, Alsolaimani R, Benseler SM, Hebert D, Khalidi N, et al. Presentation and disease course of childhood-onset versus adult-onset Takayasu arteritis. Arthritis Rheumatol. 2019;71:315–23.

Bolek EC, Kaya Akca U, Sari A, Sag E, Demir S, Kilic L, et al. Takayasu's arteritis more severe in children? Clin Exp Rheumatol. 2021;39(Suppl 129):32–8.

Clemente G, Silva CA, Sacchetti SB, Ferriani VPL, Oliveira SK, Sztajnbok F, et al. Takayasu arteritis in childhood: misdiagnoses at disease onset and associated diseases. Rheumatol Int. 2018;38:1089–94.

Di Santo M, Stelmaszewski EV, Villa A. Takayasu arteritis in paediatrics. Cardiol Young. 2018;28:354–61.

Espinoza JL, Ai S, Matsumura I. New insights on the pathogenesis of Takayasu arteritis: revisiting the microbial theory. Pathogens. 2018;7:73.

Gupta H, Kaur N, Saxena A, Jagia P, Kumar S, Gupta SK, et al. Non-specific aortoarteritis (NSAA) in children: a prospective observational study. BMJ Paediatr Open. 2021;5:e001106.

Hrisrova D, Marchev S. Takayasu arteritis: a systematic review. Acta Med Bulg. 2019;46:56–64.

Idhrees M, Thilagavathi N, Bashir M, Velayudhan BV. Management of cardiac manifestations of Takayasu arteritis. Vessel Plus. 2020;4:23.

Pugh D, Grayson P, Basu N, Dhaun N. Aortitis: recent advances, current concepts and future possibilities. Heart. 2021;107:1620–9.

Renauer P, Sawalha AH. The genetics of Takayasu arteritis. Presse Med. 2017;46:e179–87.

Russo RAG, Katsicas MM. Takayasu arteritis. Front Pediatr. 2018;6:265.

64 Takayasu's Arteritis Manifesting as Intestinal Gangrene

Pradeep Vaideeswar

64.1 Clinical History

A 2-day history of severe colicky periumbilical non-radiating pain was the chief complaint in a 23-year-old male and he was admitted in a nearby nursing home for the next 2 days. Within few hours of admission, he developed chest pain and increasing shortness of breath. Hypertension (210/110 mmHg) with atrial fibrillation was detected. The investigations that had been performed in the nursing home are given in Table 64.1. He was given antiplatelet drugs, antihypertensives, and antiarrhythmic drugs and transferred to our tertiary care center. He was admitted in poor general condition. A high-risk consent for exploratory laparotomy was taken, but the patient could not be salvaged and expired within 10 h of admission.

Table 64.1 Investigations

Hematological	Hemoglobin 14.2 g/dL Total leukocyte count 17,980/cmm Platelet count 1.70 lakhs/cmm Differential count—Neutrophil predominant (77%)
Biochemical—Routine	Serum creatinine 2.6 mg/dL Blood urea nitrogen 37.2 mg/dL Bilirubin 1.4 mg/dL (direct 0.5 mg/dL) Total protein 7.9 g/dL Albumin 4.3 g/dL Globulin 3.6 g/dL Albumin/globulin ratio 1.2 SGOT 103 IU/L SGPT 582.7 IU/L Alkaline phosphatase 67.2 IU/L Serum amylase 216 IU/L Serum lipase 1092 IU/L Sodium 135 mEq/L Potassium 3.5 mEq/L Chloride 97 mEq/L CPK-MB 880 IU/L Troponin (quantitative) >2000 ng/L
Radiological	Ultrasonography: Bulky pancreas; absent flow in the superior mesenteric artery; fluid filled bowel loops with sluggish

P. Vaideeswar (✉)
Department of Pathology (Cardiovascular and Thoracic Division), Seth Gordhandas Sunderdas Medical College and King Edward Memorial Hospital, Mumbai, India

P. Vaideeswar (ed.), *Tropical Cardiovascular Pathology*,
https://doi.org/10.1007/978-981-19-3720-0_64

64.2 Autopsy Findings

The heart was moderately enlarged in size and weighed 340 g. There was moderate enlargement of the left ventricle (LV). The transverse sections through the ventricles revealed mild concentric hypertrophy with focal congestion in the anterior papillary muscles and in the basal posterior wall. A transmural pale area was seen in the apical one-third of the posterior wall (Fig. 64.1a). All the coronary arteries were narrowed due to concentric or eccentric grey-white to pale thickening of their walls (Fig. 64.1b–d); this had been produced mainly by intimal cellular proliferation. The media was normal. The posterior wall showed a fresh transmural infarction (Fig. 64.2).

The ascending aorta and the pulmonary trunk had a normal relationship with slight dilatation of the aorta. The right coronary ostium was surrounded by pinkish-grey to pale yellow intimal plaques. The arch of aorta was slightly rigid with calcified atherosclerotic plaques. All the proximal portions of the arch arteries were atherosclerotic with calcification and stenosis or thrombotic luminal occlusion (Fig. 64.3). The proximal descending thoracic aorta, 2 cm beyond the opening of the left subclavian artery (LSA), had 3 glistening intimal plaques, beyond which the segment appeared normal. There were 2 abrupt long-segment constrictions, 9 cm of the thoracoabdominal segment, and 7 cm of the infrarenal abdominal aorta. The wall was thickened and the lumen measured 0.9–1.2 cm. The affected segments were diffusely atherosclerotic with calcification (Fig. 64.4a). There was an aneurismal dilatation of the superior

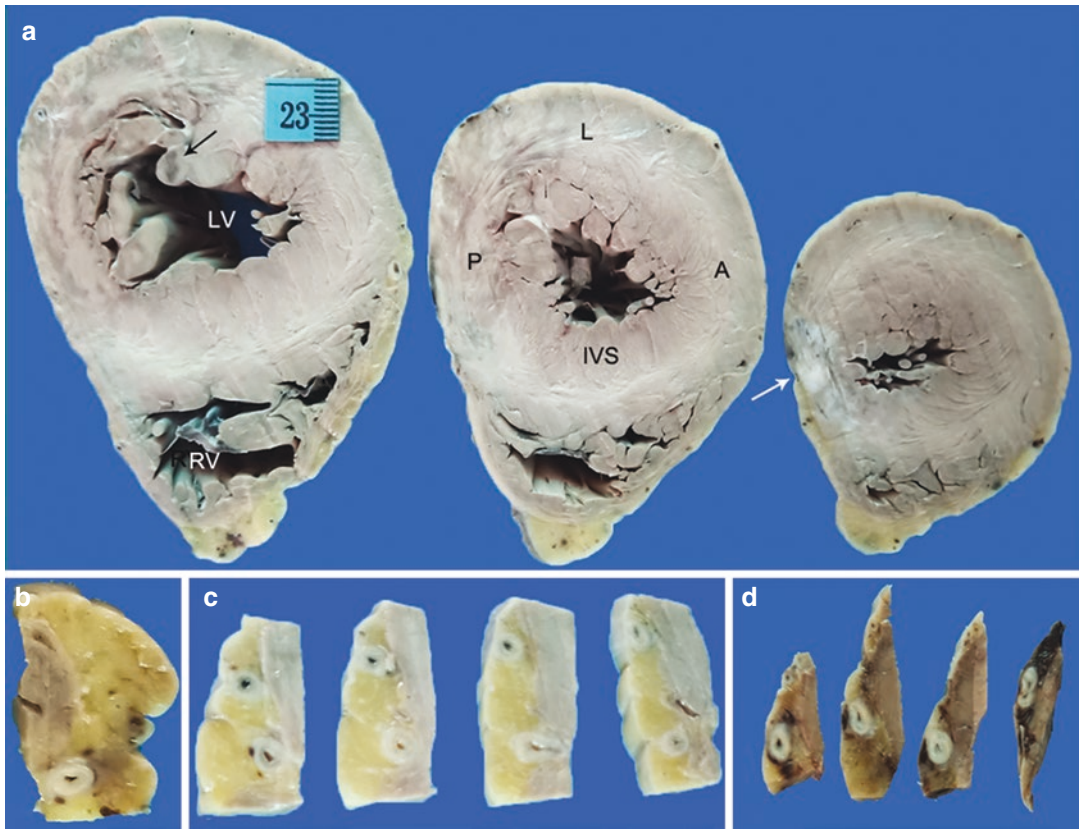

Fig. 64.1 (**a**) Transverse slices of the myocardium showing congestion of the anterior papillary muscle (black arrow) and an area of transmural scarring (white arrow) of the posterior P wall (*A* anterior wall, *IVS* interventricular septum, *L* lateral wall, *LV* left ventricle, *RV* right ventricle); Grey-white thickening of the walls with luminal narrowing of (**b**) Right, (**c**) Left anterior descending, and (**d**) Left circumflex, arteries

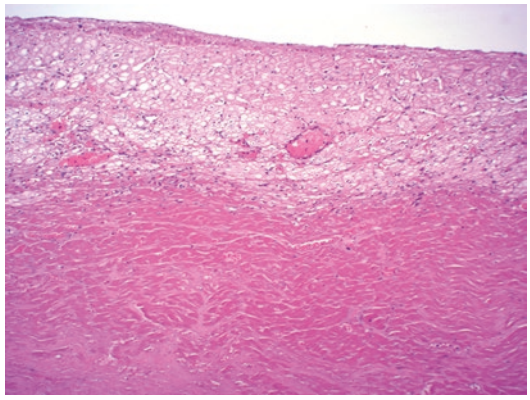

Fig. 64.2 An endocardium of normal thickness is seen with underlying band of myocytolyses with enlarged cardiomyocytes and vacuolated cytoplasm. Below this is a large area of coagulative necrosis. There are hardly any neutrophils (H&E × 200)

mesenteric artery for a length of 3 cm and a diameter of 0.9 cm with luminal thrombus (Fig. 64.4b). The left renal artery was narrowed due to concentric or eccentric grey-white to pale thickening of its walls with luminal thrombus; right renal artery was normal (Fig. 64.4b). All the affected segments revealed chronic or healed phases of Takayasu's arteritis (TA, Fig. 64.5a, b). Most of the small intestine was gangrenous (Fig. 64.5c). There was also focal acute pancreatitis. The kidneys (left kidney 65 g and right kidney 90 g) had superficial and deep scars, while the lungs showed extensive edema with multifocal hemorrhages.

Cause of Death: Acute myocardial infarction in a case of TA.

Fig. 64.3 Varying degrees of involvement of the arch arteries and their branches. Severe changes were seen in the left common carotid artery (LCCA) with occlusive thrombus in the left external carotid artery (arrows). The right subclavian artery RSA was minimally affected (*LSA* left subclavian artery, *RBCA* right brachiocephalic artery, *RCCA* right common carotid artery)

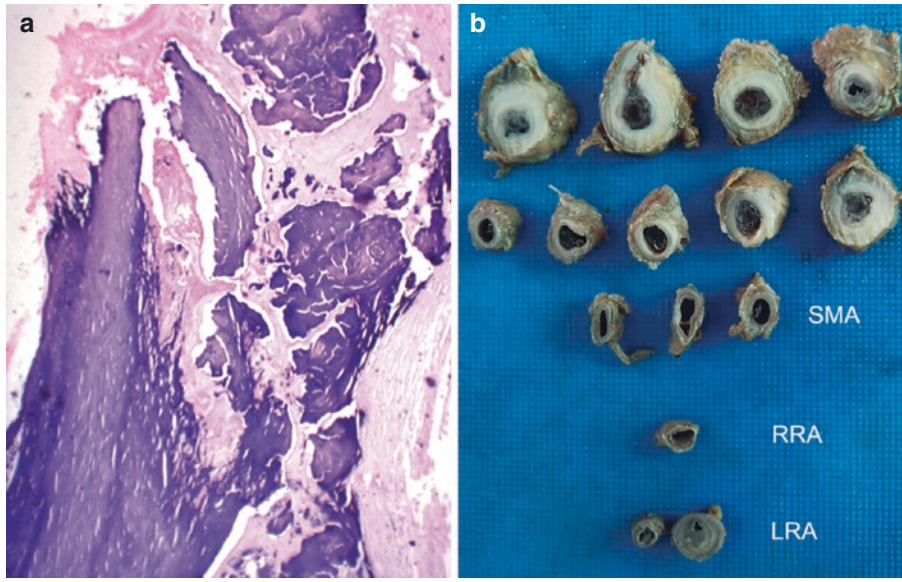

Fig. 64.4 (**a**) Aortic wall showing plates of dystrophic calcification (H&E × 100); (**b**) The superior mesenteric artery SMA is aneurysmally dilated with thickened walls and luminal thrombus. Similar but less striking changes are seen in the non-dilated left renal artery LRA. The right renal artery RRA is normal

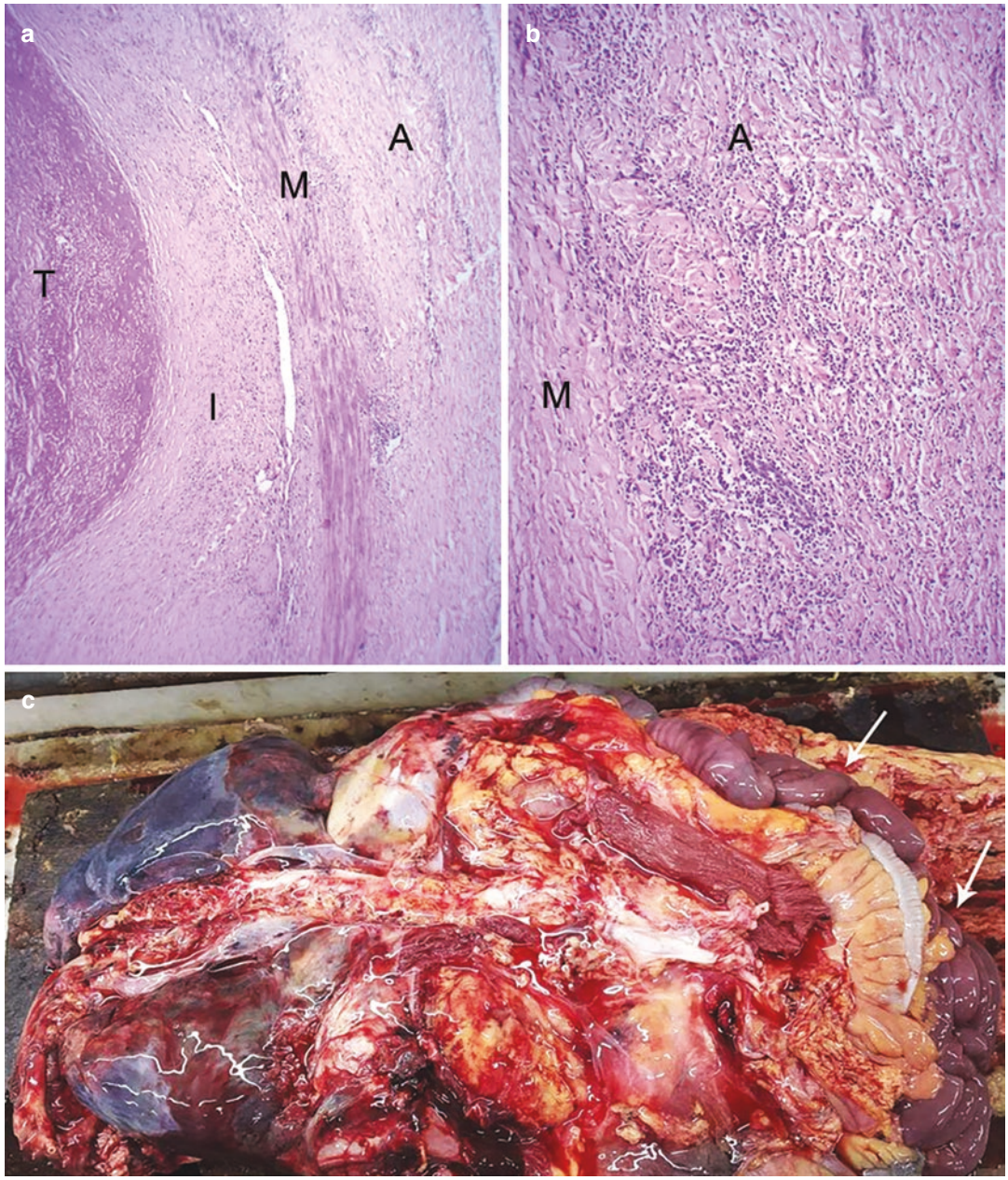

Fig. 64.5 (**a**) Thrombus T is adherent to a markedly thickened intima I. There is medial M fibrosis with separation of the smooth muscle bundles; (**b**) Adventitial A fibrosis with intense inflammatory cell infiltration; (**c**) Eviscerated viscera showing dusky appearance of the small intestinal loops (arrows)

64.3 Discussion

Multiorgan involvement (small intestinal gangrene, acute myocardial infarction, and acute pancreatitis) was noted clinically and at autopsy in this young male patient as manifestations of TA (See Chap. 63). It is the prototype of large-vessel vasculitis, which tends to be more common in the Asian subcontinent and affects young women in the second and third decades of life.

The inflammation is immune-mediated resulting in a granulomatous response that sooner or later affects all the layers of the wall (panarteritis). The ongoing inflammation and its sequelae occur in a triphasic pattern (pre-pulseless, vasculitic, and chronic) with varied clinical presentations related to arterial stenosis, occlusion, or aneurismal dilatation. In many patients, there is a diagnostic delay (median of almost 15 months) after the onset of symptoms, while some patients can remain asymptomatic.

TA has a predilection for the aorta and its major branches. The initial inflammatory nidus frequently occurs in the left subclavian artery, affecting the proximal or middle portions. In due course of time, different segments of the aorta are affected with or without associated pulmonary or coronary arterial disease (the angiographic classification, See Chap. 63) with variable geographic distribution. In the natural course of the disease, the constitutional and vasculitic symptoms are accompanied or replaced by vascular insufficiency due to insidiously developing stenotic/occlusive lesions (seen in over 90% of the individuals); aneurysms are seen in only 25% of the cases. The most common consequence is claudication of the limbs (not elicited in the history in this case) and renovascular hypertension (noted in this patient). However, this patient presented with an uncommon manifestation of mesenteric ischemia. Since inflammatory stenosis and in some cases even occlusion develops over time, a good collateral circulation develops, which is particularly true for the mesenteric circulation. These patients present with nausea, vomiting, abdominal pain, or diarrhea that suggests chronic ischemia. Even more infrequent is the acute occlusion of one or more of the splanchnic arteries with gangrene of the intestines and a fulminant outcome. Chronic and/or healed arteritis with calcification and superadded atherosclerosis affecting the arch arteries (including the left subclavian artery), thoracoabdominal aorta, and the splanchnic arteries were observed at autopsy in this patient. In addition to the stenosing lesions seen in most areas, the SMA was aneurismally dilated with a thrombotic occlusion, which resulted in the ischemic catastrophe. Such an involvement would require resection of the affected loops of intestine and revascularization of the aortoarterial segments, along with aggressive immunosuppressive therapy. Hence, acute abdominal pain in young patients needs a meticulous clinical evaluation, particularly blood pressure in all 4 limbs and appropriate thoracoabdominal imaging studies. It also should be noted that on some occasions, TA is also associated with inflammatory bowel syndromes. The vascular stenosis and ischemia also resulted in acute pancreatitis. The cause of death was, however, related to the cardiovascular complication in the form of acute myocardial infarction.

Further Reading

Hrisrova D, Marchev S. Takayasu arteritis: a systematic review. Acta Med Bulg. 2019;46:56–64.

Khan R, Arif A, SHA I, Riaz B, Jamil H. Takayasu's arteritis in a 33-year-old male. Cureus. 2021;13:e14557.

Misra DP, Krishnan N, Gochhait D, Emmanuel D, Negi VS. Takayasu arteritis (TA) first presenting with intestinal ischemia: a case report and review of gastrointestinal tract involvement (ischemic and non-ischemic) associated with TA. Rheumatol Int. 2017;37:169–75.

Morrissey S, Tan KT, Byrne JS. Takayasu arteritis with middle aortic syndrome and mesenteric ischemia treated by aortic stenting. J Vasc Surg Cases Innov Tech. 2017;3:168–70.

Pugh D, Grayson P, Basu N, Dhaun N. Aortitis: recent advances, current concepts and future possibilities. Heart. 2021;107:1620–9.

65 Takayasu's Arteritis Complicated by Chronic Aortic Dissection, False Channel Aneurysm, and Aorto-Esophageal Fistula

Pradeep Vaideeswar and Subhash Yadav

65.1 Clinical History

A 25-year-old male was admitted in the emergency services department in a gasping state and expired within 2 h. He had about eight episodes of hematemesis for a day with a massive bout before admission. There had been a past history of chest pain off and on for 3 years, for which nonsteroidal anti-inflammatory drugs had been prescribed. No investigations had been performed. A complete autopsy was performed.

65.2 Autopsy Findings

At autopsy, the heart was mildly enlarged in size (330 g) and showed mild concentric left ventricular hypertrophy. The right coronary artery had a dominant distribution; all epicardial coronary arteries showed mild glistening grey-white thickening of their walls. The intima of the ascending aorta appeared a little rigid and thickened. The transverse aorta around the ostium of left subclavian artery (LSA) showed intimal irregularity with radiating fissures. The entire right brachiocephalic artery, proximal 1.1 cm of right common carotid artery, proximal 0.8 cm of right subclavian artery, and proximal 1.5 cm of LSA appeared markedly narrowed due to glistening translucent intimal fibrosis (Fig. 65.1), confirmed on microscopy; there was extensive medial destruction and very marked adventitial fibrosis.

The proximal dilated and scarred descending thoracic aorta (DTA), 3.8 cm beyond the origin of LSA, showed a Stanford type 2 (See Chap. 60) chronic dissection that continued till the bifurcation. The aorta was inadvertently opened through the false channel, which was aneurysmally dilated (8 cm in diameter, Fig. 65.2a, b). The inner layers of the false channel showed uniform milky white cobblestoning with few adherent fresh thrombi (Fig. 65.3a). On microscopy, the nondissected thoracic aorta showing the histomorphology of

P. Vaideeswar (✉)
Department of Pathology (Cardiovascular and Thoracic Division), Seth Gordhandas Sunderdas Medical College and King Edward Memorial Hospital, Mumbai, India

S. Yadav
Department of Pathology, Tata Memorial Hospital, Mumbai, India

P. Vaideeswar (ed.), *Tropical Cardiovascular Pathology*,
https://doi.org/10.1007/978-981-19-3720-0_65

Fig. 65.1 Involvement of the arch arteries by the fibroinflammatory process (*LCCA* left common carotid artery, *LSA* left subclavian artery, *RBCA* right brachiocephalic artery, *RCCA* right common carotid artery, RSA subclavian artery)

aortitis—fibrocellular corrugated intimal thickening, medial destruction, and marked adventitial fibrosis, indicating healed phase of Takayasu's arteritis (TA) and chronic dissection (Fig. 65.3b–e). The false channel, at the level of DTA, showed a large (9 × 5 × 5 cm) saccular outpouching (Fig. 65.2a) that was attached to, and projected into, the esophagus (Fig. 65.4a). This had resulted in an aorto-esophageal fistula (AEF). The opening in the esophagus was 4 × 2 cm and was covered by blood clots with ulcerations (Fig. 65.4b). The kidneys were asymmetrical (right larger than the left) with presence of superficial cortical scarring. Other organs were normal.

Cause of Death: Hypovolemic shock following massive hematemesis due to AEF.

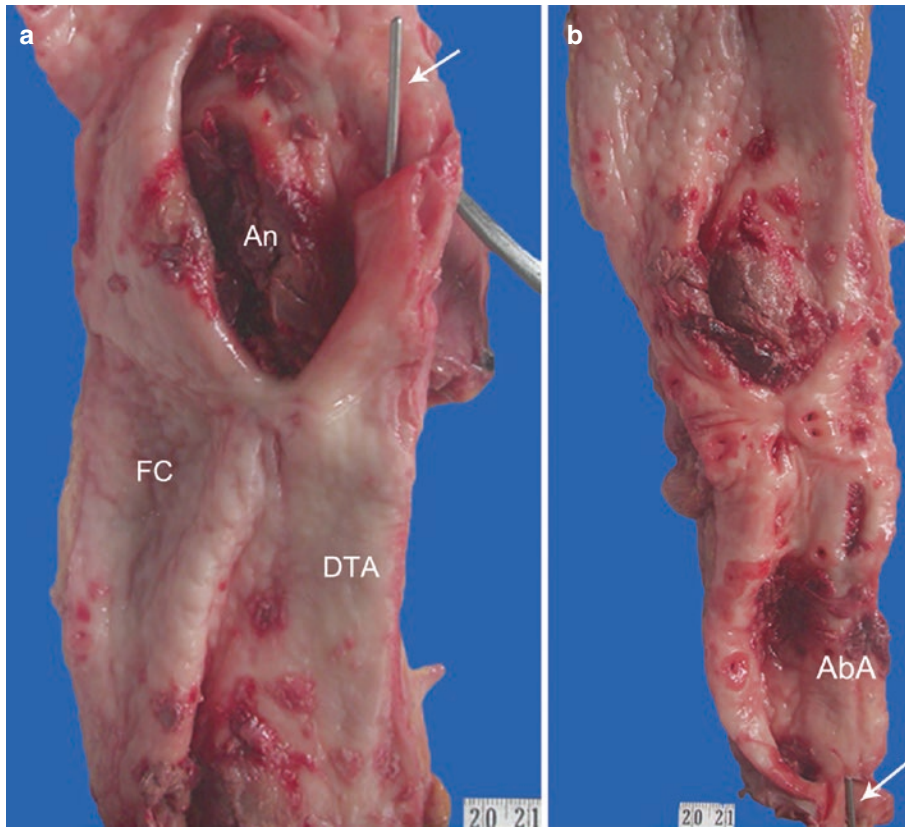

Fig. 65.2 Chronic Stanford type 2 aortic dissection. The vessel was opened through the false channel. A probe (arrow) has been inserted through the true lumen. (**a**) An aneurysm (An) is seen in the proximal part of the false channel. (**b**) Most of the visceral arteries had communication with the false channel. (*AbA* abdominal aorta, *DTA* descending thoracic aorta, *FC* false channel)

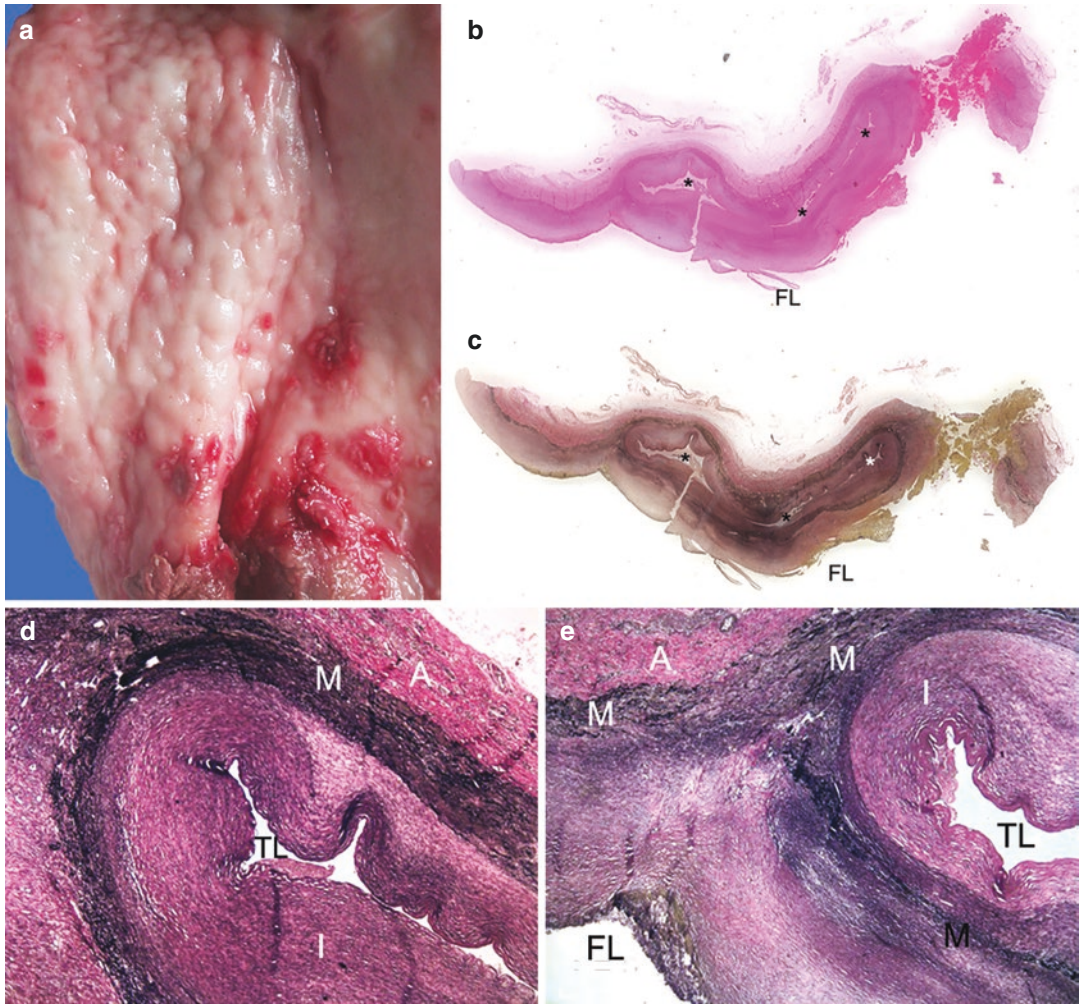

Fig. 65.3 (**a**) Cobble-stoned pseudointima of the false channel with adherent red thrombi; Scanned images of the transverse section of the abdominal aorta to show the true and false channels of the dissection—(**b**) H&E and (**c**) Elastic van Gieson; (**d**) Intimal I and adventitial A fibrosis with focal medial M destruction is present—features of healed aortitis (Elastic van Gieson × 200); (**e**) The media is split into its inner two-thirds and outer one-third. The false channel FL is lined on either side by loose fibrocellular tissue (*TL* true lumen, Elastic van Gieson × 250)

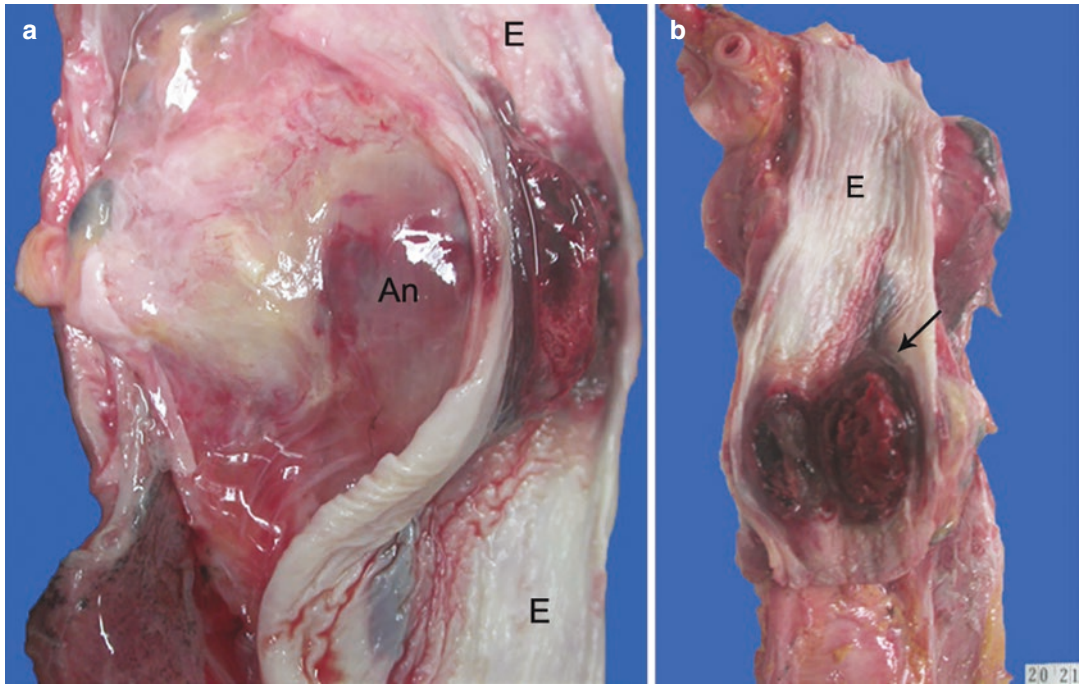

Fig. 65.4 (**a**) The saccular aneurysm An from the false channel bulges into the esophagus E; (**b**) Hemorrhagic ulcerations and blood clots (arrow) obscure the site of aorto-esophageal fistula

65.3 Discussion

The case demonstrates 3 unusual sequential complications—chronic aortic dissection, aneurysm of the false channel, and AEF, of TA. It is an example of large-vessel vasculitides with a distinct propensity of involving the aorta and its major branches. As compared to the western world, the panarteritic inflammation is frequently observed to afflict young Asian women. The pathogenesis of TA still remains uncertain and possibly occurs due to an autoimmune reaction in a background of genetic predisposition and infection. The disease manifestations depend on the aortoarterial sites of involvement and patterns of inflammatory response, which leads to the clinical phases designated as preocclusive, vasculitic, and occlusive. In the initial stages of the disease, mononuclear cells begin to accumulate at the medioadventitial junction and patients may present with constitutional symptoms. An increase in the number of cells with formation of granulomas results in destruction of the media, which may lead to tenderness or pain over the palpable arteries (angiodynia in the vasculitic phase). Progressive medial fibrosis with decreasing inflammation (chronic inflammatory stage) is associated with endarteritis obliterans, intense adventitial fibrosis, and intimal fibrocellular proliferation (healing inflammation) and is characterized by stenosis or obliteration of the vascular lumens with consequent end-organ ischemia and organ-specific symptoms. Combinations of these manifestations aided by imaging features and laboratory parameters have been adopted as diagnostic criteria for TA. Our patient had not been thoroughly investigated and a significant history of chest pain had been treated symptomatically. Presence of hypertension, the common finding in well-established TA, was not detected as the patient was admitted in shock.

Weakening and thinning of the wall due to inflammation and fibrosis can also lead to ectasia or frank aneurysm formation. Aortic dissection is an extremely rare complication with a rough estimate of 0.87% of patients with TA. Exuberant adventitial and intimal fibrotic thickening which

characterizes the healed phase produces a rigid aorta that is often resistant to the process of dissection. Hence, it is presumed that AD occurs at the peak of aortic inflammation; the reaction would also be intense. A similar scenario may have occurred in the index case and would have resulted in the chest pain. But, often the classic clinical features of AD may not be present. Majority of the dissections are Stanford type B and often chronic (See Chap. 60), as seen in this case. In general, it has been observed that about 30% of patients with Type B ADs develop aneurysms of the false channel in the thoracic or abdominal aortic segments within 5 years with fatal ruptures in 18% of the cases. Patients of TA with AD should be promptly diagnosed and treated ensuring adequate control of hypertension and ongoing inflammation of TA. Conservative treatment is advocated when there is maintenance of hemodynamic stability despite dissection, while the more complicated cases require endovascular stenting or surgical intervention. Fatal hematemesis due to AEF was noted in this unfortunate case. Though AEF has been noted in very few cases of TA, fistula developing due to rupture of the aneurysm of the false lumen of the thoracic aorta has never been documented before.

Further Reading

Hrisrova D, Marchev S. Takayasu arteritis: a systematic review. Acta Medica Bulg. 2019;46:56–64.

Pugh D, Grayson P, Basu N, Dhaun N. Aortitis: recent advances, current concepts and future possibilities. Heart. 2021;107:1620–9.

Takeno S, Ishii H, Nanashima A, Nakamura K. Aortoesophageal fistula: review of trends in the last decade. Surg Today. 2020;50:1551–9.

Wu XP, Zhu P. Clinical features of aortic dissection associated with Takayasu's arteritis. J Geriatr Cardiol. 2017;14:485–7.

Yang KQ, Yang YK, Meng X, Zhang Y, Zhang HM, Wu HY, et al. Aortic dissection in Takayasu arteritis. Am J Med Sci. 2017;353:342–52.

Tuberculous Aortitis with Ruptured Pseudoaneurysm

66

Pradeep Vaideeswar and Gayathri Amonkar

66.1 Clinical History

A 65-year-old woman, with a total ward stay of 3 days at our institute, had been referred for increasing shortness of breath. She initially had complaints of low-grade fever and loose motions for a month, followed by 4–5 episodes of hematemesis for the past 10 days with admissions in 2 private nursing homes and another tertiary-care center. A chest computed tomographic scan performed in the latter center revealed wide-necked (1.3 cm) saccular aneurysm (2.1 × 1.9 cm) arising from the posterior wall of the ascending aorta. Surrounding this aneurysm was a well-defined lobulated hypodense collection producing indentations into the superior vena cava, the pulmonary trunk, and the left atrium. This was interpreted as organized hematoma secondary to a sealed off rupture of the aneurysm. The lung parenchyma also showed bilateral patchy ground glass opacities with non-necrotic mediastinal lymphadenopathy. An endoscopy performed revealed Mallory-Weiss tears in the lower end of the esophagus.

On examination during the current admission, the patient was conscious and cooperative. The pulse rate was 96 per minute, respiratory rate 30 per minute, and blood pressure of 30 per minute. There were bilateral coarse crepitations. The heart sounds were normal. The hemoglobin was 9.8 g/dL; other laboratory investigations were normal. A two-dimensional echocardiography showed normal chambers and valves. The ejection fraction was 60%. Repeat endoscopy showed no abnormality in the esophagus. She was treated with antibiotics and antacids. Unfortunately, there was no improvement in her condition.

66.2 Autopsy Findings

The heart was kept with the aorta (400 g) and was moderately enlarged in size. There was dense adhesion between the parietal and visceral layers of the pericardium (Fig. 66.1a). In areas where the parietal layer was stripped off, the epicardial surface showed flakes of fibrinous exudates. There was a 6 × 4.5 cm bulge present above the right atrial appendage and below the origin of the right brachiocephalic artery (RBCA) in relation to the right lateral aspect of

P. Vaideeswar (✉)
Department of Pathology (Cardiovascular and Thoracic Division), Seth Gordhandas Sunderdas Medical College and King Edward Memorial Hospital, Mumbai, India

G. Amonkar
Department of Pathology, Topiwala National Medical College and BYL Nair Charitable Hospital, Mumbai, India

P. Vaideeswar (ed.), *Tropical Cardiovascular Pathology*,
https://doi.org/10.1007/978-981-19-3720-0_66

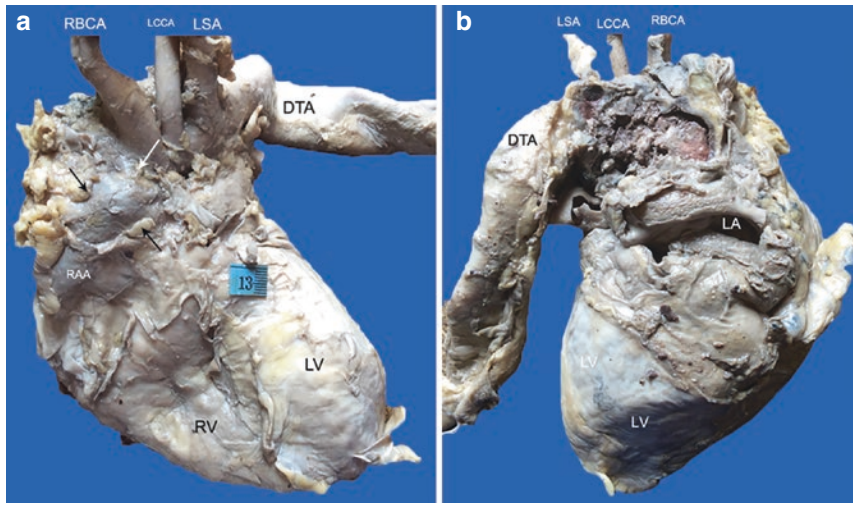

Fig. 66.1 (**a**) Anterior aspect of the heart showing dense adhesion between the layers of the pericardium. Note presence of a bulge (arrows) above the right atrial appendage RAA and towards the origin of the right brachiocephalic artery RBCA; (**b**) Blood clots are seen on the posterior aspect over the aortic arch (*DTA* descending thoracic aorta, *LCCA* left common carotid artery, *LV* left ventricle, *LSA* left subclavian artery, *RV* right ventricle)

the ascending aorta (Fig. 66.1a). On the posterior aspect, this bulge was hemorrhagic and was present over the entire aortic arch (Fig. 66.1b) with dense adherence to the trachea and the main bronchi. The bulge basically represented a pseudoaneurysm produced by a rupture of non-aneurysmal aorta with a localized hemo-mediastinum. The opening was present in the arch of aorta, 1 cm below the ostium of the RBCA (Fig. 66.2a, b) and was the result of tuberculous aortitis. There was transmural destruction of the media with large amounts of caseation necroses and focal granulomatous inflammation (Figs. 66.3 and 66.4). Adherent caseous para-aortic and paratracheal lymph nodes were present. There was no aorto-esophageal fistula. There was also tuberculous tracheitis with associated perforation and localized pneumomediastinum (as seen in the review of the CT scan). There was associated tuberculous pericarditis, pulmonary miliary tuberculosis with diffuse alveolar damage, and miliary granulomas in the liver, kidneys, spleen, and adrenals.

Cause of Death: Disseminated tuberculosis.

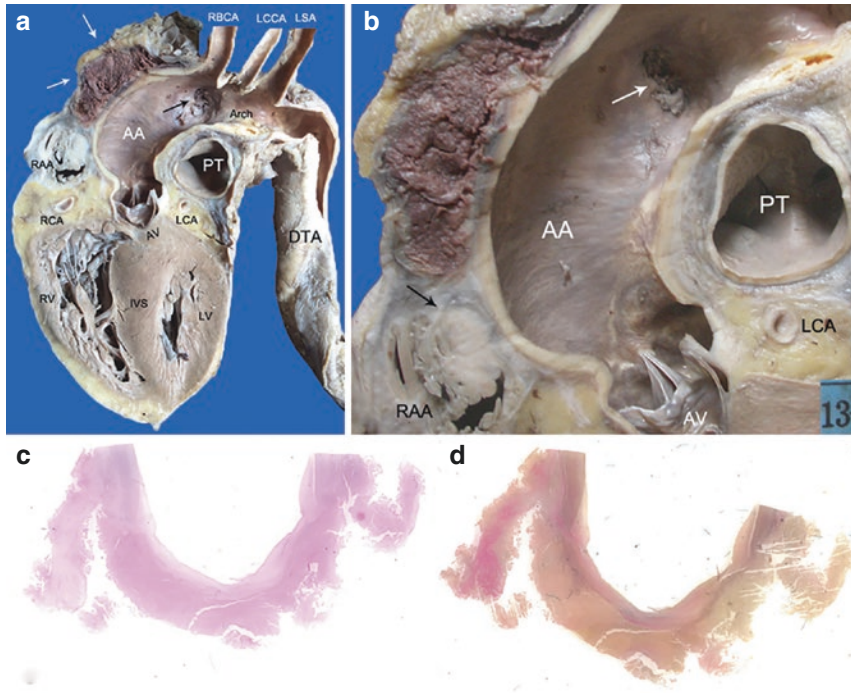

Fig. 66.2 (**a**) The heart has been longitudinally cut. There is a hematoma around the arch (white arrows) and friable thrombus below the ostium of the right brachiocephalic artery (black arrow) RBCA; (**b**) Close-up showing a perforation covered by friable thrombus (white arrow). Collection of grey-white necrosis (black arrow) partly surrounds the right atrial appendage RAA (*AA* ascending aorta, *AV* aortic valve, *DTA* descending thoracic aorta, *IVS* interventricular septum, *LCA* left circumflex artery, *LCCA* left common carotid artery, *LV* left ventricle, *LSA* left subclavian artery, *PT* pulmonary trunk, *RCA* right coronary artery, *RV* right ventricle); Scanned image of the section taken adjacent to the site of perforation—(**c**) H&E and (**d**) Elastic van Gieson

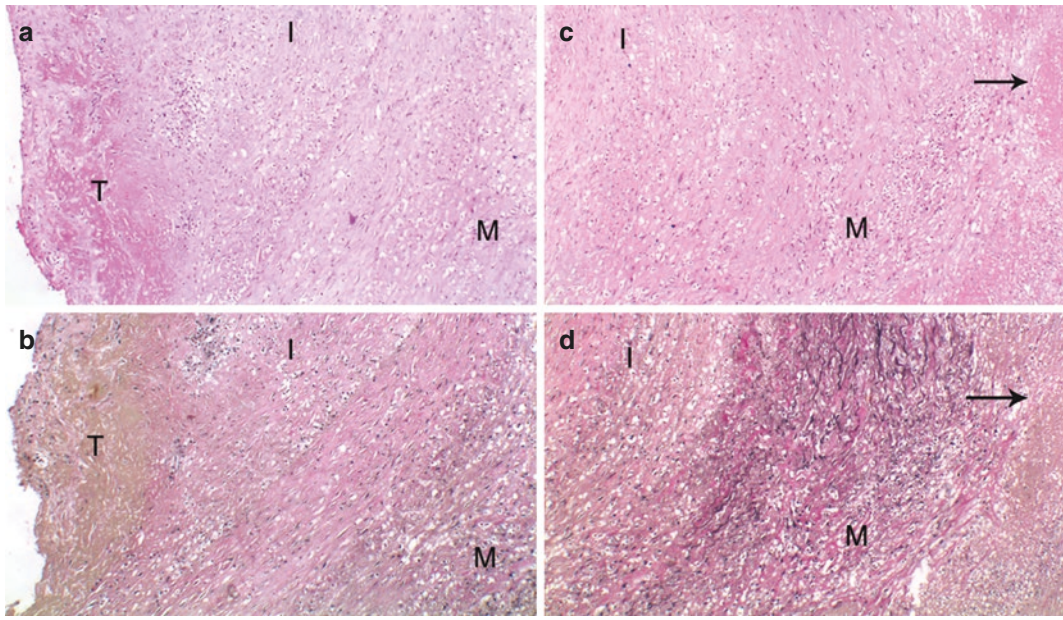

Fig. 66.3 Fibrocellular proliferation of the intima I with overlying fresh thrombus T. The underlying media M shows fibrosis and scattered inflammation with hardly any elastic fibers—(**a**) H&E × 250 and (**b**) Elastic van Gieson × 250; Destruction of the media M with subjacent caseation necrosis (arrow)—(**c**) H&E × 250 and (**d**) Elastic van Gieson × 250

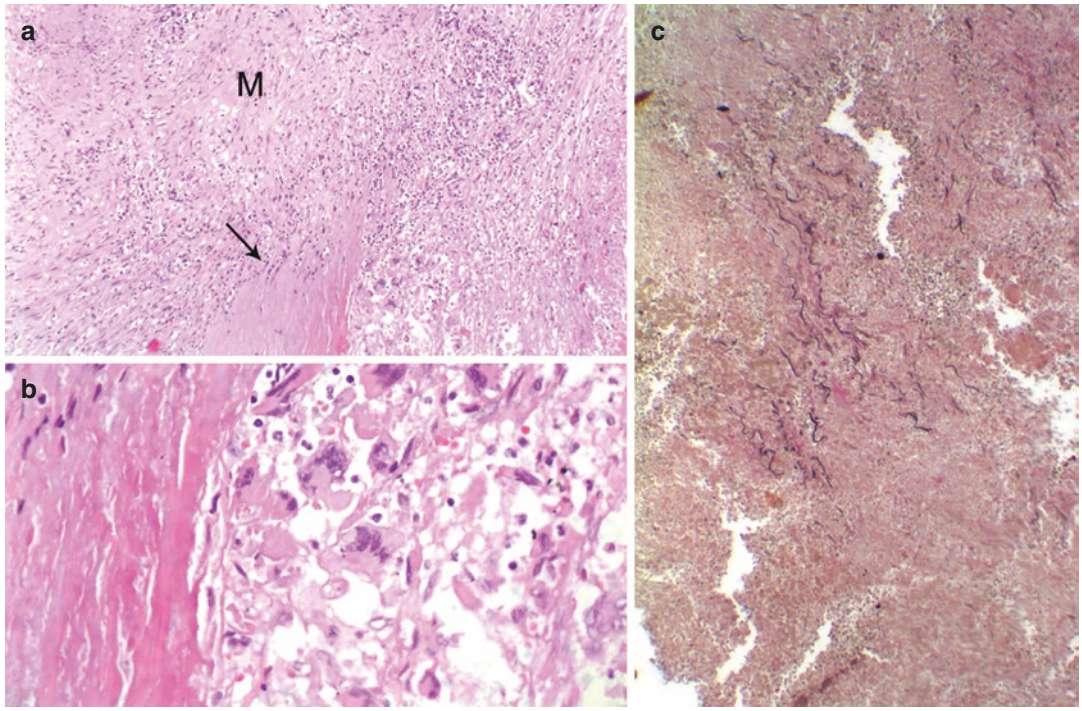

Fig. 66.4 (**a**) Transmural destruction of the media with focal granulomatous inflammation. Note a band of necrotic media (arrow, H&E × 250); (**b**) Collections of giant cells (H&E × 400); (**c**) Scattered elastic fibers within the zone of caseation necrosis (Elastic van Gieson × 250)

66.3 Discussion

Localized transmural tuberculous inflammation and destruction of the wall of the transverse aorta with formation of a pseudoaneurysm were seen as a manifestation of disseminated tuberculosis in an elderly immunocompetent woman. The involvement of the aorta with inflammation—aortitis is a feature of large-vessel vasculitis and is associated with significant morbidity. A varied etiology of aortitis results in varying geographic distribution, ages of onset, aortic segmental locations, and systemic manifestations. The diagnosis, therefore, depends on a multidisciplinary approach encompassing clinical, radiological, and laboratory criteria for accurate diagnosis. Aortitis can be broadly classified into noninfectious and infectious causes. In most instances, aortitis is noninfectious and most often represented by Takayasu's arteritis (See Chaps. 63–65) and giant-cell arteritis, where the line of therapy is directed towards immunosuppression (particularly use of steroids). In contrast to these disorders, the uncommon infectious aortitis (often acute or subacute) is potentially life-threatening due to higher rates of rupture and has to be promptly diagnosed and treated with appropriate antimicrobial therapy. The aorta is generally considered to be resistant to infective invasion, but age—or disease-related changes and compromised immunity are important predisposing factors. In general, the infection can occur as a result of hematogenous dissemination, septic embolization of the vasa vasora, or contiguous spread from adjoining structures. Most common organisms that are implicated include mainly gram-positive cocci (*Staphylococcus* and *Streptococcus* species) and gram-negative bacilli (*Salmonella* and *Escherichia* species). In the current case, the causative organism was *Mycobacterium tuberculosis*.

Tuberculosis of the cardiovascular system is the second most common manifestation of extrapulmonary disease and occurs in association with

pulmonary/pleural involvement and can rarely be seen independently. The 3 main patterns of tuberculous heart disease are pericarditis (See Chap. 2), myocarditis (See Chap. 38), and aortitis; in this patient, the aortitis was accompanied by tuberculous pericarditis. Tuberculous aortitis is an uncommon entity with an approximate incidence of 0.004% and has been reported in 32–46% of patients with miliary dissemination, as also seen in the present case. The mycobacteria can gain access into the aortic wall through systemic seeding via the vasa vasora, extension from adjacent tuberculous foci (in more than half the cases), and even direct implantation into atherosclerotic plaques. The most common pathogenetic mechanism is spread from the para-aortic structures such as the affected lymph nodes, vertebral bodies, pericardium, and also the lungs. Hence, predictably, the thoracic and abdominal segments are affected in nearly equal frequency, followed by the ascending aorta and the arch. Our patient had large caseous lymph nodes in the thorax with miliary tuberculosis as well. Histologically, there was transmural focal extension of the tuberculous inflammation into the non-aneurysmal wall leading to perforation and formation of a peri-aortic hematoma; the communication with the lumen was retained and there was walling off of the hematoma. Such a pseudoaneurysm formation occurs in close to 90% of the cases of tuberculous aortitis. True (mycotic) aneurysms usually occur when there is tuberculous inflammation in a longer segment of the aorta with weakening and subsequent dilatation.

The clinical manifestations of tuberculous aortitis can be nonspecific and constitutional as seen in patients with tuberculosis in general or specific related to the false or true aneurysms. These symptoms would be related to the location of the aneurismal disease and is due to mass effects or rupture into the surrounding space or into a viscus. It is imperative to have knowledge of this uncommon lesion that is highly fatal if it remains undiagnosed. Treatment includes both medical and surgical approaches and with this dual approach, the survival rate increases drastically up to 84–87%. In our case, the previous hematemesis was not related to an aorto-esophageal fistula, but to mucosal tears in the lower end of the esophagus. Exsanguination had also been prevented due to containment of the hematoma. Death was due to tuberculous dissemination.

Further Reading

Aebert H, Birnbaum DE. Tuberculous pseudoaneurysms of the aortic arch. J Thorac Cardiovasc Surg. 2003;125:411–2.

Deipolyi AR, Czaplicki CD, Oklu R. Inflammatory and infectious aortic diseases. Cardiovasc Diagn Ther. 2018;8(Suppl 1):S61–70.

Delaval L, Goulenok T, Achouh P, Saadoun D, Gaudric J, Pellenc Q, et al. New insights on tuberculous aortitis. J Vasc Surg. 2017;66:209–15.

Pugh D, Grayson P, Basu N, Dhaun N. Aortitis: recent advances, current concepts and future possibilities. Heart. 2021;107:1620–9.

Restrepo CS, Gonzalez TV, Brar R, Ocazionez D, Velasco ML, Reyna Lopez RA, et al. Thoracic cardiovascular complications of tuberculosis. J Comput Assist Tomogr. 2021;45:157–65.

Sharma S, Pandey NN, Sinha M, Chandrashekhara SH. Etiology, diagnosis and management of aortitis. Cardiovasc Intervent Radiol. 2020;43:1821–36.

Tuberculous Coronary Arteritis and Sudden Cardiac Death

67

Pradeep Vaideeswar and Gayathri Amonkar

67.1 Clinical History

A 24-year-old woman with episodic chest pain for the past 1 week, presented with acute respiratory distress. An ECG performed revealed ventricular fibrillation. She was immediately intubated; hemorrhagic frothy fluid flowed out of the endotracheal tube. Three DC shocks were applied with administration of atropine and adrenaline, followed by xylocaine and dopamine. The heart rate remained at 130 per minute. The hemoglobin was 7.6 g/dL; other routine investigations were normal. However, she had another cardiac arrest and expired after 6 h of admission.

67.2 Autopsy Findings

The heart was normal in size (230 g). There was patchy epicardial thickening with granular, yellowish white exudates over the course of the left anterior descending artery (LAD). The left coronary ostium showed protruding granular material. The left main coronary artery was a little ectatic (Fig. 67.1a). The lumen measured 1 cm across and was filled with friable dark-brown nonocclusive fresh thrombus. The proximal LAD showed grey-white expansion of its wall (Fig. 67.1a) for a length of 1.7 cm with critical luminal stenosis. Rest of the artery showed mild thickening of the wall. On histology, there was transmural destruction by granulomatous inflammation with foci of granular eosinophilic caseous necrosis (Fig. 67.1b, c). There was medial fibrosis and intimal fibrocellular thickening (Fig. 67.2a–d). The lumen was occluded by fresh and organizing thrombi. The myocardium showed only ischemic changes with interstitial edema. Aorta and other branches were not affected by the vasculitic process. The lungs were severely edematous with focal hemorrhage. Surprisingly, only the kidneys had multiple miliary caseating granulomas. Special stains for acid-fast bacilli were however negative.

Cause of Death: Tuberculous coronary artery vasculitis and acute myocardial ischemia.

P. Vaideeswar (✉)
Department of Pathology (Cardiovascular and Thoracic Division), Seth Gordhandas Sunderdas Medical College and King Edward Memorial Hospital, Mumbai, India

G. Amonkar
Department of Pathology, Topiwala National Medical College and BYL Nair Charitable Hospital, Mumbai, India

P. Vaideeswar (ed.), *Tropical Cardiovascular Pathology*,
https://doi.org/10.1007/978-981-19-3720-0_67

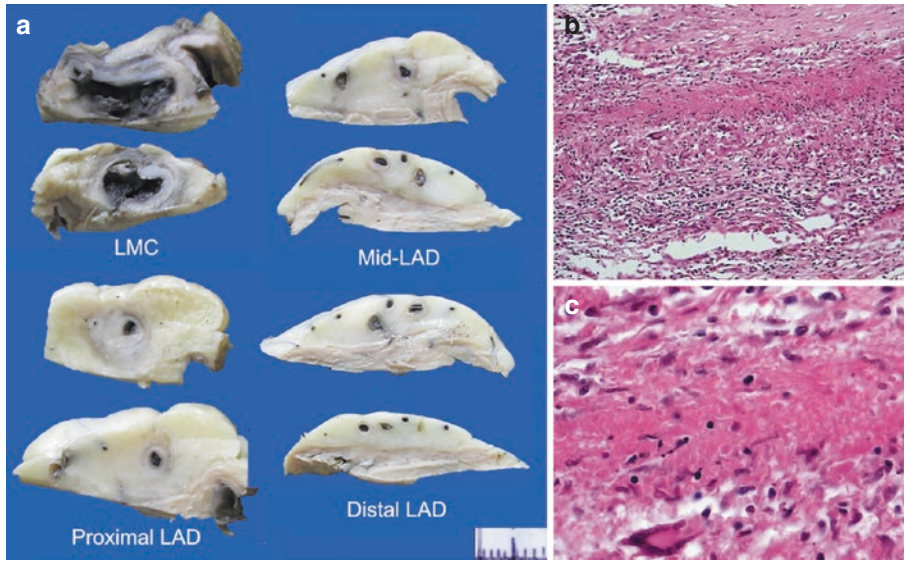

Fig. 67.1 (**a**) Serial cross sections of the coronary artery. The left main coronary LMC artery shows luminal dilatation with thrombotic occlusion. The proximal left anterior descending LAD artery has thick white walls; rest of the artery appeared almost normal; Wall of the artery showing band-like caseation necrosis with granulomatous reaction, (**b**) H&E × 250 and (**c**) H&E × 400

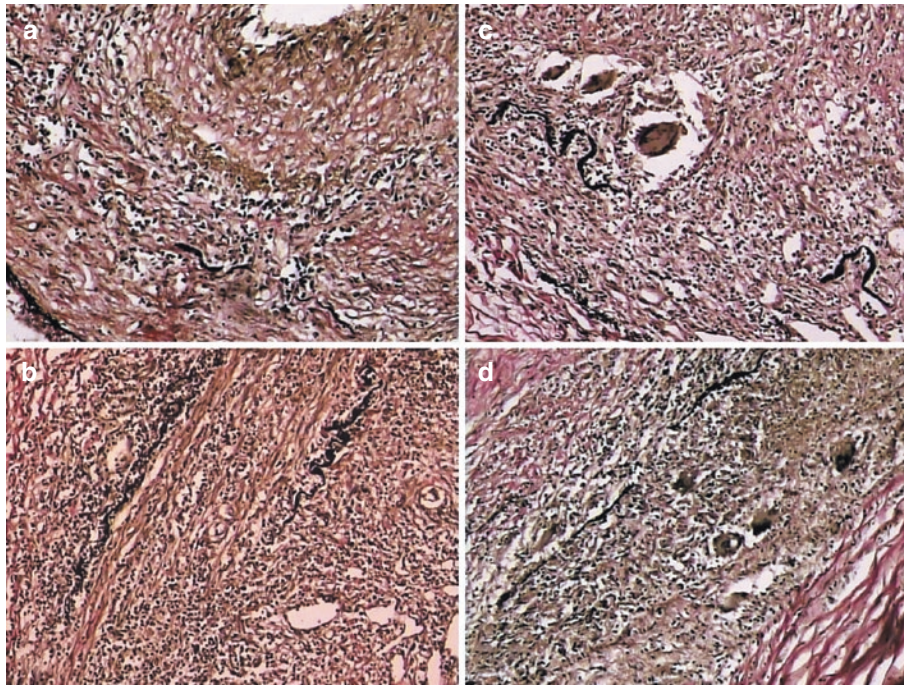

Fig. 67.2 (**a**) and (**b**) Destruction of the coronary arterial wall by inflammation and fibrosis; (**c**) and (**d**) Granulomatous inflammation is present. Note disruption of the internal elastic lamina in all the sections (Elastic van Gieson × 400)

67.3 Discussion

The young woman, who had presented with chest pain off and on in the preceding week, developed acute myocardial ischemia as a result of coronary artery vasculitis (CAV). Most of the cases of CAV occur in conjunction with systemic vasculitis, which are classified with reference to the type and the size of the vessels and also the type of inflammatory response. Even then, CAV is less common as compared to the other cardiac manifestations of systemic vasculitis such as pericarditis, myocarditis/cardiomyopathy, and valvular heart disease. The incidence of CAV varies with respect to the type of vasculitis. The most common vasculitic syndromes associated with CAV are Takayasu's arteritis (See Chaps. 63–65)/giant-cell arteritis (both large vessel vasculitis), and polyarteritis nodosa (See Chap. 74)/Kawasaki disease (both medium-sized vessel vasculitis). CAV results in spasms, stenosis, occlusion, aneurysms, rupture, or dissections of one or more of the coronary arteries. A diagnosis of CAV should be considered when young individuals present with sudden cardiac death, acute coronary syndromes, arrhythmias or conduction disturbances, and unexplained heart failure particularly in a setting of primary or secondary vasculitides. When it occurs in young individuals with no prior cardiovascular disease, isolated CAV should be kept in mind as the incidence of isolated disease is often underestimated. An infective etiology for the CAV should also be kept in mind, as was identified in this particular case caused by tuberculosis (TB).

The lungs are the most common organs affected by *Mycobacterium tuberculosis*; involvement of other organs is termed as extrapulmonary TB. In this context, though India has one of the highest burdens of TB, cardiovascular disease is uncommon with an incidence of 0.14–2% of patients with TB. It usually affects the pericardium (See Chap. 2) and myocardium (See Chap. 38) through lymphatic/hematogenous routes or spread from the adjacent tuberculous foci. Involvement of the coronary arteries by TB is vanishingly rare. Very few cases of tuberculous CAV have been documented in the literature and these had been associated with either pulmonary TB or mediastinal tuberculous lymphadenitis. However, in this young woman, there was no histological evidence of lung or mediastinal lymph node TB, and caseating granulomas seen in the kidneys suggest a hematogenous seeding of the affected coronary artery. Fibrointimal proliferation with necrotizing granulomatous inflammation indicated an ongoing process, which culminated in thrombotic occlusion and sudden death. In general, since CAV often portends a bleak outcome, a clinical suspicion, prompt diagnosis with multimodality imaging tools, and early institution of appropriate therapy can improve the outcome.

Further Reading

Chan S. An unusual case of mycobacterium tuberculous coronary arteritis and thrombosis resulting in acute myocardial infarction. Forensic Sci Med Pathol. 2018;14:390–4.

Gori T. Coronary vasculitis. Biomedicine. 2021;9:622.

Khanna K, Garikapati K, Goh DSL, Cho K, Lo P, Bhojaraja MV, et al. Coronary artery vasculitis: a review of current literature. BMC Cardiovasc Disord. 2021;21(1):7.

Paliwal P, Jain S, Ahuja A, Mittal S, Chauhan DS. Coronary arteritis as a cause of sudden cardiac death in a young girl. Autops Case Rep. 2021;11:e2021310.

Vaideeswar P, Verma R, Gupta R. Infective coronary arteritis: a pathological analysis at autopsy. Hum Pathol. 2012;43:2334–41.

Part X

Pulmonary Vascular Disorders

68 Chronic Pulmonary Thromboembolism with Membranous Nephropathy

Pradeep Vaideeswar and Lovelesh Nigam

68.1 Clinical History

A 39-year-old male patient had a long protracted medical history spanning over 3 years. In the first year, a high-resolution computed tomography (CT) and CT pulmonary angiography (CTPA) performed for 20-day progressive dyspnea revealed filling defects in subsegmental branches of right and left lower lobar pulmonary arteries. Since this was suggestive of pulmonary thromboembolism (PTE), he was started on anticoagulant therapy. In the second year and in the early part of the third year, a 2-dimensional transthoracic echocardiography revealed right atrial and ventricular dilatation, severe tricuspid regurgitation, borderline right ventricular function, severe pulmonary hypertension (126 mmHg), grade 1 left ventricular diastolic dysfunction, and paradoxical interventricular septal motion. In the latter part of the third year, he was admitted in our center with complaints of persistent dyspnea with atypical chest pain and orthopnea. On examination, he was afebrile with a pulse rate of 90 per minute, blood pressure of 114/70 mmHg, and respiratory rate of 18 per minute. There was raised jugular venous pressure and a pansystolic murmur heard on auscultation. All the hematological and biochemical investigations were within normal limits, except for a serum albumin value of 2.8 g/dL. A CTPA performed again showed dilated extrapulmonary arteries (pulmonary trunk 29 mm, right pulmonary artery 20 mm, left pulmonary artery 19 mm) with near complete occlusive thrombus in bilateral lower lobe branches and partial blockage of lingular segmental branches. He was treated with antifailure drugs, vasodilators, and anticoagulants. A pulmonary thrombectomy (Fig. 68.1a) was performed on the 13th day of admission. He had a cardiac arrest on postoperative day 01.

68.2 Autopsy Findings

The heart was mildly enlarged (320) with moderate enlargement and hypertrophy of the right-sided chambers. The tricuspid annulus was dilated with myxomatous changes in the leaflets. The pulmonary annulus was also dilated with prominent central nodules of the cusps. The pulmonary trunk was dilated and larger than the aorta with intimal thickening and irregularity; few adherent thrombi were present. The coronary arteries were normal. The intrapulmonary

P. Vaideeswar (✉)
Department of Pathology (Cardiovascular and Thoracic Division), Seth Gordhandas Sunderdas Medical College and King Edward Memorial Hospital, Mumbai, India

L. Nigam
Department of Pathology, Institute of Kidney disease and Research Center, HL Trivedi Institute of Transplantation Sciences, Gujarat University, Ahmedabad, India

P. Vaideeswar (ed.), *Tropical Cardiovascular Pathology*,
https://doi.org/10.1007/978-981-19-3720-0_68

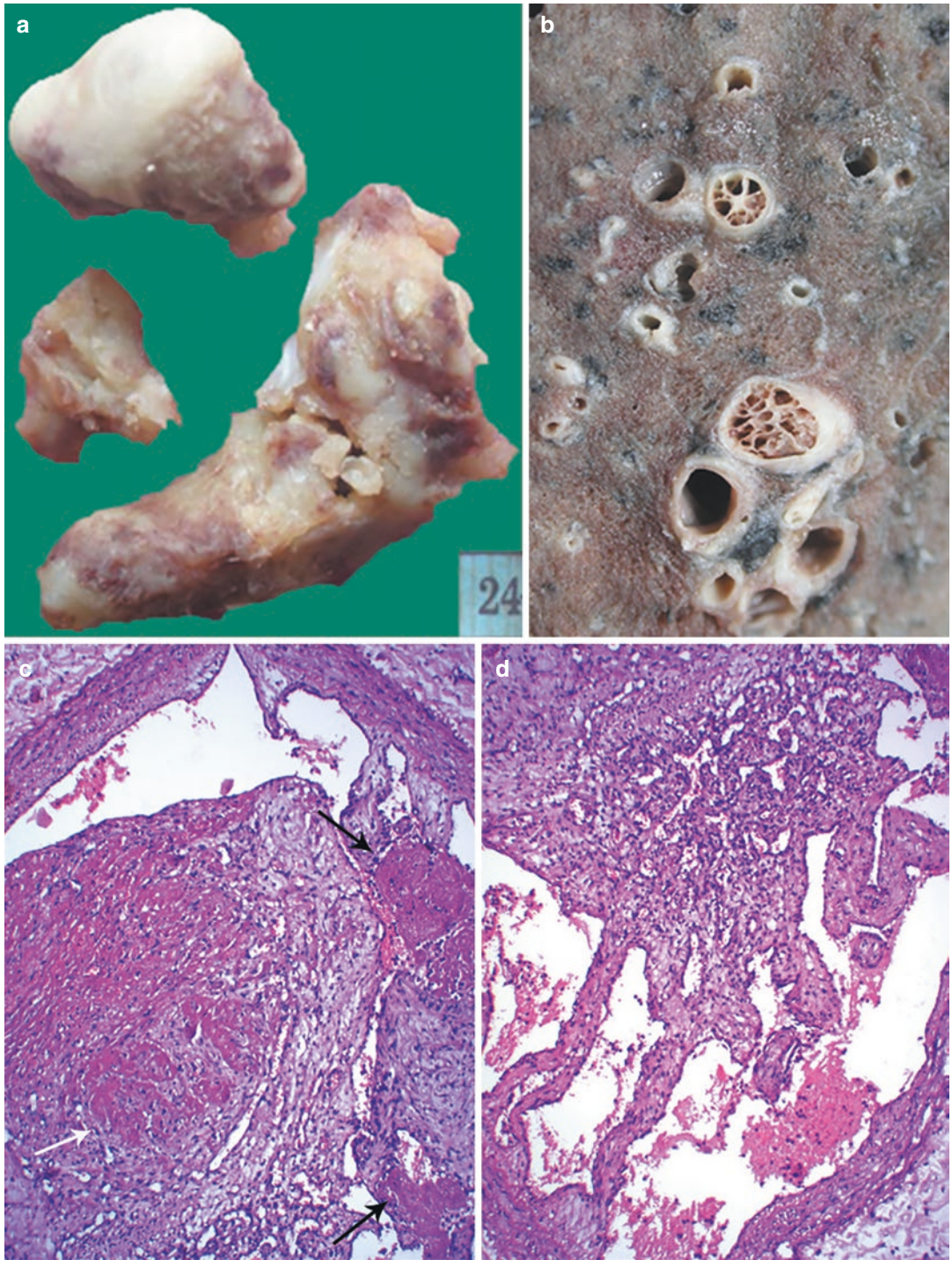

Fig. 68.1 (**a**) Curvilinear to irregular masses of thrombi excised from the pulmonary trunk; (**b**) The parenchymal arteries showing multiple sieve-like openings, the 'collander' lesions; (**c**) Organizing and recanalizing thrombus. Note presence of fresh fibrin clumps in the recanalized channels (black arrows) and within the organizing thrombus (white arrow, H&E × 250); (**d**) Part of the lumen traversed by multiple vascular channels (H&E × 250)

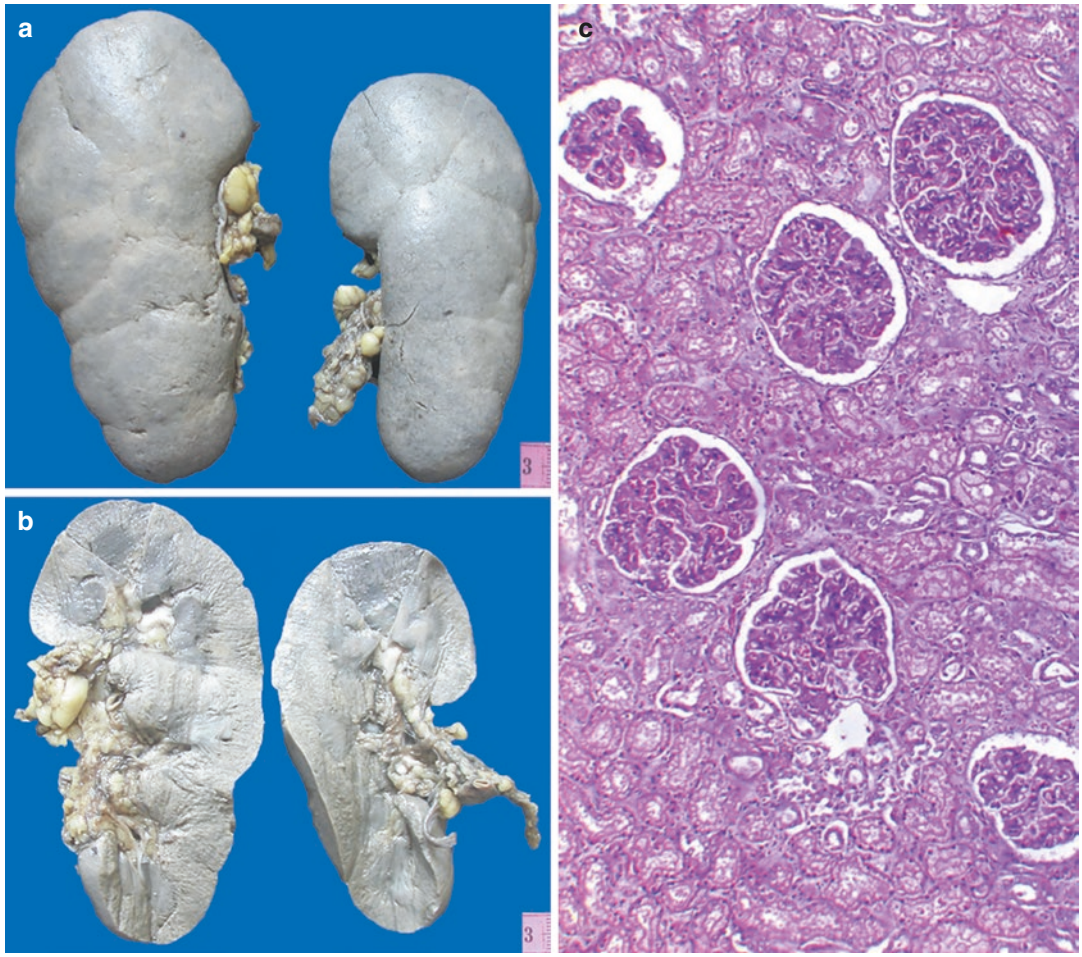

Fig. 68.2 (**a**) Pale appearing enlarged kidneys, right larger than the left; (**b**) The cut surfaces show widening and pale white appearance of the cortex; (**c**) All the glomeruli are enlarged (H&E × 250)

arteries showed gross (Fig. 68.1b) and microscopic (Fig. 68.1c, d) features of organizing and recanalizing thrombi with the formation of the characteristic 'collander lesions'. Some of the arteries including the recanalized channels also showed presence of fresh, nonocclusive, or occlusive thrombi (Fig. 68.1c). Many arterial media were of increased thickness—medial hypertrophy. These features were suggestive of chronic thromboembolic pulmonary hypertension (CTEPH). A surprising finding was bilateral enlargement of the kidneys (right kidney g and left kidney g) with a uniform pale white surface (Fig. 68.2a). On histology, there were classic features of membranous nephropathy (MN, Figs. 68.2c and 68.3a–d). Lymphocytic thyroiditis was also present (Fig. 68.3e).

Cause of Death: Right heart failure due to CTEPH.

68.3 Discussion

A young male had developed recurrent PTE, received prolonged anticoagulant therapy, and had undergone a surgical intervention before his unfortunate demise. PTE is one of the manifestations that is included under the term of 'acute

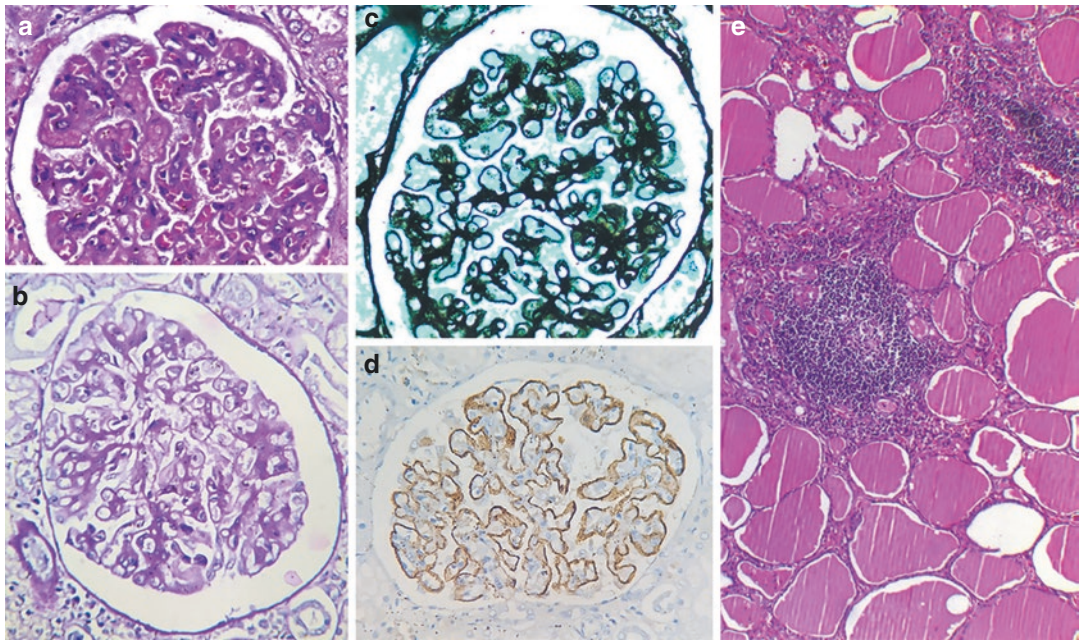

Fig. 68.3 (**a**) The enlarged glomeruli show thickening of the capillary walls (H&E × 400), highlighted by (**b**) the Periodic Schiff stain (× 400); (**c**) Silver methenamine stain demonstrating the 'spikes' which reflect the extension of the basement membrane between the subepithelial deposits (× 400); (**d**) Immunohistochemical positivity of PLA2R in the glomerular basement membrane (× 400); (**e**) Thyroid showing lymphocytic aggregates with formation of pale staining germinal center (H&E × 250)

venous thromboembolism', the second category being deep vein thrombosis (DVT). It is a life-threatening malady and is the third most common cause of death related to cardiovascular diseases, after acute coronary syndromes (See Chaps. 24–26) and cerebrovascular accidents. The estimated incidence is projected at 100–200 cases per 100,000 persons with a slight male predominance. In majority of the cases, the pulmonary arterial tree is occluded by thrombotic fragments that break free from deep vein thrombi. However, in a significant number of patients, PTE is not always preceded by DVT and there would be role for *in-situ* thrombosis of the pulmonary arteries. In addition, intracardiac thrombi that can occur in the absence of DVT are other possible sources. There was no history of DVT in our patient. Thrombi, in general, form within the vasculature secondary to changes in the blood flow, endothelial injury, and blood hypercoagulability; these factors constitute the Virchow's triad. The risk factors for this thrombogenicity may include genetic or acquired factors. The genetic causes include loss-of-function mutations in genes encoding anticoagulants such as protein C/protein S deficiency or gain-of-function mutations in genes encoding procoagulants, which involve factor V or prothrombin. Deficiencies of these factors may also occur secondary to the acquired causes of thrombophilia. In most cases, there are acquired or secondary risk factors that include prolonged immobilization, postoperative states, pregnancy, use of oral contraceptives, cancer, antiphospholipid antibodies (See Chap. 30), chronic cardiopulmonary disorders, advancing age, obesity, and a prior history of VTE. Thrombophilia in our case was in all probability produced by MN.

MN is the most common cause of nephrotic syndrome (NS, defined as proteinuria of 3.5 g/day and serum albumin <3.5 g/dL) in adults, accounting for nearly 20–40% of the cases. The mean age

of diagnosis is in the fifth decade of life, though it can be seen in all age groups. The glomerular dysfunction is attributed to deposition of immune complexes on the outer aspect of the basement membrane (subepithelial deposits). MN can either be primary (idiopathic) or secondary to drugs, malignancy, infections, systemic, or even nonrenal organ-specific autoimmune disorders. Many cases of primary MN are now seen to represent renal-limited autoimmune disease with antibodies against M-type phospholipase A2 receptor (aPLA2Rab) that have been identified in 70–80% of patients of various ethnic groups. The presence of this type of autoimmunity has been demonstrated by immunohistochemical positivity of PLA2R along the glomerular basement membrane. This patient at autopsy also demonstrated the presence of lymphocytic thyroiditis, and around 10–30% of patients with thyroidal autoimmune disorders are known to have secondary MN. Some patients with MN may have asymptomatic proteinuria, while some may exhibit a waxing and waning of the disease process. Hypoalbuminemia was seen in this patient; however, routine urine examination reports were not available. This case highlights the importance of not overlooking results of basic routine investigations that in this case might have uncovered the existence of MN. Patients with NS and MN in particular also have an increased risk of VTE. The pathogenesis is attributed to the hypercoagulable state in patients with NS, caused by increased filtration of small proteins like antithrombin III, plasminogen, protein C, and protein S, further accentuated by loss of albumin and increased hepatic synthesis of fibrinogen. There is also concomitant increase in the levels of factor V, VII, and von Willebrand factor in these patients, which along with increased platelet activation, hyperfibrinogenemia, and inhibition of plasminogen activation complicate the process. The risk of thrombosis is also related to severity and duration of NS and is seen to be increased with serum albumin concentration of $\leq$2.0 g/dL. Most common sites of thrombosis in NS include deep veins of lower limbs, inferior vena cava, renal veins, and pulmonary artery. Of all the causes of NS, patients with MN are noted to be at the highest risk for developing a thromboembolic phenomenon. Association of MN and renal vein thrombosis is more known than any other venous thrombosis. The incidence of PTE ranges from 3.3 to 11.9% in adults with NS, but its occurrence as the presenting manifestation of NS or in MN, as was seen in the index case, is unusual. Thromboembolic disorders in NS are dangerous and can progress to mortality if not medically controlled. In this patient, the subclinical MN led to recurrent pulmonary arterial thrombosis that lapsed into CTEPH.

CTEPH is one of the chief and serious manifestations of postpulmonary embolism syndrome, affecting 2–4% of patients with prior episodes of PTE. It is classified in group 4 of pulmonary hypertension (PH, See Chap. 71) and is defined as "symptomatic PH (a mean pulmonary arterial pressure of $\geq$25 mmHg or mean pulmonary artery wedge pressure (PAWP) $\leq$ 15 mmHg measured by right heart catheterization) in the presence of flow-limiting obstructive lesions within the pulmonary arteries persisting, despite effective anticoagulation therapy (as seen in the present case). It should be distinguished from another postembolic manifestation termed as chronic thromboembolic pulmonary vascular disease, where chronic vascular occlusions are associated with (near) normal pulmonary hemodynamics at rest and (marked) exercise limitations. The failure of incomplete resolution of the thrombus is multifactorial, resulting from defects in fibrinolysis and neoangiogenesis, endothelial and platelet dysfunctions, and local release of inflammatory cytokines. Interestingly, hypothyroidism is a risk factor in the development of CTEPH. Unfortunately, the thromboembolic phenomenon is also accompanied by microvascular remodeling and the final result is increased pulmonary vascular resistance, PH, increased right ventricular preload, decreased right ventricular contractility, decreased left ventricular filling due to bulge of the interventricular septum to the left, and finally right heart failure, which was the cause of death in this young patient. Pharmacotherapy combined with pulmonary endarterectomy and balloon pulmonary angioplasty play important roles in the management of CTEPH.

Further Reading

Giordano NJ, Jansson PS, Young MN, Hagan KA, Kabrhel C. Epidemiology, pathophysiology, stratification, and natural history of pulmonary embolism. Tech Vasc Interv Radiol. 2017;20:135–40.

Huisman MV, Barco S, Cannegieter SC, Le Gal G, Konstantinides SV, Reitsma RH, et al. Pulmonary embolism. Nat Rev Dis Primers. 2018;4:18028.

Klok FA, Couturaud F, Delcroix M, Humbert M. Diagnosis of chronic thromboembolic pulmonary hypertension after acute pulmonary embolism. Eur Respir J. 2020;55:2000189.

Klok FA, Delcroix M, Bogaard HJ. Chronic thromboembolic pulmonary hypertension from the perspective of patients with pulmonary embolism. J Thromb Haemost. 2018;16:1040–51.

Leslom AN, Alrawiah ZMS, Al-Asmari AMA, Alqashaneen MDA, Alahmari AOT, Al-Ahmari HBOT. Prevalence of pulmonary thromboembolism in nephrotic syndrome patients: a systematic review and meta-analysis. J Fam Med Prim Care. 2020;9:497–501.

LeVarge BL, Wright CD, Rodriguez-Lopez JM. Surgical management of acute and chronic pulmonary embolism. Clin Chest Med. 2018;39:659–67.

Marongiu F, Marneli A, Grandone E, Barcellona D. Pulmonary thrombosis: a clinical pathological entity distinct form pulmonary embolism? Semin Thromb Hemost. 2019;45:778–83.

Papamatheakis DG, Poch DS, Fernandes TM, Kerr KM, Kim NH, Fedullo PF. Chronic thromboembolic pulmonary hypertension. J Am Coll Cardiol. 2020;76:2155–69.

Trujillo H, Alonso M, Praga M. New ways of understanding membranous nephropathy. Nephron. 2020;144:261–71.

69 Pulmonary Tumor Embolism in a Case of Hepatocellular Carcinoma

Pradeep Vaideeswar

69.1 Clinical History

A 65-year-old woman had been earlier diagnosed with liver cirrhosis (posthepatitis B) complicated by portal hypertension. Abdominal distension, decreased urinary output, and bilateral pedal edema, which had been present for 'few' days, were now associated with sudden onset of shortness of breath and retrosternal chest pain. She was transferred to our center in a poor general condition (pulse 110 per minute, blood pressure 90 systolic) and expired within 20 min of admission. No investigations had been performed.

69.2 Autopsy Findings

The heart was mildly enlarged (290 g) with moderate dilatation of the right atrium and mild enlargement of the right ventricle. A large (8 × 7 × 2.5 cm) broccoli-like mass was present in the entire suprahepatic portion of the inferior vena cava (IVC, Fig. 69.1a, b). The mass was soft, friable, yellowish green, and projected into the right atrium as multiple blunt finger-like projections (Fig. 69.1a, b). The pulmonary trunk and its branches were dilated and contained friable greenish-yellow irregular tissue bits loosely present in their lumens. Smaller particulate debris was also noted in the sinuses-of-Valsalva of the pulmonary valve. This had resulted in extensive pulmonary pure tumor embolism, affecting the segmental and sub-segmental branches (Fig. 69.1c, d). The hepatic and subhepatic IVC showed the presence of mural nonocclusive thrombi (Fig. 69.1a). The portal vein and its radicles had occlusive thrombi (Fig. 69.1a). The cavo-atrial mass had originated from a multifocal hepatocellular carcinoma (HCC) in a background of macronodular cirrhosis (Fig. 69.1a). The hepatic veins were dilated but devoid of thrombi or tumor. Other findings were cholelithiasis and fibrocongestive splenomegaly.

Cause of Death: Pulmonary tumor embolism (PTuE) due to HCC.

P. Vaideeswar (✉)
Department of Pathology (Cardiovascular and Thoracic Division), Seth Gordhandas Sunderdas Medical College and King Edward Memorial Hospital, Mumbai, India

P. Vaideeswar (ed.), *Tropical Cardiovascular Pathology*,
https://doi.org/10.1007/978-981-19-3720-0_69

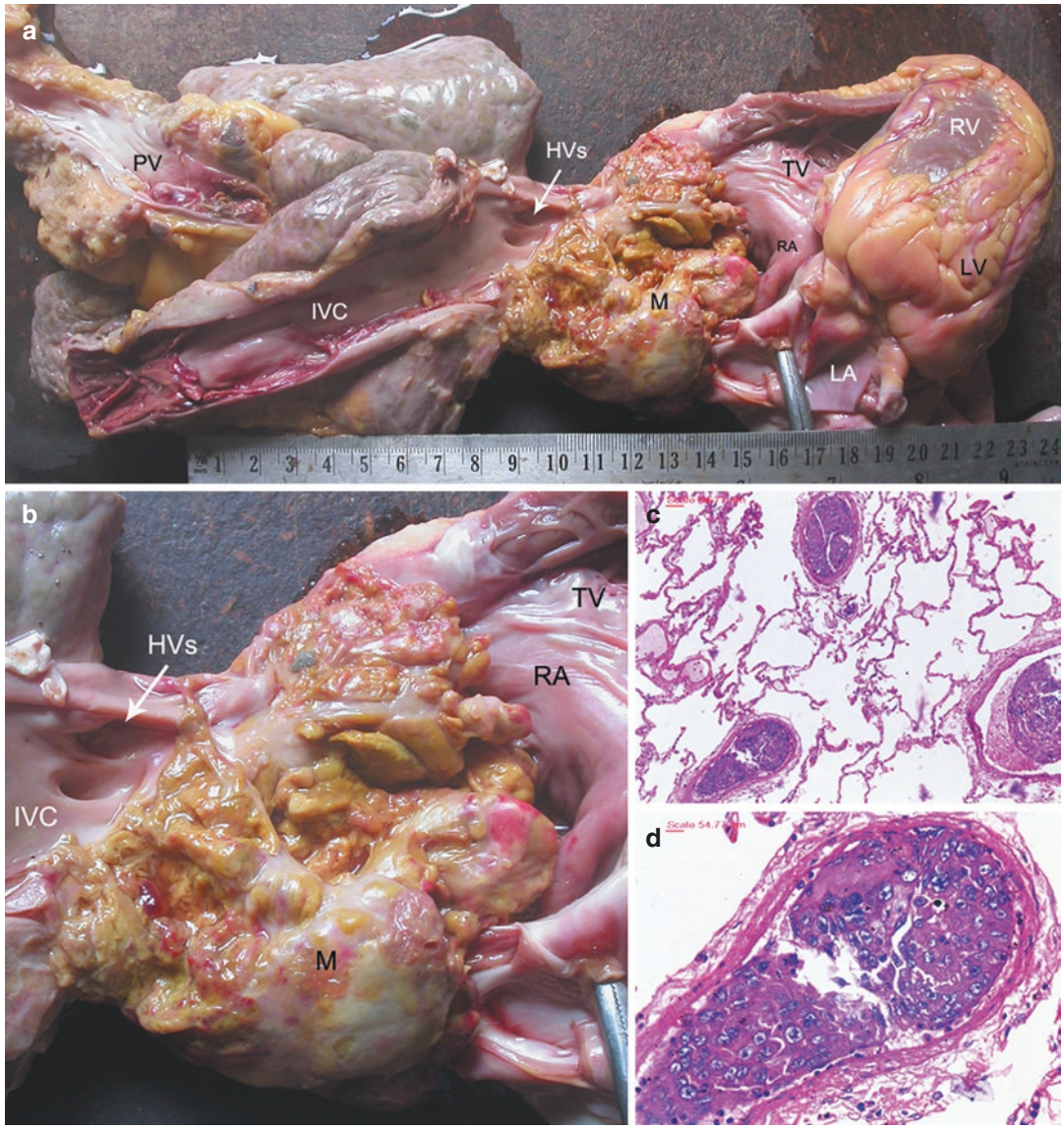

Fig. 69.1 (**a**) A large yellowish-green mass M was present at the inferior vena caval IVC—right atrial RA junction with formation of friable finger-like projections within the atrial cavity. Note the presence of mural and occlusive thrombi in the remaining portion of IVC and portal vein, respectively. The liver is small in size with macronodular cirrhosis; (**b**) Close of the cavo-atrial mass. Note extremely friable surface. The pulmonary arteries are exclusively occluded by tumor emboli, (**c**) H&E × 200 and (**d**) H&E × 400

69.3 Discussion

Mortality in this elderly woman was caused by intrapulmonary arterial obstruction produced by a shower of tumor fragments from a large cavo-atrial metastatic mass. She had a subclinical multicentric HCC, which is the commonest malignant tumor of the liver when metastatic lesions are excluded. When an acute hemodynamic compromise occurs in a cancer patient, it is frequently attributed to an underlying venous thromboembolism (VTE). This entity encompasses both deep vein thrombosis and the more ominous pulmonary thromboembolism (PTE). The thrombo-

genic potential in the cancer afflicted is also explained by the Virchow's triad, which includes endothelial dysfunction, blood flow disturbances, and alterations of the constituents of blood. Important among them is cancer-related thrombophilia (sometimes designated as type I hypercoagulability) caused particularly by enhanced activity or release of several prothrombotic factors and inflammatory cytokines, overexpression of tissue factors, and even platelet activation. In these cases, the common sites of cancer are in the pancreas, gastrointestinal tract, and lung and histologically are mainly adenocarcinomas. Other causes are treatment-related or patient-specific factors (the so-called type II hypercoagulability). WhiIe 90% of the cancer patients have thrombotic occlusion, in this case the acute pulmonary embolism was non-thrombotic in nature and was produced by fragmentation of an intraatrial metastatic tumor from the liver malignancy.

Presence of tumor cell clusters in the pulmonary arterial tree, including the alveolar septal capillaries, away from metastatic nodules and devoid of thrombosis or fibro-cellular intimal thickening (See Chap. 70) characterizes PTuE. This is seldom an antemortem diagnosis as the symptomatology mimics the more common PTE such as dyspnea, chest pain, or cardiovascular collapse. Furthermore, the routine radiological investigations used for the diagnosis of PTE cannot differentiate between thrombus and tumor within the pulmonary arteries. Hence, such a diagnosis is often rendered on postmortem examination. The incidence ranges from 3 to 26% and the wide disparity is explained on the degree of sampling of lung tissues at autopsy. But this may also not be a true incidence as all cancer deaths are not autopsied. Clinical manifestations are produced when tumor cells occlude 30% of the pulmonary arterial tree. The most common primary cancers with PTuE are breast (14.2%) and gastric cancers (13.3%), followed by HCC (12.5%). In nearly half of the cases, HCC presents as pulmonary embolism (thrombus and/or tumor). Additionally, presence of tumor thrombus in the IVC and right atrium is also infrequent (about 1.4–4.9% of patients with HCC) and this picture is usually associated with a dismal prognosis.

Further Reading

Deng D, Wu H, Wei H, Song Z, Yu Y, Zhang C, et al. Syncope as the initial presentation of pulmonary embolism in two patients with hepatocellular carcinoma: two case reports and literature review. Medicine. 2021;100:38 (e27211).

Gimbel IA, Mulder FI, Bosch FTM, Freund JE, Guman N, van Es N, et al. Pulmonary embolism at autopsy in cancer patients. J Thromb Haemost. 2021;19:1228–35.

He X, Anthony DC, Catoni Z, Cao W. Pulmonary tumor embolism: a retrospective study over a 30-year period. PLoS One. 2021;16:e0255917.

Leiva O, Newcomb R, Connors JM, Al-Samkari H. Cancer and thrombosis: new insights to an old problem. J Med Vasc. 2020;45:6S8–6S16.

Liu J, Zhang RX, Dong B, Guo K, Gao ZM, Wang LM. Hepatocellular carcinoma with inferior vena cava and right atrium thrombus: a case report. World J Clin Cases. 2021;9(26):7893–900.

Ufuk F, Kaya F, Sagtas E, Kupeli A. Non-thrombotic pulmonary embolism in emergency CT. Emerg Radiol. 2020;27:343–50.

70 Uterine Choriocarcinoma with Pulmonary Tumor Thrombotic Microangiopathy

Pradeep Vaideeswar and Mona Agnihotri

70.1 Clinical History

A 20-year-old unmarried female presented with the symptoms of progressive dyspnea (grade I to II), cough with mucoid expectoration, generalized body ache, joint pains, and weight loss of 5 kg in 2 months. This was followed by intermittent moderate grade fever with chills and vaginal bleeding for the past 15 days. There was no pedal edema, decreased urine output, loose motion, burning micturition, or facial puffiness. No history of tuberculosis or tuberculous contact was present.

On examination, the general condition was fair. The pulse rate was 150 per minute and blood pressure was 114/70 mmHg. Bilateral crepitations were heard on auscultation; rest of the systemic examination had been normal. The clinical impression had been lower respiratory tract infection, possibly tuberculosis. The investigations have been tabulated (Table 70.1). The patient was treated with augmentin, hydrocortisone, tamiflu, and emset. However, the respiratory distress worsened and she succumbed after 29 days of ward stay.

Table 70.1 Investigations

Hematological	[a]Hemoglobin 7.5 g/dL [a]Total leukocyte count 12,300/cmm Differential count: Neutrophil predominant [a]Platelet count 3 lakhs/cmm
Biochemical—Routine	[a]Serum creatinine 0.825 mg/dL [a]Blood urea nitrogen 12.25 mg/dL [a]Total proteins 6.9 g/dL [a]Total bilirubin 1.45 mg/dL [a]Direct bilirubin 0.85 mg/dL [a]SGOT 48.5 U/L [a]SGPT 25.5 U/L [a]Sodium 136 mEq/L [a]Potassium 3.65 mEq/L [a]Chloride 97.5 mEq/L [a]Alkaline phosphatase 301 U/L
Biochemical—Specialized	Creatine kinase: MB isoform 109 U/L C-reactive protein 33.7 (normal <5.0 mg/L) T_3 348.65 mmol/L (normal 6–181) T_4 > 30 mmol/dL (normal 4.5–10.9)
Serological	HIV negative HBsAg negative HCV negative Leptospirosis negative Dengue negative Anti-nuclear antibody positive 1:1280 Anti-double stranded DNA negative Cardiolipin IgG 11.01 (normal <12 GPL/mL) Cardiolipin IgM 25.52 (normal <12 MPL/mL)
Radiological	Computed tomography (CT) chest: Bilateral patchy consolidation in posterior segment of lower lobes—Infective etiology, most likely tuberculosis or vasculitis
Others	Sputum culture: Negative for acid-fast bacilli

[a]Mean values

P. Vaideeswar (✉)
Department of Pathology (Cardiovascular and Thoracic Division), Seth Gordhandas Sunderdas Medical College and King Edward Memorial Hospital, Mumbai, India

M. Agnihotri
Department of Pathology, Seth Gordhandas Sunderdas Medical College and King Edward Memorial Hospital, Mumbai, India

P. Vaideeswar (ed.), *Tropical Cardiovascular Pathology*,
https://doi.org/10.1007/978-981-19-3720-0_70

70.2 Autopsy Findings

The main pathology was found in the intra-pulmonary arteries and the female genital tract. There was extensive thrombotic occlusion of almost all the pulmonary arteries (Fig. 70.1a, b). The thrombi appeared reddish-brown and friable to pale yellow and fleshy. This had resulted in bilateral, multiple sub-pleural wedge-shaped fresh hemorrhagic infarction (Fig. 70.1a), with cavitations in some of them. This was confirmed on histo-pathological examination (Fig. 70.1c), where some of the infarcts also revealed peripheral organization, indicating healing of the necrotic zones. Apart from the fresh and recanalized/organized thrombi, many of the arteries revealed necrotic tumor tissue. The viable tumor at the periphery was characterized by an intimate admixture of mononuclear and multi-nucleated giant cells (Fig. 70.2a–c). The mononuclear cells were medium sized and polygonal with round, hyperchromatic nuclei and abundant granular to clear cytoplasm, which resembled cytotrophoblasts (Fig. 70.2d). The multi-nucleated cells had dense amphophilic cytoplasm and multiple hyperchromatic, smudged nuclei that indicated syncytiotrophoblasts (Fig. 70.2d). The tumor was completely restricted to the arterial lumens and no nodules were found in the lung parenchyma.

The uterus (Fig. 70.3a) measured 10 × 7 × 3 cm with endometrium thickness of 0.5 cm. The ovaries were enlarged with multiple cortical cysts filled with yellowish clear fluid (luteinized follicular cysts, Fig. 70.3a, b). The myometrium on the left and posterior aspect of the fundus showed a yellowish granular raw area of perforation (Fig. 70.3c), which on cut surface was pale yellow with hemorrhagic borders. This revealed necroses, clusters of choriocarcinomatous elements (Fig. 70.3d), sheets of foamy macrophages (Fig. 70.3e), hemorrhage and vascular tumor embolization (Fig. 70.3f). There were no antecedent features of pregnancy. Other organs, including the heart (weight 230 g) were unremarkable and were completely devoid of metastatic deposits.

Cause of Death: Pulmonary tumor thrombotic micro-angiopathy (PTTM) due to choriocarcinoma (CC).

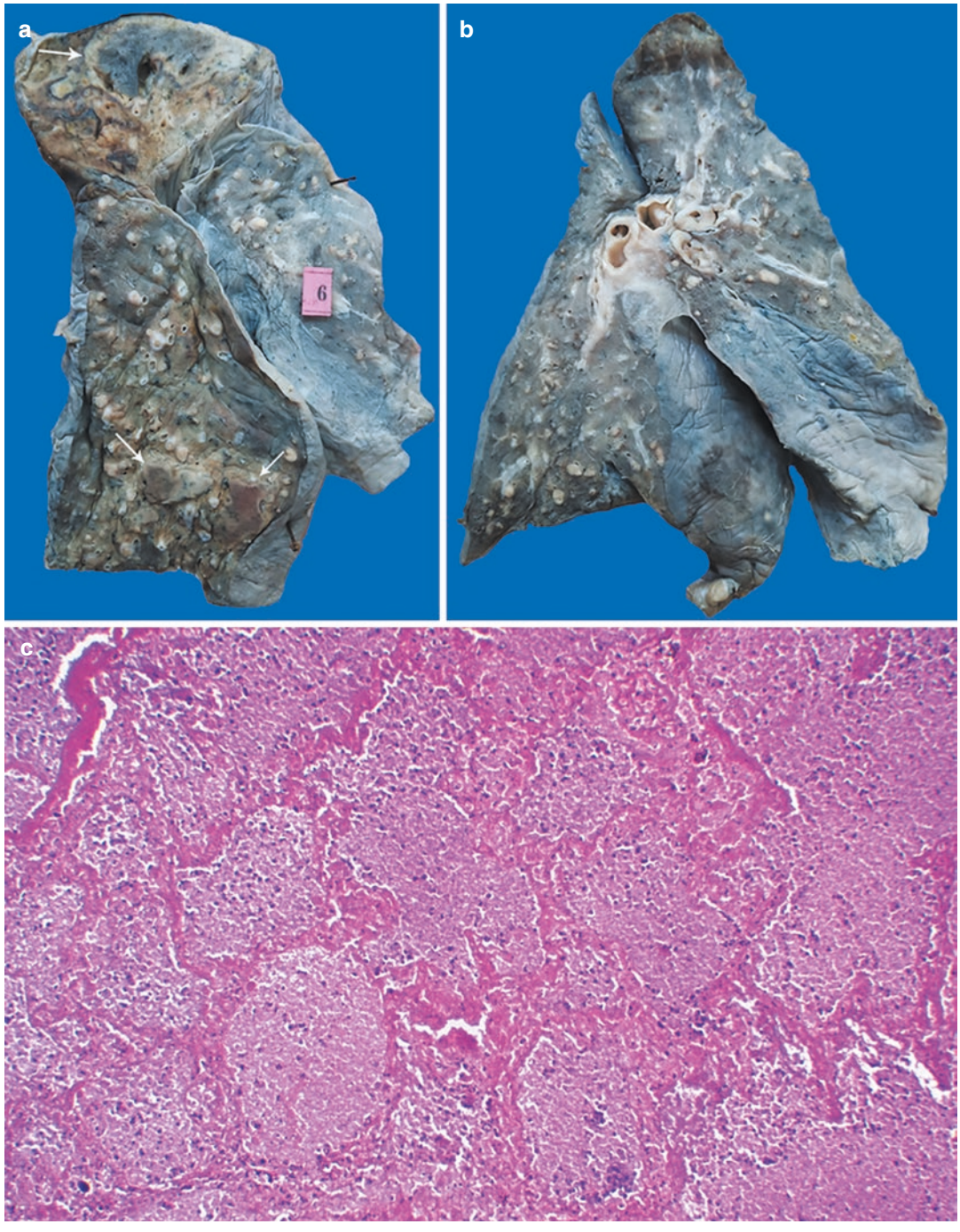

Fig. 70.1 The cut surfaces of (**a**) right and (**b**) left lungs show presence of arterial thrombotic occlusion, some of them appear pale yellow and fleshy. Note the presence of sub-pleural areas of infarctions (arrows); (**c**) hemorrhagic infarction (HE × 200)

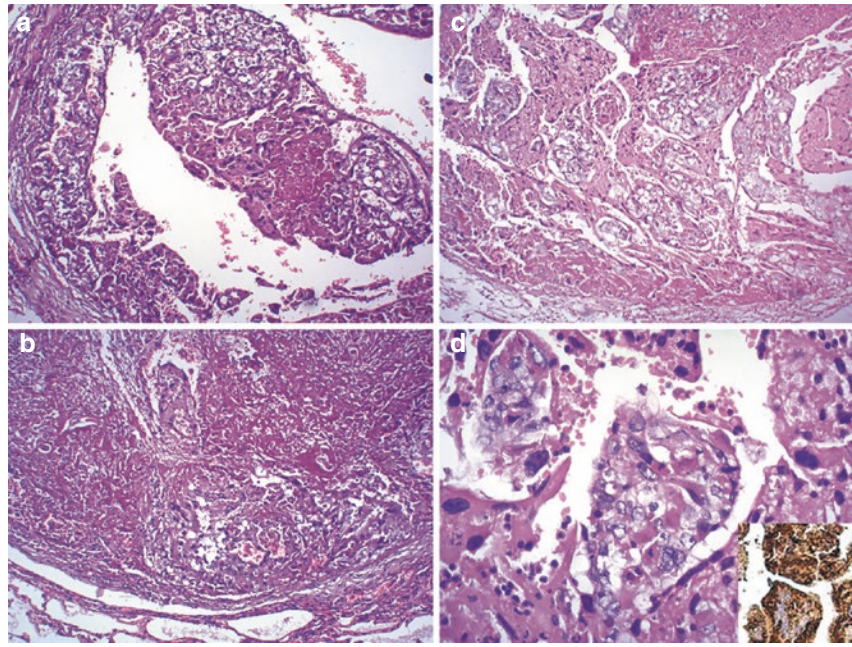

Fig. 70.2 Muscular pulmonary arteries seen in (**a**), (**b**), and (**c**) showing varying amounts of thrombotic material admixed with clusters of tumor cells (H&E × 250); (**d**) biphasic pattern—polygonal cells with hyperchromatic round nuclei and abundant granular to clear cytoplasm, the cytotrophoblasts and few large multi-nucleated cells with amphophilic cytoplasm, the syncytiotrophoblasts (H&E × 400); inset shows positive immunohistochemistry for β-HCG (× 400)

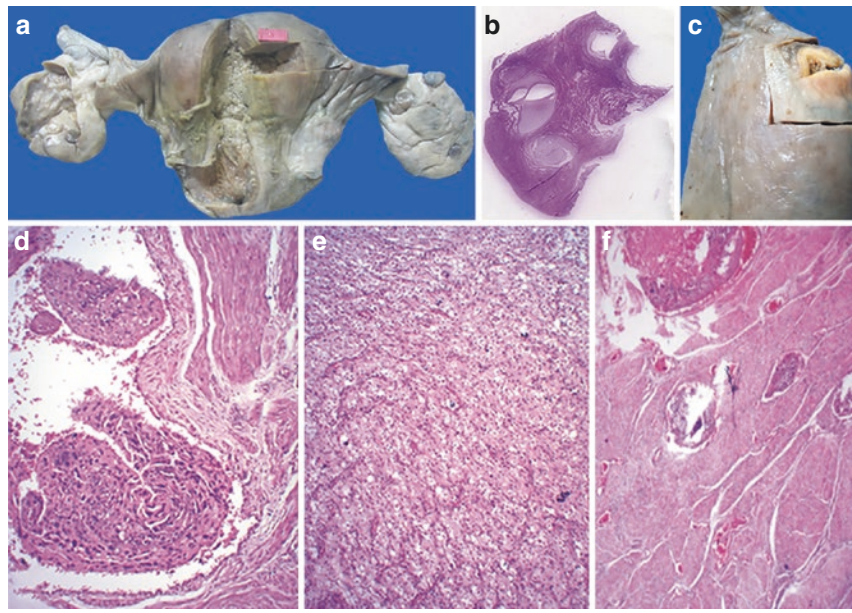

Fig. 70.3 (**a**) Uterus and bilateral adnexa. There is no endometrial hemorrhage. Both the ovaries are uniformly enlarged with multiple cysts, which on histology revealed (**b**) theca lutein cysts (Scanned slide, H&E); (**c**) the left aspect of the fundic portion of the posterior uterine wall revealed a yellow plaque with central area of rupture; multiple sections from that site revealed. (**d**) Choriocarcinomatous elements dissecting the smooth muscle bundles (H&E × 250) with (**e**) sheets of foamy macrophages (H&E × 250); (**f**) Note myometrial vascular tumor emboli (H&E × 100)

70.3 Discussion

Herein, another example of non-thrombotic pulmonary embolism (see Chap. 69) is presented, where widespread intra-luminal necrotic tumor was associated with fresh fibrin deposition accompanied by fibro-cellular proliferation. These are the characteristic features of PTTM, which represents a step beyond pulmonary tumor embolism. The entrapped tumor cells lead to endothelial injury with consequent increased local pro-coagulant activation and secretion of growth factors as well as inflammatory cytokines. There is usually a reactive myo-fibroblastic proliferation in the vascular intima. The ongoing sub-acute process leads to increased peripheral vascular resistance and pulmonary hypertension. Consequently patients present with progressive shortness of breath and cough. The clinical presentations are sub-acute respiratory failure, congestive heart failure, or even sudden death and are seen mainly in patients with mammary, gastric, or pulmonary cancers. Choriocarcinoma (CC) producing PTTM is unusual. Besides the arterial involvement, this patient had no other metastatic disease in the lungs or at other extra-pulmonary sites.

CC, a malignant trophoblastic tumor, may be gestational or non-gestational. Gestational tumors are usually seen in reproductive age group and arise from hydatidiform mole (either partial or complete) or following abortion, normal or ectopic pregnancies. Conversely, non-gestational CCs are predominantly seen as one of the components of mixed germ cell tumors. Rarely they can occur without other germ cell elements and are termed as pure NGCC. They may have gonadal or extragonadal origins. In this case, CC was present in the uterus and had apparently produced a perforation of its left posterior wall. The patient also had a history of menorrhagia. But the clinical information of previous abortion or pregnancy was not available and may have also been difficult to elicit since the patient was unmarried. Apart from abnormal uterine bleeding and metastases, patients with CCs can also present as thyrotoxicosis due to thyrotropic activity of β-human chorionic gonadotropin (HCG) and benign ovarian enlargements due to multiple luteinized follicular cysts (hyperreactolutenalis), both of which were seen in this case. But there was no correlation to presence of anti-nuclear antibodies. Since CCs respond exquisitely to chemotherapeutic agents, the treatment should be promptly initiated and hence this type of malignancy should be suspected in women of the reproductive age group with severe respiratory insufficiency or cardiovascular decompensation.

Further Reading

Godbole RH, Saggar R, Kamangar N. Pulmonary tumor thrombotic microangiopathy: a systematic review. Pulm Circ. 2019;9:2045894019851000.

Hayashi S, Abe Y, Tomita S, Nakanishi Y, Miwa S, Nakajima T, Nomoto K, Tsuneyama K, Fujimori T, Imura J. Primary non-gestational pure choriocarcinoma arising in the ovary: a case report and literature review. Oncol Lett. 2015;9(5):2109–11.

Irene M, Njoroge M, Inyangala D, Caroline M, Mariga D, Waweru W, Shahbal S, Mwika P, Kuria K, Osawa F, Lessan J. Pure non-gestational ovarian choriocarcinoma. J Pediatr Surg Case Rep. 2019;40:1–5.

Khakural P, Shrestha KR, Sapkota R, Shrestha UK. An unusual case of pulmonary embolism. J Surg Case Rep. 2015;2015(2):rjv006.

Price LC, Wells AU, Wort SJ. Pulmonary tumour thrombotic microangiopathy. Curr Opin Pulm Med. 2016;22:421–8.

Seckl MJ, Fisher RA, Salerno G, Rees H, Paradinas FJ, Foskett M, Newlands ES. Choriocarcinoma and partial hydatidiform moles. Lancet. 2000;356(9223):36–9.

Skride A, Sablinskis K, Klepetko W, Lang I. Choriocarcinoma mimicking chronic thromboembolic pulmonary hypertension. Eur Heart J. 2016;37:1480.

Stockton L, Green E, Kaur B, De Winton E. Non-gestational choriocarcinoma with widespread metastases presenting with type 1 respiratory failure in a 39-year-old female: case report and review of the literature. Case Rep Oncol. 2018;11(1):151–8.

Ufuk F, Kaya F, Sagatas E, Kupeli A. Non-thrombotic pulmonary embolism in emergency CT. Emerg Radiol. 2020;27:343–50.

Zhu Y, Yu M, Ma L, Xu H, Li FR. Choriocarcinoma-associated pulmonary thromboembolism and pulmonary hypertension: a case report. J Biomed Res. 2016;30:243–7.

Pulmonary Arterial Hypertension in an Infant

71

Pradeep Vaideeswar

71.1 Clinical History

A 2-month-old male child was brought with complaints of increased respiratory activity since the past 3 h. There had been episodes of loose motions and forehead sweating while feeding in the last 3 days. The general condition was poor with a heart rate of 60 beats per minute. The peripheral pulses could not be felt. He was tachypneic (respiratory rate of 68/min) and hypoxic (SpO_2 of 47%). Intubation was performed in view of impending respiratory failure, but he did not respond to oxygen therapy and expired within 3 h of admission.

71.2 Autopsy Findings

There was moderate cardiomegaly (78 g) due to marked right ventricular enlargement with apex formed by both ventricles (Fig. 71.1a). The great arteries had a normal relationship and the pulmonary trunk was larger than the ascending aorta (Fig. 71.1a) with a slight bulbous appearance in its proximal portion. Patent ductus arteriosus or coarctation of the aorta was not present. Surprisingly, despite this external morphology, there was also no intracardiac left-to-right shunt except for a probe patent foramen ovale (PFO). All valves and the left-sided chambers were normal.

Remarkable features were present in the lungs. Both the lungs were of normal size and shape with patchy visceral pleural opacification. Patchy congestion was seen on the cut surfaces along with unusual prominence of the intrapulmonary branches (Fig. 71.1b). The histopathology revealed large numbers of plexiform lesions (Fig. 71.2a–e) with associated moderate to marked medial hypertrophy and luminal narrowing due to concentric or eccentric fibromyxoid intimal thickening (Fig. 71.3). The veins and venules were normal. There was congestive hepatosplenomegaly; other organs were normal.

Cause of Death: Right heart failure due to severe pulmonary hypertension (PH).

71.3 Discussion

Severe PH was noted in this infant. Irrespective of the age, a mean pulmonary arterial pressure of greater than 25 mmHg (measured by cardiac catheterization at rest and at sea level) denotes PH and can present at any age from the pediatric age group to adults. The mean pressure in healthy individuals is usually 14 ± 3 mmHg, regardless of age, sex, and ethnicity. Since PH is an outcome of diverse etiologies, it has been classified

P. Vaideeswar (✉)
Department of Pathology (Cardiovascular and Thoracic Division), Seth Gordhandas Sunderdas Medical College and King Edward Memorial Hospital, Mumbai, India

P. Vaideeswar (ed.), *Tropical Cardiovascular Pathology*,
https://doi.org/10.1007/978-981-19-3720-0_71

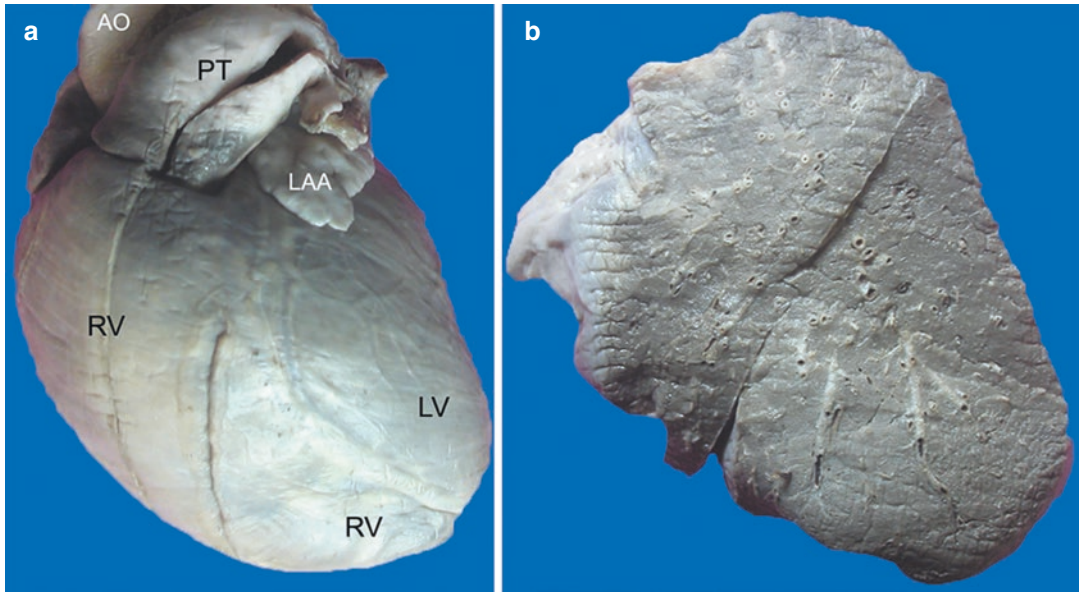

Fig. 71.1 (**a**) Moderate cardiac enlargement. There is marked enlargement of the right ventricle RV. Note that the apex is formed by both ventricles and the pulmonary trunk PT is twice the size of ascending aorta AA (LV); (**b**) Prominence of vasculature seen on the cut surface of the left lung

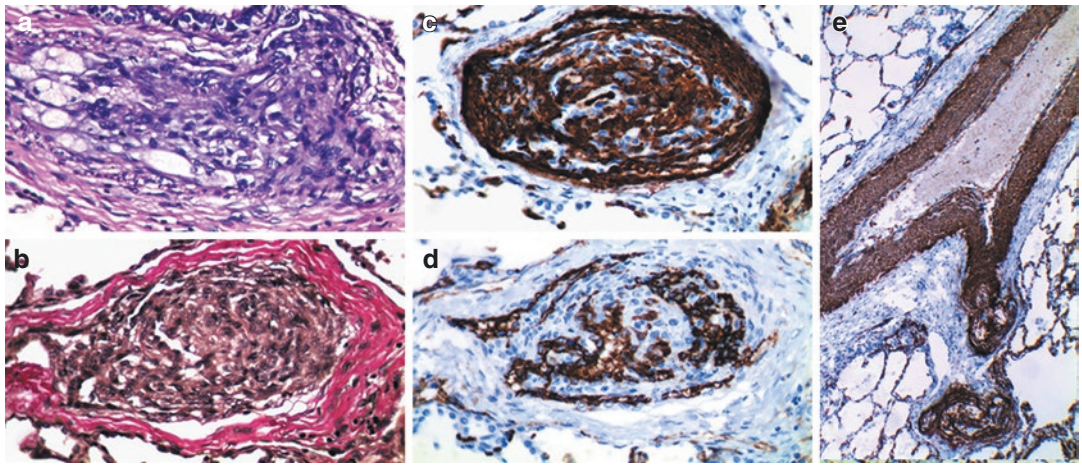

Fig. 71.2 Plexiform lesions showing a complex proliferation of cells with slit-like vascular spaces (**a**) H&E × 400 and (**b**) Elastic van Gieson × 400. There is proliferation of both smooth muscle (**c**) Smooth muscle actin (SMA immunohistochemistry × 400) and (**d**) endothelial cells (CD 31 immunohistochemistry × 400); (**e**) The cellular proliferations are seen to sprout from a large muscular artery with a thick media (SMA immunohistochemistry × 100)

by the WHO on the basis of the pathogenetic mechanisms, hemodynamic findings, and therapeutic considerations into 5 important groups: Group 1—pulmonary arterial hypertension (PAH), Group 2—PH due to left heart disease, Group 3—PH due to lung diseases and/or hypoxia, Group 4—chronic thromboembolic PH (See Chapter), and Group 5—PH due to multifactorial causes. In this infant, the PH developed as a result of extensive remodeling of the intrapulmonary arterial tree and is, therefore, an example of PAH. Apart from mean arterial pres-

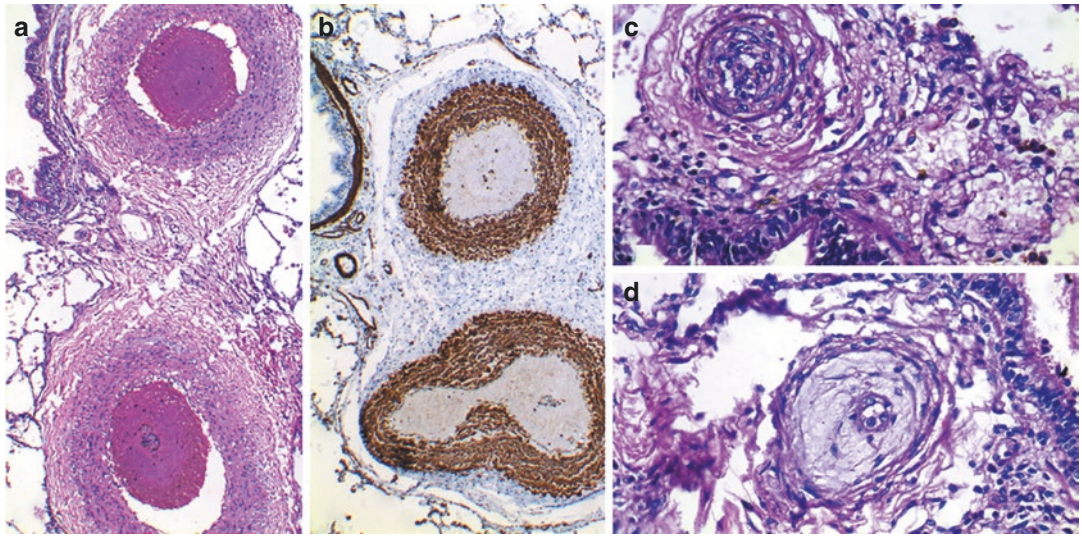

Fig. 71.3 Moderate medial hypertrophy of the muscular arteries: (**a**) H&E × 100 and (**b**) SMA immunohistochemistry × 100; Small arterial occlusion by (**c**) cellular proliferation (H&E × 400) and (**d**) myxoid tissue (H&E × 400)

sure of greater than 25 mmHg, PAH is also characterized by pulmonary artery wedge pressure of less than 15 mm Hg and indexed pulmonary vascular resistance of more than 3 Wood units (WU).

In general, pediatric PH is more frequently observed in patients with congenital heart diseases, inheritable conditions (both Group 1 causes), and developmental or maladaptive pulmonary disorders (Group 3 causes). The index case did not have any pulmonary parenchymal disease. In most children, the outcome is PAH and the overall incidence of this pediatric PAH ranges from 2 to 4 cases per million children per year. A female preponderance, that is seen in adults with PAH, is not a feature in the pediatric category. Majority of the cases of PAH in children are represented by idiopathic or hereditary subtypes and a subset caused by congenital heart diseases (CHD). Hereditary PAH often develops due to mutations in the genes coding for bone morphogenetic protein receptor 2, T-box 4-containing protein, and SRY-related HMG box transcription factor; other uncommon genetic mutations also exist. In the patients with idiopathic PAH, the genetic mutation remains to be detected. The incidence of these subsets varies from 0.47 to 1–2 cases per million children. On the other hand, PAH associated with CHD has an incidence of 2.2 cases per million children and mainly includes the unoperated and in some instances operated post-tricuspid left-to-right shunts. The PAH group also includes persistent PH of the newborn, pulmonary capillary hemangiomatosis, and pulmonary venoocclusive disease.

In this infant, there was an absence of any major congenital or acquired heart diseases. The severity of PAH could not be explained on the mere presence of a PFO. This association has been included as "those with PAH thought to be incidental to their CHD" and is indistinguishable from idiopathic/hereditary types. Since there had been no family history of PAH, appropriate material had not been kept during autopsy for identification of the casual genetic variant (See Chap. 1). Despite the varying underlying basis of PAH, the genetic, epigenetic, and environmental interactions culminate in dysregulated angiogenesis and unopposed growth of phenotypically altered, apoptosis-resistant cells with characteristic obliterative histopathological features (well brought in the index case), particularly the plexiform lesions, suggesting a 'quasi-malignancy' concept. Though they are common in PAH, such lesions

can also be seen with advanced PH in other groups, albeit rarely.

The vascular remodeling leads to symptoms such as progressive dyspnea, exercise intolerance, failure to thrive, and/or syncopal events. The diagnosis is often made when the shortness of breath is complicated by right-heart failure, clinical deterioration, and cardiac arrest. Detailed investigations like cardiac catheterization (the gold standard) could not be performed in our case and the diagnosis of severe PH was made at autopsy. The child succumbed in spite of the PFO, which would have actually been helpful in reducing the suprasystemic pulmonary arterial pressure. In untreated patients, especially in the idiopathic subset, the median survival after diagnosis is 10 months and despite the availability of new therapeutic agents and targeted drugs, the prognosis of such idiopathic and heritable PAH remains grave.

Further Reading

Cool CD, Kuebler WM, Bogaard HJ, Spiekerkoetter E, Nicolls MR, Voelkel NF. The hallmarks of severe pulmonary arterial hypertension: the cancer hypothesis—ten years later. Am J Physiol Lung Cell Mol Physiol. 2020;318:L1115–30.

Hansmann G. Pulmonary hypertension in infants, children, and young adults. J Am Coll Cardiol. 2017;69:2551–69.

Ivy D, Frank BS. Update on pediatric pulmonary arterial hypertension. Curr Opin Cardiol. 2021;36:67–79.

Pascall E, Tulloh RMR. Pulmonary hypertension in congenital heart disease. Future Cardiol. 2018;14:343–53.

Rosenzweig EB, Abman SH, Adatia I, Beghetti M, Bonnet D, Haworth S, et al. Paediatric pulmonary arterial hypertension: updates on definition, classification, diagnostics and management. Eur Respir J. 2019;53:1801916.

Simonneau G, Montani D, Celermajer DS, Denton CP, Gatzoulis MA, Krowka M, et al. Haemodynamic definitions and updated clinical classification of pulmonary hypertension. Eur Respir J. 2019;53:1801913.

Welch CL, Austin ED, Chung WK. Genes that drive the pathobiology of pediatric pulmonary arterial hypertension. Pediatr Pulmonol. 2021;56:614–20.

72 Porto-Pulmonary Hypertension in Extrahepatic Portal Vein Obstruction

Pradeep Vaideeswar, Swati Kolhe, and Manjusha Karegar

72.1 Clinical History

This male child was hospitalized at the age of 9 years for complaints of hematemesis and melena. The ultrasonography revealed massive splenomegaly, while an upper gastrointestinal endoscopy showed esophageal varices for which band ligation was performed. After few months, the patient was referred to our tertiary-care center for similar complaints. A hepatoportal Doppler study suggested portal vein thrombosis and splenomegaly with multiple collaterals. A computed tomography of the abdomen and pelvis revealed portal cavernoma and esophageal and fundic varices with moderate splenomegaly. A clinical diagnosis of extrahepatic portal vein obstruction (EHPVO) was made. When the patient was 11 years old, he was admitted for low-grade intermittent fever and cough with minimal expectoration. Sputum stained for acid-fast bacilli was negative. Symptomatic treatment was given, and the boy was discharged. There was another episode of hematemesis at the age of 12 years, for which endoscopic variceal band ligation was performed.

The current admission at the age of 14 years was for generalized weakness, yellowish discoloration of sclera and urine, disturbance of sleep, and shortness of breath for the past 15 days. His mother also complained of distractions/poor performance in studies, slow speech, and stubborn/aggressive behavior. Clinical examination revealed icterus, pallor, and splenomegaly. The hemogram revealed pancytopenia with hemoglobin of 7.5 g/dL, total leukocyte count of 4000/cmm, and platelet count of 20,000/cmm. Apart from elevated bilirubin (total 2.8 mg/dL, direct 2 mg/dL), rest of the biochemical profile had been normal. Hepatitic viral markers were negative. Within 2 days of admission, the patient deteriorated suddenly and succumbed.

72.2 Autopsy Findings

A complete autopsy was performed. The heart was moderately enlarged (weight 255 g) with marked enlargement of the right atrium and ventricle (Fig. 72.1a). The pulmonary artery was larger than the aorta (Fig. 72.1a). The pulmonary trunk and its branches were dilated with thickening of the intima. There was moderate to marked right ventricular hypertrophy (Fig. 72.1b). The cut surfaces of the lungs revealed mild prominence of the vasculature (Fig. 72.2a). Very sur-

P. Vaideeswar (✉)
Department of Pathology (Cardiovascular and Thoracic Division), Seth Gordhandas Sunderdas Medical College and King Edward Memorial Hospital, Mumbai, India

S. Kolhe · M. Karegar
Department of Pathology, Seth Gordhandas Sunderdas Medical College and King Edward Memorial Hospital, Mumbai, India

P. Vaideeswar (ed.), *Tropical Cardiovascular Pathology*,
https://doi.org/10.1007/978-981-19-3720-0_72

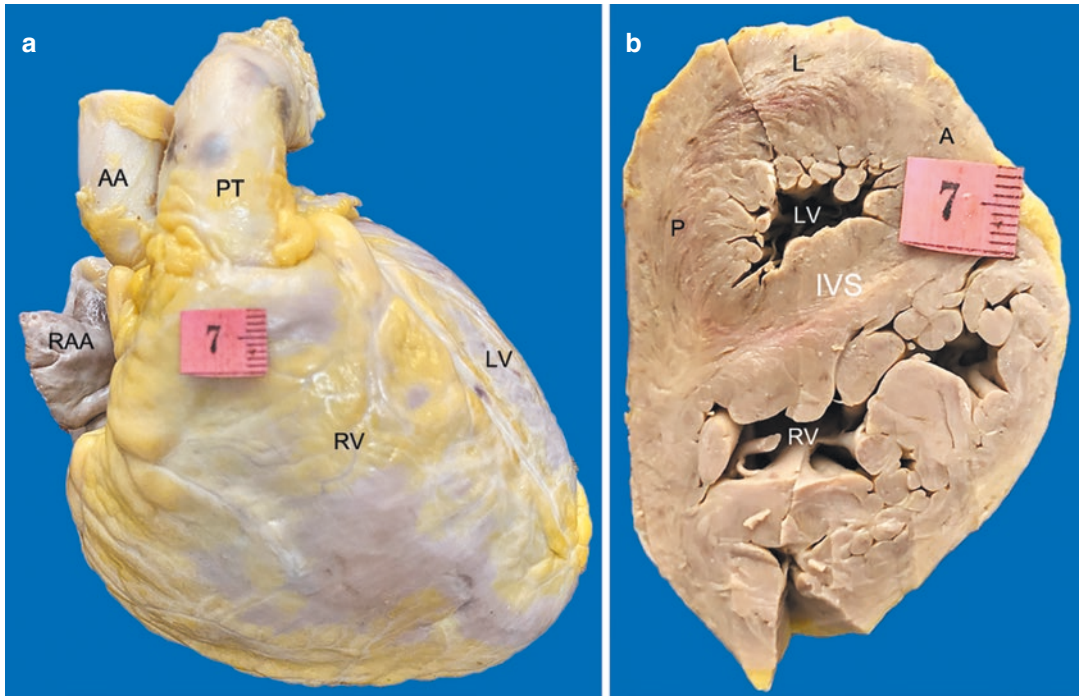

Fig. 72.1 (**a**) Moderate cardiomegaly with enlarged right-sided chambers. The apex is wholly formed by the right ventricle RV. The pulmonary trunk PT is larger than the ascending aorta AA; (**b**) Transverse slice shows moderate to marked RV hypertrophy with unduly prominent trabeculae carnae (*A* anterior wall, *IVS* interventricular septum, *L* lateral wall, *LV* left ventricle, *P* posterior wall, *RAA* right atrial appendage)

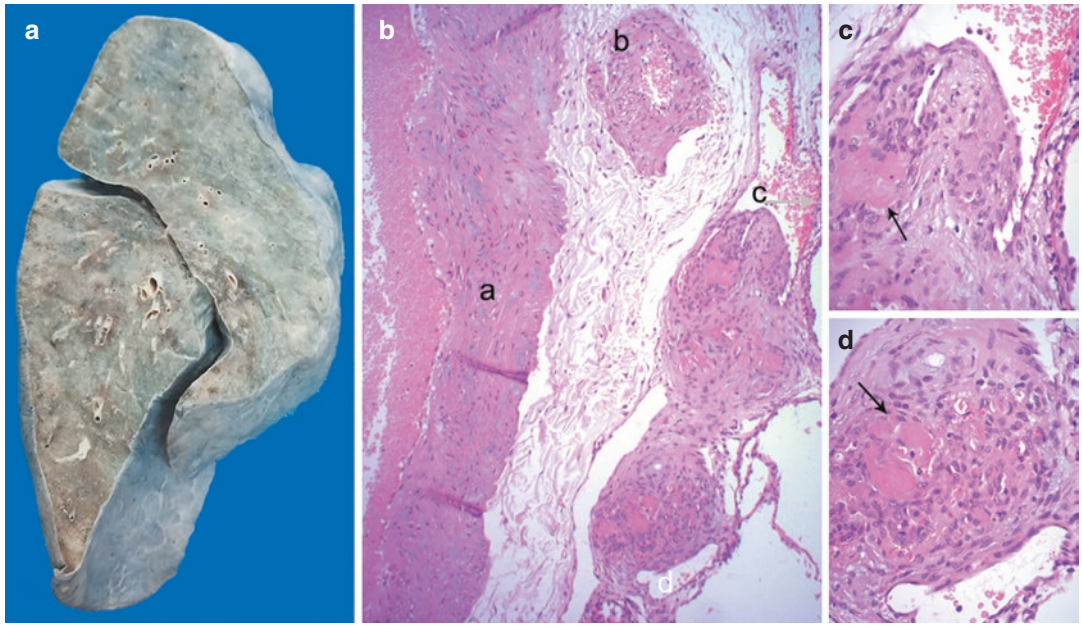

Fig. 72.2 (**A**) The cut surface of the left lung showed mild prominence of the vasculature; (**B**) (a) Large muscular artery with increased basophilic ground substance splaying apart the smooth muscle fibers, (b) Small-sized muscular artery with mild medial hypertrophy, (c and d) are the plexiform lesions with a characteristic glomeruloid configuration (H&E × 100) and their higher powers are depicted in (**C**) and (**D**) H&E × 400. Note the presence of occlusive fresh fibrin thrombi (arrows) in some of the channels

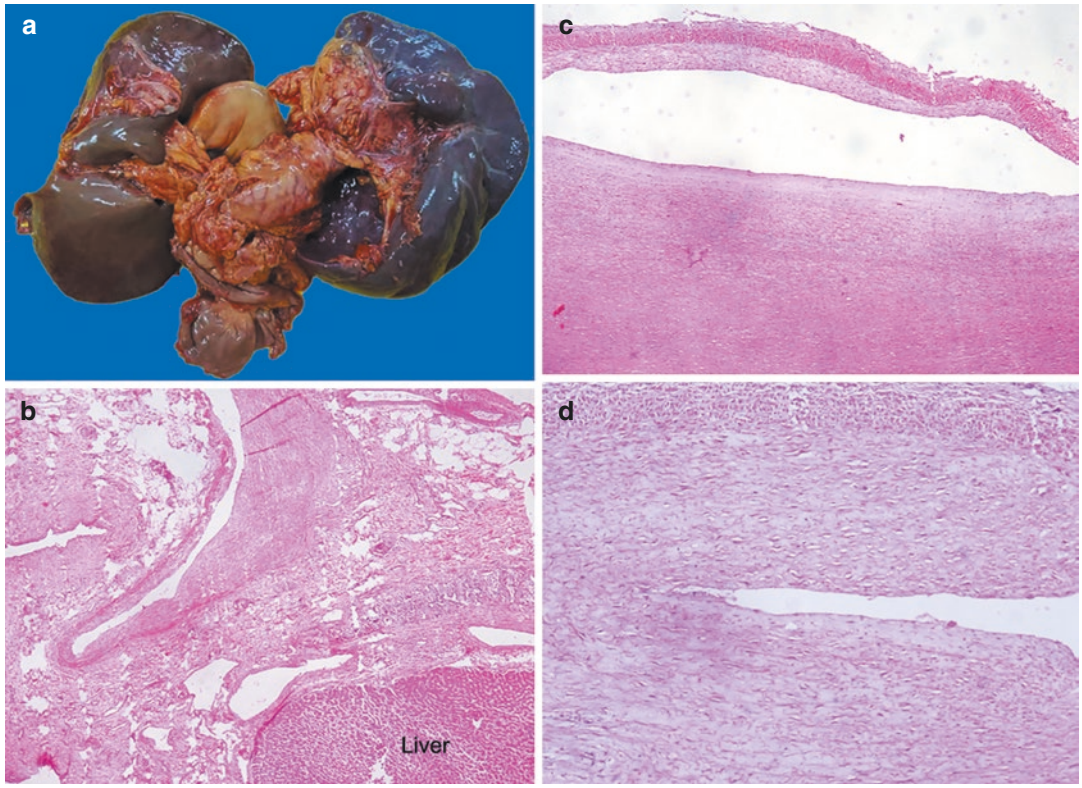

Fig. 72.3 (**a**) Hepatobiliary block showing normal-sized liver and very marked splenomegaly; (**b**) Multiple collateral venous channels at the porta-hepatis (H&E × 100); (**c**) Eccentric (H&E × 100) and (**d**) Concentric (H&E × 200) intimal thickening of the portal vein

prisingly, the histology revealed very severe remodeling of the pulmonary arteries with presence of mild to moderate medial hypertrophy with focal increases in basophilic proteoglycans (Fig. 72.2b), eccentric to concentric intimal fibrocellular proliferation, and many plexiform lesions (Fig. 72.2b–d, See Chap. 71); the small lumina within these lesions were occluded by fresh fibrin thrombi.

The liver was normal in size and had a slight yellowish discoloration (Fig. 72.3a). Changes of chronic venous congestion were accompanied by phlebosclerosis of few portal venular radicles. A hepatobiliary dissection was done. There were multiple collateral channels at the porta hepatis (Fig. 72.3b); similar channels were also seen around the thickened and partially obliterated cord-like portal vein (Fig. 72.3c, d). No thrombi were seen. The spleen (970 g, Fig. 72.3a) was markedly enlarged and congested; fibrocongestive changes with extramedullary hematopoiesis were seen on histology. Few collapsed tortuous veins were seen in submucosa of esophagus, consistent with varices. Congestive vasculopathy was present in the stomach and intestines. Other organs were unremarkable.

Cause of Death: Sudden death due to porto-pulmonary hypertension (PoPH).

72.3 Discussion

The lung histopathology in this adolescent male, a known case of EHPVO, had severe vascular changes replete with multiple plexiform lesions. This indicated the presence of PoPH, which had been missed on antemortem examination. PoPH is defined by the presence of pulmonary arterial hypertension (PAH—resting mean pulmonary artery pressure greater than 25 mmHg, raised pulmonary vascular resistance greater than 3 Wood units, and pulmonary artery wedge pres-

sure of less than 15 mmHg) associated with portal hypertension, either in the presence or absence of liver disease. It is categorized under subset of the WHO Group 1 pulmonary hypertension, within which it affects 6–18% of patients with PAH. Around 2–10% of patients with portal hypertension develop this grave complication; this incidence may be underestimated as the disease may not be clinically recognized. Vast majority of these patients have liver cirrhosis; however, there appears to be no link between the presence and severity of PoPh with the magnitude of liver injury. Interestingly, noncirrhotic causes of portal hypertension, even devoid of liver dysfunction, can also be associated with PoPH and an example here is EHPVO, which is the commonest cause for portal hypertension in children. The etiology still remains uncertain and it is believed that a subtle injury to the portal vein in early infancy or childhood provokes thrombosis and the thrombotic organization is accompanied with formation of multiple collateral channels. These are not sufficient to withstand the high flow volume of the splanchnic circulation leading to portal hypertension and porto-systemic anastomosis. In most of the patients (70%), there is sole involvement of the portal vein, while others show portal vein affection with the splenic and/or superior mesenteric veins. Most often, the children (most of them between 6 and 9 years of age) present with esophageal variceal bleeding, massive splenomegaly, and hypersplenism, which was present in this patient. There was no significant hepatic disease.

The exact pathogenesis of PoPH is not known, but it has been suggested that the porto-systemic shunts produce a dysregulation of vasoactive, proliferative, angiogenic, and pro-inflammatory substances that initially induces pulmonary arterial vasoconstriction. There is then ensuing endothelial and smooth muscle interactions. It manifests histologically as intimal proliferation, medial hypertrophy, muscularization of the arterioles, and plexiform arteriopathy, which is indistinguishable from changes produced by other causes of PAH. Diagnosis of PoPH requires a high degree of clinical suspicion. The progress of vascular stenosis and/or occlusion is insidious and majority of the patients remain asymptomatic. The clinical manifestations are mainly related to portal hypertension and/or liver disease. The most common symptom of PoPH is dyspnea, which can also result from concomitant anemia and serous cavity effusions; other symptoms include syncope, chest pain, palpitation, or features related to congestive cardiac failure. Therapy directed to PAH should be initiated early since PoPH is associated with significant morbidity and mortality. Those with liver disease may be benefited with transplantation. Our patient had manifestations related to portal hypertension for close to 5 years. Dyspnea was a recent accompaniment and he succumbed to sudden cardiac decompensation.

Further Reading

DuBrock HM, Krowka MJ. The myths and realities of portopulmonary hypertension. Hepatology. 2020;72:1455–60.

Navarro-Vergara DI, Roldan-Valadez E, Cueto-Robledo G, Jurado-Hernandez MY. Portopulmonary hypertension: prevalence, clinical and hemodynamic features. Curr Probl Cardiol. 2021;46:100747.

Sarma MS, Settharaman J. Pediatric non-cirrhotic portal hypertension: endoscopic outcome and perspectives from developing nations. World J Hepatol. 2021;12:1269–88.

Simonneau G, Montani D, Celermajer DS, Denton CP, Gatzoulis MA, Krowka K, et al. Haemodynamic definitions and updated clinical classification of pulmonary hypertension. Eur Respir J. 2019;53:1801913.

Thomas C, Glinskii V, de Jesus PV, Sahay S. Portopulmonary hypertension: from bench to bedside. Front Med. 2020;7:569413.

73 Takayasu's Disease with Predominant Pulmonary Arterial Involvement

Pradeep Vaideeswar

73.1 Clinical History

A 20-year-old male had been symptomatic for the past 2 years with grade 1 dyspnea. He had been diagnosed as a case of rheumatic heart disease (RHD) and had had been on regular penicillin prophylaxis. During the past 10 days, the dyspnea had progressed to grade 4 and was accompanied by right-sided chest pain, generalized anasarca, and ascites. On examination, the pulse rate was 96 per minute, irregular with raised jugular venous pressure. There was a diffuse, hyperdynamic apical impulse with systolic/diastolic thrill and pan-systolic/early diastolic murmur at pulmonary area. Right bundle branch block with right ventricular strain, and aneurysmal right atrium, right ventricular hypertrophy, severe tricuspid regurgitation with small left ventricle were noted on ECG and echocardiography, respectively. Computed tomographic angiography revealed thrombotic occlusion of distal right pulmonary artery. The patient was transferred to intensive care unit for continuous hemodynamic monitoring and was treated with inotropics, antifailure drugs, and anticoagulants. The patient's relatives had refused consent for thrombolytic therapy. Due to unstable hemodynamics, surgical pulmonary thrombectomy could not be considered as a viable option. The condition did not improve and was complicated by development of basal consolidation with expiry on 5th day of admission.

73.2 Autopsy Findings

At autopsy, there was moderate cardiomegaly (weight 400 g) with ballooned right atrium and marked enlargement of right ventricle (Fig. 73.1a). Both chambers had marked pearly white endocardial thickening (Fig. 73.1a) with moderate myocardial hypertrophy. The pulmonary trunk (Fig. 73.1b) and its branches were markedly dilated with extremely thick, rugose, wrinkled, grey-white intima and thick, leathery walls. The extrapulmonary branches were devoid of thrombi, but right pulmonary artery and inferior division of left pulmonary artery at their respective hila were occluded by fresh and organizing thrombi. There were no features of chronic rheumatic heart disease. Fresh thrombi were also present within some intrapulmonary branches. Dilatation of the airways, firmness at the bronchovascular bundles, and bronchopneumonia were also noted.

The pulmonary trunk and both branches showed thickening of their walls due to moderate to marked fibro-cellular intimal thickening and adventitial fibrosis (Fig. 73.1c, d). The media was attenuated with paucity/fragmentation of elastic

P. Vaideeswar (✉)
Department of Pathology (Cardiovascular and Thoracic Division), Seth Gordhandas Sunderdas Medical College and King Edward Memorial Hospital, Mumbai, India

P. Vaideeswar (ed.), *Tropical Cardiovascular Pathology*,
https://doi.org/10.1007/978-981-19-3720-0_73

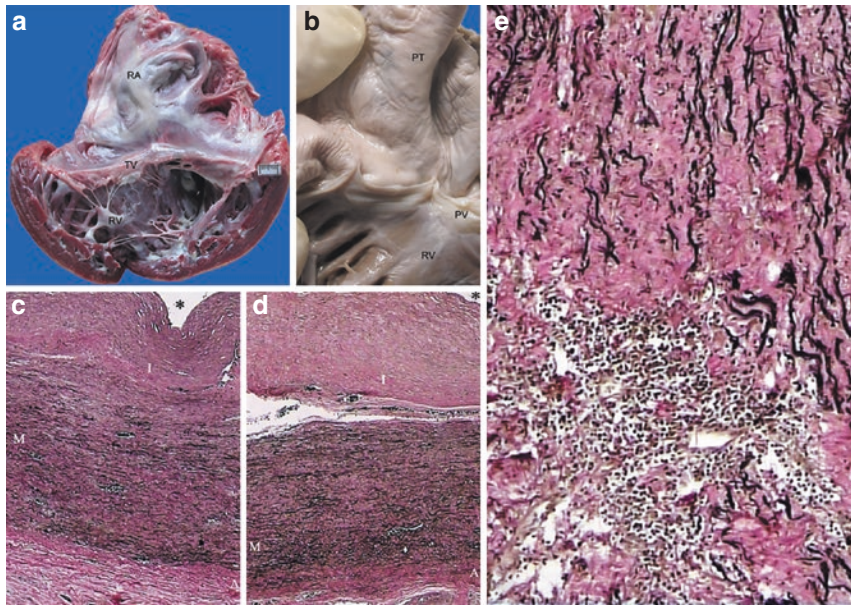

Fig. 73.1 (**a**) Opened out right ventricular RV inflow tract in the fresh state showing marked dilatation of right atrium RA and RV with dilated tricuspid annulus. Note marked patchy endocardial thickening; (**b**) Thick, wrinkled whitish intima of the pulmonary trunk PT imparting a vague tree-bark appearance (*PV* pulmonary valve, *TV* valve); (**c**) and (**d**) The wall of the main pulmonary artery showed thickened intima I with adventitial A fibrosis. The media M also shows fibrosis with paucity of elastic fibers (Elastic van Gieson × 250); (**e**) Scarred media with foci of lymphocytes (Elastic van Gieson × 400)

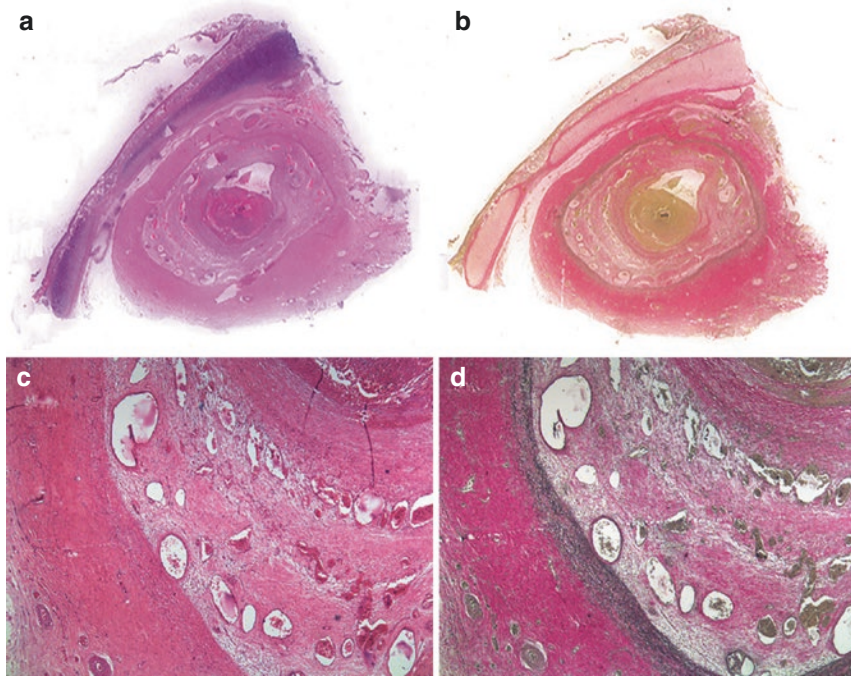

Fig. 73.2 Scanned image of the inferior division of the left pulmonary artery showing luminal occlusion by fresh and organizing thrombus, (**a**) H&E and (**b**) Elastic van Gieson; The organization shows intense collagenization towards the luminal aspect, imparting a 'vessel-in-vessel' appearance, (**c**) H&E × 100 and (**d**) Elastic van Gieson × 100

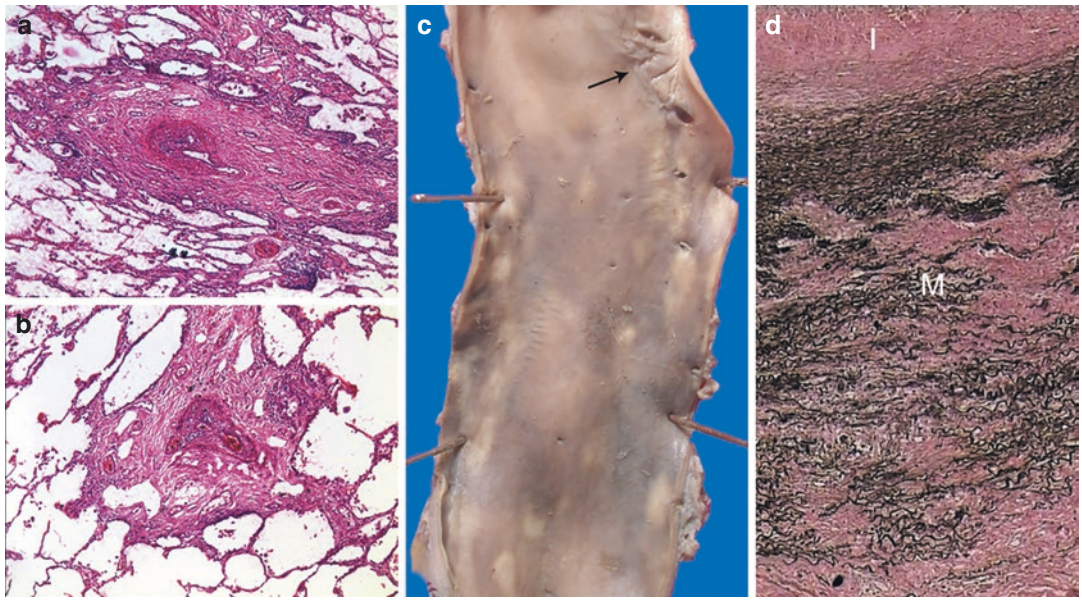

Fig. 73.3 (**a**) and (**b**) Thickening of the walls of the small muscular arteries with extensive peri-arterial fibrosis with vascularization; (**c**) Small area over the greater curvature of the proximal thoracic aorta showing intimal plaque and rugosity (arrow); (**d**) Extensive scarring of the media M with intimal fibrosis was seen in the region of the aortic pathology (Elastic van Gieson × 100)

fibers and fairly extensive collagenization (Fig. 73.1c, d). Small clusters of lymphohistiocytes were also present (Fig. 73.1e). The branch lumina had occlusive fresh thrombi superimposed over organizing thrombus, giving it a classic 'vessel-in-vessel' pattern (Fig. 73.2a–d). Similar lesions were also present in the intrapulmonary branches. A striking feature was the presence of prominent peri-arterial fibrosis (Fig. 73.3a, b), leading to ectatic bronchi/bronchioles, acute inflammation, bronchopneumonia, and simple aspergilloma. Interestingly, a small segment of cobble-stoned intima with wall thickening was present in proximal thoracic aorta (Fig. 73.3c), revealing histology of a healed aortitis (Fig. 73.3d).

Cause of Death: Right heart failure due to predominant pulmonary arterial Takayasu's arteritis (TA) with chronic thrombosis.

73.3 Discussion

A vasculitic process involving the pulmonary trunk and its extra-and intrapulmonary branches had produced the clinical features of pulmonary thromboembolism (PTE) in a young adult male. The histopathology revealed destruction of the wall with fibrosis and minimal inflammation, which was suggestive of a healed phase of Takayasu arteritis (TA). TA (See Chaps. 63–65) is an example of a large-vessel vasculitis of an unknown etiology, which targets the aorta and its major branches (including the coronary arteries) and commonly occurs in young women of usually Asian descent. The various stages (viz. active, chronic, and healed) of granulomatous or non-granulomatous pan-arteritis lead to triphasic clinical phases (i.e., pre-pulseless, vasculitic, and burnt-out). The ongoing and dissipating inflammation produces arterial stenosis, occlusion, and/or aneurysms with end-organ ischemia. The clinical presentations depend on the location and extent of the stenotic aorto-arteriopathy and hence the clinical criteria for diagnosis of TA and the angiographic classification for distribution of lesions are based primarily on the aorto-arterial disease. In this instance, the clinical scenario was entirely orchestrated by a dominant pulmonary arterial involvement.

The pulmonary artery (PA) is the second large artery to be involved by TA and there is an extremely wide range of incidence (8–80%) depending on the ethnicity of the population studied and the diagnostic modalities. It must be realized that PA involvement is often clinically overlooked since it is usually coexists with the more morbid aorto-arterial disease, particularly in Type II TA (ascending aorta, arch and its branches, and descending thoracic aorta, See Chap. 63), which warrants careful analysis of the pulmonary vasculature by noninvasive techniques like echocardiography. However, exclusive or predominant PA inflammation (which is not classified as an independent type) is rarely reported and is said to affect about one-third of the patients with TA with increased frequency in males and without racial or geographic predilection. Again, the incidence may be an overestimate as many of these patients do not have adequate follow-up to document a possibly subsequent aortic involvement. In our case, the dominant pulmonary arterial disease showed only subtle aortic involvement, which may not have been picked up by the routinely used imaging techniques.

In the reported case, there was involvement of the PA, its left and right branches, and many of the intrapulmonary arteries in both the lungs. Literature reveals a varied distribution, most often affecting the right PA along with segmental and subsegmental branches of the upper lobes. In the present case, the trunk and the proximal portions of the branches were dilated with intimal thickening and had features of healed arteritis. However, the distal portions and their intrapulmonary branches revealed stenotic and occlusive lesions with the characteristic vessel-in-vessel appearance, which was well seen. Dilatations or plexiform lesions were not seen within the lungs. Patients with predominant pulmonary vascular disease present a challenge to clinical diagnosis. Owing to the absence of the aortic disease, the insidious pulmonary arterial inflammation does not present any symptoms. The patients develop symptoms like progressive dyspnea, chest pain, or hemoptysis in the late stages of disease when there is stenosis or occlusion, which are indistinguishable from chronic thromboembolic phenomenon (See Chap. 68) with pulmonary hypertension (PH). TA-related PH is included in the subset WHO Category 4. Our patient was symptomatic for the past 2 years, but had been misdiagnosed as a case of RHD (See Chap. 5) and had a diagnosis of thromboembolism in the current admission. Some cases can also develop pulmonary infarctions or pulmonary hemorrhage, which develops due to systemic-pulmonary shunts. The shunts are better demonstrated by angiography and not well-appreciated on gross or histopathological examination. Infarction or hemorrhage was not seen at autopsy. We also noted that the peri-arterial fibrosis had also lead to ectasia of the airways and there were foci of bronchopneumonia and even fungal colonization. These superadded infections (including tuberculosis) can occur in the patients with TA of PA and the diseased parenchyma may have to be resected in some cases. Steroids are the first line of therapy in all cases of TA, which was delayed in our case leading to severe dyspnea due to PH and right heart failure. The delay in diagnosis can range from 3 to 72 months. The stenosing lesions may also require interventional or surgical pulmonary revascularization. In conclusion, pulmonary vasculitis should be borne in mind whenever young patients present with features suggestive of pulmonary arterial thrombosis or PH.

Further Reading

Adams TN, Zhanga D, Batrab K, Fitzgerald JE. Pulmonary manifestations of large, medium, and variable vessel vasculitis. Respir Med. 2018;145:182–91.

He Y, Lv N, Dang A, Cheng N. Pulmonary artery involvement in patients with Takayasu arteritis. J Rheumatol. 2020;47:264–72.

Lally L, Spiera RF. Pulmonary vasculitis. Rheum Dis Clin North Am. 2015;41:315–31.

Li Y, Lv X, Yang Y, Jiang W, Li J, Ma Z. Echocardiographic characteristics of pulmonary artery involvement in Takayasu arteritis. Echocardiography. 2017;34:340–7.

Nassera M, Cottin V. The respiratory system in autoimmune vascular diseases. Respiration. 2018;96:12–28.

Toledano K, Guralnik L, Lorber A, Ofer A, Yigla M, Rozin A, et al. Pulmonary arteries involvement in Takayasu's arteritis: two cases and literature review. Semin Arthritis Rheum. 2011;41:461–70.

Necrotizing Pulmonary Arteritis with Rheumatic Mitral Stenosis

74

Smita Divate and Pradeep Vaideeswar

74.1 Clinical History

A 26-year-old female developed intermittent high-grade fever with chills, cough with minimal mucoid expectoration, pain in and rash over, both lower limbs, and rapidly progressive dyspnea for the past 4 days. She was a known case of severe rheumatic mitral stenosis (MS, mitral valvular area of 0.9 cm^2). She had refused to undergo balloon valvotomy procedure and was not on any penidure prophylaxis. On examination, the general condition was poor with a pulse rate of 130 per minute and blood pressure of 100/60 mmHg. There was mild icterus. The lower limb lesions appeared like palpable petechiae/purpurae suggesting a vasculitic process. Chest auscultation revealed bilateral crepitations, loud first heart sound, and mid-diastolic murmur. There was mild hepatosplenomegaly. Chest radiography showed multifocal opacities in both lung fields with minimal bilateral pleural effusions. The clinical impression was infective endocarditis with bilateral pneumonia. The investigations were as follows: Hemoglobin 10.2 g/dL, total leukocyte count 15,600/cmm (80% neutrophils), blood urea nitrogen 68 mg/dL, creatinine 2.0 mg/dL, total bilirubin 4.4 mg/dL, direct bilirubin 3 mg/dL, SGOT 715 U/L, SGPT 1410 U/L, alkaline phosphatase 129 U/L, and C-reactive protein 197 mg/L. She expired within 7 h of admission. The blood culture report received after she expired showed no growth of organisms.

74.2 Autopsy Findings

The heart was moderately enlarged in size (410 g) with mild enlargement of the right atrium, moderate enlargement of the left atrium, and marked enlargement of the right ventricle. The pulmonary artery was larger than the aorta with dilatation of the artery and its branches, and associated intimal thickening. There was mild and moderate hypertrophy of the right atrium and ventricle, respectively. The tricuspid valve did not show any rheumatic involvement. The mitral orifice was markedly stenotic and measured 0.9 cm across. There was extreme fusion of both commissures with focal calcification. The valve leaflets were mildly thickened. There was only mild subvalvular pathology. The left atrial myocardium showed marked hypertrophy. The left ventricle was mild enlarged with mild hypertrophy. Commissural fusion and cuspal thickening had produced mild aortic stenosis. The histology did

S. Divate
Department of Pathology, Seth Gordhandas Sunderdas Medical College and King Edward Memorial Hospital, Mumbai, India

P. Vaideeswar (✉)
Department of Pathology (Cardiovascular and Thoracic Division), Seth Gordhandas Sunderdas Medical College and King Edward Memorial Hospital, Mumbai, India

P. Vaideeswar (ed.), *Tropical Cardiovascular Pathology*,
https://doi.org/10.1007/978-981-19-3720-0_74

not reveal any myocarditis. There were no infective vegetations.

Remarkable findings were seen in the lungs. They showed multiple subpleural, wedge-shaped hemorrhagic infarcts (Fig. 74.1a, b) with associated fibrinous exudates. The intraparenchymal pulmonary arteries particularly towards the hilar aspects appeared prominent and some of them were occluded by fresh friable red-brown thrombi (Fig. 74.1c). These were as a result of necrotizing arteritis. There was segmental to circumferential fibrinoid necroses (Fig. 74.2a, b) of varying thickness of the wall with prominent neutrophilic infiltration (Fig. 74.2c, d). The inflammation appeared to extend into the surrounding parenchyma (Fig. 74.3a). However, the intervening parenchyma did not show a pneumonic consolidation; neither were hyaline membranes or organisms seen. The muscular arteries also showed medial hypertrophy with eccentric to concentric intimal fibro-cellular thickening. Changes of venous hypertension and chronic passive venous congestion (CPVC) were present. Sample of skin revealed leukoclastic vasculitis (Fig. 74.3b). Similar vascular changes were not seen in the other organs including the kidneys. The liver showed only changes of CPVC with focal necrosis.

Cause of Death: Multiple pulmonary infarcts due to necrotizing pulmonary arteritis with thrombosis.

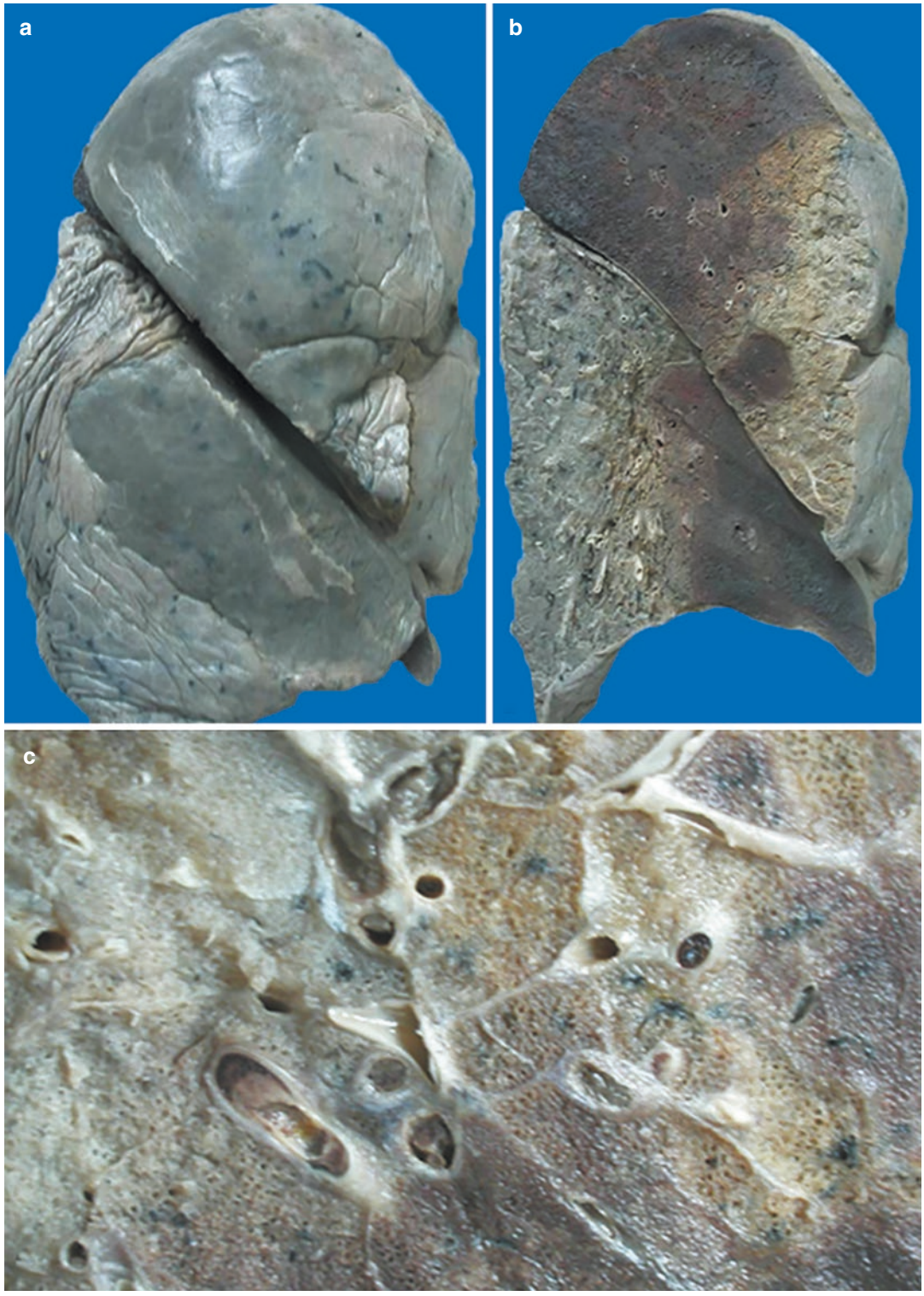

Fig. 74.1 (**a**) External surface of the right lung showing a bulge with congested pleura in the upper and basal lower lobes; (**b**) The cut surface reveals small to large subpleural hemorrhagic parenchyma in all lobes; (**c**) Occlusive fresh thrombi are seen in the pulmonary arteries

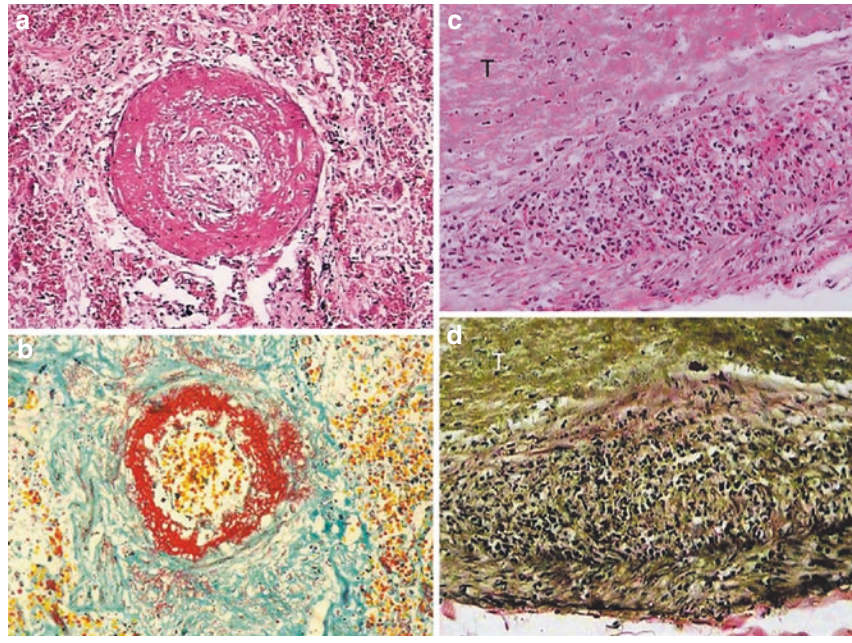

Fig. 74.2 Circumferential fibrinoid necrosis of a muscular pulmonary artery—(**a**) H&E × 250 and (**b**) Putt's fibrin stain × 250; Prominent neutrophilic infiltration is present at the intimomedial junction with overlying fresh fibrin thrombus T—(**c**) H&E × 400 and (**d**) Elastic van Gieson × 400

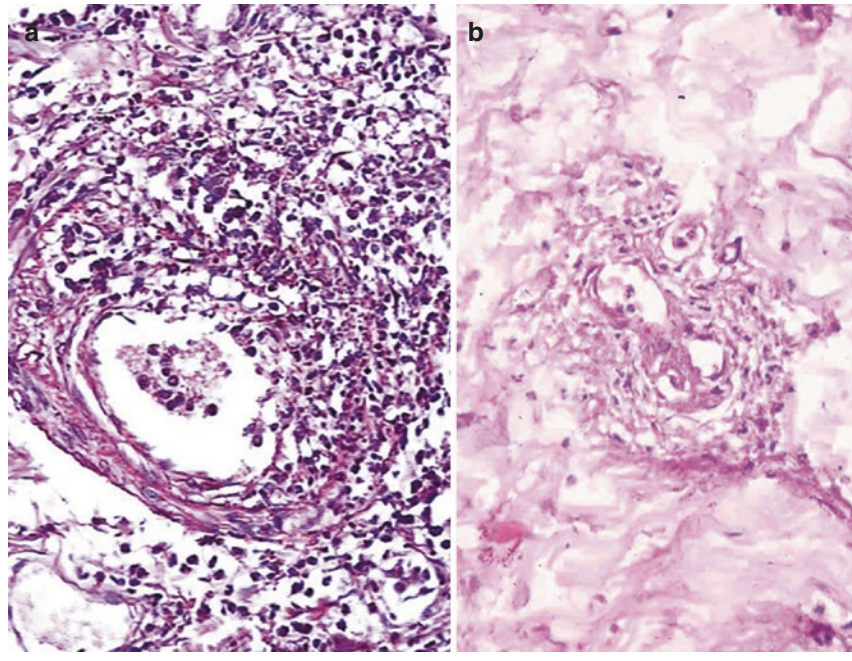

Fig. 74.3 (**a**) Necrotizing arteritis with spill-over of neutrophils into the adjacent alveolar spaces (H&E × 400); (**b**) Small-vessel vasculitis in the subcutaneous fat (H&E × 400)

74.3 Discussion

In the present case, an autopsy revealed the presence of necrotizing arteritis (NA) of the muscular pulmonary arteries in a patient with severe mitral stenosis. Necroses and inflammation of the vascular walls are features that characterize a heterogeneous group of disorders collectively called vasculitides. They often manifest with multisystem involvement with constitutional complaints and symptoms due to end-organ damage. These rare conditions may occur secondary to a variety of underlying conditions such as autoimmune diseases, infections, drugs, and malignancy or be primary vasculitides of unknown etiology. The 2012 Revised International Chapel Hill Consensus Conference Nomenclature (CHCC) of Vasculitides, most commonly used to categorize vasculitis, is primarily based on the size of blood vessel involved (large-vessel, medium-sized vessel, and small-vessel) and the underlying etiology. Primary pulmonary vasculitis is uncommon with an incidence of 20–100 cases per million persons per year and involves the extrapulmonary and intrapulmonary arteries, the parenchymal small vessels (including the capillaries), and bronchial arteries. In the lungs, small-vessel vasculitides are more common. They are often associated with antineutrophil cytoplasmic antibody (ANCA) positivity, targeting the alveolar septal capillaries. Involvement of the pulmonary vasculature by large-vessel (See Chap. 73) and medium-sized vessel vasculitis (as seen in this case) is distinctly rare.

Necrotizing arterial lesions can also be seen in advanced pulmonary arterial (precapillary) hypertension. However, it is invariably associated with other features such as obliterative intimal fibrosis or plexiform lesions. This patient had MS, which usually shows the postcapillary type of changes involving the veins and venules, along with a milder degree of medial hypertrophy of the arteries in the later stages of the stenosis. Hence, MS is unlikely to be a cause for the NA. When present as a sole feature, NA of muscular arteries is most characteristic of polyarteritis nodosa (PAN), often associated with hepatitis B infection. The CHCC defines PAN as a necrotizing inflammation involving medium-sized or small arteries, and not associated with vasculitis in smaller vessels (arterioles, capillaries, or venules) or glomerulonephritis, clearly distinguishing it from microscopic polyangiitis (an ANCA positive vasculitis). Fibrinoid necrosis with a polymorphic inflammatory infiltrate is typically seen within walls of muscular arteries, often in a segmental fashion. Destruction of the elastic lamina due to the NA leads to microaneurysms that form the hallmark lesions of PAN, identifiable by arteriography. PAN can involve single or multiple sites most commonly in the gastrointestinal system, skin, peripheral nerves, and kidneys. A leukocytoclastic vasculitis is seen in the superficial layers of the skin, while the deeper muscular arteries of the subcutaneous adipose tissue show characteristic necrotizing arteritis. Lung involvement has been reported to be rare, but tends to affect the bronchial arteries. Bronchiolitis obliterans, organizing pneumonia, and diffuse alveolar damage have also been reported in the lungs in patients with PAN. In the index case, renal and gastrointestinal involvement was absent. Such PAN lesions were also not noted in other organs. However, the skin had shown the presence of leukocytoclastic vasculitis, a feature that excludes the diagnosis of single organ pulmonary vasculitis in this case. Furthermore, an evidence of autoimmune disorders, positive blood culture, angioinvasive fungi, usage of any drugs including penicillin, and malignancy was not present. Hence, the most probable cause of the pulmonary NA in this case appears to be PAN. Underscoring the rarity of this association, the present case of PAN with severe MS has not been hitherto reported in literature to the best of our knowledge.

Further Reading

Adams TN, Zhanga D, Batrab K, Fitzgerald JE. Pulmonary manifestations of large, medium, and variable vessel vasculitis. Respir Med. 2018;145:182–91.

Casal A, Díaz-Garel J, Pereiro T, Toubes ME, Ricoy J, Valdes L. Pulmonary vasculitis. J Thorac Dis. 2018;10:5560–75.

Jennette JC, Falk RJ, Bacon PA, Basu N, Cid MC, Ferrario F, et al. 2012 revised international Chapel Hill consensus conference nomenclature of vasculitides. Arthritis Rheum. 2013;65:1–11.

Lally L, Spiera RF. Pulmonary vasculitis. Rheum Dis Clin North Am. 2015;41:315–31.

Matsumoto T, Homma S, Okada M, Kuwabara N, Kira S, Hoshi T, Uekusa T, Saiki S. The lung in polyarteritis nodosa: a pathologic study of 10 cases. Hum Pathol. 1993;24:717–24.

Zarka F, Veillette C, Makhzoum JP. A review of primary vasculitis mimickers based on the Chapel Hill consensus classification. Int J Rheumatol. 2020;2020:8392542.

Pulmonary Arterial Hypertension and Connective Tissue Disorders

75

Pradeep Vaideeswar and Smita Divate

75.1 Clinical History

A 40-year-old female was brought to the emergency services of our hospital with nonrecordable pulse and blood pressure, feeble heart sounds, and no response to deep pain. Accompanying relatives provided a history of rapidly progressive shortness of breath with chest pain on and off and multiple joint pains for the past 15 days. She had been diagnosed as a case of systemic lupus erythematosus (SLE) 3 years ago, but had not followed up in the last 2 years. She died within 2 h of admission.

The patient's personal medical file contained some records of previous assessment and investigations. A history of hair loss, photosensitivity, Raynaud's phenomenon, and dysphagia had been recorded. It was also mentioned that the patient had no skin changes of SLE or scleroderma. The hematological and biochemical investigations were as follows: Hemoglobin 12.5 g/dL, total leukocyte count 6000/cmm (differential count—neutrophils 68%, lymphocytes 30%, and eosinophils 2%), platelet count 2 lakhs/cmm, serum cholesterol 149 mg/dL, triglycerides 84 mg/dL, high density lipoproteins 24 mg/dL, and low density lipoproteins 103 mg/dL. Serological parameters revealed positive antinuclear antibodies and anti-double-stranded DNA antibodies at 1:160 and 1:80 titers, respectively, with serum complement C_3 129 mg/dL and C_4 41 mg/dL. An additional investigation retrieved was the ANA immunofluorescence test that had been recorded as showing a centromeric pattern. ECG was normal, while a high-resolution computed tomography had shown cardiomegaly, severe pulmonary hypertension (pulmonary artery diameter of 30 mm), and stigmata of old tuberculosis (scarring of bilateral upper lobes and calcified hilar lymph nodes). At that time, her records showed that she had been advised digoxin, sildenafil, atorvastatin, fruselac, low-molecular weight heparin, and aspirin.

75.2 Autopsy Findings

At autopsy, remarkable features were seen in the lungs. Both the lungs were of normal size and shape with patchy visceral pleural thickening and opacification. The cut surfaces showed very marked prominence of the pulmonary arteries with extensive thickening of the walls and near total luminal obliteration (Fig. 75.1). Some of the plaques had a distinct pale-yellow color (Fig. 75.1b). On histology, there was extreme

P. Vaideeswar (✉)
Department of Pathology (Cardiovascular and Thoracic Division), Seth Gordhandas Sunderdas Medical College and King Edward Memorial Hospital, Mumbai, India

S. Divate
Department of Pathology, Seth Gordhandas Sunderdas Medical College and King Edward Memorial Hospital, Mumbai, India

P. Vaideeswar (ed.), *Tropical Cardiovascular Pathology*,
https://doi.org/10.1007/978-981-19-3720-0_75

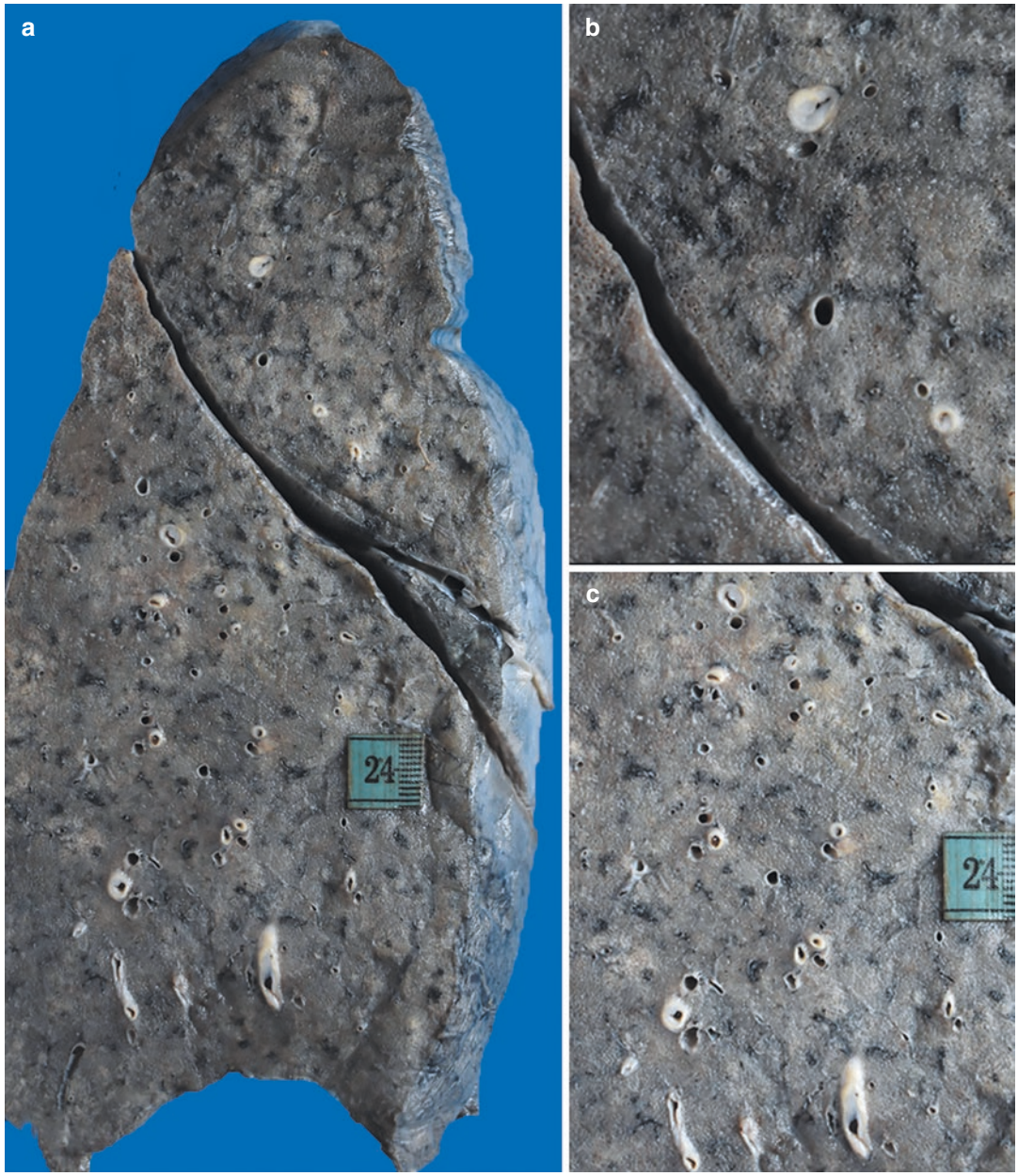

Fig. 75.1 (**a**) The cut surface of the left lung and the close-up of (**b**) left upper and (**c**) lower lobes show extreme narrowing of the pulmonary arteries of all sizes. The larger arteries show a pale hue

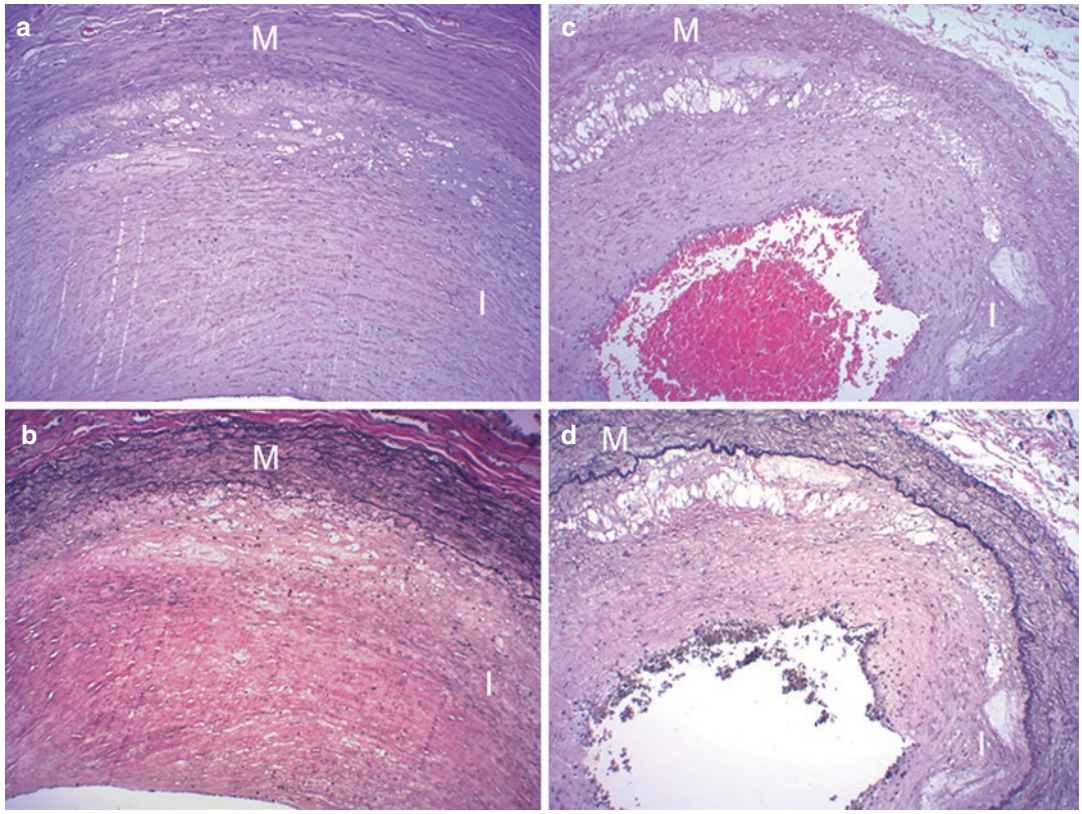

Fig. 75.2 Elastic pulmonary artery ((**a**) H&E × 100, (**b**) Elastic van Gieson × 100) and muscular pulmonary (**c**) H&E × 100, (**d**) Elastic van Gieson × 100) showing remarkable narrowing of their lumina by eccentric intimal proliferation with foamy macrophages at the basal aspects. The internal elastic lamina is intact (*I* intima, *M* media)

narrowing of the elastic and muscular arteries (Fig. 75.2) by exuberant intimal proliferation. The internal elastic lamina was largely intact. The intimal thickening was largely fibro-myxoid (Fig. 75.3a) and towards the basal aspects, there were small to large collections of foamy macrophages (Fig. 75.3b). These changes were seen in the muscular arteries of all sizes, including the arterioles; some of the arteries also showed mild medial hypertrophy (Fig. 75.3c, d). Veins and venules were normal. There was acute bronchiolitis with neutrophilic infiltration; features of interstitial lung disease were not present. The heart (250 g) showed moderate right ventricular hypertrophy with a fresh thrombus in the right atrial appendage. The pulmonary trunk was as large as the ascending aorta with intimal thickening and few atherosclerotic plaques. Renal vascular changes (Fig. 75.4) appeared to be consistent with that seen in scleroderma. Chronic passive venous congestion was present in the liver with focal hemorrhagic necroses.

Cause of Death: Right heart failure due to pulmonary arterial hypertension (PAH).

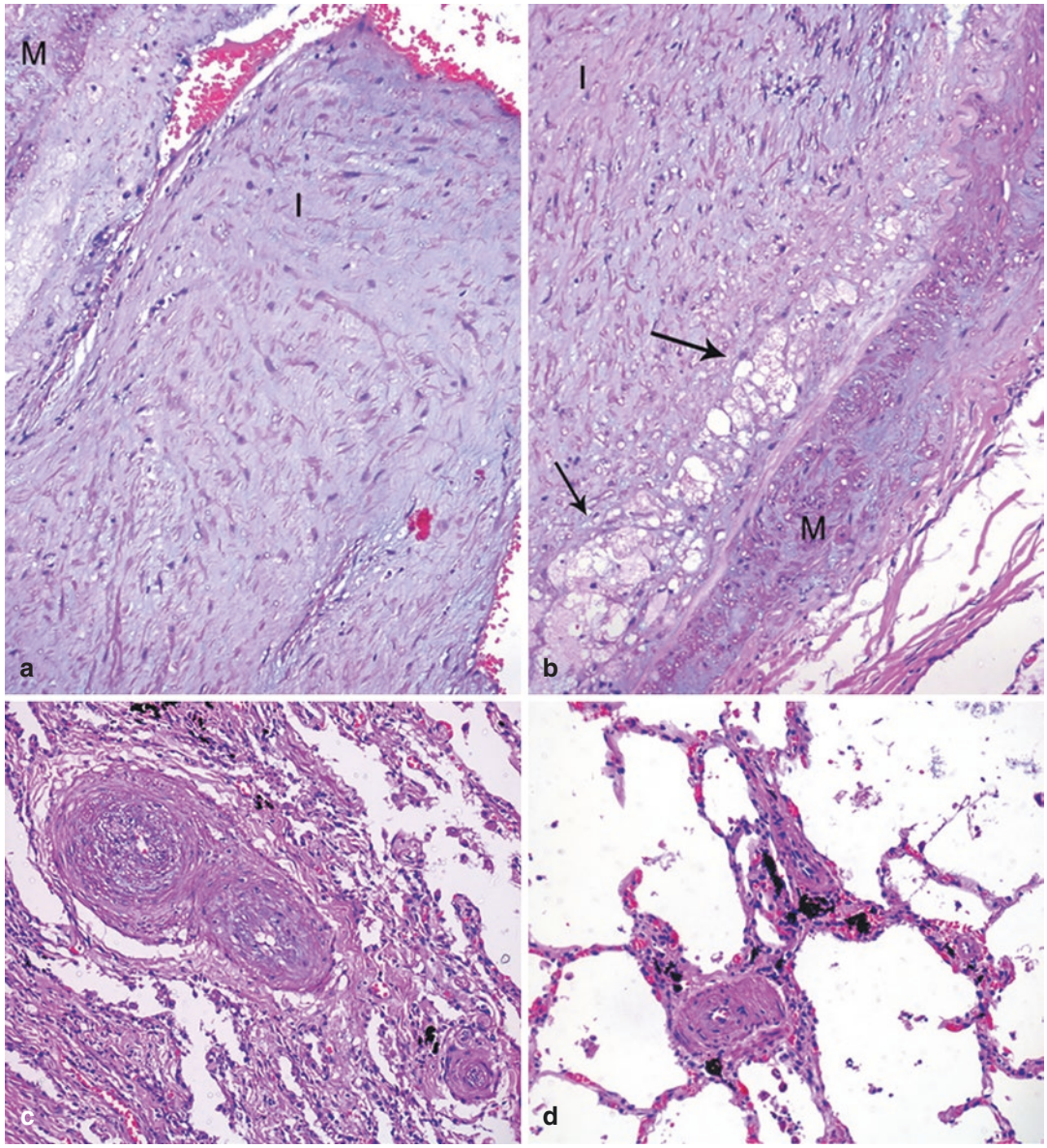

Fig. 75.3 (**a**) The intima I shows paucicellular fibromyxoid proliferation (H&E × 400); (**b**) Collections of foamy macrophages (arrows) are seen at the interface between the thickened intima I and the media M. Increased ground substances are also seen to intersect the smooth muscle bundles of the media (H&E × 400); (**c**) and (**d**) Show muscular arteries with medial hypertrophy and fibro-intimal thickening with muscularization of the arterioles (H&E × 400)

75.3 Discussion

Autopsy histopathological findings in the present case revealed features of well-established pulmonary hypertension (PH) in a setting of an autoimmune connective tissue disorder (CTD). PH, defined as an increase in the resting mean pulmonary arterial pressure of more than 25 mmHg, is classified on the basis of the hemodynamics and clinical settings. Utilizing additional parameters of pulmonary arterial wedge pressure and pulmonary vascular resistance, the PH is divided into 3

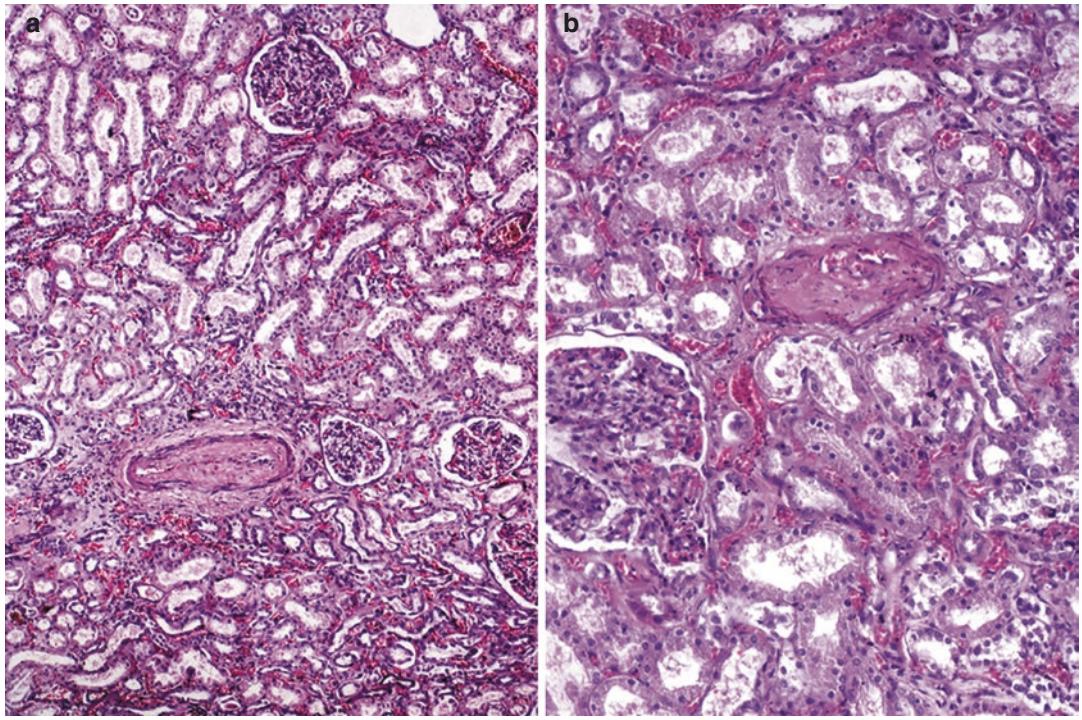

Fig. 75.4 Renal parenchyma showing intimal proliferation of the renal arteries (**a**) H&E × 200 and (**b**) H&E × 400

groups—precapillary, isolated postcapillary, and combined pre−/postcapillary PH. Five categories of PH are based on the etiopathogenetic mechanisms and therapeutic management, and they include Category 1—PAH, Category 2—PH associated with impaired left heart function, Category 3—PH secondary to underlying lung disease, Category 4—PH due to thromboembolism, and Category 5—PH arising from multifactorial causes. Though all of these can occur to a lesser or greater extent, PAH remains the most common and dreaded complication in CTD patients with reported estimates ranging from 2.8 to 32%. The proliferative remodeling of the small pulmonary arteries in PAH with CTDs is mediated by endothelial dysfunction induced by dysregulation of endothelin I, nitric oxide, and prostacyclin and elevated pro-inflammatory cytokines in a setting of autoantibodies and immune complexes. Among the CTDs, systemic sclerosis (SSc) accounts for up to 60–80% of PH, followed by mixed connective tissue disease and SLE; in other CTDs, it is estimated to be less than 1%.

SSc or scleroderma is an autoimmune disease that is characterized by a triad of small-vessel noninflammatory vasculopathy, excessive and progressive fibrosis, and a variable inflammatory infiltrate that can involve virtually any organ system. It shows a female preponderance (male-to-female ratio of 1:4–1:14) and a mean age of presentation of 50 years. Apart from the presence of ANAs, SSc patients have a host of other antibodies. Based on the degree of skin involvement, SSc is usually classified into limited (LcSSc) and diffuse (DcSSc) cutaneous forms. Earlier and frequent multiorgan involvement is seen with the diffuse subtype. Furthermore, LcSSc has an elevated titer of anticentromere antibodies, while DcSSc is associated with a predominance of anti-topoisomerase 1 (Scl-70) and anti-RNA polymerase III, antibodies. Apart from skin, the organ systems which are affected are the lungs, heart, gastrointestinal tract, kidneys, and musculoskeletal system. There is also a rare subset, SSc-sine scleroderma, where visceral involvement occurs in the absence of typical skin changes of SSc.

Despite an earlier diagnosis of SLE in our patient, there had been subsequent documentation of Raynaud's phenomenon and dysphagia and a centromeric ANA pattern had been noted; skin changes were absent. Furthermore, the available clinical information did not fulfil the classification criteria for SLE. The examination of the gastrointestinal system (including the esophagus) at autopsy did not reveal any abnormality. But primary involvement of the lungs and kidneys in this case suggested the diagnosis of the rarer variant of SSc-sine scleroderma. Unfortunately, the patient did not have thorough examination, investigations, and follow-up.

Systemic manifestations of SSc are very often seen in the lungs, as compared to the other organs. They occur in the form of interstitial lung disease (seen in 25–50% of patients) and PH, often associated with antitopoisomerase 1 antibody and anticentromere antibody positivity, respectively. Together, they are leading causes of morbidity and mortality in SSc patients. The cause of PH in these patients is extremely variable. About 8–12% of the patients with SSc have PAH (group 1), the most common pattern, seen in both subsets of SSc and associated with late onset of the disease and postmenopausal status. The arteries show prominent intimal fibrosis and medial hypertrophy; plexiform lesions are infrequent. Some patients can also show pulmonary venoocclusive like changes. PH can also develop as a complication of ILD (Group 3 PH), or left ventricular myocardial dysfunction (Group 2 PH) or as a consequence to antiphospholipid antibody (APLA)-related chronic thromboembolism (Group 4). Alarmingly, an overlap of different forms of PH can occur within the same patient. The present case revealed advanced PAH without significant interstitial lung involvement. Apart from right ventricular hypertrophy, there was no fibrosis in the left ventricular myocardium. The presence of an atrial appendage thrombus was noted in our index case. While the patient in the present case had been advised low-molecular weight heparin, there was no documentation of any test for APLA in the records retrieved. We presume that the thrombus could have been related to relative stasis in a dilated chamber in response to the severe PH. Hence, in this patient, PAH was the sole and extremely severe pulmonary manifestation and affected arteries of all sizes. As with other causes of PAH (See Chaps. 71 and 72), significant signs and symptoms occur late in the disease and hence it would be imperative to have periodic screening of these patients so that appropriate therapy targeting the vasoconstrictive/vasodilatatory mediators can be promptly instituted.

Further Reading

Attanasio U, Cuomo A, Pirozzi F, Loffredo S, Abete P, Petretta M, et al. Pulmonary hypertension phenotypes in systemic sclerosis: the right diagnosis for the right treatment. Int J Mol Sci. 2020;21:4430.

Denton CP, Khanna D. Systemic sclerosis. Lancet. 2017;390:1685–99.

Denton CP, Wells AU, Coghlan JG. Major lung complications of systemic sclerosis. Nat Rev Rheumatol. 2018;14:682.

Haque A, Kiely DG, Kovacs G, Roger Thompson AA, Condliffeet R. Pulmonary hypertension phenotypes in patients with systemic sclerosis. Eur Respir Rev. 2021;30:210053.

Johnson SR, van den Hoogen F, Devakandan K, Matucci Cerinic M, Pope JE. Systemic sclerosis: to subset or not to subset, that is the question. Eur J Rheumatol. 2020;7(Suppl 3):S222–7.

Mathai MC. Pulmonary hypertension associated with connective tissue disease. Cardiol Clin. 2022;40:29–43.

Sundaram SM, Chung L. An update on systemic sclerosis-associated pulmonary arterial hypertension: a review of the current literature. Curr Rheumatol Rep. 2018;20:10.

Vonk MC, Vandecasteele E, van Dijk AP. Pulmonary hypertension in connective tissue diseases, new evidence and challenges. Eur J Clin Invest. 2020;51:e13453.